

**Qiaohong Zu
Bo Hu (Eds.)**

LNCS 10745

Human Centered Computing

**Third International Conference, HCC 2017
Kazan, Russia, August 7–9, 2017
Revised Selected Papers**

 **Springer**

www.allitebooks.com

Commenced Publication in 1973

Founding and Former Series Editors:

Gerhard Goos, Juris Hartmanis, and Jan van Leeuwen

Editorial Board

David Hutchison

Lancaster University, Lancaster, UK

Takeo Kanade

Carnegie Mellon University, Pittsburgh, PA, USA

Josef Kittler

University of Surrey, Guildford, UK

Jon M. Kleinberg

Cornell University, Ithaca, NY, USA

Friedemann Mattern

ETH Zurich, Zurich, Switzerland

John C. Mitchell

Stanford University, Stanford, CA, USA

Moni Naor

Weizmann Institute of Science, Rehovot, Israel

C. Pandu Rangan

Indian Institute of Technology, Madras, India

Bernhard Steffen

TU Dortmund University, Dortmund, Germany

Demetri Terzopoulos

University of California, Los Angeles, CA, USA

Doug Tygar

University of California, Berkeley, CA, USA

Gerhard Weikum

Max Planck Institute for Informatics, Saarbrücken, Germany

More information about this series at <http://www.springer.com/series/7409>

Qiaohong Zu · Bo Hu (Eds.)

Human Centered Computing

Third International Conference, HCC 2017
Kazan, Russia, August 7–9, 2017
Revised Selected Papers

 Springer

Editors

Qiaohong Zu
Wuhan University of Technology
Wuhan
China

Bo Hu
Fujitsu Laboratories of Europe Ltd.
Hayes
UK

ISSN 0302-9743 ISSN 1611-3349 (electronic)
Lecture Notes in Computer Science
ISBN 978-3-319-74520-6 ISBN 978-3-319-74521-3 (eBook)
<https://doi.org/10.1007/978-3-319-74521-3>

Library of Congress Control Number: 2017964220

LNCS Sublibrary: SL3 – Information Systems and Applications, incl. Internet/Web, and HCI

© Springer International Publishing AG 2018

This work is subject to copyright. All rights are reserved by the Publisher, whether the whole or part of the material is concerned, specifically the rights of translation, reprinting, reuse of illustrations, recitation, broadcasting, reproduction on microfilms or in any other physical way, and transmission or information storage and retrieval, electronic adaptation, computer software, or by similar or dissimilar methodology now known or hereafter developed.

The use of general descriptive names, registered names, trademarks, service marks, etc. in this publication does not imply, even in the absence of a specific statement, that such names are exempt from the relevant protective laws and regulations and therefore free for general use.

The publisher, the authors and the editors are safe to assume that the advice and information in this book are believed to be true and accurate at the date of publication. Neither the publisher nor the authors or the editors give a warranty, express or implied, with respect to the material contained herein or for any errors or omissions that may have been made. The publisher remains neutral with regard to jurisdictional claims in published maps and institutional affiliations.

Printed on acid-free paper

This Springer imprint is published by Springer Nature
The registered company is Springer International Publishing AG
The registered company address is: Gewerbestrasse 11, 6330 Cham, Switzerland

Preface

In the past decade, a gradual yet steady paradigm shift was the refocusing of technologies from machine-oriented concepts, algorithms, and automats toward the maximization of human potentials and the fulfilment of human needs and human well-being. Consequently, the development of computational power and computational efficiency has been set in the context of effortless technology utilization by both individuals and societies. With the recent advances in human-machine interfaces, wireless and mobile network technologies, and data analytics, we finally set out on the long journey toward making computer services truly human-centric, instead of limiting human capacities to suit computer requirements. Instead of playing a prominent role in the behavior of individuals and societies, machines and their very existence have become ever more subtle: smart devices have been weaved into the everyday fabric; analytic power has penetrated into all aspects of our daily activities from family to work (and everything in between); and automation has begun to displace segments of our routines. For an area as active as human-centered computing, it is not possible to cover the entire thematic spectrum. Instead, the Human-Centered Computing (HCC) conference aims to present a selection of examples of new approaches, methods, and achievements that can underpin the aforementioned paradigm shift.

HCC 2017 was the third in the series, following successful events in Phnom Penh, Cambodia (2014), and Columbo, Sri Lanka (2016). The HCC 2017 papers present a balance between conceptual and empirical work, between design and evaluation studies, and between theoretical and applied research.

All HCC 2017 submissions went through rigorous paper evaluation and selection process. Each paper was peer-reviewed by the Program Committee and selected reviewers and meta-reviewed by senior Program committee members. Based on these recommendations, the program co-chairs made acceptance decisions and classified the accepted papers into the following categories: full regular papers, short papers, and position papers.

It has been another year of hard-working and selfless contribution. As the conference Organizing Committee, we are grateful to all members of the Technical Program Committee — it was their hard work that enabled us to identify a set of high-quality submissions reflecting the trends and interests of the paradigm shift. We would like to extend our gratitude to the international Advisory Committee for its invaluable advice and guidance. Finally, our special thanks also goes to the additional reviewers, student volunteers and members of the local organization team, who are the key elements that made HCC2017 a successful event.

August 2017

Max Talanov
Salvatore Distefano
Qiaohong Zu
Bo Hu
Vlada Kugurakova

Organization

Honorary Conference Chair

Airat Khasianov Kazan Federal University, Russia

Conference Co-chairs

Max Talanov ITIS, Kazan Federal University, Russia
Yong Tang South China Normal University, China

Program Committee Co-chairs

Salvatore Distefano Università degli Studi di Messina, Italy
Jing He Victoria University, Australia

Organizing Committee

Chengzhou Fu South China Normal University, China
Vlada Kugurakova Kazan Federal University, Russia
Qiaohong Zu Wuhan University of Technology, China

Publication Committee

Bo Hu Fujitsu Labs of Europe, UK
Philip Moore Birmingham City University, UK

Secretariat

Jizheng Wan Coventry University, UK

Abstracts of Invited Keynotes

IoT+AI: Opportunities and Challenges

Huadong Ma

School of Computer Science, Beijing University of Posts
and Telecommunications, Beijing, China
mhd@bupt.edu.cn

The Internet of Things (IoT) can enable the interconnection and integration of the physical world and the cyber space, and has been widely considered as the kernel technology for sensing the urban environments and providing smart services further. At the same time, the rapid development of Artificial Intelligence (AI) brings many opportunities to IoT. In this talk, we first introduce the challenges of urban sensing networks. Combining AI theory, we discuss some researches on sensing, networking and computing, and service in the IoT environment. Finally, we outline the prospects of IoT development.

Biograph

Dr. Huadong Ma is a Chang Jiang Scholar Professor and Executive Dean, School of Computer Science, Beijing University of Posts and Telecommunications (BUPT), China. He is also Director of Beijing Key Lab of Intelligent Telecommunications Software and Multimedia, BUPT. He is Chief Scientist of the project “Basic Research on the Architecture of Internet of Things” supported by the National 973 Program of China from 2010 to 2013. He received his PhD degree in Computer Science from the Institute of Computing Technology, Chinese Academy of Science in 1995. From 1999 to 2000, he held a visiting position in the Department of Electrical Engineering and Computer Science, The University of Michigan, Ann Arbor, USA. His current research focuses on sensor networks and Internet of things, multimedia computing, and he has published over 200 papers in journals (such as ACM/IEEE Transactions) or Conferences (such as IEEE INFOCOM, ACM MM) and 4 books on these fields. As a co-author, he got the best paper award in IEEE ICPADS2010 and the best student paper award in IEEE ICME2016. He was awarded National Funds for Distinguished Young Scientists in 2009. He serves for Chair of ACM SIGMOBILE China.

Machine Learning for Real-World: Is Deep Learning Enough?

Adil Khan

Department of Computer Science, Innopolis University, Innopolis,
Respublika Tatarstan, Russian Federation
a.khan@innopolis.ru

The real world is unpredictable; it is full of noise and filled with novel scenarios. Therefore, it is almost impossible to provide the machine learning models with a complete representation of such a world at the time of training, forcing us to work with an insufficient picture of our world. That is why one of the biggest problems that the field of machine learning still faces today is the inability of the learned models to generalize well to scenarios that are different from the ones seen at the time of training. In this talk, we will explore this problem in four different areas: Human Activity Recognition, Emotion Recognition in Text, User Authentication, and Medical Image Analysis. We will see the results of applying deep learning models to these problems, and discuss ways that may be used in addition to the use of such models to achieve optimum performance.

Biograph

Dr. Adil Khan is an Associate Professor in the Department of Computer Science at Innopolis University, Russia. He is also the head of Machine Learning & Knowledge Representation Lab at Innopolis. He has received his Ph.D. in Computer Engineering from Kyung Hee University, South Korea. He has over 11 years of experience in academic research and teaching. His primary research interests include machine learning, computer vision, data analytics, wearable computing, and context-aware computing. His research work, comprising over 60 articles, is published in various international conferences and journals. He is currently participating in several international research projects. He is an IEEE member and is also a reviewer for numerous IEEE, ACM, Elsevier and other international journals.

Contents

An Improved MST Clustering Algorithm Based on Membrane Computing.	1
<i>Ping Gong and Xiyu Liu</i>	
A Method for Correcting the Leaning of AR Two-Dimensional Codes Based on LSM	13
<i>Chen Miao, Shufen Liu, and Zhilin Yao</i>	
The Associated Algorithm of Target Batch Number Based on Gaussian Mixture Clustering	23
<i>Ning Liu, Shufen Liu, and Xinjia Zhang</i>	
Density Peaks Clustering Based on Improved RNA Genetic Algorithm	28
<i>Liyen Ren and Wenke Zang</i>	
Local Homogeneous Weighted Spiking Neural P Systems	34
<i>Mengmeng Liu and Feng Qi</i>	
Weight-Improved K-Means-Based Consensus Clustering	46
<i>Yanhua Wang, Laisheng Xiang, and Xiyu Liu</i>	
A Novel Trace Clustering Technique Based on Constrained Trace Alignment	53
<i>Pan Wang, Wen'an Tan, Anqiong Tang, and Kai Hu</i>	
A Fast Local Image Descriptor Based on Patch Quantization	64
<i>Tian Tian, Fan Yang, Kun Zheng, Hong Yao, and Qian Gao</i>	
A Method of Large - Scale Log Pattern Mining	76
<i>Lu Li, Yi Man, and Mo Chen</i>	
More Efficient Filtration Method for Big Data Order-Preserving Matching.	85
<i>Wenchao Jiang, Dexi Lin, Sui Lin, Chuanjie Li, and Aobing Sun</i>	
Blind Image Quality Assessment via Analysis of GLCM	95
<i>Guanghui Yue, Chunping Hou, Tongtong Ma, and Yang Yang</i>	
An Improved Ranked K-medoids Clustering Algorithm Based on a P System	102
<i>Bao Zhang, Laisheng Xiang, and Xiyu Liu</i>	

A Novel Inverse-Operation Based Group Undo/Redo Algorithm
for Feature-Based 3D Collaborative CAD Systems 108
Yuan Cheng, Fazhi He, Xiao Lv, and Weiwei Cai

Two Steps Method Using Polarization to Resist Phase Noise
for Self-interference Cancelation in Full-Duplex 118
Fangfang Liu, Xinyi Wang, Chunyan Feng, and Xiao Han

Sparse Linear Method Based Top-N Course Recommendation System
with Expert Knowledge and L_0 Regularization 130
Jinjiao Lin, Haitao Pu, Yibin Li, and Jian Lian

The Research on the Container Truck Scheduling Based on Fuzzy
Control and Ant Colony Algorithm 139
Meng Yu, Dawei Li, and Qiang Wang

Researches on the Analysis Framework of Application Layer
Communication Protocol Based on SQLite. 150
Wenyuan Xu, Hao Li, and Weifeng Xu

The Implementation of Growth Guidance Factor Diffusion via Octree
Spatial Structures for Neuronal Systems Simulation. 158
Almaz Sabitov, Fail Gafarov, Vlada Kugurakova, and Vitaly Abramov

Intelligent Perceptive QoS Based Centralized Admission Control
for Route Computing. 164
Xuejing Li, Yajuan Qin, Haohui Fu, Zhewei Zhang, and Xiaorong Lin

Research on the Shortest Path Problem Based on Improved
Genetic Algorithm. 173
Baoliang Wang, Susu Yao, Kaining Lu, and Huizhen Zhao

Semantic Web Languages for Policy Enforcement
in the Internet of Things 183
Rustem Dautov and Salvatore Distefano

Network Traffic Prediction Based on Wavelet Transform
and Genetic Algorithm. 189
Xuehui Zhao, Wanbo Zheng, Lei Ding, and Xingang Zhang

Research and Optimization of the Cluster Server Load Balancing
Technology Based on Centos 7. 201
Lei Ding, Wanbo Zheng, Shufen Liu, and Zhian Han

Base Station Location Optimization Based on Genetic Algorithm
in CAD System 208
Yanhua Wang, Laisheng Xiang, and Xiyu Liu

A Study of Optimal Multi-server System Configuration with Variate Deadlines and Rental Prices in Cloud Computing 215
Zhongfeng Kang and Bo Yang

A Composite Anomaly Detection Method for Identifying Network Element Hitches. 232
Duo Zhang, Yi Man, and Ligang Ren

D-SVM Fusion Clustering Algorithm Based on Indoor Location. 245
Zhongliang Deng, Jiachen Fan, and Jichao Jiao

Research on Evaluation of Sensor Deviations During Flight 252
Yuping Xiong, Shufen Liu, Sihua Gao, and Yemei Zhu

A Distributed Routing Algorithm for LEO Satellite Networks. 258
Jundong Ding, Yong Zhang, Ruonan Li, and Liang Zhao

Optimization of Smart Home System Based on Wireless Sensor Network 265
Xing Guo and Neng Hu

The Energy Efficiency Research of Traffic Offloading Mechanism for Green Heterogeneous Networks 274
Kaili Wu, Yifei Wei, Qiao Li, Da Guo, and Mei Song

A Game-Theoretic Approach for Joint Optimization of Sensing and Access in Cognitive Cellular Heterogeneous Networks 288
Changqing Pan, Ya'nan Xiao, Yinglei Teng, Weiqi Sun, and Xiaoqi Qin

Energy Harvesting Relay Node Deployment for Network Capacity Expansion. 301
Zhiqiang Zhang, Yifei Wei, Bo Gu, Xiaojun Wang, and Mei Song

Parameters Optimization for KFKM Clustering Algorithm Based on WiFi Indoor Positioning 311
Zhengying Hu, Lujuan Ma, Baoling Liu, and Zhi Zhang

Energy Harvesting Time Coefficient Analyze for Cognitive Radio Sensor Network Using Game Theory. 318
Mengyu Zhao, Yifei Wei, Qiao Li, Mei Song, and Ningning Liu

Traffic Paralysis Alarm System Based on Strong Associated Subnet 330
Chen Yu, Shaohui Zhu, Hanhua Chen, Ruiguo Zhang, Jiehan Zhou, and Hai Jin

Fault Recovery Algorithm Based on SDN Network	342
<i>Yi Zhang, Yifei Wei, Ruqin Huang, Bo Gu, Yue Ma, and Mei Song</i>	
Sensor Location Verification Scheme Based on Range-Free Localizations in WSNs	354
<i>Chunyu Miao, Lina Chen, and Qingzhang Chen</i>	
Design and Development of Parametric System for Planetary Reducer	364
<i>Yangpeng Chen, Menglun Tao, Dingfang Chen, Bo Li, Yanfang Yang, and Boting Chen</i>	
A Dynamic Double Threshold Based Cooperative Spectrum Sensing Strategy in Heterogeneous Cognitive Radio Networks	376
<i>Chongxiao Peng, Yifei Wei, Bo Gu, Ligang Ren, and Mei Song</i>	
A Distributed Self-adaption Cube Building Model Based on Query Log	382
<i>Meina Song, Mingkun Li, Zhuohuan Li, and Haihong E.</i>	
Property-Based Network Discovery of IoT Nodes Using Bloom Filters	394
<i>Rustem Dautov, Salvatore Distefano, Oleg Senko, and Oleg Surnin</i>	
The Personality Analysis of Characters in Vernacular Novels by SC-LIWC	400
<i>Yahui Yuan, Baobin Li, Dongdong Jiao, and Tingshao Zhu</i>	
Digging Deep Inside: An Extended Analysis of SCHOLAT E-Learning Data	410
<i>Aftab Akram, Chengzhou Fu, Yong Tang, Yuncheng Jiang, and Kun Guo</i>	
Social Network Analysis of China Computer Federation Co-author Network	422
<i>Chengzhou Fu, Weiquan Zeng, Rui Ding, Chengjie Mao, Chaobo He, and Guohua Chen</i>	
Detecting Postpartum Depression in Depressed People by Speech Features	433
<i>Jingying Wang, Xiaoyun Sui, Bin Hu, Jonathan Flint, Shuotian Bai, Yuanbo Gao, Yang Zhou, and Tingshao Zhu</i>	
Research on Network Public Opinion Propagation Mechanism Based on Sina Micro-blog	443
<i>Weidong Huang, Qian Wang, and Yixuan Wang</i>	

Scholar Recommendation Model in Large Scale Academic Social Networking Platform 453
Ming Chen, Chunying Li, Jiwei Liu, Dejie Meng, and Yong Tang

Research on Simulation for Fuel Consumption of UAV 465
Zongpu Jia, Yonghui Shi, Songyuan Gu, and Shufen Liu

Research on Meteorological Data Simulation 472
Zhenglun Wu, Shufen Liu, and Tie Bao

Anti-data Mining on Group Privacy Information 481
Fan Yang, Tian Tian, Hong Yao, Xiuyu Zhao, Tinggang Zheng, and Min Ning

Big Data Analysis of Reviews on E-commerce Based on Hadoop 492
Qiaohong Zu and Jiangming Wu

Analysis on Structural Vulnerability Under the Asymmetric Information 503
Mingshu He, Xiaojuan Wang, Jingwen You, and Zhen Wang

Combining Link and Content Correlation Learning for Cross-Modal Retrieval in Social Multimedia 516
Longtao Zhang, Fangfang Liu, and Zhimin Zeng

The Research on Touch Gestures Interaction Design for Personal Portable Computer 527
Qing Sheng, Ting Liu, Wenjun Hou, and Gengyi Wang

Research on Mobile User Dynamic Trust Model Based on Mobile Agent System 538
Weijin Jiang and Yuhui Xu

A Group Decision-Making Method Based on Evidence Theory in Uncertain Dynamic Environment 550
Weijin Jiang and Yuhui Xu

Analysis and Estimate the Effect of Knowledge on Software Reliability Distribution 561
Chunhui Yang, Yan Gao, Xuedong Kong, Dingfang Chen, Shengwu Xiong, and Jianwen Xiang

Development of Virtual Reality-Based Rock Climbing System 571
Yiming Su, Dingfang Chen, Congxing Zheng, Sihan Wang, Liwen Chang, and Jie Mei

Kinematics and Simulation Analysis of a 3-DOF Mobile Handling Robot Based ADAMS and MATLAB 582
Jingbo Hu, Dingfang Chen, Lijie Li, Jie Mei, Qin Guo, and Huafeng Shi

A New Type of 3D Printing Nozzle with PET Wire as Raw Material 588
Yawei Hong, Shaobo Li, Shupei Wu, Tianhao Huang, Guang Liu, Liwen Chang, and Yang Zhang

When Partitioning Works and When It Doesn't: An Empirical Study on Cache Way Partitioning 595
Hanfeng Qin

Track Maintenance Feedback Mechanism Based on Hadoop Big Data Analysis. 608
Yong Zhu, Jiawei Fan, Guangyue Liu, Mou Wang, and Qian Wang

Crowdsourcing and Stigmergic Approaches for (Swarm) Intelligent Transportation Systems 616
Salvatore Distefano, Giovanni Merlino, Antonio Puliafito, Davide Cerotti, and Rustem Dautov

Research on Visual Feedback Based on Natural Gesture 627
Wenjun Hou, Shupeng Zhang, and Zhiyang Jiang

Information Security Technology and Application in Logistics Traceability System of Aquatic Products Based on QR Code 638
Qiaohong Zu and Rui Chen

Quantified Self: Big Data Analysis Platform for Human Factor Efficacy Evaluation of Complex System. 648
Chaoqiang Li, Wenjun Hou, Xiaoling Chen, and Hao Li

Application of Speech Recognition Technology in Logistics Selection System. 654
Tianzheng Fu and Bin Sun

Author Index 661

An Improved MST Clustering Algorithm Based on Membrane Computing

Ping Gong and Xiyu Liu^(✉)

School of Management Science and Engineering,
Shandong Normal University, Jinan 250014, Shandong, China
gongping_sd@163.com, sdxylu@163.com

Abstract. MST clustering algorithm can detect data clusters with irregular boundaries. For a weighted complete graph the feasible solutions to the MST problem is non-unique. Membrane computing known for its characteristics of distribution and maximal parallelism can properly reduce the complexity of processing a MST of a graph. This paper combines MST clustering algorithm and membrane computing by designing a specific P system. The designed P system realizes the process of an improved MST clustering by collecting all feasible solutions to the MST problem together preserving proper edges and deleting redundant heavy edges. The improved MST clustering method efficiently enhances the quality of clustering and proved to be feasible through an instance.

Keywords: MST clustering algorithm · Membrane computing
P system

1 Introduction

Clustering is the process of partitioning a set of data objects into subsets, making each subset a cluster, such that objects in identical clusters are similar to each other, yet dissimilar to objects in other clusters. Clustering has been widely used in many applications such as business intelligence, image pattern recognition, Web search, biology, and security [1].

There are many kinds of algorithms in the literature to solve clustering problems, mainly including partitioning methods, hierarchical methods, density-based methods and grid-based methods and so on. Among various kinds of clustering methods, the minimum spanning tree (MST) clustering algorithm is known to be capable of detecting clusters with irregular boundaries, because it does not assume a spherical shaped clustering structure of the underlying data. MST constructing problems has been investigated by researchers since 1926 which also makes it a relatively mature algorithm. Many researches on this algorithm have promised close to linear time complexity of construction cost [2, 3]. Standard MST clustering algorithms basically include sorting the edges in constructed graph and removing the edges with heaviest weight. Applying MST algorithm to solve clustering problems has been investigated, but in practical applications, clustering results of MST algorithms are easy to be affected by outliers [3].

Membrane computing is a new branch of natural computing, which have been investigated and proved to be universal and efficient. Membrane computing models (named P system) are motivated by the parallel characteristic of biochemical reactions taking place in a series of regions of a living cell. This computing theory is also motivated by the mathematical convenience of this kind of parallelism. P systems owe the characteristics of distribution and maximal parallelism [4]. Thus, membrane computing approaches are more suitable applied to combinatorial problems, graph theory, and finite state problems.

On account of the non-uniqueness of feasible solutions to the MST problem and the lack of researches on MST clustering in membrane computing fields, this paper combines membrane structures with MST clustering algorithm together. Make P system an efficient computing tool during the process of solving MST clustering problem to reduce the time complexity. It is no doubt that combination will greatly improve the quality and efficiency of finding the best clustering results.

2 Preliminary

2.1 P System

Membrane computing, introduced by PAUN in 1998, takes the living cell as multi-hierarchical structural regions, which are surrounded by the so-called membranes. There are three main investigated variants of P systems, cell-like, tissue-like, and neural-like. Cell-like P System imitates the function and structure of the cells, and it includes the membrane structure, rules and objects as basic elements. Cell-like arrangements of membranes correspond to trees. And some P systems have been proposed to solve computer science related problems, like NP problems, arithmetic operations, matrix vector computation and image processing. P systems have also been proved to be effective when being studied with clustering problems [6].

Membranes divide the whole system into different regions. The skin membrane is the outermost membrane. A membrane is a basic membrane if there are no membranes in it and a membrane is a non-elemental membrane otherwise. Rules and objects exist in regions. Usually the objects are indicated by strings or characters. Rules are used to process objects or membranes in corresponding region. The rules are executed uncertainly and maximum concurrently. Cell-like P System can be further divided into three types from according to kinds of rules: transition P system, P system with communication rules and P system with active membranes [7]. The basic membrane structure is shown in Fig. 1.

In general, a P system of degree m is a construct:

$$\Pi = (V, T, C, H, \mu, w_1, w_2, \dots, w_m, (R_1, \rho_1), (R_2, \rho_2), \dots, (R_m, \rho_m))$$

Where:

1. V is an alphabet. Elements in it are called objects;
2. $T \subseteq V$ is the output objects;

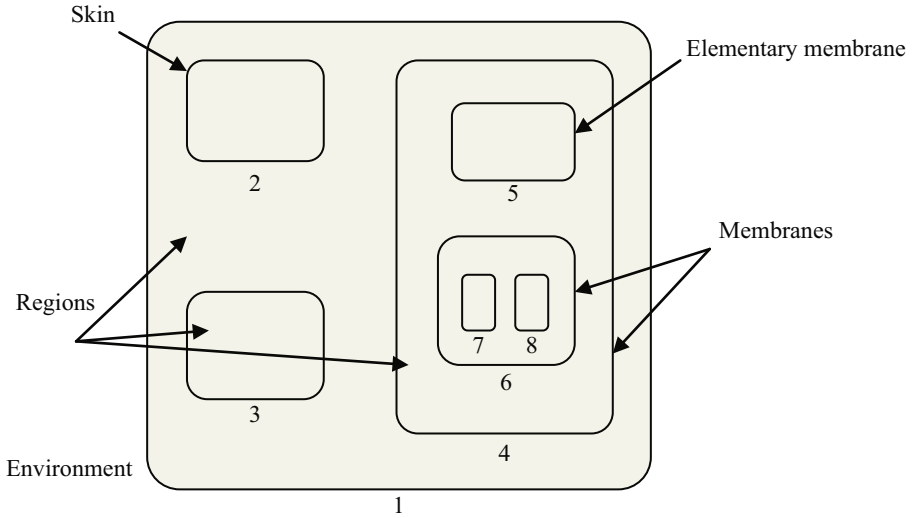


Fig. 1. The basic membrane structure

3. $C \subseteq V - T$ is the catalyst. These catalysts neither change their numbers nor their kinds in rules. But rules cannot be executed without these catalysts;
4. $H = \{1, 2, m\}$ is the set of membrane labels.
5. μ is a membrane structure; each membrane has its label;
6. $w_i (i = 1, 2, m)$ is the objects in membrane i ;
7. The basic rule is in the form of $(u \rightarrow v)$, u is a string composed of objects in V and v is a string in the form of $v = v'$ or $v = v'\delta$. v' is a string over $\{\text{here, out, in} \in V, 1 \leq j \leq m\}$.
8. R_i is the set of the rules in region i . ρ_i is the precedence relation which defines the partial order relation over R_i . High priority rule is executed prior [8].

The rules are used in maximum parallel and uncertainly in each membrane when calculating. So space of exponential growth can be generated in linear operation steps. This is very helpful to solve the computationally hard problems within feasible time. The P system will halt after some steps if no more rules can be executed and these objects in output membrane is the final result. The P system will not halt if rules are always executed, then this calculation is invalid, and there is no result being outputted [9].

2.2 MST Clustering Method

A tree is a simple structure for representing binary relationships, and any connected component of a tree is called a sub-tree. A spanning tree is an acyclic connected sub-tree of a graph G , which contains all the vertices from G . And the minimum spanning tree (MST) is the one with the minimum weight. By representing the data set in a graph, finding the corresponding minimum spanning tree, the structure characteristics of data can be got to some extent.

MST related theories have been widely used for data classification in the field of pattern recognition and image processing for about forty years. As classical algorithms rely on either the idea of grouping data around some ‘centers’ or the idea of separating data points using some regular geometric curve like a hyper-plane, they generally do not work well when the boundaries of the clusters are very complex. An MST is quite invariant to detailed geometric changes in the boundaries of clusters. As long as the relative distances between clusters do not change significantly, the shape complexity of a cluster has very little effect on the performance of our MST-based clustering algorithms. And the process is quite simple. Remove the $k-1$ largest weighted edges from the constructed minimum spanning tree, and k sub-trees obtained can just be regarded as k clusters [10]. Two key advantages in representing a set of multi-dimensional data as an MST are: 1. The simple structure of a tree facilitates efficient implementations of rigorous clustering algorithms, which otherwise are highly computationally challenging; and 2. As an MST-based clustering does not depend on detailed geometric shape of a cluster, it can overcome many of the problems faced by classical clustering algorithms.

Representing a set of multi-dimensional data points as a simple tree structure will lose some of the inter-data relationship. But during the process of simplifying the data set into a MST, essential intra-data information is remained in MST tree. Each cluster corresponds to one sub-tree, which does not overlap the representing sub-tree of any other clusters. And through MST representation, we can convert a multi-dimensional clustering problem to a tree partitioning problem, just like finding a particular set of tree edges and cutting them. And finding a globally optimal solution for a combinatorial optimization problem is often possible.

3 A P System for Improved MST Clustering Method

3.1 The Improved MST Clustering Method

MST clustering methods attempt to represents a data set into a tree graph with the minimum edge weights, then cut $k-1$ longest edges in it to form k clusters. In this section, we propose a new method to find a minimum spanning tree, and implement the MST constructing rules in a membrane system. By applying the membrane structure as a computing tool, we can find all feasible solutions to an MST problem in the process. And finally we optimize the process of cutting the longest $k-1$ edges to find a better clustering solution.

Firstly, we measure similarity between data points as distances of objects, and express in a matrix W'_{mn}

$$W'_{mn} = \begin{bmatrix} w'_{11} & w'_{12} & \cdots & w'_{1n} \\ w'_{21} & w'_{22} & \cdots & w'_{2n} \\ \cdots & \cdots & \cdots & \cdots \\ w'_{n1} & w'_{n2} & \cdots & w'_{nn} \end{bmatrix}$$

Where w'_{ij} is the distance between point a_i and a_j . To facilitate calculation, W'_{mn} is totally converted into corresponding integer matrix W_{mn} as follows:

$$W_{mn} = \begin{bmatrix} w_{11} & w_{12} & \dots & w_{1n} \\ w_{21} & w_{22} & \dots & w_{2n} \\ \dots & \dots & \dots & \dots \\ w_{n1} & w_{n2} & \dots & w_{nn} \end{bmatrix}$$

Accordingly, every w_{ij} here means the weight of edge e_{ij} connecting vertex a_i and a_j .

The first part of MST clustering process is to construct minimum spanning trees: We set V as vertex set and E as edge set, and they both are empty sets initially; rank all edges in ascending order; then add the shortest edge e_{ij} (with the smallest weight) into the set E , and accordingly add the associated two vertex a_i and a_j into the set V ; other edges are added into set E gradually, which are supposed to be connected to one of the existing vertices and with smallest weight in the remaining edges; after an edge is added into E , we add the other vertex connected to it into V ; while once there are two identical vertices in V , it means that there is a circle in tree. And this edge will be abandoned. Above steps are repeated until $|V| = n$ and $|E| = n-1$ ($|V|$ is the number of vertices in V ; $|E|$ is the number of edges in E).

For a complete graph, especially a graph with a mass of vertex, there are edges with identical weights. Therefore, the minimum spanning tree of a given complete graph is not unique and only if the shape of the minimum spanning tree is not unique. To find all feasible solutions, we are supposed to choose every different edge with the same weights every time when constructing a MST. But obviously, such enumerating process will take too much time.

One of the most advantages of membrane computing is its parallelism. Membrane structure is hierarchical, and computing rules in regions evolve react and communicate synchronously. For this reason, we apply this parallelism to constructing all minimum spanning trees of a complete graph at a time by duplicating and generating new reaction membranes with rules. When there are more than one edges can be chosen, we can construct new computing regions, where we add every feasible new edge into the tree.

When the process of adding edges and vertices to corresponding sets ends, the next step is to partition the produced MST. An edge with a large weight means that the two vertices connected by it are distinct from each other. For this reason, we choose to delete $k-1$ maximum value edges from the existed set E to form k clusters. Since there are more than one MST feasible solutions collected, for these always appearing short edges, we can conclude that they are correct elements of sub-tree which should be preserved in partitions. We rearrange edges which used to belong to set E but now appear in different membranes as parts of MST solutions with their frequency of occurrences in descending order. Then we delete redundant edges one by one. For edges with the same value, we preferentially preserve ones with higher frequency; for edges with same frequency, we preferentially delete ones with heavier weights. To make sure that every point is kept in set V , when an edge is to be deleted, the existence of two adjacent vertices must be checked. Repeat this process until $|E| = N-K$.

The procedure of our method is as below:

Input: $G = \langle V, E \rangle$, k , n

Output: k clusters

Begin:

Sort the edges with their w_{ij} in ascending order.

Select the shortest e_{ij} initially

If (the shortest e_{ij} is not unique) {

Set every shortest edge as an initial edge in different computation branches.

}

Add e_{ij} into E . Add the connected $a_i a_j$ into V .

For (e_{ij} is the next shortest edge) {

If (a_i is in V and a_j is not in V) {

Add e_{ij} into E . Add a_j into V .

} else if (a_j is in V and a_i is not in V) {

Add e_{ij} into E . Add a_i into V .

} else {

Give up e_{ij} . // to make sure the tree connected and with no circle.

}

}

If ($|V| \neq n$) {Give up this computation branch.}

Count the frequency $f_{e_{ij}}$ of edges in different V .

Sort edges with their frequency in descending order and keep the top n .

For (e_{ij}) {

If ($f_{e_{ij}} = f_{e_{ij+1}}$ and $w_{ij} > w_{ij+1}$) {Give up e_{ij} }

Until $|E| = n - k$.

}

End

3.2 Definition of the P System for Improved MST Clustering Method

P system deal with multi-sets of symbol objects in distributed and parallel manner. So we design a specific P system for the improved MST clustering method to collect all

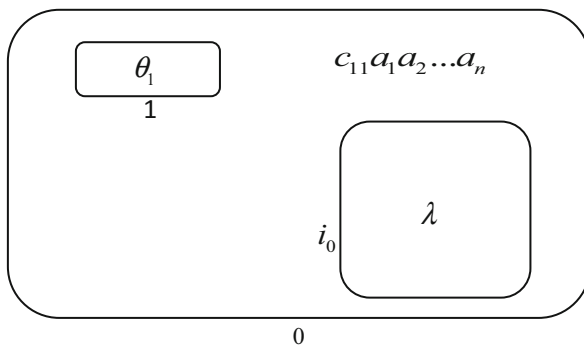


Fig. 2. The initial state of the designed P system

MST feasible solutions and partition the dataset. The designed P system is shown as Fig. 2.

$$\Pi = (O, \mu, M_0, M_1, M_{i_0}, R_0, R_1, R_{i_0}, \rho)$$

Where:

$O = \{c_{11}a_1a_2 \dots a_n\theta_1\lambda\}$ specifies the initial collection of objects in the P system;

$\mu = [{}_0[{}_1]_1 [{}_{i_0}]_{i_0}]_0$ specifies the initial membrane structure of the P system;

$M_0 = \{c_{11}a_1a_2 \dots a_n\}$ specifies the initial objects in membrane 0;

$M_1 = \{\theta_1\}$ specifies the initial object in membrane 1;

$M_{i_0} = \{\lambda\}$ specifies that there is nothing in the output membrane i_0 initially;

Rule in R_0 :

$$r_1 = \{c_{ij}a_i a_j \rightarrow c_{i(j+1)}a_i a_j [U_{ij}^{w_{ij}}]_{in1} | 1 \leq i, j \leq n\} \cup \\ \{c_{i(n+1)} \rightarrow c_{(i+1)(i+2)} | 1 \leq i, j \leq n\} \cup \{c_{n(n+1)} \rightarrow \lambda\}$$

Rules in R_1 :

$$r_2 = \{\theta_1 U_{ij}^{w_{ij}} \rightarrow \theta_1 U_{ij}^{w_{ij}-1} | 1 \leq i, j \leq n\}$$

$$r_3 = \{\zeta \theta_1 U_{ij}^t \rightarrow q_i q_j v_i v_j P_{ij} \theta_2 A_c | t = 0, 1 \leq i, j \leq n\} \\ \cup \{\zeta \theta_1 U_{i_1 j_1}^t \dots U_{i_s j_s}^t \rightarrow [q_{i_1} q_{j_1} v_{i_1} v_{j_1} P_{i_1 j_1} A_c \theta_2]_1 \dots [q_{i_s} q_{j_s} v_{i_s} v_{j_s} P_{i_s j_s} A_c \theta_2]_1 \\ | t = 0, 1 \leq i, j \leq n\}$$

$$r_4 = \{\zeta \theta_2 q_i U_{is}^{w_{is}} \rightarrow \zeta \theta_2 q_i U_{is}^{w_{is}-1} | 1 \leq i, s \leq n\} \cup \\ \{\zeta \theta_2 q_j U_{sj}^{w_{sj}} \rightarrow \zeta \theta_2 q_j U_{sj}^{w_{sj}-1} | 1 \leq s, j \leq n\}$$

$$r_5 = \{\zeta \theta_2 v_i v_s U_{is}^t \rightarrow \zeta \theta_2 v_i v_s | t = 0, 1 \leq i, s \leq n\}$$

$$\begin{aligned}
r_6 &= \{ \zeta \theta_2 v_i U'_{is} \rightarrow q_s v_i v_s \omega_s P_{is} \theta_2 | t = 0, 1 \leq i, s \leq n \} \cup \\
&\quad \{ \zeta \theta_2 v_j U'_{sj} \rightarrow q_s v_s v_j \omega_s P_{sj} \theta_2 | t = 0, 1 \leq s, j \leq n \} \\
r_7 &= \{ [\zeta \theta_2^2 v_s \omega_i P_{is} A_c]_1 \rightarrow [q_s v_s P_{is} A_c \theta_2]_1 [A_c \theta_2 \zeta]_1 | 1 \leq i, j \leq n \} \cup \\
&\quad \{ [\zeta \theta_2^2 v_s \omega_j P_{sj} A_c]_1 \rightarrow [q_s v_s P_{sj} A_c \theta_2]_1 [A_c \theta_2 \zeta]_1 | 1 \leq i, j \leq n \} \\
r_8 &= \{ \theta_2 \rightarrow d' \} \quad r_9 = \{ q_i v_i U_{ij} \rightarrow \lambda |_{d'} \} \quad r_{10} = \{ P_{ij} \rightarrow [\eta P_{ij}]_{i_0} |_{d'} \} \\
r_{11} &= \{ d' \rightarrow \delta \} \quad r_{12} = \{ \zeta \rightarrow d \} \quad r_{13} = \{ A_c \rightarrow \lambda |_d \} \\
r_{14} &= \{ d \rightarrow \delta \}
\end{aligned}$$

Rules in R_{i_0} :

$$\begin{aligned}
r_{15} &= \{ \eta^t P_{i_1 j_1}^{m_1} P_{i_2 j_2}^{m_2} \dots P_{i_t j_t}^{m_t} \rightarrow \eta^{t-1} P_{i_1 j_1}^{m_1-1} P_{i_2 j_2}^{m_2-1} \dots P_{i_t j_t}^{m_t-1} | \\
&\quad t \in N^+, m_i \in N^+, m_1 \geq m_2 \geq \dots \geq m_t, 1 \leq i, j \leq n \} \\
r_{16} &= \{ \eta^{t-m} P_{i_1 j_1}^{(m_1)'} P_{i_2 j_2}^{(m_2)'} \dots P_{i_{n-1} j_{n-1}}^{(m_{n-1})'} \rightarrow P_{i_1 j_1}^{w_{i_1 j_1}} P_{i_2 j_2}^{w_{i_2 j_2}} \dots P_{i_{n-1} j_{n-1}}^{w_{i_{n-1} j_{n-1}}} | \\
&\quad 1 \leq t, m \in N^+, m_1 \geq m_2 \geq \dots \geq m_{n-1}, 1 \leq i_s, j_s \leq n \} \\
r_{17} &= \{ P_{i_1 j_1}^{w_{i_1 j_1}} P_{i_2 j_2}^{w_{i_2 j_2}} \dots P_{i_{n-1} j_{n-1}}^{w_{i_{n-1} j_{n-1}}} \rightarrow P_{i_1 j_1}^{w_{i_1 j_1}-1} P_{i_2 j_2}^{w_{i_2 j_2}-1} \dots P_{i_{n-1} j_{n-1}}^{w_{i_{n-1} j_{n-1}}-1} \\
&\quad | 1 \leq i_s, j_s \leq n \} \\
r_{18} &= \{ P_{i_1 j_1}^{(w_{i_1 j_1})'} P_{i_2 j_2}^{(w_{i_2 j_2})'} \dots P_{i_{n-1} j_{n-1}}^{(w_{i_{n-1} j_{n-1}})'} \rightarrow \\
&\quad \eta_2 P_{i_1 j_1} P_{i_2 j_2}^{(w_{i_1 j_1})'-1} P_{i_3 j_3}^{(w_{i_2 j_2})'-1} \dots P_{i_{n-1} j_{n-1}}^{(w_{i_{n-1} j_{n-1}})'-1} \} \\
r_{19} &= \{ \eta_2^{n-k} P_{i_1 j_1} P_{i_2 j_2} \dots P_{i_{n-k} j_{n-k}} \dots P_{i_{n-1} j_{n-1}}^{(w_{i_{n-1} j_{n-1}})''} \rightarrow \\
&\quad P_{i_1 j_1} P_{i_2 j_2} \dots P_{i_{n-k} j_{n-k}} | 1 \leq i_s, j_s \leq n \}
\end{aligned}$$

By counting the amount of objects to find the shortest edges, the sorting procedure is combined with the tree construction. Meanwhile the parallelism of computation reduces the time complexity of finding all feasible solutions to $O(n)$.

3.3 Introduction of Computations

Rule r1 is executed firstly in the environment to calculate the direct distance between any two points and send it to membrane1. After objects $u_{ij}^{w_{ij}}$ are sent into membrane1, rule r_2 and r_3 are activated to identify the shortest edge from all edges and generate two related points among these $u_{ij}^{w_{ij}}$. If the number of edges with minimum weight of the complete graph is greater than 1, rule r_3 generates same new membranes (membrane1) for every initial minimum edge to continue the next steps.

Rule r_4 continually identifies edges which are connected to the existed points and calculates which the minimum one is. When $u'_{is} = 0$ appears, it means the next edge with minimum weight is find out. Adding a minimum weight edge, two identical objects v_i may appear in same membrane. That means there is a circle in the minimum spanning tree. Rule r_5 are activated to dissolve the according u_{is} to avoid forming a circle. Then rule r_6 generates relative objects to represent the edge and point.

If the number of current edges with minimum weight is greater than 1, rule r_7 activates the current membrane to divide into two, with one containing all elements including the new added edge but another with all elements except the new edge.

The number of object ζ is set as $n-1$, and as every edge is added, it reduces by 1. When there is no ζ in membrane1, it means that $n-1$ edges have been added into the graph. Object θ_2 generates object d' without the constraint of ζ which catalyzes other objects than P_{ij} to dissolve themselves. It also promote P_{ij} conveyed into membrane i_0 . While if there are objects ζ but no other edges to be added, rule r_{12} r_{13} r_{14} dissolve the current membrane and other objects.

The second computing stage of this structure happens in membrane i_0 . Rule $r_8 - r_{11}$ sends the chosen edges for a minimum spanning tree into membrane i_0 . In every membrane1, executing rule $r_8 - r_{11}$, there is a feasible solution to the minimum spanning tree. As a consequence, there will be more than $n-1$ edges existing in membrane sent to i_0 , including identical edges. Rule $r_{15} - r_{19}$ is executed in membrane i_0 . The number of object η indicates the number of edges in membrane i_0 . We choose the edge with maximum weights and highest frequency. Rule r_{18} executes until the cardinal of η_2 reducing to $n-k$ ($n-1-(k-1) = n-k$), which means there are only $n-k$ different edges left. At this time, Rule r_{19} finds out the final $n-k$ edges and preserves them in the result.

4 Instance Analysis

In order to verify whether the designed P system has better clustering effect, we introduce a simple example in this section. In this test, 10 points need to be divided into 3 clusters, and data-points in same clusters are similar to each other but dissimilar to data-points in other clusters. The example points are shown as Fig. 3.

The modified similarity matrix of this set is as below.

$$W_{1,10} = \begin{bmatrix} 0 & 1 & 1 & 8 & 10 & 13 & 10 & 10 & 17 & 25 \\ 1 & 0 & 2 & 5 & 5 & 10 & 9 & 13 & 20 & 26 \\ 1 & 2 & 0 & 5 & 9 & 8 & 5 & 5 & 10 & 16 \\ 8 & 5 & 5 & 0 & 2 & 1 & 2 & 10 & 13 & 13 \\ 10 & 5 & 9 & 2 & 0 & 5 & 8 & 20 & 25 & 25 \\ 13 & 10 & 8 & 1 & 5 & 0 & 1 & 9 & 10 & 8 \\ 10 & 9 & 5 & 2 & 8 & 1 & 0 & 4 & 5 & 5 \\ 10 & 13 & 5 & 10 & 20 & 9 & 4 & 0 & 1 & 5 \\ 17 & 20 & 10 & 13 & 25 & 10 & 5 & 1 & 0 & 2 \\ 25 & 26 & 16 & 13 & 25 & 8 & 5 & 5 & 2 & 0 \end{bmatrix}$$

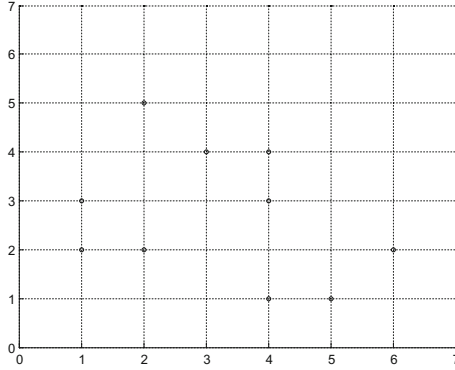


Fig. 3. Instance data set $(a_1 = (1,2), a_2 = (1,3), a_3 = (2,2), a_4 = (3,4), a_5 = (2,5), a_6 = (4,4), a_7 = (4,3), a_8 = (4,1), a_9 = (5,1), a_{10} = (6,2))$.

The designed P system realizes the minimum spanning tree clustering algorithm with its maximal parallelism and distributed manner. Now we give simple analysis of how the P system executives in this example.

At first, rule r_1 in the environment sends objects $u_{ij}^{wij} (1 \leq i, j \leq 10)$ into membrane 1 to represent distances between data-points. Among all these $u_{ij}^{wij} (1 \leq i, j \leq 10)$, rules $r_2 r_3$ pick $u_{12} u_{13} u_{46} u_{67}$ to start the construction, because they have the minimum weight 1. Therefore there are four membranel in parallel to continue next constructing steps, and each of them starts from different edges. For the membranel starting from u_{12} , the edge with next minimum weight is e_{13} . Then rule r_5 estimate whether adding e_{13} will form a circle or not. If a circle is to form, this edge will be abandoned. Otherwise, the edge is added. After the judgment, u_{13} evolves into $q_3 v_3 \omega_3 P_{13}$ according to rule r_6 . Then the next object u_{23} is to be judged. Since there are $v_1 v_2 v_3$ here, rule r_5 dissolves u_{23} , and the next edges with minimum weight 5–edges $e_{24} e_{25} e_{34} e_{27} e_{38}$ continue this process. As there are more than one objects to be added, these previous objects in the membrane is copied 5 times and membrane 1 split into 5 identical membranes according to rule r_7 . For one of them, for example, the one containing e_{25} , the next minimum edge to be added is e_{54} ; and the one containing e_{34}, e_{46} with weight 1 is next to be added. These procedures will repeat until no ζ or u_{ij} is left. Finally there are 26 minimum spanning trees constructed as shown in Fig. 4. And according to rule r_{10} , edges in these trees are sent into membrane i_0 . The membrane structure containing all feasible solutions is shown as Fig. 4.

The final partition step is executed in membrane i_0 with rules $r_{15} - r_{19}$. In this example, we can see edges in all minimum spanning tree feasible solutions including $e_{12} e_{13} e_{46} e_{78} e_{89} e_{9,10} e_{67} e_{45} e_{24} e_{25} e_{34} e_{38} e_{56} e_{37}$. They are sorted by rules in descending order by their cardinal and retained the first $9(n-1)$ edges only by rule r_{15} and r_{16} . Rule $r_{17} r_{18}$ and r_{19} pick the longest $2(k-1)$ edges – $e_{78} e_{24}$ and delete them by their weights. Finally edges $e_{12} e_{13} e_{46} e_{89} e_{9,10} e_{67} e_{45}$ are reserved in the graph. The clustering result is $\{a_1 a_2 a_3\}, \{a_4 a_5 a_6 a_7\}, \{a_8 a_9 a_{10}\}$.

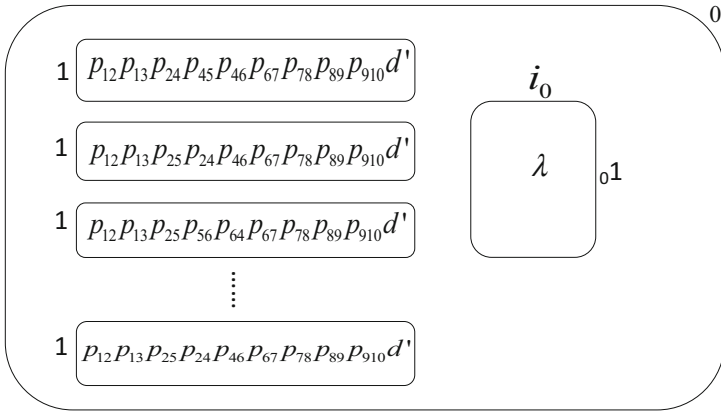


Fig. 4. configuration after applying rule r_9

5 Discussion and Future Works

In this paper, we construct a specific P system where all feasible solutions to the minimum spanning tree problem of a complete graph can be calculated. Then by integrating these feasible solutions and deleting some large weight edges the final partition result is formed in the output membrane. Through the example test, we can see that the designed P system can effectively find quality clustering result in a distributed and parallel manner. The future work is mainly focused on optimizing the process of finding solutions with the purpose of reducing identical solutions and computation complexity and making our system run more efficiently.

Acknowledgement. Project supported by National Natural Science, Foundation of China (61170038, 61472231, 61640201), Jinan, City independent innovation plan project in College and Universities, China (201401202), Ministry of education of Humanities and social science research project, China (12YJA630152), Social Science Fund Project of Shandong Province, China (11CGLJ22), outstanding youth scientist foundation project of Shandong Province, China (ZR2011FM001).

References

1. Han, J., Pei, J., Kamber, M.: Data Mining: Concepts and Techniques. Elsevier (2011)
2. Fredman, M., Willard, D.: Trans-dichotomous algorithms for minimum spanning trees and shortest paths. In: Proceedings of the 31st Annual IEEE Symposium on Foundations of Computer Science, pp. 719–725 (1990)
3. Zhong, C., Malinen, M., Miao, D., et al.: A fast minimum spanning tree algorithm based on k-means. Inf. Sci. **295**, 1–17 (2015)
4. Zhong, C., Miao, D., Wang, R.: A graph-theoretical clustering method based on two rounds of minimum spanning trees. Pattern Recogn. **43**(3), 752–766 (2010)
5. Păun, G.: Computing with membranes. J. Comput. Syst. Sci. **61**(1), 108–143 (2000)

6. Xue, J., Liu, X.: Lattice based communication P systems with applications in cluster analysis. *Soft. Comput.* **18**(7), 1425–1440 (2014)
7. Paun, G., Rozenberg, G., Salomaa, A.: *The Oxford Handbook of Membrane Computing*. Oxford University Press Inc., New York (2010)
8. Sosik, P., Rodríguez-Patón, A.: Membrane computing and complexity theory: A characterization of PSPACE. *J. Comput. Syst. Sci.* **73**(1), 137–152 (2007)
9. Zhang, G.X., Pan, L.Q.: A survey of membrane computing as a new branch of natural computing. *Chin. J. Comput.* **33**, 208–214 (2010)
10. Grygorash, O., Zhou, Y., Jorgensen, Z.: Minimum spanning tree based clustering algorithms. In: *2006 18th IEEE International Conference on Tools with Artificial Intelligence (ICTAI 2006)*, pp. 73–81. IEEE (2006)

A Method for Correcting the Leaning of AR Two-Dimensional Codes Based on LSM

Chen Miao, Shufen Liu, and Zhilin Yao^(✉)

Jilin University, Changchun, China
814274078@qq.com

Abstract. In this paper, it is inevitable that the AR two-dimensional codes obtained by the mobile device will have a tendency towards the mobile augmented reality application. A two-dimensional code tilts correction method based on least square method is proposed. After binarization preprocessing, the target two-dimensional code inclination angle is obtained by least-squares method. After further correction by bilinear interpolation, satisfactory results can be achieved. Restore the image. The experimental results show that the method can be quickly and effectively identify the target two-dimensional code, and then the corresponding three-dimensional model to enhance the reality display.

Keywords: Augmented reality · 2D code · Tilt correction
Least square method

1 Introduction

Augmented reality (AR) is with the development of virtual reality technology and produce a new kind of computer application and the technology of human-computer interaction [1]. It combines the computer-generated virtual environment with the real scene of the user by means of photoelectric display technology, interactive technology, multi-sensor technology, computer graphics and multimedia technology, so that the user can confirm from the sensory effect that the virtual environment is an integral part of the surrounding real scene. Unlike immersive virtual reality, augmented reality technology is mainly based on the existing real world, to provide users with a new sensory composite visual effects, to expand the human cognitive and perceived ability of the world. Augment reality technology not only has the strong sense of reality, modeling on small workload, and more secure and reliable.

Mobile augmented reality applications require mobile device software and hardware, using the device camera to capture real-world images, calculate the relevant information, integration of virtual scenes, and finally output to the screen, projectors and other display devices [4]. When the two-dimensional barcode image is acquired and decoded by the camera of the mobile phone, the acquired two-dimensional code is inevitably inclined. When the tilt angle exceeds a certain range, the decoded barcode can not be decoded correctly. Therefore, it is necessary to tilt the two-dimensional code.

The traditional two-dimensional code correction algorithm: Hough transform, Fourier transform [6]. The Fourier transform method uses the two-dimensional barcode tilt angle corresponding to the azimuth angle with the largest density of the Fourier space. The computational complexity is very high and is rarely used at present. Hough transform is the most commonly used method to detect the inclination angle. For the real-time processing of mobile phones using mobile phones to enhance the real-time display of 3D models may appear unpredictable error, this approach is first recorded two-dimensional code contour space coordinates, record the coordinates, the application of the minimum. The linear regression of these points by LSM gives the slope of the line, and the slope of the two-dimensional code is known. This can effectively improve the computation time.

2 Overview of 2D Code

As a new information storage and transmission technology, two-dimensional code can be used to express text and image processing information on many languages, and has the characteristics of high capacity, high density, strong error correction capability, fast positioning and automatic encoding and decoding [3]. It can not only encode the scene information associated with it to the landmarks, but also obtain the scene information on the decoding landmarks, which is obviously different from the traditional ARToolKit marker points for locating and recognizing [7]. The common mark point has QR code, like Fig. 1 shows. As a kind of two-dimensional code, QR code is based on the computer image processing technology, combined coding principle and so on, and has the function of automatic recognition read processing.

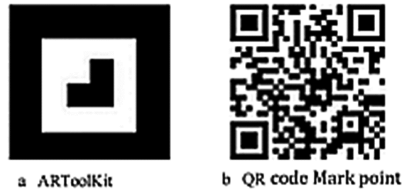


Fig. 1. Two kinds of mark points

2.1 QR Code Internal Structure

The QR code is a matrix-type two-dimensional code consisting of a square block consisting of a coding region (consisting of version information, format information and data and error correction code words) and function graphics (composed of a seek pattern, a delimiter, and a correction pattern component) [5], the coding region is a region for coding data or error correction code words, and the functional pattern refers to a specific pattern in the symbol for symbol localization and feature recognition, an imaging pattern located at three corners, It can help to determine the position, size and inclination of the symbol. The symbol is surrounded by a blank area. Figure 2 shows the internal structure

of the QR code. In the symbol, the dark module represents the binary “1”, the light module represents the binary “0” [9].

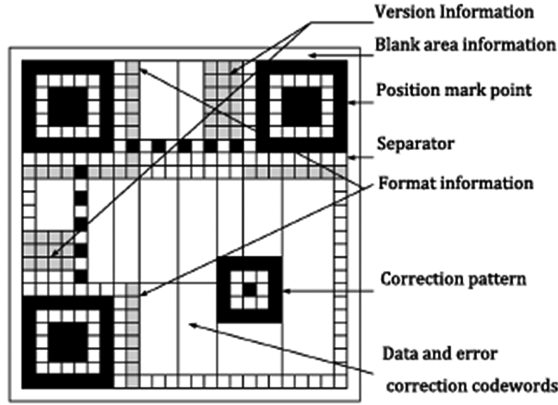


Fig. 2. QR code structure

3 The Lean Correction Principle Based on LSM

According to the structure of the QR code, firstly locate the position mark and record the space coordinates of its left boundary, construct the data set $\{X, Y\}$, where X, Y is the input vector, used to store the spatial coordinates of the boundary point of the contour [2].

After rotation, the left edge of the 2D barcode must be perpendicular to the X axis, then:

$$\min \sum_{i=1}^n (\omega(x_i, y_i) - \omega(\bar{x}, \bar{y}))^2 \quad (1)$$

According to the data set $\{X, Y\}$ constructed, it can be linear regression according to $f(x) = \omega x + b$, we can see that the regression error of sample points is:

$$e_i = f(x) - Y = \omega x = b - Y \quad (2)$$

Substitute Eq. 1 into Eq. 2

$$\begin{aligned} & \min \sum_{i=1}^n (\omega(x_i, y_i) - \omega(\bar{x}, \bar{y}))^2 \\ &= \min \sum_{i=1}^n \left(e_i - b - Y - \left(\overline{e - b - Y} \right) \right)^2 \\ &= \min \sum_{i=1}^n (e_i)^2 \end{aligned} \quad (3)$$

Therefore, only the data set $\{X, Y\}$ regression. When the inaccuracy e_i variance is minimum, the parameter ω is the tilt vector. In this way, the optimization problem of the image tilt angle is transformed into the process of regression of the data set $\{X, Y\}$ to identify the parameter ω .

Suppose there exists a univariate regression model $f(x) = ax + b$, and the regression of the random variable Y on the independent variable is $f(x)$. The univariate regression model is:

$$y = ax + b + \varepsilon \quad \varepsilon \sim N(0, \sigma^2)$$

Here parameters a, b , on the independent variables X are independent.

Let the left boundary of the boundary contour of a two-dimensional code be independent of each other by N characteristic points [6]. The deviation between the estimated value and the sample is:

$$\delta_i = y_i - f(x_i) = y_i - ax_i - b$$

By Eq. 3 we can see that when the deviation is the minimum angle is the tilt, the value is:

$$\min \delta^2 = \min \sum_{i=0}^{n-1} (y_i - ax_i - b)^2 \quad (4)$$

According to KKT conditions to obtain the optimal a, b value, that is

$$a = \frac{N \sum_{i=0}^{n-1} x_i y_i - \sum_{i=0}^{n-1} x_i \sum_{i=0}^{n-1} y_i}{N \sum_{i=0}^{n-1} x_i^2 - \sum_{i=0}^{n-1} x_i \sum_{i=0}^{n-1} x_i} \quad (5)$$

$$b = \frac{\sum_{i=0}^{n-1} x_i^2 \sum_{i=0}^{n-1} y_i - \sum_{i=0}^{n-1} x_i \sum_{i=0}^{n-1} x_i y_i}{N \sum_{i=0}^{n-1} x_i^2 - \sum_{i=0}^{n-1} x_i \sum_{i=0}^{n-1} x_i} \quad (6)$$

The value of a obtained here is the slope of the straight line after the left edge of the fitting, and the inclination angle of the two-dimensional code in the horizontal direction can be obtained.

4 QR Code Correction Process

In order to realize the detection of QR code in mobile augmented reality, we need to perform binary preprocessing of the obtained 2D code to make the later operation more accurate. And then obtains the coordinates of the boundary points of the QR code, and obtains the final image through the distortion correction, the skew correction and the bilinear interpolation mapping. Finally, the 3D model is obtained by decoding the 2D code image, and output to the screen, projector and other display devices to enhance Reality display. The flowchart is shown below (Fig. 3):

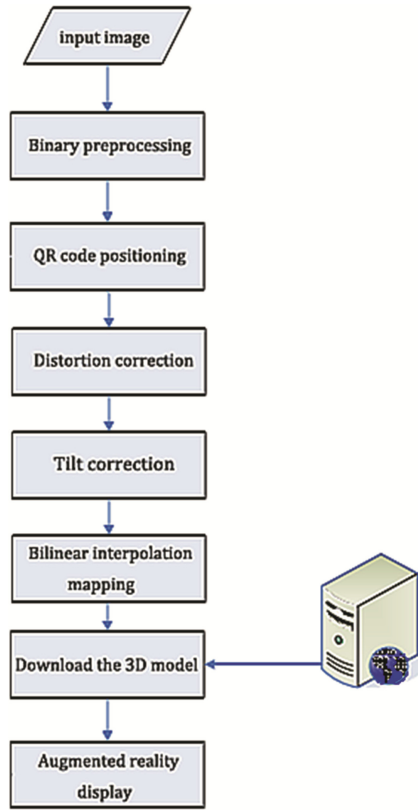


Fig. 3. Flowchart

4.1 Image Preprocessing

There are two kinds of formulas for converting the color image into grayscale image:

$$Y = 0.299R + 0.587G + 0.114B \quad (7)$$

$$Y = (R + G + B)/3 \quad (8)$$

Here, we use the formula $Y = (R + G)/2$ and ignore the B component of the two-dimensional code image gray processing. The adaptive threshold segmentation algorithm is adopted in the binarization threshold processing. The basic idea of the algorithm is that the average gray value of S pixels is calculated when traversing the whole image. When the pixel value of a pixel is lower than this value, set to black, otherwise set to white.

4.2 Barcode Location

After the bar code is binarized, the bar code needs to be positioned. According to the structure of the QR code, we take the location of the QR code, record its spatial coordinates, and construct the data set $\{X, Y\}$, where X and Y are the input variables.

4.3 Distortion Correction

In practice, the camera in take of QR code image will have different degree of distortion. Any geometric distortion can be defined by an equation that transforms the non-distorted coordinate system (X, Y) into the distortion coordinate system (X', Y') , which is generally of the form:

$$\begin{cases} x' = h_1(x, y) \\ y' = h_2(x, y) \end{cases} \quad (9)$$

Let $f(x, y)$ be the original image without distortion and $g(x, y)$ be the result of $f(x, y)$ distortion. The distortion process is known, and is defined by the functions $h_1(x, y)$ and $h_2(x, y)$

$$g(x', y') = f(x, y) \quad (10)$$

Equation (10) that should appear in the image in pixels (x, y) on the grey value due to the distortion, and appear in the (x', y') , the distortion problem might be solved by mapping transformation. In the case of known $g(x', y')$, $h_1(x, y)$ and $h_2(x, y)$, the restoration process is as follows:

1. Find the corresponding positions in $g(x', y')$ for each point (x_0, y_0) in $f(x, y)$: $(M, N) = [h_1(x_0, y_0), h_2(x_0, y_0)]$. M and N are the coordinate values of the spatial points, respectively. (M, N) does not coincide with any point in $g(x', y')$, since M and N are not necessarily integers.
2. Find the point (x_1', y_1') nearest to (M, N) in $g(x', y')$, let $f(x_0, y_0) = g(x_1', y_1')$, that is, give the grayscale values of $g(x_1', y_1')$ to $f(x_0, y_0)$, according to this way point by point until the entire image is finished, and the geometry is corrected.

4.4 Tilt Correction

After the distortion correction, we record the left border of the bar code, using (5,6) to calculate the tilt angle $\alpha = \arctan a$; After the bar code is obtained, the rotation formula, that is

$$\begin{bmatrix} x_{new} \\ y_{new} \end{bmatrix} = \begin{bmatrix} \cos a & \sin a \\ -\sin a & \cos a \end{bmatrix} \begin{bmatrix} x_{old} \\ y_{old} \end{bmatrix} \quad (11)$$

If the Eq. (11) is used directly, for a wide (W) * high (H) image, the rotation requires $4WH$ multiplication and $2WH$ addition, and the algorithm is highly computationally. In fact, for a height of H for the two-dimensional code image, the vertical direction of the projection maximum deviation is:

$$Y_{max} = H \tan a$$

The deviations for the j^{th} column and the i^{th} row in the image are, respectively (Fig. 4).

$$\Delta y_j = \left(\frac{j}{Y_{max} + 1} \right) \times W$$

$$\Delta x_i = \left(\frac{i}{X_{max} + 1} \right) \times H$$

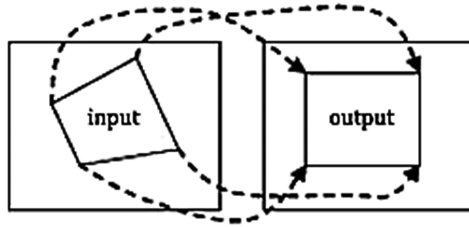


Fig. 4. Spatial mapping of control points

4.5 Bilinear Interpolation

Some points that are not in the integer position may be generated during the image rotation transformation. This requires an algorithm for gray-scale interpolation to produce a smooth mapping that maintains continuity and connectivity. Interpolation methods include the nearest neighbor interpolation, bilinear interpolation and high order interpolation. The nearest neighbor interpolation is a simple interpolation algorithm, but the nearest neighbor interpolation algorithm will produce a clear image of the zigzag boundary. For the QR code with only black and white, bilinear interpolation can be used to produce a satisfactory image restoration effect [8]. The mathematical model is shown in Fig. 5:

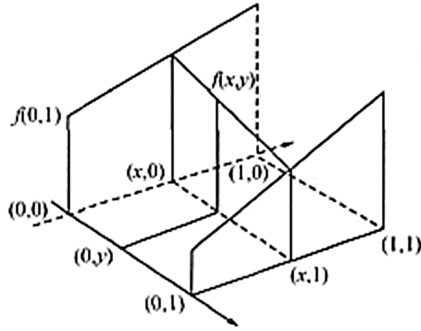


Fig. 5. Mathematical model of bilinear interpolation

First, by first-order linear interpolation:

$$f(x, 0) = f(0, 0) + x[f(1, 0) - f(0, 0)]$$

The same can be drawn:

$$f(x, 1) = f(0, 1) + x[f(1, 1) - f(0, 1)]$$

$$f(x, y) = f(x, 0) + y[f(x, 1) - f(x, 0)]$$

Merge the above three formulas:

$$f(x, y) = [f(1, 0) - f(0, 0)]x + [f(0, 1) - f(0, 0)]y + [f(1, 1) + f(0, 0) - f(0, 1) - f(1, 0)]xy + f(0, 0)$$

After this series of operations, the original two-dimensional code image into a more standard image, as shown (Fig. 6):

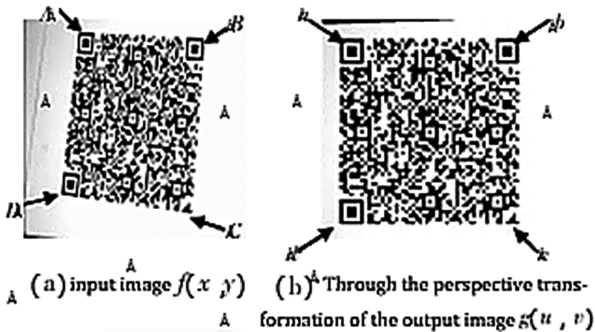


Fig. 6. Compared before and after correction

4.6 Download the 3D Model and Display It

As shown in Fig. 7, QR code content with the soldier URL address, we can easily download from the server to the corresponding three-dimensional model, and through the camera to enhance its reality display.



Fig. 7. Enhanced reality display

5 Conclusion and Outlook

This paper mainly focuses on the tilt correction method of 2-D codes in mobile AR. The LSM effectively improves the decoding time and decoding success rate. Start from the server to download the three-dimensional virtual model loaded into memory. Then, the model rendering output to the phone screen, and ultimately achieve the target QR code to enhance the reality show. However, this method only supports the identification of a single QR code. The next step is to consider a method that supports multiple QR code recognition and combine with the current excellent local feature point algorithm to realize fast and effective recognition of multiple QR codes.

References

1. Belimpasakis, P., Selonen, P., You, Y.: Bringing user-generated content from internet services to mobile augmented reality clients. In: 2010 Cloud-Mobile Convergence for Virtual Reality Workshop (CMCVR), pp. 14–17. IEEE (2010)
2. Trier, O.D., Jain, A.K.: Goal-directed evaluation of binarization methods. *IEEE Trans PAMI* **17**(12), 1191–1201 (1995)
3. Chen, Y.-Y., Shi, P.-F.: Study and application of two-dimensional bar code. *Tech. Meas. Control* **23**(12), 17–19 (2006)
4. Schmalstieg, D., Wagner, D.: Experiences with handheld augmented reality. In: Proceedings of Mixed and Augmented Reality, 6th IEEE and ACM International Symposium, pp. 3–18 (2007)

5. Liu, Y., Liu, M.-Y., Shang, Z.-H.: Multi-level thresholding method for fast response matrix codes. *Appl. Res. Comput.* **8**, 177–179 (2006)
6. Liang, Y.-H., Wang, Z.-Y.: Two-dimensional bar code tilt detection based on projection under high noise conditions. *Microcomput. Inf.* **22**, 232–234 (2006)
7. Azuma, R., Bailot, Y., Behringer, R., et al.: Recent advances in augmented reality. *Comput. Graph. Appl.* **21**(6), 34–47 (2001)
8. White, S., Feiner, S., Kopylec, J.: Virtual vouchers: prototyping a mobile augmented Reality user interface for botanical species identification. In: *IEEE Symposium on 3DUserInterfaces 2006, 3DUI2006*, pp. 119–126. IEEE (2006)
9. Pavlidis, T.: A new paper/computer interface: Two-dimensional symbologies. *IEEE Comput. Mag.* **2**, 145–151 (2000)

The Associated Algorithm of Target Batch Number Based on Gaussian Mixture Clustering

Ning Liu^(✉), Shufen Liu^(✉), and Xinjia Zhang^(✉)

Software College, Jilin University, Changchun, China
frank93@sina.cn, {liusf, zhxj}@jlu.edu.cn

Abstract. This article provides some questions about the large quantities of target track information, unclear sensor batch number, etc. referring to target fusion, and provide the clustering algorithm of Gaussian Mixture Distribution to realize the division of all the batch numbers of target track and associated operation. According to the processing to the Gaussian distribution of information by maximum likelihood estimation and through continuous iterative and refinement of the clusters divided, the tracking information detected by all radar sensors of each target batch number can be obtained precisely in the end. This algorithm provides rapid and precise working conditions for target fusion.

Keywords: Gaussian mixture distribution · Associated operation
Maximum likelihood estimation · Clustering algorithm

1 Introduction

When the formation of ship combat synergistically, naval and radars in the fleet will report all the detected objectives about the main naval, which will create influences on the warship equipment attacked precisely according to the information.

Not only this, the objectives detected by radars can only feedback its physical information and can not precisely judge the target batch number defined by human. In the current literature, radars' objective fusion rarely have research, which aims at the two sides. In order to simplify the target quantity, avoid unnecessary redundant target information. The associated algorithm of target batch number in this article will connect the prototype cluster in the ensemble learning to solve the related problems between target information and target batch number.

2 The Data Analysis

The command system of formation of ship receives periodically signals from different radars in formation. Here it is set as M pieces of sensors, with each sensor as m . It can periodically make up instructions and send N pieces of tracking information processed by itself and under the unified coordinate system. Here the ensemble of communication of multiple batches of tracking information sent by $No.m$ sensor is set as D_m and among

it, some batch of tracking information is d_{mn} (PS: $m = 1, 2, \dots$ as the tracking information detected by NO.m sensor. $n = 1, 2, \dots$ as the NO.n target detected).

3 Target Batch Correlation

Target batch correlation is the basis of target fusion. Exactly differentiating DS is the precondition of fusion algorithm accuracy. In the war of formation of ship, because it is very difficult to recognize the target without exactly differentiating a large amount of tracking information detected, the accuracy of the algorithm is very important.

Firstly define some basic knowledge. As it is mentioned earlier, target tracking information includes a great amount of data, such as a sensor' serial number, target nationality, target type, longitude and latitude, height and a series of data. Here the number of attributes is set as k and set $d_{mn} = \{x_{mn1}, x_{mn2}, \dots, x_{mnk}\}$, the NO.n target tracking information detected by NO.m radar as a k -dimensional vector. x_{mnk} is the value of NO.k of a some batch tracking information (such as, the above target type's value on x_{ijk} is "the air"), while k is the dimension of the tracking information vector.

The result of batch correlation is a list, with a batch number on each line. Batch numbers correspond to the tracking information collection under the target detected by the related sensor. The collections can not be controlled strictly or intersected and the parallel operation of these collections is D , which is all tracking information detected by all radars. Here we call every subset as a "cluster". Through this divide, each cluster stands for tracking information collection of the same target detected by the radar sensor. After the target batch correlates with tracking information, the list formed by all clusters report to fusion center to perform blend operation.

It is formally said that D can be divided into h pieces of disjoint clusters $\{C_i | i = 1, 2, \dots, h\}$, with $C_i \cap C_j \neq \emptyset$. Accordingly, each cluster's marker is set as the target batch number. We use $\lambda = \{\lambda_1, \lambda_2, \dots, \lambda_h\}$ to represent tracking information clusters' marker, including the value of λ_h as the target batch number.

Above we introduce is some basic knowledge about association algorithm. The association algorithm the article studies will be researched by connecting clusters under unsupervised learning. We just need to divide the D collection formed by all tracking information into multiple joint clusters. But we need to solve the problem of distance calculation.

3.1 Gaussian Mixture Clustering Algorithm

We know that Gaussian distribution is fixed by two parameters among it. The two parameters are mean vector μ and covariance matrix G . We define Gaussian mixture distribution first:

$$PM(x) = \sum_{i=1}^h \alpha_i p(x | \mu_i, G) \quad (3.1.1)$$

Among it, the latter part $p(x|\mu_i, G)$ is the probability density of Gaussian distribution. Suppose that all tracking information is produced by Gaussian mixture distribution, the specific process is to fix different Gaussian mixture distribution probability density according to $\alpha_1, \alpha_2, \dots, \alpha_h$. After fix the probability density function, put different tracking information in different Gaussian distributions. In here we can see that Gaussian mixture distribution is the mixed composition of multiple Gaussian distribution. Each Gaussian distribution's probability is controlled by a parameter α_h . The probability is how much the the size is about some tracking information has been specifically related to one Gaussian distribution.

It can be seen that three parameters α_i, μ_i, G among it should be fixed if defining Gaussian mixture distribution. Suppose that all tracking information has been completed the correlation, how to fix the target batch number of some tracking information, which means how to fix cluster marker of the tracking information cluster some tracking information is in. Suppose that the tracking information cluster of some tracking information d_{ij} is in is z . In Gaussian mixture distribution, z_{mn} is the Gaussian distribution some sample is in. The value range is $1 \sim h$. But we have no way to know its specific value. According to Bayes' theorem, posteriori distribution of z_{ij} is

$$\begin{aligned} PM(z_{mn} = h|d_{mn}) &= \frac{p(z_{mn} = h) \cdot PM(d_{mn}|z_{mn} = h)}{PM(d_{mn})} \\ &= \frac{\alpha_i \cdot p(d_{mn}|\mu_i, G)}{\sum_{i=1}^h \alpha_i \cdot p(d_{mn}|\mu_i, G)} \end{aligned} \tag{3.1.2}$$

Which means we have got the posteriori probability of each tracking information cluster d_{mn} is in, marked as γ_{mnz} . When we want to know the batch number of some target tracking information, it is only to find the max one the d_{mn} corresponds to.

3.2 Maximum Likelihood Estimation

To all tracking information collection D , perform maximum likelihood estimation.

$$LL(D) = \ln \left(\prod_{j=1}^m PM(x) \right) = \sum_{j=1}^m \ln \left(\sum_{i=1}^h \alpha_i \cdot p(d_{mn}|\mu_i, G) \right) \tag{3.2.1}$$

Maximum likelihood estimation is to maximize the above formula. The derivative is 0 with the maximum value. The partial derivatives of three parameters are 0 through the formula 3.2.3.

Firstly, get out the partial derivative to μ_i through the formula 3.2.3, with the values of derivatives as 0, and according to the formula 3.2.2, get out

$$\mu_i = \frac{\sum \gamma_{mnz} d_{mn}}{\sum \gamma_{mnz}} \tag{3.2.2}$$

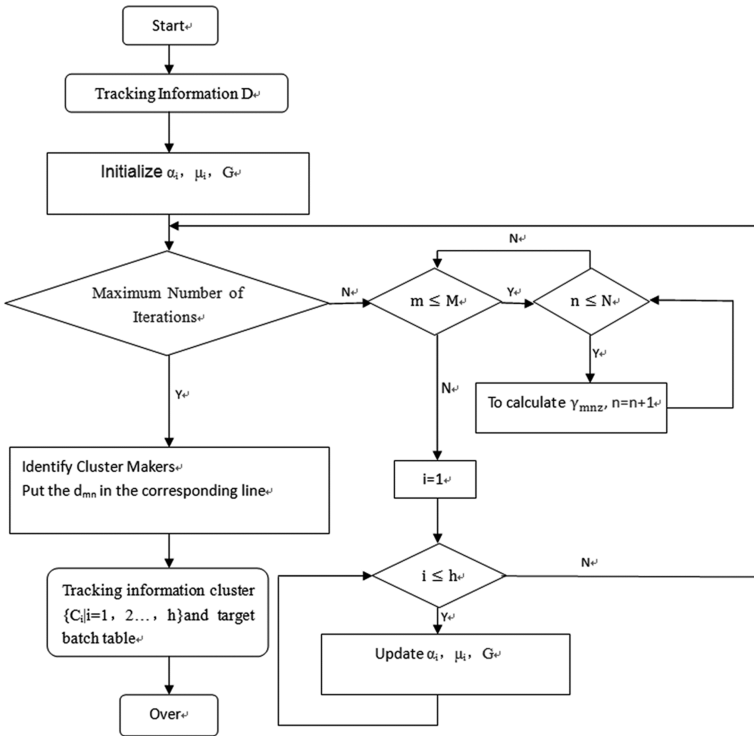
Similarly, through the derivation of G, get out of

$$G = \frac{\sum \gamma_{mn} (d_{mn} - \mu_i) (d_{mn} - \mu_i)^T}{\sum \gamma_{mnz}} \tag{3.2.3}$$

Because α_i is the related probability of target batch selected by tracking information, the sum of $\alpha_1, \alpha_2, \dots, \alpha_h$ should be 1, which all are greater than and equal to 0. According to the lagrange formalism of maximum likelihood estimation, perform α_i partial derivatives and get the values with the partial derivative as 0, get out

$$\alpha_i = \frac{1}{mn} \sum \gamma_{mnz} \tag{3.2.4}$$

After get every parameter's calculation method and use iterative process of Gaussian mixture clustering, which means getting posterior probability of each Gaussian distribution through current parameters and current tracking information. Then through the formula, update three parameters till reach the maximum value of iterative or LL(D) with a little improvement or no improvement, stop updating the parameters and finally make sure the tracking information included among every tracking information. And the corresponding marker of every tracking information is target batch. In this way, the overview that flow the target tracking information relates is shown in following figure.



4 Justification and Summary

We define a measure that evaluates the clarity of the tracking information to prove the advantages of this algorithm. Davies-Bouldin index:

$$DB = \frac{1}{h} \sum_{i=1}^h \max_{j \neq i} \left(\frac{\text{avg}(C_i) + \text{avg}(C_j)}{d_{\text{cen}}(\mu_i, \mu_j)} \right)$$

Among them, $d_{\text{cen}}(\dots)$ is to calculate the distance between the center of two clusters, $\text{avg}(C)$ is the average distance of each trace information in the cluster C . So, we can see, the denominator in the DB index is the distance between the two tracking information clusters, the larger the denominator, the lower the similarity of the two clusters, and the molecules represent the tracking information aggregation in two clusters. So, the smaller the value of the DB index, the better the result of the algorithm. In a tracking information data set of 11 ships, the results are obtained 0.32~0.33, it's better than the general information.

The algorithm promoted in this article controls all the tracking information within the k -dimension space, proceeds loop iteration and fix the collection of tracking information detected by multi sensors each target corresponds to, which realizes the connective work of precise target batch number and complete the work within the quadratic time.

References

1. Wan, S.: Clustering of multisensor data fusion method. *J. Syst. Eng. Theory Pract.* (05) (2008)
2. Xinrui, Z., he, J.: Multi-sensor information fusion technology. *Comput. Meas. Control* (09) (2007)
3. Hongfeng ailin, W., Single Showers: Research progress of foreign military information fusion theory and application. *Lightning Control* (04) (2007)
4. Ma, J., Jixiang, S.: Information fusion model of neural network to describe. *J. Avionics Technol.* (01) (1998)
5. Xin, W., Qidan, Z., Shuli, S.: Unfettered global optimal weighted measurement fusion estimation. *Comput. Eng. Appl.* (24) (2010)
6. Hu, W., Shenyuan, Y.: The multi-sensor track correlation. *Appl. Sci. Technol.* (12) (2005)

Density Peaks Clustering Based on Improved RNA Genetic Algorithm

Liyan Ren and Wenke Zang^(✉)

School of Management Science and Engineering, Shandong Normal University,
No. 88 East of Wenhua Road, Jinan 250014, Shandong, China
13395410670@163.com, zwker@163.com

Abstract. A density peaks clustering based on improved RNA genetic algorithm (DPC-RNAGA) is proposed in this paper. To overcome the problems of Clustering by fast search and find of density peaks (referred to as DPC), DPC-RNAGA uses exponential method to calculate the local density. In addition, improved RNA-GA was used to search the optimums of local density and distance. So clustering centers can be determined easily. Numerical experiments on synthetic and real-world datasets show that, DPC-RNAGA can achieve better or comparable performance on the benchmark of clustering, adjusted rand index (ARI), compared with K-means, DPC and Max_Min SD methods.

Keywords: RNA genetic algorithm · Clustering · Density peaks
Distance

1 Introduction

Clustering, a kind of unsupervised learning technique, aims at dividing a given population into groups or clusters with common characteristics, so that objects in the same cluster are similar to one another and dissimilar to objects in any other clusters. Clustering is widely used in exploratory pattern analysis, grouping, decision making, and machine learning situations, including data mining, document retrieval, image segmentation, and pattern classification [1]. Many different clustering methods exist including K-means clustering algorithm, Density-Based Spatial Clustering of Applications with Noise (DBSCAN), Affinity Propagation (AP) and so on [2, 7, 9, 10].

Recently, a novel clustering algorithm was proposed by Alex Rodriguez and Alessandro Laio [3], based on the assumption that clustering centers are surrounded by the neighbors with lower local density and that they are at a relatively large distance from any points with a higher local density. We refer to this algorithm as DPC (Density Peaks Clustering) in this paper. It was demonstrated on several test cases that DPC can efficiently find the cluster centers (i.e., the density peaks) and assign the remaining points to their appropriate clusters as well as detect outliers. Several researches have been going on around this method [4]. However, DPC does have some shortcomings. The clustering centers are only determined by the multiplication of the density and the distance, which affects the selection of the best clustering centers, what's more, the calculation of the density is highly depending on the cutoff distance d_c . That affects the generalization of the algorithm.

In order to overcome these problems, we propose a novel DPC based on RNA genetic algorithm (DPC-RNAGA). The method completes clustering by density and distance analysis based on RNA-GA, which computes density with exponential method to reduce the impact of cutoff distance and adopts RNA-GA to search the optimal thresholds of the density and distance to determine the best clustering centers. The benchmark of clustering, rand index, is taken as the fitness function. To overcome the excursion of search re-gion and accelerate convergence, a penalty factor was introduced in the RNA-GA. Meanwhile, the selective crossover operators improve the effectiveness and accuracy of the algorithm.

This paper is organized as follows: Sect. 2 briefly describes the related works of the improved algorithm which include density peaks clustering, the improvement of RNA-GA. Section 3 introduces our novel clustering algorithm DPC-RNAGA and gives a detailed analysis. Section 4 tests our proposed algorithm on several real-world datasets and synthetic datasets, and compares its performance with K-means, DPC and Max_Min SD on adjusted rand index (ARI). Section 5 draws some conclusions.

2 Related Works

The proposed DPC-RNAGA is based on DPC and RNA-GA. This section provides brief reviews of DPC and RNA-GA.

2.1 Density Peaks Clustering

Rodriguez and Laio proposed an algorithm published in Science and has appealed to many machine learning researchers. Its idea is that clustering centers are characterized by a higher density than their neighbors and by a relatively large distance from points with higher densities. This method utilizes two important quantities: One is the local density of each point i^{ρ_i} and the other is the distance from points of higher densities δ_i . In the following, we will describe the calculation of ρ_i and δ_i in detail. Assume that the data set is $X_{N \times M} = [\chi_1, \chi_2, \dots, \chi_N]^T$, where $\chi_i = [\chi_{i1}, \chi_{i2}, \dots, \chi_{iM}]^T$ is the vector with M attributes and N is the number of points. The distance matrix of the dataset needs to be computed firstly.

Let $d(\chi_i, \chi_j)$ denote the Euclidean distance between the point χ_i and χ_j , The local density of a point χ_i , denoted by ρ_i , is defined as:

$$\rho_i = \sum_j \chi(d(\chi_i, \chi_j) - d_c)$$

$$\chi(x) = \begin{cases} 1 & \text{if } x < 0 \\ 0 & \text{if } x \geq 0 \end{cases} \quad (1)$$

Where d_c is cutoff distance, ρ_i is defined as the number of points that are adjacent to the point χ_i , d_c is an adjustable parameter and the only variable in Formula (1). Here we

use the other way to calculate the local density called exponential kernel function, it is defined as follows:

$$\rho_i = \sum_{j \neq i} \exp\left(-\left(\frac{d_{ij}}{d_c}\right)^2\right) \quad (2)$$

The computation of δ_i is quite simple. The minimum distance between the point χ_i and any other points with higher densities, denoted by δ_i , is defined as:

$$\delta_i = \begin{cases} \min_{j: \rho_j > \rho_i} (d(\chi_i, \chi_j)) & \text{if } \exists j.s.t. \rho_j > \rho_i \\ \max_j (d(\chi_i, \chi_j)) & \text{if otherwise} \end{cases} \quad (3)$$

Only those points with relative high ρ_i and high δ_i are considered as clustering centers. The points with high ρ_i and high δ_i are also called as peaks. After clustering centers have been found, DPC assigns each remaining points to the same cluster as its nearest neighbor with higher density.

2.2 The Improvement of RNA Genetic Algorithm

RNA encoding and decoding. In the RNA-GA, a section of chromosome is used to encode one parameter and a chromosome is used to encode all the parameters. Specifically, a chromosome represents the values of ρ_i and δ_i in this study.

Genetic operators and penalty factor. The tournament method is adopted as the selection method in DPC-RNAGA [5]. However, in the special circumstance, It was found that the search field is biased after several experiments. So we propose the penalty factor d to get rid of inferior individuals whose fitness value stays the last d percentage of all. If the initial population is $Q_1 = \{q_1, q_2, \dots, q_m\}$, the remaining ratio of the parent generation is r , so the number of individuals remaining from the parents is $r * m$.

Selective crossover operator is designed to enhance the ability in exploring the searching space in this paper. According to the crossover probability p_c , the two parents exchange the bases between the two crossover points to produce two offspring individuals.

In this paper, we adopted the ordinary mutation operators but with adaptive probability. We divide the nucleotide bases into two parts: left and right parts. Correspondingly, the adaptive probabilities pml (left) and pmh (right) are described as follows:

$$\begin{cases} pml = a_1 + \frac{b_1}{1 + \exp[aa(g-g_0)]} \\ pmh = a_1 + \frac{b_1}{1 + \exp[-aa(g-g_0)]} \end{cases} \quad (4)$$

Where a_1 denotes the initial mutation probability of pml , b_1 denotes the range of transmutability. The parameter g is evolutionary generation, and g_0 denotes the generation where the maximum of mutation probability is reached, and aa is the speed of change.

Fitness function. In this paper, Rand index was adopted as the fitness function of RNA-GA. The Rand index is defined as the ratio of the same data pairs from the two clustering results and all the data pairs [6]. The value of rand index ranges from 0 through 1, and the value close to 1 shows that the clustering is better.

3 The Density Peaks Clustering Algorithm Based on Improved RNA-GA

The density peaks clustering algorithm based on improved RNA-GA is an adaptive way to select the best clustering centers without human intervention and reduce the impact of cutoff distance on the calculation of local density. Firstly, calculate ρ and δ of each point and then generate m couples of parameters randomly to form the initial population. After the execution of RNA-GA, we can get two thresholds. Secondly, we can determine the clustering centers according to the thresholds. Thirdly, complete the clustering by assigning remaining data points. Here we cluster the points to the same cluster as the nearest center with bigger local density. Calculate the fitness value when the clustering process is finished. The algorithm stops until the fitness value is stable or the maximum of iteration is reached.

Assuming the size of dataset is n . The iterations of RNA-GA cost most time. The complexity of each iteration is $O(n^2)$, the numbers of iteration is G_{max} . The time complexity of the algorithm is $O(mG_{max} n^2)$, the space complexity of the algorithm is due to the storage of the density and distance metrics. So the space complexity is $O(n^2)$. Compared with several typical clustering algorithms, the complexity analysis of the algorithm is shown as Table 1.

Table 1. The comparative complexity analysis of algorithms

Algorithm	Time complexity	Space complexity
DPC-RNAGA	$O(mG_{max} n^2)$	$O(n^2)$
DPC	$O(kn^2)$	$O(n^2)$
K-means	$O(ktn)$	$O(n)$
Max_Min_SD	$O(n^3)$	$O(n^2)$

From Table 1, we can see that the time complexity of DPC-RNAGA is of the same order as DPC. Although it is higher than K-means, it is still acceptable. And it doesn't affect the application of the algorithm.

4 Experiments

To evaluate our proposed algorithm, clusters created by DPC-RNAGA are compared with state of art clustering algorithms on synthetic datasets and real-word datasets. The synthetic datasets are collected at <http://cs.uef.fi/sipu/datasets/> [8]. The details of the datasets are shown in Tables 2 and 3 correspondingly.

Table 2. Synthetic datasets

Dataset	Objects	Dimensions	Classes
Aggregation	788	2	7
Spiral	312	2	3
D31	3100	2	31
flame	240	2	2

Table 3. Real-world datasets

Dataset	Objects	Dimensions	Classes
Iris	150	4	3
Wine	178	133	3
Glass	214	10	6
Seeds	210	7	3

To evaluate the performance of DPC-RNAGA, we used eight kinds of datasets and compare with K-means, DPC and Max_Min SD. The dimensions of synthetic datasets are small and the shape of clusterings is obvious. So we set that the size of the population is 50, the maximum of the genetic iteration is 30, the penalty factor is 5. However, for real-word datasets, the clusterings are mostly crossed and there are many noises. So we set that the size of the population is 100, the maximum of the genetic iteration is 30, the penalty factor is 1. The parameters of another three algorithms are set according to the actual clusterings.

In our proposed algorithms, RI is used as fitness value. Table 4 shows the RI got from four kinds of clustering algorithms dealing with eight kinds of datasets. The RI is more close to 1, the clustering result is better. The underlined RI shows the best RI for the special datasets. The experiment result shows that our proposed algorithm performs better than the other three methods.

The results show that four clustering methods perform well when the datasets is small and there are few noise points, however, when noise point appears, our proposed algorithm performs better than DPC; What's more, because real-word datasets have more noises and crosses, and the dataset is large, our proposed algorithm got better clustering results than the other three algorithms.

Table 4. Comparison of RI benchmark for 4 clustering algorithms

Dataset	RNA-GA-DPC	K-means	DPC	Max_Min_SD
Aggregation	<u>0.9993</u>	0.9234	0.9893	0.9434
Spiral	<u>1.0000</u>	0.5713	<u>1.0000</u>	0.5813
D31	<u>0.9959</u>	0.9931	0.9859	0.9934
Flame	<u>1.0000</u>	0.4524	<u>1.0000</u>	0.4829
Iris	<u>0.8923</u>	0.7342	<u>0.8923</u>	0.7931
Wine	<u>0.7350</u>	0.4219	0.6309	0.4341
Glass	<u>0.8198</u>	0.4512	0.7936	0.4621
Seeds	<u>0.7908</u>	0.6864	0.7343	0.7049

5 Conclusion

A clustering algorithm based on RNA genetic algorithm and finding density peaks was proposed in this paper. This method computes the local density of data points with the exponential kernel methods, which reduced the dependence on the parameter d_c . RNA-GA is used to search the optimal density and distance from other data point with higher density, which makes the clustering algorithms more effective. Penalty factor is added to the RNA-GA, which avoids the search region getting wrong way and accelerates convergence. The power of DPC-RNAGA was tested on several synthetic datasets and real-world datasets. The results demonstrate that DPC-RNAGA is powerful in finding clustering centers and recognizing clusters regardless of their shape and size. The comparison analysis of several clustering algorithms shows that our proposed method can be fit to many different datasets and perform better than the existing DPC, K-means and Max_Min_SD methods.

Acknowledgement. This research is supported by Excellent Young Scholars Research Fund of Shandong Normal University, China. It is also supported by Natural Science Foundation of China (No. 61472231, No. 61640201, No. 61502283, No. 61402266). And in part by the Jinan Youth Science and Technology Star Project under Grant 20120108, and in part by the soft science research on national economy and social information of Shandong, China under Grant(2015EI013).

References

1. Mohebi, A., Aghabozorgi, S.R., Teh, Y.W., Herawan, T., Yahyapour, R.: Iterative big data clustering algorithms: a review. *Softw. Pract. Exper.* **46**(1), 107–129 (2016). <https://doi.org/10.1002/spe.2341>
2. Gorunescu, F.: *Data Mining –Concepts, Models and Techniques*. ISRL, vol. 12. Springer, Heidelberg (2011). <https://doi.org/10.1007/978-3-642-19721-5>
3. Rodriguez, A., Laio, A.: Clustering by fast search and find of density peaks. *Science* **344** (6191), 1492–1496 (2014)
4. Sun, K., Geng, X., Ji, L.: Exemplar component analysis: a fast band selection method for hyperspectral imagery. *IEEE Geosci. Remote Sensing Lett.* **12**(5), 998–1002 (2015). <https://doi.org/10.1109/LGRS.2014.2372071>
5. Zhu, Q., Ning, W., Li, Z., Zhu, Q., Ning, W., Li, Z.: Circular genetic operators based RNA genetic algorithm for modeling proton exchange membrane fuel cells. *Int. J. Hydrog. Energy* **39**(31), 17779–17790 (2014)
6. Dubes, R.C.: Cluster analysis and related issues. In: *Handbook of Pattern Recognition & Computer Vision* (2015). 996 p
7. Chang, H., Yeung, D.: Robust path-based spectral clustering. *Pattern Recogn.* **41**(1), 191–203 (2008). <https://doi.org/10.1016/j.patcog.2007.04.010>
8. KBache, M.L.: Uci machine learning repository (2013). <http://archive.ics.uci.edu/ml>
9. Dubey, A.K., Gupta, U., Jain, S.: Analysis of k-means clustering approach on the breast cancer wisconsin dataset. *Int. J. Comput. Assist. Radiol. Surg.* **11**(11), 2033–2047 (2016). <https://doi.org/10.1007/s11548-016-1437-9>
10. Bian, W., Tao, D.: Max-min distance analysis by using sequential SDP relaxation for dimension reduction. *IEEE Trans. Pattern Anal. Mach. Intell.* **33**(5), 1037–1050 (2011). <https://doi.org/10.1109/TPAMI.2010.189>

Local Homogeneous Weighted Spiking Neural P Systems

Mengmeng Liu and Feng Qi^(✉)

School of Management Science and Engineering, Shandong Normal University,
No. 88 East of Wenhua Road, Jinan 250014, Shandong, China
18353110110@163.com, qfsdnu@126.com

Abstract. Homogeneous Spiking Neural P Systems (HSN P systems, for short) are a class of neural-like computing models in membrane computing, which are inspired by neurons that they are “designed” by nature to have the same “set of rules”, “working” in a uniform way to transform input into output. HSN P systems can be converted to weighted homogeneous SNP systems. In this work, based on the above two known systems, we consider a restricted variant of SN P systems called local homogeneous weighted SN P systems (LHWSN P systems, for short), where neurons in same module have the same set of rules. As a result, we prove that such systems can achieve Turing completeness. Specifically, it is proved that using only standard spiking rules is sufficient to compute and accept the family of sets of Turing computable natural numbers, moreover local homogeneity reduces the time required for the execution of the system.

Keywords: Spiking Neural P system · Weight · Local homogeneous

1 Introduction

Membrane computing [1] is one of the recent branches of natural computing, whose aim is to construct powerful computing models and intelligent algorithms by abstracting ideas from a single living cell and from complexes of cells. The obtained models are distributed and parallel computing devices, usually called P systems. There are three main classes of P systems investigated: cell-like P systems [1], tissue-like P systems [2] and neural-like P systems [3]. Spiking Neural P systems (SN P systems, for short) are a class of neural-like P systems, which are inspired by the way of biological neuron in human brain processing information and communicating with each other by means of electrical impulses (spikes) [3].

In the research of SN P system, the results mainly focus on three aspects: theory, application and implement. Theoretical level is divided into three aspects: generating sets of numbers [4–10], generating languages [11, 12], computing any Turing computable functions [13, 14]. In recent years, we have studied a variety of SNP variants and analyzed their ability to generate sets of numbers [4, 6–8, 15, 16]. Particularly, Zeng proposed the homogeneous SNP systems in 2009 [4], and proved that homogeneous SNP systems have Turing universality in generating and accepting modes. In 2015, Song proposed homogenous SNP Systems with Inhibitory Synapses (through inhibitory

synapses, spikes is converted to the anti-spikes) [16], and proved the systems have Turing universality in the case of using only the spiking rules.

Inspired by various of SNPS, this article proposed a variant of SNP system based on a new biological fact and study the ability of generating sets of numbers in two modes of the new system, besides that, we analyze the time need to execute the system. The biological fact is that although neurons are “designed” very similar, but there are still some differences between different neurons. According to functional division, neurons can be divided into three categories: sensory neurons, connecting neurons, motor neurons. In the nerve center, neuronal cell bodies having the same function gather together to regulate a physiological activity of body (the definition of nerve center). That is to say, there are some differences in the rules of the neuron, but the neurons of the same rules will be gathered together to cooperate with each other to complete a certain physiological function. We introduce this biological phenomenon into SN P systems and the SNP systems have local homogeneity.

In LHWSN P systems, the rules used by neurons in the same function module are identical, and the weights on the synapse can be positive integer and negative integer. When the spike passes through the synapse with negative weights, the spike is changed into the anti-spike and the number of the spike is doubled according to the absolute value of the weight.

In this paper, we proved that the LHWSN P systems have Turing universality. First, we conclude that the delay of rules can be removed but the systems still have Turing universality. Second, we use negative weight to express inhibitory synapse so the forgetting rule in neurons is removed. Third, the proposing of local homogeneous reduces the total time needed to execute the system.

In the next section, we introduce prerequisites and the definition of LHWSN P systems. In Sect. 3, we investigate the computation power of the system. Conclusions and remarks are drawn in Sect. 4.

2 Local Homogeneous Weighted SN P Systems

Before we introduce LHWSN P systems, we recall some necessary prerequisites. It is useful for readers to have some familiarity with basic elements of formal language theory, e.g., from [17], as well as basic concepts and notions of SN P system and register machine [18].

2.1 Background

Generally, an SN P system is composed of neurons, spikes, synapses, and rules (spiking rules and forgetting rules). A neuron can send information to its neighboring neurons by using the spiking rule. A predefined number of spikes will be removed from the neuron by using the forgetting rule, and thus they are removed out of the system. One neuron in the system is specified as the output neuron, which can emit spikes to the environment.

In the study of the computing power of SN P system, most of them are proved by simulating calculation process of the register machine. A register machine is a construct $M = (m, H, l_0, l_h, R)$, where m is the number of registers, H is the set of instruction labels, l_0 is the start label, l_h is the halt label, and R is the set of instructions. The instructions are of the following forms:

- $l_i: (\text{ADD}(r), l_j, l_k)$ (add 1 to the register r and then go to one of the instructions with label l_j and l_k , non-deterministically chosen),
- $l_i: (\text{SUB}(r), l_j, l_k)$ (if register r is non-empty, then subtract 1 from it and go to the instruction with label l_j , otherwise go to the instruction with label l_k),
- $l_h: \text{HALT}$ (halt the calculation of the register machine and regard the number in register 1 as the result of the register machine).

Register machine has two kinds of working modes: generating mode and accepting mode. In generating mode, the register machine computes number n as follows: starting M with all registers empty, the initial instruction with label l_0 is applied, and the instructions are applied as indicated by labels. When the register machine M proceeds to the halt instruction, number n stored at that time in the first register is said to be computed by M . In accepting mode (using deterministic ADD instructions), a random number is stored in the first register (other registers are empty). If the computation starting from the initial configuration eventually halts, the number is said to be accepted by M .

2.2 System Description

In this section, we define the LHWSN P system. The definition is complete, but familiarity with the basic elements of homogeneous SN P systems, anti-spikes and SNP with weights (e.g. from [4, 7, 19]) is helpful.

An LHWSN P system of degree $m \geq 1$ is a construct of the form:

$$\Pi = (O, \sigma_1, \sigma_2, \dots, \sigma_m, \text{syn}, \text{in}, \text{out})$$

Where

- $o = \{a, \bar{a}\}$ is the alphabet, where a is spike and \bar{a} is anti-spike;
- $\sigma_1, \sigma_2, \dots, \sigma_m$ are neurons of the form $\sigma_i = (n_i, R)$ with $1 \leq i \leq m$ where
 - (a) n_i is a natural number representing the initial number of spikes in σ_i ;
 - (b) R is set of rules in each neuron of the following forms:
 1. $E/a^c \rightarrow a$ is the spiking rule, where E is the regular expression over $\{a\}$. (c is integer and $c \geq 1$);
 2. $a^s \rightarrow \lambda$ is the forgetting rule, with the restriction that for any $s \geq 1$ and any spiking rule $E/a^c \rightarrow a; d$, $a^s \notin L(E)$, where $L(E)$ is set of regular languages associated with regular expression E and λ is the empty string;
 3. $a\bar{a} \rightarrow \lambda$.

- $\text{syn} \subseteq \{1, 2, \dots, m\} \times \{1, 2, \dots, m\} \times \mathbb{Z}$ (\mathbb{Z} is integer) is set of synapses between neurons, where $i \neq j$, $z \neq 0$ for each $(i, j, z) \in \text{syn}$, and for each $(i, j) \in \{1, 2, \dots, m\} \times \{1, 2, \dots, m\}$ there is at most one synapse (i, j, z) in syn .
- $\text{In}, \text{out} \in \{1, 2, \dots, m\}$ indicate the input and output neurons respectively.

In LHWSN P systems, the rules used by neurons in the same function module are identical, but the rules of different functional modules are different. A neuron may contain a number of spikes or anti-spikes, but only one of them. In LHWSN P systems, spiking rules ($E/a^c \rightarrow a$) can be applied in any neuron as follows: if neuron σ_i contains k spikes a with $a^k \in L(E)$ and $k \geq c$, the spiking rule $E/a^c \rightarrow a$ is enabled to be applied. By using the rule, c spikes a are consumed, thus $k - c$ spikes a remain in the neuron σ_i , and one spike a is sent to all neurons σ_j such that $(i, j, z) \in \text{syn}$. Rules of the form $a^s \rightarrow \lambda$, $s \geq 1$ are forgetting rules with the restriction $a^s \notin L(E)$ (that is to say, a neuron cannot apply the spiking rules and forgetting rules at the same moment), where $L(E)$ is set of regular languages associated with regular expression E and λ is the empty string. If neuron σ_i contains exactly s spikes, the forgetting rule $a^s \rightarrow \lambda$ can be applied, by which s spikes can be removed from the neuron.

The set of synapses is denoted by (i, j, z) . Specifically, neuron σ_i spikes at certain step sending a spike to neuron σ_j along the synapse (i, j, z) , if $z > 0$, neuron σ_j will receive z spikes; if $z < 0$, neuron σ_j will receive $-z$ anti-spikes. The result of a computation of the system Π is defined as the time interval of first two spikes being emitted to the environment by the output neuron at steps t_1, t_2 in the form of number $t_2 - t_1$; we say that this number is generated by Π . The set of all numbers computed in this way by Π is denoted by $N_2(\Pi)$ (the subscript 2 indicates that we only consider the distance between the first two spikes of any computation.)

An LHWSN P system Π can also work in the accepting mode. A number n is introduced in a specified neuron in the form of $f(n)$ spikes by reading spike train from the environment through the input neuron. If the computation eventually halts, then number n is said to be accepted by Π . The set of numbers accepted by Π is denoted by $N_{\text{acc}}(\Pi)$ (the subscript acc indicates the system works in the accepting mode).

We denote by $N_\alpha \text{LHW}_k \text{SNP}_m$, $\alpha \in \{2, \text{acc}\}$ all sets of numbers generated or accepted by LHWSN P systems of degree m . If the parameter m is not bounded, then it is replaced with $*$. The absolute value of the weight is not more than K .

3 The Computing Power of LHWSN P Systems

3.1 Proof of Turing Universal

In this section, we proved that the LHWSN P systems have a universal computation in the generating mode and the accepting mode. In the following proofs, a directed graph is used to represent the structure of the system: the neurons are placed in the nodes of the graph connecting with each other by the synapses; the output neuron has an outgoing synapse, emitting spikes to the environment.

Theorem 1. $N_2LHW_3SNP_* = NRE$

It is enough to prove the inclusion $NRE \subseteq N_2IHW_3SNP_*$, for the converse inclusion can be invoked from the Turing-Church thesis. In the following universality proof, a LHWSN P system Π is constructed to simulate the computation of M.

Each register r of M is represented by a neuron σ_r , whose content corresponds to the number stored in register r . Specifically, if the number stored in register r is $n \geq 0$, then neuron σ_r contains $5n$ spikes. In the initial configuration, the number stored in each register of M is 0, so that there is zero spike in neurons representing those registers. One neuron σ_{l_i} is associated with each instruction labeled l_i of M . During a computation, a neuron σ_{l_i} is spiked and start to simulate an instruction $l_i: (ADD(r), l_j, l_k)$ or $l_i: (SUB(r), l_j, l_k)$, starting with neuron σ_{l_i} activated, operating neuron σ_r as requested by ADD or SUB; then introducing spikes into neuron σ_{l_j} or neuron σ_{l_k} , which becomes active in this way. When neuron σ_{l_h} (associated with the label l_h of the halting instruction of M) is activated, a computation in M is completely simulated in Π ; the FIN module starts to output the computation result.

The LHWSN P system Π is composed of three types of modules, ADD modules, SUB modules, and a FIN modules, which are used to simulate the ADD, SUB, and HALT instructions of M .

Module SUB shown in Fig. 1. The rules for neurons of SUB module are $a \rightarrow a$ and $a^4(a^5)^+ / a^4 \rightarrow a$.

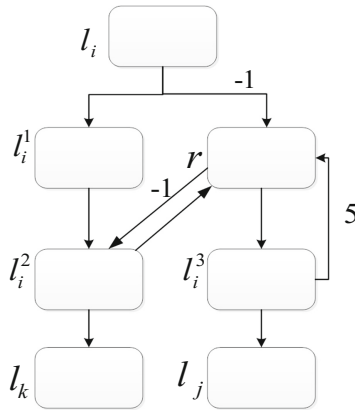


Fig. 1. The structure of SUB module

Assume at step t , the system starts to simulate a SUB instruction l_i of M . Having one spike inside, neuron σ_{l_i} fires at step t emitting a spike to neurons $\sigma_{l_i^1}$ and σ_r . The spike arriving at neuron σ_r will be changed into an anti-spike due to the negative weight, and there are the following two cases in neuron σ_r .

- Before receiving the anti-spike, if the number stored in register r is not zero, then neuron σ_r contains at least $5n$ spikes. After the annihilation, the number of spikes in neuron σ_r is decremented to $5(n - 1) + 4$, which simulates decreasing the number in register r by one. With $5(n - 1) + 4$ spikes inside, neuron σ_r fires at step $t + 1$ by using the rule $a^4(a^5)^+/a^4 \rightarrow a$ and sends one spike to neuron $\sigma_{i_2}, \sigma_{i_3}$. The spike arriving at neuron σ_{i_2} will be changed into an anti-spike due to the negative weight. Meanwhile, neuron σ_{i_2} receives one spike from neurons σ_{i_1} . The anti-spike in neuron σ_{i_2} will be annihilated by the spike from neuron σ_{i_1} . So neuron σ_{i_2} ends with no spike or anti-spike inside and remains inactive. By receiving the spike, neuron σ_{i_3} fires at step $t + 2$, and the neuron σ_{i_1} will be fired at step $t + 3$ to start to simulate instruction l_j of M . It is worth to point out that 5 spikes are sent back to neuron σ_r at step $t + 3$ from neuron σ_{i_3} , which represents that the number in register r is still n .
- Before receiving the anti-spike, if the number in register r is zero, then neuron σ_r has no spikes. After receiving the anti-spike, neuron σ_r has one anti-spike. At step $t + 1$, neuron σ_{i_1} fires sending one spike to neuron σ_{i_2} . At step $t + 2$, neuron σ_{i_2} sends a spike to neuron σ_k and neuron σ_r . In neuron σ_r , the anti-spike is annihilated, and it keeps inactive. At step $t + 3$, neuron σ_k receives a spike from neuron σ_{i_2} and becomes active, which starts to simulate instruction l_k of M .

The simulation of SUB instruction is correct: system P starts from neuron σ_i and ends in neuron σ_j (if the number stored in register r is great than 0 and decreased by one), or in neuron σ_k (if the number stored in register r is 0).

Module ADD shown in Fig. 2— simulating the ADD instruction $l_i: (ADD(r), l_j, l_k)$. The neurons of ADD module are identical, and the rules contained in the neurons are $a \rightarrow a, a^2 \rightarrow a, a^3 \rightarrow a$, and $a^3/a^2 \rightarrow a$.

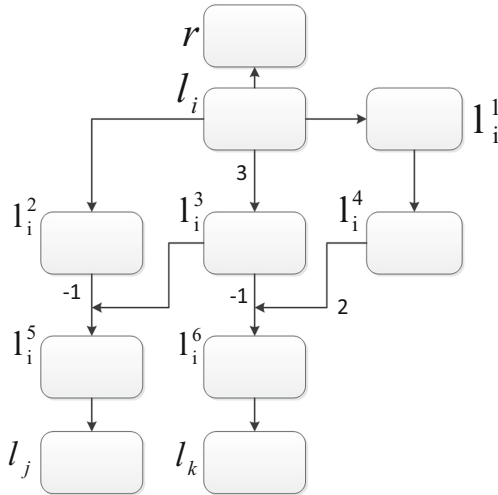


Fig. 2. The structure of ADD module

The initial instruction l_0 of M is an ADD instruction. Let us assume that at step t , an instruction $l_i: (\text{ADD}(r), l_j, l_k)$ has to be simulated, with one spike in neuron σ_{l_i} and no spike in any other neurons, except in those neurons associated with registers. Having one spike inside, neuron σ_{l_i} fires at step t sending one spike to neuron σ_{l_1} , σ_{l_2} and σ_r , and three spikes to σ_{l_3} respectively. Neuron σ_{l_i} sends one spike to neuron σ_r , which simulates increasing the number in register r by one. With three spikes inside, neuron σ_{l_3} non-deterministically chooses one of the two spiking rules $a^3 \rightarrow a$ and $a^3/a^2 \rightarrow a$ to apply at step $t + 1$, which will non-deterministically activate neuron σ_{l_k} or σ_{l_j} .

- In neuron σ_{l_3} , if rule $a^3 \rightarrow a$ is chosen to be used, then it sends one spike to neurons σ_{l_5} and σ_{l_6} , but when the spike arrives at neuron σ_{l_6} , it will be changed into an anti-spike due to the negative weight between neurons σ_{l_3} and σ_{l_6} . Neuron σ_{l_5} receives an anti-spike from neuron σ_{l_2} and a spike from neuron σ_{l_3} . So neuron σ_{l_5} ends with no spike or anti-spike inside and remains inactive. At step $t + 2$, neuron σ_{l_4} receives a spike from neuron σ_{l_4} and neuron σ_{l_6} has an anti-spike. At step $t + 3$, neuron σ_{l_6} receives two spikes from neuron σ_{l_4} . In neuron σ_{l_6} , the anti-spike inside will be annihilated by the spikes from neuron σ_{l_4} . With one spike inside, neuron σ_{l_6} fires at step $t + 3$ by using the rule $a \rightarrow a$ and sends one spike to neuron σ_{l_k} . By receiving the spike, neuron σ_{l_k} fires at step $t + 4$, simulating instruction l_k of M .
- In neuron σ_{l_3} , if rule $a^3/a^2 \rightarrow a$ is chosen to use, then after the rule is applied, neuron σ_{l_3} can spike for the second times by using rule $a \rightarrow a$. It indicates that neuron σ_{l_5} receives spike and σ_{l_6} receives anti-spike in $t + 2$ and $t + 3$ two steps. The two anti-spikes in neuron σ_{l_6} can be annihilated by the two spikes from neuron σ_{l_4} arriving at step $t + 3$. With no spike or anti-spike inside, neuron σ_{l_6} keeps inactive. In neuron σ_{l_5} , after annihilating the anti-spike inside, it has one spike and fires at step $t + 3$, sending one spike to neuron σ_{l_j} . Neuron σ_{l_j} fires at step $t + 4$ to start to simulate instruction l_j of M .

Therefore, from firing neuron σ_{l_i} , the system adds one spike to neuron σ_r and non-deterministically spikes one of neurons σ_{l_j} and σ_{l_k} ; which correctly simulates the ADD instruction $l_i: (\text{ADD}(r), l_j, l_k)$.

Module FIN shown in Fig. 3—outputting the result of computation. FIN module is composed of neurons from Fig. 4.

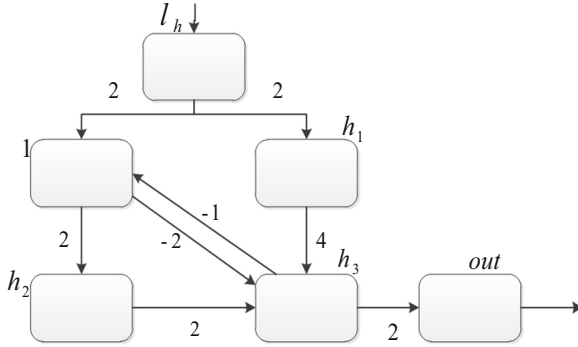


Fig. 3. The structure of FIN module

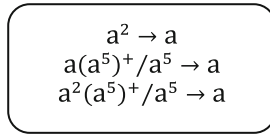


Fig. 4. The neuron of FIN module

Assume now that the computation in M halts (that is, the halting instruction is reached), which means that neuron σ_{l_h} in Π has two spikes and fires. The evolution of the numbers of spikes in the neurons during the computation of the FIN module is shown in Table 1.

Table 1. The numbers of spikes in neurons of FIN module during the process outputting the computational result.

Neuron	Step									
	t	t + 1	t + 2	t + 3	...	t + n	t + n+1	t + n+2	t + n+3	
σ_{l_h}	1	0	0	0	...	0	0	0	0	
σ_1	5n	5n + 2	5(n-1) + 2	5(n-2) + 1	...	5 + 1	1	1	0	
σ_{h_1}	0	2	0	0	...	0	0	0	0	
σ_{h_2}	0	0	2	2	...	2	2	0	0	
σ_{h_3}	0	0	2	0	...	0	0	2	0	
σ_{out}	0	0	0	2	...	0	0	0	2	

According to the function of the above three modules, it is clear that the register machine M can be correctly simulated by LHWSN P system Π . Therefore, LHWSN P systems can characterize NRE. It is also worth to mention that there are only standard spiking rules, and no forgetting rule is used. Moreover, we can see that the maximum number of rules in neurons is 4(in ADD module), so we greatly reduce the number of rules in the neurons.

Theorem 2. $N_{acc}LHW_7SNP_* = NRE$

LHWSNP systems working in accepting mode can accept any set of Turing computable natural numbers. This result is achieved by simulating register machines working in accepting mode. In the simulation, the FIN module is not necessary any more, but an INPUT module is needed to receive spike train 10^n-11 from the environment. The number n of steps elapsed between the two spikes is the number checked to be accepted. After two spikes are received, if the system finally halts, then number n is said to be accepted.

Module INPUT is shown in Fig. 5. An LHWSNP system Π' working in the accepting mode is constructed to simulate M . Each register r of M is associated with a neuron σ_r in Π' ; the rules in neuron are $a \rightarrow a$ and $a^4(a^5)^+/a^4 \rightarrow a$. The evolution of the numbers of spikes in the neurons during the computation of the INPUT module is shown in Table 2.

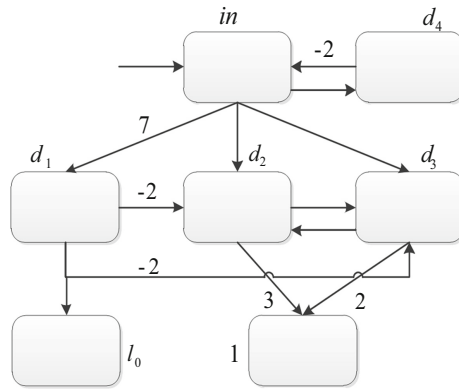


Fig. 5. The structure of INPUT module

Table 2. The numbers of spikes in the neurons of INPUT module during the process of reading spike train $10^{n-1}1$

Neuron	Step								
	t	t + 1	t + 2	t + 3	...	t + n	t + n+1	t + n+2	t + n+3
σ_{in}	14	10	8	8	...	9	5	3	3
σ_{d_1}	0	7	7	7	...	7	14	10	10
σ_{d_2}	0	1	1	1	...	1	2	0	0
σ_{d_3}	0	1	1	1	...	1	2	0	0
σ_{d_4}	0	1	0	0	...	0	1	0	0
σ_{l_0}	0	0	0	0	...	0	0	1	0
σ_1	0	0	5	5×2	...	$5(n-1)$	$5n$	$5n$	$5n$

During the process of reading spike train $10^{n-1}1$, the evolution of the numbers of spikes in the neurons of INPUT module is shown in Table 2.

In accepting module, ADD module is deterministic and its form is $(l_i:(ADD(r, l_j)))$, which is indicated in Fig. 6. The neurons of this system contain rule $a \rightarrow a$.

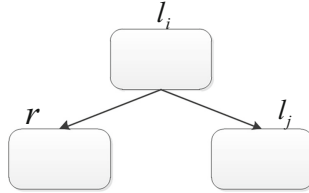


Fig. 6. The structure of deterministic ADD module

Module SUB remains unchanged (as shown in Fig. 1), module FIN is removed, with neuron σ_h remaining in the system, but without outgoing synapses. When neuron σ_h receives two spikes, it means that the computation of register machine M reaches instruction σ_h and stops. Having two spikes inside, neuron σ_h spikes ($a^2 \rightarrow a$ is enabled) without emitting any spike out and the system Π' halts.

As explained above, it is obtained that any set of natural numbers accepted by deterministic register machines can be accepted by LHWSN P system Π' .

3.2 Analysis of Results

Literature [20] proposed that spiking rules in neurons see the regular expressions as criteria of spiking and determining whether a regular expression satisfied may be a NP hard problem. This paper reduce the number of rules in neurons, greatly reducing the time of determining whether a regular expression is satisfied and then reducing the time of the whole module running.

We assume that the time to judge whether the spiking rules are satisfied is T1, and whether the forgetting rules are satisfied is T2. Each step of the system needs to determine whether the spiking and forgetting rules can be executed. In the following, We will compare the time required for LHWSNPS and HWSNPS [4] in each module.

In the ADD module of INHWSNPS, each neuron has 4 spiking rules, and the ADD module takes 5 steps from start to finish, So the total time required for the ADD module is $20T1$; In ADD module of HWSNPS, each neuron has five spiking rules and two forgetting rules, and four steps are needed to finish ADD module, so the total time is $20T1 + 8T2$. Similarly, we can calculate the time consumed by two systems in the SUB module, FIN module and INPUT module respectively. Comparison of execution time of two systems can be seen in Table 3.

Table 3. The time comparison of two system

Module Time Name	ADD module	SUB module	FIN module	INPUT module
LHWSNP	20T1	8T1	3(n+3)T1	2(n+2)T1
HWSNP	20T1+8T2	20T1+8T2	5(n+3)T1+2(n+3)T2	5(n+3)T1+2(n+3)T2

4 Final Remarks

In this work, inspired by the local homogeneity of biological neurons, we consider a restricted variant of SNP system (LHWSNP systems). In this system, each neuron in the same module has the same set of rules, which is having the local homogeneity. We investigate the computing power of LHWSNP systems. It is obtained that such systems only using standard spiking rules can achieve the Turing completeness. It reveals that we not only maintain the homogeneity of the system, but also reduce the time needed of the system.

Many problems of LHWSNP systems need further researches. It is worth to consider that whether we can reduce the category of rules in the system without losing the universality of LHWSNP systems. Also, the language generated by such systems is worthy to be studied. Moreover, the next step, we will consider use this SNP system to solve practical problems.


Acknowledgment. This work was supported by the Natural Science Foundation of China (No. 61502283). Natural Science Foundation of China (No. 61472231). Natural Science Foundation of China (No. 61640201).

References

1. Păun, G.: Computing with membranes. *J. Comput. Syst. Sci.* **61**(1), 108–143 (2000)
2. Freund, R., Păun, G., Pérez-Jiménez, M.J.: Tissue-like P systems with channel-states. *Theor. Comput. Sci.* **330**, 101–116 (2005)
3. Ionescu, M., Păun, G., Yokomori, T.: Spiking neural P systems. *Fund. Inf.* **71**(2–3), 279–308 (2006)
4. Zeng, X., Zhang, X., Pan, L.: Homogeneous spiking neural P systems. *Fundamenta Informaticae* **97**(1–2), 275–294 (2009)
5. Ibarra, O.H., Păun, A., Rodríguez-Patón, A.: Sequential SNP systems based on min/max spike number. *Theor. Comput. Sci.* **410**(s30–s32), 2982–2991 (2009)
6. Cavaliere, M., Ibarra, O.H., Păun, G., et al.: Asynchronous spiking neural P systems. *Theoret. Comput. Sci.* **410**(24), 2352–2364 (2009)
7. Pan, L., Păun, G.: Spiking neural P systems with anti-spikes. *Int. J. Comput. Commun. Control* **4**(3), 273–282 (2009)
8. Song, T., Pan, L., Păun, G.: Asynchronous spiking neural P systems with local synchronization. *Inf. Sci.* **219**, 197–207 (2013)

9. Zhang, X., Zeng, X., Pan, L.: Weighted spiking neural p systems with rules on synapses. *Fundamenta Informaticae* **134**(1–2), 201–218 (2014)
10. Song, T., Zou, Q., Liu, X., et al.: Asynchronous spiking neural P systems with rules on synapses. *Neurocomputing* **151**, 1439–1445 (2015)
11. Chen, H., Freund, R., Ionescu, M., et al.: On string languages generated by spiking neural P systems. *Fundamenta Informaticae* **75**(75), 141–162 (2007)
12. Zhang, X., Zeng, X., Pan, L.: On string languages generated by spiking neural P systems with exhaustive use of rules. *Nat. Comput.* **7**(4), 535–549 (2008)
13. Păun, A., Păun, G.: Small universal spiking neural P systems. *BioSystems* **90**(1), 48–60 (2007)
14. Pan, L., Zeng, X.: Small universal spiking neural P systems working in exhaustive mode. *IEEE Trans. NanoBiosci.* **10**(2), 99–105 (2011)
15. Song, T., Shi, X., Jinbang, X.U.: Reversible spiking neural P systems. *Front. Comput. Sci. Sel. Publ. Chin. Univ.* **7**(3), 350–358 (2013)
16. Song, T., Wang, X.: Homogenous spiking neural P systems with inhibitory synapses. *Neural Process. Lett.* **42**(1), 199–214 (2014)
17. Rozenberg, G., Salomaa, A.: *Handbook of Formal Languages: Beyond Words*. Springer, Heidelberg (1997). <https://doi.org/10.1007/978-3-642-59126-6>
18. Hopcroft, J.E., Motwani, R., Ullman, J.D.: *Introduction to automata theory, languages, and computation*, 2nd edn. *ACM Sigact News* **5**(8), 60–65 (2001)
19. Wang, J., Hoogeboom, H.J., Pan, L., et al.: spiking neural P systems with weights. *Neural Comput.* **22**(10), 2615–2646 (2010)
20. Leporati, A., Zandron, C., Ferretti, C., et al.: On the computational power of spiking neural P systems. *Int. J. Unconventional Comput.* **5**(5), 459–473 (2009)

Weight-Improved K-Means-Based Consensus Clustering

Yanhua Wang, Laisheng Xiang, and Xiyu Liu 

School of Management Science and Engineering, Shandong Normal University, Jinan, China
15554130027@163.com, xls3366@163.com, sdxyliu@163.com

Abstract. Many consensus clustering methods ensemble all the basic partitionings (BPs) with the same weight and without considering their contribution to consensus result. We use the Normalized Mutual Information (NMI) theory to design weight for BPs that participate in the integration, which highlights the contribution of the most diverse BPs. Then an efficient approach K-means is used for consensus clustering, which effectively improves the efficiency of combinatorics learning. Experiment on UCI dataset iris demonstrates the effective of the proposed algorithm in terms of clustering quality.

Keywords: Consensus clustering · K-means · Basic partitionings

1 Introduction

There is no single clustering algorithm can performs best for all data sets [1], and can discover all types of cluster shapes and structures [2]. Consensus clustering approached are able to integrate multiple clustering solutions obtained from different data sources into a unified solution, and provide a more robust, stable and accurate final result [3]. However, the previous research still has some limitations.

Firstly, high quality BPs are beneficial to the performance of consensus clustering yet the partitions with poor quality will lead to worse consensus result. But most studies tend to integrate all BPs, and they do not filter poor BPs. Secondly, the diversity between BPs also have great impact on consensus clustering, diverse BPs which means the BP that has different mutual information with other BPs will have different contribution to the consensus result. However, there are few references explore impact of the number of BPs to consensus clustering neither did they take into account the diversity of BPs into the integration process.

We proposed weight-improved K-means-based consensus clustering (WIKCC). Firstly, we design weight for each BP participating in the integration. Specifically, we generate multiple BPs and measure the quality of each BP using normalized Rand index R_n [6], and sort the BPs in the increasing order of R_n , then we explore the influence of the number of BPs on consensus clustering, based on the above exploration we can choose an appropriate number of better BPs for consensus clustering, which can minimize the number of BPs in quality assurance. After that we construct the co-occurrence matrix with the selected BPs, and calculate the similarity of two

BPs with Normalized Mutual Information (NMI) method [4] according to the co-occurrence matrix. Then weight of each BP is designed according to NMI values which reflect a single BP to overall BPs' similarity. K-means-based method [2] make special attention for its simplicity and high efficiency. So we transform consensus clustering to K-means clustering.

2 Weight Design Based on the Normalized Mutual Information

Mutual information is used to measure the shared information of the two distributions. We compute the NMI between two BPs, and the greater the value of NMI means the lower difference, which will result in lower w_i .

Given two BPs results π_i with K_i clusters, $\pi_i = \{C_1^{(i)}, C_2^{(i)}, \dots, C_{K_i}^{(i)}\}$ and π_j with K_j clusters, $\pi_j = \{C_1^{(j)}, C_2^{(j)}, \dots, C_{K_j}^{(j)}\}$ the mutual information between two results is defined as follows:

$$NMI(\pi_i, \pi_j) = \frac{2I_1(\pi_i, \pi_j)}{I_2(\pi_i) + I_2(\pi_j)} \quad (1)$$

$$I_1(\pi_i, \pi_j) = \sum_h \sum_l \frac{|C_h^{(i)} \cap C_l^{(j)}|}{n} \log \frac{n |C_h^{(i)} \cap C_l^{(j)}|}{|C_h^{(i)}| |C_l^{(j)}|} \quad (2)$$

$$I_2(\pi_i) = - \sum_h \frac{|C_h^{(i)}|}{n} \log \frac{|C_h^{(i)}|}{n} \quad (3)$$

$$I_2(\pi_j) = - \sum_l \frac{|C_l^{(j)}|}{n} \log \frac{|C_l^{(j)}|}{n} \quad (4)$$

For a single BP the average mutual information can be defined as:

$$H(\pi_i) = \frac{1}{r-1} \sum_{k=1, k \neq i}^r NMI(\pi_i, \pi_k), (i = 1, 2, \dots, r) \quad (5)$$

Where $h \in \{1, 2, \dots, k_i\}$, $l \in \{1, 2, \dots, k_j\}$ is one of the cluster result label of π_i and π_j , $|C_h^{(i)}|$, $|C_l^{(j)}|$ respectively represent the number of the data set belong to cluster $C_h^{(i)}$ in π_i and $C_l^{(j)}$ in π_j , $|C_h^{(i)} \cap C_l^{(j)}|$ is the number of the dataset belong both to $C_h^{(i)}$ and $C_l^{(j)}$, r is the number of the BPs.

The greater $H(\pi_i)$ indicate that cluster member π_i share more information with other cluster members. The weight is defined as:

$$w_m = \frac{1}{H(\pi_i)} \quad (6)$$

The normalized form is defined as:

$$w_m = \frac{w'_m}{\sum_{m=1}^r w'_m} \tag{7}$$

The weight is bigger as the greater diversity between two base clustering.

3 The Weight-Improved K-Means-Based Consensus Clustering

In this section, we first introduce the co-occurrence matrix which is used for records the situation of sharing dataset between two BPs. Table 1 shows an example.

Table 1. The co-occurrence matrix

π^*	$\pi_{iC_1^{(i)}}$	$C_2^{(i)}$...	$C_{K_i}^{(i)}$	Σ
C_1	$n_{11}^{(i)}$	$n_{12}^{(i)}$...	$n_{1K_i}^{(i)}$	n_{1+}
C_2	$n_{21}^{(i)}$	$n_{22}^{(i)}$...	$n_{2K_i}^{(i)}$	n_{2+}
...
C_K	$n_{K1}^{(i)}$	$n_{K2}^{(i)}$...	$n_{KK_i}^{(i)}$	n_{K+}
Σ	$n_{+1}^{(i)}$	$n_{+2}^{(i)}$...	$n_{+K_i}^{(i)}$	n

In Table 1, BPs: π^* and π_i contain k and k_i clusters respectively, $n_{KK_i}^{(i)}$ represents the number of the objects that belongs to both C_K and $C_{K_i}^{(i)}$, then let $n_{k+} = \sum_{j=1}^{K_i} n_{kj}^{(i)}$, $1 \leq j \leq K_i$, $1 \leq k \leq K$, $P_{kj}^{(i)} = n_{kj}^{(i)} / n$, $p_{k+} = n_{k+} / n$, and $p_{+j}^{(i)} = n_{+j}^{(i)} / n$. We can obtain a normalized co-occurrence matrix (NCM), based on which we can compute the centroid of the K-means clustering.

K-means algorithm cannot directly run on the co-occurrence matrix, so a binary data set is introduced to represent the result of r BPs. The binary data set $X_l^{(b)} = \{x_l^{(b)} | 1 \leq l \leq n\}$ as follows:

$$x_l^{(b)} = \langle x_{l,1}^{(b)}, \dots, x_{l,i}^{(b)}, \dots, x_{l,r}^{(b)} \rangle, \text{ with} \tag{8}$$

$$x_{l,i}^{(b)} = \langle x_{l,i1}^{(b)}, \dots, x_{l,ij}^{(b)}, \dots, x_{l,iK_i}^{(b)} \rangle, \text{ and} \tag{9}$$

$$x_{l,ij}^{(b)} = \begin{cases} 1, & \text{if object } l \text{ belongs to the cluster } C_j \text{ in } \pi_i \\ 0, & \text{otherwise} \end{cases}, \tag{10}$$

Where $x_l^{(b)}$ is an $n \times \sum_{i=1}^r K_i$ binary data set matrix with $\left| x_{li}^{(b)} \right| = 1$.

We use the K-means algorithm to integrate the BPs, suppose r BPs are integrated to a result π^* , m_k represent the centroid of the C_k in π^* as follows:

$$m_k = \langle m_{k,1}, \dots, m_{k,i}, \dots, m_{k,r} \rangle, \text{ with} \quad (11)$$

$$m_{k,i} = \langle m_{k,i1}, \dots, m_{k,ij}, \dots, m_{k,iK_i} \rangle, \quad (12)$$

The centroids of the K-means on X^b are represented as follows:

$$m_{k,i} = \left\langle \frac{P_{k1}^{(i)}}{P_{k+}}, \dots, \frac{P_{kj}^{(i)}}{P_{k+}}, \dots, \frac{P_{kK_i}^{(i)}}{P_{k+}} \right\rangle, \forall k, i. \quad (13)$$

The centroids can be computed by the Co-occurrence matrix, and m_k is a vector of $\sum_{i=1}^r k_i$ dimension. The element in the vector is computed by the number of shared data set between current cluster and all of the clusters of BPs.

By using the co-occurrence matrix and the binary data set the consensus clustering are transformed to the K-means clustering, that is:

$$\max \sum_{i=1}^r w_i U(\pi, \pi^*) = \min \sum_{k=1}^K \sum_{x_l \in C_k} f(x_l^{(b)}, m_k) \quad (14)$$

As shown in Fig. 1. In BPs generation phase, classic partition clustering method K-means is used, different initial number of cluster k , to generate diversified BPs. In consensus clustering phase, after generating the BPs and computing the weight for each clustering member, we can obtain the weighted co-occurrence matrix, and then we can

Algorithm WIKCC

Require:

Input: a data set of known class label

Ensure:

1. Using K-means to generate r BPs called Π
2. Construct the binary data set $X^{(t)}$ from Π
3. The Co-occurrence matrix is constructed by using BPs
4. Compute the weight of r BPs as $\{w_1, w_2, \dots, w_r\}$ by using NMI
5. Reconstruct the binary data set $X^{(t) \prime}$ using weight
6. Run K-means to cluster $X^{(t) \prime}$ into K clusters and get π^*
- 7: Return π^*

Fig. 1. Algorithm WIKCC

get the weighted binary dataset $X^{(b)'}$, by running K-means on weighted binary dataset $X^{(b)'}$, we can get final consensus result π^* .

4 Experimental Results

We present experiment on UCI dataset iris. The normalized Rand index (R_n) [6] is adopted. Its value usually range between [0,1]. The higher value, indicate that the higher quality of clustering. We demonstrate the cluster validity of WIKCC by comparing it with two well-known consensus clustering algorithms the K-means-based algorithm (KCC) [2], the hierarchical algorithm (HCC) [5].

4.1 Quality of BPs

We run K-means algorithm 100 times with the initialized number of clusters randomized within $[K, \sqrt{n}]$ to generate 100 basic partitionings (BPs) for consensus clustering; K is the true class of data set, n is the number of the instances, the squared Euclidean distance is used for the distance function, the quality of each BPs is measured by R_n , the distribution of quality of BPs is shown as Fig. 2.

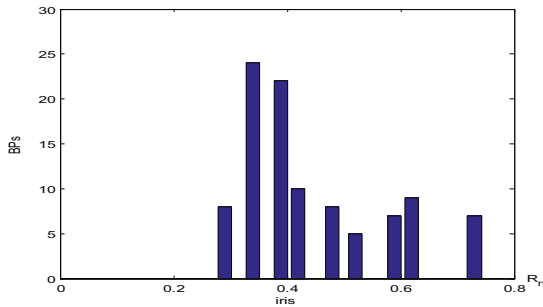


Fig. 2. Clustering quality distribution of BPs

As can be seen in Fig. 2, the distribution of the clustering quality of the BPs show that there is a large proportion of BPs with poor quality, but only quite a small proportion of BPs with relatively high quality. This shows that the incorrect pre-specified number of classes will lead to weak clustering result.

4.2 Exploration of Impact Factors

In order to determine a suitable number of BPs for WIKCC, we explore the influence of the number of BPs on consensus clustering. In the above experiment, r BPs have generated, and $r = 100$. We randomly select a part of BPs to obtain the subset \prod^r , with $r = 10, 20, \dots, 90$. For each r we do KCC [2] algorithm 100 times to get 100

consensus clustering result. The distribution of the quality of consensus clustering result for different subset is shown as Fig. 3.

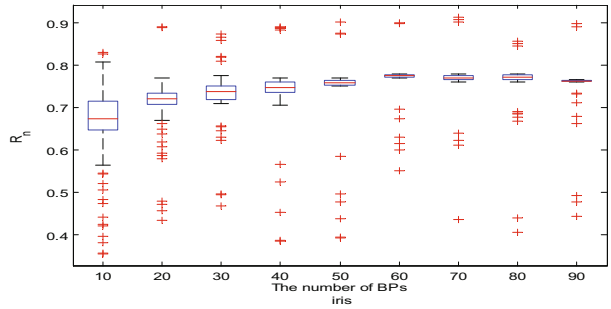


Fig. 3. Impact of the number of BPs to the consensus clustering

As shown in Fig. 3, when $r < 50$, the quality of the consensus result present increasing trend with the increase of r , but when $r > 50$ the result fluctuate in a mall range and nearly tend to be stable, it imply that 50 may be the appropriate number of BPs for WIKCC. Based on above exploration we chose the BPs with the quality of the top 50 BPs for WIKCC.

4.3 WIKCC versus Other Clustering Methods

We compare the WIKCC with KCC and HCC, we choose top 50 better BPs for each method and run on the iris dataset for 10 times.

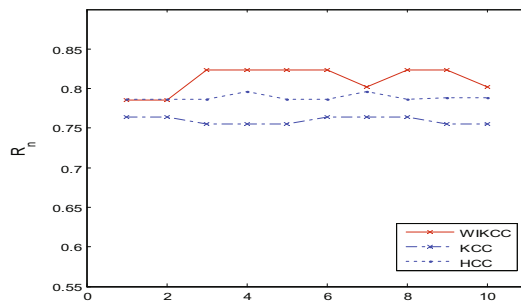


Fig. 4. WIKCC versus KCC and HCC

We can see in Fig. 4. The WIKCC shows significantly higher than KCC, and outperforms better than the HCC in term of the quality of consensus clustering. In addition, comprising the Figs. 2 and 4, we can see that consensus clustering is much better than almost all the basic clustering result obtained by K-means, this indicates that, the consensus clustering method can find the real cluster structure more accurately than a single traditional clustering algorithm by integrating the commonality of many basic

clustering results, so it can obtain a more stable and accurate clustering result by ensemble multiple weak BPS.

5 Concluding Remarks

We explore the influence of the number of BPs on the consensus clustering and chose appropriate number better BPs for WIKCC. The weight is designed by the NMI method between two BPs based on co-occurrence matrix. Finally, the experiment on iris demonstrates that WIKCC outperforms the state-of-the-art well-known KCC and HCC algorithms in terms of clustering quality. In the future, we will explore the more other factors that have influence on the performance of KCC, and we will consider more other factors when designing the weights.

Acknowledgment. Projected supported by National Natural Science Foundation of China (61472231, 61170038, 61502283, 61640201), Jinan City independent innovation plan project in College and Universities, China (201401202), Ministry of education of Humanities and social science research project, China (12YJA630152), Social Science Fund Project of Shandong Province, China (11CGLJ22, 16BGLJ06).

References

1. Strehl, A., Ghosh, J.: Cluster ensembles—a knowledge reuse framework for combining multiple partitions. *J. Mach. Learn. Res.* **3**(12), 583–617 (2002)
2. Wu, J., Liu, H., Xiong, H., et al.: K-means-based consensus clustering: a unified view. *IEEE Trans. Knowl. Data Eng.* **27**(1), 155–169 (2015)
3. Yu, Z., Luo, P., You, J., et al.: Incremental semi-supervised clustering ensemble for high dimensional data clustering. *IEEE Trans. Knowl. Data Eng.* **28**(3), 701–714 (2016)
4. Vinh, N.X., Epps, J., Bailey, J.: Information theoretic measures for clusterings comparison: is a correction for chance necessary? In: *Proceedings of the 26th Annual International Conference on Machine Learning*, pp. 1073–1080. ACM (2009)
5. Fred, A.L.N., Jain, A.K.: Combining multiple clusterings using evidence accumulation. *IEEE Trans. Pattern Anal. Mach. Intell.* **27**(6), 835–850 (2005)
6. Tan, P.-N., Steinbach, M., Kumar, V.: *Introduction to Data Mining*. Addison-Wesley, Reading (2005)

A Novel Trace Clustering Technique Based on Constrained Trace Alignment

Pan Wang^{1(✉)}, Wen'an Tan^{1,2}, Anqiong Tang², and Kai Hu³

¹ Nanjing University of Aeronautics and Astronautics, Nanjing, People's Republic of China
pwang@nuaa.edu.cn

² Shanghai Polytechnic University, Shanghai, People's Republic of China
{watan, aqtang}@sspu.edu.cn

³ Beihang University, Beijing, People's Republic of China
hukai@buaa.edu.cn

Abstract. Whenever traditional process discovery techniques are confronted with complex and flexible environments, equipping all the traces with just one single model might lead to a spaghetti-like process description. Trace clustering which splits the logs into clusters and applies discovery algorithm per cluster has affirmed to be a versatile solution for that. Nevertheless, most trace clustering techniques are not precise enough due to the indiscriminate treatment on the activities captured in traces. As a result, the impacts of some important activities are reduced and some typical information may be distorted or even lost during comparison. In this paper, we propose a novel trace clustering technique that based on constrained traces alignment and then adapt two appropriate clustering strategies into process mining perspective. And experiments on real-life event logs show that our technique has compelling outperformance in terms of process models complexity and comprehensibility.

Keywords: Constrained Trace Clustering · Trace clustering · Process mining
Business process management · Constrained Trace Alignment

1 Introduction

Process discovery is one of the most crucial process mining tasks that entails the construction of process models from event logs of information systems [1]. The most arduous challenge for process discovery is tackling the problem that discovery algorithms are unable to generate accurate and comprehensible process models out of event logs stemming from highly flexible environments.

Trace Clustering is an efficient solution, which *clusters the traces such that each of the resulting clusters corresponds to coherent sets of cases that can each be adequately represented by a process model* [3]. Figure 1 shows the basic procedure for trace clustering.

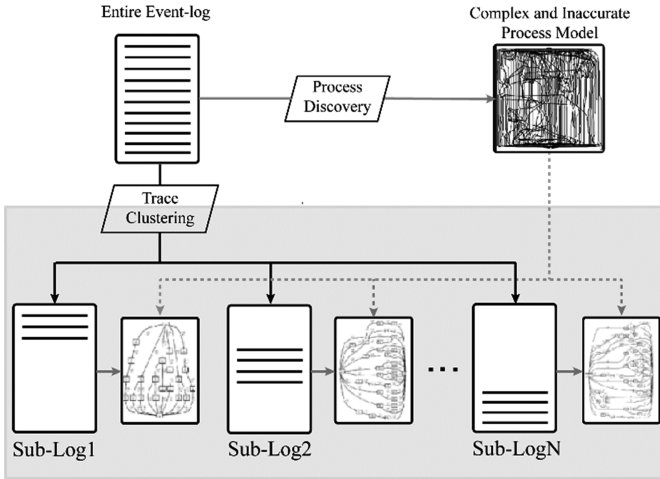


Fig. 1. Illustration of the basic procedure of trace clustering in process mining.

Nevertheless, most currently available trace clustering techniques are not precise enough due to the indiscriminate treatment on the activities captured in traces. As a result, the impacts of some important activities are reduced and some typical process information may be distorted or even lost during comparison.

To address the drawback, this paper presents a novel similarity measurement based on constrained traces alignment. First, some typical causal sequences that reflect the “backbone” of process are identified. Then, these sequences are exploited as constraints to guarantee the priority of important activities in traces. Subsequently, we suggest two clustering strategies that agree with the process mining perspective. The agglomerative hierarchical clustering (AHC) was selected for its embedded flexibility on abstraction level to provide us an overall insight into the complex process. And the spectral clustering has a good recommendation about the number of clusters corresponding to the generic abstraction level.

In brief, this work contributes by proposing a novel constrained trace similarity measurement to guarantee the priority of important process episodes and subsequently adapting two appropriate clustering techniques into process mining perspective. In addition, experiments on real-life logs prove the improvements achieved by our method relative to six existing methods.

The rest of the paper is organized as follows: Sect. 2 provides a brief overview of related works. Next, Sect. 3 introduces our novel constrained trace similarity measurement and the process-adaptive clustering strategies we selected. And Sect. 4 discusses the experiment results. Finally, Sect. 5 draws conclusions and spells out directions for future work.

2 Related Work

The main distinction between trace clustering techniques is the clustering bias (distance/similarity measures) they proposed. Existing approaches in literature can be classified into two major categories.

2.1 Distance-Based Trace Clustering

2.1.1 Vector-Based Trace Clustering

Vector-based trace clustering approaches transform traces into a vector space. Then, clustering can be achieved combining different distance metrics in the vector space. Greco et al. [8] were pioneers in study of clustering log traces within the process mining domain. They make trace clusters through the vector space over the activities and their transitions to discover expressive process models at the first attempt. They also introduced a notion of disjunctive workflow schemas (DWS) for divisive trace clustering [5]. Song et al. [13] elaborated on constructing so-called profiles associated with multiple trace perspectives as the feature vector.

2.1.2 Context-Aware Trace Clustering

Context-aware trace clustering approaches regard the entire trace as a whole sequence which implies all the process context information. Then various string edit distance metrics can be applied on it in conjunction with standard clustering techniques. In [2], Bose and van der Aalst propose a generic edit distance which derives specific edit operation costs so as to take into account the behavior in traces. The context-aware method is further developed in [3], it leverages conserved patterns or subsequences as feature sets to describe the characteristic of a certain trace.

2.2 Model-Based Trace Clustering

2.2.1 Sequence Clustering

Sequence clustering algorithm creates first-order Markov chains for clusters cooperating with the expectation-maximization (EM) algorithm to determine the assignment of a certain sequence. It has been used to automatically group large protein datasets to search for homologous gene sequences in bioinformatics. This technique was migrated into trace clustering by [6].

2.2.2 Active Trace Clustering

Active trace clustering inherits the underlying idea of sequence clustering [15]. Therein a trace is added to the current cluster if the model discovered from the cluster including that trace satisfies the target threshold of fitness. An optimal distribution of execution traces over a given number of clusters is achieved whereby the combined accuracy of the associated process models is maximized. In this way, the quality of process model discovered is under control. More extension on it has been developed to support further objectives in [7].

3 Approach Design

Distance/similarity measurement and clustering strategy with its specific characteristics are both important cluster-theoretical aspects. Therefore, we introduce our approach in the two steps. The framework of the approach in this paper is depicted in Fig. 2.

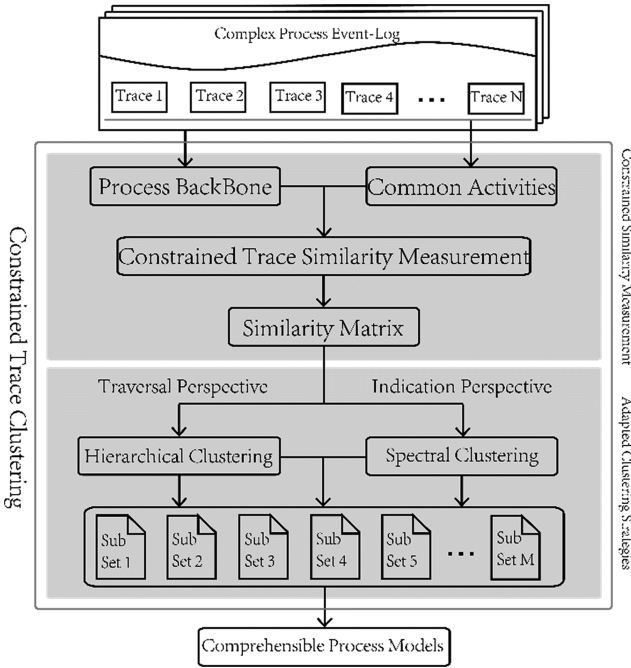


Fig. 2. Framework of Constrained Trace Clustering.

3.1 Similarity Measurement Based on Constrained Traces Alignment

Just as noted by [10], “specifying an appropriate dissimilarity measure is far more important than choice of clustering algorithm. This aspect of the problem is emphasized less in the clustering literature since it depends on domain knowledge specifics.” Therefore, it is inevitable to refine the distance/similarity metrics in trace clustering for providing more appropriate information to the clustering algorithm.

We can perceive that identifying some significant behaviors in traces will assist in mining better sub-process models by clustering the traces based on those significant behaviors. However, due to the indiscriminate treatment on behaviors in traces and the lack of domain knowledge, capturing them directly from event logs seems to be a difficult task.

Fortunately, the association rules in data mining shed light on this tough task. Employing the association rules, we are able to reveal the “backbone” of process. Then, some typical causal sequences that reflect the process backbone are identified and

exploited as constraints to guarantee the priority of significant behaviors during similarity comparison.

3.1.1 Dependency Measures to Reveal Process Backbone

Definition 1. (Dependency Measures) Let L be an event log over A . a and b are activities that occur in L , i.e.; $|\sigma|$ denotes the length of the trace.

$|a \succ_L b|$ is the number of times a is directly followed by b in, i.e.,

$$|a \succ_L b| = \sum_{\sigma \in L} L(\sigma) \times |\{1 \leq i \leq |\sigma| \mid \sigma(i) = a \wedge \sigma(i+1) = b\}| \quad (1)$$

$|a \Rightarrow_L b|$ is the value of the dependency relation between a and b :

$$|a \Rightarrow_L b| = \begin{cases} \frac{|a \succ_L b| - |b \succ_L a|}{|a \succ_L b| + |b \succ_L a| + 1} & \text{if } a \neq b \\ \frac{|a \succ_L a|}{|a \succ_L a| + 1} & \text{if } a = b \end{cases} \quad (2)$$

$|a \Rightarrow_L b|$ produces a value between -1 and 1 . If $|a \Rightarrow_L b|$ is close to 1 , then there is a strong positive dependency between a and b .

By setting μ , the threshold of $|a \succ_L b|$, we can filter out the infrequent items. And when $|a \Rightarrow_L b|$ meets certain thresholds ν , we specified that there is a connection between a and b .

To illustrate the basic concepts, we use the following event log L :

$$L = [\langle a, d, e, f, g, i \rangle^{16}, \langle a, b, e, f, i \rangle^1, \langle a, c, e, f, h, i \rangle^1, \langle a, c, b, e, f, h, i \rangle^{12}, \langle a, e, f, g, i \rangle^5, \langle d, d, a, d, e, f, g, i \rangle^1, \langle a, b, c, e, f, h, i \rangle^{13}, \langle a, d, d, d, e, f, g, i \rangle^1]$$

Figure 3(A) depicts the dependency graph corresponding to the threshold of $\mu = 2$, $\nu = 0.7$. And Fig. 3(B) is another dependency graph with the threshold of $\mu = 5$, $\nu = 0.85$. Obviously, the dependency graph does not show the routing logic but it reveals the “backbone” of the process model. The derived dependency graph (denote as G) is then used as a reference to reveal the general order of some typical activities.



Fig. 3. Dependency graphs according to the dependency measures.

3.1.2 Constrained Similarity Measurement

Let A_i represents the set of activities that involved in trace σ_i (known as Alphabet) while B represents the set of activities that involved in the “process backbone”. $A_i \cap A_j \cap B$ are the common activities between σ_i and σ_j with respect to the “process backbone”. Referring to the dependency graph mentioned above, we can get the causal sequences of them. For example, the involved common activities between traces $\langle d, d, a, d, e, f, g, i \rangle$, $\langle a, d, d, d, e, f, g, i \rangle$ in L and the dependency graph are $\langle a, d, e, f, g, i \rangle$, their constraints are shown as the black highlights in Fig. 4. We call these common activities that attached with causal sequences as typical behaviors.

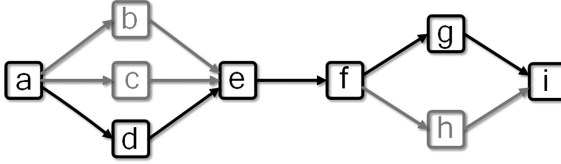


Fig. 4. Illustration of constraint instance.

These behaviors provide an approximation of the essence of the both comparing traces in a global perspective. Next, we utilize them as constraint conditions to guarantee the priority of typical behaviors between traces. In the following, the typical behaviors between traces σ_i and σ_j concerning the process backbone are denoted as $C_{i,j}$.

Definition 2. (Constrained Similarity Measurement) σ_i and σ_j are two traces, the constraints of them are $C_{i,j}$. Then, the similarity of σ_i and σ_j , $Sim(\sigma_i, \sigma_j)$ is defined as:

$$Sim(\sigma_i, \sigma_j) = \frac{length(CLCS(\sigma_i, \sigma_j, C_{i,j}))}{\max(length(\sigma_i), length(\sigma_j))} \quad (3)$$

The constrained measurement is relied on the constrained longest common sequences (CLCS). The CLCS has already been applied in bioinformatics for the computation of the homology of two biological sequences. For more details about CLCS, please refer to [14].

3.2 Adapted Trace Clustering Strategies

Traditional trace clustering only adapts data-centric clustering algorithms. However, as described in [3], the most important evaluation dimension for trace clustering is from a process discovery perspective. This entails the compatibility with process features on the adopted clustering strategies. Here, we suggest two apposite clustering strategies for different applications.

3.2.1 Agglomerative Hierarchical Clustering

Thanks to the hierarchical characteristic of AHC algorithm, it pertinently agrees with the *continuum* ranging from unstructured processes to structured processes. The bottom of AHC means clusters corresponding to each trace whose processes mined are surely structured while the top represents the only cluster that contains everything whose process mined is usually unstructured when confronted with flexible environment. Thus, we are able to ascertain the applicable level as desired or traverse all the hierarchy straightforward to gain an overall insight into the complex process.

The method we adopt is proposed by [4] termed as GuideTreeMiner. The GuideTreeMiner uses AHC algorithm to build a guide tree (also known as dendrogram). Any horizontal line spanning over the dendrogram corresponds to a practical clustering at a specific abstraction level.

3.2.2 Spectral Clustering

Except for hierarchical clustering algorithms, most of the trace clustering require predefined parameters for clustering such as the amount of clusters, the maximum cluster size etc. The truth is the definition of these specialized parameters are far from easy for general users due to the lack of domain knowledge. Actually, even for experts, it's also not a trivial work as well owing to the complexity and flexibility of real-life process. Against this background, the spectral clustering was selected as it provides a good recommendation about the number of clusters [11] which can guide us to a generic abstraction level.

It's worth point out that the *affinity* matrix always calculated as *Gaussian kernel*, however, it doesn't reflect the nature of processes. So, in this work, it is calculated as the constrained similarity described in the previous section. Likewise, the *laplacian* is often normalized, but duo to the robustness of constrained similarity measurement against infrequency and the pursuit of stable clustering indication, we select the non-normalized *laplacian*. As for the indication about the cluster number k , it can be recognized whereby the sudden drop in the eigenvalues. Actually, in many cases, the two solutions can be used in union.

4 Experiments

4.1 Experiment Configuration and Evaluation Criterion

We used the ProM¹ framework which has been developed to support process mining algorithms to perform the experiments. The data is from Dutch Financial Institute². And we adopted the HeuristicsMiner to derive the process model as it has the best capability to deal with real-life event logs. The approaches to compare with are presented as follows: DWS Mining [5], Trace Clustering [13], GuideTree Miner [2, 3], Sequence Clustering [6] and ActiTraC [15].

¹ <http://www.processmining.org>.

² <http://www.win.tue.nl/bpi/doku.php?id=2012:challenge>.

We evaluate the results with respect to their model complexity, as they are measured by a comprehensive list of metrics reported in [12]:

1. $|A|$ signifies the number of arcs in the process model.
2. $|N|$ signifies the number of nodes in the process model.
3. $|CN| = |A| - |N| + 1$ signifies the cyclomatic number of the process model.
4. $CNC = \frac{|A|}{|N|}$ signifies the coefficient of connectivity of the process model.
5. $\Delta = \frac{|A|}{|N| \cdot |N-1|}$ signifies the density of the process model.

4.2 Clustering Results

We made comparisons with different number of clusters for three different abstraction levels. Here, level 1 represents the original trace set, i.e. there is only one cluster. Level 2 stands for 2/3/4 clusters while level 3 contains 5/6/7 clusters. We calculated $|A|$ by taking their corresponding nodes weighted average and the same as $|N|$.

The aggregated results are presented in Table 1. All the data has been depicted to the radarplots in Fig. 5. We can see that all cluster techniques lead to models with lower complexity than the original log file. However, the DWS, the ActiTraC and the Trace Clustering approaches lead to clusters whose models have higher density values than the unclustered one though they perform well in the other metrics. The smaller area and more balanced capabilities shown in the radarplots from two abstraction levels proved the effectiveness of our constraints.

Table 1. The aggregated clustering results

Abstraction level	Method	Cluster number	A	N	CNC	CN	Δ
Level 1	Unclustered	1	141.0	36.0	3.917	106.0	0.112
Level 2	SC	3	101.3	35.7	2.838	65.6	0.082
	DWS	4(Std.)	62.3	22.5	2.769	39.8	0.129
	TC	3(1-3)	50.0	16.7	2.994	33.3	0.191
	ATC	4(3-Std.)	21.5	12.0	1.792	9.5	0.163
	GED	3	86.6	34.6	2.503	52.0	0.074
	MRA	3	94.4	34.6	2.728	59.8	0.081
	Co-TC	3	86.5	35.3	2.450	51.2	0.071
Level 3	SC	6	74.5	34.7	2.147	39.8	0.064
	DWS	6(5-5-5-10)	41.7	19.0	2.195	22.7	0.122
	ATC	7(6-Std.)	15.6	10.1	1.544	5.5	0.170
	GED	6	76.5	33.6	2.277	42.9	0.070
	MRA	6	82.3	33.9	2.428	48.4	0.074
	Co-TC	6	73.5	33.1	2.221	39.4	0.069

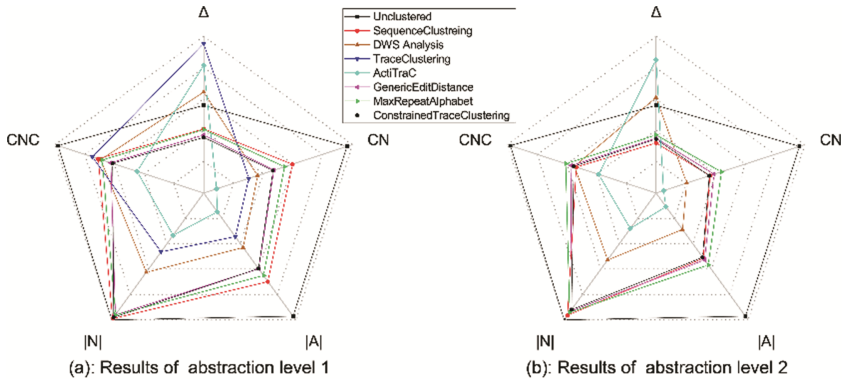


Fig. 5. Radarplots of different trace clustering techniques.

Moreover, Fig. 6 depicts Constrained Trace Clustering at different levels. With the increasing number of clusters, there is only a little improvement in all aspects. Considering the extra elaboration on more clusters, it is inefficient and meaningless to set the number of clusters to a higher value. This is consistent with the spectral clustering. Just as the eigenvalues scatterplot shown in Fig. 7, only the first three clusters are well separated. Therefore, the spectral clustering can guide us to correctly capture the right level of abstraction by providing a good recommendation about the number of clusters instead of the iterations on different hierarchies.

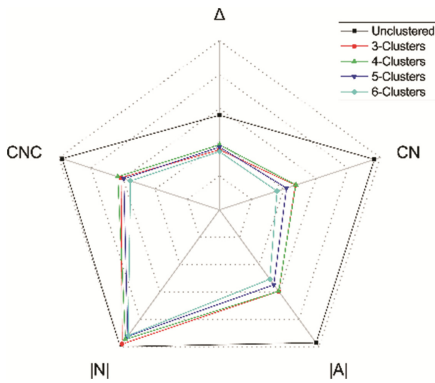


Fig. 6. Constrained Trace Clustering from different abstraction levels.

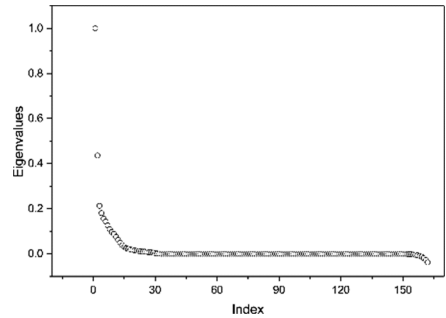


Fig. 7. Similarity matrix eigenvalues.

In a nutshell, all these experiments confirm the effectiveness and efficiency of Constrained Trace Clustering to deliver comprehensible process models from the flexible and complex logs.

5 Conclusions and Future Perspectives

In this paper, we contribute to trace clustering techniques by imposing constraints on trace similarity/distance measurements to guarantee the priority of important activities in traces. By this means, significant process information is preserved as much as possible such that more accurate trace similarity measurement will be obtained. Moreover, we integrate two clustering strategies that agree with the process mining perspective to cluster these traces.

There are still a number of challenging issues remain open for future research work. Firstly, more refined similarity/distance measurements that felicitously agree with the process domain knowledge are encouraged. On the issues of processing sequence data, we should learn from bioinformatics which has more mature applications on sequence data mining. Another direction of research might be that of integrating advanced clustering strategies, as currently available techniques only adapt traditional data clustering techniques which are data-centric instead of process-centric into process mining. More generally, designing ad hoc clustering strategies usually leads to more suitable clustering results. Finally, trace clustering techniques only take into account of sorting in the horizontal direction, it would be promising to combine with techniques that focus on abstraction in the vertical direction, such as FuzzyMiner [9] which enforces cartography to the process mining by means of clustering activities.

Acknowledgment. This work is supported in part by the National Natural Science Foundation of China under Grant No. 61672022, Key Disciplines of Computer Science and Technology of Shanghai Polytechnic University under Grant No. XXKZD1604, the Fundamental Research Funds for the Central Universities and Foundation of Graduate Innovation of Shanghai Polytechnic University, and Foundation of Graduate Innovation Center in NUAA under Grant No. kfj20161601.

References

1. Aalst, W.V.D.: *Process Mining: Discovery, Conformance and Enhancement of Business Processes*. Springer, Heidelberg (2011)
2. Bose, R.P.J.C., van der Aalst, W.M.P.: Context aware trace clustering: towards improving process mining results. In: *SIAM International Conference on Data Mining*, pp. 401–412 (2009)
3. Bose, R.P.J.C., van der Aalst, W.M.P.: Trace clustering based on conserved patterns: towards achieving better process models. In: Rinderle-Ma, S., Sadiq, S., Leymann, F. (eds.) *BPM 2009*. LNBP, vol. 43, pp. 170–181. Springer, Heidelberg (2010). https://doi.org/10.1007/978-3-642-12186-9_16
4. Bose, R.P.J.C., van der Aalst, W.M.P.: Trace alignment in process mining: opportunities for process diagnostics. In: Hull, R., Mendling, J., Tai, S. (eds.) *BPM 2010*. LNCS, vol. 6336, pp. 227–242. Springer, Heidelberg (2010). https://doi.org/10.1007/978-3-642-15618-2_17
5. de Medeiros, A.K.A., Guzzo, A., Greco, G., van der Aalst, W.M.P., Weijters, A.J.M.M., van Dongen, B.F., Saccà, D.: Process mining based on clustering: a quest for precision. In: ter Hofstede, A., Benatallah, B., Paik, H.-Y. (eds.) *BPM 2007*. LNCS, vol. 4928, pp. 17–29. Springer, Heidelberg (2008). https://doi.org/10.1007/978-3-540-78238-4_4

6. Ferreira, D.R.: Applied sequence clustering techniques for process mining. In: Handbook of Research on Business Process Modeling, pp. 492–513 (2009)
7. García Bañuelos, L., Dumas, M., La Rosa, M., De Weerd, J., Ekanayake, C.C.: Controlled automated discovery of collections of business process models. *Inf. Syst.* **46**, 85–101 (2014)
8. Greco, G., Guzzo, A., Pontieri, L., Sacca, D.: Discovering expressive process models by clustering log traces. *IEEE Trans. Knowl. Data Eng.* **18**, 1010–1027 (2006)
9. Günther, C.W., van der Aalst, W.M.P.: Fuzzy mining – adaptive process simplification based on multi-perspective metrics. In: Alonso, G., Dadam, P., Rosemann, M. (eds.) BPM 2007. LNCS, vol. 4714, pp. 328–343. Springer, Heidelberg (2007). https://doi.org/10.1007/978-3-540-75183-0_24
10. Hastie, T., Friedman, J., Tibshirani, R.: The Elements of Statistical Learning, vol. 167. Springer, New York (2009). <https://doi.org/10.1007/978-0-387-21606-5>
11. von Luxbur, U.: A tutorial on spectral clustering. *Stat. Comput.* **17**, 395–416 (2007)
12. Reijers, H.A., Mendling, J.: A study into the factors that influence the understandability of business process models. *Trans. Sys. Man Cyber. Part A* **41**, 449–462 (2011)
13. Song, M., Günther, C.W., van der Aalst, W.M.P.: Trace clustering in process mining. In: Ardagna, D., Mecella, M., Yang, J. (eds.) BPM 2008. LNBIP, vol. 17, pp. 109–120. Springer, Heidelberg (2009). https://doi.org/10.1007/978-3-642-00328-8_11
14. Tsai, Y.T.: The constrained common subsequence problem. *Inf. Process. Lett.* **88**, 173–176 (2003)
15. Weerd, J.D., Broucke, S.V., Vanthienen, J., Baesens, B.: Active trace clustering for improved process discovery. *IEEE Trans. Knowl. Data Eng.* **25**, 2708–2720 (2013)

A Fast Local Image Descriptor Based on Patch Quantization

Tian Tian¹(✉), Fan Yang¹, Kun Zheng², Hong Yao¹(✉), and Qian Gao³

¹ College of Computer Science, China University of Geosciences,
No. 388 Lumo Road, Wuhan 430074, China
{tiantian,yaohong}@cug.edu.cn

² Faculty of Information Engineering, China University of Geosciences,
No. 388 Lumo Road, Wuhan 430074, China

³ School of Mathematics and Statistics,
Huazhong University of Science and Technology,
No. 1037 Luoyu Road, Wuhan 430074, China

Abstract. Representing local image patches is a key step in many applications of computer vision, while fast and effective description methods are always required by real-time image processing. Motivated by the fact that quantization compresses information while preserving primary structures, in this paper, we propose to use vector quantization (VQ) on local patch descriptor building. Compared to conventional approaches that compress floating-point features with VQ, we produce local integer descriptors very fast directly based on simple quantization methods. Experimental results on a publicly available dataset show that the present method is efficient both to build and to match. It achieves comparable performance to some typical floating-point and binary descriptors such as SIFT and BRIEF, offering a novel solution to fast local image representation except for bit test created in BRIEF.

Keywords: Local image descriptor · Vector quantization
Feature matching · Cumulative distribution function

1 Introduction

As one of the vital problems in image processing and understanding, image representation is a core research of many computer vision applications, such as image registration, image retrieval, and object classification. This task can be generally divided into two main steps: the extraction of feature points and the description of these keypoints [9]. During the past decades, Scale Invariant Feature Transform (SIFT) [11] proposed by Lowe was once a benchmark for its excellent performance. And Speeded Up Robust Features (SURF) [2] which exhibits much higher efficiency than SIFT has then become a *de facto* standard.

SURF addresses the issue of speed, but, since the SURF feature is still a vector of floating point values, the storage and computation of features is still expensive. Thus, a number of techniques are proposed from different aspects to reduce memory consumption and speed up matching of features. The first direct

way is to work with short descriptors, which is obtained by applying dimensionality reduction on computed features. Principal Component Analysis (PCA) or Linear Discriminant Embedding (LDE) [8] can be easily used to reduce descriptor size without loss in recognition performance [13]. Another way to shorten a descriptor is to quantize its floating-point coordinates into integers [20] or binarize the feature with a few of bits. Quantization is a simple additional operation yielding better memory gain and faster matching, and both CHoG [5] and PQ-WGLOH [21] use vector quantization to build compact descriptors. Binarization motivated by Locality Sensitive Hashing (LSH) [6] is usually achieved by using hash functions to turn floating-point vectors into binary strings. Such implementation especially on SIFT and GIST [15] can be easily found in the literatures of improving existing features [14, 19].

Though different approaches of dimensionality reduction are added, the construction of original full descriptor is still indispensable. In other words, the substantial amount of time-consuming computation has not be reduced yet. With the development of mobile devices, algorithms with low computation complexity are in great demand. Binary Robust Independent Elementary Features (BRIEF) proposed by Calonder et al. [4] constructs the descriptor by directly comparing pairwise pixel intensities to produce a binary string for an image patch. Other outstanding features based on bit test include Oriented steered BRIEF (ORB) [16], Binary Robust Invariant Scalable Keypoints (BRISK) [10], Fast Retina Keypoint (FREAK) [1], etc.

Different from BRIEF-like descriptors, Locally Uniform Comparison Image Descriptor (LUCID) [22] attempts to describe an image patch from the view of order permutation of pixel intensities. The employment of permutation brings in a better resistance to monotonic brightness changes, meanwhile the linear-time construction and integer representation of LUCID descriptor lead to a good time efficiency. Local Image Permutation Interval Descriptor (LIPID) [18] improved the robustness of LUCID by means of zone division. These descriptors create fast and short patch representation in a different way from bit test.

As we know, many descriptors are constructed based on gradient, histogram, bit comparison and filtering. Quantization is also utilized as a postprocessing step to shorten a descriptor as we have mentioned above. But to our knowledge, no one makes a direct use of it in descriptor building. In this paper, we show that a local image patch can be described by virtue of patch quantization, which produces a descriptor that is very fast both to build and to match. We study two simple ways to implement the patch vector quantization and compare the respective performance. The experimental results show that the proposed method is sufficient to obtain good matching results, as long as invariance to large in-plane rotations is not a requirement. Moreover, the quantization-based method employs integer descriptors which avoid floating point computation, so it is promising to be time efficient. In the rest of this paper, Sect. 2 will describe the overall methodology, experimental results and discussions are provided in Sect. 3, and conclusions are drawn in Sect. 4.

2 Methods

2.1 Image Patch Quantization

Quantization methods have been thoroughly studied in the field of signal processing, including the coding and compression of different signals. Image quantization represents the image with finite gray levels, whose idea is exactly the same as we desire for image descriptors – represent the most primary information with less data. Inspired by this, we attempt to use vector quantization on image patches for descriptor construction. Quantizing an image patch refers to the quantization of the gray scales. A scalar quantization can be understood as a mapping of an input into a finite number of output. A straight forward way is the uniform quantization, which divides the gray scales equally. It is the simplest and fastest way of implementation, and the intensity mapping function for pixels within a patch is as following:

$$f(p) = \left\lfloor \frac{(p(x, y) - minv) N_q}{maxv - minv + 1} \right\rfloor \quad (1)$$

where

$$minv = \min_{(x, y) \in P} p(x, y), \quad maxv = \max_{(x, y) \in P} p(x, y) \quad (2)$$

and $p(x, y)$ is the pixel intensity in a patch P , N_q is the number of quantization levels, and $\lfloor \cdot \rfloor$ refers to rounding down.

Though the above method is a fast and reasonable solution, it may be too simple and crude for not taking intensity distribution into account. Another way to quantize the patch lays emphasis on equal pixel quantities. This non-uniform quantization divides the gray scales into disjoint intervals of equal probability by virtue of the Cumulative distribution function (CDF) [3]. The original histogram of an image patch counts the number of pixels whose intensities fall into each gray level, which can be depicted as:

$$N(i) = N(p(x, y) = i) \quad (3)$$

and the CDF of it is calculated as:

$$CDF(i) = \sum_{j=minv}^i N(j) \quad (4)$$

where $minv$ is defined in Eq. (2). CDF counts the number of pixels whose intensities are below each gray level, which provides us an expression for quantity partition. For a CDF function, it is obvious that $CDF(maxv) = N_{patch}$ (pixel number of the whole patch), and $CDF(minv) = N(minv)$ (number of pixels with the smallest intensity). So the intensity mapping function can be written in two forms:

$$f(p) = \left[\frac{(CDF(i) - CDF(minv)) N_q}{CDF(maxv) - CDF(minv) + 1} \right] \quad (5)$$

$$= \left[\frac{(CDF(i) - N(minv)) N_q}{N_{patch} - N(minv) + 1} \right] \quad (6)$$

Figure 1 illustrates how these two quantization methods work by plotting histograms of an image patch and lines which indicate the dividing gray levels. Figure 1a shows that the first method sets uniform threshold levels within the range of gray levels. Figure 1b and c describe the process of the second approach. Figure 1b plots the CDF we use to get threshold levels which ensures an equivalent number of pixels in each interval. The green horizontal lines in Fig. 1b indicate the uniform partition on pixel quantities, and intersection points of these lines and CDF function show the locations of thresholds (red lines). Figure 1c shows these non-uniform thresholds which are obtained in Fig. 1b on gray scales. Sum of pixels within each interval is approximately the same.

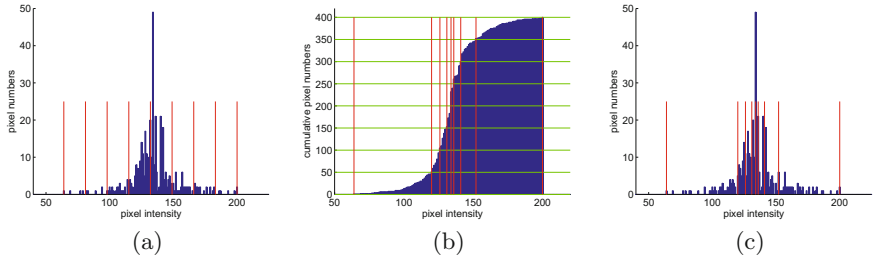


Fig. 1. Illustration of quantization approaches on image histograms. (a) Quantization based on equal division on gray levels. (b) Cumulative distribution function and equal division on pixel numbers. (c) Quantization based on equal pixel quantities. (Color figure online)

2.2 Descriptor Construction

Once the intensity mapping function is given, we can obtain a matrix by mapping all pixels into new values within the patch. Then by vectorizing it, we get the feature vector as the patch descriptor. Our descriptors take the form of integers, within the range of 0 to N_q , where N_q equals the number of quantization levels. A diagram shown as Fig. 2 depicts the descriptor construction process.

The main parameters our descriptors may concern should be the quantization levels and patch size. Too few levels will result in a loss of feature distinctiveness, but an excess of levels will also overlook the intention of feature extraction. As for the size of an image patch, a proper size is also demanded. Oversize patches will no longer contribute to description effectiveness but cause a waste on computation power. Usually, parameters are always trade-offs between precision and recall, accuracy and efficiency. We provide some experiments on parameter

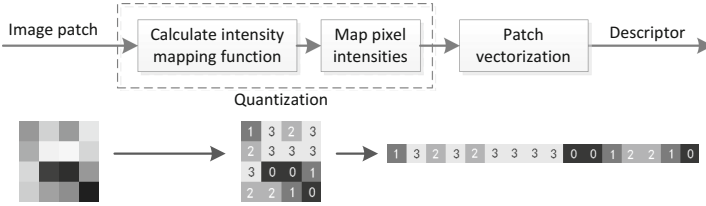


Fig. 2. The process of descriptor construction.

selection in Sect. 3.2, from which, some empirical parameters can be concluded for practical uses.

We discover the descriptor quantized via CDF is actually a order-permutation-based method, which should be invariant to monotonic illumination changes [17]. As we know in combinatorics, permutation is a bijective mapping of a finite set onto itself. It can be understood as a sequence involving every element in the finite set which appears only once. We use $X = (x_1, x_2, \dots, x_n)$ to denote the vector of an image patch, and vectorization is arbitrary (e.g. row-major) but fixed for all patches. Let $Z = (0, \dots, 0, 1, \dots, 1, \dots, N_q - 1, \dots, N_q - 1)$ be a vector associated with X , where Z contains all the quantized values of each element (pixel intensity) in X . Z is a fixed vector and we define a bijective mapping or action π to denote the corresponding relationship between X and Z via the mapping function in Eq. (6). From the CDF-based quantization process, we know that this action basically concerns the orders of the elements rather than the values. Hence, the descriptor D is a permutation on Z , where π^{-1} is applied on Z . As we imagine, the descriptor based on patch quantization via CDF is promising to be robust to monotonic changes.

3 Experiments

In this section, we compare our method with several competing descriptors, and a real-world dataset that is publicly available is employed in the experiments. Parameters of the quantization-based descriptors are discussed, and performance evaluation including recognition rates and computation time is studied.

3.1 Experiment Setup

Our methods are tested on the widely-used datasets introduced by Mikolajczyk and Schmid [13], as shown in Fig. 3. The dataset contains several image sequences, each sequence includes six images of a same scene, with varying degrees of a same image transformation. They are designed to test robustness to typical image disturbances that often occurs in real-world scenarios. For all sequences, we consider five image pairs by matching the first image to the remaining five ones. Our quantization-based methods are marked as Q1 (uniform quantization) and Q2 (using CDF). All the experiments are implemented by OpenCV 2.4.4 on a PC with

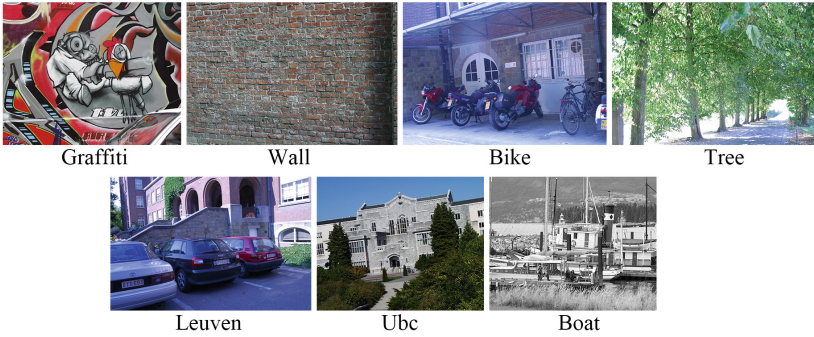


Fig. 3. Oxford dataset introduced by Mikolajczyk and Schmid.

2.93 GHz i7 CPU and Windows 7 Professional 64-bit OS, since OpenCV provides a convenient implementation of most state-of-the-art features.

Although our descriptor can be computed on arbitrary kinds of keypoint detector, we first carry out the comparison on SURF points. And in the situation that considers scaling and rotation correction, we would rather employ the AGAST [12] detector that BRISK feature uses for its fast speed. After keypoints are extracted from each images, 1000 points are selected from them based on their rankings of Harris corner measure [7]. We evaluate the performance of descriptors using the recognition rate as BRIEF does. As for the strategy to determine what is a correct match, we choose the Nearest Neighbor Distance Ratio (NNDR) [13]. This strategy is more strict than the Nearest Neighbor one, and produce less but more accurate correspondences. The distance ratio is set as 0.9 in all the experiments.

3.2 Parameter Selection

We first test the impact of parameters in our methods in order to find a group of well-performed parameters. Figure 4 plots the variations of patch size and number of quantization levels when the other parameter is fixed. As the patch size increases, recognition rate of image pair matching is improving explicitly. The curves increase as an exponential function and approach the upper limit when the patch size is above 16. Hereafter, larger patch size will not contribute to an obvious improvement on performance but bring in more computation requirement. Results of Quantization levels have the similar findings as the former parameter. Recognition rate increases rapidly when the quantization level grows under 8, but starts to level off with slight fluctuations after that. To sum up, we consider a patch of 16×16 which is quantized to 8 levels is a good choice of empirical parameters. Therefore, we use this group of parameters in the latter tests against other descriptors.

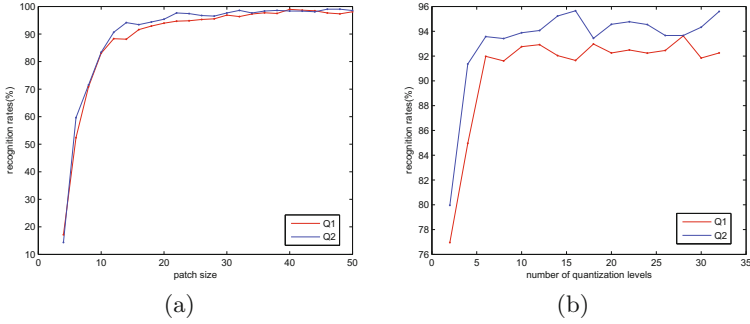


Fig. 4. Impact of parameter variations in quantization-based descriptors. (a) Recognition rate changes as patch size alters, number of quantization level is fixed to 8. (b) Recognition rate changes as number of quantization level alters, a 16×16 patch size is selected. Experiments are carried out on image pair Wall 1 and 2.

3.3 Performance Evaluation

Because our original descriptor does not correct for scale and orientation, we first carry out a performance evaluation of several comparable but competing description approaches. Chief among them are SURF and BRIEF descriptors provided by OpenCV. The single-scale and orientation-ignored (U stands for upright) SURF (SU-SURF) is also employed for a fair comparison. Moreover, we supplement LIPID rather than LUCID as a representative of permutation-based description methods since LIPID is more robust than LUCID. Note that all methods involved in this comparison except SURF are scale and orientation ignored, while SURF is included as a reference of rotation and scale invariant feature. In addition, the SURF keypoints are detected for all descriptors as we have explained above, and Boat sequence for zoom and rotation test is also ignored here. Results of recognition rates are given by Fig. 5.

Our methods outperform most of the others on Wall, Leuven and Ubc images. For the two sequences of image blur, our algorithms work very well on minor distortions but degrade faster than BRIEF and SURF. SURF features which are based on gradient truly suffer a lot from image blurring. As for the Graffiti sequence, most involved descriptors cannot undergo such an extreme affine warping. Q1 and Q2 show obvious advantages on texture scene images and compression artifacts. Q2 performs much better than Q1 on monotonic illumination changes probably because Q2 descriptor inherits inherent robustness from order permutation, and LIPID shows a talent on Leuven sequence because it is also permutation-based. Overall, our quantization-based descriptors perform well on many different deformations, and Q2 based on non-uniform quantization shows a better recognition accuracy than Q1.

With consideration of correcting orientation and scale for the descriptors, we further compare several state-of-the-art invariant features in the following experiment. SIFT and SURF are benchmarks of the scale and rotation invariant features, while BRISK is a remarkable binary feature that handles the invariance

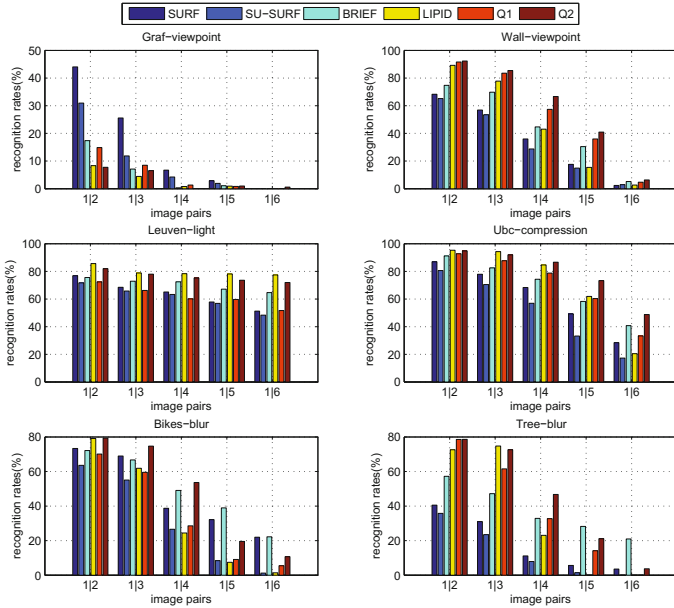


Fig. 5. Recognition rates of different description methods

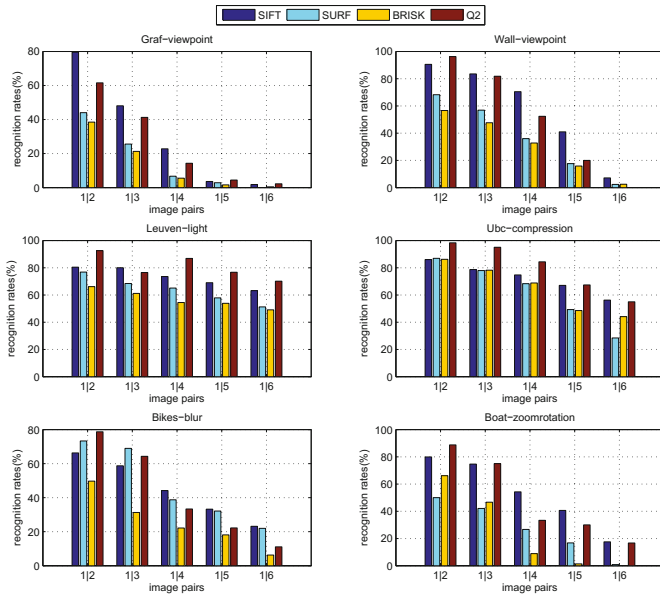


Fig. 6. Recognition rates of orientation and scale corrected methods

problem well. On account of the overall better performance of CDF-based descriptor in the previous experiment, only Q2 is tested during this part. All the features participated in use their own keypoint detectors, and Q2 employs the multi-scale AGAST detector that BRISK uses [10] for its best speed. Results of these four features are shown in Fig. 6. From the rates, it is concluded that the quantization-based descriptor outperforms SURF and BRISK in most cases. SIFT feature shows better results than Q2 in viewpoint change sequence, but poorer ones than the latter under light changes and compression artifacts. For the severe blurring pairs, multi-scale AGAST detector has a poor repeatability, therefore Q2 performs well on slight image blur pairs and degrades rapidly ever after. As for scale and rotation changes, AGAST detector is inferior to SIFT detector on orientation consistency, so the quantization-based feature shows a tendency that it outperforms SIFT under small deformation while yields poorer results than SIFT as the deformation increases.

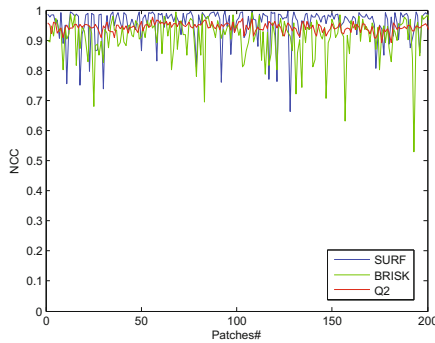


Fig. 7. NCC values for patches from Wall image

We further evaluate the noise resistance of our descriptor. We add Gaussian noise of zero mean and 0.01 variance into Wall 1 image, and extract feature vectors from the original image and the additive noise image respectively. Approximate 200 keypoints are detected in the original image and descriptors of these 200 patches are computed. SURF, BRISK and our method are involved for evaluation, and Normalized Cross Correlation (NCC) is used to measure the similarity of the two feature vectors before and after adding noise. As shown in Fig. 7, the NCC value of our method is higher than BRISK but lower than SURF, which shows that SURF is the most sensitive to image noises. As BRISK employs Gaussian smooth before the descriptor building (pixel sampling and bit comparison), it is more robust to Gaussian noise in our evaluation. The real matching experiment shown in Fig. 8 further illustrates the noise resistance of the involved features. The wall images added with different degree of noises are matched to itself, and the recognition rates are computed and plotted as the variance of Gaussian noise varies. As the noise increases, BRISK shows the best resistance, and performance of SURF has the most severe degradation. Our method retains

good performance under slight noise and begins to degrade gradually when noise keeps increasing.

Finally we provide the time efficiency estimation of the proposed method. Time complexity and CPU running time are included as the evaluation of time analysis. The uniform quantization can be computed in linear time with no doubt, and no extra space is need either. And the CDF-based quantization requires an auxiliary array to store the CDF function, which is also $O(n)$ in time complexity. Merely, it operates two linear-time computations, one for the CDF and the other for the mapping, hence it should be more time-consuming than the uniform one. Table 1 lists the description and matching time of different descriptors on image pair Wall 1-2. For each image, top 1000 points are selected according to Harris measure from SURF keypoints, and time shown in the table is the average computation time per point. For a fair assessment, only description time is compared here and all the descriptors except SURF do not take scale and rotation into account in the description process. It is seen from the table that the Q1 quantization method shows a definite superiority on description time consumption. Though Q2 requires more time than the former, it shares a similar rank with BRIEF. In general, our methods perform competitively well as state-of-the-art features and require very little computation time.

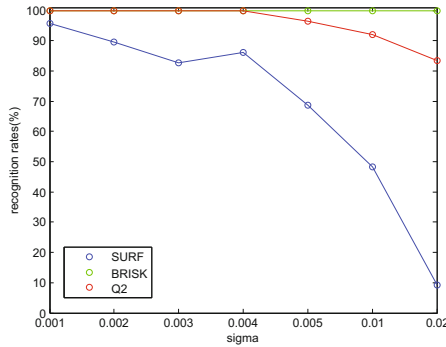


Fig. 8. Recognition performance under different degrees of Gaussian noises.

Table 1. Comparison of computational timings.

	SURF	SU-SURF	BRIEF	LIPID	Q1	Q2
Description time (ms)	1.99	1.43	0.30	1.04	0.12	0.31
Matching norm	L2	L2	Hamming	L1	L1	L1
Matching time (ms)	0.13	0.37	0.35	0.28	0.12	0.11

4 Conclusion

In this paper, we present a simple quantization-based description method for local image patch. More detailed, we propose two different ways to carry out quantization based on uniform thresholds on either gray scales or pixel quantities. Generally, descriptors using both quantization methods have very good time efficiency, and perform well on texture scene, illumination changes, compression distortions and image blurring. Specifically, the CDF-based descriptor requires more computation time yet yields better results. We think it is a feasible attempt to introduce quantization into fast descriptor building besides bit sampling and comparison of BRIEF-like descriptors and intensity permutation of LUCID-like descriptors. The quantization-based methods have similar advantages as permutation-based descriptors and consume as little computation power as binary ones. Our method can be applied as an alternative of SURF-like and BRIEF-like descriptor under the circumstance of real-time requirement, limited computation power and minor image deformation. Future work may aim at developing the robustness to undergo greater deformation and warping, and binarized construction methods utilizing quantization is worthy to be discovered for better storage efficiency.

Acknowledgement. This work is supported by the National Natural Science Foundation of China under Grant 61672474 and 41701417, the Fundamental Research Funds for the Central Universities - China University of Geosciences (Wuhan), the Provincial Natural Science Foundation of Hubei Province of China under Grant 2016CFB278 and 2015CFB400, the China Postdoctoral Science Foundation under Grant 2016M602390, and the Open Research Project of Hubei Key Laboratory of Intelligent Geo-Information Processing (KLIGIP1608).

References

1. Alahi, A., Ortiz, R., Vandergheynst, P.: FREAK: fast retina keypoint. In: 2012 IEEE Conference on Computer Vision and Pattern Recognition (CVPR), pp. 510–517. IEEE (2012)
2. Bay, H., Tuytelaars, T., Van Gool, L.: SURF: speeded up robust features. In: Leonardis, A., Bischof, H., Pinz, A. (eds.) ECCV 2006, Part I. LNCS, vol. 3951, pp. 404–417. Springer, Heidelberg (2006). https://doi.org/10.1007/11744023_32
3. Bjornson, E., Ottersten, B.: Post-user-selection quantization and estimation of correlated frobenius and spectral channel norms. In: IEEE 19th International Symposium on Personal, Indoor and Mobile Radio Communications (PIMRC 2008), pp. 1–6. IEEE (2008)
4. Calonder, M., Lepetit, V., Strecha, C., Fua, P.: BRIEF: binary robust independent elementary features. In: Daniilidis, K., Maragos, P., Paragios, N. (eds.) ECCV 2010, Part IV. LNCS, vol. 6314, pp. 778–792. Springer, Heidelberg (2010). https://doi.org/10.1007/978-3-642-15561-1_56
5. Chandrasekhar, V., Takacs, G., Chen, D.M., Tsai, S.S., Reznik, Y., Grzeszczuk, R., Girod, B.: Compressed histogram of gradients: a low-bitrate descriptor. *Int. J. Comput. Vis.* **96**(3), 384–399 (2012)

6. Gionis, A., Indyk, P., Motwani, R., et al.: Similarity search in high dimensions via hashing. In: VLDB, vol. 99, pp. 518–529 (1999)
7. Harris, C., Stephens, M.: A combined corner and edge detector. In: Alvey Vision Conference, Manchester, UK, vol. 15, p. 50 (1988)
8. Hua, G., Brown, M., Winder, S.: Discriminant embedding for local image descriptors. In: IEEE 11th International Conference on Computer Vision (ICCV 2007), pp. 1–8. IEEE (2007)
9. Huang, Z., Kang, W., Wu, Q., Chen, X.: A new descriptor resistant to affine transformation and monotonic intensity change. *Comput. Vis. Image Underst.* **120**, 117–125 (2014)
10. Leutenegger, S., Chli, M., Siegwart, R.Y.: BRISK: binary robust invariant scalable keypoints. In: 2011 IEEE International Conference on Computer Vision (ICCV), pp. 2548–2555. IEEE (2011)
11. Lowe, D.G.: Object recognition from local scale-invariant features. In: The proceedings of the seventh IEEE International Conference on Computer Vision, vol. 2, pp. 1150–1157. IEEE (1999)
12. Mair, E., Hager, G.D., Burschka, D., Suppa, M., Hirzinger, G.: Adaptive and generic corner detection based on the accelerated segment test. In: Daniilidis, K., Maragos, P., Paragios, N. (eds.) ECCV 2010, Part II. LNCS, vol. 6312, pp. 183–196. Springer, Heidelberg (2010). https://doi.org/10.1007/978-3-642-15552-9_14
13. Mikolajczyk, K., Schmid, C.: A performance evaluation of local descriptors. *IEEE Trans. Pattern Anal. Mach. Intell.* **27**(10), 1615–1630 (2005)
14. Ni, Z.S.: B-SIFT: a binary sift based local image feature descriptor. In: 2012 Fourth International Conference on Digital Home, pp. 117–121. IEEE (2012)
15. Oliva, A., Torralba, A.: Modeling the shape of the scene: a holistic representation of the spatial envelope. *Int. J. Comput. Vis.* **42**(3), 145–175 (2001)
16. Rublee, E., Rabaud, V., Konolige, K., Bradski, G.: ORB: an efficient alternative to SIFT or SURF. In: 2011 IEEE International Conference on Computer Vision (ICCV), pp. 2564–2571. IEEE (2011)
17. Singh, M., Parameswaran, V., Ramesh, V.: Order consistent change detection via fast statistical significance testing. In: IEEE Conference on Computer Vision and Pattern Recognition (CVPR 2008), pp. 1–8. IEEE (2008)
18. Tian, T., Sethi, I., Ming, D., Zhang, Y., Ma, J.: LIPID: local image permutation interval descriptor. In: 2013 12th International Conference on Machine Learning and Applications (ICMLA), vol. 2, pp. 513–518. IEEE (2013)
19. Torralba, A., Fergus, R., Weiss, Y.: Small codes and large image databases for recognition. In: IEEE Conference on Computer Vision and Pattern Recognition (CVPR 2008), pp. 1–8. IEEE (2008)
20. Tuytelaars, T., Schmid, C.: Vector quantizing feature space with a regular lattice. In: IEEE 11th International Conference on Computer Vision (ICCV 2007), pp. 1–8. IEEE (2007)
21. Wang, C., Duan, L.Y., Wang, Y., Gao, W.: PQ-WGLOH: a bit-rate scalable local feature descriptor. In: 2012 IEEE International Conference on Acoustics, Speech and Signal Processing (ICASSP), pp. 941–944. IEEE (2012)
22. Ziegler, A., Christiansen, E., Kriegman, D., Belongie, S.J.: Locally uniform comparison image descriptor. In: *Advances in Neural Information Processing Systems*, pp. 1–9 (2012)

A Method of Large - Scale Log Pattern Mining

Lu Li^{1(✉)}, Yi Man¹, and Mo Chen²

- ¹ School of Electronic Engineering, Beijing University of Posts and Telecommunications, Beijing 100876, China
SallyLi0863@163.com
- ² Institute of Network Technology, Beijing University of Posts and Telecommunications, Beijing 100876, China

Abstract. With the development of the telecommunication network, more and more devices are used in the network, which has been a burden for the network operation and maintenance. At the same time, network devices generate large amounts of log data every day, recording the activities of each device in detail. As a result, the log can reflect the performance of network state, and sometimes, we can predict the occurrence of network failure based on the log. However, since the log has such features: big volume, multi-source heterogeneous and difficult to understand, people have not reasonably used it to analyze and predict network failure. Therefore, we propose a method for structuring a large number of device logs in the short term, and use the data generated from a real communication device network to verify the effect. Besides, we compare our method with the traditional log parsers, such as regular expressions, LogSig, etc. to demonstrate the efficient processing performance and accurate pattern extraction analysis for massive network device logs.

Keywords: Big data · Log parser · Telecommunication network equipment
Word2vec

1 Introduction

With the rapid development of telecommunications technology, the telecommunications network is more complex and the network business is more diverse. At the same time, the mining for a large amount data generated by network has also attracted the attention of many people. Network devices log contains a lot of information, which can represent the operating state and healthy degree of network. However, because of the volume and characteristic of the log data, the researchers have not achieved remarkable results. For example, all the equipment in an operator can produce about 2 TB log data in a province in one day, and these log are written by seven different vendors with different formats (Fig. 1).

Obviously, without the instructions and the guidance of the professionals, raw log message produced by telecommunication network equipment, as shown in the following example, is difficult for the operator to understand the exact meaning of these logs, not to mention using it to carry out further work.

```

Jul 26 18:12:42: {6/LP}: %ASESDK-5-NOTICE: 35208 3 NOTICE
sgwcd_SEOS_ssc:libsscdoperations.UpdateBearerOperation: , MmeTeid=1073584140, LCOR=0,
Cause=10 (2)
Jul 26 17:34:41: {8/LP}: %ASESDK-4-WARNING: gtpcd[7909]:gc-0/8/1:8242 <DAPP>:
<11>: !!!WARN: Gx_WarnUnknownAvpReceived: GX: Received and ignored unknown AVP, Route-
Record (code 282, vendor 0). (cmdCode=RAR(258), appld=PCC(16777238),
hopByHopId=212199767, e ...

```

Fig. 1. Typical raw telecommunication device log data

At present, there are several methods to deal with log, and methods based on the pattern are widely used in log analysis. In this method, one raw log message can be divided into two parts: the constant part and the variable part. For telecommunication network equipment log, the variable part contains a lot of valid information, such as the location of the module that issued the log, the actions performed by the operator, and the time of the log. However, when the volume of log increases to a certain extent, due to the huge variable data, despite using this method, the results will take up a lot of storage space.

Therefore, we investigated the various log preprocess methods and for the characteristics of the network device logs, we have taken certain ways based on the natural language model, making complex log becomes more suitable for storing and mining. In order to validate our method, we used it and several other typical log parser to compare the result in the test set of different kinds of logs and the real network device data set, which proves the accuracy and efficiency of our method.

2 Log Parser

2.1 Parser Methods

There are three kinds of methods that are mainly used for log data parser.

2.1.1 Methods Based on Regular Expression

In the traditional log processing methods, regular expression is often used to extract a specific field. Many programming languages support the use of regular expressions for string manipulation. It can develop the structured data to process the log, so that a large number of non-structural or semi-structured information is discarded. And this kind of method is not flexible enough, basically for some specific log need to be processed.

2.1.2 Methods Based on Pattern

The log data is automatically generated by the program in the device, which is often composed by constant strings and variable parameters, so the log data has obvious semi-structured features. By generating and comparing the existing set of patterns, the words in the log are divided into log template words and variable words, so that we can find the abnormal parameters in the data set (Fig. 2).

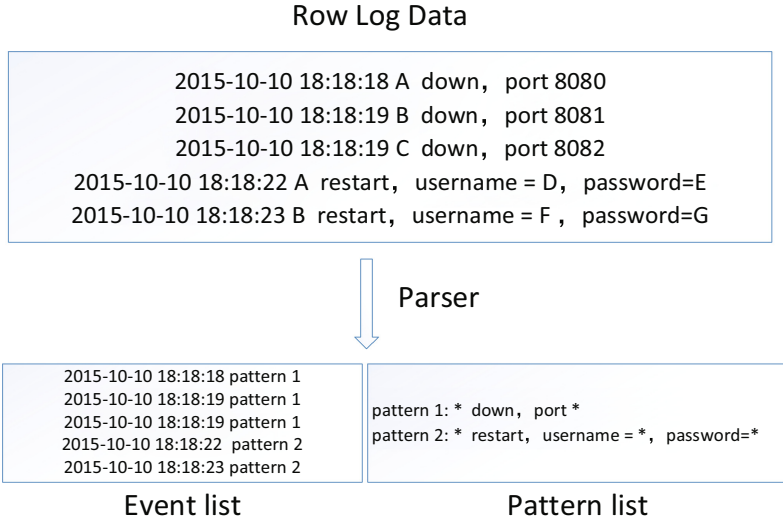


Fig. 2. The object of methods based on pattern

For example, in [5], the author proposes a STE method to judge whether it is a log template word or a variable word based on the location and length of the word in the log text, which can determine the log pattern.

This is the usual method for log analysis, and its speed is faster and performance is better, but because the device log parameters varies and the data format is very irregular, leading to the poor quality and large redundancy for the pattern set, which has a great impact on the effect of the data mining work.

2.1.3 Methods Based on Data Mining

At present, many studies apply the data mining algorithm to the log process, for example, [6] applied the k-center clustering algorithm to analyze the ITS system log data to analyze the internal structure of the ITS system. In [7], by using the clustering algorithm, a log pattern recognition algorithm based on distributed platform is designed to improve the speed and efficiency of log recognition.

However, at present there is not suitable data mining method for telecommunication network device log analysis.

2.2 Three Typical Parsers

In order to verify the performance of our parser, we chose three typical parsers to compare with ours. And these parser’s source code can be find in the [1].

2.2.1 LKE

This method is proposed to parse free-form text log for anomaly detection in distributed systems, and it is made up by the following steps: (1) remove the parameters according

to the established rules (2) measure raw log similarity by the weighted edit distance (3) cluster similar raw log keys together (4) Log template generation [2].

2.2.2 IPLoM

This method is proposed for automatic event log analysis, which includes three step hierarchical partitioning process: (1) Partition by log length. The first step is to use the token count heuristic to partition the log messages, because the log messages that have the same line format are likely to have the same token length (2) Partition by token position. By counting the words in the same position, the method will sort the log by the count. (3) Partition by search for mapping. By searching for mapping relationships between the set of unique tokens in two token positions, the log is divided into smaller partition. (4) Log template generation [3].

2.2.3 LogSig

To understand and optimize system behaviors, LogSig is proposed to generate system events from textual log messages. LogSig works in three steps: (1) Word pair generation. Raw log data are converted to a set of word pairs to record both the word and its position. (2) Log Clustering. Based on the word pairs, a potential value is calculated for each log message to decide which cluster the log message potentially belongs to. (3) Log template generation. In each cluster, the log messages are leveraged to generate a log template [1, 4].

2.3 Our Parser

Telecommunication device log data often have the following characteristics: (1) Complex parameters. Most of the parameters are numbers. (2) Short text. Most of logs are short sentences or parameters list, and the sentence are irregular. The longest sentence is no more than 30 words. (3) Difficult to understand. Without professional instruction book, it is difficult to identify the meaning of the log.

According to the characteristics of the raw data, our analytical method has three steps. First, remove all the punctuations, numbers and the words containing numbers. Second, compute the Hash value of the processed text, to obtain unique Hash value of each log text. Third, by comparing the hash values, the log is merged into the same log pattern, and we can obtain the log pattern table and the simplified log event sequence. Fourth, use the edit distance to merge the log patterns again and rewrite the log event sequence.

2.4 Parser Practice

2.4.1 In the Five Kinds of Log Data Set

We use five different log data, which come from different log systems (BGL, HPC, HDFS, Zookeeper and Proxifier), each kind log data contains two thousand lines [1], and we used our parser and three other parsers to compare the result. In the experiment, we used the same environment and code language to come to the following results.

From the results we can see that for the small data set of log data, IPLoM algorithm show a great advantage in speed, our algorithm is running faster than the other two parsers. In terms of accuracy, our parser has an advantage in the analysis of certain logs (Figs. 3 and 4).

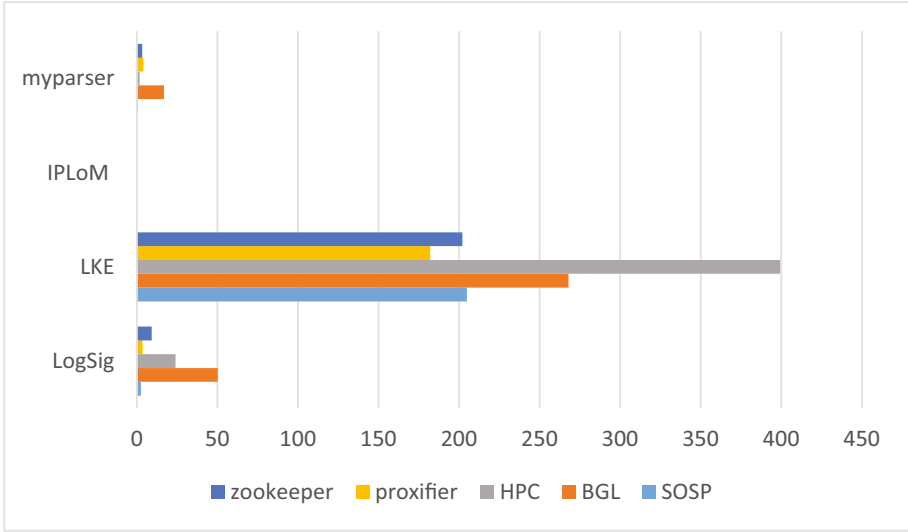


Fig. 3. The running time of four parsers

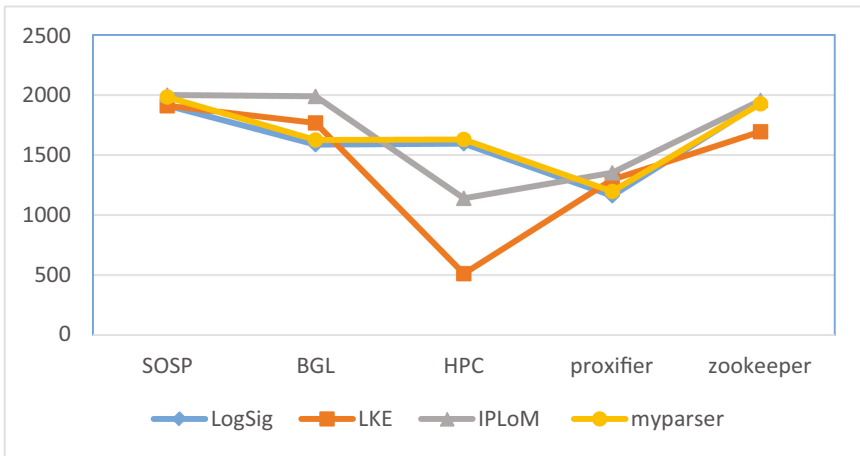


Fig. 4. The accuracy of four parsers

2.4.2 In the Large-Scale Log Data Set

We still experimented with actual data set on, because the actual data set is very large, we use thousandth log in one day, 750 M data, containing more than 7 million log data (Table 1).

Table 1. The running time of four parsers on big data set

Parser name	Time(s)
LogSig	38581
LKE	–
IPLoM	376
My parser	7673

We listed the running time of each parser, where LKE was unable to perform log parsing due to memory overflow, and we could see that IPLoM still had a great advantage in speed, but when there was no standard regular expressions, its results contain a lot of redundancy. Our parser will give less redundant and more accurate results within a tolerable time range.

2.4.3 Summary

Comparing our performance with the other three classic parsers, we found that although our parser was not as fast as IPLoM, it showed good adaptability and speed when dealing with a large number of telecommunications device logs data. After that, we have carried out further data mining to understand the data and find the information in the log data.

3 Log Analysis

3.1 Background

3.1.1 Word Vector

To apply the machine learning method to the natural language processing field, the most basic problem is the representation of the language symbol. So far, the most commonly used method for natural language processing is One-hot Representation, which means that n words are n-dimensional vectors, each vector is 1 in a dimension and the other dimension is zero. However, this method will cause the lexical gap problem, there is no connection between words and words.

Therefore, the Distributed Representation method is proposed, that is, using low-dimensional real vector to represent vocabulary. The biggest advantage of Distributed Representation is that it can make meaning-related words relatively similar in distance. At the same time, the word vector will show many special properties, as shown below (Fig. 5).

$$V(\text{King}) - V(\text{Queen}) \approx V(\text{man}) - V(\text{woman})$$

Fig. 5. An application of word vector

3.1.2 Neural Network Language Model

Bengio Yoshua proposed a neural network algorithm using a three-layer neural network to build the model, the purpose of the model is to predict the next word w_t by former $n - 1$ words. At the bottom are the former $n - 1$ words ($w_{t-n+1} \sim w_{t-1}$), and $C(w)$ means the vector of the word w . The input layer of the network is to concatenate the $n-1$ vectors to a $(n - 1) * m$ dimensions vector, which is labeled x . The second layer of the network is obtained directly by using $d + Hx$, where d is the offset term, and the initialization value is random, using \tanh as the activation function (Fig. 6).

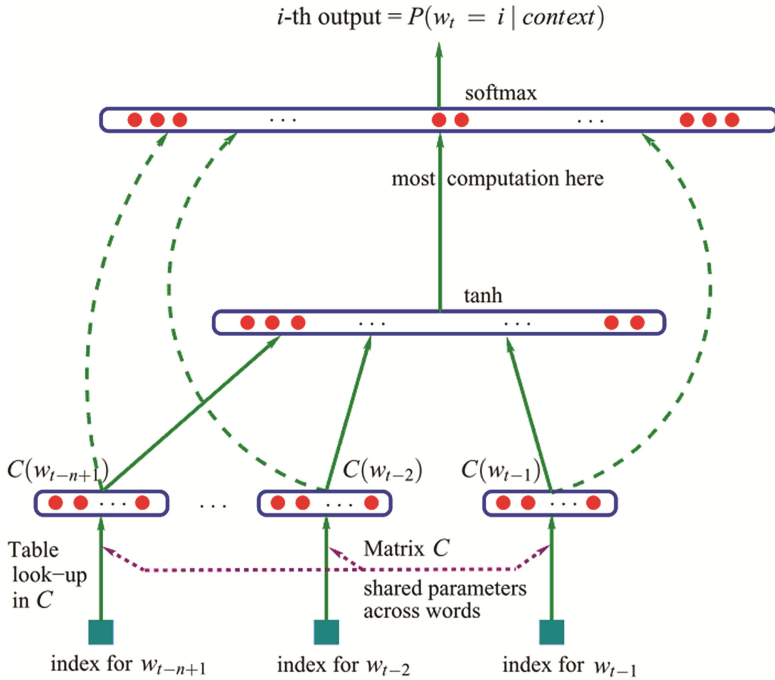


Fig. 6. Neural network structure proposed by Bengio Yoshua

The third layer of the network is represented by the node Y_i , using the softmax function to normalize the output value into probability, and the final Y is calculated as:

$$Y = b + Wx + U * \tanh(d + Hx)$$

U is the parameter from the hidden layer to the output layer, the majority of the model compute operation is centered on the matrix multiplication of the U and hidden layers. Finally, we use the stochastic gradient descent method to optimize the model, then we can get word vector [8].

3.1.3 Word2vec

Word2vec is a tool launched by Google to calculate words vector, which has been gained comprehensive attention because of its efficiency and convenience. It is based on the neural network and the natural language model. By the relationship between words and sentences, it can calculate a word vector for each word, and we can compare the word similarity by the distance between the word vectors. Based on the principle of word2vec, we have present a log mining method that can get literally similar logs or logs containing a log of important links.

3.2 Use Word2vec in the Log Process

3.2.1 The Method

We use our parser to parse certain carrier’s seven-day telecommunication device log data. (1) Firstly, we parse the log data into a log pattern set and a log event data table. (2) Then, we list one-day log pattern number in order of their time sequence, as the word2vec sentence, and we see each log pattern as word in word2vec. Through the word2vec tool we calculate the word vector for each pattern. (3) Finally, we derive a similar pattern set by comparing the Euclidean distance between the word vectors and comparing the similarity between patterns.

3.2.2 The Result

We optimized the parameters of word2vec for structure log data. When using the Skip-Gram model, the vector dimension is 50 dimensions and the window size is 5, we find that the word vector is more accurate when looking for similar data patterns. At the same time, we choose the vectors whose cosine similarity is greater than 0.9 as a similar pattern. Finally, we get a number of similar patterns, and these similar patterns is of great significance in the problem analysis (Table 2 and Fig. 7).

Table 2. The parameters of word2vec

CBOW	Size	Window	Negative	HS	Sample	Threads	Binary	Iter
0	50	5	0	1	1.00E-04	20	0	100

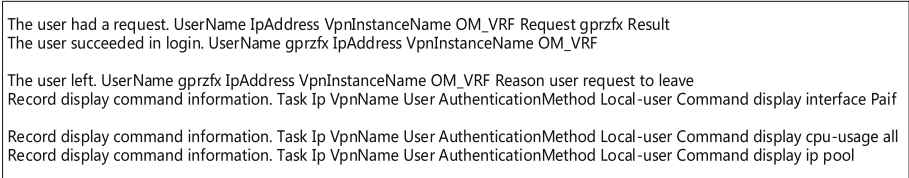


Fig. 7. The similar log pattern produced by word2vec

In the results, we can find that some similar log patterns produced by word2vec have literal similarity, which means that word2vec can help us to optimize the log parsing and find else log patterns need to be classified except which has the different digital parameters or whose edit distance is less than a certain value. At the same time, word2vec

can help us discover log patterns that are literally unrelated but have similar meanings or links, which is of great importance to subsequent log analysis.

4 Conclusion

Our algorithm uses the neural network language model for the first time to analyze the telecommunication equipment log, and obtains the similarity pattern. At the same time, we design the log analysis method to adapt to the log of the telecommunication equipment, and verify the effectiveness of the method by experiment.

Through the experiment and the comparison of the results, we can find that our parser obtains a better analytical effect for the telecommunications server log data in the tolerable time. Subsequent analysis, whether using word2vec for similar patterns discovery, or the use of other data mining methods to explore, such as abnormal point recognition and correlation analysis, can be based on our processing results for analysis.

However, our analytical methods are also deficient, for example, we can find patterns that have similar characteristics in the order of occurrence, but how these patterns are applied specifically to some telecommunications systems problem, such as system error prediction, auto log analysis system without expert, we also need to continue exploring and researching.

References

1. He, P., et al.: An evaluation study on log parsing and its use in log mining. In: IEEE/IFIP International Conference on Dependable Systems and Networks. IEEE Computer Society, pp. 654–661 (2016)
2. Fu, Q., Lou, J., Wang, Y., Li, J.: Execution anomaly detection in distributed systems through unstructured log analysis. In: Proceedings of International Conference on Data Mining, ICDM 2009 (2009)
3. Makanju, A., Zincir-Heywood, A., Milios, E.: Clustering event logs using iterative partitioning. In: Proceedings of International Conference on Knowledge Discovery and Data Mining, KDD 2009 (2009)
4. Tang, L., Li, T., Perng, C.: LogSig: generating system events from raw textual logs. In: Proceedings of ACM International Conference on Information and Knowledge Management, CIKM 2011, pp. 785–794 (2011)
5. Kimura, T., Ishibashi, K., Mori, T., Shiomoto, K.: Spatio-temporal factorization of log data for understanding network events. In: INFOCOM 2014 Proceedings. IEEE (2014)
6. Juneja, P., Kundra, D., Sureka, A.: Anvaya: an algorithm and case-study on improving the goodness of software process models generated by mining event-log data in issue tracking systems. *Support. Care Cancer* **6**(6), 539–541 (2015)
7. Hamooni, H., Debnath, B., Xu, J., et al.: LogMine: fast pattern recognition for log analytics. In: CIKM (2016)
8. Bengio, Y., et al.: A neural probabilistic language model. *J. Mach. Learn. Res.* **3**(6), 113 (2003)

More Efficient Filtration Method for Big Data Order-Preserving Matching

Wenchao Jiang^(✉), Dexi Lin, Sui Lin, Chuanjie Li, and Aobing Sun

School of Computer Science and Technology, Guangdong University of Technology,
Guangzhou 510006, China
jiangwenchao@gdut.edu.cn

Abstract. Data matching and retrieval aims at finding out similar substrings with the pattern P in the given data set T . This problem has wide applications in big data analysis. A liberalized verification rule is proposed first, and then a similarity computing based order preserving matching method is presented. Theory analysis indicates our method runs in linear. Furthermore, the experimental results show that our method can improve effectively the precision ratio and the recall ratio. More qualified matching results can be detected compared with the state of the art of this problem.

Keywords: Pattern recognition · Order-preserving matching · Similarity retrieval

1 Introduction

Fast and accurate data matching and retrieval is one of the key problems in big data applications such as video retrieval, stock analysis and prediction. Based on the context and application scenarios, the data objections can be abstracted into a series of vectors with different properties. Furthermore, the different properties can be integrated into a number through reduction or conversion. Consequently, data matching problem will be transformed into string or number matching problem which is one kind of well known problems in pattern recognition. Given a set of numbers T of length n and a pattern P of length m , both being numbers or strings over a finite alphabet Σ , the task of string matching is to find all the substrings u in T which have the same relative order as P , and $|u| = |P|$. For example, let $P = (10, 22, 15, 30, 20, 18, 27)$ and $T = (22, 85, 79, 24, 42, 27, 62, 40, 32, 47, 69, 55, 25)$, then the relative order of P matches the substring $u = (24, 42, 27, 62, 40, 32, 47)$ of T [1].

Several online [3–7] and one offline solution [2] have been proposed for the string matching problem. Kim et al. [3] and Kubica et al. [4] presented solutions based on the Knuth-Morris-Pratt algorithm (KMP) [8], the KMP algorithm is mutated such that it determines if the text contains substring with the same relative order as that of the pattern using the order-borders table. Kim et al. [3] utilized the prefix representation method to find the rank of each number in the prefix, and this method was further optimized using the nearest neighbor representation to overcome the overhead involved in computing

the rank function. Later, Cho et al. [5, 6] gave a sublinear solution based on the bad character heuristic of the Boyer-Moore algorithm [9]. Almost at the same time, Belazzougui et al. [7] derived an optimal sublinear solution. The state of the art for this problem is the filtration method [1] which is presented by Chhabra et al. All the verification rules in previous researching demanded the values and the positions of the numbers in both T and P must be coherent strictly. So, some actual matching results may be discarded. Moreover, almost all the earlier researching were focused on the time complexity analysis while ignored the precision ratio analysis and recall ratio analysis. They didn't research whether some actual matching results were missing despite the algorithm became more and more fast.

In view of the above problem, a similarity computing based string or number order preserving matching method is presented. Based on the preprocessing, i.e. binary transforming and filtration, our method proposes a novel verification rule which can guarantee more candidate results can be found out. Then, a similarity computing based sorting method is presented which can ensure all the matching results are listed according to the similarities with the pattern P. Theory analysis indicates our method is sublinear. The experimental results show that our method can improve effectively the precision ratio and the recall ratio compared with the newest method at present.

This paper is organized as follows. Section 2 presents our solution. Section 2.4 analyses our approach. The experimental results are given and discussed in Sect. 3. Section 4 concludes this paper.

2 Our Solution

2.1 Problem Description and Motivation

The state of the art for order-preserving matching is the filtration method [1] which was presented by Chhabra et al. We call the filtration method as MT.C in this paper. The MT.C transform the original data T and the pattern P into binary string T' and P' according to formulation (1). Then searching for the substring with the same relative order with P in T can be transformed into searching P' in the analogously T'. In the above example, P' = 101001 and T' = 100101001100. Each occurrence is a match candidate which is verified following the numerical order of the positions in the original pattern P.

$$t_i = \begin{cases} 1, & t_{i-1} < t_i \\ 0, & t_i \leq t_{i+1} \end{cases}, \quad t_i \in T; \quad p_i = \begin{cases} 1, & p_{i-1} < p_i \\ 0, & p_i \leq p_{i+1} \end{cases}, \quad p_i \in P \quad (1)$$

The MT.C method made the matching process simpler and more efficient than the earlier solutions. However, some deficiencies could be found because of the too harsh filtration and verification rules. The MT.C method required the order of the numbers is strictly coherent according to the values and the corresponding positions in P and T. For example, as shown in Fig. 1(a), the MT.C method can't find the differences between T and P if the max-number increases or the mini-number decreases immensely in T. Moreover, as shown in Fig. 1(b), the MT.C method can't find the differences either if

certain subsection data in T jumps suddenly while the variation trend maintains as a whole. Furthermore, to find out the matching substrings from the candidate strings which were produced through filtration algorithm, the numbers of P must be sorted, and the verification processing demands the positions and the size relations between T and P must be coherent strictly. This rule would result in the looseness of some actual matching substrings. As shown in Fig. 1(c), according to the MT.C method, the gray node x in T can only change between dashed line a and dashed line b which represent the right neighbor y and the left neighbor z respectively in the sorting of T. Once the gray node x changes above the dashed line a or down the dashed line b, the MT.C method will regard that T is not matching with P. Then the corresponding substring will be discarded consequently. Actually, we can find that this is not the case especially when $|y-z|$ is small enough. For example, when x changes to x' which is slightly larger than y or changes to x'' which is slightly smaller than z, the MT.C method will discard the substring. But we think the substring is still similar with P in most actual applications such as data retrieval.

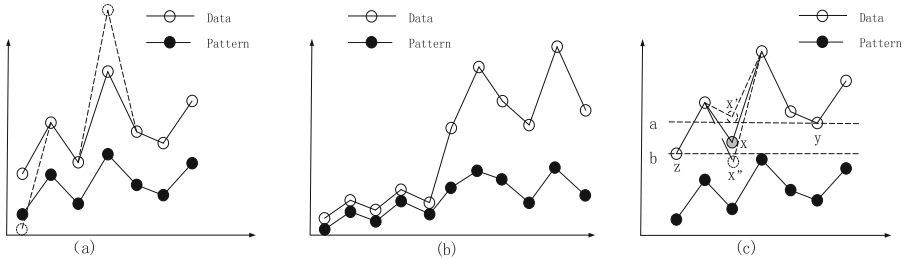


Fig. 1. Problem description

2.2 Our Solution

Problem definition of string or number matching in [1] is described as following: Two strings $u = u_1u_2\dots u_m$ and $v = v_1v_2\dots v_m$ of the same length over Σ are called order-isomorphic, written $u \approx v$, if formulation (2) holds.

$$u_i \leq u_j \Leftrightarrow v_i \leq v_j \text{ for } 1 \leq i, j \leq m. \tag{2}$$

This rule demands all numbers in u and v are strictly coherent with both the sizes and their positions. So, some actual matching results would be discarded as shown in Fig. 1(c). To overcome this deficiency, a different rule is presented as following. Two strings $u = u_1u_2\dots u_m$ and $v = v_1v_2\dots v_m$ of the same length over Σ . The numbers of $v = v_1v_2\dots v_m$ are sorted firstly and the result is a sequential table r as formulation (3).

$$r = \{v_{r_{|i|}} | v_{r_{|i|}} \leq v_{r_{|j|}}, 1 \leq i < j \leq m\} \tag{3}$$

$$\begin{aligned}
 |u_{r[i]} - u_{r[i-1]}| &\leq \frac{|u_{r[i+1]} - u_{r[i-1]}|}{2} \text{ or} \\
 |u_{r[i+1]} - u_{r[i]}| &\leq \frac{|u_{r[i+1]} - u_{r[i-1]}|}{2} \text{ for } v_{r[i-1]} \leq v_{r[i]} \leq v_{r[i+1]}, 1 \leq i \leq m.
 \end{aligned}
 \tag{4}$$

Two strings u and v are called order-isomorphic, written $u \approx v$, if formulation (4) holds. Apparently, multiple matching results would be found out according to formulation (4) once the pattern is given. But, the similar extent of the multiple matching results are different. To distinguish the similar level of multiple candidate results, a similarity computing method should be given based on the optimized verification method. Considering the possible concussion range of some numbers in T which have the same positions with relevant numbers in P . The similarity function f , as shown in Fig. 2, between the candidate substring u and the pattern P is defined as formulation (5).

$$f(u, P) = \sum |g(u_i) - g(p_i)|, \quad 1 \leq i \leq m.
 \tag{5}$$

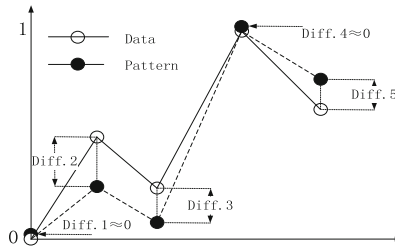


Fig. 2. Data reduction

Where, u_i and p_i are the relevant numbers which have the same position order in the candidate substring u and the pattern P . m is the length of u and P . g is the reduction function, shown in formulation (6), which can reduce all the numbers in u and p into the same zone $[0,1]$. $\text{Min}(u)$ and $\text{Min}(P)$ are separately the Min -values in u and P . $\text{Max}(u)$ and $\text{Max}(P)$ are separately the Max -values in u and P .

$$u_i - \text{Min}(u)/\text{Max}(u) - \text{Min}(u) \text{ or } p_i - \text{Min}(P)/\text{Max}(P) - \text{Min}(P)
 \tag{6}$$

As shown in Fig. 2, the similarity between the candidate substring u and the pattern P can be computed easily as the sum of all the differences, represented by $\text{Diff}.i$ ($1 \leq i \leq n$), between the relevant nodes of u and P according to formulation (5).

2.3 The Proposed Algorithm

As described above, our solution includes four steps: binary transformation, filtration, verification and similarity computing. The binary transformation can be processed according to [1], and the filtration can be conducted using any exact string matching algorithm. Supposing the binary transformation and filtration have been finished, the

pseudo-code of our solution based on the optimization and the similarity computing can be described as Algorithm 1 and Algorithm 2.

Algorithm 1: Computing the similarity

- 1) $X_t = \text{AnticipationBinary}(T_r)$;
 - 2) $X_p = \text{AnticipationBinary}(P)$;
 - 3) For $i=0$ to length;
 - 4) $\text{Sum} += \text{Abs}(X_t[i] - X_p[i])$;
 - 5) Return Sum.
-

Algorithm 2: AnticipationBinary is reduction function

- 1) input A;
 - 2) $\text{Max} = A.\text{Max}$;
 - 3) $\text{Min} = A.\text{Min}$;
 - 4) For $i=0$ to length
 - 5) If ($\text{Max} == \text{Min}$);
 - 6) $B[i] = 0$;
 - 7) else
 - 8) $B[i] = (A[i] - \text{Min}) / (\text{Max} - \text{Min})$;
 - 9) Return B.
-

2.4 Algorithm Analysis

Our solution, represented as MS, include four steps: Binary Transformation (BT), filtration, verification and Similarity Computing (SC). So, the time complexity of our solution $O(MS)$ can be represented as following.

$$O(M_S) = O(BT) + O(\text{filtration}) + O(\text{verification}) + O(SC)$$

Compared with [1], the main differences of our solution are the verification and similarity computing. Furthermore, the main modification in verification is a liberalized verification rule is implemented and more matching results can be detected. So, the time complexity of verification doesn't be changed and only the $O(SC)$ need be analyzed.

Supposing the numbers in P and T are integers and they are statistically independent of each other and the distribution of numbers is discrete uniform. Supposing $LT = n$, $LP = m$. In the worst case, the similarity computing process requires $O(m(n-m))$ similarity computing operations. In most cases, LT is usually very large while LP is usually a constant small enough. So, $O(m(n-m)) \approx O(nm)$ on average which is equal with $MT.C$ method. So, we can conclude $O(MS) = O(MT.C)$ which are all sublinear.

3 Experimental Results

Our experiments used linear string matching algorithm KMP [8] as the filtration method. The tests were run on single node of Tianhe-2 super computer with configuration CPU E5-2692 v2 12*2 2.20 GHz. All the algorithms were implemented in C# in the 64-bit mode.

3.1 Effectiveness

To explain the superiority of our method, two special data sets are generated based on one basic data set. The basic data set was given as $T = (10, 14, 12, 15, 13, 28, 36, 32, 24, 38, 26)$ and $P = (10, 14, 12, 15, 13, 19, 21, 20, 17, 22, 18)$. The first special data set shown in Fig. 3(a) was generated by multiplying n ($1 < n < 100$) to the last six numbers in T. The second special data set shown in Fig. 3(b) was generated by multiplying n ($1 < n < 100$) to only the 10th number in T.

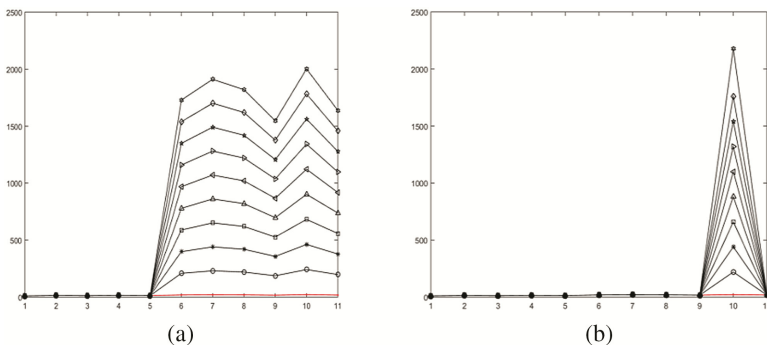


Fig. 3. Data set samples

From Fig. 3(a) and (b), we can find that the data T and the pattern P become more and more dissimilar with the increasing of n. But, the MT.C method couldn't find the differences among them. Through computing the similarities between T and P according to the technologies presented in Sect. 2, the variation trend of the similarity between T and P with the increasing of n was shown in Fig. 4. According to the definition of similarity shown as formulation (5), the more bigger the value of the similarity is, the more dissimilar the substring is compared with P. We can find that the similarity increases with the increasing of n and becomes converging with the infinite increasing of n. The point of inflection means that the data set T couldn't be considered similar with P according to our method. At the same time, we can find that the points of inflection are different with different data sets. So there is no stable point of inflection for different data sets in our method. The appearance of the point of inflection depend on the data set itself.

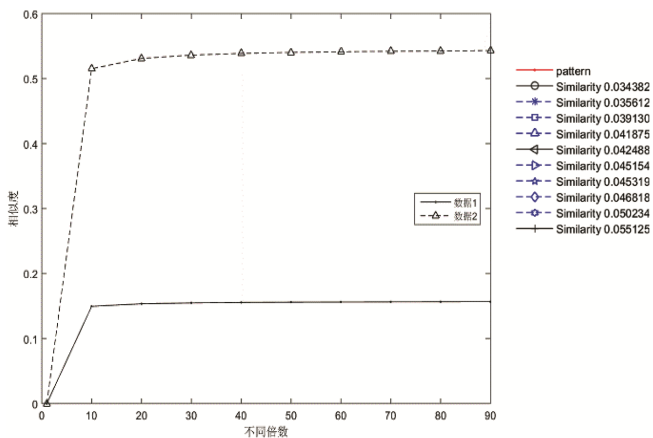


Fig. 4. Similarity convergence

Imitating the data generation method in [1], we generated two special data set and one random data set. The random data set contains 100000000 random integers between 0 and 230. The lengths of patterns (LP) were picked as 10, 15 and 30. The experimental results showed that our method can find more matching substrings than the MT.C method. For example, when the pattern length was picked as 10, the MT.C method can only find 15 results. However, our method can find 135 results which were sorted according to the similarities. The first 10 most similar results were shown in Figs. 5, 6 and 7 separately when the length of pattern were picked as 10, 15 and 30. The red line represents the pattern, and the blue lines represent the missing results using MT.C method while are detected using our solution. The black lines represent the matching results which can be detected using both MT.C method and our solution.

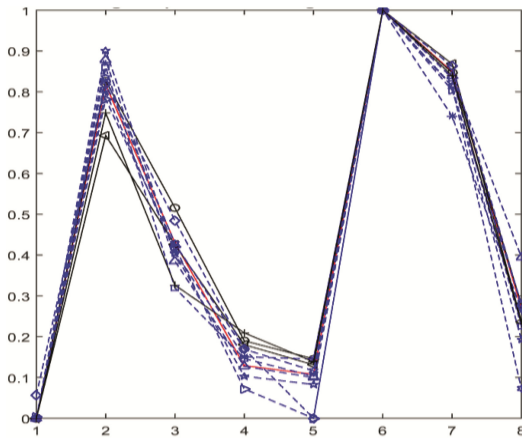


Fig. 5. The most similar 10 results ($L_p = 10$)

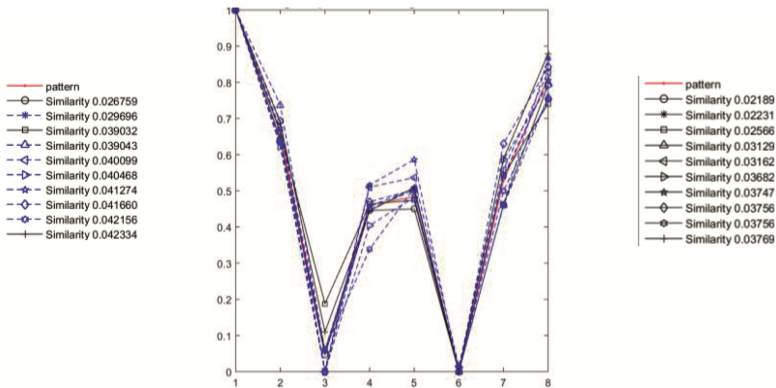


Fig. 6. The most similar 10 results ($L_p = 15$)

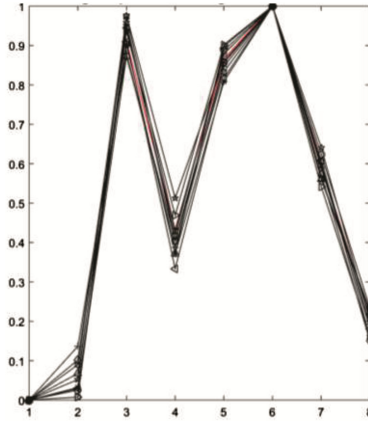


Fig. 7. The most similar 10 results ($L_p = 30$)

3.2 Time Consuming

Furthermore, to compare the time consuming between our method and the MT.C method. We enlarged the length of T from 10000000 to 49000000 gradually with an increment of 1000000. Ten experiments were conducted and the average time consuming was computed with the different lengths of patterns such as 5, 30 and 50. The statistical results were shown in Fig. 8. Because our method could find more results than the MT.C method, and more similarity computing operations were needed. So the overall executing time appear a small amount of growth on equal conditions. But, the executing time growth decreased quickly with the increasing of the length of the pattern. Because the number of matching results decreased quickly with the increasing of the length of the pattern.

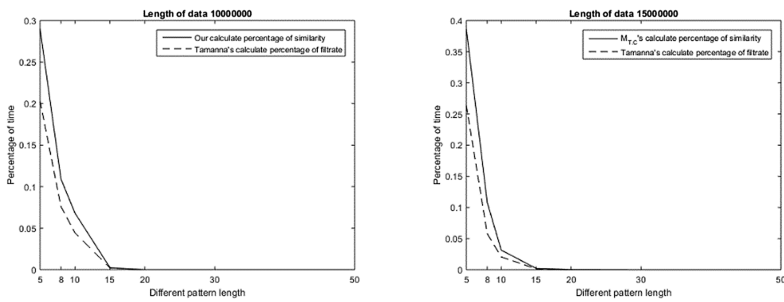


Fig. 8. Comparison of average time consuming

4 Conclusion

Fast and accurate data matching and retrieval is a key problem in big data applications such as video retrieval, stock analysis and bioinformatics etc. A similarity computing based string or number order preserving matching method is presented. Theory analysis indicates our method is sublinear. Furthermore, the experimental results show that our method can improve effectively the precision ratio and the recall ratio compared with the newest method at present under the same conditions. Compared with former research works for order-preserving matching problem, our solution liberalized the verification rules on certain extent and so more qualified matching results can be detected and found out.

Acknowledgements. This work is supported by Guangdong Province Natural Science Foundation (2016A030313703) and Guangdong Province science and technology program (2015B010109001, 2015B010131001, 2016B030305002, 2016YFB10005000, 2017B090901005, 2017A070712016).

References

1. Chhabra, T., Tarhio, J.: A filtration method for order-preserving matching. *Inf. Process. Lett.* **116**(2), 71–74 (2016)
2. Chhabra, T., Külekci, M.O., Tarhio, J.: Alternative algorithms for order-preserving matching. In: *Prague Stringology Conference* (2015)
3. Chhabra, T., Giaquinta, E., Tarhio, J.: Filtration algorithms for approximate order-preserving matching. In: Iliopoulos, C., Puglisi, S., Yilmaz, E. (eds.) *SPIRE 2015*. LNCS, vol. 9309, pp. 177–187. Springer, Cham (2015). https://doi.org/10.1007/978-3-319-23826-5_18
4. Cantone, D., Faro, S., Külekci, M.O.: An efficient skip-search approach to the order-preserving pattern matching problem. In: *Prague Stringology Conference* (2015)
5. Knuth, D.E., Morris, J.H., Pratt, V.R.: Fast pattern matching in strings. *SIAM J. Comput.* **6**(2), 323–350 (1977)
6. Crochemore, M., Iliopoulos, C.S., Kociumaka, T., Kubica, M., Langiu, A., Pissis, Solon P., Radoszewski, J., Rytter, W., Waleń, T.: Order-preserving incomplete suffix trees and order-preserving indexes. In: Kurland, O., Lewenstein, M., Porat, E. (eds.) *SPIRE 2013*. LNCS, vol. 8214, pp. 84–95. Springer, Cham (2013). https://doi.org/10.1007/978-3-319-02432-5_13
7. Kim, J., Eades, P., Fleischer, R., et al.: Order-preserving matching. *Theoret. Comput. Sci.* **525**(4), 68–79 (2013)
8. Boyer, R.S.: A fast string searching algorithm. *Commun. ACM* **20**(10), 762–772 (1977)
9. Cho, S., Na, J.C., Park, K., Sim, J.S.: Fast order-preserving pattern matching. In: Widmayer, P., Xu, Y., Zhu, B. (eds.) *COCOA 2013*. LNCS, vol. 8287, pp. 295–305. Springer, Cham (2013). https://doi.org/10.1007/978-3-319-03780-6_26
10. Cho, S., Na, J.C., Park, K., et al.: A fast algorithm for order-preserving pattern matching. *Inf. Process. Lett.* **115**(2), 397–402 (2015)
11. Belazzougui, D., Pierrot, A., Raffinot, M., Vialette, S.: Single and multiple consecutive permutation motif search. In: Cai, L., Cheng, S.-W., Lam, T.-W. (eds.) *ISAAC 2013*. LNCS, vol. 8283, pp. 66–77. Springer, Heidelberg (2013). https://doi.org/10.1007/978-3-642-45030-3_7

Blind Image Quality Assessment via Analysis of GLCM

Guanghui Yue^(✉), Chunping Hou, Tongtong Ma, and Yang Yang

School of Electrical and Information Engineering, Tianjin University, Tianjin, China
{yueguanghui, hcp, matongtong, yang_yang}@tju.edu.cn

Abstract. Blind image quality assessment (BIQA) assesses the perceptual quality of the distorted image without any information about its original reference image. Features, in consistent with human visual system (HVS), have been proved effective for BIQA. Motivated by this, we propose a novel general purpose BIQA approach. Firstly, considering that HVS is sensitive to image texture and edge, the image gradient and wavelet decomposition is computed. Secondly, taking the direction sensitivity of HVS into account, the gray level co-occurrence matrixes (GLCMs) are calculated in two directions at four scales on the computed feature maps, i.e., gradient and wavelet decomposition maps, as well as the image itself. Then, four features are extracted for each of GLCM matrix. Finally, a regression model is established to map image features to subjective opinion scores. Extensive experiments are conducted on LIVE II, TID2013 and CSIQ databases, and show that the proposed method is superior to the state-of-the-art BIQA methods and comparable to SSIM and PSNR.

Keywords: Blind image quality assessment (BIQA)
Gray level co-occurrence matrix (GLCM) · Human visual system (HVS)
Image structure

1 Introduction

At present, digital images, as the carrier of massive information, have greatly enriched people's life as well as drastically facilitated the communication among people [1, 2]. Yet image distortion remains a stubborn problem in image transmission system. Therefore, it is indispensable to establish efficient methods for image quality assessment (IQA).

Generally, IQA method can be split into two major categories: subjective and objective assessment methods. Currently, objective IQA algorithm has been widely studied because it is easy to implement and portability. Given the available information of the pristine image, objective assessment method can be further classified into full-reference IQA (FR-IQA), reduced-reference IQA (RR-IQA) and no-reference IQA (NR-IQA). Since both FR-IQA and RR-IQA methods use information of the original reference image, so they are limited to special situations. In this paper, we mainly focus on the NR-IQA method.

At present, NR-IQA method can be broadly divided into two classes, i.e., training-based opinion-aware metric and opinion-unaware metric. The former one requires a training process to create a regression model for predicting image quality. For example,

Moorthy and Bovik [3] proposed a two-step framework that called BIQL. Specifically, each distortion type was trained with a regression model. In such case, the distortion type of image can be obtained through these models. Subsequently, the image statistical properties are gradually applied into IQA and have been proved effectively. For instance, Saad *et al.* [4] provided a NR-IQA algorithm under the hypothesis that the statistics features of discrete cosine transform (DCT) coefficients change regularly along with image quality. Although these methods have achieved meaningful performance, they require training procedure. To tackle the problem, metrics, which don't require human opinion scores and any regression model, have been proposed. Xue *et al.* [5] used a set of cluster centroid with quality label as a codebook to predict image quality, called QAC. Natural image quality evaluator (NIQE) [6] established a completely blind BIQA metric by fitting the quality-aware features to a multivariate Gaussian (MVG) model. Although the training process is not required, their performances need to be further improved. In this paper, we propose a new blind image quality assessment method based on training.

It should be mentioned that the above methods mainly rely on mathematical statistics method but without full consideration of the HVS characteristics. GLCM can effectively describe image feature by measuring statistical characteristic of image in multi-direction and multi-scale. By considering characteristics of HVS and the variety of computing method for GLCM, this paper presents a simple yet effective BIQA metric. Figure 1 shows the pipeline of our method. It can be divided into the following three parts: calculation of GLCM, feature extraction and image quality prediction.

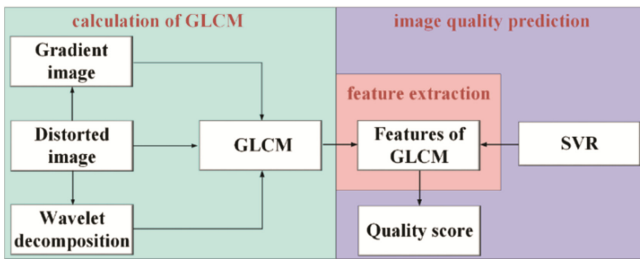


Fig. 1. The pipeline of the proposed method

2 The Proposed Method

2.1 Feature Map Extraction

(1) Gradient map and wavelet transform

Given a color image, firstly, it is transformed into grayscale, which is denoted by $I(x, y)$. The direction templates in the horizontal and vertical directions are denoted by T_x and T_y

$$T_x = [-1 \ 0 \ 1] \tag{1}$$

$$T_y = T_x' \quad (2)$$

where ‘ \prime ’ denotes transpose.

Then, the gradient components in the horizontal and vertical directions, denoted by G_x and G_y , are computed as:

$$G_x = T_x * I \quad (3)$$

$$G_y = T_y * I \quad (4)$$

where ‘ $*$ ’ denotes convolution. Finally, the gradient map G is calculated as:

$$G = \frac{|G_x| + |G_y|}{2} \quad (5)$$

Wavelet transform decomposes image into multi-scale and multi-direction. The image is usually transformed along horizontal, vertical and diagonal directions. And then the decomposition sub-graphs in those three directions are usually denoted by HL, LH and HH, respectively [15]. In this paper, the wavelet decomposition scale is set to 1, which gets good results.

As image distortion always induces the structural degradation, we desire to evaluate image quality by utilizing image structure information. Image gradient and decomposition sub-graphs are complementary to each other in representing rich image structure. On the one hand, image gradient describes the global image structure while misses orientation information. On the other hand, wavelet decomposition reflects image features in different orientation, while ignores global structure. Hence, their combination ensures integrity of the image structure information.

(2) GLCM matrix calculation

Usually, image distortion brings about a significant change of image statistic characteristics. GLCM can provide image statistic characteristics in different directions and at different scales in spatial domain, so it can describe image characteristics from various aspects. Based on this, in this paper, the GLCM matrixes of the above image structure maps are calculated.

The GLCM is composed of the joint probability density between image gray tones. There are three important parameters in GLCM: angle (θ), quantized gray tones (L) and distance (d). Firstly, the image is quantized to L gray tones. Then, the probability of occurrences of the pair of gray tones i and j in original image is expressed in $P(i, j, d, \theta)$ ($i = 1, 2, \dots, L, j = 1, 2, \dots, L$). Each entry (i, j) is depart at a distance d in angle θ . Finally, the GLCM can be denoted as $[P(i, j, d, \theta)]_{L \times L}$, where $P(i, j, d, \theta)$ is the element of $[P(i, j, d, \theta)]_{L \times L}$ in the i -th row and j -th column.

2.2 Feature Extraction

In [7], fourteen features were extracted from GLCM to represent image properties from multiple perspectives. Currently, researchers usually used part of them in view of the

redundancy among them [8]. In this paper, we employ four commonly used features, namely contrast, energy, correlation, and homogeneity, to extract quality sensitive features for IQA. Those four selected features involve local and global image characteristics. Among them, contrast and energy describe the overall characteristics of the image. Specifically, contrast describes image definition. Energy reflects the image distribution as well as roughness. On the contrary, correlation and homogeneity are local image descriptors. Concretely, correlation illustrates the local correlation of image grayscale. Homogeneity measures local change of image grayscale. Overall, the selected features can reflect both local and global features of image, to a certain extent. Therefore, they can be applied into IQA problem.

Although we have demonstrated the feasibility of GLCM in IQA problem, how to choose the parameters, i.e., θ , L , d , is still a thorny problem. Research shows that HVS is more sensitive to the horizontal and vertical image information than the oblique direction [9]. Moreover, different viewing distances produce various perception for HVS. HVS focuses on outline of image at large viewing distance, while at small distance, it will pay attention to image details [10]. And for GLCM, small scale in GLCM can describe characteristics of fine image structure, while large scale obtains characteristics of rough image structure. Inspired by these, we extract GLCM in multi-direction and multi-scale. Specifically, θ is set as 0° and 90° to highlight the sensitive direction of HVS, the distance d is set as 1, 2, 4, and 8 for simulating the variation of viewing distance, and L is set as 8. Since distortion also corrupts the brightness information, to avoid its loss, we also extract the above features on distorted image. Overall, the GLCM for gradient image, decomposed high-frequency sub-images (HL, LH and HH after one scale wavelet decomposition) and distorted image is calculated in two directions (0° and 90°) at 4 scales, resulting in eight GLCM matrices for each calculated image. A total of 40 GLCM matrices are attained, followed by four features extraction for each GLCM matrices.

2.3 Image Quality Assessment

After the feature extraction, the realization of image quality assessment is based on a regression model. Specifically, the train samples is denoted as $T = \{(F_1, D_1), (F_2, D_2), \dots, (F_i, D_i), \dots, (F_m, D_m)\}$, where i is the index of the train images, $F_i \in R^n$ represents image feature vectors and D_i denotes image opinion scores. The array T is trained to learn a model. Then, the obtained regression model can be used to predict image quality. Its mapping function can be abbreviated as $D_i = model(F_i)$, where F_i is the feature vector of the test image and D_i is the predicted quality score. In our metric, we employ support vector regression (SVR) to evaluate image quality. The LIBSVM toolbox is utilized to implement Epsilon-SVR with kernel of radial basis function [11].

3 Experiment Results and Analysis

3.1 Experiment Setup

The proposed method is tested on three public databases: LIVE II [12], TID2013 [13] and CSIQ [14] database. In LIVE II database, we test the proposed algorithm on all of the five distortion types, i.e., JPEG2000 compression (JP2K), JPEG compression (JPEG), white noise (WN), Gaussian blur (Gblur) and transmission errors in the JP2K using Fast-fading Rayleigh channel model (FF). In TID2013 and CSIQ databases, four distortion types are tested, namely JP2K, JPEG, WN and Gblur. Three general IQA criteria, i.e., Spearman rank order correlation coefficient (SROCC), Pearson linear correlation coefficient (PLCC) and root-mean-squared error (RMSE), are employed for performance evaluation. A better performance means a value close to 1 for PLCC and SROCC while a value close to 0 for RMSE.

In order to verify the effectiveness of the proposed method, we select two public FR algorithms (SSIM [15] and PSNR) and several mainstream NR methods (QAC [5], BIQI [3], ILNIQE [14], GM-LOG [16] and YCLTYCbCr [17]) for comparison. For ROI-BRISQUE, because the source code is not obtained, we directly use the experiment results on LIVE II database provided in the original paper for comparison. Since the proposed method is based on training, we divide the image set into two non-overlapping image sets: training set and testing set. The training set contains 80% of the reference images and corresponding distortion versions of them, and the testing set is comprised by the residual images. After the random train-test split is repeated 1000 times, the median performance is taken as the final results.

3.2 Experiment Results

Table 1 shows the performance tested on the entire database. For better observation, the top three performed algorithms are highlighted in bold. As we can see, the performance of the proposed method always lies in top three. In fact, compared with those IQA methods in Table 1, our method achieves the best performance in all three databases.

Table 1. SROCC, PLCC and RMSE (median value across 1000 train-test trials) of SSIM, PSNR, QAC, BIQI, NIQE, ILNIQE, GM-LOG and YCLT-YCbCr on the overall database of LIVE II, TID2013 and CSIQ respectively.

Database	Metric	SSIM	PSNR	QAC	BIQI	IL-NIQE	GM-LOG	YCLT-YCbCr	Pro.
LIVE II	PLCC	0.9397	0.9122	0.8755	0.8909	0.9011	0.9539	0.9354	0.9581
	SROCC	0.9244	0.8000	0.8803	0.8899	0.8996	0.9503	0.9348	0.9524
	RMSE	7.9001	14.0604	11.1677	10.5236	12.1186	8.1723	5.9386	6.6445
CSIQ	PLCC	0.9294	0.9281	0.8645	0.9101	0.8991	0.9408	0.8980	0.9482
	SROCC	0.9274	0.8550	0.8338	0.8925	0.8854	0.9228	0.8869	0.9432
	RMSE	0.1040	0.1483	0.1411	0.1198	0.1491	0.0950	0.1295	0.0890
TID2013	PLCC	0.8591	0.9149	0.8273	0.8048	0.9001	0.9439	0.8789	0.9512
	SROCC	0.8291	0.9058	0.8188	0.7846	0.8714	0.9282	0.8690	0.9377
	RMSE	0.7232	0.5908	0.7670	0.8254	0.6728	0.4629	0.9017	0.4293

4 Conclusion

In this paper, we propose a simple yet efficient blind IQA metric based on GLCM statistic model of image structure. To verify the performance of our proposed method, we conducted a set of experiments on LIVE II, CSIQ and TID2013 databases. We apply it on the entire database, and the experimental results demonstrate that our predicted scores is more accuracy than two public FR-IQA algorithms and the mainstream NR-IQA methods. In summary, we can draw the conclusion that the proposed method obtains excellent performance in BIQA.

Acknowledgement. This work was supported by the National Natural Science Foundation of China under Grant 61471262, the International (Regional) Cooperation and Exchange under Grant 61520106002.

References

1. Gu, K., Lin, W.S., Zhai, G.T., Yang, X.K.: No reference quality metric of contrast-distorted images based on information maximization. *IEEE Trans. Cybern.* **47**, 4559–4565 (2016)
2. Gu, K., Zhai, G.T., Yang, X.K., Zhang, W.J.: Using free energy principle for blind image quality assessment. *IEEE Trans. Multimed.* **17**(1), 50–63 (2015)
3. Moorthy, A.K., Bovik, A.C.: A two-step framework for constructing blind image quality indices. *IEEE Signal Process. Lett.* **17**(5), 513–516 (2010)
4. Saad, M.A., Bovik, A.C., Charrier, C.: Blind image quality assessment: a natural scene statistics approach in the DCT domain. *IEEE Trans. Image Process.* **21**(8), 3339–3352 (2012)
5. Xue, W.F., Zhang, L., Mou, X.Q.: Learning without human scores for blind image quality assessment. In: *Computer Vision and Pattern Recognition*, pp. 995–1002 (2013)
6. Mittal, A., Soundararajan, R., Bovik, A.C.: Making a completely blind image quality analyzer. *IEEE Signal Process. Lett.* **20**(3), 209–212 (2013)
7. Haralick, R.M., Shanmugam, K., Dinstein, I.: Textural features for image classification. *IEEE Trans. Syst. Man Cybern.* **smc-3**(6), 610–621 (1973)
8. Gadelmawla, E.S.: A vision system for surface roughness characterization using the gray level co-occurrence matrix. *NDT E Int.* **37**(7), 577–588 (2004)
9. Lambrecht, C.J.V.D.B., Verscheure, O.: Perceptual quality measure using a spatiotemporal model of the human visual system. In: *Electronic Imaging: Science & Technology*, pp. 450–461. International Society for Optics and Photonics (1996)
10. Gu, K., Wang, S.Q., Yang, H., Lin, W.S.: Saliency guided quality assessment of screen content images. *IEEE Trans. Multimed.* **18**(6), 1 (2016)
11. Chang, C.C., Lin, C.J.: LIBSVM: a library for support vector machines. *ACM Trans. Intell. Syst. Technol.* **2**(3), 389–396 (2007). Article 27
12. Sheikh, H.R., Sabir, M.F., Bovik, A.C.: A statistical evaluation of recent full reference image quality assessment algorithms. *IEEE Trans. Image Process.* **15**(11), 3440–3451 (2006)
13. Ponomarenko, N., Lukin, V., Zelensky, A., Egiazarian, K., Carli, M., Battisti, F.: TID2008—a database for evaluation of full-reference visual quality assessment metrics. *Adv. Mod. Radioelectron.* **10**(4), 30–45 (2009)
14. Larson, E.C., Chandler, D.M.: Categorical image quality (CSIQ) database (2010). <http://vision.okstate.edu/csiq>

15. Wang, Z., Bovik, A.C., Sheikh, H.R., Simoncelli, E.P.: Image quality assessment: from error visibility to structural similarity. *IEEE Trans. Image Process.* **13**(4), 600–612 (2004)
16. Xue, W., Mou, X., Zhang, L., Bovik, A.C., Feng, X.: Blind image quality assessment using joint statistics of gradient magnitude and Laplacian features. *IEEE Trans. Image Process.* **23**(11), 4850–4862 (2014)
17. Wu, Q.B., Li, H.L., Meng, F.M., Ngan, K.N., Luo, B., Huang, C., Zeng, B.: Blind image quality assessment based on multichannel feature fusion and label transfer. *IEEE Trans. Circuits Syst. Video Technol.* **26**(3), 425–440 (2016)

An Improved Ranked K-medoids Clustering Algorithm Based on a P System

Bao Zhang, Laisheng Xiang, and Xiyu Liu^(✉)

School of Management Science and Engineering, Shandong Normal University,
Jinan 250014, China

zhangbao_sup@163.com, sdxyliu@163.com

Abstract. In this paper an improved ranked K-medoids algorithm by a specific cell-like P system is proposed which extends the application of membrane computing. First, we use the maximum distance method to choose the initial clustering medoids, maximum distance method which is based on the fact that the farthest initial medoids were the least likely assigned in the same cluster. And then, we realize this algorithm by a specific P system. P system is adequate to solve clustering problem for its high parallelism and lower computational time complexity. By computation of the designed system, one possible clustering result is obtained in a non-deterministic and maximal parallel way. Through example verification, our algorithm can improve the quality of clustering.

Keywords: Ranked K-medoids · Maximum distance · P system clustering

1 Introduction

Clustering is a rapidly developing area which contributes to research field including data mining, machine learning, spatial database technology, biology and marketing and so on [1]. Clustering analysis is the process of dividing a set of objects into none-overlapping subsets [1].

Up to now, many kinds of approaches of clustering has appeared, for instance hierarchical [2], partitioning [3], density-based [4], model-based [5] and grid-based [6]. As a partitioning clustering algorithm, ranked K-medoids algorithm has strong robustness and high accuracy in contrast to traditional K-medoids algorithm [2]. In this algorithm K medoids are selected randomly, in this way, two or more medoids will be assigned to one cluster easily. When this phenomenon appeared, one of them was left behind, and others should be relocated.

As a new branch of natural computing, membrane computing is a cross-discipline topic incorporating computer science, biology, artificial intelligence and so on. It has the advantage of parallelism so it can lessen the time complexity and improve the process speed of massive data sets [8, 9].

In this paper, a new version of ranked k-medoids algorithms is proposed in order to escaping from local optimum. When select the initial medoids we use the method called “Maximum Distance Method”, by this method we select the accuracy medoids at the beginning. To realize this algorithm we designed a specific cell-like P system.

The rest of the paper is organized as follows. Section 2 presents a variant of the ranked k-medoids algorithm. Section 3 design a specific P system to realize the algorithm we proposed. Finally, Sect. 4 makes conclusions.

2 The Improved Ranked K-medoids Clustering Based on Maximum Distance Method

2.1 Maximum Distance Method

In ranked K-medoids clustering the initial medoids are selected randomly, when more than one medoids are assigned to the same cluster one of them is left and others relocated. It wastes a lot of time, to solve this problem we use the method of maximum distance.

Maximum distance method based the fact as follows: (1) objects who are far from each other is less likely to assigned to the same cluster. Based on this fact, firstly we calculated the distance between every two objects, and two objects who has the maximum distance are chosen as the initial clustering center. In the remained (N-2) sample points, select the object as the third cluster center when the product of the distance to the first two initial centers is maximum. The fourth cluster center is selected like before, and so on, we can find the k initial cluster centers.

2.2 Ranked K-medoids Based on Maximum Distance Method

In this paper, a new ranked K-medoids clustering algorithm based on maximum distance method is proposed

1. Calculate the similarities among pairs of objects based on the similarity metric.
2. Calculate R matrix by sorting the similarity values and store the indexes of similar objects from the most similar to the least similar in sorted index matrix.
3. Select k medoids use the maximum distance method.
4. Select the group of the most similar objects to each medoid, using sorted index matrix (The number of members of the group is determined by an input parameter m).
5. Calculate the hostility values of every object in those groups
6. Choose object with the maximum hostility value as the new medoid.
7. Assign each object to the most similar medoid.

3 P System for the Improved Ranked K-medoids Algorithm

3.1 Construction of the Specific P System

$$\Pi = (O, M_0, M_1, M_2, \dots, M_k, ch, c_0, \rho)$$

Where:

$$O = (\alpha_{11}, \gamma_{1,0}, \theta_1, \xi_1, a_1, a_2, \dots, a_n, \vartheta_0)$$

$$ch = [[]_1 []_2, \dots, []_k []_{c_0}]$$

$$\sigma_0 = (w_{0,0}, R_0)$$

$$w_{0,0} = \alpha_{11}, \gamma_{1,0}, \theta_1, \xi_1, a_1, a_2, \dots, a_n, \beta_{12}$$

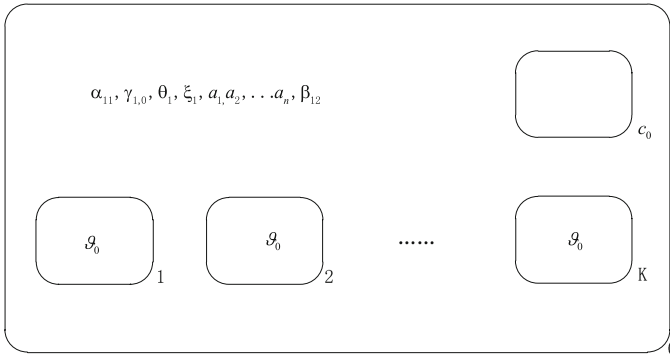


Fig. 1. Membrane structure

R_0 :

$$\begin{aligned}
 r_1 &= \left\{ \alpha_{ij} a_i a_j \rightarrow \alpha_{i(j+1)} a_i a_j U_{ij}^{\alpha_{ij}} \mid 1 \leq i, j \leq n \right\} \\
 &\quad \cup \left\{ \alpha_{i(n+1)} \rightarrow \alpha_{(i+1),1} \mid 1 \leq i \leq n \right\} \cup \left\{ \alpha_{n(n+1)} \rightarrow \lambda \right\} \\
 r_2 &= U_{11}^{w_{11}} \rightarrow D_{11}^{w_{11}} U_{11}^{w_{11}} \\
 r_3 &= \left\{ \beta_{ij}^h U_{ij}^{w_{ij}} U_{i(j+1)}^{w_{i(j+1)}} \rightarrow \beta_{i(j+1)}^{h+w_{ij}-w_{i(j+1)}} U_{ij}^{w_{ij}} U_{i(j+1)}^{w_{i(j+1)}} \right\} \cup \left\{ \beta_{i(n+1)}^h \rightarrow \beta_{i(i+1)} \right\} \\
 &\quad \mid 0 < i < j \leq n \\
 r_4 &= \left\{ \beta_{ij}^h D_{ij}^{w_{ij}} U_{i(j+1)}^{w_{i(j+1)}} \gamma_p \rightarrow \beta_{i(j+1)}^h U_{ij}^{w_{ij}} D_{i(j+1)}^{w_{i(j+1)}} \gamma_{p+1} \mid h' < 0, 0 < i < j < n \right\} \\
 &\quad \cup \left\{ \gamma_p D_{ij}^{w_{ij}} a_i a_j \rightarrow (A_i)_1 (A_j)_2 \mid p = (n-1)! \right\} \\
 r_5 &= \left\{ \eta^q U_{11}^{w_{11}} U_{12}^{w_{12}} \dots U_{1n}^{w_{1n}} U_{21}^{w_{21}} \dots U_{nn}^{w_{nn}} \rightarrow \right\} \\
 &\quad \left\{ \eta^{q-w_{ij}} U_{11}^{w_{11}} U_{12}^{w_{12}} \dots U_{1n}^{w_{1n}} U_{21}^{w_{21}} \dots U_{nn}^{w_{nn}} \right\} \\
 &\quad \cup \left\{ \eta^{q-w_{ij}} a_j \rightarrow (A_j)_t \mid 2 < t \leq k \right\}
 \end{aligned}$$

$$\begin{aligned}
 r_6 &= \left\{ \begin{aligned} &U_{ij}^{\omega_{ij}} \gamma_{i,q} \rightarrow \gamma_{i,q+1} \left(\zeta_{ij}^{q+1} \right)_{in_1} \left(\zeta_{ij}^{q+1} \right)_{in_2} \dots \left(\zeta_{ij}^{q+1} \right)_{in_k} \zeta_{ij}^{q+1} \\ &|\omega_{ij} = 0, 1 \leq i, j \leq n, 0 \leq q < n \end{aligned} \right\} \\
 &\cup \left\{ \gamma_{i,(n+1)} \rightarrow \gamma_{(i+1),0} | 1 \leq i \leq n \right\} \cup \left\{ \gamma_{n(n+1)} \rightarrow e \right\} \\
 r_7 &= \left\{ \gamma_{i,q} U_{i1}^{\omega_{i1}} U_{i2}^{\omega_{i2}} \dots U_{in}^{\omega_{in}} \rightarrow \gamma_{i,q} U_{i1}^{\omega_{i1}-1} U_{i2}^{\omega_{i2}-1} \dots U_{in}^{\omega_{in}-1} | 1 \leq i \leq n, 0 \leq q \leq n \right\} \\
 r_8 &= \left\{ \chi_r A_{ri} a_j \zeta_{ij}^p \zeta_p \rightarrow \chi_r A_{ri} (G_{pj})_{in_t} \zeta_{p+1} | 1 \leq i, j \leq n, 1 \leq t \leq k, 1 \leq p \leq m \right\} \\
 r_9 &= \left\{ \chi_{k+1} \zeta_m \rightarrow \zeta_1 (\eta_1)_{in_1} (\eta_1)_{in_2} \dots (\eta_1)_{in_k} \right\} \\
 r_{10} &= \left\{ \begin{aligned} &\left(d^k a_i A_{1j_1} A_{2j_2} \dots A_{kj_k} U_{ij_1}^{\omega_{ij_1}} U_{ij_2}^{\omega_{ij_2}} \dots U_{ij_k}^{\omega_{ij_k}} \rightarrow \right)_{a_i} \\ &\left(d^k (a_i)_{in_p} (A_{1j_1})_{in_1} (A_{2j_2})_{in_2} \dots (A_{kj_k})_{in_k} \right)_{a_i} \\ &|\omega_{ij_p} = 0, 1 \leq j_1, j_2, \dots, j_k \leq n \end{aligned} \right\} \\
 r_{11} &= \left\{ \begin{aligned} &U_{ij_1}^{\omega_{ij_1}} U_{ij_2}^{\omega_{ij_2}} \dots U_{ij_k}^{\omega_{ij_k}} \rightarrow U_{ij_1}^{\omega_{ij_1}-1} U_{ij_2}^{\omega_{ij_2}-1} \dots U_{ij_k}^{\omega_{ij_k}-1} \\ &|\omega_{ij_h} = 0, 1 \leq j_1, j_2, \dots, j_k \leq n \end{aligned} \right\} \\
 r_{12} &= \left\{ d^k \rightarrow (\beta)_{in_1} (\beta)_{in_2} \dots (\beta)_{in_k} | 1 \leq i \leq n, 0 \leq j \leq k \right\} \cup \left\{ \zeta \zeta \rightarrow \lambda \right\}
 \end{aligned}$$

$\sigma_i = (w_{i,0}, R_i)$, $1 \leq i \leq k$ Where:

$$w_{t,0} = \vartheta_0$$

$$R_t (1 \leq t \leq k) :$$

$$\begin{aligned}
 r'_1 &= \left\{ (\beta \varphi \rightarrow \beta \varphi a_i)_{a_i} | 1 \leq i \leq n, \varphi \subseteq O_{ij} \cup \{a_p | 1 \leq p \leq n\} \right\} \\
 r'_2 &= \left\{ \beta \varphi \rightarrow (\beta \varphi)_{in_{c_0}} | \varphi \subseteq O_{ij} \cup \{a_p | 1 \leq p \leq n\} \right\} \cup \left\{ \zeta \rightarrow \lambda \right\} \\
 r'_3 &= \left\{ \begin{aligned} &A_p G_{1j_1} G_{2j_2} \dots G_{mj_m} \zeta_{pj_1}^{q_1} \zeta_{pj_2}^{q_2} \dots \zeta_{pj_m}^{q_m} \rightarrow A_p G_{1j_1} G_{2j_2} \dots G_{mj_m} \zeta_{pj_1}^{q_1} \zeta_{pj_2}^{q_2} \dots \zeta_{pj_m}^{q_m} \zeta_p^{Q_p} \\ &| 1 \leq j_1, j_2, \dots, j_m, p \leq n, 1 \leq t \leq k \end{aligned} \right\} \\
 r'_4 &= \left\{ \begin{aligned} &\left(\eta_i G_{ij_1} G_{1j_1} G_{2j_2} \dots G_{(i-1)j_{(i-1)}} G_{(i+1)j_{(i+1)}} \dots \right) \\ &\left(G_{mj_m} A_p \zeta_{j_1}^{q_1} \zeta_{j_2}^{q_2} \dots \zeta_{j_{(i-1)}}^{q_{(i-1)}} \zeta_{j_{(i+1)}}^{q_{(i+1)}} \dots \zeta_{j_m}^{q_m} \zeta_{j_p}^{Q_p} \rightarrow \right) \\ &\left(\eta_i G_{ij_1} G_{1j_1} G_{2j_2} \dots G_{(i-1)j_{(i-1)}} G_{(i+1)j_{(i+1)}} \dots \right) \\ &\left(G_{mj_m} A_p \zeta_{j_1}^{q_1} \zeta_{j_2}^{q_2} \dots \zeta_{j_{(i-1)}}^{q_{(i-1)}} \zeta_{j_{(i+1)}}^{q_{(i+1)}} \dots \zeta_{j_m}^{q_m} \zeta_{j_i}^{Q_i} \right) \\ &| 1 \leq j_1, j_2, \dots, j_m, p \leq n, 1 \leq i \leq m \end{aligned} \right\} \\
 r'_5 &= \left\{ \begin{aligned} &\vartheta_h A_p G_{ij_1} \zeta_p^{Q_p} \zeta_{j_i}^{Q_i} \rightarrow \vartheta_{h+Q_i-Q_p} A_p G_{ij_1} \zeta_p^{Q_p} \zeta_{j_i}^{Q_i} \\ &| 1 \leq t \leq k, 1 \leq j_i, p \leq n, 1 \leq i \leq m \end{aligned} \right\} \\
 r'_6 &= \left\{ \vartheta_h A_p G_{ij_1} \rightarrow \vartheta_0 G_{ip} A_{ij_1} \mu | h' > 0, 1 \leq p, j_i \leq n, 1 \leq i \leq m, 1 \leq t \leq k \right\} \\
 &\cup \left\{ \vartheta_{h'} \rightarrow \vartheta_0 v | h' \leq 0 \right\} \cup \left\{ \eta_i \rightarrow \eta_{i+1} \right\} \cup \left\{ \eta_{m+1} \rightarrow \lambda \right\} \\
 r'_7 &= \left\{ \zeta_p^{Q_p} \zeta_{j_i}^{Q_i} \rightarrow \lambda | 1 \leq j_i, p \leq n \right\} \\
 r'_8 &= \left\{ \begin{aligned} &\mu^i v^j G_{1j_1} G_{2j_2} \dots G_{mj_m} A_p \zeta \rightarrow (b a_{j_1} a_{j_2} \dots a_{j_m} A_p \lambda_1)_{in_0} | 1 \leq j_1, j_2, \dots, j_m, p \leq n, 1 \leq t \leq k \\ &\cup \left\{ (v^i A_p \rightarrow (A_p d)_{out})_{-|\mu^i} | 1 \leq i, j \leq n \right\} \end{aligned} \right\}
 \end{aligned}$$

$$\rho = \{r_i > r_j | 1 \leq i < j \leq 11\} \cup \{r'_i > r'_j | 1 \leq i < j \leq 8\}$$

The P system we construct include membrane M_0 , membrane $M_t(1 \leq t \leq k)$, $W_{0,0}$ is the initial multiset that include in the membrane M_0 , and $a_1, a_2 \dots a_n$ represent the objects in a given data set. R_0 represents the rules in membrane M_0 (Fig. 1).

3.2 Experiment and Results

In order to give a better interpretation of our P system model for the improved ranked K-medoids clustering, we take an example to simulate the procedure of the P system. There are 12 points (Fig. 2):

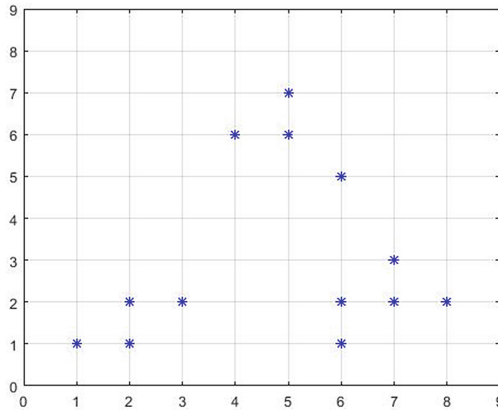


Fig. 2. The initial state of the points

The P system is supposed to distribute the points into 3 clusters with the given parameter m of the value 3. Diagram 2 depicts the original state of the 13 points.

First, calculate the distance between every two points, then find points (1, 1), (5, 7), (8, 2) that satisfy maximum distance method. After that, the rules in three membranes are executed at the same time and find the final clustering medoids by hostility values. Finally, sent the objects to the nearest clusters.

Eventually, the clustering result was attained that the 13 points were classified into 3 clusters. And the clustering effect sketch is shown in Fig. 3.

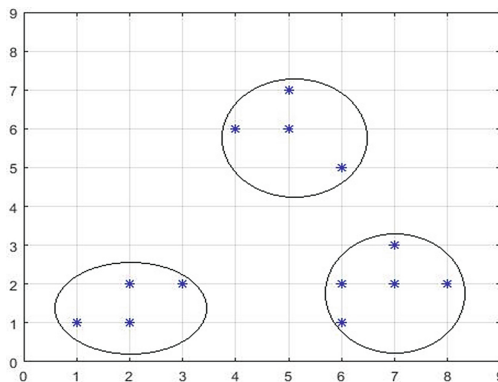


Fig. 3. The final clustering result

4 Conclusions

Ranked K-medoids is a novel partitioning clustering algorithm, it propose a novel new term named hostility value. The medoid is update in each iteration finally it will find the center of the clusters, objects will be assigned to the nearest cluster.

This paper present a new ranked K-medoids algorithm that based on the maximum distance method, by this method we can find the suitable initial medoids. By this mean we don't need to relocate the medoids that are assigned to the same cluster, and profit from characteristic great parallelism of P system, so that the time of iteration is shorten.

Acknowledgment. This work is supported by the Natural Science Foundation of China (Nos. 61170038, 61472231, 61402187, 61502535, and 61572523).

References

1. Han, J., Kambr, M.: Data mining concepts and techniques, Elsevier Inc., USA (2012). ch. 8
2. Razavi Zadegan, S.M., Mirzaie, M., Sadoughi, F.: Ranked k-medoids: a fast and accurate rank-based partitioning algorithm for clustering large datasets. *Knowl.-Based Syst.* **39**(2), 133–143 (2013)
3. Zhang, T.: BIRCH: an efficient data clustering method for very large databases. *ACM SIGMOD Record* **25**(2), 103–114 (1996)
4. Kaufman, L., Rousseeuw, P.J.: Finding Groups in Data: An Introduction to Cluster Analysis (1991)
5. Sander, J., Ester, M., Kriegel, H.P., et al.: Density-based clustering in spatial databases: the algorithm GDBSCAN and its applications. *Data Min. Knowl. Disc.* **2**(2), 169–194 (1998)
6. Fraley, C., Raftery, A.E.: Model-based clustering, discriminant analysis, and density estimation. *J. Am. Stat. Assoc.* **97**(458), 611–631 (2002)
7. Wang, W., Yang, J., Muntz, R.R.: STING: a statistical information grid approach to spatial data mining. In: International Conference on Very Large Data Bases, pp. 186–195. Morgan Kaufmann Publishers Inc. (1997)
8. Peng, H., Wang, J., Pérez-Jiménez, M.J., et al.: An unsupervised learning algorithm for membrane computing. *Inf. Sci.* **304**(C), 80–91 (2015)
9. Niu, Y., Xiao, J., Jiang, Y.: Time-free solution to 3-coloring problem using tissue P systems. *Chin. J. Electron.* **25**(3), 407–412 (2016)

A Novel Inverse-Operation Based Group Undo/Redo Algorithm for Feature-Based 3D Collaborative CAD Systems

Yuan Cheng¹, Fazhi He^{2(✉)}, Xiao Lv², and Weiwei Cai²

¹ School of Information Management, Wuhan University, Wuhan, China

² School of Computer Science, Wuhan University, Wuhan, China
fzhe@whu.edu.cn

Abstract. Supporting group Undo/Redo with high performance in a 3D designing environment still remains a challenge. The question is how to recover the document state as if an operation is never executed. In this paper, we are going to propose an inverse-operation based group Undo/Redo solution for feature-based 3D collaborative CAD systems. It allows a 3D part to be manipulated locally. We developed an ontology in the CAD domain so as to describe common elements in typical feature-based CAD systems. By classifying features according to how they affect a volume, feature modeling operations are categorized into four groups. We are able to create inverse operations for operations belonging to the same category. The proposed methods are tested in a prototype system with case study.

Keywords: Feature-based collaborative CAD · Group Undo/Redo
Inverse operation · Ontology

1 Introduction

Feature-based modeling approaches have played a relevant role for qualitative knowledge specification and integration in collaborative designing since the 70s [1–3], and feature-based CAD systems are currently considered the state-of-art technologies for product modeling [4–7]. Undo/Redo is a standard and core function for nearly all human-computer interaction applications. It can help to remove some erroneous operations and enable a user to explore a new system by try-and-failure. Most importantly, undo/redo is an essential tool to grant that a document is the result of designers' intentions by removing the effects of undesired operations. An Undo/Redo mechanism should understand which operation is to be undone when a user issues an undo command by different interaction methods. Besides, the undo effect demands that the result of a certain operation is eliminated as if it has never been executed. This leaves us a question that how the effect of an undo target be removed from the 3D model. Our previous study investigate both full-rerun and full checkpoint strategy[8, 9], although the correctness of our group Undo/Redo algorithms can be promised, the performance is still not satisfying.

Treating Undo as an inverse operation is a prevailing strategy for collaborative document and graphic editing. The inverse operation is executed on the current document directly. The document does not need to be rolled back and forth which is considered to be more efficient than the previously mentioned two undo strategies. This mechanism depends largely on two conditions. One is that there should be quite a limited number of primitive operations. For example, in collaborative document editing, there are simply two primitive operations, say insert and delete, which are regarded as the inverse operation of each other [10]. The other one is that an object from the document should be easily located and distinguished from other objects. A feature-based CAD application retains a large quantity of feature modeling operations. Generating an inverse operation for every feature modeling operation still remains a challenge.

In this paper, we are going to propose an inverse-operation based group undo/redo approach to serve the purpose of both intention preservation and high performance. The basic idea is to generate inverse operations by building a domain ontology and classifying the modeling operations into quite a limited number of groups. An Inverse operation is generated in a uniformed way for an operation category but not for any specific operation. The remaining of this paper is organized as follows. Section 2 reviews the related works from the perspective of current group undo methods and ontologies build in the CAD domains. In Sect. 3, the ontology constructed in the CAD domain is introduced. Section 4 provides a detailed description of how to create inverse operations different feature groups. Section 5 includes the experiments to illustrate the our group Undo/Redo approach based on the inverse-operation model. Conclusions and limitations are given.

2 Related Works

Several undo models are proposed for multi-user Undo/Redo. Each model sets a framework for developing specific undo and redo algorithms. The script model [11] is one of the earliest group Undo/Redo solutions. Regional undo was also applied in spreadsheets [12] by allowing users to select a part of the spreadsheet and perform undo on the cells. Treating an undo as a concurrent inverse operation is another popular solution for group undo. For the first time, Berlage introduced the selective undo model that adds the reverse operation of the selected command to the current context [13]. In collaborative textual editors, delete and insert can be the inverse operation for each other. DistEdit [14] is the first OT based selective undo solution. The undo target is transposed to the end of the history buffer and the inverse command of the transposed operation is executed. The adopted [15, 16] also considered an inverse as the concurrent operation of operations generated after O. Neither DisEdit nor adOPTed supports the full featured selective undo. Sun has proposed the framework of AnyUndo to support “Anytime, Anywhere undo”. The proposed algorithms GOTO and COT both integrate do and selective undo [17, 18]. Azurite [19, 20], provides general selective undo in a code editor. Azurite uses the inverse model, by adding the inverse text editing operation to the end of the history, and provides a variety of user interfaces to resolve conflicts. Logoot-Undo [21] is the group undo algorithm supporting AnyUndo under the CRDT framework.

The document is manipulated at the line-level. The effects of that an inserted line is undone is actually controlled by changing the visibility of the line. Conflicts between two concurrent undos are therefore avoided because if an undo cannot find a line given its unique identifier, it can therefore be discarded.

Applying the inverse model to graphical editors seems easier than to painting systems. On one hand, in an object-oriented system, the inverse operation can be easily generated by retrieving the designing history, and then executing some system defined operation by using the properties of the graphical object before the latest modification [13, 22]. In pixel-based drawing systems, such as Photoshop, it is the historical information of every pixel that needs to be recorded which is resource consuming. In Wang's solution for undo in bitmap systems [23], only pixels of the drawing area and connections between operations are recorded. Aquamarine [24, 25] is a system developed on the basis of Photoshop for selective undo using the script model. Another undo scheme developed under the script model is the group Undo/Redo method for 3D collaborative CAD systems developed by our previous research [25].

3 Ontology-Based Inverse Operation Generation

We build an ontology, called Part Feature Ontology (PFO), to describe the semantics of a part from the perspectives of individual settings and parameter values. We also intend to use this ontology to categorize features in a 3D collaborative CAD system. The classes defined in PFO are: modeling feature, topology info, B-rep Operation, Reference Info and Sketch Info. Six relations are defined, which are: is-a, has-topology-attribute, has-reference-attribute, has-boolean-operation, as-dependency-attribute, and has-sketch. We categorize features according to their effects on the volume. The subclasses of modeling feature include convex feature, concave feature, edge transition feature and primitive feature.

3.1 Inverse Operation for Convex Features

The inverse operation of a convex feature creating operation is to remove any topological entities that extrude outward the datum plane without considering the shape of the feature. The construction process of the inverse operation is presented in Algorithm 1.

Algorithm 1 The inverse operation for convex feature creating operations

Function Inverse(O)

- 1: Obtain the topological entities that belong to the feature created by O. Typically, these topological entities are protrusive above the original part model. This is accomplished by parsing the semantic descriptor OWL file FD_O with OWL API parser so as to obtain the attribute TopologicalFaceSet;
 - 2: For every topological face f from the TopologicalFaceSet, execute the $delete(f)$ so as to remove the revealed faces from the part model;
 - 3: Detect the broken area on the datum plane, create a face in the same shape, and merge the face with the plane.
 - 4: return ;
-

Figure 1 gives us an example. Three feature instances are added to the same base block feature by different modeling methods. O_1 adds the convex feature by sweeping the face f_p along a curve. O_2 adds the convex feature by rotating. O_3 adds the feature by extruding. The features are in different forms. It is worth noting that, in some situations, when deleting some revealed faces from the boundary, there leaves a broken area on the datum plane. In this case, the plane should be repaired. As it is illustrated in Fig. 2, when the revealed faces from the round protrusion are deleted, there leaves a circular broken area on the datum plane where the protrusion located.

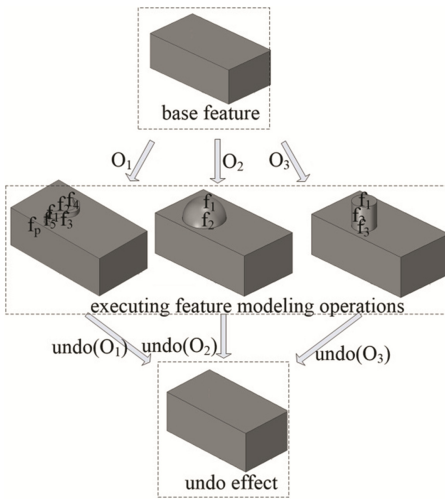


Fig. 1. Inverse operations for different convex feature instances

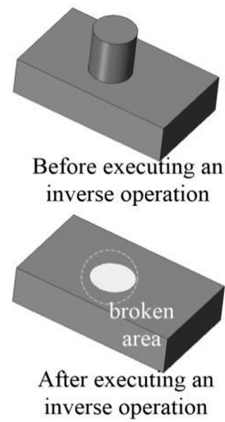


Fig. 2. An example of the broken area

3.2 Inverse Operation for Concave Feature Creating Operations

The inverse operation of a concave feature creating operation is to re-fill in any hollow space it creates on the part model. Inspired by the definition of the bounding box widely used in 3D modeling, we intend to find the Minimum Wrapping Solid, noted as MWS for brevity, for a hollow space of any form. An MWS is actually a solid with the smallest volume which contains all the points from the depression feature. Then, by uniting the MWS with the part model, the hollow space is re-filled. The formal definition for the Minimum Wrapping Solid is given in the following.

In Fig. 3, we give several examples of the MWSs for different types of depression features with different forms. O_1 creates a cubic slot. O_2 creates a round hole. O_3 creates a sink hole. For the sake of creating an MWS, geometry-related information, such as the radius and length of a simple hole, the width, length and height of a block, is more critical than topology-related information.

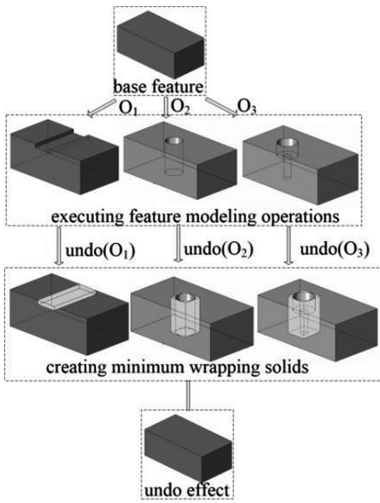


Fig. 3. Inverse operations for different concave feature instances

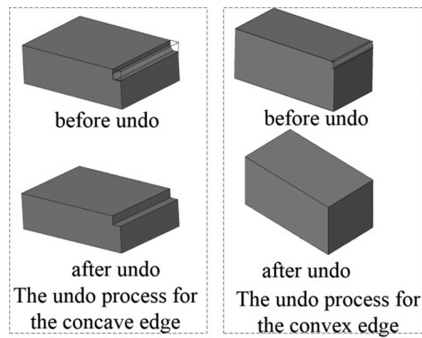


Fig. 4. Inverse operations for different edge transition feature instances

Algorithm 2 The inverse operation for concave feature creating operations

Function Inverse(O)

- 1: Parse the FD_O and extract the information, namely, the category the feature instance belongs to, the dimension parameters and the reference information.
 - 2: The MWS for the concave feature is constructed. It is then transformed to the proper position by using the same reference information extracted in step 1;
 - 3: Unite the MWS with the current part model so as to refill the hollow space that O created;
 - 4: Delete faces from the MWS that are extruding outward the part and repair the broken area;
 - 5: return ;
-

3.3 Inverse Operation for Edge Transition Feature Creating Operations

We devise the inverse operations by considering how an edge transition is created. As it is illustrated in Fig. 4, an edge transition is created in two different situations: (1) On the left side of the Fig., a concave edge is chosen for edge transition which appears to difference a small volume from the part; (2) On the right side of the Fig., a convex edge is chosen and the result appears to add a volume so the two orthogonal faces connect smoothly. The procedure of creating inverse operations for different edge transition occasions is given in Algorithm 3.

Algorithm 3 The inverse operation for edge transition feature creating operations

Function Inverse(O)

- 1: Parse the FD_O and extract the information, namely, the category the feature instance belongs to, the dimension parameters.
 - 2: The MWS for the transition edge is constructed. It is then transformed to the proper position;
 - 3: If O selects a convex edge for edge transition, the MWS is united with the part. if O selects a concave edge for edge transition, the MWS is subtracted from the part;
 - 4: return ;
-

4 Experiments

In this example, three geographically dispersed sites build and modify models with both do and undo operations. How the boundary of the part evolves with the continuous execution of both do and undo at each site is given in Fig. 5 and the expected effect of every operation is described in details in Table 1. Whenever an operation is performed, the related hybrid feature descriptor is generated. Observed from Fig. 5, the collaboration activity involves three stages. The operations issued in the first stage are pure modeling operations. The second stage contains concurrent do and undo. The third stage is a typical scenario of concurrent undo. The emphasis will be laid on the group undo process.

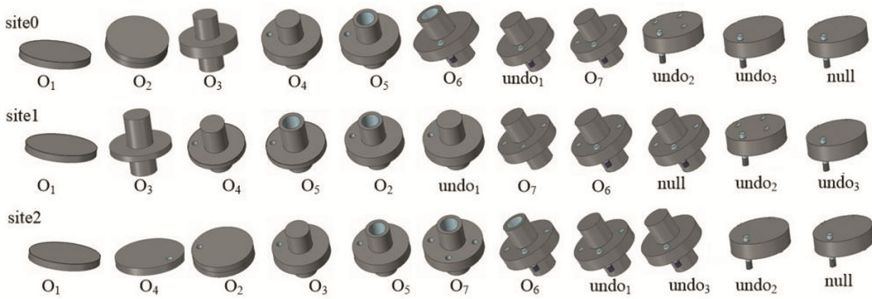


Fig. 5. A typical scenario of the collaborative modeling process

When undo is issued by site1, its intention is to delete the round hole feature created by O_5 from site1. It is carried out immediately at site1. The undo command is sent to other sites in the form of $UNDO(\langle 1, 1 \rangle, \langle 1, 3 \rangle)$. Being an instance of a concave feature, the MWS for the round hole is created given the length of the hole and the radius of the circular end-face. The MWS is then transformed given the locating information containing in the reference information descriptor of FD_{O_5} . By uniting it with the part, O_5 is successfully undone. When undo1 is received by a remote site, O_5 is then identified with the assistance of the tuple $\langle 1, 3 \rangle$. The undo process is carried in the same process with how the undo is performed at the local site site1.

Undo2 and undo3 are concurrently generated at site0 and site2. However, they are not in a conflictive relation. Undo2's intention is to delete the round protrusion created by O_3 from site1. It is carried out immediately at site0. The undo command is sent to other sites in the form of $UNDO(\langle 0, 1 \rangle, \langle 1, 1 \rangle)$. The revealed faces from the round protrusion are deleted. Then, the broken area left on the base feature is repaired. The topology information are required are from FD_{O_3} . When undo2 is received by a remote site, O_3 is then picked out with the assistance of the tuple $\langle 1, 1 \rangle$.

Table 1. Operation descriptions

Feature modeling operation	Operation effect
O ₁	Create the base cylinder feature
O ₂	Create another cylinder with the same radius on top of the base feature
O ₃	Create a round protrusion across the base cylinder
O ₄	Create a round hole within the base cylinder
O ₅	Create a round hole within the round protrusion built by O ₃
O ₆	Create a round cylinder crossing the hole generated by O ₃ . The end of the cylinder is decorated by spiral line.
O ₇	A mirror operation is invoked to generate another three holes around the round protrusion generated by O ₃ . Since now the four holes are symmetric with the center of the round protrusion. Then we can say O ₇ depends on O ₄ .

The intention of undo3 is to delete the small round hole within the base cylinder created by O₄ from site1. It is carried out immediately at site2 and sent to other sites in the form of UNDO($\langle 2, 1 \rangle, \langle 2, 1 \rangle$). The MWS for this round hole is created given its length and the radius. It is then transformed given the same reference information acquired from FD_{O₄}. By uniting it with the part, O₄ is successfully undone. O₇ is undone as well because of its dependency relation with O₄.

5 Conclusions

In this paper, we propose a novel inverse-operation based group Undo/Redo algorithm for feature-based 3D collaborative CAD systems. This work is the first to apply the inverse model to the domain of 3D environment. We built an ontology in the CAD domain and developed classes with sub-classes to describe general entities in the feature-based 3D CAD environment. Using these concepts and their relations, we generate a hybrid descriptor to record the information of a feature. For a convex feature, we delete the topological entities it creates and repair the broken area after its deletion. For a concave feature of any shape, we re-fill the hollow space by creating the minimum wrapping solid and uniting it with the part. This group Undo/Redo solution gives an opportunity to modify a part locally. Our future work is to deal with the attribute dependency and attribute conflicts among features.

Acknowledgement. The work is supported by the National Natural Science Foundation of China (NSFC Grant Nos. 61472289 and 61502353) and Youth Innovation Corps Fund of Humanities and Social Sciences, Wuhan University. The authors would like to thank all the reviewers for their constructive comments and suggestions.

References

1. He, F., Han, S.: A method and tool for human-human interaction and instant collaboration in CSCW-based CAD. *Comput. Ind.* **57**(8), 740–751 (2006)
2. Jing, S., He, F., Han, S., et al.: A method for topological entity correspondence in a replicated collaborative CAD system. *Comput. Ind.* **60**(7), 467–475 (2009)
3. Li, X., He, F., Cai, X., et al.: CAD data exchange based on the recovery of feature modelling procedure. *Int. J. Comput. Integr. Manuf.* **25**(10), 874–887 (2012)
4. Li, X., He, F., Cai, X., et al.: A method for topological entity matching in the integration of heterogeneous CAD systems. *Integr. Comput. Aided Eng.* **20**(1), 15–30 (2013)
5. Zhang, D., He, F., Han, S., et al.: Quantitative optimization of interoperability during feature-based data exchange. *Integr. Comput. Aided Eng.* **23**(1), 31–50 (2016)
6. Wu, Y., He, F., Zhang, D., et al.: Service-oriented feature-based data exchange for cloud-based design and manufacturing. *IEEE Trans. Serv. Comput.* **PP**(99), 1 (2015)
7. Wu, Y., He, F., Han, S.: Collaborative CAD synchronization based on a symmetric and consistent modeling procedure. *Symmetry* **9**(4), 59 (2017)
8. Cheng, Y., He, F., Cai, X., et al.: A group Undo/Redo method in 3D collaborative modeling systems with performance evaluation. *J. Netw. Comput. Appl.* **36**(6), 1512–1522 (2013)
9. Cheng, Y., He, F., Wu, Y., et al.: Meta-operation conflict resolution for human-human interaction in collaborative feature-based CAD systems. *Cluster Comput.* **19**(1), 237–253 (2016)
10. Ressel, M., Nitsche-Ruhland, D., Gunzenhauser, R.: An integrating, transformation-oriented approach to concurrency control and undo in group editors. In: *Proceeding of Conference on Computer Supported Cooperative Work (CSCW)*, pp. 288–297 (1996)
11. Archer Jr., J.E., Conway, R., Schneider, F.B.: User recovery and reversal in interactive systems. *ACM Trans. Program. Lang. Syst.* **6**(1), 1–19 (1984)
12. Kawasaki, Y., Igarashi, T.: Regional undo for spreadsheets (Demo). In: *2004 Adjunct Proceedings UIST*, 2 pages (2004)
13. Berlage, T., Genau, A.A.: Framework for shared applications with a replicated architecture. In: *1993 ACM UIST, Atlanta, GA*, pp. 249–257 (1993)
14. Prakash, A., Knister, M.J.: A framework for undoing actions in collaborative systems. *ACM Trans. Comp.-Hum. Inter.* **1**(4), 295–330 (1994)
15. Ressel, M., Gunzenhauser, R.: Reducing the problems of group undo. In: *ACM Conference on Supporting Group Work* (1999)
16. Ressel, M., Nitsche-Ruhland, D., Gunzenhauser, R.: An integrating, transformation oriented approach to concurrency control and undo in group editors. In: *Proceeding of ACM conference on computer supported co-operative work, November 1996*, pp. 288–297 (1996)
17. Sun, C.Z.: Undo as concurrent inverse in group editors. *ACM Trans. Comput. Hum. Interact.* **9**(4), 309–361 (2002)
18. Sun, D., Sun, C.: Context-based operational transformation in distributed collaborative editing systems. *IEEE Trans. Parallel Distrib. Syst.* **20**(10), 1454–1470 (2009)
19. Yoon, Y., Koo, S., Myers, B.A.: Visualization of fine-grained code change history. In: *IEEE VL/HCC 2013*, pp. 119–126 (2013)
20. Yoon, Y., Myers, B.A.: Supporting selective undo in a code editor. In: *ICSE 2015, Florence, Italy* (2015)
21. Weiss, S., Urso, P., Molli, P., et al.: Logoot-undo: distributed collaborative editing system on P2P networks. *IEEE Trans. Parallel Distrib. Syst.* **21**(8), 1162–1174 (2010)
22. Myers, B.A.: Scripting graphical applications by demonstration. In: *SIGCHI 1998*, pp. 534–541 (1998)

23. Wang, X.Y., Bu, J.J., Chen, C.: Achieving undo in bitmap-based collaborative graphics editing systems. In: The 2002 ACM Conference on Computer Supported Cooperative Work (2002)
24. Myers, B.A., Lai, A., Le, T.M., et al.: Selective undo support for painting applications. In: Human Factors in Computing Systems, pp. 4227–4236 (2015)
25. www.cs.cmu.edu/NatProg/aquamarine.html

Two Steps Method Using Polarization to Resist Phase Noise for Self-interference Cancellation in Full-Duplex

Fangfang Liu¹(✉), Xinyi Wang¹, Chunyan Feng¹, and Xiao Han²

¹ Beijing Laboratory of Advanced Information Networks,
Beijing University of Posts and Telecommunications, Beijing 100876, China
fliu@bupt.edu.cn

² Network Technology Research Institution, China Unicom, Beijing, China

Abstract. Phase noise caused by the local oscillator affects both the cancellation of self-interference and the reception of the desired signal. In this paper, a novel two steps method exploiting polarization is proposed to resist the effect of phase noise on the self-interference cancellation in full-duplex. This method can convert the multiplicative noise to additive noise with polarization signal processing in two steps, which can cancel the effect of phase noise on both the self-interference and desired signal. It should be noted that this method needs no prior information of the phase noise. Theory analysis and numerical simulations show that the effect of phase noise is reduced and the amount of cancellation is also evaluated in condition of different phase noise values.

Keywords: Full duplex · Self-interference cancellation · Phase noise
Polarization

1 Introduction

Full-duplex is a modality of communication that allows a node to transmit and receive signal simultaneously at the same frequency band. It has higher spectral efficiency, higher throughput, and lower transmission delay than the traditional half duplex system, which satisfies the requirements of 5G very well [1–5]. However, massive self-interference (SI) caused by the local transmitter coupling into the local receiver is an inevitable problem to resolve. Self-interference transmitted through a short path is 15–100 dB stronger than the desired signal [6]. Therefore the cancellation of self-interference is one of the key factors influencing the full-duplex communication. Moreover, it has been demonstrated that the phase noise is one of the bottleneck of the self-interference cancellation [7].

Currently, relevant scholars put forward many self-interference cancellation methods at the receiver, which can be classified into three categories, antenna

This work is supported by Chinese National Nature Science Foundations (61501050) and (61271177).

cancelation [2, 5, 9], radio frequency cancelation (RFC) [1, 3, 6, 8], and digital cancelation [10–13]. Antenna cancelation and radio frequency cancelation is on the premise of ignoring the phase noise, then the self-interference can be suppressed to 10–15 dB stronger than the desired signal. Digital cancelation utilizes one pilot signal to track the phase noise and uses compensation structure to improve the amount of self-interference cancelation. The effect of phase noise caused by separate local oscillator or the same local oscillator on self-interference cancelation is analyzed [10]. Inter carrier interference (ICI) and common phase error (CPE) caused by the phase noise is handled through estimating and compensating the phase noise, the amount of cancelation can be improved 7–10 dB in [11, 12]. The closed-form solution between the amount of cancelation and 3 dB bandwidth of phase noise is derived [13]. However, the existing methods dealing with phase noise only focus on self-interference signal but ignore the effect of phase noise on the desired signal. In this paper, a novel polarization self-interference cancelation method is proposed to cancel the effect of phase noise both on the self-interference signal and the desired signal without any prior information of the phase noise.

The polarization state (PS) of the signal is a substantive character which can be used to carry information such as time, frequency, space, and code character [14]. Polarization modulation technology have been proposed, and the oblique projection filtering is used to distinguish the desired signal from the noise [15]. The PS of the signal is decided by the amplitude ratio and phase difference. Taking advantage of the PS definition, the basic idea of this paper is that, phase noise does not affect the phase difference between the two branches but only affect the absolute phase, thus the phase noise has no effect on the PS of the signal. We have proved the theoretical feasibility in the previous work [16], and we will further consider the effect of phase noise on both self-interference and desired signal in this paper.

In this paper, the PS of the signal can be used to cancel the effect of the phase noise on the self-interference and desired signals, since it is not affected by the phase noise. The algorithm can be divided into two steps by converting the multiplicative noise to additive noise with polarization signal processing. The first step is converting the effect of phase noise on the self-interference signal to the desired signal and white noise, and using the reconstructed signal feedback from transmitter to cancel the self-interference signal. The second step is converting the effect of phase noise on the desired signal to white noise, then recovering the desired signal. Both of the two steps does not need the prior information of the phase noise. This method uses the polarization matching to receive the desired signal and improve the amount of self-interference cancelation. Theory analysis and numerical simulation show the effect of phase noise on self-interference cancelation. The amount of cancelation can be improved by 0–10 dB in condition of the different phase noise values. This paper mainly analyzes the effect of phase noise on the self-interference cancelation, other parameters like the nonlinearity of power amplifier of transmitter and receiver, I/Q (in phase and

quadrature components) imbalance, and the quantization noise of ADC (analog to digital converter) are ignored.

The rest of the paper is organized as follows. The full-duplex communication system model and signal model of polarization is presented in Sect. 2. In Sect. 3, the self-interference cancellation of two steps against phase noise based on polarization signal processing is proposed. Simulation results are presented in Sect. 4 to demonstrate the effectiveness of the proposed scheme. Finally, conclusions are captured in Sect. 5.

2 System and Signal Model

2.1 System Model

Full-duplex communication link is established between two nodes as shown in Fig. 1. A significant difference between the polarization full-duplex model and the traditional full-duplex communication model is introducing a Polarization Control Module (PCM) at the transmitter. After Code Modulation Module (CMM), the signal enters into the PCM. PCM is composed of Power Division Unit (PDU) and Phase Shifting Unit (PSU), amplitude ratio can be controlled by PDU and phase difference can be controlled by PSU. The signal can obtain a specific PS after PCM, then enters into the D/A conversion module. The up-converted signal, which is affected by phase noise, enters into the orthogonal dual polarized antenna. The orthogonal polarization antenna is adopted at receiver, thus the mixed signal is affected by phase noise when down-converted at the receiver. The effect of phase noise will be analyzed in following signal model. After the self-interference cancellation, the mixed signal enters into the Demodulation Module (DM).

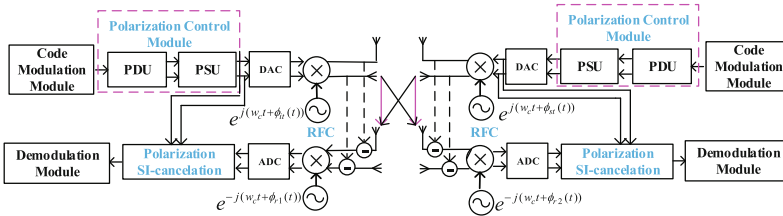


Fig. 1. Full-duplex communication system model of polarization

2.2 Signal Model

Jones vector is used to express polarization state of the signal, the polarization state of the desired signal and self-interference are $\mathbf{P}_s \in \mathbf{C}^{2 \times 1}$ and $\mathbf{P}_I \in \mathbf{C}^{2 \times 1}$ respectively, and the desired signal \mathbf{S}_t and self-interference \mathbf{I}_t are

$$\mathbf{S}_t = \mathbf{P}_s s(t) = [\cos(\varepsilon_s), \sin(\varepsilon_s) e^{j\delta_s}]^T s(t), \quad (1)$$

$$\mathbf{I}_t = \mathbf{P}_r i(t) = [\cos(\varepsilon_i) \sin(\varepsilon_i) e^{j\delta_i}]^T i(t), \quad (2)$$

where ε_s and ε_i express the polarization angles, δ_s and δ_i express the phase angles of the desired and self-interference signals respectively. $s(t)$ and $i(t)$ express the desired signal and self-interference in time domains.

$$s(t) = a(t) e^{jw_c t} e^{j\phi_{st}(t)}, \quad (3)$$

$$i(t) = b(t) e^{jw_c t} e^{j\phi_{it}(t)}, \quad (4)$$

where $a(t)$ and $b(t)$ represent the amplitude of the desired and self-interference signals respectively, and w_c is the carrier frequency. $\phi_{st}(t)$ and $\phi_{it}(t)$ represent the phase noise respectively, then the desired and self-interference signals in polarization domain are

$$\mathbf{S}_t = \begin{bmatrix} a(t) \cos(\varepsilon_s) e^{j(w_c t + \phi_{st}(t))} \\ a(t) \sin(\varepsilon_s) e^{j(w_c t + \phi_{st}(t) + \delta_s)} \end{bmatrix} = \begin{bmatrix} E_{hs} e^{jw_c t} \\ E_{vs} e^{j(w_c t + \delta_s)} \end{bmatrix} e^{j\phi_{st}(t)}, \quad (5)$$

$$\mathbf{I}_t = \begin{bmatrix} b(t) \cos(\varepsilon_i) e^{j(w_c t + \phi_{it}(t))} \\ b(t) \sin(\varepsilon_i) e^{j(w_c t + \phi_{it}(t) + \delta_i)} \end{bmatrix} = \begin{bmatrix} E_{hi} e^{jw_c t} \\ E_{vi} e^{j(w_c t + \delta_i)} \end{bmatrix} e^{j\phi_{it}(t)}, \quad (6)$$

where $E_{hs} = a(t) \cos(\varepsilon_s)$ and $E_{vs} = a(t) \sin(\varepsilon_s)$ represent the H and V branch of the desired signal, $E_{hi} = b(t) \cos(\varepsilon_i)$ and $E_{vi} = b(t) \sin(\varepsilon_i)$ represent the H and V branch of self-interference, suppose the channel satisfies Gauss distribution and the noise is additive white Gaussian noise $\mathbf{N}(t)$, and the mixed signal at the receiver.

$$\mathbf{y}(t) = \mathbf{S}_r(t) + \mathbf{I}_r(t) + \mathbf{N}(t), \quad (7)$$

$\mathbf{S}_r(t)$ and $\mathbf{I}_r(t)$ represents the desired and the interference signals at the receiver. After been down-converted, the equivalent signal at baseband can be written as

$$\mathbf{y}_L(t) = \mathbf{S}_r(t) e^{j\phi_r(t)} + \mathbf{I}_r(t) e^{j\phi_r(t)} + \mathbf{N}_L(t), \quad (8)$$

where $\phi_r(t)$ represents the phase noise caused by local oscillator at the receiver, $\mathbf{N}_L(t)$ expresses the white noise at baseband. Then Eq. (8) can be written as

$$\begin{aligned} \mathbf{y}_L(t) &= \begin{bmatrix} E_{hi} \\ E_{vi} e^{j\delta_i} \end{bmatrix} e^{j(\phi_{it}(t) + \phi_r(t))} \\ &+ \begin{bmatrix} E_{hs} \\ E_{vs} e^{j\delta_s} \end{bmatrix} e^{j(\phi_{st}(t) + \phi_r(t))} + \begin{bmatrix} N_{hL}(t) \\ N_{vL}(t) \end{bmatrix}, \end{aligned} \quad (9)$$

where the $N_{hL}(t)$ and $N_{vL}(t)$ express the H and V branch of $\mathbf{N}_L(t)$, and the two branches satisfies Gaussian distribution of random variable, $N_{hL}(t)$ and $N_{vL}(t)$ are independent and identical with mean 0 and variance is $\sigma^2/2$.

3 Two Steps Method of Self-interference Cancellation

The signal enters into the orthogonal dual-polarization antenna through the AWGN channel. Then the signal passed from the mixer down-converts to the

base band, which is affected by phase noise. The traditional algorithm is estimation and compensation [11–13], thus the estimation error of phase noise will affect the cancelation of self-interference. The proposed elimination algorithm in domain of polarization is shown in Fig. 2. This method can be achieved by converting the multiplicative noise to additive noise with polarization signal processing in two steps. The first step is converting the effect of phase noise on the self-interference to the desired signal and the white noise using stokes vector processing in polarization domain, then using the reconstructed signal to cancel the self-interference signal. The second step is recovering the desired signal using the same principle. Then the mixed signal enters into the Match Receiving module (MR), at last it enters into the Demodulation Module (DM).

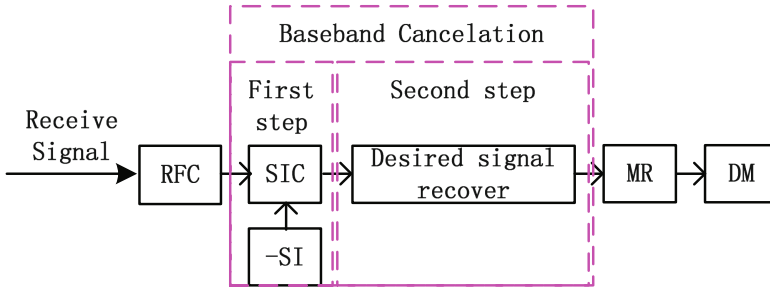


Fig. 2. The self-interference elimination algorithm

3.1 Eliminating the Effect of Phase Noise on Self-interference

After the mixed signal being down-converted, the mixed signal is expressed as Eq. (9), in which the $[N_{hL}(t) N_{vL}(t)]^T$ can be written as Eq. (10).

$$\begin{bmatrix} N_{hL}(t) \\ N_{vL}(t) \end{bmatrix} = \begin{bmatrix} n_{hc} + jn_{hs} \\ n_{vc} + jn_{vs} \end{bmatrix} \quad (10)$$

The n_{hc} and n_{hs} express the in-phase and quadrature components of $N_{hL}(t)$, the n_{vc} and n_{vs} has the similar expression. In order to analyze conveniently, the signal transformed through stokes, as expression (11).

$$\begin{aligned} S_1 &= |y_{LH}(t)|^2 - |y_{LV}(t)|^2 \\ S_2 &= 2 |y_{LH}(t)| |y_{LV}(t)| \cos(\varphi_{y_{LH}}(t) - \varphi_{y_{LV}}(t)) \\ S_3 &= 2 |y_{LH}(t)| |y_{LV}(t)| \sin(\varphi_{y_{LH}}(t) - \varphi_{y_{LV}}(t)), \end{aligned} \quad (11)$$

where S_1, S_2, S_3 express the three components of stokes. $y_{LH}(t)$ and $y_{LV}(t)$ express the H and V branch of $\mathbf{y}_L(t)$. Through (9) and (11), $\mathbf{y}_L(t)$ expressed as

$$\begin{aligned}
 S_1 = & (E_{hi}^2 - E_{vi}^2) + (E_{hs}^2 - E_{vs}^2) + (n_{hc}^2 + n_{hs}^2) - (n_{vc}^2 + n_{vs}^2) \\
 & + 2(E_{hi}E_{hs} \cos(\phi_{st}(t) - \phi_{it}(t)) - E_{vi}E_{vs} \cos(\phi_{st}(t) - \phi_{it}(t) + (\delta_s - \delta_i))) \\
 & + 2 \begin{bmatrix} E_{hs} \cos(\phi_{st}(t) - \phi_{it}(t)) + E_{hi} \\ E_{hs} \sin(\phi_{st}(t) - \phi_{it}(t)) \end{bmatrix}^T \\
 & \cdot \begin{bmatrix} \cos(\phi_{it}(t) + \phi_r(t)) & \sin(\phi_{it}(t) + \phi_r(t)) \\ -\sin(\phi_{it}(t) + \phi_r(t)) & \cos(\phi_{it}(t) + \phi_r(t)) \end{bmatrix} \begin{bmatrix} n_{hc} \\ n_{hs} \end{bmatrix} \\
 & - 2 \begin{bmatrix} E_{vs} \cos(\delta_s + \phi_{st}(t) - \phi_{it}(t)) + E_{vi} \cos(\delta_i) \\ E_{vs} \sin(\delta_s + \phi_{st}(t) - \phi_{it}(t)) + E_{vi} \sin(\delta_i) \end{bmatrix}^T \\
 & \cdot \begin{bmatrix} \cos(\phi_{it}(t) + \phi_r(t)) & \sin(\phi_{it}(t) + \phi_r(t)) \\ -\sin(\phi_{it}(t) + \phi_r(t)) & \cos(\phi_{it}(t) + \phi_r(t)) \end{bmatrix} \begin{bmatrix} n_{vc} \\ n_{vs} \end{bmatrix}, \tag{12}
 \end{aligned}$$

$$\begin{aligned}
 S_2 = & 2(E_{hs}E_{vs} \cos(\delta_s) + E_{hs}E_{vi} \cos(\phi_{st}(t) - \phi_{it}(t) - \delta_i) \\
 & + E_{hi}E_{vs} \cos(\phi_{st}(t) - \phi_{it}(t) + \delta_s) + E_{hi}E_{vi} \cos(\delta_i)) + n_{hc}n_{vc} + n_{hs}n_{vs} \\
 & + 2 \begin{bmatrix} E_{vs} \cos(\phi_{st}(t) - \phi_{it}(t) + \delta_s) + E_{vi} \cos(\delta_i) \\ E_{vs} \sin(\phi_{st}(t) - \phi_{it}(t) + \delta_s) + E_{vi} \sin(\delta_i) \end{bmatrix}^T \\
 & \cdot \begin{bmatrix} \cos(\phi_{it}(t) + \phi_r(t)) & \sin(\phi_{it}(t) + \phi_r(t)) \\ -\sin(\phi_{it}(t) + \phi_r(t)) & \cos(\phi_{it}(t) + \phi_r(t)) \end{bmatrix} \begin{bmatrix} n_{hc} \\ n_{hs} \end{bmatrix} \\
 & + 2 \begin{bmatrix} E_{hs} \cos(\phi_{st}(t) - \phi_{it}(t)) + E_{hi} \\ E_{hs} \sin(\phi_{st}(t) - \phi_{it}(t)) \end{bmatrix}^T \\
 & \cdot \begin{bmatrix} \cos(\phi_{it}(t) + \phi_r(t)) & \sin(\phi_{it}(t) + \phi_r(t)) \\ -\sin(\phi_{it}(t) + \phi_r(t)) & \cos(\phi_{it}(t) + \phi_r(t)) \end{bmatrix} \begin{bmatrix} n_{vc} \\ n_{vs} \end{bmatrix}, \tag{13}
 \end{aligned}$$

$$\begin{aligned}
 S_3 = & 2(E_{hs}E_{vs} \sin(-\delta_s) + E_{hs}E_{vi} \sin(\phi_{st}(t) - \phi_{it}(t) - \delta_i) \\
 & - E_{hi}E_{vs} \sin(\phi_{st}(t) - \phi_{it}(t) + \delta_s) - E_{hi}E_{vi} \sin(\delta_i)) + n_{hs}n_{vc} - n_{hc}n_{vs} \\
 & + 2 \begin{bmatrix} -E_{vs} \sin(\phi_{st}(t) - \phi_{it}(t) + \delta_s) - E_{vi} \sin(\delta_i) \\ E_{vs} \cos(\phi_{st}(t) - \phi_{it}(t) + \delta_s) + E_{vi} \cos(\delta_i) \end{bmatrix}^T \\
 & \cdot \begin{bmatrix} \cos(\phi_{it}(t) + \phi_r(t)) & \sin(\phi_{it}(t) + \phi_r(t)) \\ -\sin(\phi_{it}(t) + \phi_r(t)) & \cos(\phi_{it}(t) + \phi_r(t)) \end{bmatrix} \begin{bmatrix} n_{hc} \\ n_{hs} \end{bmatrix} \\
 & + 2 \begin{bmatrix} E_{hs} \sin(\phi_{st}(t) - \phi_{it}(t)) \\ -E_{hs} \cos(\phi_{st}(t) - \phi_{it}(t)) + E_{hi} \end{bmatrix}^T \\
 & \cdot \begin{bmatrix} \cos(\phi_{it}(t) + \phi_r(t)) & \sin(\phi_{it}(t) + \phi_r(t)) \\ -\sin(\phi_{it}(t) + \phi_r(t)) & \cos(\phi_{it}(t) + \phi_r(t)) \end{bmatrix} \begin{bmatrix} n_{vc} \\ n_{vs} \end{bmatrix}, \tag{14}
 \end{aligned}$$

while

$$\begin{bmatrix} n_{hc1} \\ n_{hs1} \end{bmatrix} = \begin{bmatrix} \cos(\phi_{it}(t) + \phi_r(t)) & \sin(\phi_{it}(t) + \phi_r(t)) \\ -\sin(\phi_{it}(t) + \phi_r(t)) & \cos(\phi_{it}(t) + \phi_r(t)) \end{bmatrix} \cdot \begin{bmatrix} n_{hc} \\ n_{hs} \end{bmatrix}, \tag{15}$$

$$\begin{bmatrix} n_{vc1} \\ n_{vs1} \end{bmatrix} = \begin{bmatrix} \cos(\phi_{it}(t) + \phi_r(t)) & \sin(\phi_{it}(t) + \phi_r(t)) \\ -\sin(\phi_{it}(t) + \phi_r(t)) & \cos(\phi_{it}(t) + \phi_r(t)) \end{bmatrix} \cdot \begin{bmatrix} n_{vc} \\ n_{vs} \end{bmatrix}, \tag{16}$$

$\begin{bmatrix} n_{hc1} & n_{hs1} \end{bmatrix}^T$ and $\begin{bmatrix} n_{vc1} & n_{vs1} \end{bmatrix}^T$ express the H and V branch of white noise after the first rotation. According to the rotation characteristics unitary matrix

[14], $[n_{hc1} \ n_{hs1}]^T$ and $[n_{vc1} \ n_{vs1}]^T$ have the same distribution with $[n_{hc} \ n_{hs}]^T$ and $[n_{vc} \ n_{vs}]^T$, then the $\mathbf{y}_L(\mathbf{t})$ can be calculated as

$$\mathbf{y}_L(\mathbf{t}) = \begin{bmatrix} E_{hi} \\ E_{vi}e^{j\delta_i} \end{bmatrix} + \begin{bmatrix} E_{hs} \\ E_{vs}e^{j\delta_s} \end{bmatrix} e^{j(\phi_{st}(t)-\phi_{it}(t))} + \begin{bmatrix} N_{hL1}(t) \\ N_{vL1}(t) \end{bmatrix}, \quad (17)$$

the $N_{hL1}(t) = n_{hc1} + jn_{hs1}$, $N_{vL1}(t) = n_{vc1} + jn_{vs1}$. Comparing Eqs. (9) and (17), the phase noise of self-interference is converted to the desired signal and white noise, and the distribution of white noise has not changed. In the first rotation, it is not simply multiply the $e^{-j(\phi_{it}(t)+\phi_r(t))}$ both sides of the Eq. (9). because the $\phi_{it}(t)$, $\phi_{st}(t)$, $\phi_r(t)$ is unknown. It just uses the character of phase noise in frequency domain. Therefore it is unnecessary to estimate phase noise in this paper, which is the strong aspect compared with the method in time and frequency domain. Using the canceling signal $\mathbf{y}_{cl}(\mathbf{t})$ from transmitter through wired feedback, the residual signal is Eq. (18).

$$\begin{aligned} \mathbf{y}_{LR}(\mathbf{t}) &= \mathbf{y}_L(\mathbf{t}) - \mathbf{y}_{cl}(\mathbf{t}) \\ &= \begin{bmatrix} E_{hi} \\ E_{vi}e^{j\delta_i} \end{bmatrix} + \begin{bmatrix} E_{hs} \\ E_{vs}e^{j\delta_s} \end{bmatrix} e^{j(\phi_{st}(t)-\phi_{it}(t))} + \begin{bmatrix} N_{hL1}(t) \\ N_{vL1}(t) \end{bmatrix} - \begin{bmatrix} E_{hi} \\ E_{vi}e^{j\delta_i} \end{bmatrix} \\ &= \begin{bmatrix} E_{hs} \\ E_{vs}e^{j\delta_s} \end{bmatrix} e^{j(\phi_{st}(t)-\phi_{it}(t))} + \begin{bmatrix} N_{hL1}(t) \\ N_{vL1}(t) \end{bmatrix}, \end{aligned} \quad (18)$$

where the $\mathbf{y}_{LR}(\mathbf{t})$ represents the residual signal cancelled by the first step. From Eq. (18), the self-interference is cancelled. However, the phase noise is converted to the desired signal, which will be solved in B.

3.2 Eliminating the Effect of Phase Noise on Desired Signal

Suppose:

$$\begin{bmatrix} n_{hc2} \\ n_{hs2} \end{bmatrix} = \begin{bmatrix} \cos(\phi_{st}(t) - \phi_{it}(t)) & \sin(\phi_{st}(t) - \phi_{it}(t)) \\ -\sin(\phi_{st}(t) - \phi_{it}(t)) & \cos(\phi_{st}(t) - \phi_{it}(t)) \end{bmatrix} \cdot \begin{bmatrix} n_{hc1} \\ n_{hs1} \end{bmatrix}, \quad (19)$$

$$\begin{bmatrix} n_{vc2} \\ n_{vs2} \end{bmatrix} = \begin{bmatrix} \cos(\phi_{st}(t) - \phi_{it}(t)) & \sin(\phi_{st}(t) - \phi_{it}(t)) \\ -\sin(\phi_{st}(t) - \phi_{it}(t)) & \cos(\phi_{st}(t) - \phi_{it}(t)) \end{bmatrix} \cdot \begin{bmatrix} n_{vc1} \\ n_{vs1} \end{bmatrix}, \quad (20)$$

$[n_{hc2} \ n_{hs2}]^T$ and $[n_{vc2} \ n_{vs2}]^T$ express the H and V branch of white noise after the second rotation. Using the same method as the first step, the Eq. (18) can be written as Eq. (21).

$$\mathbf{y}_{LR}(\mathbf{t}) = \begin{bmatrix} E_{hs} \\ E_{vs}e^{j\delta_s} \end{bmatrix} + \begin{bmatrix} N_{hL2}(t) \\ N_{vL2}(t) \end{bmatrix}, \quad (21)$$

In Eq. (21), the $N_{hL2}(t) = n_{hc2} + jn_{hs2}$, $N_{vL2}(t) = n_{vc2} + jn_{vs2}$. From the Eq. (21), the effect of phase noise on the desired signal is converted to white noise,

and the distribution of white noise has not changed. Then using the minimum variance criterion, we can get the polarization state of the desired signal. Then the polarization of the desired signal can be written as Eq. (22).

$$\hat{\mathbf{P}}_{\mathbf{s}} = [\cos(\varepsilon_s) \sin(\varepsilon_s) e^{j\delta_s}]^T, \quad (22)$$

$\hat{\mathbf{P}}_{\mathbf{s}}$ is the polarization of the desired signal estimated at the receiver. After the (MR), the mixed signal changed as Eq. (23).

$$\begin{aligned} \mathbf{y}_{\text{LR1}}(\mathbf{t}) &= \hat{\mathbf{P}}_{\mathbf{s1}} \cdot \mathbf{y}_{\text{LR}}(\mathbf{t}) \\ &= \begin{bmatrix} \cos(\varepsilon_s) \\ \sin(\varepsilon_s) e^{-j\delta_s} \end{bmatrix}^T \cdot \left\{ \begin{bmatrix} E_{hs} \\ E_{vs} e^{j\delta_s} \end{bmatrix} + \begin{bmatrix} N_{hL2}(t) \\ N_{vL2}(t) \end{bmatrix} \right\} \\ &= [\cos(\varepsilon_s) \sin(\varepsilon_s) e^{-j\delta_s}] \begin{bmatrix} E_{hs} \\ E_{vs} e^{j\delta_s} \end{bmatrix} + [\cos(\varepsilon_s) \sin(\varepsilon_s) e^{-j\delta_s}] \begin{bmatrix} N_{hL2}(t) \\ N_{vL2}(t) \end{bmatrix} \\ &= s(t) + n_o(t), \end{aligned} \quad (23)$$

In Eq. (23), the $\mathbf{y}_{\text{LR1}}(\mathbf{t})$ is the mixed signal after MR, $\hat{\mathbf{P}}_{\mathbf{s1}}$ is the Hermitian Transpose of $\hat{\mathbf{P}}_{\mathbf{s}}$, $n_o(t)$ is the white noise after MR.

$$n_o(t) = [\cos(\varepsilon_s) \sin(\varepsilon_s) e^{-j\delta_s}] \begin{bmatrix} N_{hL2}(t) \\ N_{vL2}(t) \end{bmatrix} \quad (24)$$

After the MR, the desired signal $s(t)$ has been recovered. From the Eq. (23), the phase noise caused by the local oscillator of transmitter and receiver is canceled. The white noise is full polarization after the MR, thus the power of white noise keeps only in half. In the meanwhile, the amount of self-interference cancelation is calculated as Eq. (25).

$$\eta_{\text{SINR}} (\text{dB}) = 10 \log \left[\frac{\text{SINR}_{\text{out}}}{\text{SINR}_{\text{in}}} \right], \quad (25)$$

η_{SINR} (dB) expresses the amount of self-interference cancelation. SINR_{in} and SINR_{out} express the ratio between the desired signal and self-interference add white noise before and after signal processing at the receiver. Then the Eq. (25) can be written as Eq. (26).

$$\eta_{\text{SINR}} (\text{dB}) = 10 \log \left[2 \left(1 + \frac{b^2(t)}{\sigma^2} \right) \right]. \quad (26)$$

Comparing the Eq. (26) and the amount of self-interference cancelation in [7, 9, 10, 12], the phase noise caused by the local oscillator of transmitter and the receiver is canceled, and the amount of self-interference cancelation is improved.

4 Simulation Scenarios, Results and Analysis

Co-simulation between MATLAB and Advanced Design System (ADS) is used to verify the performance of self-interference cancelation method proposed in this

paper. This part shows the effect of phase noise on the signal and the process of how to cancel the effect of the phase noise intuitively.

In this section, the ratio between H and V branch is set as 1, the phase difference is set as 45 in degree. The variance of phase noise is set as 0.018 in radian. The effect of phase noise on the self-interference is shown in Figs. 3 and 4. The spectrum of the self-interference without phase noise is shown in Fig. 3, then Fig. 4 shows the spectrum of self-interference effected by phase noise. By comparing Figs. 3 and 4, we can obtain that the spectrum of self-interference has been spreaded due to the phase noise. The center power value of the self-interference decreased. The total power of the signal unchanged at the same time. The effect of phase noise on the desired signal is the same as the self-interference.

The waveform of the mixed signal at the receiver in time domain is shown in Fig. 5(a). The self-interference is 90 dB higher than the desired signal. Because of

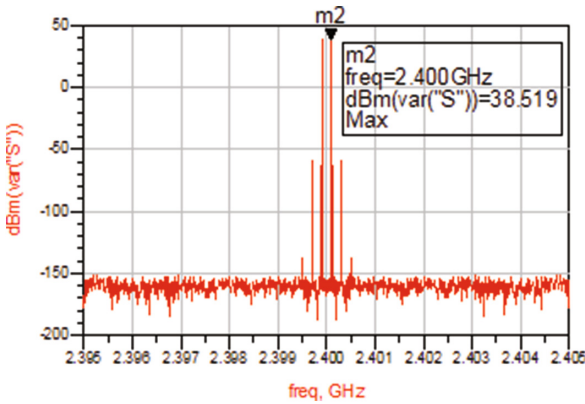


Fig. 3. The spectrum of self-interference without phase noise

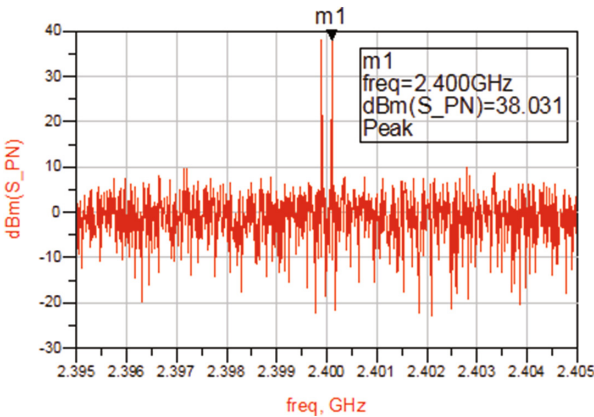


Fig. 4. The spectrum of self-interference effected by phase noise

the effect of the self-interference, phase noise and white noise, the desired signal has been distorted seriously. After the first step cancellation, the self-interference is canceled, whose phase noise is converted to the desired signal and white noise as shown in Fig. 5(b). After cancellation by the second step, the phase noise of the desired signal is converted to the white noise as shown in Fig. 5(c). After the two steps, the effect of phase noise on self-interference cancellation is canceled, and the desired signal is recovered.

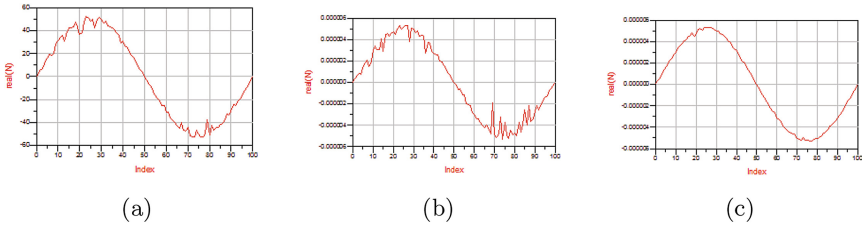


Fig. 5. Waveform of the mixed signal before cancellation (a), after the first cancellation (b), after the second cancellation (c)

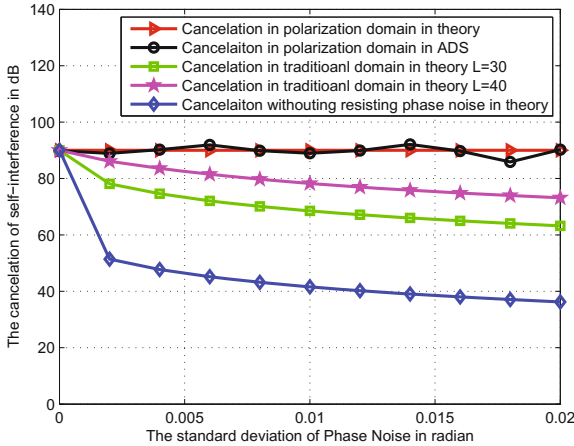


Fig. 6. The cancellation affected by phase noise (Color figure online)

Figure 6 shows the effect of phase noise on the self-interference cancellation. In Fig. 6, the abscissa expresses the standard deviation of phase noise, ordinate expresses the amount of cancellation in dB. The signal interference noise ratio (SINR) is set as 90 dB. The blue (rhombus) line expresses the relationship between the amount of self-interference cancellation and the standard deviation of phase noise without the method of suppression [7], the amount of cancellation

decreased as the power of phase noise increased. The green (rectangle) and pink (pentagram) lines express the amount of cancelation affected by phase noise after traditional self-interference elimination algorithm [11, 12]. Although the amount of cancelation increased under the condition without suppression, it decreased when the phase noise increases. The red (triangle) line expresses the amount of self-interference cancelation using the method proposed in this paper. The black (roundness) line expresses the amount of self-interference cancelation simulated in ADS. These two lines suggest that by utilizing the cancelation algorithm proposed in this paper, the amount of cancelation remained unchanged as the phase noise increased. We can conclude that the effect of phase noise on the cancelation of self-interference has been canceled by using the two steps method algorithm proposed in this paper.

5 Conclusion

Based on the unitary matrix rotation characteristics in polarization domain, the method in this paper has canceled the effect of phase noise on the self-interference cancelation and recovering of the desired signal. This method can be achieved by converting the multiplicative noise to additive noise with polarization signal processing in two steps. The first step is converting the effect of phase noise on the self-interference to the desired signal and the white noise using stokes vector processing in polarization domain, then using the reconstructed signal to cancel the self-interference signal. The second step is recovering the desired signal using the same principle. Theory analysis and numerical simulation show that effect of phase noise on self-interference cancelation is canceled, and the amount of cancelation is improved on the premise of recovering the desired signal.

References

1. Zhang, Z., Long, K., Vasilakos, A.V., Hanzo, L.: Full-duplex wireless communications: challenges, solutions, and future research directions. *Proc. IEEE* **104**, 1369–1409 (2016)
2. Everett, E., Sahai, A., Sabharwal, A.: Passive self-interference suppression for full-duplex infrastructure nodes. *IEEE Trans. Wireless Commun.* (2013, in press)
3. Debaillie, B., van den Broek, D.-J., Lavn, C., van Liempd, B., Klumperink, E.A.M., Palacios, C., Craninckx, J., Nauta, B.: Analog/RF solutions enabling compact full-duplex radios. *IEEE J. Sel. Areas Commun.* **32**(9), 1662–1673 (2014)
4. Liu, G., Yu, F.R., Ji, H., Leung, V.C.M., Li, X.: In-band full-duplex relaying for 5G cellular networks with wireless virtualization. *IEEE Netw.* **29**, 54–61 (2015)
5. Foroozanfard, E., Franek, O., Tatomirescu, A., Tsakalaki, E., de Carvalho, E., Pedersen, G.F.: Full-duplex MIMO system based on antenna cancellation technique. *Electron. Lett.* **50**(16), 1116–1117 (2014)
6. Sahai, A., Patel, G., Sabwarwal, A.: Pushing the limits of full duplex: design and real-time implementation. Rice University, Technical report REE1104 (2011)
7. Sahai, A., Patel, G., Dick, C., Sabharwal, A.: On the impact of phase noise on active cancelation in wireless full-duplex. *IEEE Trans. Veh. Technol.* **62**(9), 4494–4510 (2013)

8. Wang, J., Zhao, H., Tang, Y.: A RF adaptive least mean square algorithm for self-interference cancellation in co-frequency co-time full duplex systems. In: IEEE Symposium Transactions on Communications (2014)
9. Duarte, M., Dick, C., Sabharwal, A.: Experiment-driven characterization of full-duplex wireless systems. *IEEE Trans. Wireless Commun.* **11**(12), 4296–4307 (2012)
10. Syrjala, V., Valkama, M., Anttila, L., Riihonen, T., Korpi, D.: Analysis of oscillator phase-noise effects on self-interference cancellation in full-duplex OFDM radio transceivers. *IEEE Trans. Wireless Commun.* **13**(6), 2977–2990 (2014)
11. Syrjala, V., Yamamoto, K.: Self-interference cancellation in full-duplex radio transceivers with oscillator phase noise. In: *European Wireless* (2014)
12. Ahmed, E., Eltawil, A.M., Sabharwal, A.: Self-interference cancellation with phase noise induced ICI suppression for full-duplex systems. In: *Signal Processing for Communications Symposium, GLOBECOM* (2013)
13. Shao, S., Quan, X., Shen, Y., Tang, Y.: Effect on phase noise of digital self-interference cancellation in wireless full duplex. In: *IEEE International Conference on Acoustic, Speech and Signal Processing (ICASSP)* (2014)
14. Zhuang, Z., Xiao, S., Wang, X.: *Radar Polarization Information Processing and Application*. National Defense Industry Press, Beijing (1999)
15. Cao, B., Zhang, Q.Y., Jin, L.: Polarization division multiple access with polarization modulation for LOS wireless communications. *EURASIP J. Wireless Commun. Network.* (2011)
16. Liu, F., Jia, S., Guo, C., Feng, C.: Exploiting polarization to resist phase noise for digital self-interference cancellation in full-duplex. In: *IEEE International Conference on Communications (ICC)* (2016)
17. Benedetto, S., Poggiolin, P.: Theory of polarization shift keying modulation. *IEEE Trans. Commun.* **40**(4), 708–721 (1992)

Sparse Linear Method Based Top-N Course Recommendation System with Expert Knowledge and L_0 Regularization

Jinjiao Lin^{1,2}, Haitao Pu³, Yibin Li¹, and Jian Lian^{3(✉)}

¹ School of Control and Engineering, Shandong University, Jinan, China

² Shandong University of Finance and Economics, Jinan, China

³ Shandong University of Science and Technology, Qingdao, China
lianjianlianjian@163.com

Abstract. In this paper, we propose an approach of course recommender system for the subject of information management speciality in China. We collect the data relative to the course enrollment for specific set of students. The sparse linear method (SLIM) is introduced in our approach to generate the top-N recommendations of courses for students. Furthermore, the L_0 regularization terms were presented in our proposed optimization method based on the observation of the entries in recommendation system matrix. Expert knowledge based comparing experiments between state-of-the-art methods and our method are conducted to evaluate the performance of our method. Experimental results show that our proposed method outperforms state-of-the-art methods both in accuracy and efficiency.

Keywords: Course recommender system · Sparse linear method
Expert knowledge

1 Introduction

The emergence and rapid development of Internet have greatly affected the traditional viewpoint on choosing courses by providing detailed course information. As the number of courses conforming to the students' has tremendously increased, the above-mentioned problem has become how to determine the courses mostly suitable for the students accurately and efficiently. A plethora of methods and algorithms [2, 3, 11, 15] for course recommendation have been proposed to deal with this problem. Most of the methods designed for recommendation system can be grouped into three categories, including collaborative [1, 8], content-based [7, 14], and knowledge-based [5, 8, 17], which have been applied in different fields such as [4] proposed a collaborative filtering embedded with an artificial immune system to the course recommendation for college students. The rating from professor was exploited as ground truth to examine the results.

Inspired by the idea form [4] and the optimization framework in [9], we propose a sparse linear based method for top-N course recommendation with expert knowledge as the ground truth. This method extracts the coefficient matrix for the courses in the

recommender system from the student/course matrix by solving a regularized optimization problem. The sparseness is exploited to represent the sparse characteristics of recommendation coefficient matrix. Sparse linear method (SLIM) [9] was proposed to top-N recommender systems, which is rarely exploited in course recommender systems. Due to the characteristics of course recommendation system in Chinese University, our method focuses on the accuracy more than the efficiency. It is different from the previously proposed SLIM based methods [6, 9, 10, 18], which mainly addresses the real-time applications of top-N recommender systems. The framework of our proposed course recommender system is shown in Fig. 1.

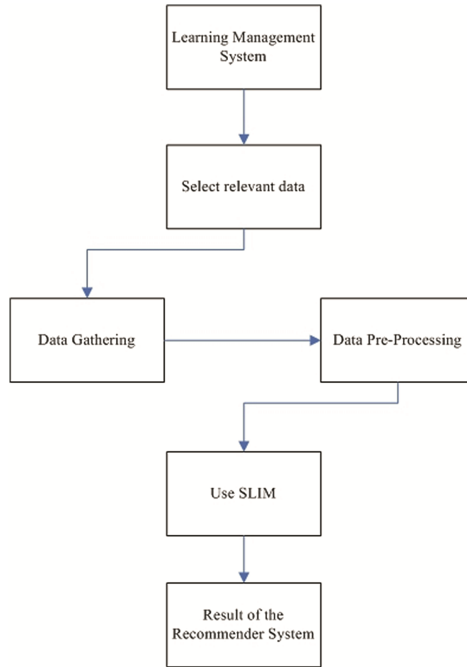


Fig. 1. The framework of our proposed course recommender system

According to our observation about common recommendation system matrix, most of the entries are assigned the same value (zero or one), and the gradients of neighboring entries also hold the same value (zero or one). Therefore, the sparse counting strategy of L_0 regularization terms [16] were included into the optimization framework of SLIM. The L_0 terms can globally constrain the non-zero values of entries and the gradients in the recommendation system matrix, which is the main contribution of our proposed method. Different from the previously proposed regularization terms (the L_1 and L_2 terms), the L_0 term can maintain the subtle relationship between the entries in recommendation system matrix.

After the process of data gathering as shown in Fig. 1, comparing experiments between state-of-the-art methods and our method are conducted. Consequently, both the

experimental results of state-of-the-art methods and our method are evaluated with the course recommendations presented by seven experts with voting strategy.

The rest of the paper is organized as follows. In Sect. 2, we describe the details of our proposed method. In Sect. 3 the dataset that we used in our experiments and the experimental results are presented. In Sect. 4 the discussion and conclusion are given.

2 Our Method

2.1 The Formation of the Method

In the following content, t_j and s_i are introduced to denote each course and each student in course recommender system, respectively. The whole student-course taken will be represented by a matrix A of size $m \times n$, in which the entry is 1 or 0 (1 denotes that the student has taken the course, 0 vice versa).

In this paper, we introduce a Sparse Linear Method (SLIM) to implement top-N course recommendation. In this approach, the score of course recommendation on each un-taken student/course item t_j of a student s_i is computed as a sparse aggregation of items that have been taken by s_i , which is shown in Eq. (1).

$$\bar{a}_{ij} = a_i^T w_j \quad (1)$$

where \bar{a} is the initial course selection of a specific student and w_j is the sparse vector of aggregation coefficients. The model of SLIM with matrix is represented as:

$$\bar{A} = AW \quad (2)$$

Where \bar{A} is the initial value of student/course matrix, A denotes the latent binary student-course item matrix, W denotes the $n \times n$ sparse matrix of aggregation coefficients, in which j -th column corresponds to w_j as in Eq. (1), and each row of $C(c_i)$ is the course recommendation scores on all courses for student s_i . The final course recommendation result of each student is completed through sorting the non-taken courses in decreasing order, and the top-N courses in the sequences are recommended.

In our method, the initial student/course matrix is extracted from the learning management system of a specific University in China. With the extracted student/course matrix of size $m \times n$, the sparse matrix W size of $n \times n$ in Eq. (2) is iteratively optimized by alternate minimization method. Different from the objective function previously proposed in [9] shown in Eq. (3), our proposed method is shown in Eq. (4).

$$\min_{w \geq 0} \frac{1}{2} \|A - AW\|_2^2 + \frac{\beta_1}{2} \|W\|_F^2 + \lambda_1 \|A\|_1 \quad (3)$$

$$\min_{w \geq 0} \frac{1}{2} \|A - AW\|_2^2 + \frac{\beta_2}{2} \|W\|_F^2 + \lambda_2 \|A\|_0 + \mu |\nabla A|_0 \quad (4)$$

Where $\|\cdot\|_F$ denotes the Frobenius norm for matrix, $\|W\|_1$ is the item-wise L_1 norm, $\|W\|_0$ denotes the entry-wise L_0 norm that stands for the number of entries with zero

value. The data term $\|A - AW\|$ is exploited to measure the difference between the calculated model and the training dataset. The $L_F - norm$, $L_1 - norm$, and $L_0 - norm$ are exploited to regularize the entries of the coefficient matrix W , A , and ∇A , respectively. The parameters β_1 , β_2 , λ_2 , and μ are used to constrain the weights of regularization terms in the objective functions.

In our proposed final objective function, the L_F norm is introduced to transfer the optimization problem into elastic net problem [19], which prevents the potential over fitting. Moreover, the L_1 norm in Eq. (3) is changed to L_0 norm in our proposed objective function. This novel norm L_0 [12, 13, 16] is introduced to constrain the sparseness of the A and ∇A .

Due to the independency of the columns in matrix W , the final objective function in Eq. (4) is decoupled into a set of objective functions as follows:

$$\min_{w_j \geq 0, w_{j,j}=0} \frac{1}{2} \|a_j - a_j w_j\|_2^2 + \frac{\beta_2}{2} \|w_j\|_F^2 + \lambda_2 \|a_j\|_0 + \mu \|\nabla a_j\|_0 \tag{5}$$

where a_j is the j -th column of matrix A , w_j denotes j -th column of matrix W . As there are two unknown variables in each Eq. (5), which is a typical ill-posed problem. Thus, this problem need to be solved by alternate minimization method. In each iteration, one of the two variables is fixed and the other variable is optimized.

2.2 The Solver of Our Proposed Method

Subproblem1: computing w_j

The w_j computation sub-problem is represented by the minimization of Eq. (6):

$$\frac{1}{2} \|a_j - a_j w_j\|_2^2 + \frac{\beta_2}{2} \|w_j\|_F^2 \tag{6}$$

Through eliminating the L_0 terms in Eq. (5), the function Eq. (6) has a global minimum, which can be computed by gradient descent. The analytical solution to Eq. (6) is shown in Eq. (7):

$$w_j = F^{-1} \left(\frac{F(a_j)}{F(a_j) + \frac{\beta_2}{2} (F(\partial_x)^* \cdot F(\partial_x) + F(\partial_y)^* \cdot F(\partial_y))} \right) \tag{7}$$

where $F(\cdot)$ and $F^{-1}(\cdot)$ denotes the Fast Fourier Transform (FFT) and reverse FFT, respectively. $F(\cdot)^*$ is the complex conjugate of $F(\cdot)$.

Sub-problem 2: computing a_j and ∇a_j

With the intermediate outcome of w_j , the a_j and ∇a_j can be computed by Eq. (8):

$$\frac{1}{2}\|a_j - a_j w_j\|_2^2 + \lambda_2 \|a_j\|_0 + \mu \|\nabla a_j\|_0 \quad (8)$$

By introducing two auxiliary variables h and v corresponding to the column vector a_j and ∇a_j . The sub-problem can be transformed into Eq. (9):

$$\frac{1}{2}\|a_j - a_j w_j\|_2^2 + \lambda_2 \|a_j - h\|_2^2 + \mu \|\nabla a_j - v\|_2^2 + \lambda (\|h\|_0 + \|v\|_0) \quad (9)$$

To testify the performance of our proposed method, comparing experiments between state-of-the-art methods and our method are carried out with gathered dataset and expert knowledge. In the following section, the experiments are described in detail.

3 Experimental Results

3.1 Datasets

In order to testify the performance of our proposed method and implement the method in practical scenarios, we gather the data from five classes of information management specialty for the learning management system of our University. The data records of the

Table 1. The initial dataset from the five classes

No.	SPSS	CH	Eng	LA	PT	DB	CC	PE	C	Acc	CS
1	1	1	1	0	1	0	1	1	0	1	0
2	0	1	1	0	1	0	1	1	1	1	0
3	0	1	1	0	1	1	0	1	0	1	0
4	0	1	1	0	1	1	0	1	1	1	0
5	1	1	1	1	1	0	0	1	1	1	0
6	1	1	1	1	1	0	0	1	1	1	1
7	0	1	1	1	1	0	0	1	1	1	1
8	1	1	1	1	1	1	0	1	0	1	1
9	1	1	1	0	1	1	1	1	0	1	0
10	1	1	1	0	1	1	1	1	0	1	0
11	0	1	1	0	1	0	1	1	0	1	0
12	0	1	1	0	1	1	0	1	0	1	1
13	0	1	1	1	1	0	1	1	0	1	1
14	1	1	1	1	1	1	1	1	0	1	1
15	1	1	1	1	1	1	1	1	0	1	1
16	0	1	1	0	1	1	1	1	0	1	1
17	1	1	1	1	1	1	1	1	0	1	1
18	0	1	1	1	1	0	1	1	0	1	0
19	1	1	1	0	1	1	1	1	0	1	0
20	0	1	1	1	1	0	1	1	0	1	1

courses and students were extracted from the Department of Management Information System, Shandong University of Finance and Economics and the Department of Electronic Engineering Information Technology at Shandong University of Sci&Tech. The most important information of the courses and students is mainly about the grades corresponding to the courses. All of the students from the information management specialty are freshmen in our University. Most of them have taken the courses of the first year in their curriculum except three students have failed to go up to the next grade. Thus, firstly we eliminate the records of the three students. Meanwhile, we collect the knowledge including the programming skill that they have mastered through a questionnaire. The courses that they have taken and the content that have grasped are combined in the final dataset. A part of the dataset is shown in Table 1, where 1 denotes that the s_i student has mastered the t_j course, and 0 denotes the opposite.

After gathering the data of the students from the five classes, comparing experiments between state-of-the-art methods and our method are conducted. We choose several state-of-the-art methods including collaborative filtering methods itemkNN, userkNN, and the matrix factorization methods PureSVD.

3.2 Measurement

The knowledge from several experts on the courses in information management specialty are adopted as ground truth in the experimental process. To measure the performance of the comparing methods, we introduce the Hit Rate (HR) and the Average Reciprocal Hit-Rank (ARHR) in the experiments, which are defined as shown in Eqs. (11) and (12).

$$HR = \frac{\#hits}{\#students} \quad (11)$$

where $\#hits$ denotes the number of students whose course in the testing set is recommended by the expert, too. $\#students$ denotes the number of all students in the dataset.

$$ARHR = \frac{1}{\#students} \sum_{i=1}^{\#hits} \frac{1}{p_i} \quad (12)$$

Where p_i is the ordered recommendation list.

3.3 Experimental Results

In this section, the experimental results calculated from the practical dataset. Table 2 shows the experimental results of the comparing methods in top-N course recommendation.

Table 2. The performance of the comparing methods

Methods	HR_1	$ARHR_1$	HR_2	$ARHR_2$	HR_3	$ARHR_3$	HR_4	$ARHR_4$	HR_5	$ARHR_5$
itemkN	0.18	0.13	0.19	0.14	0.20	0.13	0.18	0.13	0.19	0.14
N										
Itemprob	0.21	0.15	0.19	0.16	0.21	0.14	0.19	0.12	0.17	0.13
PureSVD	0.09	0.11	0.10	0.12	0.12	0.12	0.17	0.14	0.18	0.15
SLIM	0.24	0.16	0.17	0.18	0.24	0.19	0.16	0.14	0.17	0.15
ours	0.27	0.17	0.19	0.17	0.25	0.18	0.20	0.14	0.19	0.15

Where $HR_i, ARHR_i$ denotes the performance for $class_i$, respectively. The experimental results shown in Table 2 demonstrate that our proposed method outperforms state-of-the-art methods in most of course recommendations both in the HR and ARHR. It shows that the sparse regularization term based on the prior knowledge from the observation in our method are suitable for solving the problem of course recommendation.

In order to illustrate the performance of our proposed method according to the number of courses and topics included in the experimental testing. It shows in Fig. 2 that a higher accuracy is obtained when the number of courses increases. Meanwhile, the courses included in our experiments are divided into 32 different topics, Fig. 3 shows that the accuracy is also higher when there are more relative courses.

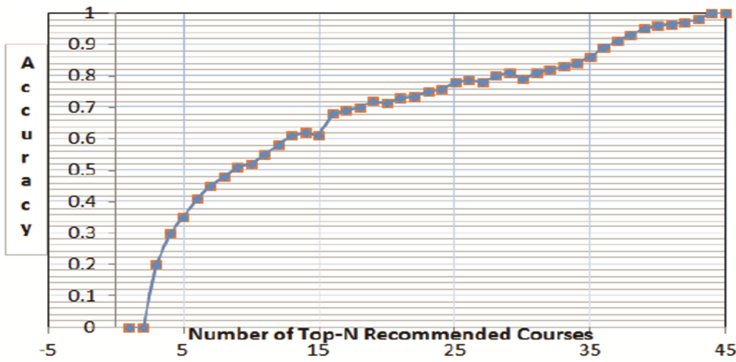


Fig. 2. Accuracy of our proposed recommendation system method due to the number of courses

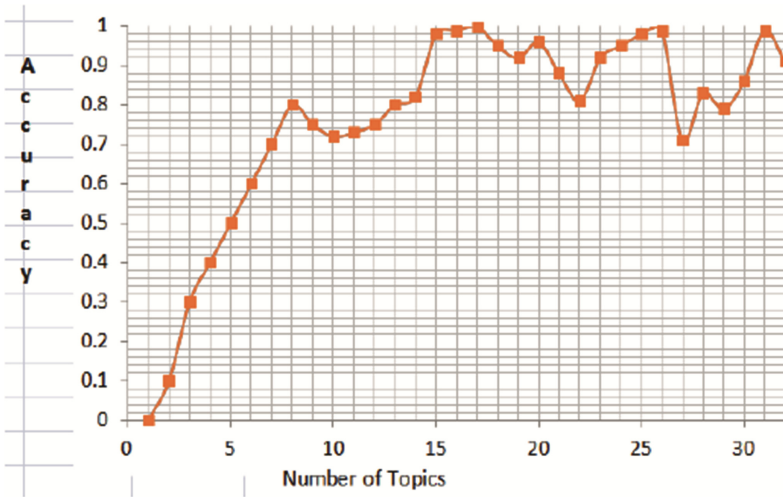


Fig. 3. Accuracy of our proposed recommendation system method due to the number of topics

4 Conclusion

In this paper, we propose an approach of course recommendation. In our method, the SLIM was introduced and a novel L_0 regularization term was exploited in SLIM. Meanwhile, the alternate minimization strategy is exploited to optimize the outcome of our method. To testify the performance of our method, comparing experiments on students from five different classes between state-of-the-art methods and our method are conducted. The experimental results show that our method outperforms the other previously proposed methods.

The proposed method was be mainly used to implement the course recommendation for the Universities in China. However, it also can b exploited in other relative fields. In the future, more applications of our approach would be investigated. Other future work includes the modification of the objective function in our method including the other regularization terms and different optimization strategy.

Acknowledgments. This work was financially supported by the Teaching Reform Research Project of Undergraduate Colleges and Universities of Shandong Province (2015M111, 2015M110, Z2016Z036) and the Teaching Reform Research Project of Shandong University of Finance and Economics (2891470), Teaching Reform Research Project of Undergraduate Colleges and Universities of Shandong Province (2015M136), SDUST Young Teachers Teaching Talent Training Plan (BJRC20160509); SDUST Excellent Teaching Team Construction Plan; Teaching research project of Shandong University of Science and Technology (JG201509 and qx2013286); Shandong Province Science and Technology Major Project (No. 2015ZDX X0801A02).

Disclosures. The authors declare no conflict of interest. The founding sponsors had no role in the design of the study; in the collection, analyses, or interpretation of data; in the writing of the manuscript, and in the decision to publish the results.

References

1. Ahn, H.: Utilizing popularity characteristics for product recommendation. *Int. J. Electron. Commer.* **11**(2), 59–80 (2006)
2. Albadaerah, A., Alsakran, J.: An automated recommender system for course selection. *Int. J. Adv. Comput. Sci. Appl.* **7**(3) (2016)
3. Aher, S.B., Lobo, L.M.R.J.: A comparative study of association rule algorithms for course recommender system in e-learning. *Int. J. Comput. Appl.* **39**(1), 48–52 (2012)
4. Chang, P., Lin, C., Chen, M.: A hybrid course recommendation system by integrating collaborative filtering and artificial immune systems. *Algorithms* **9**(3), 47 (2016)
5. Chen, Y., Cheng, L., Chuang, C.: A group recommendation system with consideration of interactions among group members. *Expert Syst. Appl.* **34**(3), 2082–2090 (2008)
6. Christakopoulou, E., Karypis, G.: HOSLIM: higher-order sparse linear method for top- N recommender systems. In: Tseng, V.S., Ho, T.B., Zhou, Z.-H., Chen, A.L.P., Kao, H.-Y. (eds.) PAKDD 2014. LNCS (LNAI), vol. 8444, pp. 38–49. Springer, Cham (2014). https://doi.org/10.1007/978-3-319-06605-9_4
7. Kim, E., Kim, M., Ryu, J.: Collaborative filtering based on neural networks using similarity. In: Wang, J., Liao, X.-F., Yi, Z. (eds.) ISNN 2005. LNCS, vol. 3498, pp. 355–360. Springer, Heidelberg (2005). https://doi.org/10.1007/11427469_57
8. McLaughlin, M., Herlocker, J.L.: A collaborative filtering algorithm and evaluation metric that accurately model the user experience, pp. 329–336 (2004)
9. Ning, X., Karypis, G.: SLIM: sparse linear methods for top- n recommender systems, pp. 497–506 (2011)
10. Ning, X., Karypis, G.: Sparse linear methods with side information for top- n recommendations, pp. 155–162 (2012)
11. Omahony, M.P., Smyth, B.: A recommender system for on-line course enrolment: an initial study, pp. 133–136 (2007)
12. Pan, J., Hu, Z., Su, Z., Yang, M.: Deblurring text images via L₀-regularized intensity and gradient prior, pp. 2901–2908 (2014)
13. Pan, J., Lim, J., Su, Z., Yang, M.H.: L₀-regularized object representation for visual tracking. In: Proceedings of the British Machine Vision Conference. BMVA Press (2014)
14. Philip, S., Shola, P.B., John, A.O.: Application of content-based approach in research paper recommendation system for a digital library. *Int. J. Adv. Comput. Sci. Appl.* **5**(10) (2014)
15. Sunil, L., Saini, D.K.: Design of a recommender system for web based learning, pp. 363–368 (2013)
16. Xu, L., Lu, C., Xu, Y., Jia, J.: Image smoothing via L₀ gradient minimization. In: International Conference on Computer Graphics and Interactive Techniques, vol. 30, No. 6 (2011). 174
17. Yap, G., Tan, A., Pang, H.: Dynamically-optimized context in recommender systems, pp. 265–272 (2005)
18. Zheng, Y., Mobasher, B., Burke, R.: CSLIM: contextual slim recommendation algorithms, pp. 301–304 (2014)
19. Zou, H., Hastie, T.: Regularization and variable selection via the elastic net. *J. Roy. Stat. Soc. Ser. B-Stat. Methodol.* **67**(2), 301–332 (2005)

The Research on the Container Truck Scheduling Based on Fuzzy Control and Ant Colony Algorithm

Meng Yu, Dawei Li^(✉), and Qiang Wang

School of Logistics Engineering, Wuhan University of Technology, Wuhan, China
ymmona@126.com, 1054386503@qq.com

Abstract. This paper studies a Container Trucks (CTs) dynamic dispatching strategy in which multiple tasks are matched with multiple CTs and proposes Multi-Agent contract net protocols based on two-way negotiation mechanism. It could assign optimal tasks to CTs through tendering, bidding and contracting of tasks. Fuzzy set theory and method is adopted to couple multiple factors on the tasks to assess to their dispatching emergency degree in the process. One of the factors is the distance from the current position of CT to the loading/unloading position. Through judging obstruction status by using related data of the GPRS system, the steps of ant colony algorithm are designed to find the predicted travel distance of the optimal route. After fuzzification and defuzzification in MATLAB, the decision query table of dispatching plan is obtained. Finally, a case study is given to describe the scheduling scheme in detail.

Keywords: Container truck dynamic scheduling · Multi- agent system
Fuzzy control · Ant colony algorithm · Path optimization

1 Introduction

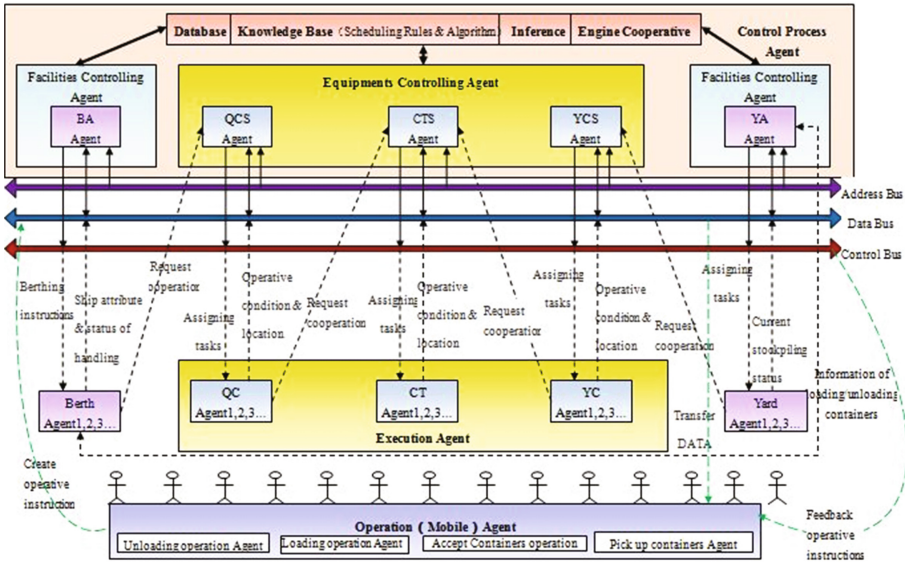
The loading/unloading equipment at most container terminals in China are mainly Quay Cranes (QCs), Yard Cranes (YCs) and CTs. The scheduling system of CTs is well known to possess complex logistics system characteristics for there are many factors effecting scheduling, such as time, space, resources, and uncertain factors. Optimize the scheduling system is meaningful, which can improve the efficiency of loading and unloading.

The physical entity resource network and the control decision-making information network were integrated into the modeling and optimization architecture using Harvard architecture and Agent based computing [1, 2]. In [3], Relationship between transport tasks and service of CTS has been taken as a contract net using the fuzzy set theory and method. The dispatching model based on Contract Network Protocol (CNP) using bidirectional negotiation is provided and fuzzy reasoning process of dispatching decisions is suggested. But the distance from the current position of CT to the loading/unloading position is calculated by the established coordinate system. In the case of road congestion, CT should choose a smooth route, so the distance should be the length of the route. Recently, the path planning problem is a hot research area [4, 5], the main algorithms used are genetic algorithm, ant colony algorithm and so on.

This paper proposes Multi-Agent contract net protocols based on two-way negotiation mechanism. The fuzzy control system is designed to couple multiple factors on the tasks to assess to their dispatching emergency degree. The steps of ant colony algorithm considering obstruction status were designed to find the optimal route. After fuzzification and defuzzification, the decision query table of dispatching plan is obtained.

2 MAS Framework of Container Terminal Scheduling

Container terminal consists of containers, ships, handling equipment (QC, YC, and CT) communication equipment, berths, container yards and human resource, etc. Superior and subordinate subsystems have command and obedience relationships, and parallel subsystems have collaboration, consultation, competitive relationships. Figure 1 shows the hierarchical structure of the whole system.



BA-Berth Assigning; QCS-Quay Cranes Scheduling; CTS-Container Trucks Scheduling; YCS-Yard Cranes Scheduling; YA- Yard Allocating

Fig. 1. Framework of container terminal schedule system based on Multi-Agent

As we can see, there are three types of individual agents, namely Control Agent (fixed), Execution Agent (moving with wireless mobile terminal) and Operation (Mobile) Agent (dynamically generated).

Operation Agents are created dynamically and freely by the Central Processing Agent throughout the whole system just like computer software, and they are assigned by the Control Agent, executed by the Execution Agent.

3 Dynamic Dispatching Strategy

In the traditional static scheduling mode, the truck is unloaded at half of the distance. A dynamic dispatching strategy in which multiple tasks are matched with multiple CTs is adapted in this study, which can guarantee the truck in the idle state can be quickly put into the operation point which needs trucks. So how to arrange a truck for the task should be considered. In this paper, considering the load of communication and consultation efficiency in system, Multi-Agent contract net protocols based on two-way negotiation mechanism was adopted to achieve the best arrangement. Figure 2 shows the contract net.

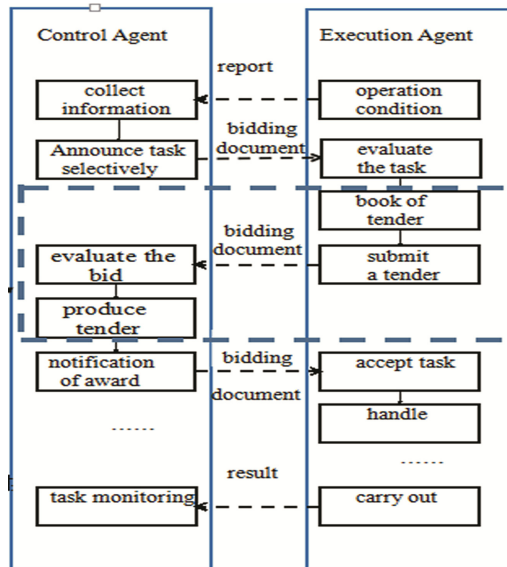


Fig. 2. Contract net

In the contract negotiation protocol Agent network, different types of equipment in collaboration between the task request and response with announcing, bidding, and awarding in contract net. In evaluating tender, fuzzy set theory and method is adopted to couple multiple factors on the tasks to assess to their dispatching emergency degree. The higher evaluation of dispatching emergency is, the greater probability to select the CT is.

4 Fuzzy Set Theory and Method

The structure of fuzzy reasoning controller is shown in Fig. 3. Here are the two inputs, namely, predicted travel distance, priority of handling operation. The output is dispatching emergency degree. Dispatching decision knowledge set consists of n subset, $R_1, R_2, \dots R_n$. Each subset contains some knowledge of dispatching decision, which is described in a matrix form according to certain rules. The input information is given according to bidding document and database of Agents. The meaning or interpretation of the function module is based on the input linguistic variables to determine its value corresponding fuzzy sets A_1, A_2 ; Effect of fuzzy reasoning is to use and expertise subset $R_1, R_2, \dots R_n$, and the information of synthesis module A to obtain comprehensive information on the fuzzy relation composition operations in order to generate output result. The result is also indicated by fuzzy sets. Linguistic matching function with the fuzzy decision module is translate the result into output language, or the result of this reasoning is converted to exact amount of that task dispatching emergency degree, to which Agents can refer to bid.

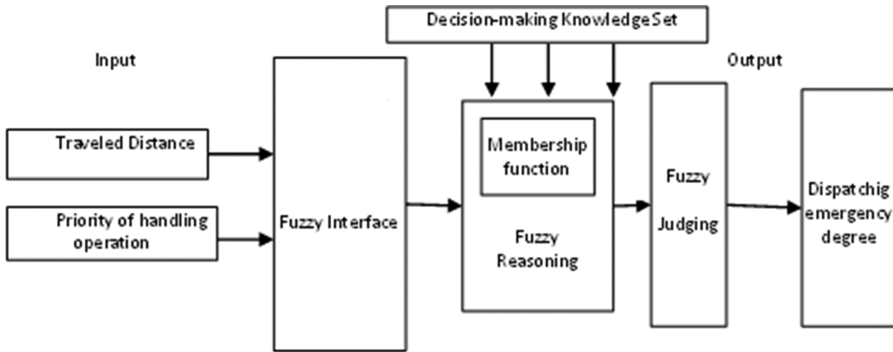


Fig. 3. Modal of fuzzy assessment for distributing tasks

Heavy weights and the closed space on the dock make the truck more likely to be involved in traffic crash which leads to road congestion. So the travel time and distance from the current position of CT to the loading/unloading position cannot just calculated according to the shortest route. Through judging obstruction status, the steps of ant colony algorithm were designed to find the optimal route. Then the predicted travel distance and time can be calculated.

4.1 The Ant Colony Algorithm Design for the Optimal Route of Container Truck Definition and Control of Congestion

Definition and Control of Congestion. Traffic flow model is a kind of math equation to express the correlation of traffic parameters like speed, density and flux etc. Obstruction status can be judged according to related data gathered by GPRS. Take the spur track $i \rightarrow j$ for instance.

$$u_{ij} = u_{ijf} (1 - k_{ij}/k_{ij0})$$

$$q_{ij} = k_{ij} u_{ij}$$

- u_{ij} : The vehicle speed
 u_{ijf} : The free driving speed
 k_{ij} : The vehicle density
 k_{ij0} : The jam density
 q_{ij} : The traffic flux

Suppose the average minimum distance headway at the port of congestion density as h_{ijs} , and average minimum time headway as h_{ijt} , then

$$k_{ij0} = 1000/h_{ijs}$$

$$q_{ijm} = 3600/h_{ijt}; k_{ijm} = k_{ij0}/2$$

$$u_{ijm} = q_{ijm}/k_{ijm}$$

- q_{ijm} : The maximum traffic capability
 k_{ijm} : The corresponding density
 u_{ijm} : Critical speed of the congestion

The judging procedure about the congestion for the spur track is as follows:

- Step 1: If $q_{ij} > q_{ijm}$, then switch to step 3, otherwise, switch to step 2.
 Step 2: If $u_{ij} < u_{ijf}$, then switch to step 3.
 Step 3: The spur track is under congestion, and the jam knots are recorded in the congestion table Ck .

Confirming Principle of Allowed Knot Set *allowedk*. Considering the reality of dock, the container is abstracted into some grids. The dynamic control over the change of ants position comes to be true through modifying Relation Matrices by utilizing coordinate to confirm the direct pre-knot or sub-knot.

The allowed knot set *allowedk* equals n minus Ck and Pk at knot i for ant number k , in which n is the total number of knots and Pk is the knots passed by ant k . There is no repetition at the same knot for the consequent knots considering the traffic rules of container terminals.

The Steps of Ant Colony Algorithm of Optimal Route for Container Trucks.

- Step 1: Initialization. To set up a starting point and ending point and set the maximum number of cycles $Nmax$. To initialize the control parameters α , β , Q (user-defined). At the initial, m ants are randomly put on n nodes and the amount of information on each path is equal. The data gathered by GPRS for every spur track are: u_{ij} , h_{ijs} , h_{ijt} , q_{ij} .

Step 2: Put the initial knot of ant k into Pk to search till find target knot. If does, end the loop, and turn to step 3. If doesn't find the target knot, determine $allowed_k$ and work out the transfer probability p_{ij}^k , then adjust knot and keep searching.

The transfer probability from knot i to j of ant k can be defined as:

$$p_{ij}^k = \begin{cases} \frac{\tau_{ij}^\alpha \eta_{ij}^\beta}{\sum_{s \in allowed_k} \tau_{is}^\alpha \eta_{is}^\beta}, & s \in allowed_k \\ 0, & else \end{cases}$$

Step 3: End a loop iteration when the last ant find the target knot and record the length Lk .

Step 4: Update the pheromone intensity

If the arrival time is between t and $t + I$, the pheromone intensity is to be updated according to the following formula:

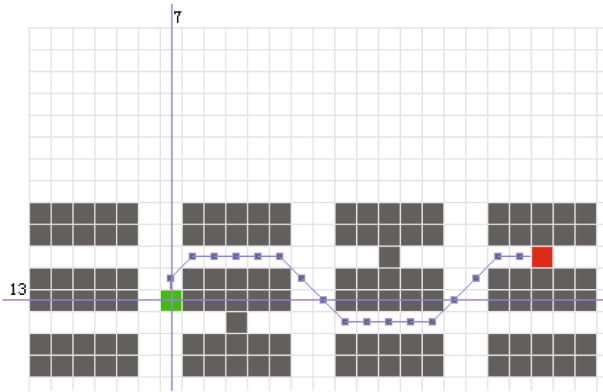
$$\begin{aligned} \tau_{ij}(t + 1) &= \rho \tau_{ij}(t) + \Delta \tau_{ij} \\ \Delta \tau_{ij} &= \sum_{k=1}^m \Delta \tau_{ij}^k \\ \Delta \tau_{ij}^k &= \begin{cases} \frac{Q}{Lk} & \text{if } e(i, j) \in T_k(t) \\ 0 & else \end{cases} \end{aligned}$$

Q is a constant denoting the pheromone intensity. Lk is the gross route length covered in repetition by the ant number k . ρ symbolizes the left-over elements of pheromone, and ρ ought to be defined as a number less than 1 in order to avoid the endless accumulating of pheromone.

Step 5: To compare all the routes passed by the ants and the minimum route length is the optimal route. To output the result, the algorithm is to be ceased.

Case Analysis. The optimal route and the shortest route are shown in Figs. 4 and 5, respectively.

The speed of the spur tracks which are under the congestion is 10 km/h, and the speed of other spur tracks are 25 km/h. The length of each grid in the map is 50 m, and the oblique line is simplified into two straight segments. The travel time and distance between the current position of CT to the loading/unloading position are calculated. The distance and time of the optimal route is respectively 1.25 km, 0.05 h, and the shortest route respectively 0.95 km, 0.06 h. The application of ant colony algorithm can help to search out the optimal route while the route is under the congestion. The study of optimal route is helpful in instructing the running of container trucks so as to avoid or relieve traffic congestion.



■: The starting point; ■: The ending point; ■: The container;

Fig. 4. Chart of the optimal route

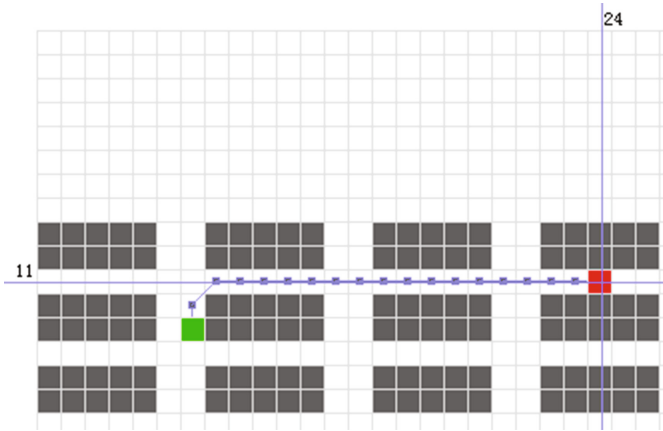


Fig. 5. Chart of the shortest route

4.2 Fuzzification

Fuzzification of Distance. Table 1 shows container truck steer distance partition.

Table 1. Container truck steer distance partition

Class	1	2	3	4	5	6	7	8
R	(0, 100]	(100, 300]	(300, 500]	(500, 700]	(700, 900]	(900, 1200]	(1200, 1500]	>1500

R represents distance. According to the actual situation, the distance is segregated into 8 grade: 1, 2, 3, 4, 5, 6, 7, 8. The fuzzy linguistic value is defined as very near, near, nearer, general, far, farther, very far, extremely far, and the corresponding fuzzy set is N1, N2, N3, N, R3, R2, R1, VR. According to the distribution of discrete points, the triangular membership function is adopted for its convenience.

Fuzzification of Priority of Handling Operation. Suppose P as the artificially defined priority, N as the number of arranged CTs, and L as the priority of handling operation.

$$L = P - N$$

The fuzzy linguistic value is defined as unimportant, a little important, important, very important and extremely important, and the corresponding fuzzy set is P1, P2, P3, P4, VP.

Fuzzification of Dispatching Emergency Degree. Suppose S as dispatching emergency degree. The fuzzy linguistic value is defined as very low, lower, low, general, high, higher, very high, and the corresponding fuzzy set is D1, D2, D3, M, M2, M1, VM.

Determination of Fuzzy Rules. Scheduling principle:

- (1) Dispatcher’s assignment is preferential;
- (2) The important task has priority;
- (3) The close distance is preferential;
- (4) The requirements of QCs are preferential.

The experience of terminal scheduling engineers and operators is summarized, so that the fuzzy rules can maximally reflect the actual scheduling principle of terminal. Table 2 shows the rule table for fuzzy control.

Table 2. Rule table for fuzzy control

S	N1	N2	N3	N	R3	R2	R1	VR
P1	D2	D2	D2	D2	D2	D1	D1	D1
P2	D3	D3	D3	D3	D2	D2	D1	D1
P3	M2	M	M	M	D3	D3	D2	D2
P4	M1	M2	M2	M2	M	M	D3	D2
VP	VM	M1	M1	M2	M2	M	M	D3

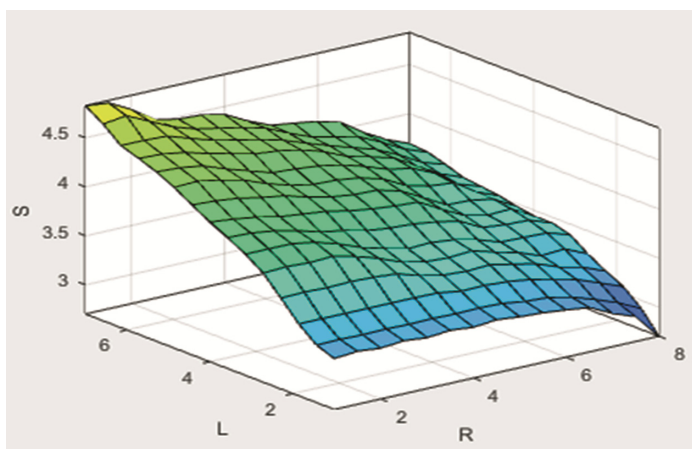
Fuzzy Inference and Defuzzification. Method of centroid is used in this system. Clear outputs corresponding to each of the input values are calculated through MATLAB tool. Table 3 shows the decision query table.

In practical work, the terminal management system can directly query the table for the dispatching emergency degree.

Table 3. Decision query table

S	1	2	3	4	5	6	7	8
1	3.22	3.22	3.22	3.22	3.22	3.18	3.04	2.7
2	3.5	3.5	3.5	3.48	3.43	3.39	3.27	3.1
3	3.9	3.9	3.81	3.65	3.59	3.53	3.43	3.35
4	4.13	4.07	4	3.92	3.87	3.72	3.56	3.44
5	4.38	4.34	4.19	4.08	4.03	3.85	3.78	3.52
6	4.54	4.51	4.39	4.31	4.14	4.01	3.81	3.59
7	4.83	4.68	4.48	4.42	4.2	4.13	3.91	3.69

Figure 6 shows the relationship between R, L and S in MATLAB.

**Fig. 6.** System output result schematic

The two axis represents the input of the system (L, R), and the vertical axis represents the output (S). It can be seen from this figure that S increases with the decrease of L and R. Space surface is smooth, illustrating the design of membership functions and fuzzy rules are basically correct.

5 Case Analysis

There are four operations requested, shown in Table 4, and three idle CT, shown in Table 5. After CT dispatching Agent announce the four tasks, three free CT Agents gain task dispatching emergency degree by fuzzy reasoning controller, shown in Tables 6, 7 and 8.

Table 4. The information of cooperative request for transporting

Task serial number	Request equipment number	Task priority	Loading container number
1	QC105	5	CHPU2306280
2	QC111	4	SNBU476253
3	YC203	4	U4688360
4	YC208	3	AM2U4166740

Table 5. The information of idle CTs

CT number	Operating state
CT301	idle
CT311	idle
CT312	idle

Table 6. Task dispatching emergency degree evaluated by agent of CT301

CT number	Request equipment number	Task priority	Distance	Task dispatching emergency degree
CT301	QC105	5	300	4.34
CT301	QC111	4	900	3.87
CT301	YC203	4	950	3.72
CT301	Y208	3	1250	3.43

Table 7. Task dispatching emergency degree evaluated by agent of CT311

CT number	Request equipment number	Task priority	Distance	Task dispatching emergency degree
CT311	QC105	5	850	4.03
CT311	QC111	4	850	3.87
CT311	YC203	4	950	3.72
CT311	YC208	3	650	3.65

Table 8. Task dispatching emergency degree evaluated by agent of CT312

CT number	Request equipment number	Task priority	Distance	Task dispatching emergency degree
CT312	QC105	5	700	4.08
CT312	YC208	3	100	3.9
CT312	YC203	4	700	3.87
CT312	QC111	4	1100	3.72

Three CT Agents bid to QC105 whose emergency degree is the highest. CT dispatching Agent evaluates these bidders, shown in Table 9. As the table shown,

evaluated dispatching emergency degree of CT301 is the highest (shown in Table 9), CT dispatching Agent rewards Agent of CT301 and meanwhile refuses to application of CT311 and CT312.

Table 9. Task dispatching emergency degree sort of QC105

Request equipment number	CT number	Task important degree	Distance	Task dispatching emergency degree
QC105	CT301	5	300	4.34
QC105	CT312	5	700	4.08
QC105	CT311	5	850	4.03

Then CT311 and CT312 select tasks to bid, whose dispatching assessed value of emergency is the highest among the remaining, namely QC111 and YC208. CT dispatching Agent respectively issue orders to CT311 and CT312 after evaluating.

6 Conclusion

A model of container terminal scheduling system was established based on Multi-Agent and how to dispatch Container Trucks (CTs) in dynamic dispatching strategy was studied. Relationship between transport tasks and service of CTs has been taken as a contract net using the fuzzy theory and method of optimum allocation of multiple tasks to multiple CTs, and the bidirectional negotiation mechanism was adopted. It coupled multiple factors on the tasks to get the assessment score of dispatching emergency. Through judging obstruction status by using related data of the GPRS system, the steps of ant colony algorithm were designed to calculate the distance of the optimal route. Further research is necessary to study on the method considering more practical factors before it can be applied in practice and the optimization of algorithm.

Acknowledgements. This paper has been funded by the National Natural Science Foundation of China (No. 71672137 and No. 61503291).

References

1. Li, B., Li, W.: Container terminal logistics systems collaborative scheduling based on multi-agent systems. *Comput. Integr. Manuf. Syst.* **17**, 2502–2513 (2011)
2. Li, B., Li, W., Zhang, Y.: Agent-based modeling and simulation for vehicle dispatching at container terminals. *J. Syst. Simul.* **20**(19), 5158–5161 (2008)
3. Meng, Y., Shaomei, W.: Study on scheduling system based on multi-agent of container terminal. In: *Proceedings 2006 10th International Conference on Computer Supported Cooperative Work in Design*, Nanjing, China, pp. 579–584 (2006)
4. Li, G.R., Yang, D.B., Ren, D.W.: Path optimization algorithm of dynamic scheduling for container truck. *Jiaotong Yunshu Gongcheng Xuebao* **12**(3), 86–91 (2012)
5. Cao, Q., Zhao, F.: Port trucks route optimization based on GA-ACO. *Syst. Eng. Theor. Pract.* **33**(7), 1820–1828 (2013)

Researches on the Analysis Framework of Application Layer Communication Protocol Based on SQLite

Wenyuan Xu¹, Hao Li¹, and Weifeng Xu^{2(✉)}

¹ China Shipbuilding Industry Systems Engineering Research Institute, Beijing, China
xwy0987@sina.com

² School of Control and Computer Engineering, North China Electric Power University,
Hebei, China
weifengxu@163.com

Abstract. Since the concept of mobile Internet, big data and cloud computing has been proposed, the format of the information undergoes a tremendous change, information gradually appear problems in large quantities, the complexity and the data form is not fixed. This is not a small impact and challenge to the traditional fixed form protocol analysis. Dynamic processing and analysis of data is very important for the data processing flexibility, easy scalability and better fault tolerance. Dynamic is mainly reflected in the dynamics of dynamic definition, dynamic analysis and dynamic processing. In the dynamic analysis of the data, you don't need to set the specific format of the data in the program, only the framework of dynamic analysis need to be constructed in the sending and receiving programs, the programs can read the format of data automatically, and get the content of data easily. This approach can make the program more suitable for the current application in size and flexibility than the traditional form of a fixed communication protocol analysis. Redundant structures does not need to add into the programs, which is no longer processing data passively. Data transmission becomes more convenient, because the data format needn't to be taken care when the administrator wants to transfer the data.

Keywords: SQLite · Communication protocol · Dynamic analysis
Message buffer

1 Instruction

At present, the format of messages transmitted between application processes on different terminal systems is mostly defined in programs, and it can't be changed when users transmit messages with application processes, the flexibility of dynamically define message format is lacked [1]. Once a user modified the message format, changes to the format of messages in code layer by program developers would be required, and part of communication procedure of application would need to be retested, this process will consume a lot of manpower and material resources [5]. The format of the information undergoes a tremendous change, information gradually appear problems in large quantities, the complexity and the data form is not fixed. This is not a small impact and challenge to the traditional fixed

form protocol analysis. Dynamic processing and analysis of data is very important for the data processing flexibility, easy scalability and better fault tolerance.

The analysis framework of application layer communication protocol based on SQLite [6], which is proposed in this paper, presents the format of message defined in the program in the form of database table, users can configure the table flexibly according to needs, and dynamically analyze it when in using. The whole framework contains protocol development process, dynamic object generation process, protocol analysis process, message combination sending process, message receiving process, data stored procedure, communication process. Dynamic is mainly reflected in the dynamic definition of communication protocol, dynamic analysis and dynamic processing. In the dynamic analysis of the data, you don't need to set the specific format of the data in the program, only the framework of dynamic analysis need to be constructed in the sending and receiving programs, the programs can read the format of data automatically, and get the content of data easily. This approach can make the program more suitable for the current application in size and flexibility than the traditional form of a fixed communication protocol analysis. Redundant structures does not need to add into the programs, which is no longer processing data passively. Data transmission becomes more convenient, because the data format needn't to be taken care when the administrator wants to transfer the data.

In view of the SQLite memory database belongs to the lightweight database, with superiorities such as less resource consumption, portability, security, reliability, zero management costs and so on, we will use the SQLite memory data as the base carrier to implement the message format storage and high-speed information buffer in this paper.

2 SQLite Database Technology

SQLite memory database is an embedded database engine. Specifically suitable for appropriate data access on a variety of equipment with limited resources (such as mobile phones, pads and other intelligent devices) [3, 7]. It follows the ACID relational database management system, its design goal is embedded, and now has been applied in many embedded products, and its source code is abundant on the official website. SQLite memory database takes up very few resources, the memory is only occupied in the order of 100 k bytes in the embedded device [8]. It can be supported by mainstream desktop operating systems like Windows/Linux/Unix and all the mobile operating system platforms, and can be combined with plenty of programming languages, such as C#, C/C+, PHP, Java and ODBC interface, and it is faster than MySQL and PostgreSQL, which are two of the world famous open source database management systems [4]. The SQLite supports the most of the SQL92 syntax, and allows developers to use SQL statements to manipulate data in the database, and the SQLite is just a file, that doesn't need to be installed or started the server processes as databases like Oracle and MySQL. It has the following characteristics:

- (1) Lightweight: The SQLite is a built-in database, all the database operations can be completed by it with a dynamic library.
- (2) Portability: The SQLite can be run in a variety of environments, we can see from the source code provided by the official website, not only the desktop side, but also the mobile side is covered by the mainstream platform.

- (3) Security and Reliability: When a certain data need to be accessed by multiple processes simultaneously, data in the database can be read but cannot be written at the same time by these processes, which ensures the reliability of the data.
- (4) Green software: Another feature of SQLite is green: its core engine doesn't rely on any third-party software, and installation does not be required. So a lot of trouble can be saved at the time of deployment.
- (5) Easy to manage: The various data information in SQLite involve graphics, tables and other files are isolated from each other, to ensure the mutual interference would not take place, and also facilitate the operations on the database.

3 Overall Structure of the Application Layer Communication Protocol Analysis Framework

3.1 Architecture Design of Analysis Framework

Figure 1 shows the architecture design of the application layer communication protocol analysis framework. In this framework, the definition between the sender and receiver is very vague, so we do not deliberately distinguish the sender or receiver.

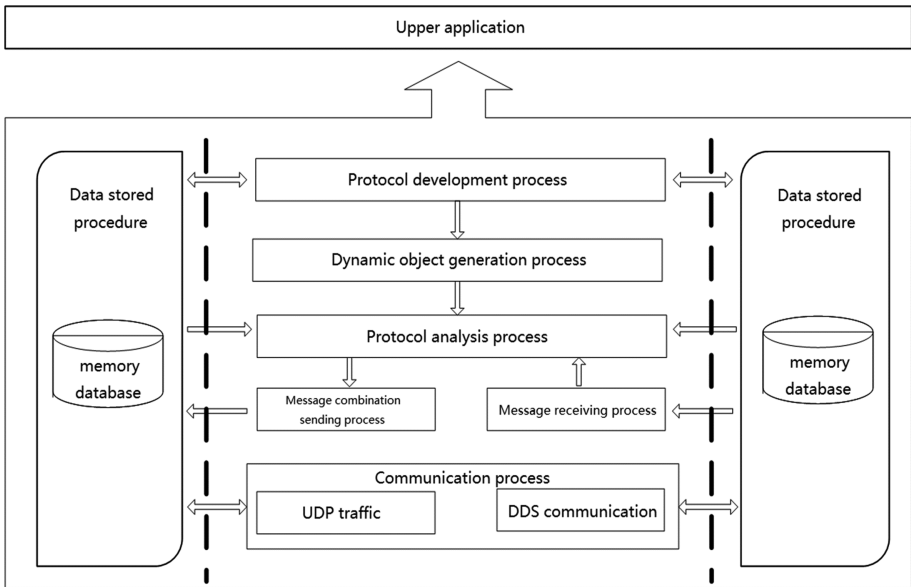


Fig. 1. Overall structure of the application layer communication protocol analysis framework

Firstly the framework provides the user with a data table that can be created and modified, and this table stipulates the format in which the protocol is created. The protocol can be analyzed by software after it has been created, that is, getting into the protocol analysis process. During the protocol analysis process, the object of each

attribute in the protocol is generated by starting the dynamic object generation process. The message combination sending process should be started if the simulation software needed to send data after the protocol has been analyzed.

During the message sending process, the UDP or DDS [2] interface in communication process will not be called directly for data transmission, but starts the data stored procedure firstly, stores the data to be sent into the memory database, and then throw a specific message to the communication process, which initiates the send function after receiving this message, retrieves the data to be sent from the memory database and sends it to the destination. If a message sent by the external software is received by the communication process of the simulation software, this message would not be analyzed but the raw string should be stored in the memory database firstly after the UDP or DDS communication interface receives the information, and then a specific message should be thrown by protocol analysis process which retrieves the raw string data from the memory database and initiates the protocol analysis function to complete the analysis of the message after receiving it. In the analysis process, message is associated with the specific agreement according to the information identification, and finally completes the analysis of information according to the protocol. The data which have been analyzed would be stored in the memory database again after the analysis process, and then a specific message should be sent to inform the business application layer to complete the corresponding business functions, such as display, calculation and so on.

3.2 Communication Process Based on Framework

The basic communication process of the software based on framework implementation has been shown in Fig. 2. As can be seen from the figure, both the data sending and

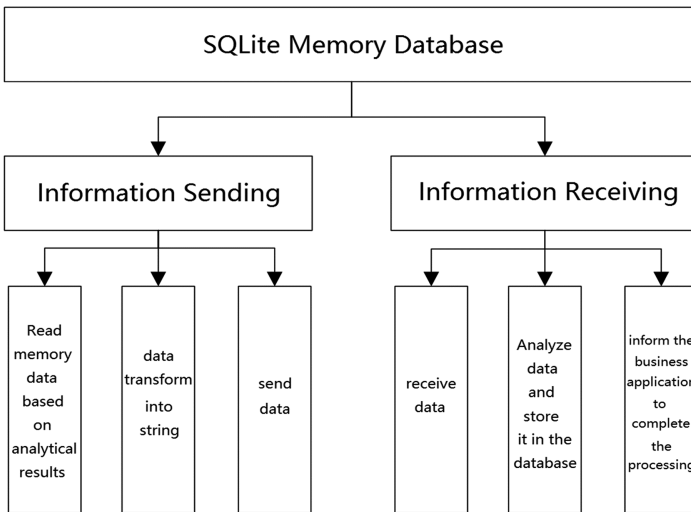


Fig. 2. Information sending and receiving process

receiving is centered on SQLite memory database. Taking memory data as the center is an another important feature of the framework proposed in this paper.

4 Analysis Method of Application Layer Communication Protocol

4.1 Protocol Configuration Process

In the analysis method of application layer communication protocol, information is configured according to the information format, and the received information is identified to accomplish the analysis of the received information and the formatted storage of the information, and the analysis method has the function of calling the business application in real time through the service manage center. Users configured by the communication protocol can configure through the configuration files dynamically, the real-time information and business application scheduling relationship users can also configure dynamically through the configuration file.

The purpose of configuring the information protocol is that the information protocol can be dynamically configured by the software developer. The framework can analyze the received information according to the identity of the configuration pair and the message after the information protocol is configured in database. The configuration of the information protocol is configured by the developers of the simulation software. The configuration is as follows:

(1) Information index configuration

Database name: Config.db

Database path: main_project_directory\Bin\Win32\Config

Database table: MessageDictionary

When configuring the information protocol, the basic information in the information index table should be configured at first. As shown in Table 1, RecNo in the configuration table is the information number automatically generated by database; ID is the protocol number (not repeatable); Name is the information protocol name; and ReMark is the information protocol description.

(2) Information protocol configuration

Database name: StructMessage.db

Database path: main_project_directory\Bin\Win32\Config

Database table: MessageDictionary

Table 1. An example of the protocol configuration

ID	EName	Srartindex	Byte count	Type
1	InFoN	0	16	Char[]
2	InFoId	16	1	Char[]
3	ShipGauge	24	4	FLOAT
4	WindSpeek	28	4	FLOAT
5	WindCourse	32	4	DOUBLE

Each information establishes a protocol configuration table which is named by the name of the information protocol (name of the Name item) in the MessageDictionary table.

As shown in Table 1, RecNo in the configuration table is the protocol field number automatically generated by database; ID is the field number in the protocol (not repeatable); EnName is the English name of field; startIndex is the number of the first byte of the field in the entire protocol, the byte of protocol is numbered from “0”; ByteCount is a count of bytes occupied by the field; Type is the field type; Rule is an additional processing instructions of the field; and ReMark is the field description.

4.2 Protocol Analysis Implementation

- (1) Dynamic generation of the object:

```
ClassCreator::ClassCreator(constchar *cName, CreateClass cc)
{
    static std::map<std::string, CreateClass> s_classMap;
    pMap = &s_classMap;
    map<std::string, CreateClass>::iterator it = pMap->(className);
    if (it == pMap->end())
    {(*pMap)[className] = cc;}
}
```

This code is a dynamic generation of the object, and the object needs to be generated before dynamically analyzing in order to call the analysis process.

- (2) Process of dynamic analysis

```
bool CStructMessage::ParseMessage(unsigned char* pBuf)
{
    for(int i = 0; i < m_StructMessageVec. size(); i++)
    {m_StructMessageVec[i]->SetValue(pBuf);}
    return true;
}
```

Through using a for-loop on valid data in the database, this code analyzes each segment of data into an available value, and combines this values into a valid string for transmission in the next step.

5 Message Buffer Design

The whole system is divided into three modules by function in order to implement the message buffer: first, Socket communication module, the module is mainly used to accept and transmit messages which require to be buffered, such as string, structure, etc.; second, SQLite message access module, the module is to access messages, which need to be buffered, in the SQLite database; third, the forwarding module of Windows message mechanism, the module generates a message reminder in the process and then distributes it; The overall structure is shown in Fig. 3.

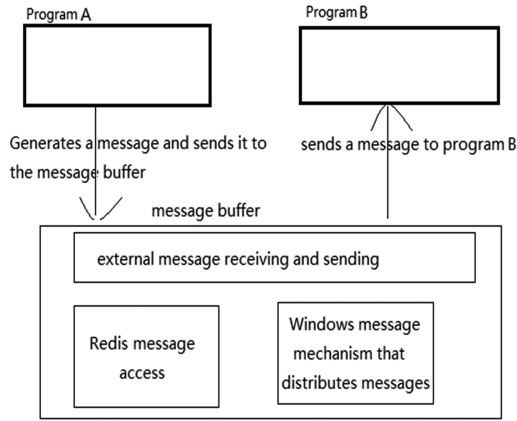


Fig. 3. Structure of the message buffer

In the implementation of the message buffer, communicating between programs is needed, so the Socket network communication technique has been used. Messages are transmitted through the sockets between the program A and the message buffer. Sockets programming can be used in three ways, streaming socket (SOCK_STREAM), datagram socket (SOCK_DGRAM), raw socket (SOCK_RAW); this program is designed based on UDP socket programming uses streaming sockets. The following describes the specific implementation of the program: The programming steps of the sender of program A: 1, Load the socket library, and create the socket (WSAStartup()/socket()); 2, send the connect request to the receiver of buffer (connect()); 3, communicate to the receiver of the message buffer (send()/recv()); 4, close the socket, and close the loaded socket library (closesocket()/WSACleanup()).

When the message has been received by the message buffer through the socket, it will be stored in the SQLite database according to the type, the stored messages has different types, so the SQLite message storage operations are not same, too. Step 1: load/release the Winsock library; Step 2: connect to the SQLite; Step 3: different storage operations are performed according to different message types.

When the message has been stored in the SQLite database, the system will send message reminder to different windows based on the different types of messages, which involves the windows message mechanism and dialog window design with MFC, and this will be introduced in next two sections. Messages will be processed by MFC window after the window receives a message reminder, but due to the limitation of design, the message processing in this experiment is simply simulated, which selects messages from SQLite database and displays them to the MFC Edit controls.

6 Conclusions

The analysis framework of application layer communication protocol based on SQLite, which is proposed in this paper, presents the format of message defined in the program

in the form of database table, users can configure the table flexibly according to needs, and dynamically analyze it when in using.

The framework that is proposed in this paper can make the program more suitable for the current application in size and flexibility than the traditional form of a fixed communication protocol analysis. Based on the framework we proposed, redundant structures does not need to add into the programs, which is no longer processing data passively. Data transmission becomes more convenient, because the data format needn't to be taken care when the administrator wants to transfer the data.

However, this paper only uses one type of database, SQLite, and only implements one kind of communication mode, UDP, so that the application scope of this framework is still limited. In the future work, increasing the type of database and expanding the communication model will be an important way to develop this framework.

References

1. Harrison, T., Pyarali, I.: An object behavioral pattern for demultiplexing and dispatching handlers for asynchronous events. In: 4th Pattern Languages of Programming Conference in Allerton Park, Illinois, 2–5 September 1997 (1997)
2. An, K., Gokhale, A.: A cloud-enabled coordination service for internet-scale OMG DDS applications. In: Proceedings of the 8th ACM International Conference on Distributed Event-Based Systems, New York (2014)
3. Hunt, P., Konar, M., Junqueira, F.P., Reed, B.: ZooKeeper: wait-free coordination for internet-scalesystems. In: Proceedings of the 2010 USENIX Conference on USENIX Annual Technical Conference, vol. 8, p. 11 (2010)
4. Li, M., Ye, F., Kim, M., Chen, H., Lei, H.: A scalable and elastic publish/subscribe service. In: 2011 IEEE International Parallel and Distributed Processing Symposium (IPDPS), pp. 1254–1265 (2011)
5. Mei, H., Shen, J.-R.: Progress of research on software architecture. *J. Softw.* **17**(06), 1257–1275 (2006)
6. Lin, M.: Design and Implementation of a Personal Address Book Management System Based on SQLite. Jilin University (2015)
7. Tong, S.: Study on Application of Mobile Meter Reading Technology Based on SQLite. Jilin University (2015)
8. Yang, X.: Design and Implementation of Beidou Navigation System Based on SQLite Database. Lanzhou University (2015)

The Implementation of Growth Guidance Factor Diffusion via Octree Spatial Structures for Neuronal Systems Simulation

Almaz Sabitov, Fail Gafarov, Vlada Kugurakova^(✉), and Vitaly Abramov

Kazan Federal University, Kazan, Russian Federation
lina211090@gmail.com, fgafarov1977@gmail.com,
vlada.kugurakova@gmail.com, ivitazour@gmail.com

Abstract. The BioDynaMo project was created in CERN OpenLab V and aims to become a general platform for computer simulations for biological research. Important development stage was the code modernization by changing the architecture in a way to utilize multiple levels of parallelism offered by today's hardware. Individual neurons are implemented as spherical (for the soma) and cylindrical (for neurites) elements that have appropriate mechanical properties. The extracellular space is discretized, and allows for the diffusion of extracellular signaling molecules, as well as the physical interactions of the many developing neurons. This paper describes methods of the real-time growing brain dynamics simulation for BioDynaMo project, a specially the implementation of growth guidance factor diffusion via octree spatial structures.

Keywords: Biodynamo · Growth guidance factor · Diffusion · Octree
Octree spatial structures · Neuronal systems simulation

1 Introduction

The BioDynaMo project [2] aims at a general platform for computer simulations for biological research. It is collaboration between CERN, Newcastle university, Innopolis university and Kazan state university where all sides take possible part in the project according their professional skills. The main idea of the project was to close the gap between very specialized applications and highly scalable systems to give life scientists access to the rapidly growing computational resource [1]. Since the scientific investigations require extensive computer resources, this platform should be executable on hybrid cloud computing systems, allowing for the efficient use of state-of-the-art computing technology.

First development stage was the code modernization based by neurodevelopmental simulation software Cortex3D [15] transforming the application from Java to C++ and changing the architecture in a way to utilize multiple levels of parallelism offered by today's hardware.

In the current state of the project distributed teams working on first iteration: developing spatial organization layer [7] using *Octree Encoding* with simulation of neuronal growing and extracellular diffusion and visualisation of these processes.

These tools designed for modeling the development of large realistic neural networks like as the neocortex, in a physical 3D space. Neurons arise by the replication and migration of precursors that mature into cells that can expand axons and dendrites. Individual neurons are represented through spherical (for the soma) and cylindrical (for neurites) elements that have appropriate mechanical properties. The growth functions of each neuron are encapsulated in set of predefined modules that are automatically distributed across its segments during growth. The extracellular space is also discretized, and allows for the diffusion of extracellular signaling molecules, as well as the physical interactions of all developing neurons.

Typical approaches for space discretization include logically structured grids, block structured and overlapping grids, unstructured grids, and octrees. Structured (regular) grids are relatively easy to implement, have low memory requirements but limited adaptivity, whereas unstructured grids can conform to complex geometries and enable non-uniform discretization.

Unstructured grids also have the overhead by explicitly storing element-node connectivity information and in general being cache inefficient because of random access. Regular grids are easy to generate but can be quite expensive when the solution of the PDE problem is highly localized, and localized solutions can be executed more efficiently using unstructured grids. Octrees [12] offer us a good balance between adaptivity and good performance. They are more flexible than regular grids, the overhead of constructing element-to-node connectivity information is lower than in unstructured grids, and they allow calculations without the use of matrix's.

In this work we focus on reducing the time to build data octree structures, memory overhead and time to perform numerical solution of diffusion equation using these data structures.

2 Octree Data Structure

An octree is a tree data structure that is used for spatial decomposition in which every node (*octant*) has maximum eight children (see, Fig. 1). They are analogous to binary trees (maximum 2 children per node) in 1D and quadtrees (maximum 4 children per node) in 2D. The only octant with no parents is the *root*, and an octant with no children is called a *leaf*. An octant with one or more children is called an *interior octant*, octants with the same parents called *siblings*. *Complete* octrees are octrees in which every interior octant has exactly eight children. The depth of an octant from the root is referred to as its *level*. Octrees can be effectively used to partition cuboid regions, and these regions are referred to as the domain of the tree. Geometric modeling technique called *Octree Encoding* firstly was presented in [10] at 1981.

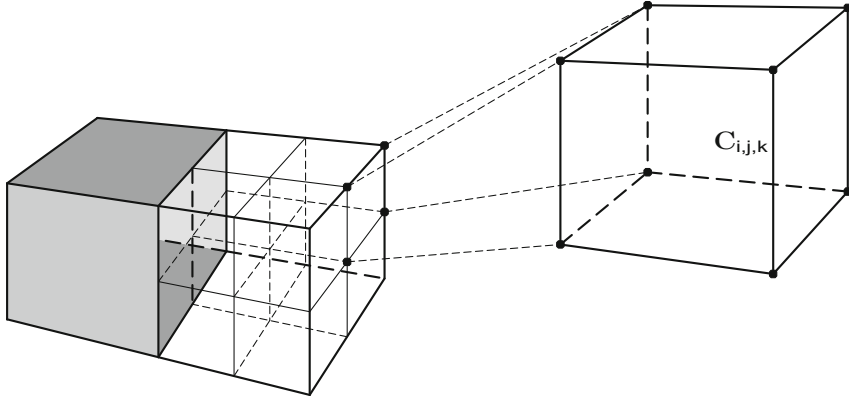


Fig. 1. *Left:* One large cell neighboring 8 smaller cells. The c_i represent the x components of the intermediate concentration c defined at the cell faces. *Right:* Zoom of one computational cell. The concentration components are defined on the cell faces, while the pressure is defined at the center of the cell.

3 Diffusion Simulation Using an Octree

Diffusible extracellular signaling molecules plays important role in developing neuronal systems. They are synthesized in by different sources in neuronal tissue and reach their target due to diffusion process. These signals can be further combined and modulated by processing of the molecule both directly at the cell surface and by the mechanisms of intracellular signaling which are activated [4]. Simulating the diffusion of growth guidance factors in the 3D model space is a difficult problem, and computationally expensive [9, 14]. To keep diffusion computationally tractable, the diffusion space must be quantized at a resolution that somehow matches the precision required by the cellular detection mechanisms, cellular density, etc. Various physical and biological processes are modeled using parabolic equations. The finite element method is a popular technique for solving parabolic partial differential equations (PDEs) numerically. Finite element methods requires grid generation to generate function approximation spaces.

The concentration $c_i = c_i(\mathbf{r}_j - \mathbf{r}_i, t)$ of growth guidance factor at the point \mathbf{r}_j in the moment t depends on the concentration of growth guidance factor released by i -th cell located at the point \mathbf{r}_i . The concentration obeys standard diffusion equation

$$\frac{\partial c_i}{\partial t} - D^2 \Delta_d c_i + k c_i = J_i(\mathbf{r}_j, t). \quad (1)$$

Here D^2 – the diffusion coefficient, k is the degradation coefficient, Δ_d is the Laplace operator in 3D space, and the quantity $J_i(\mathbf{r}_j, t)$ means the source [6].

Figure 1 illustrates unrestricted octree data structure (see e.g. [12]) with a standard grid arrangement [8]. This is convenient since interpolations are more difficult with cell centered data (see e.g. [13]). Coarsening is performed from the smaller cells to the larger

cells, i.e. from the leaves to the root. This procedure shown by algorithmic pseudo-code (see, Algorithm 1).

```

Data: Octree data structure.
Result: Diffusion process.
1 // Produce Substances Step, where  $J$  – produce coefficient is unique for
  different substances.
2 for  $\forall$  Source do
3   |  $Concentration \leftarrow +J_{Source}$ 
4   | if  $Concentration > 1$  then
5   |   |  $Concentration \leftarrow 1$ 
6   |   end
7   end
8 // Diffusion Step, where  $D^2$  is the diffusion coefficient.
9 for  $\forall$  Octree.Leaf do
10  |  $Concentration \leftarrow +\frac{1}{6}D^2 \times (Neighbor - Current)$ 
11 end
12 // Decay Step, where  $k$  is the degradation coefficient.
13 for  $\forall$  Octree.Leaf do
14  |  $Concentration \leftarrow \times(1 - k)$ 
15 end
    
```

Algorithm 1: Pseudo-code for *produce substances*, *diffusion* and *decay* steps of simulation using **octree**.

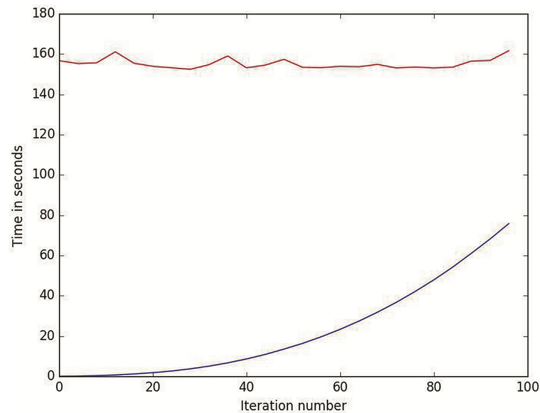


Fig. 2. The dependence of diffusion step solving time on number of octree nodes: The red line – regular grid, blue line – octree structure.

4 Results

We simulated the diffusion process with 100,000 nodes for a regular grid and using octree spatial structures. Figure 2 demonstrates the time dependence of diffusion problem solution from number of octree nodes. Comparing the results of these two modes, one can observe the efficiency of using octree on large number of nodes. By using octree spatial structures we get a significant reduction in computation time.

In Fig. 3 shows the results of simulation as a contour plot of substance concentration for system containing two sources. The the 2D snapshots are shown for 4 time moments. The diffusion process is implemented realistically what can be seen in the Fig. 3.

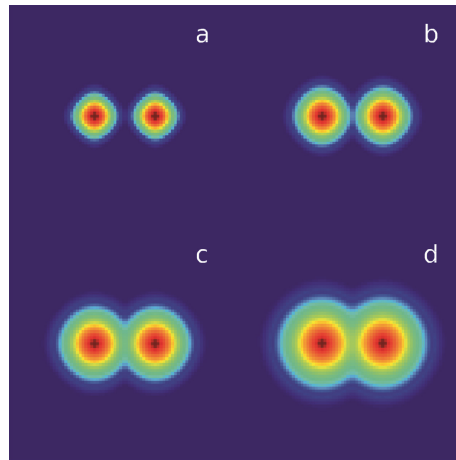


Fig. 3. Visualisation of the diffusion process of two sources for 4 different iterations a) 15, b) 26, c) 41, d) 70.

5 Conclusion

In computational physics, there has been plenty of work using either multilevel grids or adaptive mesh refinement to improve the computational efficiency.

Quadtree or octree-based adaptive refinement have also proposed in [3, 5, 11]. An octree-based algorithm for diffusion process simulation, developed in this work, is used for modeling growth and development in neural networks [15]. This method adaptively subdivides the whole simulation volume into multiple subregions using an octree. Each leaf node in the octree also holds a uniform subgrid which is the basic unit for simulation. A novel node subdivision and merging scheme is developed to dynamically adjust the octree during each iteration of the simulation.

Further development of the project involves the development of octree algorithms to perform in the cloud using parallel computations. The next stage in the development of diffusion of substances will be devoted to the realization of existing algorithms by using methods of parallel calculations.

Acknowledgements. This work was funded by the subsidy of the Russian Government to support the Program of competitive growth of Kazan Federal University among world class academic centers and universities.

References

1. BioDynaMo. Code Repository on GitHub. <https://github.com/BioDynaMo/biodynamo/>
2. Breitwieser, L., Bauer, R., Di Meglio, A., Johard, L., Kaiser, M., Manca, M., Mazzara, M., Rademakers, F., Talanov, M.: The biodynamo project: creating a platform for large-scale reproducible biological simulations. In: CEUR Workshop Proceedings, vol. 1686 (2016)
3. Charlton, E.P., Powell, K.G.: An octree solution to conservation-laws over arbitrary regions (oscar). In: 35th Aerospace Sciences Meeting and Exhibit (1997)
4. Chilton, J.K.: Molecular mechanisms of axon guidance. *Dev. Biol.* **292**(1), 13–24 (2006)
5. Coirier, W.J.: An adaptively-refined, cartesian, cell-based scheme for the euler and navier-stokes equations (1994)
6. Crank, J.: *The Mathematics of Diffusion*, 2nd edn. Clarendon Press, Oxford (1975)
7. Dmitrenok, I., Drobnyy, V., Johard, L., Mazzara, M.: Evaluation of spatial trees for simulation of biological tissue. CoRR, abs/1611.03358 (2016)
8. Harlow, F.H., Welch, J.E.: Numerical calculation of time-dependent viscous incompressible flow of fluid with free surface. *Phys. Fluids* **8**(12), 2182–2189 (1965)
9. Hentschel, H.G., van Ooyen, A.: Models of axon guidance and bundling during development. *Proc. Biol. Sci.* **266**(1434), 2231–2238 (1999)
10. Meagher, D.: Geometric modeling using octree encoding. *Comput. Graph. Process.* **19**(2), 129–147 (1982)
11. Melton, J.E., Enomoto, F.Y., Berger, M.J.: 3D automatic cartesian grid generation for euler flows. In: 11th Computational Fluid Dynamics Conference 1993, pp. 959–969 (1993)
12. Samet, H.: *The Design and Analysis of Spatial Data Structures*. Addison-Wesley, Massachusetts (1990)
13. Strain, J.: Fast tree-based redistancing for level set computations. *J. Comput. Phys.* **152**(2), 664–686 (1999)
14. Suleymanov, Y., Gafarov, F., Khusnutdinov, N.: Modeling of interstitial branching of axonal networks. *J. Integr. Neurosci.* **12**(01), 103–116 (2013)
15. Zubler, F., Douglas, R.: A framework for modeling the growth and development of neurons and networks. *Front. Comput. Neurosci.* **3**, 25 (2009)

Intelligent Perceptive QoS Based Centralized Admission Control for Route Computing

Xuejing Li^(✉), Yajuan Qin, Haohui Fu, Zhewei Zhang, and Xiaorong Lin

School of Electronic and Information Engineering, Beijing Jiaotong University,
Beijing 100044, China
15111045@bjtu.edu.cn

Abstract. For the diversity of applications and traffic, the requirement of Quality of Service (QoS) is various. In order to improve utilization of resource, performance of the network and experience of users, the QoS aware routing approaches have been researched. As the Software Defined Networking (SDN) emerging and the machine learning developing, this paper proposes a mechanism based on flow classification and routing strategy selection. This architecture is running as modules on SDN controller. In Mininet platform, we conducted experiments on POX controller to verify effective of our design and test the performance. The measuring results show that throughput and delay of the network is distinct while using different routing theory.

Keywords: Demand perception · Flow classification · Route computing
Strategy controlling · Dynamic updating

1 Introduction

For the rapid development trend, high bandwidth and low delay requirements are major challenges with the emergence of new techniques like mobile communication and 5G. Since the network traffic is increasing due to a wider spectrum of new applications, it is important to address the essential trade-off problem of appropriate allocation of restrict network resources and relatively efficient routing computing method. The QoS demands required by different applications are diversity, and there are various flows existed in same application. In addition, even in the similar types of applications there exists some different QoS demand flows. For instance, real-time multimedia applications usually require high QoS demands on bandwidth and delay but are tolerant to packet loss rate, while the high definition video streaming and the online competitive gaming have high data rate need and strict latency guarantee respectively. Furthermore, in the scenario of multimedia delivered network, there are diverse specific types of flows such as, video, audio, imaging, etc.

Custom route of path decision should be made for each flow according to its QoS requirements and network conditions, which is conducive to the suitable assignment of limited network resource. On the one hand, if every flow selects the shortest path greedily, it would bring about local congestion so that the subsequent coming packets may be dropped. On the other hand, more packets could be accepted with balancing

network traffic although it may consume excessive resource and derive long propagation delay. Therefore, the routing theory needs to be customized for some special flows according to the perception of QoS requirements and the detection of network conditions in union, which is conducive to optimal QoS guarantee and network resource orchestration [1, 2].

Moreover, there is no one algorithm can outperform all the remaining ones in every case, while there are always some scenarios where an algorithm performs well. However, the QoS aware theory makes the routing algorithm even more complex considering with classifying various flows to match dynamic and adaptive strategy respectively. Hence, the routing strategy should be trade-off between the optimality and simplicity without too much processing overhead or memory consumption due to its high complexity. Compared to some steadily and inflexible strategy aiming to realize better average performance, we present a novel mechanism to improve the network performance and reduce the computing complexity to some extent.

Considering traffic distribution state, QoS requirements of flows and dynamic available bandwidth resource, the proposed strategy enhances the high utilization of the overall resource at the cost of increasing resource consumed by individual flows. And to find the minimum cost path, the evaluation results show that it alleviates the performance degeneration and simultaneously improves the utilization of whole network resource.

SDN architecture consists of three layers: forwarding layer, control layer and application layer, as shown in Fig. 1. Physical switch is the crucial element of the forwarding layer, which takes on all the performance of forwarding data in accordance with the forwarding rules in flow tables provided by the controller. Besides, the centralized control plane is core layer of the network which takes the responsibility of topology discovery, traffic classification, strategy formulation and network configuration. Therefore, the network traffic is allocated to the paths operated directly by OpenFlow switches, where the flow-handling rules are installed by the central SDN controller [3].

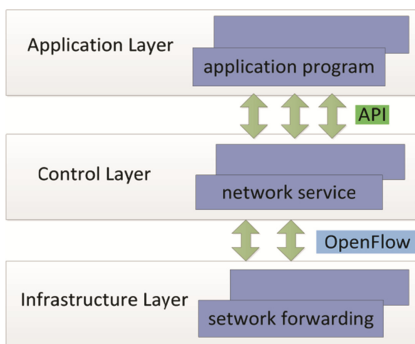


Fig. 1. SDN architecture

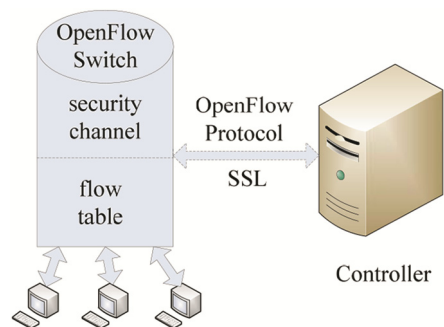


Fig. 2. The construction of OpenFlow switch

The OpenFlow switch is composed by three components including flow table, secure channel and OpenFlow protocol as illustrated in Fig. 2. Flow table contains the flow-oriented forwarding rules issued by the relevant controller. Secure channel ensures the

interaction between the switch and the controller. And OpenFlow protocol regulates messages in secure channel to realize functions, like traffic statistics collection, access control and network configuration.

As the SDN architecture can provide global visibility of network resources and inherent programmable interfaces, some explorations on the fusion of SDN and other technology have been carried out. Although some concepts have been presented several years ago, there are still many issues worth to be researching further, such as efficient self-organized routing mechanism, network resource management, QoS perception and environment forecasting [4–6].

SDN is a promising concept with the powerful advantage to introduce new dimensions of flexibility and adaptability in current communication networks. For instance, the realization of QoS aware routing becomes possible in an agile and dynamic manner. Although some routing algorithms have been well researched, they were not applied in communication networks due to its high implementation complexity and realization costs. We propose the QoS-aware resource management routing mechanism, which seems to be promising to provide better network resource management, traffic control, and application classification [7].

SDN paradigm radically transforms network architecture and provides some characteristics of programmable, efficient, fine-grained, dynamic, accurate, global-viewed, and superior computational capacity. All of these features prompt the development of network with using advanced optimization algorithm.

Computational intensive machine learning algorithms integrate several online routing algorithms for the real-time control of new connection requests. Depending on the available resource and status of the traffic, the cognitive computing could classify the flows and make adaptive routing strategies. Since new variables and additional constraints are emerging over time, the routing mechanism is supposed to utilize machine learning techniques to select the best sequence of accommodative decisions, while considering the anticipative future scenarios for improving the performance of network. In this paper, the proposed dynamic adaptive QoS-aware routing mechanism is constrained with available network resource and distinct flow requirements upon SDN platform [8, 9].

The rest of this paper is organized as follows. Section 2 proposes implementation of the QoS-aware routing mechanism with algorithms in detail. Section 3 describes the simulations. Section 4 analyzes the experimental results and evaluates the performance. Finally, Sect. 5 outlines the future researches and makes a conclusion.

2 Implementation and Algorithm

Our QoS aware routing selection computing mechanism consists of five modules, including Traffic Measurement Module, Flow Classification Module, Topology Detection Module, Routing Selection Module, and Configuration Updating Module, which are working collaboratively on SDN controller.

First, the module Traffic Measurement collects these information of flow statistics from the forwarding layer. Then, Flow Classification module differentiates the QoS

requirements like bandwidth of real-time traffic based on analyzing the flow statistics information using data mining technique, such as K-means algorithm. Moreover, Topology Detection module gathers all the up-to-date information of the link state from switches, such as delay and bandwidth, with using traffic monitoring tools like sFlow or NetFlow. Furthermore, Routing Selection module includes two parts. On the one part, the smaller bandwidth demanding flows match to the routing algorithm of Bandwidth Reserved Shortest Path (BRSP). On the other part, the larger bandwidth demanding flows match to the routing algorithm of Load Balancing Considered Polling Path (LBCPP). Finally, the Configuration Update module updates the strategies by rotating above processes if the degree of the variation exceeds the setting threshold.

2.1 Traffic Measurement Module

Applications supporting various multimedia data have specific QoS requirements on bandwidth, delay and packet loss. And the module is responsible for collecting information about the traffic type. For instance, the applications like high definition video streaming or online competitive gaming, have high demand of data rate and strict demand of latency respectively.

2.2 Flow Classification Module

This module holds the purpose to find the reasonable and effective flow classification theory according to the perception of flow's QoS requirements and the detection of link states from nodes. To trade off the complexity and the practicability of mechanism, the module measures the bandwidth requirement of flows, and calculates a critical value to divide the flows into two types.

In order to classify the flows rationally, the clustering algorithm of machine learning is employed in this process. The K-means classification method make the previous traffic flows to fall into categories, such as mice prior flows and inferior elephant flows. When new flows reach the switches, the flows will be matched to the suitable class and forwarded along the path based on the adaptive theory.

It is inevitable that the status of flows is changing ongoing. For instance, if the size enlarges and the amount increases, the mechanism should reserve more bandwidth to guarantee for the mice flows admission. Therefore, the residual network resource remained for the elephant flows should be confined to release more resource for the mice flows with priority.

2.3 Topology Detection Module

An OpenFlow-enabled network can be modeled as a network graph $G = (S, E)$, where S represents OpenFlow-enabled switches and E indicates the link edge between two adjacent switches. Link state of edge is comprised of the link capacity, link delay, and link available bandwidth.

Our mechanism attempts to avoid traffic congestion when incoming flow is added to the link. Cost of a link is calculated according to link capacity, link utilization, and

required bandwidth of incoming flow. This principle ensures that the link with lower utilization rate has smaller cost value. When link utilization comes near the link capacity, it will become expensive to occupy this link.

2.4 Routing Selection Module

The routing algorithms are committed to find the most feasible path for meeting the specific QoS requirements, which is differentiated depending on flow types: bandwidth-sensitive traffic, delay-sensitive traffic, and others type traffic. A feasible path can provide sufficient resource for the demands. However, flows of diverse requirements adapt to different optimal routing theory. Therefore, in the case of the QoS requirements being perceived, the proposed algorithms would assign the flow an optimal route which is beneficial to both the traffic quality and network performance. As explained following, the module consists of two routing algorithms.

The routing algorithm of BRST is matched to the smaller bandwidth demand flows, which are delay sensitive, bandwidth constrained, and packet loss intolerance. Reserved bandwidth-guarantee could provide small jitter and low packet loss for some special flow in some multimedia applications. We find the path with the smallest delay for delay-sensitive flows. With consuming the reserved bandwidth, this theory could find the optimal route which can assure admission guarantee for the flow with higher priority, and compute the shortest paths for the smallest propagation delay. Considering the demand of the actual network, we adopt the Bellman-Ford algorithm to realize our BRST algorithm. If there is no feasible path, the other routing theory would be employed to find a path to ensure the delivery of the flow temporarily. And the update module starts to modify the corresponding information and settings immediately.

On the contrary, the routing LBCPP is matched to the larger bandwidth demand flows which is bandwidth sensitive, delay constrained, and with moderate packet loss torment. The lager bandwidth is provided to improving the performance of network with load balancing theory. The routing algorithm of our mechanism attempts to avoid traffic congestion whether the states of the network or the features of traffic are changed. After the bandwidth reserved previously, the module uses the residual network resource to find the available paths from source to destination. And the optimal paths with enough bandwidth are figured out based on the delay constraint and packet loss. Since we consider hop counts as the only impact of propagation delay, we set the hop constraint not exceeding the 1.2 times value of that in the shortest path. We use a Top-K paths selection algorithm thinking about available bandwidth, delay, and utilization rate to decide the route by round robin method. Path load balancing is used for distributing workload to reinforce network reliability and optimize network resource utilization.

2.5 Configuration Updating Module

Due to the instability and the resource restriction of network environment, more attentions should be paid to the continuously emerging variation. For accommodating the variance with regard to the distribution of the flows and the condition of the network over time, the routing theory should be dynamically adjusted the critical value of flow

classification and the amount of reserved bandwidth. Meanwhile, the flow table installed in the switches should be updated necessarily for efficient network usage.

In the module, the update process would be triggered if the classification metric or the reserved bandwidth is out-of-date, which means that the variance is exceeding the threshold of extent or time. If some flows matching the first routing algorithm cannot find feasible path using the reserved bandwidth, the flow would use the other routing theory to ensure forwarding temporarily. And the reserved bandwidth should be increased to avoid packet losing with providing better QoS.

In addition, the traffic forwarding rules in flow table are generated by the central controller and installed to the corresponding OpenFlow-enabled switches. As the network traffic and topology are unpredictable, the flow table will be dynamically updated to keep consistent with the employed strategy. On one hand, paths are timely evaluated whether new flow arrives or network changes. On the other hand, the global statistical information is timely updated and the flow table is set to delete overtime entries. We employ suitable period and threshold of updating theory to trade off the consistency of real-time state information and overhead of frequently updating communication in the control plane.

3 Simulation and Setting

In order to evaluate the proposed architecture of SDN-based mechanism, it is implemented in POX platform and Mininet simulator to emulate the network topology. POX is a software platform for rapid exploiting and prototyping of network controller developed by Python, which could invoke scripts to operate corresponding modules to derive the adaptive actions. Mininet provides a lightweight test bed for developing OpenFlow applications to help users to create a realistic virtual network, including a collection of hosts, Open vSwitches and network links on a single machine [10, 11].

And the whole simulation is running on an experimental computer with the operating system of Ubuntu 14.04. Therefore, the computing performance is influenced by the physical machine with essential parameters, such as Intel Core i5-4590 CPU @ 3.30 GHz, and 4.00 GB RAM.

In practice, data is commonly delivered to destination through multi-hop path in the complex topology. For the sake of simplifying the simulation, we conducted experiments in the topology graph showed in the Fig. 3. In the Topology, we set H1 and H2

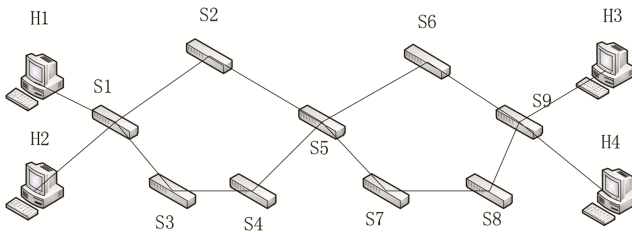


Fig. 3. Topology graph of simulation

as clients, while H3 and H4 as servers. Meanwhile, 9 Open vSwitches were built as the OpenFlow-enabled switches. And the bandwidth of each link was given to 10 Mbps.

Under stationary condition, the flow distribution and the network state are invariable over time. We conduct experiments on the condition to test algorithms of our theory. Under dynamic condition, the moment of flows arrival processes could follow the distributions like Poisson. If the size of the flows is given, the departure time of flow related to the transmission delay could be equivalent to the bandwidth demand which is set as Normal distribution. This work conduct experiments on Mininet to evaluate our mechanism and compare the results in custom dynamic condition, in which the UDP traffic of 5 Mbps is emulated as background flow from H1 to H3 by using the command of `iperf`. Using single routing algorithm, the throughput and delay are measured respectively when sudden flows are generated at some point.

4 Evaluation and Analysis

In the case of the application of real time multimedia, QoS metrics with respect to bandwidth, delay, delay jitter, and packet loss ratio are usually taken as major concerns of receivers, while the senders care more about the traffic transmission in high load and high randomness. For the network management, the network performance depends on the metrics, such as average link utilization, resource consuming, packet loss ratio, throughput, device energy efficiency, and average end-to-end delay. Therefore, the QoS aware routing problem could be converted to the multiple objective programming, which is to find a minimum cost of object with satisfying some QoS constraints.

In this paper, we focus on two metrics namely throughput and delay. Under stationary condition, intuitively, our classified synthesized routing QoS mechanism has larger throughput than BRST and smaller delay than LBCPP. Under custom dynamic condition with adding background flows through the shortest path at the time of 50 s and removing the flows at the time of 110 s, we compare the throughput and delay between the two unclassified single routings as shown in Figs. 4 and 5. When the background flows inject in the network, we could find that the throughput with BRST collapsed obviously, while the other algorithm of LBCPP shows a higher throughput at same time. Similarly, the latency of the BRST increases more evidently than the other. Therefore, from H2 to H4, the results show that the proposed routing mechanism could reduce the delay for prior mice-flows and increase the throughput for inferior elephant-flows. In the future, we will employ the other dynamic condition with injecting the background traffic subjected to Poisson distribution or Normal distribution.

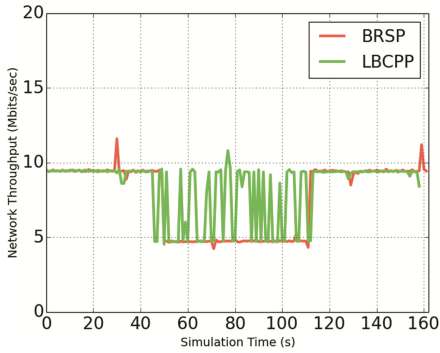


Fig. 4. Throughput comparison

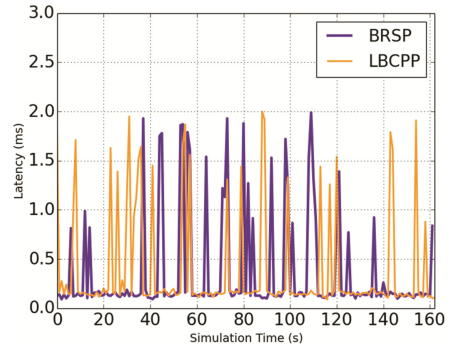


Fig. 5. Delay comparison

5 Conclusion and Future Work

Based on the fusion of techniques, this work presents an intelligent perceptive QoS mechanism for forwarding the diverse flows with the adaptive routing. The architecture consists of five modules which are collaborating together on SDN controller. First, it finds the feasible classification among flows according to the requirements of the bandwidth. Second, for the delay sensitive flows, the theory is made with bandwidth reservation for finding the shortest path in order to guarantee the delay demand and reduce packet loss rate caused by propagation in network. Third, for the bandwidth sensitive flows, the multipath polling method of load balance considered multipath is applied to improve the network performance. Finally, it updates an adjustable traffic classification threshold so as to keep optimal for both network performance and service quality.

In the future work, we would employ and exploit other computing algorithms to implement the proposed mechanism. In the paper, the machine learning technology named K-means clustering is used to classify the flows by finding the most suitable dividing metrics for the previous period. Since the flow classification named 2-means may not be efficient, other skills like reinforcement learning would be used to find the optimal adaptive dividing metrics with real-time feedback. Moreover, in the updating module, the predicted method could be exploited to get the potential growing tendency of traffic features for more appropriate classification. In addition, the machine learning could also be applied in the controller analysis, admission control, and packet security.

References

1. Vissicchio, S., Tilmans, O., Vanbever, L., et al.: Central control over distributed routing. In: SIGCOMM 2015, 17–21 August, vol. 45, no. 5, pp. 43–56 (2015)
2. Han, L., Sun, S., Joo, B., et al.: QoS-aware routing mechanism in OpenFlow-enabled wireless multimedia sensor networks. *Int. J. Distributed Sensor Netw.* **12**(7), 9378120 (2016)
3. OpenFlow Specification. Open Networking Foundation. <https://www.opennetworking.org/sdn-resources/onfspecifications/openflow>

4. Liu, J., Li, J., Shou, G., et al.: SDN based load balancing mechanism for elephant flow in data center networks. In: International Symposium on Wireless Personal Multimedia Communications, pp. 486–490. IEEE (2014)
5. Craig, A., Nandy, B., Lambadaris, I., et al.: Load balancing for multicast traffic in SDN using real-time link cost modification. In: IEEE International Conference on Communications, pp. 5789–5795. IEEE (2015)
6. Li, J., Chang, X., Ren, Y., et al.: An effective path load balancing mechanism based on SDN. In: IEEE International Conference on Trust, Security and Privacy in Computing and Communications, pp. 527–533. IEEE (2014)
7. Durner, R., Blenk, A., Kellerer, W.: Performance study of dynamic QoS management for OpenFlow-enabled SDN switches. In: IEEE International Symposium on Quality of Service, pp. 177–182. IEEE (2015)
8. Mizrahi, T., Saat, E., Moses, Y.: Timed consistent network updates in software-defined networks. *IEEE/ACM Trans. Netw.* **24**, 1–14 (2016)
9. Abu Alsheikh, M., Lin, S., Niyato, D., et al.: Machine learning in wireless sensor networks: algorithms, strategies, and applications. *IEEE Commun. Surv. Tutor.* **16**(4), 1996–2018 (2014)
10. Mininet. <http://mininet.org/>
11. POX. <http://www.noxrepo.org/pox/about-pox/>

Research on the Shortest Path Problem Based on Improved Genetic Algorithm

Baoliang Wang^{1(✉)}, Susu Yao², Kaining Lu¹, and Huizhen Zhao¹

¹ Information and Network Center, Tianjin University, Tianjin 300072, China
{wbl, knlu, tdee79}@tju.edu.cn

² School of Electrical and Information Engineering, Tianjin University, Tianjin 300072, China
yaosusu@tju.edu.cn

Abstract. Aiming at the complex large-scale shortest path problem, a modified genetic learning algorithm has been offered. Firstly, in order to prevent premature convergence of evolution population, a new fitness function for the shortest path is proposed. At the same time, to ensure the global search ability of the algorithm a selection method of crossover probability is proposed. And to ensure the local search ability of genetic algorithm a selection method of mutation probability is proposed. The experimental results show that the modified genetic algorithm has a better success rate compared with the traditional algorithm.

Keywords: Genetic algorithm · Shortest path · Fitness function
Crossover operator · Mutation operator

1 Introduction

The shortest path problem has been widely employed in many fields, such as intelligent transportation [1], computer networks [2], robot path planning [3, 4] and so on. For the shortest path problem, there are many deterministic algorithms, such as Dijkstra algorithm [5] and Ford algorithm [6]. However, in the practical application, the size of the shortest path problem is expanding, the constraint condition of the shortest path problem is increasing, and the complexity of the influencing factors is also increasing. The above leads to the difficulty of solving the shortest path is also increasing. In the traditional algorithm, it is difficult to effectively find a perfect solution to quickly find the optimal solution or suboptimal solution. For the shortest path problem of large scale, the intelligent algorithm can satisfy the user's time and precision conditions to obtain the optimal or suboptimal solution.

Genetic algorithm (GA) has good adaptability, robustness and flexibility [7]. In this paper, we use genetic algorithm to solve the shortest path problem. But, there are some problems in genetic algorithm, such as premature convergence and weak local search ability, low efficiency and low precision. These problems are caused by the irrational design of population scale, the irrational design of fitness function and the irrational selection of cross probability and mutation probability. In order to solve the above problems, two kinds of fitness function transformation methods are designed, and the crossover probability and mutation probability selection strategies

are optimized. The effectiveness of the algorithm to deal with the shortest path problem is verified by simulation experiments.

2 Genetic Algorithm

The shortest path genetic algorithm consists of the following five parts: (1) the genetic representation of the shortest path problem, (2) the encoding and decoding of the shortest path problem, (3) designing an fitness function according to the merits of each chromosome, (4) designing the genetic operators which used to change the genetic structure of offspring, usually include selection, crossover, mutation and so on, (5) parameters setting, including population size, probability of applying genetic operator, etc. The keys to solve the shortest path problem based on GA are the design of the fitness function, the setting of the crossover operator and the mutation operator.

Genetic algorithm [8, 9] is an algorithm to simulate the biological evolution process to find the optimal solution. Its main advantage lies in its good adaptability, robustness and flexibility. First, as a kind of intelligent search algorithm, the optimization process of genetic algorithms do not have much mathematical requirements. The genetic algorithm is modeled according to the specific problem, and the solution is found by evolution without having to consider the specific internal operation problem. So it has a good adaptability. And it borrows the evolutionary idea of biogenetics can carry out global search very efficiently. The computational complexity of genetic algorithm is small

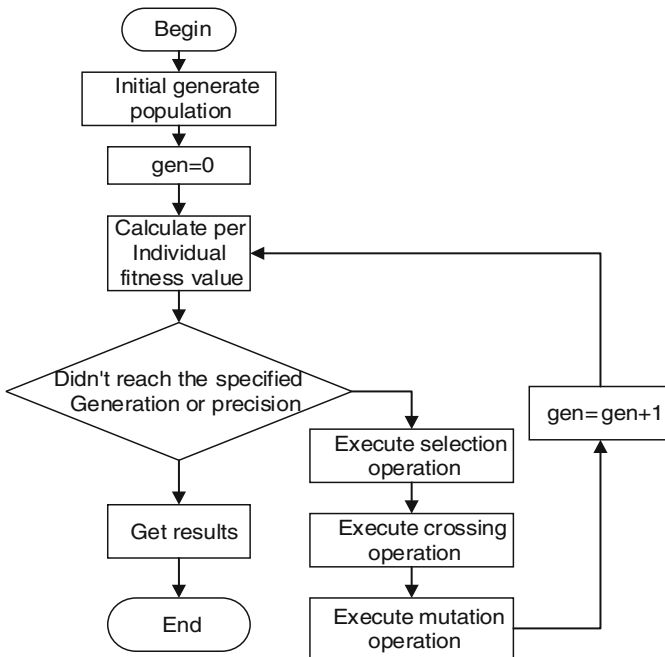


Fig. 1. Genetic algorithm flow chart

Compared with the traditional algorithm. At the same time, the genetic algorithm can be hybridized with other related heuristic algorithms, which can be flexible to deal with practical problems.

The basic process of genetic algorithm as shown in Fig. 1, including initial population, crossover, mutation, selection and so on. Individuals evolve in the direction of higher fitness by crossover, mutation and selection operations to find the optimal solution or suboptimal solution [10].

3 Optimization Design of Genetic Algorithm

3.1 Genetic Representation

Coding is a key factor to improve the efficiency and success rate of genetic algorithms. In this paper, we use the priority coding method to represent the shortest path problem. The advantage of the priority coding method is that any encoding has a corresponding path; most crossover operations are very easy to implement; there is no loop after crossing.

Encoding: Randomly generate sequences to form the original chromosomes. The length is the total number of points in the graph. According to the coding pseudo-code, we can get the random sequence which named "chromosome". The node ID in Fig. 2 is a random sequence containing 11 points. The specific encoding pseudo code is as Table 1.

Table 1. Priority encoding pseudo code

Encoding Pseudo Code:

```

for(i=1:to n)
    chromosome[i]=i;
for(i=1 to n/2)
    repeat
        q=random(1,n);
        p=random(1,n);
    until p!=q;
    swap(chromosome[p],chromosome[q]);
end

```

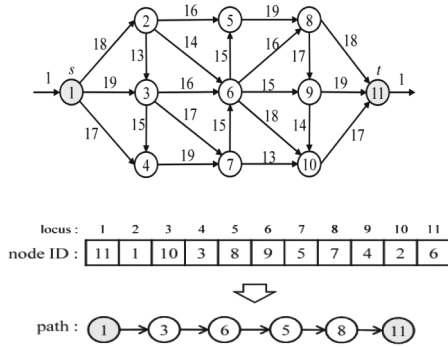


Fig. 2. Priority decoding and encoding process

Decoding: The decoding process similar to the depth traversal algorithm. Take the Fig. 2 as an example, firstly, according to the topology of the path, we can see that node

Table 2. Priority encoding pseudo code

Decoding Pseudo Code

Initialize $i=1;l=1;path[l]=1;$

while $S_1 \neq \emptyset$

$temp_j = \max(\text{chromosome}[j], j \in S_i);$

if($\text{chromosome}[temp_j] \neq 0$)

$path[l] = temp_j;$

$l = l + 1;$

$\text{chromosome}[temp_j] = 0;$

$i = temp_j;$

else

$S_i = S_i \setminus temp_j; // \text{delete } temp_j \text{ from } S_i$

$\text{chromosome}[i] = 0;$

if($(l < 1) \vee l = 1$); break;

$i = \text{chromosome}[l];$

end

1's son nodes are node 2, node 3 and node 4. In the node ID, We can get their value, ID [2] = 1, ID [3] = 10, ID [4] = 3. Secondly, choose the maximum value from the son nodes of node 1, and then change the path to 1-3. Thirdly, repeat the first two steps until find the shortest path. So we can get path 1-3-6-5-8-11 based on the node ID. Decoding method pseudo code is as Table 2.

3.2 Fitness Function

The fitness function determines the evolution direction of the GA process. And it has a great effect on the convergence speed of a GA process. In the paper, our coding method of the shortest path algorithm containing the designated points is the priority coding method, so a chromosome can be successfully decoded corresponds to an actual path. A path is a correct solution when the number of designated points in this path meet the requirements. Therefore, we sets the fitness function to the number of the designated points in the path. The direction of evolution is the direction of the path that contains the number of designated points must be more and more. The fitness function does not use the weight of the path as a reference, the above selection way may cause a larger weight to be included in the found feasible solutions. For the above defects, the algorithm is used to compare the many feasible solutions, and the optimal solution is chosen as the global optimal solution.

3.2.1 Exponential Transformation

$$\begin{cases} f'(i) = e^{-\alpha f(i)} \\ \alpha = \sqrt[t]{f_{avg} + \varepsilon}, m = 1 + \lg(T) \end{cases} \quad (1)$$

Where $f(i)$ represents the i th chromosome's original fitness value, $f'(i)$ represents the new fitness value of $f(i)$ to adapt to exponential transformation, α is an exponential transformation coefficient which is a positive number of dynamic changes that gradually increase as evolutionary generation increases, t is the current chromosome evolutionary generation, T is the largest genetic generation, f_{avg} is the average fitness which is the average value of $f(i)$, ε is a positive number which small enough.

According to the analysis of the fitness function, we can see that $f(i)$ is a non-negative number. In the process of population evolution, f_{avg} in the early evolution is very large and α is small. With the evolution of the population, f_{avg} gradually reduced, and the evolution of the current generation t is increased. According to this trend, the transformation of fitness function can be guaranteed α gradually increase. Therefore, the fitness function is an adaptive dynamic adjustment function.

3.2.2 Logistic Curve Function Transformation Method

The expression of logistic curve function is $y = \frac{1}{1 + e^x}$. According to the logistics curve in Fig. 3, it can be seen that the function range is between 0 and 1. At the same time, the function value is between 0.5 and 1 when the value of x is less than 0, and the function value is between the range of 0 and 0.5 when the value of x is larger than 0.

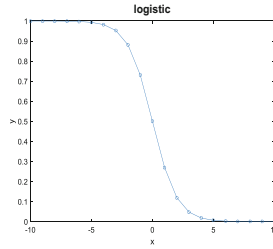


Fig. 3. Logistic curve

As can be seen from Fig. 3 the logistic function gets a value of either 1 or a value of 0 when the value of x is outside the $[-10, 10]$. If the logistic function is used as fitness function directly, the fitness value of many chromosomes will be close to 1 or 0, so that majority of the chromosomes in the population are less competitive which will lead to precocious phenomenon. In order to avoid the premature phenomenon, a new fitness function is designed for the logistics function.

$$f^*(i) = \begin{cases} \frac{1}{1 + \exp((f - f_{avg})/c)} & g \geq 30\%n \\ \frac{1}{1 + \exp(f - f_{avg})} & g < 30\%n \end{cases} \quad (2)$$

where $f^*(i)$ is a new fitness value of the i th chromosome obtained by logistic function transformation, $f(i)$ is the original fitness value of the i th chromosome, f_{avg} is the average value of the current population $f(i)$, g indicates the number of chromosomes where the difference outside range $(-10, 10)$, c is the order of magnitude of the maximum value of $|f - f_{avg}|$.

The above two kinds of fitness function to meet the general fitness function necessary conditions. At the same time, relative to other fitness function, they have the following properties: (1) the fitness function is a nonnegative number, so the objective function can be regarded directly as the original fitness function, regardless of its positive or negative; (2) the original fitness function value is inversely proportional to the value of the new fitness function, that is, the greater the value of the original fitness function the smaller the value of the new fitness function; (3) to ensure that most of the chromosomes in the population are highly competitive, and the probability of premature appearance is reduced.

3.3 Crossover Operator

In the genetic algorithm, the crossover operator has a great effect on the global searching ability and convergence ability. In this paper, we presents a new cross probability setting method. Firstly, in order to prevent the destruction of the excellent individual gene in the population, we make the excellent individual directly as the next generation of individuals. In this paper, we assume that the first 30% chromosomes in the population are the excellent individuals. Secondly, in order to reduce invalid crossover, the remaining

chromosomes adopt the non-equal probability pairing strategy, we use the correlation function in Formula 3 to calculate the correlation between chromosomes. A higher crossover probability is set for two chromosomes with uncorrelated correlations.

First of all, we selected a chromosome X that had not been operated by crossover, and then calculated the correlation index between X and other non-overlapping chromosomes. According to the correlation index, the probability of crossover between the selected chromosome and X was calculated. The roulette wheel method is chosen as the selection operator. So, we can get the chromosomes that cross with X .

a. Correlation index function

$$r(X, Y) = \sum_{j=1}^m x_j \oplus y_j, x_j \oplus y_j = \begin{cases} 0, x_j = y_j \\ 1, x_j \neq y_j \end{cases} \quad (3)$$

Where Y_i is a chromosome that has not been crossed, m is the total number of genes in the two chromosome which has the larger number of genes, $r(X, Y_i)$ is indicated that the number of genes is not the same between X and Y_i , the greater the $r(X, Y_i)$, the smaller correlation between X , and Y_i , and the smaller the probability of invalid crossover operation will be reduced.

b. The crossover probability of chromosome Y_i selected to cross with chromosome X

$$p(Y_i|X) = \frac{1}{m} \left(1 + \lambda \frac{r(X, Y_i) - r_{avg}}{r_{max} - r_{avg}} \right), i \in [1, m] \quad (4)$$

Where $r_{avg} = \frac{1}{m} \sum_{i=1}^m r(X, Y_i)$, $r_{max} = \max\{r(X, Y_i), i = 1, 2, \dots, m\}$, $r_{min} = \min\{r(X, Y_i), i = 1, 2, \dots, m\}$, λ is a constant, and $0 \leq \lambda \leq 1$.

3.4 Mutation Operator

The mutation operator is an auxiliary method, and it has an effect on the local search ability of genetic algorithm. Therefore, the algorithm perform a mutation on a small fraction of the chromosomes. The Formula 5 is used to calculate the mutation probability of each chromosome. We sorted the individuals from small to large by mutation probability. The first 15% individuals are selected to mutation, thus is, the mutation probability set to 15%.

$$p_m = \begin{cases} p_{m1}, f < f_{avg} \\ p_{m1} - \frac{(p_{m1} - p_{m2})k_1(f_{max} - f)}{f_{max} - f_{avg}}, f \geq f_{avg} \end{cases} \quad (5)$$

Where $p_{m1} = 0.1$, $p_{m2} = 0.001$, k_1 is a constant, and $0 < k_1 < 1$, f_{\max} is the largest fitness value in the population, f_{avg} is the average fitness value of population, f is the new fitness value of the chromosome.

4 Experimental Analysis

4.1 The Influence of the Crossover Operator

In order to verify the influence of the crossover operator, the improved genetic algorithm using the new crossover operator is compared with the traditional genetic algorithm. The results in Table 3 are the average of 100 tests. According to Table 3, it can be seen that the new crossover operator can improve the accuracy of the genetic algorithm, and can effectively avoid the algorithm into the local optimal solution.

Table 3. Performance comparison of improved GA and traditional GA

Algorithm	Average convergence generations	Optimal solution ratio
Traditional GA	78	0.61
Improved GA	42	0.94

4.2 The Modified Genetic Algorithm Analysis

In order to verify the validity of the algorithm, the Dijkstra algorithm is compared with the improved genetic algorithm. In Table 5, the optimal solution and the suboptimal solution represent the average of the success cases, and the time represents the average time of the cases. The genetic algorithm parameter settings: population size of about 1000 which slightly fluctuate for specific cases, mutation probability is 15%.

As can be seen from Tables 4 and 5, the genetic algorithm has a better success rate than Dijkstra algorithm, and is more effective under large-scale data. Although the probability of genetic algorithm to get the optimal solution is 100% in theory. Because it is difficult to meet the individual diversity in the population in practical application, the success rate cannot reach 100%.

Table 4. Dijkstra algorithm simulation results

Nodes	Number of designated points	Number of success/number of experiments	Traversal completion time
20	7	4/5	<1 ms
50	10	4/5	3 ms
100	15	4/6	31 ms
200	15	8/10	90 ms
300	20	7/10	320 ms

Table 5. Genetic algorithm simulation results

Nodes	Designated points	Success/all	Suboptimal solution/optimal solution	Suboptimal solution time/optimal solution time
20	7	5/5	1/2	11 ms/11 ms
50	10	5/5	1/3	52 ms/63 ms
100	15	6/6	3/23	325 ms/3 s
200	15	9/10	6/41	325 ms/36 s
300	20	9/10	21/83	42 s/203 s
500	30	8/10	56/127	167 s/361 s

From the experimental results, we can see that the genetic algorithm has a high computational cost compared with the traditional algorithm. The improved genetic algorithm is much more expensive than Dijkstra algorithm, especially the optimal solution cost. For the above-mentioned problem, we can adopt pruning strategy. First, we cut the size of the graph and reduce the size of the graph. And then, we can use the genetic algorithm mentioned in this paper in the results of the pruning. So that we can reduce the computational cost in the case of guaranteed algorithm search capabilities.

5 Concluding

The shortest path problem is an active research area. In this paper, we modify the fitness function of genetic algorithm, and then design a new selection method for crossover probability and a new selection method for mutation probability. These improvements make the genetic algorithm have a good success rate. At the same time, the algorithm proposed in this paper can easily combine with the pruning algorithm. So that we can effectively reduce the computational complexity and guarantee the search ability of the shortest path problem. However, this paper only considers the constraint condition of designated points, the algorithm also has room for improvement.

References

1. Ko, Y.D., Jang, Y.J., Min, S.L.: The optimal economic design of the wireless powered intelligent transportation system using genetic algorithm considering nonlinear cost function. *Comput. Ind. Eng.* **89**(C), 67–79 (2015)
2. Chitra, C., Subbaraj, P.: A nondominated sorting genetic algorithm solution for shortest path routing problem in computer networks. *Expert Syst. Appl.* **39**(1), 1518–1525 (2012)
3. Cheng, H.: Obstacle avoidance shortest path algorithm and its application. *Electron. Des. Eng.* **16**, 56–60 (2013). (in Chinese)
4. Qi, X., Liu, S.: Selection algorithm for QoS routing based on k-shortest paths. *J. Jilin Univ. (Eng. Technol. Ed.)* **05**, 526–530 (2005). (in Chinese)
5. Dijkstra, E.W.: A note on two problems in connexion with graphs. *Numer. Math.* **1**(1), 269–271 (1959)
6. Bellman, R.: On a routing problem. *Q. Appl. Math.* **16**, 87–90 (1958)
7. Lin, L., Gen, M.: Priority-based genetic algorithm for shortest path routing problem in OSPF. *Stud. Comput. Intell.* **187**, 91–103 (2009)

8. Holland, J.H.: *Adaptation in Natural Artificial Systems*, pp. 1–17. MIT Press, Cambridge (1975)
9. Cao, Z.: The study on exhaust algorithm, search algorithm, dynamic design for 0–1 Knapsack problem. *Comput. Knowl. Technol.* **5**(12), 3193–3198 (2009). (in Chinese)
10. Srinivas, M., Patnaik, L.: Adaptive probabilities of crossover and mutation in genetic algorithm. *IEEE Trans. Syst. Man Cybern.* **24**(4), 656–666 (1994)

Semantic Web Languages for Policy Enforcement in the Internet of Things

Rustem Dautov^{1,2}(✉) and Salvatore Distefano^{1,3}

¹ Higher Institute of Information Technology and Information Systems (ITIS),
Kazan Federal University (KFU), Kazan, Russia

{rdautov,s_distefano}@it.kfu.ru

² South-East European Research Centre (SEERC), The University of Sheffield,
International Faculty CITY College, Thessaloniki, Greece

³ University of Messina, Messina, Italy

sdistefano@unime.it

Abstract. To enable device compatibility, interoperability and integration in the Internet of Things (IoT), several ontological frameworks have been developed, using the Semantic Web technologies – a common and widely-adopted toolkit for addressing the heterogeneity issues in complex IT systems. These ontologies aim to provide a common vocabulary of terms to be universally adopted by the IoT community. Defined using the Web Ontology Language – a language underpinned by the Description Logics – these vocabularies, however, seem to neglect the automated reasoning support, which comes along with this semantic approach to model IoT environments. To bridge this gap, this paper builds upon the existing work in the area of semantic modelling for the IoT, and proposes utilising IoT ontologies to define and enforce policies, thus benefiting from the built-in support for automated reasoning.

Keywords: Internet of Things · Semantic Web · Policy management
Web Ontology Language · Semantic Web Rule Language · Reasoning

1 Introduction

While challenges associated with timely processing of sensor data have been relatively successfully tackled by the advances in networking and hardware technologies, the challenge of properly handling data representation and semantics of IoT descriptions and sensor observations is still pressing. In the presence of multiple organisations for standardisation, as well as various hardware and software vendors, overcoming the resulting heterogeneity remains one of the major concerns for the IoT community. Moreover, apart from the syntactic heterogeneity (i.e. heterogeneity in the data representation, such as, for example, differences in data formats/encodings), we can also distinguish heterogeneity in the semantics of the data [2]. For example, different units of measurement and metric systems are common causes for incompatibility and integrity problems.

As a potential workaround to the IoT heterogeneity problem and yet-to-come standards, the research community started investigating potential ways of creating semantic modelling languages, which would provide an overarching modelling framework and bridge formerly-disjoint heterogeneous IoT systems. Such modelling languages can be seen as common vocabularies of terms, which are expected to be used by IoT practitioners to enable compatibility and interoperability when integrating IoT solutions. Simply put, two disjoint system would be able to ‘communicate’ to each other by expressing their data and interfaces, using a common suitable modelling language. A representative example of how this lack of unified data representation has been addressed in the context of the IoT is the *Semantic Sensor Web* – a promising combination of two research areas, the Semantic Web and the Sensor Web [6]. Using the Semantic Web technology stack to represent data in a uniform and homogeneous manner, it provides enhanced meaning for sensor descriptions and observations so as to facilitate data analysis and situation awareness [3]. One of the main outcomes of this initiative was the Semantic Sensor Network (SSN) ontology – a thorough modelling vocabulary, jointly developed by a wide group of researchers.

From this perspective, however, Semantic Web ontologies do not differ much from other modelling approaches (e.g. UML or XML) that provide a taxonomy of terms and relationships, to be used as ‘building blocks’ when describing the IoT domain. A major advantage of the Semantic Web languages, which is frequently neglected in this context, is the support for *automated formal analysis*, underpinned by the built-in reasoning capabilities of the Web Ontology Language (OWL), which is one of the key enabling technology for the Semantic Web [4]. By representing data in terms of OWL classes and properties, one can perform reasoning tasks over this data and benefit from an already existing, highly-optimised and reliable analysis mechanism. In this light, this paper is trying to tap into this idle potential for automated reasoning, and presents an approach to policy management and enforcement in the IoT context, using existing IoT ontologies and corresponding reasoning support. As it will be further described below, the proposed approach is expected to benefit from separation of concerns, extensibility, human readability, as well as increased reliability, automation, and opportunities for reuse.

2 Background: Semantic Web Languages

The Semantic Web [1] is the extension of the World Wide Web that enables people to share content beyond the boundaries of applications and websites. This is typically achieved through the inclusion of semantic content in web pages, which thereby converts the existing Web, dominated by unstructured and semi-structured documents, into a web of meaningful machine-readable information. The Semantic Web is realised through the combination of certain key technologies [4], whereas the presented research specifically focuses on the Web Ontology Language (OWL) and the Semantic Web Rule Languages (SWRL) as the two potential ways of defining and enforcing policies in the context of the IoT.

OWL is a family of knowledge representation languages used to formally define an ontology – “a formal, explicit specification of a shared conceptualisation” [7]. Typically, an ontology is seen as a combination of a terminology component (i.e. TBox) and an assertion component (i.e. ABox), which are used to describe two different types of statements in ontologies. The TBox contains definitions of classes and properties, whereas the ABox contains definitions of instances of those classes. Together, the TBox and the ABox constitute the knowledge base of an ontology. OWL provides advanced constructs to describe resources on the Semantic Web. This way, it is possible to explicitly and formally define knowledge (i.e. concepts, relations, properties, instances, etc.) and basic rules in order to reason about this knowledge. OWL allows stating additional constraints, such as cardinality, restrictions of values, or characteristics of properties such as transitivity. OWL languages are characterised by formal semantics – they are based on *Description Logics* (DLs) and thus bring reasoning power to the Semantic Web. **SWRL** extends OWL with even more expressiveness, as it allows defining rules in the form of implication between an antecedent (body) and consequent (head). It means that whenever the conditions specified in the body of a rule hold, then the conditions specified in the head must also hold.

To date, a number of IoT ontologies have been developed using OWL. More specifically, IoT-Lite ontology¹ is a lightweight instantiation of the SSN ontology, actively developed by the World Wide Web Consortium. It describes the key IoT concepts to allow interoperability and discovery of sensory data in heterogeneous IoT platforms. This ontology reduces the complexity of other IoT models by describing only the main concepts of the IoT domain. This means that following the Semantic Web principles of linking and reusing existing ontologies and datasets, it is possible to extend the core vocabulary with other relevant concepts, defined in other ontologies if/when needed. This way, ontology engineers can simply import an existing, established, and trusted ontology, instead of ‘re-inventing the wheel’.

3 Sample Scenario

The following use case scenario demonstrates the proposed idea of leveraging the idle potential of OWL ontologies and focuses on a complex IoT system composed of multiple sensing devices, deployed both indoors and outdoors. Some of these devices are temperature sensors installed in rooms within a building. It is assumed that whenever any of these temperature sensors indicates a value exceeding a dangerous level of 50°, the situation has to be classified as critical, and thus needs taking reactive actions. A possible way to handle this scenario would be to define explicit policies for every single temperature sensor within the building. In the worst case, such policies would be either ‘hard-coded’ with numerous **if/then** operators (i.e. any modifications would lead to the source code recompilation), or defined declaratively (i.e. stored in some kind of configuration file to be dynamically fetched by the analysis component). In both cases, however, the resulting knowledge base would be saturated by the excessive

¹ <https://www.w3.org/Submission/iot-lite/>.

number of hardly manageable and possibly conflicting policies. An alternative solution is based on using the reasoning capabilities of OWL and SWRL to classify observed IoT data as instances of specific classes. More specifically, with this use case we demonstrate three different types of automated classification:²

— *Defined classes*: underpinned by the DLs, OWL allows creating so-called *defined* classes via a set of necessary and sufficient conditions. This means that the reasoner will classify any entity with a required set of sufficient properties as an instance of a specific class, even if this class membership was not defined explicitly. The defined class `RoomDevice` is demonstrated in Listing 1.1, which should be read as “if `sd` is a sensing device and has a rectangular coverage area, then `sd` is a device installed in a room”.

Listing 1.1. Defined OWL class `RoomDevice`.

```
ssn:SensingDevice(?sd) AND iot:Rectangle(?r)
    AND iot:hasCoverage(?d,?r) ≡
iot:RoomDevice(?sd)
```

— *OWL subclasses*: OWL also provides a simpler and more explicit way of defining classes and subclass relationships. It supports multiple and transitive inheritance, and, as in many other programming languages, subclasses inherit all the properties of their parent classes. The code snippet in Listing 1.2 contains two definitions. The first definition simply states that any temperature sensor is a sensing device. The second definition illustrates the transitive inheritance through a subclass hierarchy that states – in simple words – that if a device is installed in a room, then it is automatically assumed to be installed in a building as well, which in turn means it is an indoor device.

Listing 1.2. Defining OWL subclass relationships.

```
iot:TemperatureSensor IS A ssn:SensingDevice
iot:RoomDevice IS A iot:BuildingDevice IS A iot:IndoorDevice
```

— *SWRL classification*: SWRL allows defining more expressive rules, as illustrated by Listing 1.3. In simple words, the code snippet reads that if there is an indoor device `id`, indicating that its measured value has exceeded 50°, the current observation has to be classified as critical.

Listing 1.3. Defining the class `CriticalObservation` using SWRL.

```
iot:IndoorDevice(?id) AND ssn:Observation(?o) AND dul:Value(?v)
    AND iot:observes(?id,?o) AND ssn:hasValue(?o, ?v)
    AND swrl:greaterThan(?v, 50) THEN
iot:CriticalObservation(?o)
```

² The notations `ssn`, `iot`, and `dul` are established shortcuts for imported OWL ontologies, where corresponding concepts are defined.

SSN ontology (`ssn`): <http://purl.oclc.org/NET/ssnx/ssn>.

IoT-Lite ontology (`iot`): <http://purl.oclc.org/NET/UNIS/fiware/iot-lite> DOLCE

Ontology (`dul`): <http://loa.istc.cnr.it/ontologies/DOLCE-Lite.owl>.

Taking together all three definitions, we now assume that there is a temperature sensor `ts` reporting a temperature level of 60° in its covered rectangular area. The automated reasoner will follow the steps below:

1. Since `TemperatureSensor` is a subclass of `SensingDevice`, `ts` is classified as a `SensingDevice` (Listing 1.2).
2. Since `ts` is a `SensingDevice` and has a rectangular coverage area, it is classified as a `RoomDevice` (Listing 1.1).
3. Since `RoomDevice` is a subclass of `BuildingDevice`, which is a subclass of `IndoorDevice`, `ts` is classified as an instance of `IndoorDevice` (Listing 1.2).
4. Since the measured observation of an `IndoorDevice` `ts` is greater than 50° , this observation is classified as `CriticalObservation` (Listing 1.3).

This way, the reasoning engine is able to detect a critical situation by inferring implicit facts from the limited explicit information. It is worth noting that using generic rules for a wide range of devices, as in the example above, does not affect the flexibility of the proposed approach and its ability to define fine-grained, targeted policies for individual devices. Apart from inheritance, OWL also supports overwriting parent properties by subclasses. This means that it is possible to enforce device-specific policies, which will overwrite the default behaviour and apply only to those specific devices. This way, flexible policy enforcement at various granularity levels can be achieved.

4 Discussion and Conclusion

The presented approach discusses the idle potential of existing IoT ontologies to be used in the context of policy enforcement mechanisms. Semantic Web is underpinned by Description Logics, which offer automated reasoning support. This means that IoT engineers can use existing ontological classes and properties to define policies, and, as a result, benefit from the built-in policy enforcement mechanisms. More specifically, the following benefits can be identified [2]:

- *Separation of concerns*: desirably, a policy enforcement mechanism is expected to (i) separate the knowledge base and policies from the actual enforcement of these policies, and (ii) allow the definition of the knowledge base in a declarative, loosely-coupled manner. The presented approach addresses these requirements and enables policy modifications ‘on the fly’ in a seamless, transparent manner – that is, without recompiling, redeploying and restarting the whole software system. In particular, to apply changes, it is only required to add corresponding OWL/SWRL rules to the policy base. As opposed to the existing (potentially hard-coded) approaches, the declarative approach is seen as a considerable benefit, which enables minimum interruptions caused by potential modifications.
- *Human readability and ease of use*: the Semantic Web research targets at making information on the Web to be both human- and machine-readable, with languages which are characterised by an easy-to-understand syntax, as well as the visual editors for effortless and straight-forward knowledge engineering. OWL

ontologies are known to be used in a wide range of scientific domains (for example, see [5] for an overview of biomedical ontologies), which are not necessarily closely connected to computer science, and allows even for non-professional programmers (i.e. domain specialists) to design policies.

— *Extensibility*: IoT systems may be composed of an extreme number of smart devices spread over a large area (e.g. traffic sensors distributed across a city-wide road network) and have the capacity to be easily extended (as modern cities continue to grow in size, more and more sensors are being deployed to support their associated traffic surveillance requirements). To address this scalability issue, the proposed semantic approach, using the declarative definition, can extend the knowledge base to integrate newly-added devices in a seamless, transparent, and non-blocking manner. The same applies to the reverse process – once old services are retired and do not need to be considered anymore, the corresponding policies can be seamlessly removed from the knowledge base, so as not to overload the reasoning processes.

— *Increase in reuse, automation and reliability*: policy enforcement mechanisms already exist in the form of automated reasoners for OWL/SWRL languages, and the proposed approach aims to build on these capabilities. Since the reasoning process is automated and performed by an existing reasoning engine, it is expected to be free from so-called ‘human factors’ and more reliable, assuming, of course, the validity of ontologies and policies. Arguably, as the policy base grows in size and complexity, its accurate and prompt maintenance becomes a pressing concern so as to avoid potential policy conflicts.

References

1. Berners-Lee, T., Hendler, J., Lassila, O., et al.: The semantic web. *Sci. Am.* **284**(5), 28–37 (2001)
2. Dautov, R., Kourtesis, D., Paraskakis, I., Stannett, M.: Addressing self-management in cloud platforms: a semantic sensor web approach. In: Proceedings of the 2013 International Workshop on Hot topics in Cloud Services, pp. 11–18. ACM (2013)
3. Dautov, R., Paraskakis, I., Stannett, M.: Towards a framework for monitoring cloud application platforms as sensor networks. *Cluster Comput.* **17**(4), 1203–1213 (2014)
4. Hitzler, P., Krötzsch, M., Rudolph, S.: Foundations of Semantic Web Technologies. Chapman & Hall/CRC, Boca Raton (2009)
5. Rubin, D.L., Shah, N.H., Noy, N.F.: Biomedical ontologies: a functional perspective. *Briefings Bioinf.* **9**(1), 75–90 (2008)
6. Sheth, A., Henson, C., Sahoo, S.S.: Semantic sensor web. *IEEE Internet Comput.* **12**(4), 78–83 (2008)
7. Studer, R., Benjamins, V.R., Fensel, D.: Knowledge engineering: Principles and methods. *Data Knowl. Eng.* **25**(1–2), 161–197 (1998)

Network Traffic Prediction Based on Wavelet Transform and Genetic Algorithm

Xuehui Zhao, Wanbo Zheng^(✉), Lei Ding, and Xingang Zhang

College of Computer Science and Technology, Jilin University, Changchun, China
442014097@qq.com, zwb@jlu.edu.cn

Abstract. The traditional network traffic prediction is based on the establishment of a linear model, which can't describe the changes of network traffic accurately, resulting in low prediction accuracy. This paper proposes a new model of network traffic prediction based on wavelet transform and Genetic Algorithm. Firstly, after a wavelet decomposition, network traffic is turned into many stable components. Secondly, using BP neural network to predict each stable component, and optimizing neural network by genetic algorithm. Finally, all the prediction of components is combined to achieve highly-accurate traffic prediction. The experimental results show that the model has a better predictive effect.

Keywords: BP neural network · Wavelet transform · Network traffic prediction Time series · Genetic algorithms

1 Introduction

Network traffic data is a kind of time-series data. The analysis of traffic data can help people know the running status of the network, which can do it more reasonably in bandwidth allocation, control flow, routing control, and error control [1]. Thus, it is an effective way to improve QoS (Quality of Service).

Today's network traffic presents some characteristics as nonlinear, abrupt and non-stationary. The first-generation network traffic prediction models, such as Markov model, Poisson model, AR model and ARMA model, can't describe the non-stationary characteristics of traffic. Meanwhile the prediction accuracy is too low to be suitable for the current network traffic prediction [1].

Later, a second-generation traffic prediction model, such as FARIMA, gray model, neural network model, wavelet model, and support vector machine (SVM), which can capture long-run and non-linear flow characteristics [2]. But there are still some shortcomings, for instance, FARIMA can't describe the non-stationary characteristics of traffic; neural network model requires more training samples, and the algorithm is complex; gray model only applies in the occasions which original sequence changes not fast, according to the exponential law.

In order to overcome the limitation of single model and describe the characteristics of network data more accurately, some hybrid models have been proposed, such as gray neural network model [3], wavelet combined with neural network model [4], wavelet combined with time series model [5], and more complex combination of wavelet, neural

network and time series model [6] etc. In some cases, the complex combination of model methods may not reduce the forecast error of component. Although the method improves the accuracy of prediction, the complexity will increase at the same time. This model is suitable for occasions that require higher prediction accuracy and less time.

In this paper, a traffic prediction model combining wavelet transform and neural network is proposed and optimized by genetic algorithm. Firstly, process the traffic data by the wavelet decomposition, then the time series data will be decomposed into relatively simple components, for smoothing the original signal. Secondly, the BP neural network is used to predict the high frequency components and low frequency components respectively. Considering the shortcomings of slow convergence and local optimization, the genetic algorithm with good global search ability is used to optimize the weights and thresholds. Finally, the component is reconstructed to obtain the final prediction result. Experiments show that wavelet decomposition can effectively increase the signal stability, and BP neural network for non-linear changes in traffic has a better prediction effect. Meanwhile, the introduction of genetic algorithms accelerates the BP neural network convergence rate, and improve the prediction accuracy.

2 Technical Overview

2.1 Wavelet Decomposition and Reconstruction

Wavelet decomposition is proposed by Meyer and Mallat. Time series data are decomposed into two parts: low frequency and high frequency coefficient.

The decomposition of time series is achieved by Mallat algorithm, and the decomposition relationship is as follows:

$$\begin{cases} a_{j+1} = h_0 * a_j \\ d_{j+1} = h_1 * d_j \end{cases} \quad j = 0, 1, \dots \quad (1)$$

In the formula, h_0 represents a low-pass decomposition filter; h_1 represents a high-pass analysis filter; $*$ represents a convolution operator; a_j represents the low-frequency coefficients; d_j represents frequency coefficients. When $j = 0$, the original time series a_0 through h_0 and h_1 , after several decomposition, can be decomposed into the low frequency and high frequency coefficients of the original time series.

The wavelet reconstruction relations are as follows:

$$\begin{cases} A_j = g_0 * a_j \\ D_j = g_1 * d_j \end{cases} \quad j = 0, 1, \dots \quad (2)$$

In the formula, g_0 and g_1 represents a low-pass reconstruction filter and a high-pass reconstruction filter respectively; A_j represents a low-frequency component; D_j represents a high-frequency component.

Thus, the relation between the original time series S and A_j, D_j is as follows:

$$S = A_j + D_j \quad (3)$$

2.2 BP Neural Network

BP neural network is a hierarchical feed-forward network, and the training algorithm is back-propagation algorithm (referred to BP algorithm). This is a supervised learning method, and the basic idea is the least-squares algorithm. Using root mean square error (referred to RMSE) and gradient descent method to correct the network connection weight. The purpose is to minimize the RMSE between the actual and the specified output [9]. The principle is shown in Fig. 1.

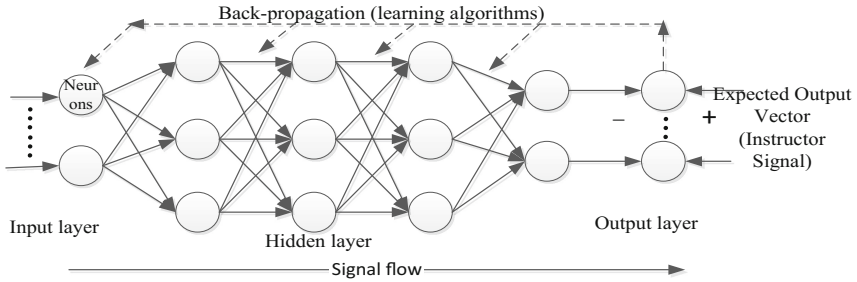


Fig. 1. BP neural network

The number of hidden layer neurons can be determined by the formula $m = \sqrt{l + n + a}$, and a is an integer between [1, 10].

2.3 Genetic Algorithm

The genetic algorithm (referred to GA) treats possible solutions in the problem space as chromosome individuals in the population, and encodes each individual into a symbol string. According to the fitness function, the value is calculated and then evolved from generation to generation. After simulating biological evolution, selecting, crossover, mutation and so on, the optimal solution [5] is obtained.

This paper discusses the weight optimization, including the following steps:

1. population initialization

Individuals are encoded with real numbers, and their encoding lengths are the sum of the number of network ownership values and the number of thresholds:

$$S = l \times m + m \times n + m + n \tag{4}$$

In the formula, S is the code length, and l, m, n are the number of neurons in the input layer, hidden layer, and output layer respectively.

2. fitness function

$$F = k \left(\sum_{i=1}^n \text{abs}(y_i - o_i) \right) \tag{5}$$

In the formula, n is the number of output node in the network output layer, k is the coefficient used to adjust the range of fitness values, y_i is the expected output of the i th node of BP neural network, o_i is the i th node prediction output.

3. selecting

We use the roulette method based on individual fitness selection strategy.

$$P_i = \frac{k}{F_i \sum_{j=1}^n \frac{k}{F_j}} \quad (6)$$

In the formula, P_i is the selection probability of each individual, k is coefficient, n is the number of individuals, F_i is the fitness value of individual i .

4. crossover

In this paper, the real cross method, that is, the k th chromosome a_k and the l th chromosome a_l in the j -bit cross operation method is as follows:

$$\begin{cases} a_{kj} = a_{kj}(1 - b) + a_{lj}b \\ a_{lj} = a_{lj}(1 - b) + a_{kj}b \end{cases} \quad (7)$$

In the formula, b is a random number between $[0,1]$.

5. mutation

$$a_{ij} = \begin{cases} a_{ij} + (a_{ij} - a_{\max}) \times f(g) & r \geq 0.5 \\ a_{ij} + (a_{\min} - a_{ij}) \times f(g) & r < 0.5 \end{cases} \quad (8)$$

$$f(g) = r_2(1 - g/G_{\max})$$

In the formula, a_{ij} is to the j th gene in the i th individual, a_{\max} is the upper bound of the gene a_{ij} , a_{\min} is the lower bound of the gene a_{ij} , r_2 is a random number, g is the current number of iterations, G_{\max} is the maximum evolution number, r is a random number between $[0,1]$.

3 Design of Traffic Prediction Model Based on Wavelet Decomposition and Genetic Algorithm

3.1 Model Ideas

The network traffic data is self-similar (single fractal) on a large time scale, while multi-fractals appears on a smaller scale [10]. The model in this paper firstly processes the flow data by wavelet decomposition, and the prediction model is composed of BP neural network, as shown in Fig. 2. Genetic algorithm is introduced to optimize the weights and thresholds of neural networks [11].

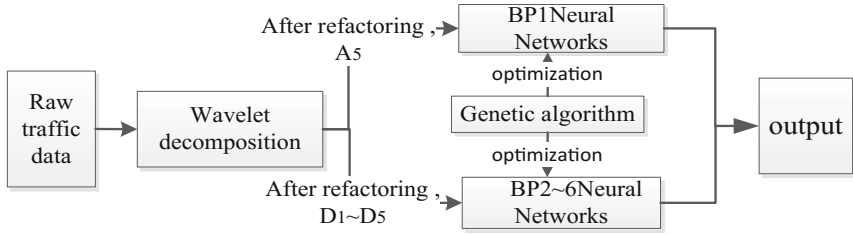


Fig. 2. Schematic diagram of network traffic prediction model

To optimize the BP neural network by genetic algorithm, the specific process is shown in Fig. 3:

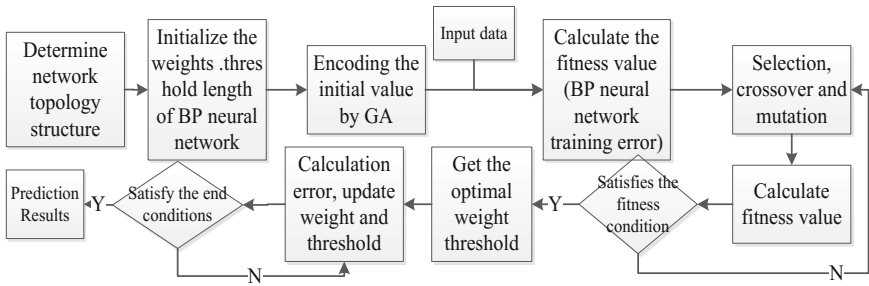


Fig. 3. Flow of GA optimizing BP neural network

3.2 Model Steps

- Step 1: Wavelet decomposition. The wavelet transform is performed on the input traffic data by the formula (1) Mallet algorithm. By using the Wavelet Toolbox in MATLAB, the decomposition level is L , the low-frequency and high-frequency components with stationary features at time k are obtained, as $\{D_1(k), D_2(k) \dots D_L(k), A_L(k)\}$. The original signal $S = D_1 + D_2 + D_3 + \dots D_L + A_L$;
- Step 2: Initialize BP1, BP2, BP3...BP(L + 1) neural network. They have three layers: input layer has 24 neurons, single hidden layer, output layer has 12 neurons;
- Step 3: Preprocessing $A_L(k), D_1(k), D_2(k) \dots D_L(k)$, and the samples of each neural network are constructed for training;
- Step 4: Training neural network BP1 optimized by genetic algorithm. $A_L(k)$ is the input of BP1 neural network, $A_L(k + T)$ at $k + T$ time is the expected value of the network. The training process is shown in Fig. 2;
- Step 5: Training BP2, BP3...BP(L + 1) optimized by genetic algorithm. $D_1(k)$ is the input of BP2 neural network, $D_1(k + T)$ is the expected value at time $k + T$, $D_2(k)$ is the input of BP3, $D_2(k + T)$ is the expected value at time $k + T$, and so on.
- Step 6: Input the test data flow, combined $L + 1$ component (high-frequency and low-frequency components) obtained from neural network prediction, and

comparing the actual results. Among them, the error of component prediction is not only positive but negative. After combination, part of the error can be offset.

4 Network Traffic Prediction Model Implementation

4.1 Wavelet Decomposition

In this paper, network traffic data comes from the CERNET backbone network center in Northeast China, which is offered by China Education and Research Network. Using the Shenyang-Changchun 30 days of data (from April 31, 2016 to May 29, 2016), as shown in Fig. 4. Network traffic is in units of GB, and selecting 2 h as the acquisition time granularity, that is, 12 points a day, 30 days a total of 360 points.

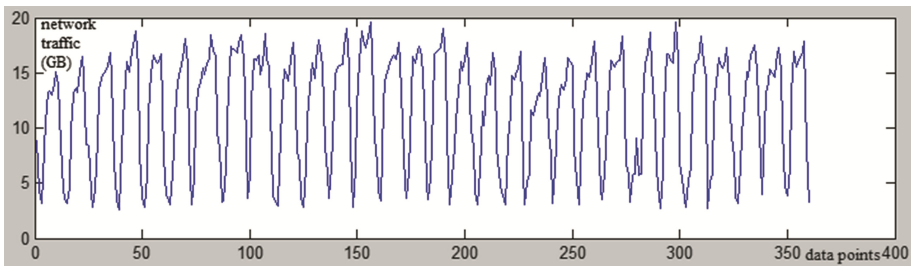


Fig. 4. Graph of real traffic data

For the data flow in Fig. 4, wavelet transform is performed using the formula (1) (2). Selecting db4 as Wavelet base, decomposition scale $L = 5$, the high-frequency and low-frequency component are $\{D_1(k), D_2(k), D_3(k), D_4(k), D_5(k), A_5(k)\}$ and the original signal $S = D_1 + D_2 + D_3 + D_4 + D_5 + A_5$, as the results shown in Fig. 5.

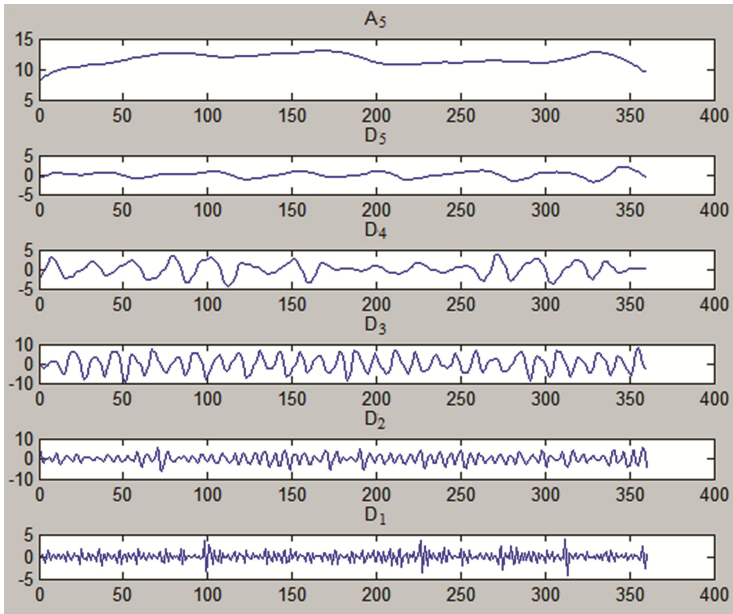


Fig. 5. Data signal after wavelet transform

4.2 Preprocessing of Traffic Data Sequence

In order to speed up the convergence rate of neural network and improve the prediction accuracy, the normalized network flow data after wavelet decomposition is processed [12]. The formula is:

$$X' = \left[\frac{X - X_{\min}}{X_{\max} - X_{\min}} \right] \tag{9}$$

The normalized data is within the range of [0,1], X_{\max} and X_{\min} are the maximum and minimum values respectively in the network traffic data set, X' is the normalized value, X is the original value of the variable.

4.3 The Sample Construction of Neural Network

$X_{i,j}$ represents the network traffic on the i th day at j time, X_i represents the network traffic on the i th day. The network traffic data is $X = \{(X_{1,1}, X_{1,2}, \dots, X_{1,n}), (X_{2,1}, X_{2,2}, \dots, X_{2,n}), \dots, (X_{m,1}, X_{m,2}, \dots, X_{m,n}), \dots\}$; The specified k learning samples is $P = ((X_1, X_2, \dots, X_j); (X_2, X_3, \dots, X_{j+1}); \dots; (X_k, X_{k+1}, \dots, X_{k+j-1}))$; The corresponding k teaching samples $T = (X_{j+1}; X_{j+2}; \dots; X_{j+k})$. The purpose of learning is to correct the weight, using the error between the neural network output corresponding to the k learning samples P_1, P_2, \dots, P_k and the corresponding teacher samples T_1, T_2, \dots, T_k , so that the output is close

to the expected teacher sample. X_{i+j} is a seasonal time series with j as the cycle, T_i is the teacher sample, the relationship between the two is $T_i = X_{i+j}$.

In this paper, $m = 30$, $n = 12$ and $n = 2$, the input layer of network training uses 24 neurons, the flow of 2d is mapped respectively; the output layer uses 12 neurons, mapping the future 1d flow.

4.4 Training Neural Networks

After several debugging experiments, BP1 neural network is determined as a $24 \times 12 \times 12$ three-layer structure, and the excitation functions of input layer, hidden layer and output layer are purelin; BP2 is a $24 \times 16 \times 12$ three-layer structure, and the excitation functions are tansig, tansig, purelin; BP3, BP4, BP5 is a $24 \times 10 \times 12$ three-layer structure, and the excitation functions are tansig, tansig, purelin; BP6 neural network is a $24 \times 16 \times 12$ three-layer structure, and excitation function, training function is the same as BP3. The training functions of these neural networks are trainlm, the maximum training times are 2000, the neural network target error is $1e^{-4}$, the learning rate is set to 0.3, and the rest is the default value.

In this paper, GAOT is used to program the genetic algorithm. The flow of the algorithm is shown in Fig. 3, and the objective function is performed according to the fitness function, the formula (5). Population size is set to 50, genetic algebra is 100, real coding, mutation is the probability of 0.09, and the rest is the default value.

5 Traffic Prediction and Analysis of Results

The data of the first 20d(days) were selected for training, and the data of the last 10d(the last 120 points) were used for testing. The flow time series of 30d is:

$$X = \{t_1 = (t_{1,1}, t_{1,2}, \dots, t_{1,12}); t_2 = (t_{2,1}, t_{2,2}, \dots, t_{2,12}); \dots; t_{30} = (t_{30,1}, t_{30,2}, \dots, t_{30,12})\};$$

The learning samples: $P = \{(t_1, t_2); (t_2, t_3); \dots; (t_{18}, t_{19})\}$, and the corresponding teaching samples: $T = \{t_3, t_4, \dots, t_{20}\}$. The network is predicted after learning, using t_{19} (network traffic on day 19) and t_{20} (network traffic on day 20) to predict traffic on day 21, and using t_{20} and t_{21} to predict traffic on day 22, and so on.

Figures 6 and 7 show the results of the short-term prediction of the last 120 data 1 day in advance. Figure 6 is a comparison of the new model without genetic algorithm (GA) optimization, and Fig. 7 is the comparison chart of new model after GA optimization. The abscissa is the detection point and the ordinate is network traffic (GB).

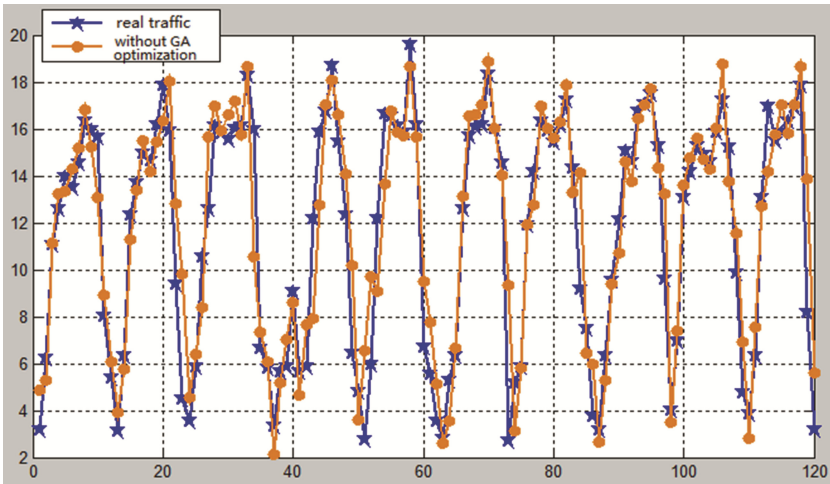


Fig. 6. Unoptimized fitting figure of 1d short-term prediction

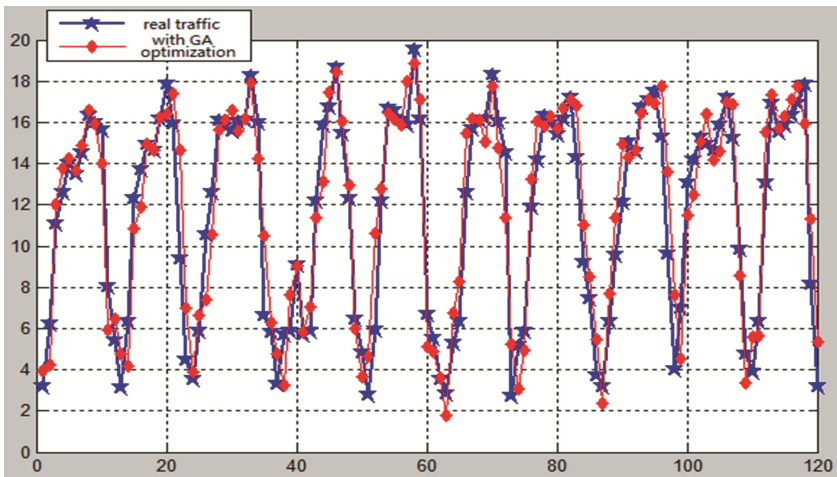


Fig. 7. GA optimized fitting figure of 1d short-term prediction

The prediction results of Fig. 6 shows that the new model has a higher prediction accuracy and a better degree of fit. Figure 7 shows that the new model is satisfactory. To clarify the performance of the new model, the results of the model performance parameters using GA or not are listed in Table 1.

Table 1. Parameters of model performance

Model	MSE	MAE	RMSE	R-square
New model without GA (1d)	3.3507	1.2670	1.8305	0.9027
New model with GA (1d)	2.6736	1.2583	1.6351	0.9680

MSE is the mean square error, MAE is the absolute error, RMSE is the root mean square error, and R-square is the determination coefficient.

From Table 1, we can see that the MSE of the new model is reduced by 20.21%, comparing the new model without the optimization, and the prediction accuracy is improved. Meanwhile, the coefficient of determination of the new model is increased by 7.23%, which improves the fitting degree. This indicates that genetic algorithm is feasible and effective to optimize the new model.

Although the genetic algorithm needs time to run, it speeds up the neural network convergence rate, and improve the prediction accuracy. The comparison of training times and running time are shown in Table 2.

Table 2. Compare training times and running time

The name of neural network	New model without GA optimization		New model with GA optimization	
	Training times	Running time(s)	Training times	Running time(s)
BP1	45	22.37	35	20.56
BP2	10	9.57	5	16.97
BP3	13	9.13	10	10.22
BP4	10	8.32	8	14.17
BP5	22	15.13	10	12.71
BP6	12	7.37	6	10.56

The above results prove the validity of using genetic algorithm. The new model can predict the traffic of t_{21} and t_{22} according to t_{19} , t_{20} and so on. The prediction results are shown in Fig. 8.

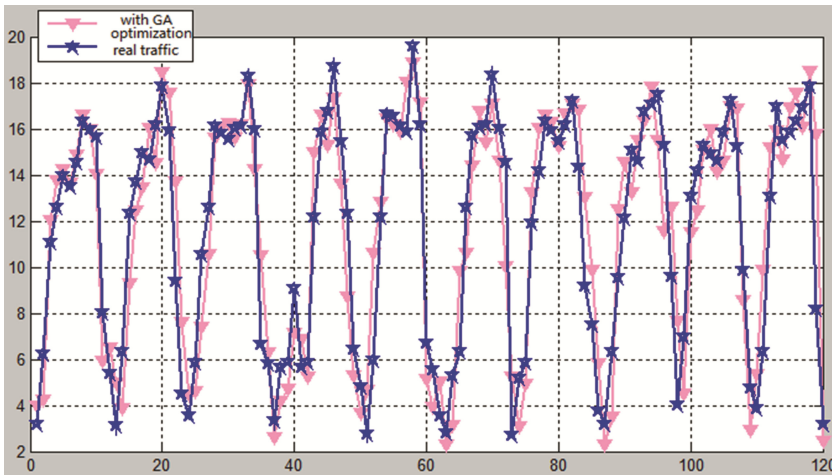


Fig. 8. GA optimized fitting figure of 2d short-term prediction

Using new model with GA optimization to realize the short-term forecast 3 days in advance, as shown in Fig. 9.

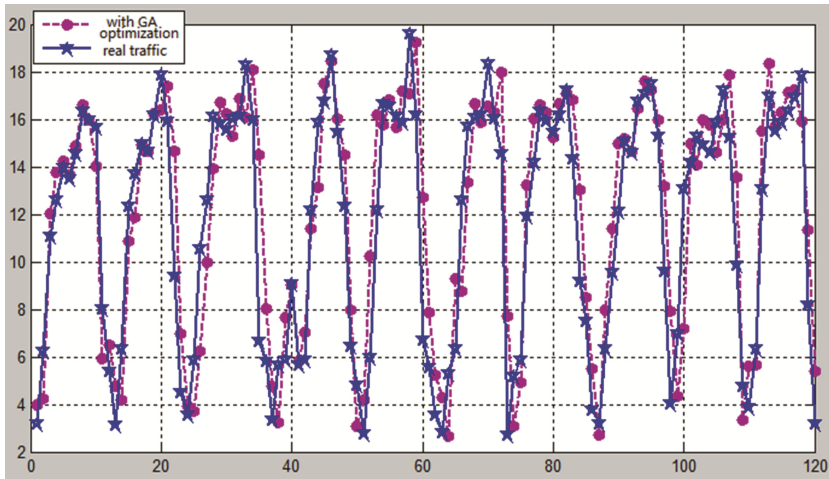


Fig. 9. GA optimized fitting figure of 3d short-term prediction

The parameters of the new model performance with GA optimization are listed, which is 2d and 3d predicted in advance, as shown in Table 3.

Table 3. Parameters of model performance

Model	MSE	MAE	RMSE	R-square
New model with GA (2d)	3.8539	1.5591	1.9631	0.8476
New model with GA (3d)	4.7562	1.6605	2.1809	0.8119

From Tables 2 and 3, we can see that the new model has higher accuracy and better fitting degree in short-term prediction. Although the fitting of the 3d prediction curve of Fig. 9 is not superior to Figs. 7 and 8, the trend of the flow rate can be roughly described, with little effect.

6 Conclusion

The results of MATLAB simulation show that the network traffic prediction model based on wavelet decomposition and genetic algorithm has good accuracy and it is an effective prediction model, which is mainly embodied in:

1. After wavelet decomposition, the original signal becomes more simple and has good stability, which provides the stability for BP neural network prediction;
2. The traditional time series analysis method is difficult to ensure high accuracy. For non-linear traffic flow, BP neural network prediction is better;
3. Genetic algorithm can improve the defects of BP neural networks, which can easily fall into the local optimal solution and the convergence rate.

However, the model in this paper is rather complicated. The high-frequency and low-frequency components obtained by wavelet decomposition are predicted by neural network, and the computational cost of prediction is large, which affects efficiency of the model. Therefore, in the case of the high accuracy, to further improve the efficiency of the model is the future research direction of this paper.

References

1. Wang, Z.X., Sun, Y.G., Chen, Z.Q., Yuan, Z.Z.: Study of predicting network traffic using fuzzy neural networks. *J. Chin. Inst. Commun.* **3**(26), 136–140 (2005)
2. Hou, J.L.: Prediction for network traffic based on Elman neural network. *Comput. Simul.* **28**(7), 154 (2010)
3. Liu, X.W., Fang, X.M., Qin, Z.H., Ye, C., Xie, M.: A short-term forecasting algorithm for network traffic based on chaos theory and SVM. *J. Netw. Syst. Manag.* **19**, 427–447 (2011)
4. Cao, J.H., Liu, Y.: Network traffic prediction based on grey neural network integrated model. *Comput. Eng. Appl.* **05**, 155–157 (2008)
5. Chen, Z.W., Guo, Z.W.: Simulation realization of prediction model based on wavelet neural network. *Comput. Simul.* **25**(6), 147–150 (2008)
6. Zhang, H., Wang, X.: Modeling and forecasting for network traffic based on wavelet decomposition. *Appl. Res. Comput.* **08**, 3134–3136 (2012)
7. Li, D.D., Zhang, R.T., Wang, C.C., Xiao, D.P.: A new network traffic prediction model based on ant colony algorithm in cognitive networks. *ACTA ELECTRONICASINI -CA* **10**, 2245–2250 (2011)
8. Bai, X.Y., Ye, X.M., Jiang, H.: Network traffic predicting based on wavelet transform and autoregressive model. *Comput. Sci.* **07**, 47–49 (2007)
9. Deng, K.L., Zhao, Z.Y.: Research and Simulation of stock price prediction mode based on genetic algorithm BP neural network. *Comput. Simul.* **26**(5), 317 (2009)
10. Boris, T., Nicolas, D.: Self-similar processes in communications networks. *IEEE Trans. Inf. Theory* **44**, 1713–1725 (1998)
11. Yao, M.H.: Application of improved genetic algorithm in optimizing BP neural networks weights. *Comput. Eng. Appl.* **24**, 49–54 (2013)
12. Dang, X.C., Hao, Z.J.: Prediction for network traffic based on modified Elman neural network. *J. Comput. Appl.* **10**, 2648–2652 (2010)

Research and Optimization of the Cluster Server Load Balancing Technology Based on Centos 7

Lei Ding^(✉), Wanbo Zheng, Shufen Liu, and Zhian Han

School of Computer Science and Technology, Jilin University,
No. 2699, Qianjin Avenue, Qianweinan District,
Changchun, Jilin, People's Republic of China
dinglei0828@qq.com

Abstract. The paper is to observe Weighted Least-Connection Algorithm, a default one of load balancing scheduling algorithms, and point out its deficiencies by establishing Linux Virtual System under Centos 7. Then we also improve the factors that influence weight based on above. During the experiment, not only is the throughput of system increased, but also the responding time shortened. It optimizes the performance and improves the stability of the whole system consequently in brief.

Keywords: Load balance · Scheduling · Cluster · WLC algorithm
Throughput rate

1 Preface

With present information on the Internet is growing at a geometric rate, parallel architecture technique of distribute web cluster service is also growing more mature. Most service vendors establish cluster system through Linux, which can effectively settle many concurrent requests to balance load and fix bugs in time [1]. This text relates to the latest released version of Centos 7, which manages and assigns tasks by using default load balance schedule of LVS and ip_vs module.

The management applications abroad at the earliest were obsoleted to settle with unbalanced load among multi servers, because deployment of each machine was verbose, such as Zeus [2]. After that, load balance production based on software and hardware appeared, like Barracuda and Load Directors, which started early on load technique issue and maintained leading position.

LVS was a free software project. It started and studied by Wen-song Zhang, a doctor of National University of Defense Technology. It covered more than ten kinds of load scheduling algorithms with IP load balance technique mainly. Therefore, LVS came first on the list of load management system for cluster as well as had great fame home and abroad with characters of scalability, reliability and manageability [3, 4].

In the study of Weighted Least-Connect Scheduling, we thought that ratio between client connections and own weight for every server could not measure load capacity accurately. Therefore, we introduced extra factors such as CPU, memory, hard disk, etc.

Most web service involved internet I/O resource, which also reflected part of real load for each server. We should consider all those factors together above and make a rational division of upcoming task for load balancer to enhance performance of the whole system. In next section, we introduce the traditional WLC algorithm and the improved version.

2 Load Balancing Scheduling Algorithm

There are three ways such as *VS/NAT*, *VS/TUN* and *VS/DR* to realize LVS under IP load balancing technique. *VS/DR* could avoid load balancer being the system bottleneck. It could also reduce the complexity of configuration sometimes. The following is the *VS/DR* architecture diagram of this experiment, as shown in Fig. 1.

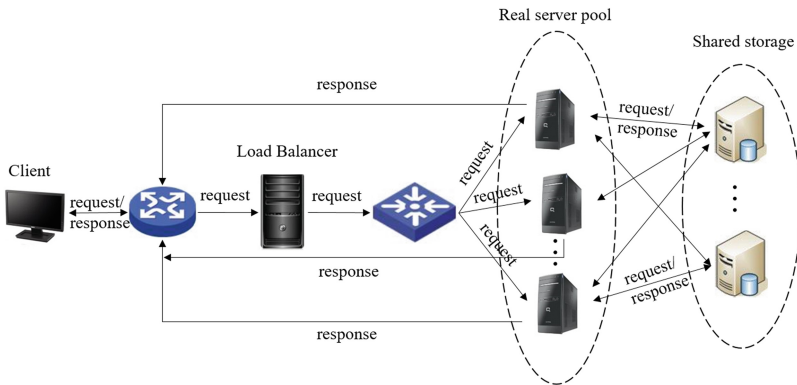


Fig. 1. *VS/DR* architecture

2.1 Traditional Weighted Least-Connection Scheduling Algorithm

More than ten traditional load balance-scheduling algorithms are built-in for Centos 7, most of which use Weighted Least-Connection Scheduling as default [5]. The schedule is the superset of the Least-Connection one. The server S_i ($i = 0, 1, \dots, n$) uses weight $W(S_i)$ as its performance with default 1, uses $C(S_i)$ as the current number of connections and use $Csum$ as the $\sum C(S_i)$. The condition as shown in formula (1) indicates a new task assigned to S_m next.

$$\frac{C(S_m)/Csum}{W(S_m)} = \min\left\{\frac{C(S_i)/Csum}{W(S_i)}\right\} \quad (1)$$

As $Csum$ from each side is extremely similar and efficiency of multiplication exceed division, then we could simplify it to formula (2) [6].

$$C(S_m) * W(S_i) > C(S_i) * W(S_m) \quad (2)$$

WLC’s aim is to find the server S_i in server pool with the minimal value of C/W , and then assign the new task to it. However, it is not reliable by just using the connections and weight as we discussed above. Administrator with much experience must change the value of weight manually during the whole procedure. Therefore, we introduce and adopt the improved WLC algorithm in next section.

2.2 Improved WLC Algorithm

The parameters such as CPU, memory and disk of servers are introduced to estimate their real load and update weight automatically in the improved version. $L(S_i)$ represents load seizure rate, $P(S_i)$ represents performance of hardware, $F(S_i)$ indicates performance of network. $P(S_i)$ and $F(S_i)$ should be concerned together to explain whole performance better. Usually, $P(S_i)$ which indicates for hardware would change little with increasing pressure, so we could assume it as static variable and send it to load balancer once. However, $F(S_i)$ dynamically change by throughput rate and TTLB factors, it could be send back with $L(S_i)$ together. The calculate formula is shown as below [7].

$$L(S_i) = \lambda_1 * Lcpu(S_i) + \lambda_2 * Lmem(S_i) + \lambda_3 * Ldisk(S_i) \tag{3}$$

$$P(S_i) = \mu_1 * Pcpu(S_i) + \mu_2 * Pmem(S_i) + \mu_3 * Pdisk(S_i) \tag{4}$$

$$F(S_i) = \gamma_1 * Ftlb(S_i) + \gamma_2 * Ftr(S_i) \tag{5}$$

The λ, μ, γ represent the percentage of each item, whose range in $(0, 1)$ and sum is 1. We could assign them specific values into the above formulas to reduce the complexity and benefit for control variables. Therefore, load weight of server could be estimated as formula (6). $W(S_i)$ is proportional to $L(S_i)$ while it is in inverse proportional to $F(S_i)$. Load balancer collects $L(S_i)$ and $F(S_i)$ of each server while new time slice ΔT begins [8].

$$W(S_i) = \frac{L(S_i)}{P(S_i) * F(S_i)} \tag{6}$$

In order to improve fault tolerance and avoid server becoming overload during ΔT while a new task comes, we put forward the concept of load redundancy to indicate extra load that server could hold [9, 10]. Load redundancy represents the max extra capacity within a slice of Δt as formula (7) [5].

$$R(S_i) = \frac{P(S_i) * F(S_i) * \Delta t}{L(S_i)} \tag{7}$$

Δt ’s range is expected to be [5, 10] seconds. On the one hand, Δt to be small would bring extra computation frequently, on the other hand, it would be too large to reflect the redundancy timely. Load balancer also needs to set an initial minimal redundancy threshold $Rmin$ and a binary sort tree, only the $R(S_i)$ which is equal or greater than

threshold could be added in that data structure. Every node of the tree has chance to receive new task, but we optimally choose the largest value of $R(Si)$, which means we choose the smallest $W(Si)$ with less load pressure [5, 12].

$P(Si)$ and $F(Si)$ could be estimated by software in next section. $L(Si)$ has three factors which change as time goes on, here are intuitive ways to get these values respectively below.

- (1) Real-time CPU utilization rate considers differences within two close moment from the file “/proc/stat” on a Linux server, the content shows many kinds of time slices whose unit are *jiffies*. Formula (8) shows *totalTime* for CPU.

$$totalTime = user + nice + system + idle + iowait + irq + softirq + stealstolen + guest \quad (8)$$

We set *totalTime* as $T1$, *idle* to $I1$. Then after a period of a very short time, we calculate *totalTime*, *idle* again and set them to $T2$, $I2$ respectively. Finally, formula (9) shows the CPU utilization rate.

$$Lcpu(Si) = \frac{(T2 - T1) - (I2 - I1)}{T2 - T1} \quad (9)$$

- (2) The memory information of Centos 7 is stored in “/proc/meminfo”. Formula (10) shows the free memory of Linux, and formula (11) shows the occupancy rate of memory which *MemTotal* indicates the total memory size.

$$Mfree = Memfree + Buffers + Cached \quad (10)$$

$$Lmem(Si) = \frac{MemTotal - Mfree}{MemTotal} \quad (11)$$

- (3) We can install “iotop” software to check whole I/O occupancy rate under Linux. The command “iotop-o” shows all processes/threads which include I/O operations. We focus the column named “IO>” and assign the sum to $Ldisk(Si)$.

$$Ldisk(Si) = \sum_{tid=1}^n IO(tid) \quad (12)$$

The communication between load balancer and servers use TCP socket [11]. Server, a TCP client, sends message $L(Si)$, $R(Si)$ and $F(Si)$ regularly but $P(Si)$ only once. Load balancer, a TCP server, receives values of each server and calculates new $W(Si)$ and $R(Si)$. If $R(Si) > Rmin$, we put this server into the tree. If $R(Si) < Rmin$, then we remove this server out of the tree [5]. Traversing the tree in order ensures the smaller node we pick up can deal with a new task easier.

2.3 Result of Experiment

We use various kinds of software such as “AIDA64”, “CPU-Z”, “Web Application Stress Tool” to estimate $P(S_i)$ with scores and $F(S_i)$ like Figs. 2 and 3 [12]. The experiment imitates the operations of login, add, refresh, and quit in sequence on the bookmarking website we build before which was written by PHP.

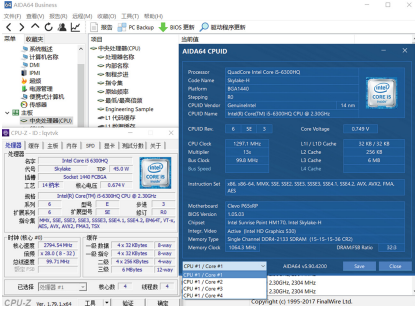


Fig. 2. AIDA64

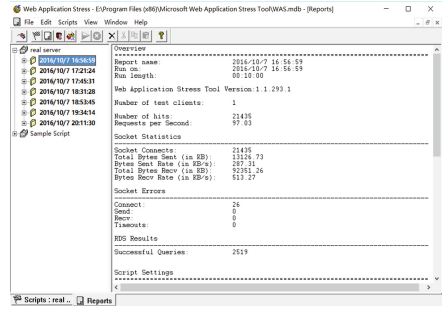


Fig. 3. Web application stress tool

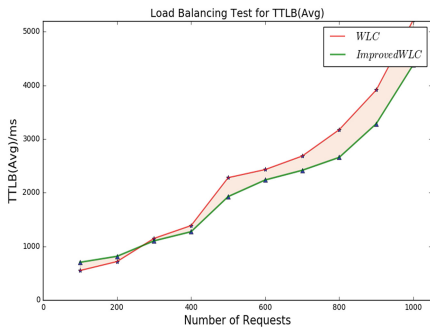


Fig. 4. TTLB average response time



Fig. 5. Bytes received rate

Firstly, we assign $\lambda_1 = 0.4$, $\lambda_2 = 0.3$, $\lambda_3 = 0.3$, $\mu_1 = 0.5$, $\mu_2 = 0.4$, $\mu_3 = 0.1$, $\gamma_1 = 0.4$, $\gamma_2 = 0.6$ and $\Delta t = 10$ s. Then we collect average response time and throughput with increasing number of requests. Figures 4 and 5 show the trend lines.

The improved algorithm when request quantity after 271 is superior to the traditional in Fig. 4. Frequent calculation and update operations need extra time in the early period, but it shorts the response time with more rational strategy to assign tasks. The throughput increases first and decrease later in Fig. 5, the improved is superior the traditional after about 267. It reaches maximum at about 410 because the system achieves saturation gradually with increasing requests.

Secondly, we discuss about the factors λ , γ in $L(Si)$ and $F(Si)$ with the same 800 requests respectively as Tables 1 and 2 below.

Table 1. λ factor

$\lambda_2 \backslash \lambda_1$ ttlb	0.1	0.3	0.6	0.8
0.1	1894.36	2017.12	2398.40	2658.32
0.3	2271.24	2475.67	2825.21	—
0.6	3093.45	3317.04	—	—
0.8	3717.72	—	—	—

Table 2. γ factor

γ_1	$F(Si)$
0.2	1204.68
0.5	963.57
0.8	673.90

Table 1 shows changes of TTLB while providing λ with different percent. λ_1 has more influence than λ_2 and $(1 - \lambda_1 - \lambda_2)$, so CPU may have the highest priority. It is similar in Table 2 with γ . Setting appropriate factors can improve the situation [13]. Boundary values could not generate reliable result.

Finally, according to these analyses above, the improved algorithm lifts about 15–18% of load balancing performance in cluster environment. It is benefit for improving stability and efficiency of the whole system.

3 Conclusion

This paper introduces the approach to enhance performance of cluster system and offers better concurrency service after improving Weighted Least-Connection Scheduling. Estimating weights reasonably and filtrating statistical data for delivering task accelerate procedure of response smoothly. The improved one contributes to science experiment and business such as neural network, big data analysis, e-commerce, virtual host service, etc. However, there are still many problems to solve [1, 12], such as understanding more influenced factors fully, improving speed, etc. We will break the limitation and strong the algorithm with the development of technology in the future.

References

1. Semchedine, F., Bouallouche-Medjkoune, L., Aïssani, D.: Task assignment policies in distributed server systems. *J. Netw. Comput. Appl.* **34**(4), 1123–1130 (2011)
2. Cardellini, V., Colajanni, M., Yu, P.S.: Dynamic load balancing on web-server systems. *IEEE Internet Comput.* **3**(3), 28–39 (1999)
3. Zhang, W., Wu, T., Jin, S., Wu, Q.: Design and implementation of a virtual internet server. *J. Softw.* (2001). (in Chinese)
4. Zhang, W.: Research and implementation of scalable network services. *Comput. Eng. Sci.* (2001). (in Chinese)

5. Bryhni, H.: A comparison of load balancing techniques for scalable web servers. *IEEE Network* **14**(4), 58–64 (2001)
6. Penmatsa, S., Cronopoulos, A.T.: Dynamic multi user load balancing in distributed systems. In: *IEEE International Parallel and Distributed Processing Symposium* (2007)
7. Wang, H.: *Research on Adaptive Load Balancing Scheduling Strategy in Web Server Cluster System*. Jilin University, Changchun (2013). (in Chinese)
8. Lu, J., Chen, Z., Liu, A.: A dynamic regulation weight value scheme for LVS. *J. Comput. Eng.* **14**, 038 (2006). (in Chinese)
9. Wang, J., Pan, L., Li, X.: Dynamic feedback scheduling algorithm in LVS. *J. Comput. Eng.* **19**, 014 (2005). (in Chinese)
10. Sheng, G.Q., Wu, S.J., Ping, M.X., Chan, W.D., Min, Z.: Design and realization of dynamic load balancing based on Linux Virtual System. *J. Comput. Res. Dev.* **6**, 002 (2004). (in Chinese)
11. Chun, W.: *Core Python Applications Programming*. 3rd edn. Prentice Hall (2012)
12. Wang, C., Dong, L., Jia, L.: Load balance algorithm for web cluster system. *J. Comput. Eng.* **36**(2), 102–104 (2010). (in Chinese)
13. Guo, C., Yan, P.: A dynamic load balancing algorithm for heterogeneous web server cluster. *Chin. J. Comput.* **2**, 004 (2005). (in Chinese)

Base Station Location Optimization Based on Genetic Algorithm in CAD System

Yanhua Wang^(✉), Laisheng Xiang, and Xiyu Liu

College of Management Science and Engineering, Shandong Normal University, Jinan, China
15554130027@163.com, xls3366@163.com, sdxyliu@163.com

Abstract. A good base station deployment plan can help network operators save cost and increase total revenue significantly under the premise of ensuring network quality. But in the past, base station location planning is often manually based on the engineer's experience. It has a lower efficiency and very high error rate. In this paper, a new method based on genetic algorithm is proposed to optimize base station location. In our work, a CAD system based Google Earth and ACIS is designed to provide data for Genetic algorithm and display the location of base station in the reconstructed terrain. This system which takes three-dimensional geographic coordinates as the input of the algorithm is advanced and different from the traditional method which only uses two-dimensional coordinates, that is, this three-dimensional system can better display the base station location and take the height into consideration. The proposed method is based on a mathematical model of base station location. Genetic Algorithm is used to find the solution of this model so that it can effectively reduce the error rate of base station location.

Keywords: Genetic Algorithm · Base station planning · Coverage · ACIS
Google earth · CAD system

1 Introduction

Excellent base station location plan for operators can help to get the best results in the mobile communications market in the increasingly fierce competition [1]. Early plan and design of the base station is mainly by the network optimization engineer based on experience and field measurements to choose [3, 4]. Obviously, this method is not very scientific. Over-reliance on subjective factors, led to the results often far from the actual optimum configuration. Telecommunication base station automatic programming CAD system based Genetic Algorithm proposed in this paper is based on Windows platform.

The process of solve the problem of base station planning as follows. First, use Microsoft visual studio, *Xtreme Toolkit Pro*, ACIS/HOOPS to build the development environment. Second, using com technology import Google earth into the development environment and accessing and transforming Google earth coordinates which include longitude, latitude, and elevation. Third, use ACIS/HOOPS technology to reconstruct Three-Dimensional Terrain according to the transformed coordinates. At the same time, establish a multi-objective mathematical model about base station planning according

to geographic information and produce base station primary scheme using genetic algorithm. At last, it uses ACIS/HOOPS modeling techniques to display the primary scheme on the reconstructed terrain 1. Structure of the process is shown in Fig. 1:

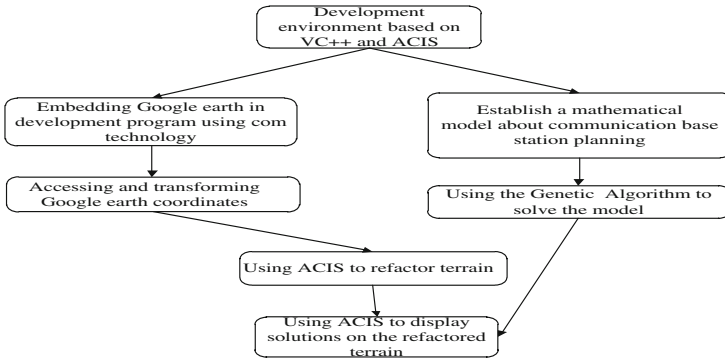


Fig. 1. Flow chart of base station location optimization

2 Terrain Reconstruction by Google Earth and ACIS Technology

ACIS is a development platform based on C++ structure graphics system, Developers can use these classes and functions construct a Three-Dimensional software system for end users. Google Earth provides a set of COM components that can be embedded into visual studio development platform by the COM technology [2]. Through the secondary development of Google Earth, you can get the actual terrain’s height, latitude and longitude information that was shown in Fig. 2 which can be converted into a three-dimensional coordinate that is shown in Fig. 3 of the screen of the CAD system so that it can simplify the data and facilitate the calculation when the transformed coordinates of the screen as the input of algorithm. After running the optimization algorithm, the optimal position of the output of the base station can be converted to the actual elevation, latitude and longitude coordinates.

```

The extracted coordinates.txt x    transformed coordinates.txt x
1  x=-1.00 y=-1.00 h=0.0316 d=130.5840
2  x=-1.00 y=-0.97 h=0.0323 d=130.5840
3  x=-1.00 y=-0.94 h=0.0329 d=130.5840
4  x=-1.00 y=-0.91 h=0.0336 d=130.5840
5  x=-1.00 y=-0.89 h=0.0344 d=130.5840
6  x=-1.00 y=-0.86 h=0.0351 d=130.5840
7  x=-1.00 y=-0.83 h=0.0358 d=130.5840
8  x=-1.00 y=-0.80 h=0.0366 d=130.5840
9  x=-1.00 y=-0.77 h=0.0373 d=130.5840
10 x=-1.00 y=-0.74 h=0.0380 d=130.5840
11 x=-1.00 y=-0.71 h=0.0388 d=130.5840
12 x=-1.00 y=-0.69 h=0.0395 d=130.5840
13 x=-1.00 y=-0.66 h=0.0402 d=130.5840
14 x=-1.00 y=-0.63 h=0.0409 d=130.5840
15 x=-1.00 y=-0.60 h=0.0417 d=130.5840
    
```

Fig. 2. The extracted actual coordinates

```

The extracted coordinates.txt x    transformed coordinates.txt x
1  B=117.0198829878 L=36.4970193010 H=144.587
2  B=117.0199017391 L=36.4981932428 H=147.588
3  B=117.0199204825 L=36.4993665838 H=150.587
4  B=117.0199397257 L=36.5005395673 H=153.665
5  B=117.0199607694 L=36.5017127824 H=157.024
6  B=117.0199818085 L=36.5028853160 H=160.382
7  B=117.0200028287 L=36.5040571917 H=163.737
8  B=117.0200238340 L=36.5052283955 H=167.091
9  B=117.0200448395 L=36.5063989278 H=170.443
10 B=117.0200658265 L=36.5075687948 H=173.793
11 B=117.0200867997 L=36.5087379963 H=177.141
12 B=117.0201077685 L=36.5099065283 H=180.487
13 B=117.0201285058 L=36.5110743255 H=183.810
14 B=117.0201490736 L=36.5122414092 H=187.114
15 B=117.0201696289 L=36.5134078344 H=190.417
    
```

Fig. 3. The transformed screen coordinates

The transformed screen coordinates can be used to reconstruct the terrain by ACIS technology with `api_face_spl_apprx`, `api_face_plane` and `api_loft_faces` interface. The reconstructed terrain was shown in the Fig. 4, the actual terrain was shown in the Fig. 5. The reconstructed terrain was used to show the plan of base station location in Three-dimensional 3.



Fig. 4. The actual terrain

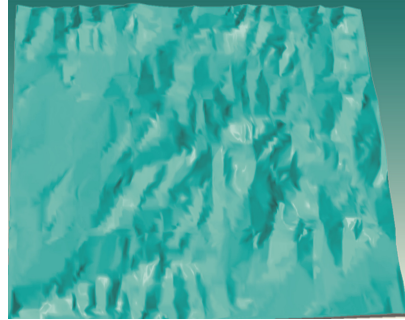


Fig. 5. The reconstructed terrain

3 The Mathematical Model of Base Station Location

3.1 Coverage Rate Statement and Formulation

Coverage rate is calculated by using the number of demand points which are covered, divided by the total number of the demand points of the terrain points [4]. To avoid a repeat count of demand points, we just put the demand point included in the base station's coverage area which has the nearest distance from the demand point compared to other base stations. To formulate coverage targets we defined as follows: U is the set of all demand points; j is the demand points which $j \in U$, T is the set of all base stations; i is the base station which $i \in T$. d_{ij} is the distance between base station i and demand point j , r_i is coverage radius of base station i , the coverage area of base station i , denoted by C_i , is defined as the collection of demand points which is within the coverage area of i and has the shortest distance from i among all the base stations. Formally stated, C_i is given by:

$$C_i = \{j \in U | d_{ij} \leq r_i \wedge (d_{ij} \leq d_{i'j}, \forall i' \in T \wedge i' \neq i)\} \tag{1}$$

The ultimate goal of optimizing the coverage is achieve full coverage of all user points by using the minimum number of base stations.

In the actual experiment, we defined f_{CT} as a function of the base station coverage goals. The total number of all demand points covered by all base stations is given by $\sum_{i \in T} C_i$. The total number of all demand points deployed on the terrain is denoted by $|U|$. When $f_{CT} = 1$, all demand points in the terrain are fully covered. However, a $f_{CT} = 0.95$ is quite acceptable. Although a $f_{CT} = 1$ is too costly to achieve, f_{CT} is maximized in the model. f_{CT} is defined as follows:

$$\text{Max}f_{CT} = \frac{\sum_{i \in T} C_i}{|U|} \quad (2)$$

3.2 Cost Statement

Cost is a very important objective optimization goals, the investment of base station planning is about two-thirds of the total investment of the whole network. Therefore, a lower cost of base station planning can effectively reduce the total network investment so that it can enhance the competitiveness of the enterprise communication. The cost of the base station planning is mainly from the built of base stations. In condition of each base station has a fixed cost, the number of base stations becomes the most important optimization goals.

In order to prevent the waste of the base station, the number of base station we calculated by divide the terrain area by the area of the base station. There are three different radii of base stations, so the number of base stations in the interval [20, 30] inner. By experiment, when the number is 25, the cost is optimal.

4 Model Solving Based on Genetic Algorithm

Genetic algorithm is one of the four main branches of evolutionary computation. It is also the main evolutionary algorithm developed rapidly in the last ten years. Genetic algorithm with evolutionary strategy, evolutionary programming and genetic programming had been rapid development and gradually to integration, and formed a new computational theory of simulated evolution [5, 6].

In the genetic algorithm, simulate the evolution of biological processes, chromosomes or individuals of the population perform crossover and mutation operations [7]. The implementation of basic genetic manipulation need to use the selection, crossover and mutation of the three types of genetic operators. Thus, the genetic algorithm is also considered as a random search algorithm. But it is also a process through iterative optimization, with self-adapting characteristics.

In the process of solve the mathematic model by Genetic Algorithm, we use floating point encoding to encod $X_i = \{x_{i1}, x_{i2}, x_{i3} \dots, x_{i,3m-2}, x_{i,3m-1}, x_{i,3m}\}$ ($m = |TS|$) is the encoding of i -th chromosome of GA algorithm ($x_{i,3m-2}, x_{i,3m-1}, x_{i,3m}$) $\in X_i$ ($k = 1 \dots m$) is the three-dimensional coordinates of k -th base station. $F = f_{CT}$ is the objective function of entire system, so $F(X_i)$ is the fitness value of i -th chromosome, That is a measure of the solution of deployment of m base stations in the planning region. The fitness value is closer to 1, indicating that the program closer to the optimal. Algorithm flow chart is shown in Fig. 6.

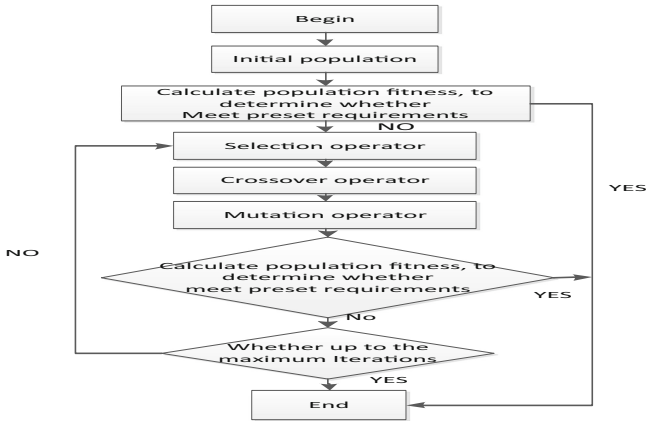


Fig. 6. Genetic Algorithm flow chart

In the CAD system, we design a dialog to run the Genetic Algorithm which is shown in Fig. 7. The maximum Iterations input box is used to set the maximum number of iterations. Color setting input box is used to set the color of base station. First we design the maximum iterations is 100. The Genetic Algorithm didn't up to the optimal result and stopped at the 100th generation. The result which the base station's color is green is shown in Fig. 8. Second we design the maximum iterations is 1000. The Genetic Algorithm up to the optimal result and stopped at the 523th generation. The result which the base station's color is red is shown in Fig. 8. The cycle is the signal of each base station.

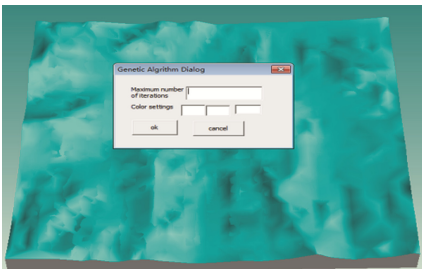


Fig. 7. Genetic Algorithm dialog

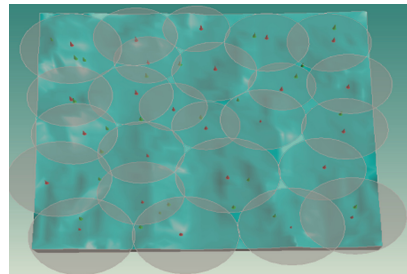


Fig. 8. The plan of base station location (Color figure online)

The iterative process of the Genetic Algorithm is shown in Fig. 9, we use 25 base station and iterated 300 times, the coverage rate is as shown in the Fig. 9.

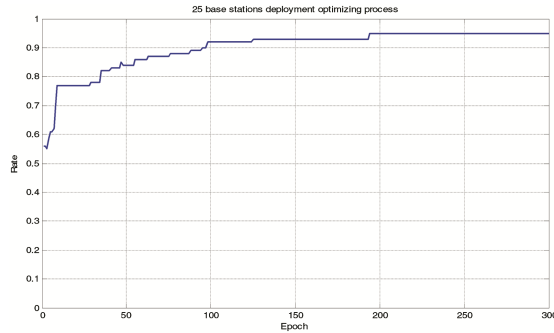


Fig. 9. Iterative process of the Genetic Algorithm

5 Conclusions

In this paper, we proposed a new method based genetic algorithm to make base station location plan. At this time, we developed a CAD system based Google Earth and ACIS to provide data for Genetic Algorithm and demonstrate base station location plan in the reconstructed terrain which is Three-dimensional.

The future work will continue research on improving traditional intelligent optimization algorithm and implement it on a three-dimensional CAD system. Meanwhile, the mathematic model of base station plan will be further design. The genetic algorithm will be improved.

Acknowledgment. Projected supported by National Natural Science Foundation of China (61472231, 61170038, 61502283, 61640201), Jinan City independent innovation plan project in College and Universities, China (201401202), Ministry of education of Humanities and social science research project, China (12YJA630152), Social Science Fund Project of Shandong Province, China (11CGLJ22, 16BGLJ06).

References

1. Xie, Q., Liu, X., Yan, X.: Research on station location optimization CAD system based on the cooperative mode. In: Zu, Q., Hu, B. (eds.) HCC 2016. LNCS, vol. 9567, pp. 930–935. Springer, Cham (2016). https://doi.org/10.1007/978-3-319-31854-7_102
2. Xie, Q., Liu, X., Yan, X.: Base station location optimization based on the Google Earth and ACIS. In: Zu, Q., Hu, B. (eds.) HCC 2016. LNCS, vol. 9567, pp. 487–496. Springer, Cham (2016). https://doi.org/10.1007/978-3-319-31854-7_44
3. Ren, S., Li, X., Liu, X.: The 3D visual research of improved DEM data based on Google Earth and ACIS. In: Zu, Q., Vargas-Vera, M., Hu, B. (eds.) ICPCA/SWS 2013. LNCS, vol. 8351, pp. 497–507. Springer, Cham (2014). https://doi.org/10.1007/978-3-319-09265-2_51
4. Tao, M., et al.: SA-PSO based optimizing reader deployment in large-scale RFID Systems. *J. Netw. Comput. Appl.* **52**, 90–100 (2015)

5. Fogel, L.J., Owens, A.J., Walsh, M.J.: *Artificial Intelligence Through Simulated Evolution*. John Wiley & Sons, New York (1966)
6. Schwefel, H.-P.: *Numerical Optimization of Computer Models*. John Wiley & Sons Inc., New York (1981)
7. Golberg, D.E.: *Genetic Algorithms in Search, Optimization, and Machine Learning*. Addison Wesley, Boston (1989)

A Study of Optimal Multi-server System Configuration with Variate Deadlines and Rental Prices in Cloud Computing

Zhongfeng Kang and Bo Yang^(✉)

School of Computer Science and Engineering, University of Electronic Science and Technology of China, Chengdu 611731, Sichuan, People's Republic of China
kzhf921203@163.com, yangbo@uestc.edu.cn

Abstract. Cloud computing is becoming more and more popular and attracts considerable attention. In the three-tier cloud environment, an important problem is to determine the optimal multi-server system configuration so that the profit of the service provider can be maximized. In related work, the maximum allowed waiting time of service is assumed to be a constant, and the rental price is also assumed to be constant for all servers despite the fact that different servers have different execution speeds. These assumptions may not be valid in realistic cloud environments. In this paper, we propose an optimization model to determine the optimal configuration of the multi-server system. There are two major differences of the proposed model with that of the existing work. First, the maximum allowed waiting time is not a constant and may change with different service requests. Second, the situation that the servers with different execution speed may have different rental prices is taken into account. Experiments are carried out to verify the performance of the proposed optimization model. The results show that the proposed optimization model can help the service provider gain more profit than the existing work.

Keywords: Multi-server system · Profit maximization
Maximum allowed waiting time · Response time · Rental price

1 Introduction

Cloud computing is becoming more and more popular and attracts considerable attention [5]. In a cloud computing environment, there are three tiers, i.e., infrastructure providers, service providers, and consumers (see Fig. 1) [1, 2]. An infrastructure provider maintains the basic hardware and software resources. A service provider could rent a certain scale of software and hardware resources from infrastructure providers and provides services to consumers. Consumers can submit their service requests to the service provider and pay them based on the quantity and the quality of the services. In above cloud computing environment, the problem of optimal multi-server system configuration for profit maximization is introduced as a significant, new research topic in computer science [3–5]. The configuration of a multi-server system is characterized by two basic features, i.e., the size of the multi-server system (the number of rented servers)

and the execution speed of the multi-server system (execution speed of the rented servers) [3]. The key issue of the multi-server system configuration problem is to determine the optimal size and execution speed of the multi-server system such that the service provider can gain the maximum profit.

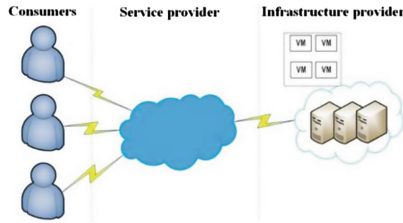


Fig. 1. The three tiers cloud environment.

Like any other business, the profit is the most important issue to a service provider. The service provider's profit is determined by two parts, i.e., the gained revenue and the corresponding cost, the revenue minus the cost is its profit. For a service provider, the revenue is the sum of the charge to the consumers, and the cost is the rental cost paid to the infrastructure providers plus the electricity cost caused by energy consumption. The charge to a consumer is related to the quantity and the quality of the service, that is, if the quality of the service is guaranteed, the service is fully charged, otherwise, if the quality of the service request is lower than the promised Quality of Service (QoS), the service provider serve the service request for free as a penalty of low service quality [3, 6, 7]. The electricity cost is linearly proportional to the number of the servers and to the square of the server speed [8, 9].

Many existing works have been done on the problem of multi-server system configuration for profit maximization in the literature [3–5]. Cao et al. [3] proposed a single renting scheme to configure the multi-server system. Using this scheme, the servers in the multi-server system are all long-term rented servers, so the system is lack of elasticity and easily leads to resource waste and consumer loss. To overcome this weakness, Mei et al. [4] proposed a combined renting scheme. Using combined server renting scheme, the main computing capacity is provided by long-term rented servers, and the rest is provided by short-term rented servers. In this service system, when a consumer submits a service request, the service request will be first put into a queue and wait in the queue until it can be served by any server. But in order to satisfy the QoS requirement, the waiting time of each service request in the queue must be limited within a certain range, which is named the maximum allowed waiting time and is determined by the service lever agreement (SLA). To guarantee the QoS, the service request should be started no later than the maximum allowed waiting time. So, for a service request in the queue, if its waiting time has reached the maximum allowed waiting time, system temporarily rents a short-term server to provide service and the short-term server is freed when the service is finished. But in Mei et al.'s study, the maximum allowed waiting time for all service requests is deemed to be the same, that is, the service requests in the multi-server system have equal maximum allowed waiting

times. This assumption may not be realistic. Therefore, this paper takes into account the condition that different service requests may have different maximum allowed waiting time.

In Mei et al.'s work [4], the servers with different execution speed is deemed to have the same rental price. Thus the rental cost in their work is only related to the number of the rented servers. But more realistically, the rental price of the server may depend on the execution speed. Hence, the rental cost is not only related to the number of rented servers but also the execution speed of the rented servers, i.e., the more (less, respectively) number of the rented server is, the more (less, respectively) rental cost is, also the faster (slower, respectively) execution speed of rented server is, the more (less, respectively) rental cost is.

In this paper, the problem of optimal multi-server system configuration for profit maximization is studied as an optimization model. In this optimization model, the conditions that the maximum allowed waiting times may be variables and the rental price of the server may be changed with the execution speed of the rented server are taken into account. The contribution of the paper is summarized as follows.

The maximum allowed waiting times of different service requests are deemed to be no longer a constant but random variables.

The condition that the rental price for different execution speed server may be different is taken into consideration. And a rental price model is proposed.

An optimization model is proposed to solve the problem of optimal multi-server system configuration for profit maximization.

Experimental studies are conducted to verify the performance of the proposed optimization model. The results show that the proposed optimization model proposed in this paper can result in more profit than that of existing work.

The rest of the paper is organized as follows. Section 2 presents the relevant models and rental scheme, including a three-tier cloud environment model, a multi-server system model, an energy consumption model and a combined renting scheme. In Sect. 3, an important probability used in this paper is calculated. Section 4 describes the rental price model. Section 5 establishes an optimization model to solve the problem of optimal multi-server system configuration for profit maximization. Section 6 verifies the performance of the proposed model through comparison with that of existing model. Finally, Sect. 7 concludes the work.

2 The Cloud Environment, Models and Renting Scheme

This section introduces three relevant models, namely a three-tier cloud environment model, a multi-server system model and an energy consumption model, and a combined renting scheme.

2.1 Three-Tier Cloud Environment Model

In this paper, we study the multi-server system configuration problem under three-tier cloud computing environment, in which there are three tiers, i.e., infrastructure providers, service providers, and consumers [3, 4, 15], as shown in Fig. 1. The infrastructure

provider maintains the basic hardware and software resources. The service provider rents a certain scale of software and hardware resources from infrastructure providers and builds its service platform to provide services to consumers. Consumers submit their service requests to the service provider and pay based on the quantity and the quality of the services. The infrastructure provides two kinds of resources renting schemes, i.e., long-term renting and short-term renting, and the rental price per server per unit period of time with long-term renting is much cheaper than that with short-term renting [4]. For a service provider, the gained revenue is the sum of charge to consumers, and the cost involved is the rental cost paid to the infrastructure providers plus the electricity cost caused by energy consumption. Thus the profit is generated from the gap between the revenue and the cost [3, 5].

2.2 Multi-server System Model

The cloud service provider is considered to be a multi-server system with a service request queue [17]. The multi-server system consists of m long-term rented identical servers and it can extend by temporarily renting short-term servers from infrastructure provider [4], therefore, the multi-server system may have two parts, i.e., long-term rented servers (the *long-term part*) and possible short-term rented servers (the *short-term part*). Each server in the multi-server system has an execution speed of s (unit: billion instructions per second) [4]. The long-term part of the multi-server system can be modeled by an $M/M/m$ queuing system [5, 18].

This paper makes the following assumptions, which are adopted for the multi-server system. These assumption are also use in related studies [3, 4].

- (i) Service requests arrive according to a Poisson process, with arrival rate λ (measured by the number of service requests arrived per second). It means that the inter-arrival times are independent and identically distributed (i.i.d.) exponential random variables (r.v.'s) with mean $1/\lambda$.
- (ii) The multi-server system maintains a queue with infinite capacity.
- (iii) Different service requests may have different service sizes (measured by the number of billion instructions), denoted by r_i ($i \in \{1,2,3,\dots\}$), which are i.i.d. exponential r.v.'s with parameter μ .
- (iv) Each service request can only be served by one server that may be long-term or short-term rented.
- (v) The first-come-first-served (FCFS) queuing discipline is adopted.

Denote by $N(t)$ the total number of service requests that arrives during the time interval $(0,t]$, with mean $E[N(t)] = \lambda t$.

Denote by $N_s(t)$ and $N_l(t)$ the number of the service requests that served by the short-term and long-term servers, respectively, during the time interval $(0, t]$.

An arrived service request is put into the queue and waits in the queue until it can be handled by any available server. Then, the working process of the system can be modeled as Fig. 2.

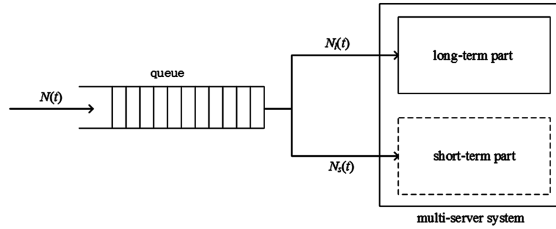


Fig. 2. The working process of the system.

According to assumption (iii), the mean of r_i is $\bar{r} = E(r_i) = \frac{1}{\mu}$ (unit: billion instructions), and the execution times of the services on the multi-server system, $x_i = \frac{r_i}{s}$ ($i \in \{1,2,3,\dots\}$), are i.i.d. exponential r.v.'s, with mean $\bar{x} = E(x_i) = \frac{\bar{r}}{s} = \frac{1}{\mu s}$ (unit: second).

The system service intensity means the average percentage of time that a server of the multi-server system is busy. Denote by ρ the system service intensity, which can be given by

$$\rho = \frac{\lambda \bar{r}}{ms} = \frac{\lambda}{m\mu s}, \tag{1}$$

According to [5, 10], ρ should be no more than 1, i.e., $\frac{\lambda}{\mu} \leq ms$.

Denote by W_i the waiting time of service request i in the queue. The cumulative distribution function (c.d.f.) of W_i , $F_{W_i}(t)$, can be derived from $M/M/m$ queuing system theory [11], which is

$$F_{W_i}(t) = 1 - \frac{\pi_m}{1 - \rho} e^{-m\delta(1-\rho)t}, \tag{2}$$

where

$$\pi_m = \frac{(m\rho)^m}{m!} \left[\sum_{k=0}^{m-1} \frac{(m\rho)^k}{k!} + \frac{(m\rho)^m}{m!(1-\rho)} \right]^{-1}.$$

2.3 Energy Consumption Model

The cost of a service provider consists of two major parts, i.e., the rental cost paid to the infrastructure provider and the electricity cost caused by energy consumption. The cost of energy consumption is determined by the electricity price and the amount of energy consumption.

Denote by ψ the price of unit energy (unit: cents per Watt). The power consumption of modern processor can be divided into two parts, dynamic power P_d (unit: Watt) and

static power P^* (unit: Watt) [12]. The dynamic power model used in the paper is given by Eq. (3), which is also used in [3–5].

$$P_d = \xi s^\alpha \quad (3)$$

When $\xi = 9.4192$ and $\alpha = 2.0$, the value of power consumption is close to the value of the Intel Pentium M processor [13]. Therefore, the power per unit period of time for a busy server is

$$P = P_d + P^*. \quad (4)$$

2.4 Combined Renting Scheme

The renting scheme combines long-term renting with short-term renting for the multi-server system [4]. The main service capacity of the multi-server system is provided by long-term rented servers, due to the low rental price; and the rest service capacity is provided by short-term rented servers. Algorithm 1 shows the combined renting scheme.

Algorithm 1. Combined renting scheme

1. A multi-server system with m servers and speed s is running and waiting for the events as follows
 2. A queue Q is initialized as empty
 3. **Event** - A service request arrives
 4. Put it at the end of queue Q and records its maximum allowed waiting time and the timer starts counting its waiting time
 5. **End Event**
 6. **Event** - A server becomes idle
 7. Search if the queue Q is empty
 8. **if true then**
 9. Wait for a new service request
 10. **else**
 11. Take the first service request from queue Q and assign it to the idle server
 12. **end if**
 13. **end Event**
 14. **Event** - The maximum allowed waiting time of a request is achieved
 15. Take this request from queue Q and rent a temporary server to execute the request
 16. **End Event**
 17. **Event** - A service on the temporary server is completed
 18. Release the temporary server
 19. **End Event**
-

Denote by W_i^m (unit: second) the maximum allowed waiting time of service request i in the queue before it is served. When a consumer submits a service request i to the system which is then put into the queue, the system records W_i^m and starts counting its waiting time W_i . The requests are assigned and executed on the long-term rented servers according to FCFS discipline. Once W_i of service request i reaches W_i^m , a temporary short-term server is rented from infrastructure provider to process the request [4]. The time that spending on renting activity is very short, so this time is ignored in this paper.

As the long-term part is modeled as an $M/M/m$ queuing system, then the multi-server system builds on the combined renting scheme can be modeled as an $M/M/m$ queuing system with impatient consumers [4]. Denote by $pe(\overline{W_i < W_i^m})$ the steady-state probability that W_i reaches W_i^m for service request i . Then, service request i will be served on a temporary short-term rented server according to the probability $pe(\overline{W_i < W_i^m})$, and will be served on the long-term part according to the probability $1 - pe(\overline{W_i < W_i^m})$. $pe(\overline{W_i < W_i^m})$ can be calculated next section.

3 $pe(\overline{W_i < W_i^m})$ Under Variate Maximum Allowed Waiting Time

In related work [4, 5, 7], W_i^m for all i in the queue is assumed to be a constant. This assumption may not be realistic, such as for a service request i , the maximum allowed response time may be shorter than W_i^m , which will lead to lower QoS. So the condition that the W_i^m may change with different service requests is considered.

In this paper, the QoS of service request i is reflected by the response time T_i (unit: second). Denote by T_i^m (unit: second) the maximum allowed response time that service request i can tolerate before it is completed. T_i^m is assumed to be linearly proportional to the service size r_i , namely $T_i^m \propto r_i$, i.e., $T_i^m = d \cdot r_i$, where d is a positive constant and determined by the service-level agreement (SLA). It can be noted that the waiting time plus the execution time is the response time, i.e., $T_i = W_i + x_i$. Then

$$W_i^m = T_i^m - x_i = kr_i, \tag{5}$$

where

$$k = \frac{ds - 1}{s}. \tag{6}$$

According to assumption (iii), the service sizes r_i 's are i.i.d. exponential r.v.'s with the parameter μ , so W_i^m ($i \in \{1,2,3,\dots\}$) are i.i.d. exponential r.v.'s with the parameter μ/k . The probability density function (p.d.f.) of W_i^m is

$$f_{W_i^m}(t) = \frac{\mu}{k} e^{-\frac{\mu}{k}t}, \tag{7}$$

and the mean of W_i^m is k/μ , where k is given by Eq. (6).

According to [10], the probability of the event $W_i < W_i^m$ is:

$$\Pr(W_i < W_i^m) = \int_0^\infty F_{w_i}(t) f_{W_i^m}(t) dt. \tag{8}$$

Substitute (2) and (7) into (8), and after some manipulation, we have

$$\Pr(W_i < W_i^m) = 1 - \frac{\pi_m \mu}{(1 - \rho)[km\delta(1 - \rho) + \mu]}. \tag{9}$$

Therefore, the probability of complementary event of $W_i < W_i^m$, $\Pr(\overline{W_i < W_i^m})$, is:

$$\Pr(\overline{W_i < W_i^m}) = 1 - \Pr(W_i < W_i^m) = \frac{\pi_m \mu}{(1 - \rho)[km\delta(1 - \rho) + \mu]}. \tag{10}$$

In $\Pr(\overline{W_i < W_i^m})$, all service requests, in spite of exceeding their maximum allowed waiting times, will be waiting in the queue. However, in the combined rented scheme multi-server system, the service request whose waiting time reaches its maximum allowed waiting time will be removed out of the queue and assigned to a temporary short-term server, which will reduce the waiting time of the following requests. Therefore, it will reduce the probability that the waiting time reaches maximum allowed waiting time of the following service requests. According to [11], $pe(\overline{W_i < W_i^m})$ is as:

$$pe(\overline{W_i < W_i^m}) = \frac{(1 - \rho) \Pr(\overline{W_i < W_i^m})}{1 - \rho \Pr(\overline{W_i < W_i^m})}, \tag{11}$$

where ρ is given by (1), $\Pr(\overline{W_i < W_i^m})$ is given by (10).

It can be seen from (5), (6), (10) and (11) that $pe(\overline{W_i < W_i^m})$ is affected by d . Figure 3 illustrates the $pe(\overline{W_i < W_i^m})$ with different d , where $\lambda = 5.99$, $\mu = 1$, $m = 6$ and $s = 1$ [4].

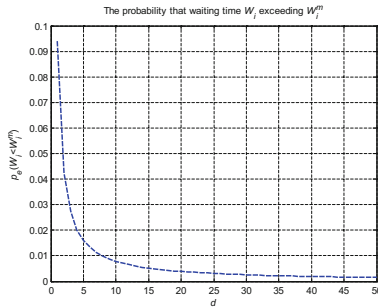


Fig. 3. The probability of W_i exceeding W_i^m .

4 Rental Price Model

In this section, a new rental price model is described. In related work [4], Mei et al. deemed that the servers with different execution speed have the same rental price. Hence, they assume all long-term servers have the same rental price β (unit: cents per second) for

each server, and all short-term servers have the same rental price γ (unit: cents per second) for each server as well, where $\beta < \gamma$. This assumption may not be realistic.

In practice, the rental price for a server normally changes with the execution speed of the server, i.e., a server with higher execution speed normally has a higher rental price. In this paper, this condition is taken into account. Denote by s_0 (unit: billion instructions per second) the baseline execution speed [3]. The rental price of a long-term rented server with execution speed s_0 is β_0 (unit: cents per second), and the rental price of a short-term rented server with execution speed s_0 is γ_0 (unit: cents per second), where $\beta_0 < \gamma_0$. The infrastructure provider maintains some kinds of servers with different execution speed s . s can be either higher or lower than s_0 , but $s \in S$, where S is the set of the possible execution speed. The service provider can select any kind of server with the speed limited in S to rent.

Assume that there are two relation expressions between execution speed and the rental price for long-term rented server and short-term rented server, respectively, as follows:

$$\frac{\beta}{\beta_0} = \left(\frac{s}{s_0}\right)^\tau \tag{12}$$

$$\frac{\gamma}{\gamma_0} = \left(\frac{s}{s_0}\right)^\tau \tag{13}$$

Hence, the rental price of a long-term or short-term rented with the execution speed s can get from (12) and (13), respectively, as follows:

$$\beta = \beta_0 \left(\frac{s}{s_0}\right)^\tau = \frac{\beta_0}{s_0^\tau} s^\tau \tag{14}$$

$$\gamma = \gamma_0 \left(\frac{s}{s_0}\right)^\tau = \frac{\gamma_0}{s_0^\tau} s^\tau \tag{15}$$

Figure 4 shows the rental price β and γ with different execution speed, where $s_0 = 1.0$, $\beta_0 = 1.5$ and $\gamma_0 = 3.0$. In Fig. 4, $\tau = 0.5$ and $\tau = 1$ for (a) and (b), respectively.

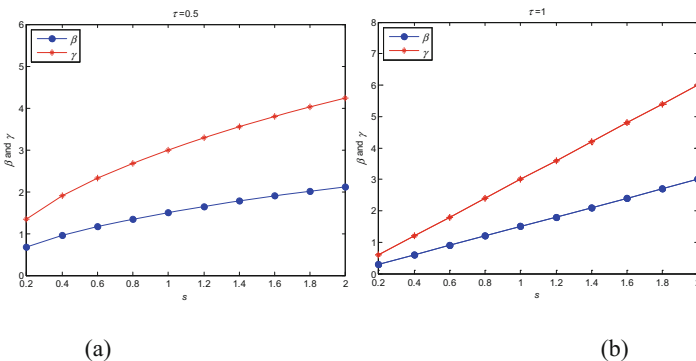


Fig. 4. Rental prices β and γ with different execution speeds s .

5 Optimal Multi-server System Configuration

To determine the optimal configuration (m, s) , the optimal number m and execution speed s of the servers in the multi-server system, such that the service provider can gain the maximum profit, an optimization model will be established in this section.

Denote by $pf(t)$ (unit: cents) and $R(t)$ (unit: cents) the profit and the revenue of the multi-server system during the time interval $(0, t]$, respectively. Denote by $C_l(t)$ and $C_s(t)$ the cost of the multi-server system on long-term servers and the short-term servers respective during the time interval $(0, t]$, including the rental cost and the electricity cost. Then the profit of multi-server system during the time interval $(0, t]$ can be calculated as:

$$pf(t) = R(t) - C_s(t) - C_l(t). \quad (16)$$

The mean of $pf(t)$ is

$$E[pf(t)] = E[R(t)] - E[C_s(t)] - E[C_l(t)]. \quad (17)$$

According to [10], the follow proposition can be got.

Proposition 1. $\{N_s(t)\}$ and $\{N_l(t)\}$ are both Poisson processes having respective rate $\lambda p_e(\overline{W_i < W_i^m})$ and $\lambda[1 - p_e(\overline{W_i < W_i^m})]$. Furthermore, the two processes are independent.

According to Proposition 1, the mean of $N_s(t)$ is

$$E[N_s(t)] = \lambda p_e(\overline{W_i < W_i^m}) \cdot t, \quad (18)$$

and the mean of $N_l(t)$ is

$$E[N_l(t)] = \lambda[1 - p_e(\overline{W_i < W_i^m})] \cdot t. \quad (19)$$

As the combined rented scheme can guarantee the QoS to all service requests, in steady-state, the revenue during the time interval $(0, t]$ can be represented as

$$R(t) = \sum_{i=1}^{N(t)} ar_i, \quad (20)$$

where a is a positive constant, which indicates the price per billion instructions (unit: cents per billion instructions).

According to [10], $R(t)$ is a compound Poisson process, with the mean

$$E[R(t)] = a\lambda t \cdot E(r_i) = \frac{a\lambda t}{\mu}. \quad (21)$$

The cost on the short-term rented servers in steady-state, $C_s(t)$, is calculated as:

$$C_s(t) = \sum_{i=1}^{N_s(t)} \frac{r_i}{s} (\gamma + \psi P) = \frac{\gamma + \psi P}{s} \sum_{i=1}^{N_s(t)} r_i, \quad (22)$$

where P is given by (4), γ is given by (15), ψ is introduced in Sect. 2.3.

According to (18) and (21), we have

$$E[C_s(t)] = \frac{\gamma + \psi P}{s} \cdot E\left[\sum_{i=1}^{N_s(t)} r_i\right] = \frac{\gamma + \psi P}{s\mu} \lambda p_e(\overline{W_i < W_i^m}) \cdot t. \quad (23)$$

The cost on the long-term rented servers in steady-state, $C_l(t)$, is calculated as:

$$C_l(t) = m\beta t + \psi p_l(t), \quad (24)$$

where

$$P_l(t) = m \cdot \left(\frac{\sum_{i=1}^{N_l(t)} r_i}{ms} P_d + P^* t \right), \quad (25)$$

and β is given by (14). In Eq. (25), P_d is given by (3), and P^* is introduced in Sect. 2.3.

According to (19), we have

$$E\left[\sum_{i=1}^{N_l(t)} r\right] = [1 - p_e(\overline{W_i < W_i^m})] \lambda t \cdot E(r) = \frac{[1 - p_e(\overline{W_i < W_i^m})] \lambda t}{\mu}, \quad (26)$$

then

$$\begin{aligned} E[P_l(t)] &= m \cdot \left\{ \frac{[1 - p_e(\overline{W_i < W_i^m})] \lambda t}{m\mu s} P_d + P^* t \right\} \\ &= m \cdot \{ [1 - p_e(\overline{W_i < W_i^m})] \rho P_d + P^* \} t, \end{aligned} \quad (27)$$

furthermore,

$$\begin{aligned} E[C_l(t)] &= m\beta t + \psi \cdot E[P_l(t)] \\ &= m \cdot \{ \beta + \psi [(1 - p_e(\overline{W_i < W_i^m})) \rho P_d + P^*] \} t. \end{aligned} \quad (28)$$

Therefore, substitute (3), (21), (23) and (28) into (17), we have

$$\begin{aligned} E[pf(t)] &= \frac{a\lambda t}{\mu} - \frac{\gamma + cP}{s\mu} \lambda p_e(\overline{W_i < W_i^m}) t \\ &\quad - m \cdot \{ \beta + \psi [(1 - p_e(\overline{W_i < W_i^m})) \rho \zeta s^\alpha + P^*] \} t. \end{aligned} \quad (29)$$

Then

$$\frac{E[pf(t)]}{t} = \frac{a\lambda}{\mu} - \frac{\gamma + cP}{s\mu} \lambda p_e(\overline{W_i < W_i^m}) - m \cdot \{\beta + \psi[(1 - p_e(\overline{W_i < W_i^m}))\rho \zeta s^\alpha + P^*]\}. \tag{30}$$

The key issue of the multi-server system configuration problem is to determine the optimal values of m and s of the servers so that the service provider can get the maximum profit. As the profit can be calculated as follows:

$$pf(m, s) = \frac{a\lambda}{\mu} - \left(\frac{\gamma_0 s^{\tau-1}}{s_0^\tau \mu} + \frac{cP}{s\mu} \right) \cdot \lambda p_e(\overline{W_i < W_i^m}) - m \cdot \left\{ \frac{\beta_0}{s_0^\tau} s^\tau + \psi[(1 - p_e(\overline{W_i < W_i^m}))\rho \zeta s^\alpha + P^*] \right\}. \tag{31}$$

The problem of optimal multi-server system configuration for profit maximization can be established as the following optimization model:

$$\text{Maximize } pf(m, s) \tag{32}$$

Subject to

$$\frac{\lambda}{\mu} \leq ms; \tag{33}$$

$$m \in \{1, 2, 3, \dots\}; \tag{34}$$

$$s \in S. \tag{35}$$

Equations (33)–(35) are the constraints of the established optimization model. Equation (33) indicates that the system service intensity is less than 1. Equation (34) denotes that the number of servers should be positive integer. The available execution speed levels of the server are limited in set S , which is indicated by Eq. (35). In the following section, some experiments are studied to testify the performance of the proposed optimization model.

6 Experimental Study

The proposed optimization model can be solved by any optimization algorithms, such as Genetic Algorithm, Ant Colony Algorithm, Simulated Annealing Algorithm, etc. In this paper, we use Genetic Algorithm to solve the optimization model and compare the results with those obtained from the optimization model in [4].

In [4], W_i^m , β and γ are all deemed to be constant. In order to increase the practicality of the proposed optimization model than [4], the conditions that the maximum allowed waiting times of services are r.v.’s and the rental price changed with the

execution speed are taken into account. In order to distinguish the proposed optimization model and the compared model, the proposed model is named as new model and the compared model is named as old model in this paper.

In order to use optimal algorithm to solve the new model and old model, it is necessary to get a closed-form expression of π_m . In this paper, we use the same closed-form expression as [3, 4], which is $\sum_{k=0}^{m-1} \frac{(m\rho)^k}{k!} \approx e^{m\rho}$. This expression is accurate when m is not too small and s is not to large [14]. According to Stirling's approximation of $m!$, i.e., $\sqrt{2\pi m} \left(\frac{m}{e}\right)^m$ [16], one closed-form expression of π_m is given by $\pi_m = \frac{1-\rho}{(1-\rho)\sqrt{2\pi m} \left(\frac{m}{e}\right)^m + 1}$. In the following, we solve new model and old model based on above closed-form expression of π_m .

6.1 Parameters Setting

In the compared old model, $\lambda = 5.99, a = 15, P^* = 3, c = 0.3, \alpha = 2.0, \xi = 9.41292, \bar{r} = 1, D = 5, \beta = 1.5, \gamma = 3$ and $S = \{0.2, 0.4, \dots, 2\}$ [4].

In the proposed new model, $\lambda, a, P^*, \xi, \alpha$ and S are sat as the same value with old model. $\psi = 0.3, \beta_0 = 1.5, \gamma_0 = 3, s_0 = 1, \mu = 1$, so that the mean of service size r in our proposed new model equals with the mean service size \bar{r} in Mei et al.'s work, namely $E(r) = \bar{r} = 1$, and set $d = \frac{1}{s} + 5$, so that $k = 5$ and $E(W_i^m) = D = 5$.

Denote by (m^*, s^*) and pf^* the optimal configuration and maximum profit respective to old model. Denote by (m, s) and pf the optimal configuration and maximum profit respective to new model. The profit of configuration (m^*, s^*) obtained in new model is denoted by pf' .

6.2 Performance Comparison

Table 1 shows the obtained optimal configuration and maximum profit of old model. It can be seen from Table 1, when the multi-server system rents 10 long-term servers with execution speed 1 billion instructions per second, the service provider can gain maximum profit 57.9124 cents interval a unit period time.

Table 1. The optimal configuration and maximum profit obtained from old model.

m^*	s^*	pf^*
6	1	57.9124

The QoS to services is guaranteed by the both models, so the revenue keeps same constant in both models.

In the first experiment, we explore the difference between configuration (m, s) and (m^*, s^*) , and the difference between profit pf and pf' , with different s_0 when parameter $\tau = 1$. The results are showed in Table 2. And Fig. 5a shows the changing trend of pf and pf' with different s_0 when $\tau = 1$. We can see that the figure shows the increasing trend of pf and pf' when s_0 is increasing from 0.2 to 2. That is because with the

Table 2. The difference between configurations (m, s) and (m^*, s^*) , and the difference between profits pf and pf' , with different s_0 when $\tau = 1$.

s_0	0.2	0.4	0.6	0.8	1.0	1.2	1.4	1.6	1.8	2
(m, s)	(10,0.6)	(10,0.6)	(10,0.6)	(10,0.6)	(10,0.6)	(10,0.6)	(10,0.6)	(10,0.6)	(10,0.6)	(10,0.6)
pf	23.1808	46.8233	54.7041	58.6445	61.0087	62.5849	63.7107	64.5551	65.2118	65.7372
(m^*, s^*)	(6,1.0)	(6,1.0)	(6,1.0)	(6,1.0)	(6,1.0)	(6,1.0)	(6,1.0)	(6,1.0)	(6,1.0)	(6,1.0)
pf'	19.9803	43.6800	51.5799	55.5299	57.8999	59.4798	60.6084	61.4548	62.1131	62.6398

increment of s_0 , the rental prices β and γ are both decreased. Hence the cost on long-term servers and short-term servers are both decreased when the number and execution speed of servers remain unchanged. In addition, the obtained profit pf to the new model proposed by this paper is always greater than the pf' , which indicates that the new model can gain more profit than old model by more reasonable configuration. It is can be seen from Table 2, the optimal configuration obtained from new model is 10 servers with 0.6 execution speed, while that obtained from compared old model is 6 servers with 1.0 execution speed.

Table 3. The difference between configurations (m, s) and (m^*, s^*) , and the difference between profits pf and pf' , with different s_0 when $\tau = 1.5$.

s_0	0.2	0.4	0.6	0.8	1.0	1.2	1.4	1.6	1.8	2
(m, s)	(30,0.2)	(15,0.4)	(15,0.4)	(15,0.4)	(15,0.4)	(10,0.6)	(10,0.6)	(10,0.6)	(10,0.6)	(10,0.6)
pf	11.8929	45.6617	56.4112	60.9118	63.2843	64.8931	66.0435	66.8462	67.4324	67.8758
(m^*, s^*)	(6,1.0)	(6,1.0)	(6,1.0)	(6,1.0)	(6,1.0)	(6,1.0)	(6,1.0)	(6,1.0)	(6,1.0)	(6,1.0)
pf'	-38.608	29.9072	46.9823	54.1312	57.8999	60.1681	61.6569	62.6957	63.4542	64.0281

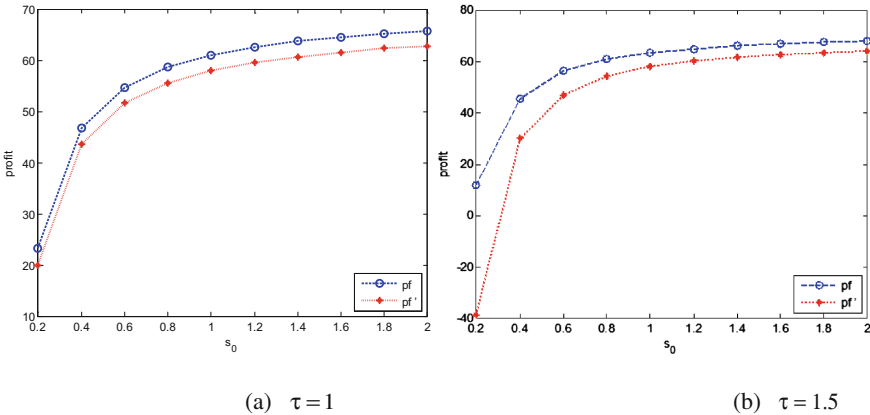


Fig. 5. The pf and pf' with different s_0 .

In the second experiment, the configurations (m, s) and (m^*, s^*) , the profits pf and pf' are compared, with different s_0 when $\tau = 1.5$, and the result is shown in Table 3. Figure 5b shows the changing trends of pf and pf' with different s_0 when $\tau = 1.5$. It can

be seen that the changing trends of two curves are similar from Fig. 5a. When s_0 is 0.2, the value of pf' is a negative. Which indicates that the optimal configuration gained from old model isn't much truthful, when $\tau = 1.5$, and $s_0 = 0.2$.

In the third experiment, we explore the difference between configuration (m, s) and (m^*, s^*) , and the difference between profit pf and pf' , with different τ when $s_0 = 0.6$. And the results are showed in Table 4. We can see that the configuration (m, s) changes from (6, 1) to (15, 0.4), when τ changes from 0.5 to 1.5, then (m, s) remain unchanged when τ increases. Figure 6a shows the changing trends of profit pf and pf' with different τ when $s_0 = 0.6$. It is can be seen from the figure, the two curves show different changing trends, i.e., the pf shows increased trend, but pf' shows decreased trend. That is because when s is greater or less than 0.6, β and γ show different trend with the increasing of τ , i.e. β and γ show decreased trend when s is greater than 0.6, but show increased trend when s is greater than 0.6. Furthermore, pf and pf' shows different changing trends.

Table 4. The difference between configurations (m, s) and (m^*, s^*) , and the difference between profits pf and pf' , with different τ when $s_0 = 0.6$.

τ	0.5	1	1.5	2	2.5
(m, s)	(6,1)	(10,0.6)	(15,0.4)	(15,0.4)	(15,0.4)
pf	55.1413	54.7041	56.4112	58.7676	61.1497
(m^*, s^*)	(6,1.0)	(6,1.0)	(6,1.0)	(6,1.0)	(6,1.0)
pf'	55.1413	51.5799	46.9823	41.0467	33.3840

Table 5 shows the results of the difference between configuration (m, s) and (m^*, s^*) , and the difference between profit pf and pf' are explored with a given τ when $s_0 = 1.2$. Figure 6b shows the changing trends of profit pf and pf' with different τ when $s_0 = 1.2$. From the figure, we can see that the profit pf and pf' show increasing trend when τ is increasing from 0.5 to 2.5. That is because with the increasing of τ , β and γ are both decreased when s is not more than 1.0. It is shown in Table 4, s and s^* are not more than 1, so β and γ are both decreased with the increase of τ in both configurations. Although with the increase of the number of servers the rental cost shows increase trend, the decrease trend is deeper with the increase of the execution speed of servers, so the rental cost integrally shows increase trend. As a consequence, the profit of the multi-server system increases. In addition, the profit obtained of our proposed new model is greater than the profit of compared old model. And with the increasing of τ from 0.5 to 2.5, the gap is more and more great. It is can be seen from Table 4, the optimal configuration obtained from this paper proposed new model is 10 servers with 0.6 execution speed when τ is 0.5 and 1, 15 servers with 0.4 execution speed when τ is from 1.5 to 2.5, while the counterpart obtained from compared old model is 6 servers with 1 execution speed. In essence, the difference of configuration leads to the gap of profit.

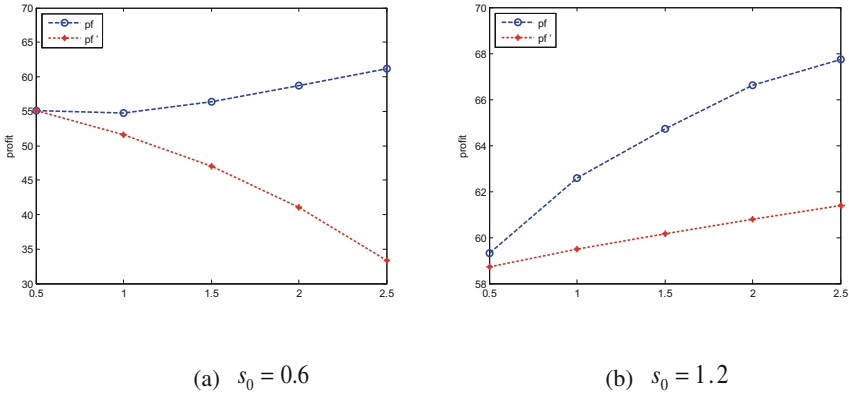


Fig. 6. The pf and pf' with different τ .

Table 5. The difference between configurations (m, s) and (m^*, s^*) and the difference between profits pf and pf' with different τ when $s_0 = 1.2$.

τ	0.5	1	1.5	2	2.5
(m, s)	(10,0.6)	(10,0.6)	(15,0.4)	(15,0.4)	(15,0.4)
pf	59.3206	62.5849	64.7123	66.6311	67.7390
(m^*, s^*)	(6,1.0)	(6,1.0)	(6,1.0)	(6,1.0)	(6,1.0)
pf'	58.7258	59.4798	60.1681	60.7965	61.3701

7 Conclusions

The problem of optimal multi-server system configuration for profit maximization in a three-tier cloud environment is investigated in this paper. We propose an optimization model to determine the optimal configuration such that the service provider can gain the maximum profit. There are two major differences with existing work. First, the maximum allowed waiting time is deemed random variable, which may change with the different service request. Second, the condition that the rental price of different execution speed may be different is taken into consideration. In addition, the performance of our proposed optimization model is verified by many experiments. The results of experiments show that the optimization model proposed in this paper can help the service provider gain more profit than existing work.

Acknowledgements. This work is supported by Sichuan Provincial Project of International Scientific and Technical Exchange and Research Collaboration Programs (Project No. 2016H H0023).

References

1. Lee, Y.C., Wang, C., Zomaya, A.Y., Zhou, B.B.: Profit-driven service request scheduling in clouds. In: Proceedings of the 10th IEEE/ACM International Conference on Cluster, Cloud and Grid Computing, pp. 15–24 (2010)
2. Chen, J., Wang, C., Zhou, B.B., Sun, L., Lee, Y.C., Zomaya, A.Y.: Tradeoffs between profit and customer satisfaction for service provisioning in the cloud. In: Proceedings of the 20th International Symposium on High Performance Distributed Computing, pp. 229–238. ACM (2011)
3. Cao, J., Hwang, K., Li, K., Zomaya, A.Y.: Optimal multiserver configuration for profit maximization in cloud computing. *IEEE Trans. Parallel Distrib. Syst.* **24**(6), 1087–1096 (2013)
4. Mei, J., Li, K., Ouyang, A., Li, K.: A profit maximization scheme with guaranteed quality of service in cloud computing. *IEEE Trans. Comput.* **64**(11), 3064–3078 (2015)
5. Li, K., Mei, J., Li, K.: A fund-constrained investment scheme for profit maximization in cloud computing. *IEEE Trans. Serv. Comput.* (2016). *IEEE Early Access Articles*
6. Ghamkhari, M., Mohsenian-Rad, H.: Energy and performance management of green data centers: a profit maximization approach. *IEEE Trans. Smart Grid* **4**(2), 1017–1025 (2013)
7. Liu, Z., Wang, S., Sun, Q., Zou, H., Yang, F.: Cost-aware cloud service request scheduling for SaaS providers. *Comput. J.* **57**, 291–301 (2013)
8. de Langen, P., Juurlink, B.: Leakage-aware multiprocessor scheduling. *J. Sig. Process. Syst.* **57**(1), 73–88 (2009)
9. Mei, J., Li, K., Hu, J., Yin, S., Sha, E.H.-M.: Energy-aware preemptive scheduling algorithm for sporadic tasks on DVS platform. *Microprocess. Microsyst.* **37**(1), 99–112 (2013)
10. Ross, S.M.: *Introduction to Probability Models*, 11th edn. Elsevier, London (2014)
11. Boots, N.K., Tijms, H.: An M/M/c queue with impatient customers. *Top* **7**(2), 213–220 (1999)
12. Ding, Y., Qin, X., Liu, L., Wang, T.: Energy efficient scheduling of virtual machines in cloud with deadline constraint. *Future Gener. Comput. Syst.* **50**, 62–74 (2015)
13. Enhanced Intel® SpeedStep® technology for the Intel® Pentium® M processor. White Paper, Intel, March 2004
14. Li, K.: Optimal configuration of a multicore server processor for managing the power and performance tradeoff. *J. Supercomput.* **61**(1), 189–214 (2012)
15. Chen, J., Wang, C., Zhou, B.B., Lee, Y.C., Zomaya, A.Y.: Tradeoffs between profit and customer satisfaction for service provisioning in the cloud (2011)
16. https://en.wikipedia.org/wiki/Stirling's_approximation (2016)
17. Ghamkhari, M., Mohsenian-Rad, H.: Energy and performance management of green data centers: a profit maximization approach. *IEEE Trans. Smart Grid* **4**(2), 1017–1025 (2013)
18. Li, K., Liu, C., Zomaya, A.Y.: A framework of price bidding configurations for resource usage in cloud computing. *IEEE Trans. Parallel Distrib. Syst.* **27**(8), 2168–2181 (2016)

A Composite Anomaly Detection Method for Identifying Network Element Hitches

Duo Zhang¹(✉), Yi Man¹, and Ligang Ren²

¹ ICN & CAD Center, Beijing University of Posts and Telecommunications, Beijing, China

zhangduobupt@163.com

² China Unicom System Integration Limited Corporation, Beijing Branch, Beijing, China

15611030998@wo.com.cn

Abstract. Based on time-series detection algorithm, this paper puts forward a new analysis method for identify Network Element (NE) hitches. Aiming at specific characteristics of the NE, this paper propose a model which consider seasonal timing characteristics and impact of current data from recent data. Considering of multi-dimensional characteristics of NE, a density-based discovery algorithm is introduced into the modeling process. Experiments on the actual data coming from operates demonstrate the effectiveness and accuracy of the proposed methods.

Keywords: Big data · Abnormity detection · Network element management

1 Introduction

In the field of network management, fault warning is a very advanced subject. First of all, the traditional method to deal with faults is to remedy the situation after malfunction, which is neither predictable nor effective. In this situation, operation and maintenance work will faces many difficulties. As a direct manifestation of devices status, the data which comes from network element can reflect the state of the device. In addition, it can helps operators to analyze and make decisions more accurately.

The data structure and data mining are carried out to explore the abnormal data in the network equipment, which can helps user to quickly identify the possible failure and achieve the target of early warning. Nevertheless, there are great challenges analyst will meet in operator's network management environment, because of the diversity and complexity of the data comes from network elements. It's also worth mentioning that the method to get structured log data has objective impact on the result of anomaly detection. Consequently, a comprehensive anomaly identification scheme for network element log data is required for operation and maintenance work.

Taking into account the different needs of operator business analysis, we propose diverse analytics solutions to match different business scenarios. In this paper, we propose a time-series-based abnormity detection method for identify network element hitches. Meanwhile, we propose a solution to meet the needs of high dimension analysis. In the experimental phase, we use actual fault data provided by the operator to

evaluate the precision of our algorithm. The experiment results indicate that our methods can find abnormal state of network element efficiently and accurately.

2 Related Work

The current anomaly detection algorithms can be divided into four categories: statistical method, clustering-based method, distance-based method and density-based method. Meanwhile, density-based anomaly detection is a hot topic in this field. Based on the local density anomaly detection algorithm [1] proposed by Breunig in 2000. Following researchers gradually improved and developed the algorithm to make it suitable for different scenarios. Some researchers attempted to use inexpensive local statistics to reduce the sensitivity of choosing parameter k [2]. In the paper of Lazarevic [3], Local Outlier Factor (LOF) is used on multiple projections and combines the results for improved detection qualities in high dimensions. [4, 5] presents effective methods to measure the similarity between objects, which can increase the stability and precision of outlier detection. But these algorithms is difficult to support large-scale data processing needs, because of the complexity of the network element's log data. Alternatively, considering of the time characteristics of log data, timing analysis is another feasible way to detect anomalies. In the field of time series analysis, moving average model, linear regression model, polynomial regression model and exponential smoothing are common algorithms for time series analysis. In statistics, a moving average (MA) is a calculation to analyze data points by creating series of averages of different subsets of the full data set [6]. The weighted moving average model (WMA) is commonly used in the analysis of natural sciences and economics [7, 8]. Besides these, linear regression was the first type of regression analysis to be studied rigorously, and to be used extensively in practical applications [9]. The polynomial regression model which is advanced by Gergonne [10, 11] had been applied extensively in a lot of professions. Exponential smoothing was first suggested by Robert Goodell Brown in 1956 [12], and one of the commonly used model is known as "Brown's simple exponential smoothing" [13]. In exponential smoothing model, the current time can be suspected by the past time, while the impact of recent time is stronger than remote time. Another practical model to analysis time series is autoregressive integrated moving average model (ARIMA) [14, 15], this model can predict the future value of a specified time series on the basis of its past performance, but the basic ARIMA can't retain the seasonal characteristics of a time series.

All above models have their own advantages in time series analysis, and are effective mediums for anomaly detection. In the process of analysis of network element's log data, both statistical method and density-based method can be reasonable applied based on their properties.

3 Anomaly Detection Based on Network Element Log Data

3.1 Anomaly Detection Solution Design

There are different concerns in the process of network element hitches detection. To fit different demands from network management analysts, we propose a composite anomaly detection method to identify network element hitches. The anomaly detection procedure is showed in Fig. 1.

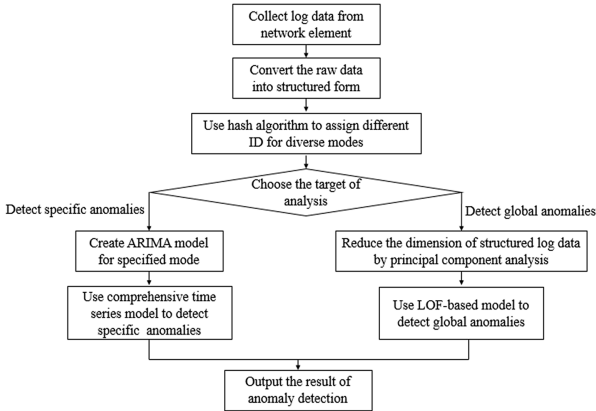


Fig. 1. Anomaly detection procedure

If network management analysts would like to detect anomaly for a specific mode, they can choose our time-series-based scheme. In the process of specific anomaly detection, we combine qualitative analysis with quantitative analysis. On one hand, generally determine the presence of abnormal period by creating ARIMA model. On the other hand, use our comprehensive time series model to detect specific anomalies. If network management analysts would like to contain the features of network element in analysis process as much as possible, they may choose our LOF-based scheme. Considering of high dimension input, we use principal component analysis (PCA) to reduce the dimension and retain characteristics of raw data. In this scheme, analysts can get global anomalies from log data.

3.2 Qualitative Analysis Based on ARIMA Model

In autoregressive integrated moving average model [15], the data sequence formed by the prediction object over time is regarded as a random sequence. Once the model is identified, it can be used to predict the future value from the past and present values of the time series.

- The autoregressive integrated moving average model is defined as

$$ARIMA(p, d, q) \quad (1)$$

p denotes autoregressive lagged item, q denotes moving average lagged item, and d denotes the order of difference. In our method we use ARIMA model to draw the curve of specific mode which can help us find suspected anomalies qualitatively.

3.3 Quantitative Analysis Based on Comprehensive Time Series Model

We can define current time t , the predicted value of our comprehensive time series model P_t is comprehensive decided by the continuous time smoothing factor C_t and the seasonal average factor S_t . The continuous time smoothing factor C_t represents the impact of recent trends on current time. While the seasonal average factor takes into the impact from the same period.

- The continuous time smoothing factor C_t is defined as

$$C_t = \beta y_t + (1 - \beta)C_{t-1} \quad (2)$$

where y_t is the measured value at time t and β denotes the weight coefficient which can measure the impact of recent trends on current time.

- The seasonal average factor S_t is defined as

$$S_t = \bar{Y}_t = \frac{1}{n} \sum_{i=1}^n Y_i \quad (3)$$

Y_i denotes the time units which are at the same period of Y_t , n denotes the number of time units we concerned about.

- The predicted value of comprehensive time series model P_t is defined as

$$\begin{aligned} & \max_{\alpha} [\alpha C_t + (1 - \alpha)S_t] \\ & \text{s.t. } \alpha \geq 0. \end{aligned} \quad (4)$$

In this manner, we can reduce the influence of single factor on predicting value, also increase the tolerance of extremely value. Is easy to understand that P_t retains the impact of recent trends and the relevance of data in the same period, which can predict the value of specified mode's time series at time t reasonably and effectively.

3.4 High Dimensionality Data Processing Scheme

Considering of multi-dimensional characteristics of NE, we introduce a LOF-based algorithm to detect global outliers, which can encapsulate properties as node attributes. In the actual network management scenario, traditional LOF-based algorithm can't solve the problem when the data volume is extremely huge. In other words, the

structured log data from network element has a large variety of characteristics, the traditional LOF algorithm will meet the performance bottleneck in computing process. Therefore, the PCA method is used to reduce the dimensions of input data, while preserving the feature information of multi dimension data.

We use Euclidean distance to measure the difference between network element's log data in different periods.

$$d(x(t_1) - x(t_2)) = \sqrt{\sum_{i=1}^n (x_i(t_1) - x_i(t_2))^2} \quad (5)$$

The abnormal degree of log data is measured by local outlier factor (LOF) [1]. And the local outlier factor (LOF) is defined as

$$LOF_k(p) = \frac{\sum_{o \in N_k(p)} \frac{lrd_k(o)}{lrd_k(p)}}{|N_k(p)|} \quad (6)$$

where $N_k(p)$ denotes the k -distance neighborhood of p . In other words, $N_k(p)$ contains every element whose distance from p is not greater than the k -distance. The k -distance of p is defined as the distance $d(p, o)$ between p and an object o such that there are at least k objects $m \in D d(p, m) \leq d(p, o)$, and there are at most $k - 1$ objects $m \in D d(p, m) < d(p, o)$

The local reachability density of p is defined as

$$lrd_k(p) = \frac{|N_k(p)|}{\sum_{o \in N_k(p)} rd_k(p, o)} \quad (7)$$

where the reachability distance of object p with respect to object o is defined as

$$rd_k(p, o) = \max[k - \text{distance}(o), d(p, o)] \quad (8)$$

For a specified network element, the statistical distribution of log modes per hour form snapshots which can reflect the status of the network element. According to the definition of local outlier factor (LOF) [1], the higher the value of local outlier factor, the more likely the object is an anomaly. Based on this, we abstract the status of network element per hour as objects (denoted as $x(t)$) which can calculate their abnormal degree by LOF. Getting the values of LOF for every $x(t)$, we can infer the occurrence time of anomalies.

3.5 Scheme Characteristic Analysis

Our model is based on time series analysis, taking into account the comprehensive effect of continuous temporal and seasonal timing. In our model, we use the optimization algorithm to optimize the parameters, which can avoid the impact of extreme value. It's suitable for network management personnel who are familiar with specific

abnormal patterns of NE's log data. Obviously, for network management analysts this method is effective, accurate and targeted-oriented. And that is to say, this model can effectively find the anomaly of specific log mode.

The global abnormality detection of network element considering of multiple attributes of network logs, which can retain the comprehensive information of network element's log data. But the existence of relevance and the mutual influence between attributes also has effects on detect results. Therefore, it's suitable for network management personnel have a global perception of abnormality. And that is to say, network management personnel can choose to find targeted anomaly and global abnormality flexibly according to different scenarios.

4 Experiments

4.1 The Analysis of Algorithm

To detect anomalies of the specific mode, we input the time series of a specific mode, y_t denote the frequency of the mode per hour. After input the time series, the comprehensive time series analysis algorithm will find which time units are anomalies (Tables 1 and 2).

Table 1. The comprehensive time series analysis algorithm

Input the time series $y_1, y_2, y_3, \dots, y_t \dots y_n$ of a specific mode
for each time unit y_t do
compute the continuous time smoothing factor C_t
compute the seasonal average factor S_t
for each possible α do
calculate $\alpha C_t + (1 - \alpha) S_t$ with the parameter α
if $\alpha C_t + (1 - \alpha) S_t > max$ then
$max \leftarrow \alpha C_t + (1 - \alpha) S_t$
$P_t \leftarrow max$
for each P_t do
if $ P_t - y_t $ is greater than threshold then
put y_t into output list
Return a list of anomalies of the specific mode

Considering of high dimension input, we use LOF-based model to find global anomalies.

Table 2. LOF-based anomaly detection algorithm

Input the set of the statuses of network element per hour	$x(1), x(2), x(3) \dots x(t) \dots x(n)$, and
the detection threshold	δ
reduce dimensions by principal component analysis	
for each $x(t)$ do	
compute the local outlier factor (LOF) of $x(t)$,denoted as	$Lof(t)$
for each $Lof(t)$	
if $Lof(t) > \delta$ then	
put $x(t)$ into output list	
Return a list of global anomalies	

4.2 Log Data Structure

Word2Vec is used to distinguish the difference between logging modes, meanwhile to get structured log data. We use the SQL aggregation statement to aggregate the data to get the frequency of modes per hour. The result of aggregation operation is showed in Table 3.

As can be seen in Table 3, all log modes are coded by hash algorithm, the last column indicates the frequency of modes per hour. In order to satisfy our analysis conditions, we convert the data to the following format.

In Table 4, the frequency of diverse log modes can be abstracted as attributes of log status in Network Element. This form is useful for network management to positioning specific log mode. Moreover, it can be processed by dimensional reduction algorithms when the dimension of attributes is extremely high.

4.3 ARIMA Analysis on Operator Actual Data

In this part, we use ARIMA-based model to qualitative analysis the time series of the specific log mode. In order to facilitate the description we select one of the specific log modes which network management analysts are interested in. The analysis method of other log modes are just the same (Table 5).

Firstly, we select a specific log mode as input for ARIMA model. Secondly, we generate the distribution curve of Autocorrelation Function (ACF) and Partial Autocorrelation Function (PACF) of the log mode's time series.

In Fig. 2, the Autocorrelation Function (ACF) trend decay and the Partial Autocorrelation Function (PACF) truncate after 1 order. This specific mode satisfaction the distribution of ARIMA(1,0,0). Therefore, we can create an ARIMA(1,0,0) model, and draw the curves of raw data and the predicted data of ARIMA.

As can be seen in Fig. 3, ARIMA(1,0,0) model well captured the trend of the time-series of the specific log mode. Moreover, we can find that there are great differences between the raw data and predicted data. So we can conclude that there are suspected anomalies in 2016-8-17 and 2016-8-19.

Table 3. Input data structure

8f6da0d89a8252e01944d8863786d52b	2016-08-16 00	1103
a631a85c804c2bdc2afc80c596b0e005	2016-08-16 00	724
661770dbcd0394f8db00ddd74352c007	2016-08-16 00	723
78e3e5d53db84e87a09a3996b09fdbb2	2016-08-16 00	719
f24f62eeb789199b9b2e467df3bl876b	2016-08-16 00	410
fd7997adb870d78fa830348b5514fc0d	2016-08-16 00	238
4586e5d1ace7df6ac23cce10ee8dfdb4	2016-08-16 00	143
ff4b2749ab7483d8f9a7a89d70e08c43	2016-08-16 00	143
478458696bcf7c72812ee5e623dedfda	2016-08-16 00	132
13e208b8db3b0c2f9d956c02253cab1aa	2016-08-16 00	132
f4094a94a79a121bcd8a10960fe34a61	2016-08-16 00	126
8424707d0420cadee4c97ef4af2ef9f4	2016-08-16 00	112
f20e457d2828982ee27a640362891d63	2016-08-16 00	89
C3f091f048a28894fea7d50660dd6942	2016-08-16 00	89
e008518e807af2bcc2356cf7ecd57b22	2016-08-16 00	89
004f4855ba92c8781a6b8c2014fd9c2	2016-08-16 00	60
75849e828d2b48945d6a6453485b59ac	2016-08-16 00	15
731c019558bf9ed8ff96dc892e9b5325	2016-08-16 00	15
9d256115355016cf657aa064a9f04862	2016-08-16 00	12
6dbe23d02c718ad2118aef94479dl32b	2016-08-16 00	11
1dd5ddd339089a28a3b1c41dabfa87eb	2016-08-16 00	11
1b78efaa73d320280808e0b361b206bd	2016-08-16 00	11
13b97cb2bc33bd94b82e2c6b9c637725	2016-08-16 00	8
609c79b375b6a32fa86a56f4136e5734	2016-08-16 00	8
a15aa8107c651ce08ce8375746717ed1	2016-08-16 00	8

Table 4. Input data transformation

log node	day	0040d4231004f6855205393daef0081f851f00d17cc5c00eaca2ff60wd3-c9c01196a8af01802332f0275abeb102c8082c034fbd4d0381059d403fabb1c04520686c05	0	0	0	0	0	0	0	0	0	0	0	0	0	0	0	0	0
2016-08-16 00	1	60	0	0	0	0	0	0	0	0	0	0	0	0	0	0	0	0	0
2016-08-16 01	1	40	0	0	0	0	0	0	0	0	0	0	0	0	0	0	0	0	0
2016-08-16 02	1	60	0	0	0	0	0	0	0	0	0	0	0	0	0	0	0	0	0
2016-08-16 03	1	56	0	0	0	0	0	0	0	0	0	0	0	0	0	0	0	0	0
2016-08-16 04	1	52	0	0	0	0	0	0	0	0	0	0	0	0	0	0	0	0	0
2016-08-16 05	1	60	0	0	0	0	0	0	0	0	0	0	0	0	0	0	0	0	0
2016-08-16 06	1	52	0	0	0	0	0	0	0	0	0	0	0	0	0	0	0	0	0
2016-08-16 07	1	60	0	0	0	0	0	0	0	0	0	0	0	0	0	0	0	0	0
2016-08-16 08	1	56	0	0	0	0	0	0	0	0	0	0	0	0	0	0	0	0	0
2016-08-16 09	1	56	0	0	0	0	0	0	0	0	0	0	0	0	0	0	0	0	0
2016-08-16 10	1	56	0	0	0	0	0	0	0	0	0	0	0	0	0	0	0	0	0
2016-08-16 11	1	56	0	0	0	0	0	0	0	0	0	0	0	0	0	0	0	0	0
2016-08-16 12	1	60	0	0	0	0	0	0	0	0	0	0	0	0	0	0	0	0	0
2016-08-16 13	1	52	0	0	0	0	0	0	0	0	0	0	0	0	0	0	0	0	0
2016-08-16 14	1	60	0	0	1	1	0	0	0	0	0	10	0	0	0	0	0	0	0
2016-08-16 15	1	44	0	0	0	0	0	0	0	0	0	0	0	0	0	0	0	0	0
2016-08-16 16	1	60	0	0	0	0	0	0	0	0	0	0	0	0	0	0	0	0	0
2016-08-16 17	1	56	0	0	0	0	0	0	0	0	0	0	0	0	0	0	0	0	0
2016-08-16 18	1	60	0	0	0	0	0	0	0	0	0	0	0	0	0	0	0	0	0
2016-08-16 19	1	72	0	0	0	0	0	0	0	0	0	0	0	0	0	0	0	0	0
2016-08-16 20	1	52	0	0	0	0	0	0	0	0	0	0	0	0	0	0	0	0	0
2016-08-16 21	1	60	0	0	0	0	0	0	0	0	0	0	0	0	0	0	0	0	0
2016-08-16 22	1	56	0	0	0	0	0	0	0	0	0	0	0	0	0	0	0	0	0
2016-08-16 23	1	52	0	0	0	0	0	0	0	0	0	1	0	0	0	0	0	0	1

Table 5. The specified mode

	GG	GR
df0	40dc1d901e25a7ff0d19c9354e70d7a5	47845809e4
0		413 132
0		448 144
0		448 144
0		448 144
0		448 144
0		451 144
0		448 144
0		448 144
0		408 120
0		408 144
0		448 144
0		448 144
0		449 144
0		448 144
0		448 144
0		448 144
0		448 144
0		419 130
0		448 144
0		448 144
0		453 144
0		440 151

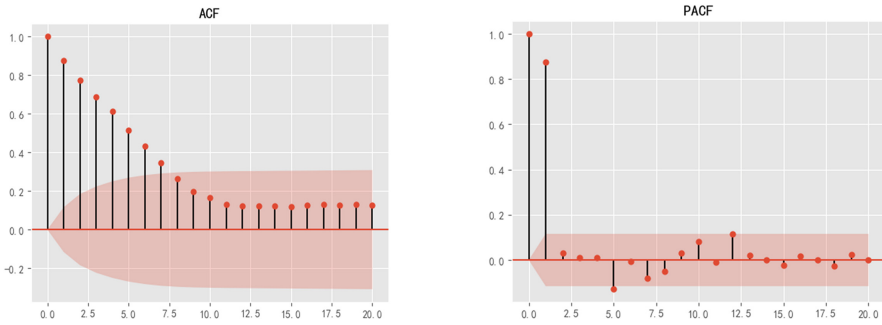


Fig. 2. Autocorrelation Function (ACF) and Partial Autocorrelation Function (PACF) of specific log mode

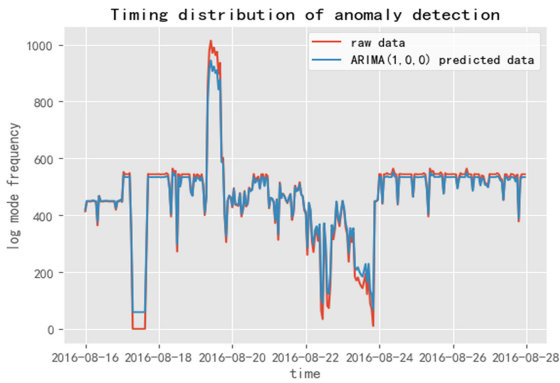


Fig. 3. Timing distribution of anomaly detection

4.4 Comprehensive Time Series Analysis on Operator’s Actual Data

After get the presence of abnormal period, furthermore, we use our comprehensive time series analysis method to quantitative find the anomalies. In this part we compare our algorithm with other common time-series-based algorithms. We choose the log data from network elements which has occurred hitches in recent year. For SAEGW1304, the specified time range is 2016-08-16 00:00 to 2016-08-27 23:00. For another network element SZHSAEGW105BEr, the time range is 2016-09-02 00:00 to 2016-10-11 23:00.

Experimental results show that our Comprehensive Time Series method can improve precision ratio to find anomalies of network element, but recall ratio greatly.

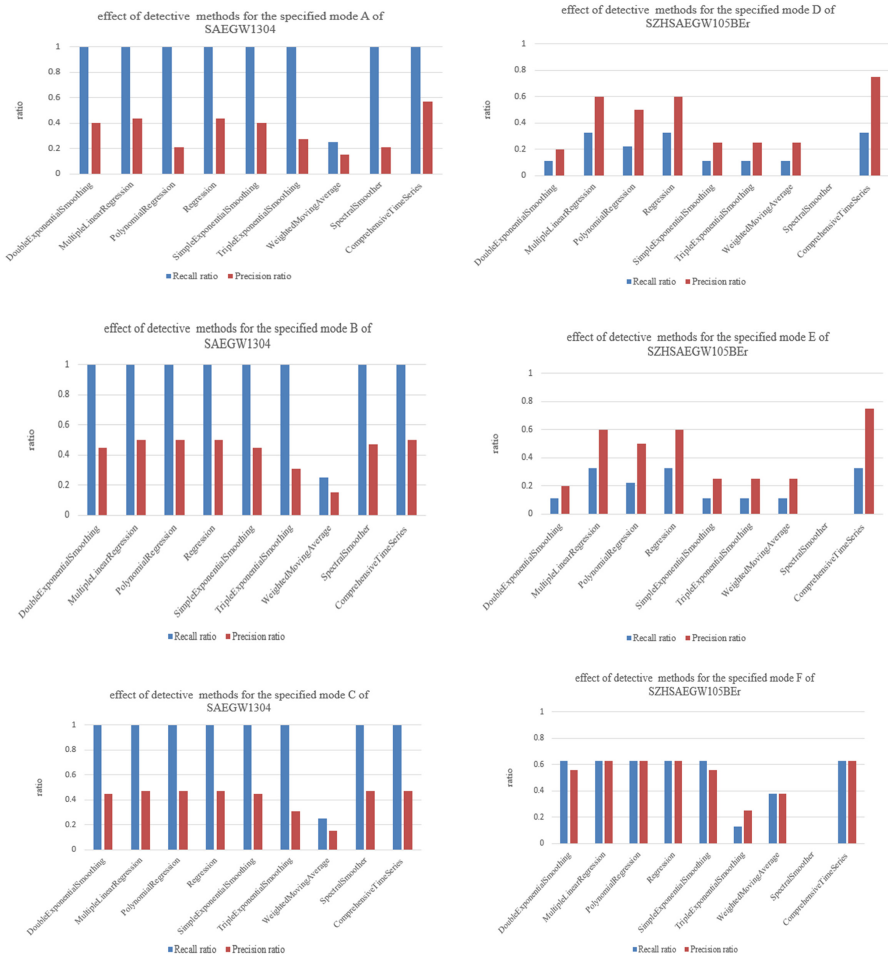


Fig. 4. Algorithm efficiency evaluation for SAEGW1304 and SZHSAEGW105BEr

4.5 High Dimensionality Data Processing Scheme to Find Global Abnormity

In LOF-based anomaly detection process, the frequency of diverse log modes can be abstracted as attributes of log status in Network Element. We use LOF to measure the degree of outlier, meanwhile find global anomalies of log data.

In Fig. 5, we can find that 2016-8-17 00:00 and 2016-8-16 23:00 are the global anomalies of log data, which caused the hitch of Network Element (SAEGW1304). Obviously, this method considering of multiple attributes of network logs, which can retain the comprehensive information of network element’s log data. But the existence of relevance and the mutual influence between attributes also has effects on detect results.

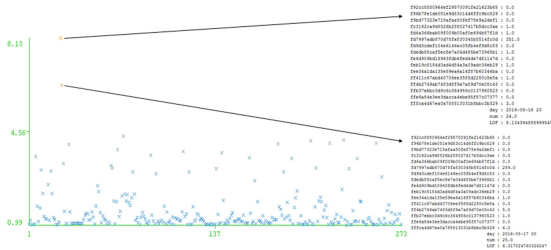


Fig. 5. High dimensionality anomaly detection

4.6 Actual Case Verification

In order to evaluate the accuracy of our detection method, we select a real case provided by the operator. Applying our detection method on log data from network element (SAEGW1304), we can verify the effectiveness of our method.

As can be seen in Tables 6 and 7, Comprehensive Time Series method detect the anomalies by 100% recall ratio. Moreover, Fig. 4 shows that the precision ratio for detection is higher than other common algorithms. Therefore, we can verify the effectiveness of our method detection the abnormal status from SAEGW1304’s log data.

Table 6. The record of hitches of SAEGW1304

Event description	Associated log time	NE label	Data description
A hitch occurred in Power Supply Bureau’s network environment Guangzhou’s network element SAEGW1304	August 16, 2016 22:00-August 17, 2016 14:00	SAEGW1304	The data to be analyzed comes from SAEGW1304’s log data

Table 7. Comprehensive Time Series method detection result

46dclid901e25a7ff0d19c9354e76d7a33	FALSE	2016-08-17 04
46dclid901e25a7ff0d19c9354e76d7a34	FALSE	2016-08-17 05
46dclid901e25a7ff0d19c9354e76d7a35	FALSE	2016-08-17 06
46dclid901e25a7ff0d19c9354e76d7a36	TRUE	2016-08-17 07
46dclid901e25a7ff0d19c9354e76d7a37	TRUE	2016-08-17 08
46dclid901e25a7ff0d19c9354e76d7a38	TRUE	2016-08-17 09
46dclid901e25a7ff0d19c9354e76d7a39	TRUE	2016-08-17 10
46dclid901e25a7ff0d19c9354e76d7a40	TRUE	2016-08-17 11
40dclid901e25a7ff0d19c9354e76d7a41	TRUE	2016-08-17 12
46dclid901e25a7ff0d19c9354e76d7a42	TRUE	2016-08-17 13
46dclid901e25a7ff0d19c9354e76d7a43	TRUE	2016-08-17 14
46dclid901e25a7ff0d19c9354e76d7a44	TRUE	2016-08-17 15
46dclid901e25a7ff0d19c9354e76d7a45	FALSE	2016-08-17 16
46dclid901e25a7ff0d19c9354e76d7a46	FALSE	2016-08-17 17
46dclid901e25a7ff0d19c9354e76d7a47	FALSE	2016-08-17 18

5 Conclusion

In the background of efficient system operation and maintenance, we propose diverse analytics solutions to match different business scenario. In our method, the frequency characteristics of log data are abstracted as attributes of network elements' attributes. Applying data mining algorithms to this data, we detect the specific anomalies and global anomalies to fit different demands from network management analysts. The result of our analysis method is verified by actual data, meanwhile is useful for operators' fault early warning system. It can be expected to find more interesting and results along these lines, since the log data of network element contains abundant information.

References

1. Breunig, M.: LOF: identifying density-based local outliers. *ACM SIGMOD Rec.* **29**(2), 93–104 (2000)
2. Kriegel, H.P., Schubert, E., Zimek, A.: LoOP:local outlier probabilities. In: *ACM Conference on Information and Knowledge Management, CIKM 2009, Hong Kong, China, DBLP*, pp. 1649–1652, November 2009
3. Lazarevic, A., Kumar, V.: Feature bagging for outlier detection. In: *Eleventh ACM SIGKDD International Conference on Knowledge Discovery in Data Mining*, pp. 157–166. ACM (2005)
4. Schubert, E., Wojdanowski, R., Zimek, A., et al.: On evaluation of outlier rankings and outlier scores. In: *Proceedings of the 2012 SIAM International Conference on Data Mining*, pp. 1047–1058 (2012)
5. Guan, H., Li, Q., Yan, Z., et al.: SLOF: identify density-based local outliers in big data. In: *Web Information System and Application Conference*, pp. 61–66. IEEE (2015)

6. Booth, E.G., Mount, J.F., Viers, J.H.: Hydrologic variability of the cosumnes river floodplain. *San Francisco Estuary Watershed Sci.* **4**(2), 1–19 (2006)
7. Domańska, J., Domański, A., Czachórski, T.: Fluid flow analysis of RED algorithm with modified weighted moving average. In: Dudin, A., Klimenok, V., Tsarenkov, G., Dudin, S. (eds.) *BWWQT 2013*. CCIS, vol. 356, pp. 50–58. Springer, Heidelberg (2013). https://doi.org/10.1007/978-3-642-35980-4_7
8. Glabadanidis, P.: Market timing with moving averages. *Int. Rev. Finance* **15**(3), 387–425 (2015)
9. Yan, X., Su, X., World Scientific: *Linear Regression Analysis [Electronic Resource]: Theory and Computing* (2009)
10. Gergonne, J.D.: The application of the method of least squares to the interpolation of sequences. *Historia Mathematica* **1**(4), 439–447 (1974)
11. Stigler, S.M.: Gergonne's 1815 paper on the design and analysis of polynomial regression experiments. *Historia Mathematica* **1**(4), 431–439 (1974)
12. Brown, R.G.: *Exponential Smoothing for Predicting Demand*, p. 15. Arthur D. Little Inc., Cambridge (1956)
13. Brown, R.G.: Smoothing, forecasting and prediction of discrete time series. *J. R. Stat. Soc.* **127**(2) (1964)
14. Mills, T.C.: *Time Series Techniques for Economists*. Cambridge University Press, Cambridge (1990)
15. Jenkins, G.M.: *Autoregressive-Integrated Moving Average (ARIMA) Models*. *Encyclopedia of Statistical Sciences*. Wiley, New York (2004)

D-SVM Fusion Clustering Algorithm Based on Indoor Location

Zhongliang Deng, Jiachen Fan^(✉), and Jichao Jiao

Beijing University of Posts and Telecommunications, Beijing, China
406908388@qq.com, {jiachenf, hwj1505}@bupt.edu.cn

Abstract. Traditional fingerprint orientation clustering algorithms often use k means clustering algorithm, but as a result of fingerprint and objective factors of volatile characteristics over time, k-means cannot adapt to change at any time in fingerprint, and cannot be generated adaptive clustering cluster number, cause the matching accuracy is not high. This paper adopts a based on support vector machine (SVM) and DBSCAN clustering algorithm, can generate continuously adapt to changing the optimal hyperplane fingerprint model, solved the fingerprint fluctuating lead to the problem of matching result is bad, and can be automatically generated in the process of matching classification number of clusters, based on statistical density characteristics of DBSCAN selection matching probability model, to improve the positioning of the matching accuracy, reduced the amount of time matching positioning, positioning accuracy can be up to 2.04 m in the range of 57%, relative k-means 6.1 m increased by 52.3%, improve the positioning accuracy.

Keywords: Location fingerprint · Clustering algorithm · SVM

1 Introduction

With the rapid development of mobile Internet and mobile terminal equipment, indoor positioning has become the front of data information technology research [1]. Under the support of the world's four major satellite navigation systems, outdoor location services have been widely into people's lives. While 80% of the daily time in indoor activities, with the increasing number of large buildings, indoor location services in commercial applications, public safety and other aspects of the application of the most broad prospects. In indoor environments, satellite system signals cannot be used due to building occlusion and multipath [1]. At present, location fingerprint location based on signal strength (RSSI) is widely used in indoor positioning. Fingerprint localization makes use of the fingerprint feature of multipath non line of sight caused by the complex indoor architecture, and improves the positioning accuracy under the traditional positioning problem.

Indoor positioning method (AOA, Arrival, of angle of arrival and time of arrival (Angle) location TOA, Time of Arrive) location, time difference of arrival (TDOA Time, Difference of, TDOA/AOA Arrival) positioning hybrid positioning, based on the received signal strength indicator (RSSI, Received Signal Strength Indication) location. TOA, TDOA positioning requires high-precision hardware synchronization, AOA

positioning requires directional antenna, and in the NLOS environment affected by multipath serious. WiFi positioning widely used RSSI technology, generally based on fingerprint matching positioning. The indoor environment is complex, but the pattern remained unchanged, the characteristics of the wireless signal formed in the specific position (the number of signals, phase, intensity) showed a special high, as the only “fingerprint” to identify the location, then according to the fingerprint matching algorithm to calculate the position.

Improve the accuracy of fingerprint matching can generally improve the stability of RSSI fingerprint database, optimize the fingerprint database structure and improve the clustering algorithm three aspects. Starting from clustering algorithm, the traditional K-means.

Is based on the concept of data partitioning, can not be adaptive optimization matching model, ignoring the data model should continue to change with the test vector changes. Positioning accuracy is easily affected by time weather and objective factors, positioning accuracy is difficult to further improve.

2 Matching Positioning Method for Position Fingerprint

This method is generally divided into off-line training and online matching stage. The off-line training phase of the mobile device to acquire the RSSI sequence, AP sequence signal intensity and location information for the RSSI signal vector and stored in the fingerprint database, the formation of space vector space according to a certain density of fingerprint acquisition point position information (Fig. 1).

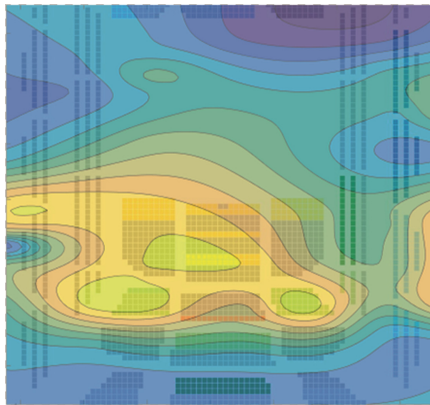


Fig. 1. Single AP signal intensity distribution of National Grand Theater

3 Several Data Clustering Methods

When the amount of fingerprint data is large, clustering algorithm is widely used to optimize the structure of fingerprint database. Generally based on the data mean division

method, density based density method, data model based machine learning methods. This paper uses divisive hierarchical clustering algorithm, the entire data set as a cluster, and then use the adaptive mesh split into multiple clusters in data modeling, the entire data set model, using two different clustering algorithms are fused to play two kinds of localization algorithm advantages, makes the use of the smallest the data space to get the location information of the most useful, to improve the positioning accuracy.

3.1 K-means Clustering Based on Data Mean

For the K nearest neighbor method, the K nearest neighbor points are given different weights according to certain rules:

$$\begin{cases} (\hat{x}, \hat{y}) = \frac{1}{K} \sum_{i=1}^K w_i(x_i, y_i) \\ \sum_{i=1}^k w_i = 1 \end{cases} \quad (1)$$

- (1) We need to give K neighbor points different weights to improve the system positioning accuracy, learn from the classic signal positioning algorithm based on active RFID system. The system selects some reference points and arrangement of reference tags in the positioning area, the signal strength compared to the tag and reference tag values, obtained several reference tags to be located closest to the label, and then based on these coordinates weighted reference tags to estimate the coordinates positioning label. Using the weight design idea of the system, the weights are redesigned.
- (2) The size of the Euclidean distance D square reflects the weight change, the smaller the D, the greater the weight, and directly depends on the current Euclidean distance Di, enhanced the Euclidean distance Di weight ratio (Fig. 2).

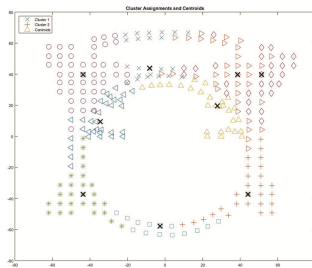


Fig. 2. National Grand Theater K-means clustering results

3.2 Density Based DBSCAN Algorithm

(1) (Eps neighborhood) given a data object P, P Eps neighborhood defined as the core of P, Eps radius of the D dimensional hypersphere sphere region, that is, Numbered lists should use the “Numbered Item” style.

$$N_{Eps}(p) = \{q \in D | dist(p, q) \leq Eps\} \tag{2}$$

Data point density and DBSCAN group connected to a cluster. The density of points m/nV , M is the number of data points that N input falls in a small region around the point and V is the area of the volume. The region is considered to be a hypersphere radius, so the MinPts threshold density can be determined by specifying a parameter.

For given and MinPts values, DBSCAN finds a dense point input set and expands it by merging adjacent dense regions. A point can be a dense (core) or non-dense point (non core business point). Non-dense point is a boundary point dense region or noisy pattern.

In the plane space data density space vector set as fingerprint clustering based on density clustering algorithm, the number of clusters is not need to set in advance, so this method is suitable for clustering point distribution of unknown data sets clustering. Based on density of DBSCAN is a widely used mesh algorithm, the super ball algorithm number of data samples within the region to measure the regional density of the fast. DBSCAN algorithm can discover clusters of arbitrary shape, and effective identification of singular points. The discovery of DBSCAN cluster grid data and characteristics, and each cluster according to the data of different densities of different probability markers, matching the priority of such arrangement has probability sequence cluster set the maximum probability in the process of matching, the matching accuracy is very good optimization (Fig. 3).

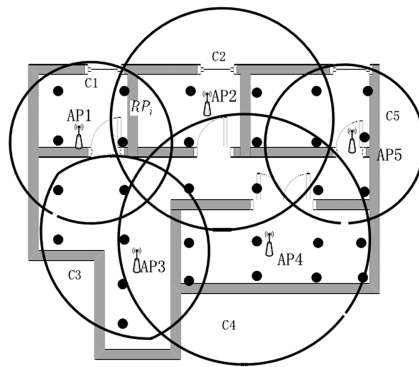


Fig. 3. Grid partition result

3.3 SVM (Support Vector Machine) Clustering Based on Data Model

After using DBSCAN to divide the grid, then use SVM to build the data model to carry on second levels of clustering. The training set is linear SVM, assuming that the size of N training set consists of two parts, respectively for the class and, if that is marked, if, if there is marked. Ultra flat $g(x)$ the training vector is correct classification of the training sample set is linearly separable

$$\begin{cases} g(x) = \omega x + b = 0; \\ \omega x_i + b \geq 1(y_i = 1); \\ \omega x_i + b \leq -1(y_i = -1). \end{cases} \quad (4)$$

When the training set is nonlinear, the input feature space by a nonlinear function is mapped to a higher dimensional space m , $X \in R^n \rightarrow X \in R^m$ these classes can be used to classify a hyperplane and get discriminant function.

$$\omega \Phi(x) + b = 0 \quad (5)$$

Discriminant function:

$$f(x) = \text{sign}[\omega \Phi(x) + b] \geq 1 - \xi_i \quad (6)$$

In the formula C is the parameter, the objective function should look for the maximum hyperplane as far as possible and the guarantee data point deviation quantity is smallest, parameter C controls before two weights.

4 DBSCAN-SVM Clustering Algorithm

4.1 Research Method

A support vector machine based on combination of DBSCAN and indoor positioning method, which is characterized by the largest cluster DBSCAN quickly find the advantage and advantage of support vector machine to solve the super plane model, to achieve the desired effect of clustering. The original data points using DBSCAN to select all kinds of density density cluster and number based on the traditional local mesh according to the substitution, the purpose of doing so can eliminate the singularity and little area quickly, so as to optimize the positioning accuracy and matching speed.

4.2 Implementation Methods

The original data points using density based DBSCAN select various density clusters. After finding the clusters of various shapes at the fastest speed, the singular points are excluded and the probability density of each cluster is sorted. In the matching process, the cluster with higher probability is preferred (Fig. 4).

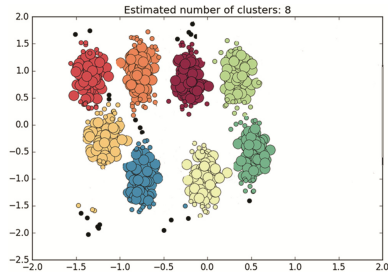


Fig. 4. DBSCAN first layer clustering results

4.2.1 Cluster Combination

Divides the good class cluster according to the number to carry on 22 combinations.

Then the SVM classifier is used to classify the 22 clusters, and the total number of classification models is $N(N - 1)/2$.

To find the best hyperplane classification, the next step is to solve a constrained extreme value problem:

SVM optimal classification surface problem can be described as:

$$\begin{cases} \min(\frac{1}{2}\|\omega\|^2) \\ s, t, y_i(\omega r_i^T + b) \geq 1 \end{cases} \quad i = 1, 2, \dots, n \quad (7)$$

By means of formula (6), we can solve an optimal hyperplane of classifying the data of the two kinds according to the mathematical model. Before the N data samples obtained by the cluster, with permutations and combinations into the SVM classifier training, $N(N - 1)/2$ hyperplane model DBSCAN (Fig. 5).

$$\begin{cases} \min \Theta(\omega) = \frac{1}{2}\|\omega\|^2 + C \sum_{i=1}^N \xi_i; \\ y_i(\omega\Phi(x_i) + b) \geq 1 - \xi_i \\ (\xi_i \geq 0, i = 1, 2, \dots, N), \end{cases} \quad (8)$$

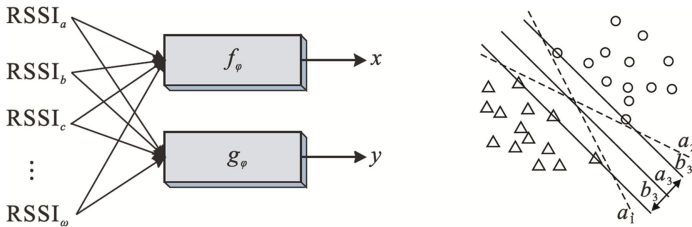


Fig. 5. Fingerprint database statistical positioning results and optimal classification plane sketch map

The penalty function can be described as the distance between the hyperplane model and the measured point in order to avoid over fitting the correction factor to the distance.

4.2.2 Location Process

The signal intensity received by the positioning point is input into the established model, and the probability density method is used to select the maximum probability density model. The first step, based on the probability of the K regions obtained by classification, calculates the weights (Fig. 6).

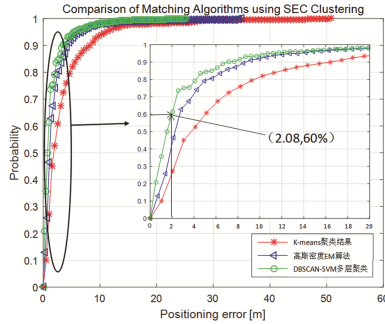


Fig. 6. Error cumulative distribution function

5 Conclusion

This paper introduces a fusion clustering algorithm in indoor positioning applications, used to solve the existing RSSI volatility, quickly find clusters. After testing, can effectively increase the matching accuracy, reduce matching time, improve positioning accuracy.

References

1. Deng, Z., Yu, Y., Yuan, X., et al.: Indoor positioning status and development trend study. *China Commun.* **10**, 50–63 (2013)
2. Zheng, R., Deng, Z., et al.: Analysis of positioning error in multipath environment. In: *China Satellite Navigation Academic Annual Meeting* (2015)
3. Ning, J.J.: An adaptive SA-DBSCAN: of density clustering algorithm. *Univ. Acad. Sci.* **26**(4), 530–538 (2009)
4. Zhou, J., Li, W., Jin, L., et al.: Design of indoor positioning system based on KNN-SVM algorithm. *J. Huazhong Univ. Sci. Technol. Nat. Sci. Ed.* **S1**, 517–520 (2015)
5. Zhang, B., He, Z.: New method of SVM multi classification based on support vector data description. *Comput. Appl. Res.* **24**, 46–48 (2007)
6. Li, S.: *Application research on indoor location technology based on WiFi*. Nanjing Normal University (2014)
7. Zhou, F.: *Design and implementation of positioning system based on WiFi technology*. Beijing University of Post and Telecommunication, p. 12 (2009)

Research on Evaluation of Sensor Deviations During Flight

Yuping Xiong¹, Shufen Liu², Sihua Gao^{2(✉)}, and Yemei Zhu³

¹ System Engineering Research Institute of China State, Shipbuilding Corporation, Beijing, China

² College of Computer Science and Technology, Jilin University, Changchun, China
13756651430@163.com

³ Chinese Journal of Electronics, Beijing 100036, China

Abstract. Aircrafts have been widely used in recent years with the rapid developments in economies. In consideration of aircraft security and the importance of navigation information, numerous sensors have been utilized for aircraft tracking. Deviations are easily produced by sensors and have significant influence on information accuracy. The existing literature on methods to monitor sensors and evaluate their deviations is limited. In this paper, the information detected by sensors is compared to the reference trajectory. Subsequently, a novel method to calculate deviations and errors is proposed. To validate the reliability of the evaluation results, the Chi Square test is integrated into the research method. A statistical method is also proposed to identify the existence of deviations between two sensors.

Keywords: Sensors · Deviations · Chi Square test · Test statistics

1 Introduction

Aircrafts have been widely used in economies, and flight safety has gained increased importance and attention. Many types of sensors have been deployed to acquire and monitor location information in different domains, such as the military, medical care, and environmental management. Multiple sensors are generally used to identify geographical coordinates precisely. However, various environmental factors can cause sensor deviation, which results in inaccurate data collection. These factors should be considered when deploying sensor probes. Thus, the calculation and the analysis of sensor deviations are crucial issues.

In most recent studies, sensors are considered as suitable tools to investigate aircraft information. In [1], the airspeed sensors were used to reconstruct the approach-path deviations through triangulation and the flow sensors controlled the touchdown phase. The authors in [2] demonstrated a trajectory recommendation framework that relied on various sensors. The authors of [3] reported that trajectories were difficult to predict the precise location of thrown objects. A sensor system, which received data from distance sensors, was responsible for detecting the deviations between the actual and predicted values. Then an algorithm to measure the in-between points during flights was proposed. The authors of [4] used inertial sensors to gather optical flow information and presented a set of novel navigation techniques to estimate the ground velocity and altitude of

aircrafts. Two formulations were proposed to calculate aircraft velocity and altitude. A novel method that used a ToF [5] camera to detect an aerial target was proposed in [6]. On the basis of a special requirement, the sky was considered as noise in the image and the target could be recognized from a model of complete randomness, thus illustrating the robustness of sensor detection with respect to the number of false alarms. In addition, the authors conducted a study to analyze the detection performance. In [7], the accuracy of sensors was noted. The authors proposed a linear covariance technique to predict the accuracy of altitude determination systems for flights. The authors also carried out a study to analyse the performance of the detection. In [8], a radar sensor was placed onto a UAV, which calculated the position deviations of aircrafts from a theoretical trajectory. A SAR processor and navigation system determined the difference between theoretical and actual values.

To the best of our knowledge, the literature on the evaluation of sensor deviations is limited. In the present research, we build the reference trajectory and propose a novel method to calculate and evaluate the deviations for each sensor. The feasibility of the obtained data is evaluated through residual analysis using the Chi Square test. We also propose a statistical method to determine whether the deviations exist between two sensors or not.

The rest of this paper is organized as follows. Section 1 discusses the potential application of sensors in the aviation industry and the importance of evaluation methods. Section 2 presents the proposed calculation and evaluation methods. Section 3 presents the statistical method for detecting the deviations for each sensor. Finally, the study is concluded in Sect. 4.

2 Deviation Calculation and Evaluation

To obtain the deviation, we should build a reference trajectory first. The reference data need to be transformed according to the local sensor framework. If the total number of points tracked by two sensors is larger than 50, then high-accuracy sensors are used to plan the trajectory. The reference time is calculated as follows:

$$Time_{ref} = \frac{(Min(time_1) + Max(time_2))}{2} \tag{1}$$

The reference trajectory of a sensor is built through the least square fitting of a polynomial. We sum up of the values in the set deviation. The sensor deviation is equal to the average of values. In order to calculate the deviation between two sensors, the deviation for each sensor corresponding to the reference trajectory should be obtained. The tracks of sensor S_x are recorded in the set ξ_{S_x} . The deviation of sensor S_x can be defined as follows:

$$b_{S_x|r_t} = \xi_{S_x}^- = \frac{\sum S_x}{N_{S_x}} \tag{2}$$

where $b_{s_x|r_i}$ and $\bar{\xi}_{s_x}$ are the deviation between S_x and the reference trajectory. The sum of values in the set ξ_{S_x} is expressed as Σ_{S_x} , and variable N_{S_x} is the number of the points tracked by sensor S_x . The deviation between sensor s_1 and s_2 is defined as follows:

$$b_{s_1|s_2} = b_{s_2|r_i} - b_{s_1|r_i} \tag{3}$$

The errors induced by the deviations could be obtained simultaneously by calculating the standard deviations of a sensor as follows:

$$\sigma_x = \sqrt{\frac{1}{N_x} \Sigma (\xi_x - \bar{\xi}_x)^2} \tag{4}$$

The variable $\sigma_{\bar{x}}$ denotes the average value of the standard deviations:

$$\sigma_{\bar{x}} = \frac{\sigma_x}{\sqrt{N_x}} \tag{5}$$

The standard deviation for each sensor could be obtained easily. After acquiring the standard deviations for sensors s_1 and s_2 , the errors induced by the deviations between these two sensors can be calculated as follows:

$$\sigma_{evaluate} = \sqrt{\sigma_{s_1}^2 + \sigma_{s_2}^2} \tag{6}$$

Subsequently, the methods to achieve the research objective are tested because the sensor errors are obviously normally distributed. In this paper, residual analysis is first utilized to identify the feasibility of the data. Then, the residual error is tested by Chi Square test. The residual error must first satisfy the test above to obtain accurate data and information. Otherwise, the deviation is discarded. Sensors have different precisions. Thus, the difference for each sensor should be normalized. The normalized difference of sensor X is defined as follows:

$$\xi_x^* = \frac{\xi_x}{\sigma'_x} \tag{7}$$

where σ'_x is the sample-standard-deviation. Normalization is applied on the two sets, and the results are sorted and stored in the set σ^{**} .

The normalized differences and their order are analyzed. The possible samples are divided into discrete areas, which are used to calculate the expectation of samples. The Chi Square test is conducted to identify the consistency of samples and expectation distributions, that is:

$$\chi_e^2 = \sum_{i=1}^k \frac{(n_e - n_s)^2}{n_e} \tag{8}$$

where k is the number of discrete areas and n_e is the distribution of the expectation. The distribution of samples is expressed by n_s . Subsequently, X_e^2 is compared to the hypothetical threshold. If the threshold is not exceeded, the distributions of the samples are considered consistent with the expected distributions. Otherwise, the residual error could not be used further.

3 Surveillance of Deviations

Apart from evaluating the deviations, the results from calculations also can also help in monitoring the state of sensors. In this study, a statistical method is employed to identify whether the deviations exist between the two sensors. Two aspects are considered in detecting deviations: the detection for a single sample and the detection for accumulated samples. Both are described in the next sections.

3.1 Detection for a Single Sample

The detection for a single sample transforms the reference trajectory and deviation calculation data, such as distance, orientation, and elevation, into the same coordinate systems. Unlike the deviation estimates, the result of deviation calculation constructs a test statistic that is used to identify the consistency of the deviation for the reference track in a statistically significant way. If the statistic is greater than the predefined threshold value, the probability of significant deviation between the two sensors is greater. Otherwise, the obvious deviation is not considered. Three steps are required to detect a single sample: calculation of deviation, calculation of test statistics, and calculation of examination. Each step is described in the following sub-sections.

3.1.1 Calculating the Deviation

For parameter p , the method to obtain the deviation is similar to the method used in calculating sensor deviations. The difference between the data tracked from sensors and the reference value is obtained by

$$\xi_{p,s}(i) = (p_s(i) - \bar{p}(i)) \tag{9}$$

where $\xi_{p,s}(i)$ indicates the difference of sensor s at point i . p_s is the parameter (e.g., distance, orientation, and elevation). The reference value of parameter p is expressed by $\bar{p}(i)$, which can be formulated as follows:

$$\bar{p}(i) = \sum_{j=0}^{j=n} c_j (t_j - t_{ref})^j \tag{10}$$

where t_j is the measured time for point j and c_j is the polynomial coefficient calculated by reference trajectory. The duration for constructing reference trajectory is expressed by t_{ref} .

3.1.2 Calculating the Test Statistics

The Student method is utilized to monitor the deviations between two sensors. We define a variable t_p , as the result of monitoring in terms of parameter p , that is:

$$t_p = \frac{\bar{\xi}_{p,1} - \bar{\xi}_{p,2}}{\sqrt{(n_1 - 1)\sigma_{p,1}^2 + (n_2 - 1)\sigma_{p,2}^2}} \sqrt{\frac{(n_1 + n_2 - 2)n_1n_2}{n_1 + n_2}} \tag{11}$$

As for parameter p , the existence of obvious deviation is considered if t_p is larger than T_{n_1} . If t_p is less than T_{n_2} , the two sensors are considered to be working cooperatively without deviation. Otherwise, the present study is unable to determine whether deviation exists between the two sensors or not (i.e., in terms of parameter p). In this case, the detection for accumulated samples is used to investigate the deviation between the two sensors.

3.2 Detection for Accumulated Samples

The detected data, such as starts, stops, average difference are recorded. Then, the results of the detection for each single sample are counted. For the two sensors, the detection for accumulated samples can be defined as follows:

$$t_c = \frac{\Sigma_{p,1} - \Sigma_{p,2}}{\sqrt{(N_1 - 1)\sigma_{p,1}^2 + (N_2 - 1)\sigma_{p,2}^2}} \sqrt{\frac{(N_1 + N_2 - 2)N_1N_2}{N_1 + N_2}} \tag{12}$$

where t_c is the detection result of the accumulated samples. The standard deviation is expressed by $\sigma_{p,s}$. The variable N_s is the number of records for parameter p . The total number of data, which determines the existence of deviation, is stored in variable k_1 . Similarly, the total number of data without deviation is k_2 . If $k_1 \leq 2 \times k_2$, the accumulated result is considered ambiguous and the accumulated samples will be detected in further tests.

The multiple data calculation method is used to monitor the deviation between two sensors. We combine the results of tests, and then achieve the cumulative tests statistic. The multiple data calculation method is defined as follows:

$$N_m = n_1 + n_2 \tag{13}$$

$$A_m = \frac{w_1a_1 + w_2a_2}{w_1 + w_2} \tag{14}$$

$$\sigma_m = \sqrt{w_1 + w_2} \tag{15}$$

$$w_x = \frac{1}{\sigma_x^2} \tag{16}$$

where a_x is the average value of sensor x , and the variance is expressed by σ_x . n_x are the points of sensor x .

4 Conclusion

This paper discussed the importance of the track points during flight and presented several practical methods to analyze the accuracy of the data obtained by sensors. We first constructed the reference trajectory, and then transformed the tracked data into the same coordinates system. The deviation between two sensors was evaluated, and then the Chi Square method was used to investigate the correctness of the deviation evaluation. In addition, we proposed a statistical method to identify whether the deviation exists between sensors or not. Future work may consider more realistic situations, more algorithms to calculate deviation, and more evaluation methods to determine the accuracy of deviations.

References

1. Trittler, M., Rothermel, T., Fichter, W.: Autopilot for landing small fixed-wing unmanned aerial vehicles with optical sensors. *J. Guidance Control Dyn.* **39**(9), 2011–2021 (2016)
2. Yeung, S., Madria, S.K., Linderman, M.: A trajectory recommendation system via optimizing sensors utilization in airborne systems (demo paper). In: Claramunt, C., Schneider, M., Wong, R.C.-W., Xiong, L., Loh, W.-K., Shahabi, C., Li, K.-J. (eds.) *SSTD 2015. LNCS*, vol. 9239, pp. 508–513. Springer, Cham (2015). https://doi.org/10.1007/978-3-319-22363-6_31
3. Frank, T., Janoske, U., Schroedter, C.: Detection of position and orientation of flying cylinder shaped objects by distance sensors. In: 2011 IEEE International Conference on Mechatronics (2011)
4. Rhudy, M.B., Gu, Y.: Unmanned aerial vehicle navigation using wide-field optical flow and inertial sensors. *J. Robot.* **2015** (2015)
5. Hussmann, S., Huhn, P., Hermanski, A.: Systematic distance deviation error compensation for a ToF-camera in the close-up range. In: *I2MTC - International Instrumentation and Measurement Technology Conference* (2012)
6. Rodríguez-Jiménez, S., Burrus, N., Abderrahim, M.: A-contrario detection of aerial target using a Time-of-Flight camera. In: *Sensor Signal Processing for Defence, SSPD 2012* (2012)
7. Blomqvist, J., Fullmerb, R.: The influence of uncertainties of attitude sensors on attitude determination accuracy by linear covariance analysis. *The International Society for Optical Engineering* (2010)
8. Labowski, M., Kaniewski, P., Konatowski, S.: Estimation of flight path deviations for sar radar installed on UAV. *Metrol. Meas. Syst.* **23**(3), 383–391 (2016)

A Distributed Routing Algorithm for LEO Satellite Networks

Jundong Ding¹, Yong Zhang^{1(✉)}, Ruonan Li¹, and Liang Zhao²

¹ Beijing Key Laboratory of Space-Ground Interconnection and Convergence, Beijing University of Posts and Telecommunications (BUPT), Xitucheng Road No. 10, Beijing 100876, China
{dingjundong, yongzhang, liruanan}@bupt.edu.cn

² China Electronic Appliance Corporation, Beijing, China
zhaol@ceac.com.cn

Abstract. Satellite networks support a wide range of service and provide global coverage. Moreover, LEO satellites, which have global coverage potential, have caused great attention in the field of satellite communication. Due to satellites' mobility, an efficient and stable routing algorithm is necessary for transmission in satellite networks. In this paper, a Distributed Multi-Path Routing algorithm (DMPR) using Earth-fixed satellite systems is proposed. DMPR adopts the Polar orbit constellation in which each satellite has four ISLs (inter satellite link) with the neighbor satellites. A traffic-light is set for every ISL to judge the blocking while avoiding some busy path and reducing the delay.

Keywords: Low earth orbit · Polar orbit constellation
Distributed multipath routing · Traffic light

1 Introduction

Satellite networks are becoming important in the field of communication, especially the LEO satellites. Compared to the terrestrial networks, the LEO satellites have global coverage potential. Besides, they can also offer services with lower latency than the geostationary satellites. Therefore, the LEO satellites communication has aroused great interest in academia and industry.

The satellites' topologies are dynamic with frequent link switching and interruption. Since the satellite constellation is determined in advance, the topologies will be predictable. These characteristics, different from terrestrial networks, bring many difficulties in routing design. Many schemes have been proposed from researchers since the 1990s [1]. Topological control strategy can generally be adopted to shield the topology's dynamic. There are two topology control strategies: Virtual topology [2, 3] and virtual node [4, 5]. Virtual node strategy in which use the concept of satellite logical location form a global virtual networks. Each node in the network is virtual node, which is serviced by the nearest satellite.

Werner [6] introduces the DT-DVTR routing algorithm (Discrete-Time Dynamic Virtual Topology Routing) in the LEO satellites networks. They divided the routing strategy into two processes: firstly, they set a virtual topology for all successive time

intervals of the system period, providing instantaneous sets of alternative paths between all source destination node pairs; secondly path sequences over a series of time intervals are chosen from that according to certain optimization procedures. Korçak [7] proposed a multistate virtual network (MSVN) topology, provided formal mathematical model for it and discussed its contribution to the overall system availability. Then Lu et al. [8] formalized and optimized the virtual topology based on virtual node strategy while elaborating its important features.

There are many distributed routing algorithms [9, 10] based on virtual nodes. A datagram routing algorithm is proposed for LEO satellite networks where routing decisions are made on per-packet basis. Henderson and Kartz [11] has proposed a distributed routing algorithm in which they flood a link state packet only as the routing radius for a given satellite and then they choose the best path using Dijkstra algorithm.

This paper is organized as follows: Sect. 2 introduces the satellite network architecture that has the Earth-fixed footprints. Section 3 proposes the new routing strategy. Section 4 presents the simulation result of the new routing algorithm and in the end Sect. 5 summarizes this paper.

2 Satellite Network Architecture

The satellite network adopts the Walker star [12] constellation which is composed of N polar orbits (planes), each with M satellites at low distances from the Earth. The planes are separated from each other with the same angular distance of $360^\circ/(2 * N)$. They cross each other only over the North and South poles. The satellites of each plane are separated from each other with an angular distance of $360^\circ/M$. Due to the circular planes, the satellites in the same plane have the same radius all the times. In this paper N is 6 and M is 12.

Each satellite has four neighboring satellites: two in the same orbit and two in the left and right planes. So each satellite has four transmission directions which means that when deciding the next hop node each satellite has four choices.

In our analysis of virtual topology dynamics, we consider a satellite orbit with N_{SAT} satellites that have Earth-fixed footprints, and serve for total of N_{FP} footprint areas along the orbit. The footprint means the ground area is serviced by satellites. Firstly, average number of satellites per footprint area (N_f^{sat}) is calculated as

$$N_f^{sat} = N_{SAT}/N_{FP} \quad (1)$$

In traditional VN (virtual node) concept, N_{SAT} is equal to N_{FP} , i.e., there exists a single satellite for each footprint, namely $N_f^{sat} = 1$. However, for the sake of increasing system availability, this paper also considers the case where there is more than one satellite per footprint. Target on improving the transmission success rate while simplifying the handover process, we set N_f^{sat} to 2 as shown in Fig. 1.

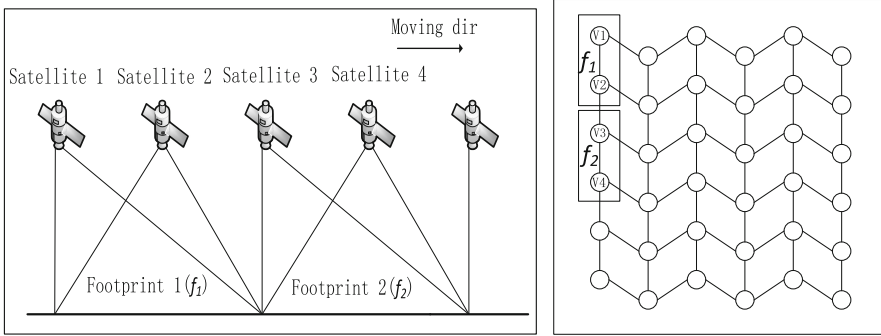


Fig. 1. The satellite system and virtual network with $N_f^{sat} = 2$

In the virtual networks, we use $\langle \mathbf{n}, \mathbf{m} \rangle$ ($\mathbf{n} = 1, 2, N; \mathbf{m} = 1, 2, M/2$) to represent the virtual footprint. Each satellite will also be assigned a corresponding address as the basis for the transmission. Taking into account the mobility of satellites, the satellites' coordinates need to be updated periodically. Ignoring the impact of the Earth's rotation, we only update the value of \mathbf{m} . There are $M/2$ footprints in each orbit, hence each satellite has $M/2$ different \mathbf{m} values. The satellite updating period (T_{upd}^{sat}) can be updated as:

$$T_{upd}^{sat} = T_{sat} / (M/2) = 2 \cdot T_{sat} / M \tag{2}$$

Where T_{sat} means the satellite movement period.

3 Routing Strategy

DMPR routing algorithm is a kind of distributed routing algorithm. Therefore, each satellite node can independently determine their next hop node depending on ISL congestion. For the satellites, a buffer queue for each ISL was set to temporarily store packets sent to the next hop satellite through this ISL. A buffer traffic is also set to represent the congestion condition for this ISL. To select the next hop node (or the transmission direction) the satellite will consider the current satellite's congestion status of a buffer queue.

Figure 2(a) shows how to set the color of traffic light according congestion. In our algorithm, there are only two types of traffic light color: "GREEN" and "RED". First of all, $BQ(n)$ ($n = 1, 2, 3, 4$; meaning there are 4 ISL in every satellite) is defined as the buffer queue of satellite at direction n . And the buffer queue occupancy rate $BOQR$ is defined as the rate of packets' number in the queue to the length of the queue. So $BOQR_n$ represents the occupancy rate of $BQ(n)$. Then we define a threshold T to distinguish the two status. When $BOQR_n$ grows beyond T , the queue is considered to be congested and the traffic light turns to "RED". There is a special situation: when the satellite checks $BQ(n)$, $BOQR_n$ is very close to but still below T , so the traffic light remains "GREEN". Just after checking, $BOQR_n$ is beyond T , but the satellite has

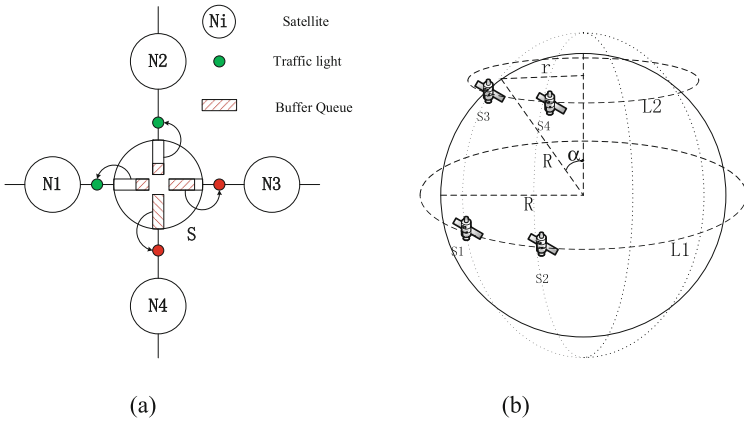


Fig. 2. Traffic light color setting scheme (Color figure online)

to stay wrong status for Δt (checking interval). To ensure that $BOQR_n$ will not exceed T during this checking interval, T should meet:-

$$T \cdot L \cdot APS \geq (I - O)_{max} \cdot \Delta t \tag{3}$$

Where L represents the size of buffer queue, APS represents average packets size, and $(I - O)_{max}$ denotes the maximum difference between input and output traffic rates.

When the satellite moves to high latitudes, the distance between them is closer than the low latitudes as shown in Fig. 2(b). The distance between satellites in orbit $L2$ can be described by: $d = \pi \times (R \times \sin\alpha + h) \div N$

(R means the Earth radius, h means the satellites height and N means the number of orbits).

According to Shannon formula, the channel capacity can be described by:

$$R_d = B \cdot \log\left(1 + \frac{S}{N}\right) = B \cdot \log\left(1 + \frac{P_D \cdot h_{ss}}{\sigma^2}\right) \tag{4}$$

h_{ss} means channel gain and $h_{ss} \sim E(d^{-\alpha})$. It can be seen satellites' channel capacity in high latitudes is larger than low latitudes. So the buffer size of inter-ISL can be set higher when satellites moves to high latitudes. This means when satellites serving for different footprint their inter-ISL buffer size change dynamically.

The routing algorithm begins with sending data from the terrestrial device to the satellite. Each terrestrial device can send data to 2 different satellites, because every footprint is served by two satellites. When the current satellite determines the next hop node, it will compare the footprint's coordinate to decide the direction.

$\langle \mathbf{n}_d, \mathbf{m}_d \rangle$ is the destination footprint coordinate and $\langle \mathbf{n}_i, \mathbf{m}_i \rangle$ as the current satellite's footprint coordinate. The current satellite will choose at most two directions to transfer data. The vertical and horizontal movements are described by

$$d_v = \begin{cases} +1, & \text{upward} \\ 0, & \text{no movemet} \\ -1, & \text{downward} \end{cases} \quad d_h = \begin{cases} +1, & \text{right} \\ 0, & \text{no movement} \\ -1, & \text{left} \end{cases} \quad (5)$$

During a date receiving processing, firstly current satellite will check whether the same data has been received. After checking, satellites can avoid transferring the same data twice, so it can save source and improve the system’s performance. If not, it will compare its own footprint coordinate with the destination coordinate to choose the direction. For example, if $m_i > m_d$, $d_v = +1$ means the current satellite chooses upward as the backup direction. If $n_i < n_d$, $d_h = +1$ means the current satellite chooses right as the backup direction (Table 1).

Table 1. Direction selection scheme

$m_i > m_d$	$m_i = m_d$	$m_i < m_d$	$n_i < n_d$	$n_i = n_d$	$n_i > n_d$
$d_v = +1$	$d_v = 0$	$d_v = -1$	$d_h = +1$	$d_h = 0$	$d_h = -1$

After choosing two backup directions, the satellite will enhance direction by taking congestion into account. If the backup ISL’s traffic light is “GREEN”, the satellite will transfer data through this ISL. If the backup ISL’s traffic light is “RED”, the satellite will discard this ISL.

4 Simulation and Evaluation

In this section, we mainly analyze the performance of satellite transmission delay and success rate. In satellite communications, congestion and satellite failure are important factors affecting data transmission. In this experiment, the average one-hop ISL propagation delay is set to 14 ms. When the ISL is set to “GREEN”, the maximum queuing delay is set to 10 ms. When the ISL is set to “RED”, maximum queuing delay is set to

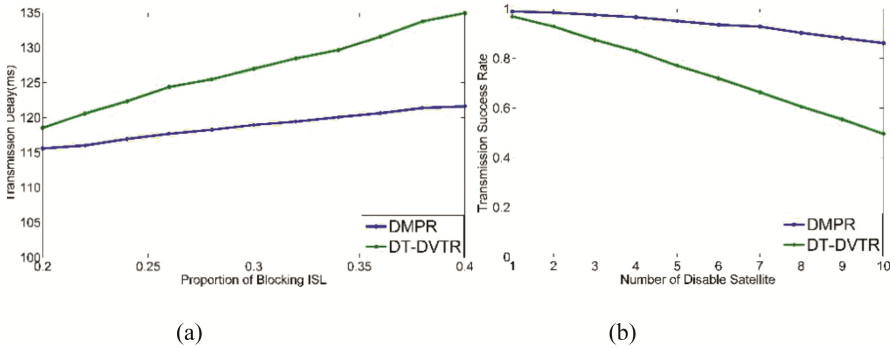


Fig. 3. Simulation of transmission delay and success rate

30 ms. In simulation, inter-orbit link's buffer size is set dynamically. Satellites' buffer size ($BQ(n)$) is 20% smaller than higher latitudes, so does the threshold T .

Figure 3(a) shows the two routing algorithm's latency increases with the proportion of blocking ISL. DMPR's latency is shorter than DT-DVTR's obviously. When the link is blocking, the satellite will wait which will increase queuing delay using DT-DVTR routing. So the impact of blocking on the delay is small while DT-DVTR's delay increases rapidly with the increase in proportion.

In DMPR routing algorithm each satellite node has at most two choices when selecting next node. Even if a node fails, it can also find an alternative node for transmission which can mitigate the adverse effects caused by node failures. So in the Fig. 3(b), it shows the success rate of DMPR is higher than DT-DVTR's especially when the number of disabled satellite exceeds 5.

5 Conclusion

In this paper, we have proposed a new distributed routing algorithm for LEO satellite networks. When choosing the next hop satellite node, the satellite will take congestion into account. So our routing strategy has an advantage in reducing latency when encountering congestion. Meanwhile, this routing algorithm can guarantee the success rate when the node fails.

Acknowledgements. The author would like to thank to the reviewers for their detailed suggestions. This work is supported by the National Natural Science Foundation of China under Grant No. 61171097.

References

1. Taleb, T., Jamalipour, A., Kato, N., Nemoto, Y.: IP traffic load distribution in N GEO broadband satellite networks – (invited paper). In: Yolum, G, G, T., G, F., O, Z., C. (eds.) ISCS 2005. LNCS, vol. 3733, pp. 113–123. Springer, Heidelberg (2005). https://doi.org/10.1007/11569596_14
2. Gounder, V.V., Prakash, R., Abu-Amara, H.: Routing in LEO-based satellite networks (1999)
3. Fischer, D., Basin, D., Engel, T.: Topology dynamics and routing for predictable mobile networks. In: IEEE International Conference on Network Protocols, pp. 207–217. IEEE Xplore (2008)
4. Mauger, R., Rosenberg, C.: QoS guarantees for multimedia services on a TDMA-based satellite network. *Commun. Mag. IEEE* **35**(7), 56–65 (1997)
5. Ekici, E., Akyildiz, I.F., Bender, M.D.: A distributed routing algorithm for datagram traffic in LEO satellite networks. *IEEE/ACM Trans. Netw.* **9**(2), 137–147 (2001)
6. Werner, M.: A dynamic routing concept for ATM-based satellite personal communication networks. *IEEE J. Sel. Areas Commun.* **15**(8), 1636–1648 (1997)
7. Korçak, Ö., Alagöz, F.: Virtual topology dynamics and handover mechanisms in Earth-fixed LEO satellite systems. *Comput. Netw.* **53**(9), 1497–1511 (2009). *The International Journal of Computer & Telecommunications Networking*

8. Lu, Y., Sun, F., Zhao, Y.: Virtual topology for LEO satellite networks based on earth-fixed footprint mode. *IEEE Commun. Lett.* **17**(2), 357–360 (2013)
9. Wang, K., Yi, K., et al.: Packet routing algorithm for polar orbit LEO satellite constellation network. *Sci. Chin. Inf. Sci.* **49**(1), 103–127 (2006)
10. Papapetrou, E., Pavlidou, F.N.: Distributed load-aware routing in LEO satellite networks. In: 2008 Global Telecommunications Conference, IEEE GLOBECOM, pp. 1–5. IEEE Xplore (2008)
11. Henderson, T.R., Katz, R.H.: On distributed, geographic-based packet routing for LEO satellite networks. In: 2000 Global Telecommunications Conference, IEEE GLOBECOM 2000, vol. 2, pp. 1119–1123. IEEE Xplore (2000)
12. Wang, J., Li, L., Zhou, M.: Topological dynamics characterization for LEO satellite networks. *Comput. Netw.* **51**(1), 43–53 (2007)

Optimization of Smart Home System Based on Wireless Sensor Network

Xing Guo^(✉) and Neng Hu^(✉)

School of Logistics Engineering, Wuhan University of Technology,
Wuhan 430063, People's Republic of China
2633283313@qq.com 419443370@qq.com

Abstract. In this paper, smart home is the research object. It analysed the intelligent acquisition for monitoring data, put forward a kind of solution for remote monitoring system based on wireless sensor network, and designed a set of perfect intelligent remote monitoring system by using the mobile terminal platform. This system can achieve a series of basic functions, including monitoring, automatic adjustment, alarm and control for the home appliances, which can provide comprehensive and reliable home environment information for the home users and meanwhile achieve remote control for home appliances. Finally, the smart home monitoring system was deployed and tested, the test results show that the system can achieve the basic functions of the modern smart home and has the unique advantages in performance, cost, versatility, scalability and other aspects.

Keywords: Smart home · Wireless sensor · ZigBee · HTML5 · WebSocket

1 Introduction

With the rapid development of wireless sensor network, smart phone communication and Internet technology, the remote wireless mobile home monitoring system will become one of the mainstream smart home network [1]. The smart home system needs a lot of information acquisition and transmission. Introducing the wireless sensor network technology into the construction of smart home can build a “home appliance network” with adaptive control function for smart home [2]. This network can not only make the smart appliances conduct mutual coordination, but also be interacted with the external network. Therefore, users can achieve the remote control of the smart appliances through this network.

At present, the domestic and foreign major operators are integrating resources and carrying out innovative business to occupy the smart home market [3–5]. Although the smart home industry is developing relatively quickly, the present level of development is uneven. It is faced with many problems like the lack of unified industry standards, expensive price, complex operation and the leakage of information which restrict the development of the smart home industry [6, 7]. In this research, the field research was conducted to find out the deficiencies of the current smart home system. And the environmental parameters required for the monitoring system were determined through the

analysis of actual functional requirements. Combined with ZigBee wireless network communication technology and the research of the intelligent collection for monitoring data by sensors, a set of perfect intelligent remote monitoring system for smart home was designed through the mobile terminal platform. And the debugging environment was deployed to analyze and verify the research results.

2 Overall Design

The overall design is based on the research about the wireless sensor network technology, wireless data communication technology, HTML5, WebSocket and other related theoretical basis [8]. Combined with corporate field research and actual functional requirements analysis, the overall design of the smart home monitoring system based on the wireless sensor network was determined generally, as shown in Fig. 1.

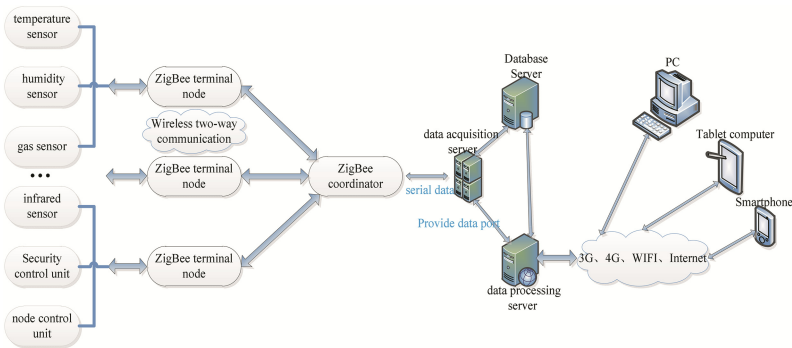


Fig. 1. Overall design

The system collects the required information of the family environment by the related sensors and controls the switch of the household electrical appliances by the controller modules. In this system, the sensor modules and the controller modules are connected to the ZigBee terminal equipment. The data transmission is based on the ZigBee wireless network and the ZigBee center coordinator. The ZigBee center coordinator is connected to the server through the serial ports. It can save the data collected from the sensors into the server database or sent the data to the client directly. According to the implementation process of the system, the overall scheme includes the front-end sensors and the controllers module design, the ZigBee wireless sensor network design, the data transmission module design, the server program design, the data interaction module design, and the client application software design.

3 Wireless Sensor Network Design

3.1 ZigBee Wireless Network Design

The ZigBee wireless transmission module of this system used TI wireless RF chip called CC2530F256 as the core chip. CC2530F256 is compatible with the ZigBee protocol stack, providing a powerful and complete ZigBee solution. Because the transmission distance is relatively short and the family housing area is limited, the system just needs relatively small sensor nodes and a simple data transmission structure, which does not need the router nodes to extend the network coverage area [9]. Meanwhile the position and the number of the household appliances are easy to change, which will change the network state. Therefore, under the premise of the communication requirements, considering the cost of the equipment and the simple structure, this system used the star topology to build the smart home wireless network. The star topology wireless network consists of a ZigBee full-function central coordinator and several terminal functional devices. And the data transmission is based on the principle of ZigBee wireless data transmission.

In this paper, the DS18B20 temperature sensor module was selected as an example to introduce the concrete design process of the data acquisition and transmission software. First, the system obtained the collected data from the terminal device. Then the data was transmitted to the central coordinator. Finally, the coordinator sent the data to the sever module through the serial ports. In order to observe the results of data acquisition expediently, the coordinator used LCD to display the collected data values. Meanwhile the data in the terminal nodes and the coordinator node was sent to the computer through the serial ports and shown by serial debugging assistant. In order to enhance the system layout and installation convenience, meanwhile reducing energy consumption, the data acquisition nodes all used the battery power [5, 10]. The node modules will go into sleep mode in leisure time and be wake up when the system needs data acquisition or transmission. The entire workflow is shown in Fig. 2.

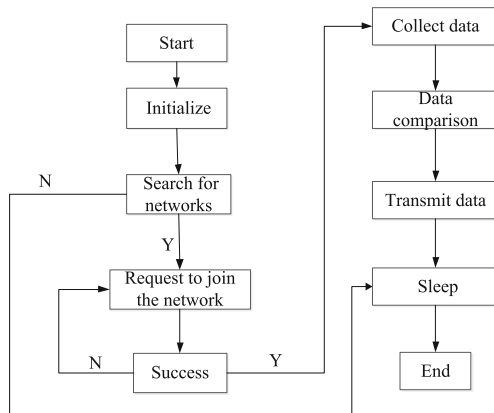


Fig. 2. Temperature sensor node workflow

3.2 Development and Encryption of the Data Communication Protocol

The data communication protocol was designed to solve all kinds of problems of the parameters transmission, ensure the integrity, reliability and security of the data, and achieve the data transmission function between the modules. Based on the basic Modbus communication protocol, the system used the same structure to define the different command codes. According to the concrete data and the specific functions, the system customized a complete communication protocol, which can make the system more standard and perfect. In order to make the communication protocol defined by the system possess scalability, the functional code fields were set in the message component unit, and the functional code table was established to manage the functional codes defined by the system. The developers only need to add the functional codes in the code table when they want to add new function in the protocol, which will not affect the previous communication protocol and functions.

In order to avoid the interference of the external equipment and ensure the confidentiality and the security of the data in the process of network communication, the security and encrypted transmission of the data in the smart home network are the importance of the research. There are three basic encryption keys of the ZigBee network data, including the main key, the link key and the network key. According to the actual application, the key is generated by the network layer and the application layer. The security keys can be shared between the layers, which can reduce the storage requirement. The system used CC2530 chip as the ZigBee module of the wireless transceiver. And the data encryption and decryption of CC2530 can be achieved through the coprocessor supported by AES (Advanced Encryption Standard).

4 Design of the Monitoring System

4.1 Design of the Functional Modules

According to the demand analysis of the system, the smart home monitoring system can be divided into five main functional modules, including real-time monitoring module, security alarm module, scene mode, basic information management and user management. These five functional modules can not only achieve the real-time monitoring data display, alarm for abnormality, linkage control and historical data display, but also achieve the statistical processing, analysis and diagnosis of the massive monitoring data to search potential effective information intelligently. In the meantime, this system can provide the mode selection, information management and scalability. The overall functional structure of the system is shown in Fig. 3.

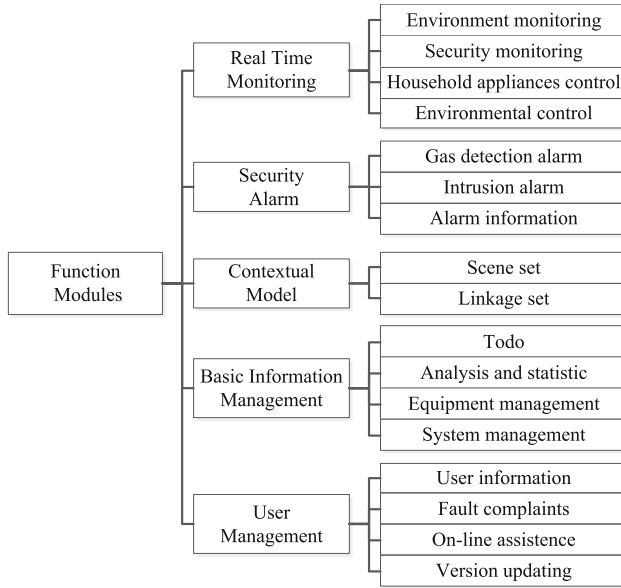


Fig. 3. Overall system functional structure

4.2 Acquisition and Processing of the Server Data

The server used multithreading serial communication technology to obtain the induction layer data. In the data communication process, a variety of serial operations were placed in different threads, and every thread was only responsible for the corresponding serial operation. The main thread was responsible for the coordination and management of the auxiliary threads, which can use the CPU in fast switching between various threads. Therefore, the system can achieve the concurrent execution and multi-task mechanism to reduce the occupancy rate of the CPU. This mechanism can improve the utilization of the serial ports and efficiency of data transmission, which can greatly improve the data request and processing ability of the server.

In order to solve the common problems of the database like operating frequently and low query efficiency, the system used the cache mechanism to save the collected data. The cache mechanism saved the data in the cache memory. Returning data from the cache memory is quicker than querying database, so it can greatly improve the performance of the server application. In the process of operation, the database will start data cache dependency. When the server requests the latest data collected by the sensor, it will write the data to the cache and update the cache. And setting the key index “CacheKey” when the system writes cache can improve query execution efficiency of the data in the cache. The concrete process of data storage adopting data cache mechanism is shown in Fig. 4.

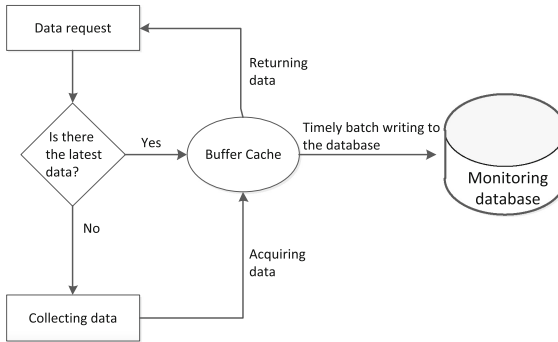


Fig. 4. Flow chart of cache data storage

4.3 Information Interaction of the Client and Server

For the basic operations which don't need high operation frequency and real-time requirements, such as user login, obtaining the equipment information, querying the historical data and other operations, the client used Ajax asynchronous loading technology to invoke the Web Service from the server and obtain the basic information. In order to make the system client and server can transmit data cross platform and cross language, this system used lightweight data exchange format "Json" to achieve the data exchange between them.

As for viewing and operating the data in real-time monitoring system, it needs client and server keep persistent connection and constantly obtain the real-time updated data from the sensor layer, which has high requirements for real-time communication, so this system designed the WebSocket full duplex bidirectional communication technology to achieve real-time monitoring. First, this system enabled a thread in the server to open the WebSocket network service and used the delegation method to open or close the WebSocket connection. Then it obtained the IP address of the machine and established the monitoring ports. Finally, the system regarded the two values as the parameter values of the WebSocket server address to transmit data. For the realization of the system client, the system used the HTML user interface. After the WebSocket connection between the client and the server, the two sides will be able to achieve continuous two-way communication with a high utilization ratio.

5 Application Test and Verification of the System

5.1 Communication Distance and Packet Loss Rate Test

In order to compare the performance of the ZigBee communication system in different environments, the test was divided into indoor test and outdoor test, which conducted a number of tests in different indoor rooms and outdoor open occasions to ensure the accuracy of the results. In each distance test process, the ZigBee terminal node data

transmission frequency was set as 3 s/times, and a total of 500 data was sent to the coordinator. The average value of the test results was shown in Table 1.

Table 1. Communication distance and data packet loss rate of the ZigBee module

Test environment	Communication distance(m)	Number of terminal data transmission	Number of coordinator data reception	Number of test	Average packet loss rate(%)
Indoor	15	500	500	10	0
	20	500	500	10	0
	25	500	500	10	0
	30	500	498	10	0.4
Outdoor	30	500	500	10	0
	50	500	496	10	0.8
	70	500	473	10	5.4
	100	500	447	10	10.6

As we can see from the test results, by using the system based on the ZigBee wireless sensor network, when the communication didn't meet interference in the outdoor environment, the packets loss rate was very low within a 50 m range. When the node distance was more than 70 m, the packet loss rate will increase a little. While in indoor environment, when the transmission distance was less than 25 m, the packet loss rate was about 0%. The results show that the data transmission of the designed ZigBee network has high reliability, and it can meet the requirements of data transmission in the general family environment.

5.2 WebSocket Real-Time Communication Verification

In order to examine the communication efficiency and real-time of the WebSocket technology which was used in the smart home monitoring system, the Ajax polling based on HTTP protocol and the real-time communication framework based on the WebSocket were set up. In this test, the data request and response information of two kinds of scheme in the process of communication were analyzed and compared through the Chrome browser network tools. Then the test case was designed by using the Jmeter pressure test tools, which simulated the communication between the client and the server to compare the network throughput and delay of two methods.

5.2.1 Network Throughput

In this two test schemes, the same data in test was used to ensure that the server sent to the client in the same actual data size. The Jmeter test tool was used to get data size through the Ajax polling and WebSocket, and then we can observe the changes of network throughput in four cases. The results were shown in Fig. 5. As we can see from this picture, with the increase of the load and the flow, the network traffic caused by the Ajax polling was very huge. The WebSocket scheme caused much smaller network

throughput than the traditional Ajax polling scheme, which has great performance advantages.

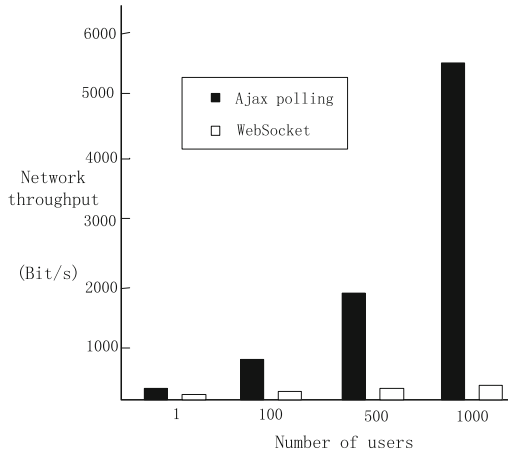


Fig. 5. Network throughput comparison of Ajax polling and WebSocket

5.2.2 Network Delay

After the completion of the test, we entered into the “view result tree” of the Jmeter test tool to count the connection time and loading time consumed in the communication process and calculate the network delay time of this two communication schemes. In order to ensure the accuracy of the test results, several experiments were carried out in each test case. The data delay time was collected to take the average value of the results. Network delay test results were shown in Table 2.

Table 2. Average delay time of the test results

Number of users	Real-time application scheme	Number of messages transmission	Total delay time (ms)	Average delay time (ms)
1	Ajax polling	1000	8025	8.02
	WebSocket	1000	4832	4.83
100	Ajax polling	1000	29757	29.75
	WebSocket	1000	8364	8.36
500	Ajax polling	1000	187074	187.07
	WebSocket	1000	12639	12.63
1000	Ajax polling	1000	472283	472.28
	WebSocket	1000	16482	16.48

According to the comparison of the above two kinds of real-time communication schemes and analysis of the results, the real-time application based on WebSocket communication scheme performs better than the current widely-used Ajax long polling

technology in the aspects of message delay time and network throughput. WebSocket technology can decrease the network throughput greatly, and take advantage of the stable long connection mode to reduce the communication delay time, which has a high efficiency in the real-time monitoring system of the smart home.

6 Conclusion

This paper introduced the wireless sensors into the system, which greatly simplified the structure of the system and improve flexibility. It used the serial debugging assistant to test the communication distance and the data packet loss rate of the wireless network set up by ZigBee equipment, and completed the ZigBee communication module test and WebSocket communication test in the smart home system. It verified the stability and safety of the ZigBee wireless network. Then, the real-time communication framework of Ajax polling and WebSocket were constructed respectively, and the network throughput and the network delay of the two schemes were tested through Chrome browser and Jmeter pressure test tool, which proved the advantages of WebSocket technology in system real-time monitoring. Finally, the on-line overall test for the entire smart home system was conducted through the different mobile terminals. The system worked well and met the design requirements, which achieved the basic expected functions of the smart home system.

Acknowledgment. This paper was supported by the project in the Hubei Science and Technology Pillar Program (No. 2015BKA222).

References

1. Lai, W.: Intelligent home system design. *Comput. Knowl. Technol.* **08**, 23–25 (2015)
2. Xie, Y., Pei, L., Wu, T.: Internet of Things in the application of intelligent home. *Instrum. Technol.* **03**, 46–49 (2015)
3. Zhao, Y.: Intelligent home system in the Internet of Things. *Internet Things* **05**, 32–35 (2013)
4. Alam, M., Reaz, M., Ali, M.: A review of smart homes-past, present, and future. *IEEE Trans. Syst. Man Cybern.* **42**(6), 12–16 (2012)
5. Zhu, M., Li, N.: Development status and future analysis of intelligent home. *Telev. Technol.* **04**, 82–85, +96 (2015)
6. Bitterman, N., Shach-Pinsly, D.: Smart home - a challenge for architects and designers. *Architect. Sci. Rev.* **58**, 266–274 (2015)
7. Wu, L., Wei, Y., Yajie, M.: Development status analysis of domestic and international intelligent home market. *Mod. Telecommun. Technol.* **12**, 71–74 (2014)
8. Zou, S.: Study on the key technology of intelligent home system based on wireless sensor network. South China University of Technology (2013)
9. Nagpal, P.: Key actors in the mobile phone industry: the smart phone wars. *Acad. Inf. Manag. Sci. J.* **17**(1), 87 (2014)
10. Liu, L., Hu, B., Li, L.: Energy conservation algorithms for maintaining coverage and connectivity in wireless sensor networks. *IET Commun.* **4**(7), 786–800 (2010)

The Energy Efficiency Research of Traffic Offloading Mechanism for Green Heterogeneous Networks

Kaili Wu^(✉), Yifei Wei^(✉), Qiao Li, Da Guo, and Mei Song

School of Electronic Engineering, Beijing University of Posts and Telecommunications,
Beijing, China

{kaili, weiyifei, liqiao1989, guoda, songm}@bupt.edu.cn

Abstract. Opportunistic Network as a novel networking, taking advantage of meeting opportunities of mobile nodes, completes the message transmission from the source node to the destination node through the way of each hop. Mobility model decides how the nodes move and is used to analyze network performance with various protocols, such as routing protocols, data dissemination protocols, etc. Currently many mobility models are proposed by researchers. To evaluate these mobility models, an analysis method is proposed. So we propose a method by analyzing mobile distance to assess node mobility models. This paper firstly introduced the commonly used mobility models based on ONE simulation platform, and then a calculation method of node mobile distance is put forward. Next, it was simulated and discussed that we have considered the nodes mobility features by mobile distance. Finally, we use the node contact duration and node inter-contact time as a validation, to make an evaluation for node mobility model.

Keywords: Energy harvesting · Green communications
Heterogeneous cellular networks · Traffic offloading

1 Introduction

Recent years, the energy consumption problem of communication network gradually becomes the research focus in the industry and academia [1, 2]. How to reduce the energy consumption of communication network and improve the energy efficiency of communication system have become a hot topic in the current field of communication research. Heterogeneous network is expected to play an important role in the future communication network [3, 4]. In heterogeneous network, it can be introduced a number of different types of small site equipment, such as micro base station (Micro), Pico base station (Pico), family base station (Femto) and wifi access points, it can strengthen the overlying cover of certain areas, improve network capacity. These small sites are often deployed in the place which are closer with the users, can provide service for users with far less power consumption than Macro. Despite the high network capacity, the dense SBSs also require huge power supply, causing heavy burdens to both the network operators and the power grid [5].

To deal with the cumbersome energy consumption, energy harvesting (EH) technology can be introduced into HCNs. Specifically, the emerging EH-SBSs, which are equipped with EH devices (like solar panels or wind turbines) exploit renewable energy as

supplementary or alternative power sources, have received great attentions from both academia and industry [6]. How to fully utilize the harvested energy to maximize network energy efficiency while satisfying the quality of service (QoS) requirements is a critical issue.

Traffic offloading problem is one of the hot issues in heterogeneous network. [7, 8] analyzes the relationship between the traffic offloading and customer service quality, and puts forward the traffic offloading incentive mechanism based on reverse auction model, can guarantee the quality of customer service, increase the amount of data offloading of the system. Literature [9] puts forward offloading users which have high requirements of service quality to femto to reduce the energy consumption of the macro, and analyzes the relationship between the system energy efficiency and the distance between the neighborhood. Literature [10] analyzes the system power consumption influence of different traffic density by different amount of micro. But [9, 10] only consider the static traffic loading scenario, without considering the dynamic changes of the business. [11] considers the offloading when in the wifi enabled small cell case.

Although traffic offloading technology has been extensively investigated in on-grid cellular networks, the conventional offloading methods cannot be applied when EH is applied. Instead, traffic offloading technology of green heterogeneous cellular networks needs to be devised, the operation of each cell is optimized individually based on their renewable energy supply. Different from existing works, we focus on the design of traffic offloading for green HCNs with multiple SBSs powered by diverse energy sources. We aim to maximize the network energy efficiency while satisfying the QoS requirement of every user. To this end, users are dynamically offloaded from the MBS to the SBSs, based on the statistical information of traffic intensity and energy arrival rate, based on which the optimal traffic offloading amount are obtained.

The reminder of the paper is organized as follows. System model is introduced in Sect. 2. Section 3 analyzes the power demand and supply for SBSs with EH devices. Then, the energy efficiency maximization problem for the single-SBS case is studied in Sect. 4. Simulation results are presented in Sect. 5, followed by the conclusion in Sect. 6.

2 System Model

In this section, the details of the HCN with different energy supply are presented as follows.

2.1 Network Model

With EH technology employed, a typical scenario of HCN is shown in Fig. 1, where different types of SBSs and wifi access points are deployed in addition to the conventional MBS to enhance network capacity. Based on the energy source, SBSs can be classified into two types: (1) HSBSs powered jointly by energy harvesting devices and power grid; and (2) RSBSs powered solely by harvested renewable energy (like solar and wind power). Wifi access points are powered only by conventional energy. Denote by N_H and N_R the number of HSBSs and RSBSs, respectively, denote by $B_H = \{1, 2, \dots, N_H\}$, $B_R = \{1, 2, \dots, N_R\}$ the set of HSBSs and RSBSs respectively, let

$B = \{B_H, B_R\}$ be the set of all SBSs. Denote by W_a the number of wifi access points, denote by $B_w = \{W_1, W_2, \dots, W_a\}$ the set of wifi access points. SBSn serves a circular area with radius $D_{s,n}$, and the small cells are assumed to have no overlaps with each other. The MBS is always active to guarantee the basic coverage, whereas SBSs and wifi access points can be dynamically activated for traffic offloading or deactivated for energy saving, depending on the traffic and energy status.

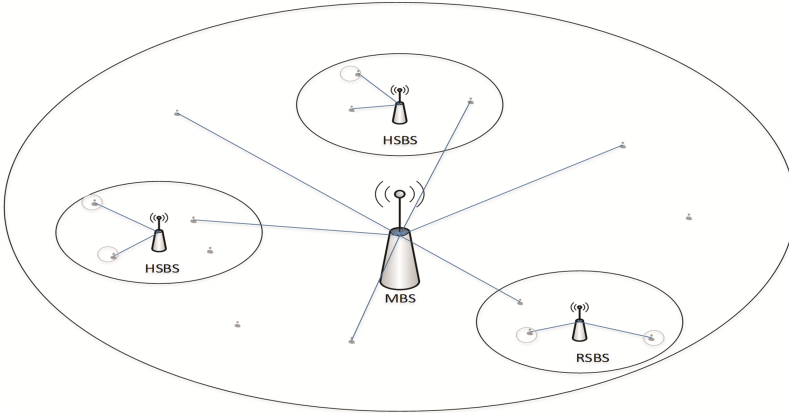


Fig. 1. Illustration of a HCN with diverse energy sources

2.2 Traffic Model

The user distribution in spatial domain is modeled as a nonhomogeneous Poisson Point Process (PPP), whose density at time t is $\rho_0(t)$ in small cell n and $\rho_n(t)$ outside of all small cells. As shown in Fig. 1, users located outside of the small cells can only be served by the MBS, while users within small cells can be partly or fully offloaded to the corresponding SBS or the wifi access points. Thus, users can be classified into three types based on the serving BS, wifi access points and location: (1) Macro-Macro Users (MMUs), users which are located outside of small cells and served by the MBS; (2) SBS-SBS Users (SSUs), users located within small cells and offloaded to the SBS; (3) Macro-SBS Users (MSUs), users located in small cells but served by the MBS. (4) WIFI-WIFI Users (WWUs), users located within small cells and offloaded to the wifi access points.

As for spectrum resource, the bandwidths available to the MBS-tier and SBS-tier are orthogonal to avoid cross-tier interference. Denote by W_m , W_s , and W_w the system bandwidth available to the MBS, each SBS and wifi access points, respectively. At the SBSn, the bandwidth actually utilized is denoted as $w_{ss,n} \leq W_s$, which is allocated to its SSUs equally for fairness. At the MBS, W_m is further divided into different orthogonal portions: w_{mm} for serving MMUs and $w_{ms,n}$ for serving MSUs in small cell n , where $w_{mm} + \sum_{n=1}^{N_H+N_R} w_{ms,n} \leq W_m$. At the wifi access points, the bandwidth actually utilized is denoted as $w_{ww,n} \leq W_w$.

2.3 Wireless Communication Model

If user u is served by SBS n , its received SINR is given by [12]

$$\gamma_{ss,nu} = \frac{P_{Ts}w_u}{W_s} \frac{d_{nu}^{-\alpha_s} h_{nu}}{(\theta_s + 1)\sigma^2 w_u} \quad (1)$$

where P_{Ts} is the transmit power level of the SBS, w_u is the bandwidth allocated to user u , d_{nu} is the distance between user u and SBS n , α_s is the path loss exponent of the SBS-tier, h_{nu} is an exponential random variable with unit mean reflecting the effect of Rayleigh fading, θ_s is the ratio of inter-cell interference to noise among SBSs, and σ^2 is the noise power density. As each SBS allocates bandwidth equally to its associated users, the achievable data rate of a generic user u is as follows:

$$r_{ss,nu} = w_{ss,nu} \log_2(1 + \gamma_{ss,nu}) \quad (2)$$

where $w_{ss,nu}$ denotes the bandwidth allocated to each user from SBS n .

Similarly, if user u is served by the MBS as a MMU or MSU, its received SINR is given by

$$\gamma_{m,u} = \frac{P_{Tm}w_u}{W_m} \frac{d_{mu}^{-\alpha_m} h_{mu}}{(\theta_m + 1)\sigma^2 w_u} \quad (3)$$

where P_{Tm} is the transmit power level of the MBS, d_{mu} is the distance between user u and the MBS, α_m is the path loss exponent of the MBS-tier, θ_m is the interference to noise ratio from other MBSs, and h_{mu} reflects Rayleigh fading with the same probability distribution as h_{nu} .

Then, the achievable data rate of user u is given by

$$r_{mm,u} = w_{mm,u} \log_2(1 + \gamma_{m,u}) \quad \text{for MMU} \quad (4)$$

$$r_{ms,nu} = w_{ms,nu} \log_2(1 + \gamma_{m,u}) \quad \text{for MSU} \quad (5)$$

where $w_{mm,u}$ and $w_{ms,nu}$ denote the bandwidth allocated to each user from MBS.

If user u is served by wifi access points, its received SINR is given by

$$\gamma_{w,nu} = \frac{P_w w_u}{W_w} \frac{d_{wu}^{-\alpha_w} h_{wu}}{(\theta_w + 1)\sigma^2 w_u} \quad (6)$$

As each wifi access point allocates bandwidth equally to its associated users, the achievable data rate of a generic user u is as follows:

$$r_{w,nu} = w_{w,nu} \log_2(1 + \gamma_{w,nu}) \quad (7)$$

3 Analysis of Power Supply and Demand

3.1 Green Power Consumption

BSs can work in either active mode or sleep mode, with different power consumption parameters. According to [13], the power consumption of a BS in active mode can be modeled as:

$$P_{BS} = P_C + \frac{w}{W}\beta P_T \quad (8)$$

where P_C denotes static power consumption including the baseband processor, the cooling system and etc., suppose the static power consumption of wifi access points is 0, coefficient β is the inverse of power amplifier efficiency factor, W is the available system bandwidth and w is the bandwidth of utilized subcarriers. P_T is the transmit power level and is treated as a system parameter, while we control the RF power by adjusting the utilized bandwidth w .

3.2 Green Energy Supply Model

In this work, we optimize the amount of offloaded traffic, the ON-OFF state, and the RF power of each SBS at the large time scale, based on the stochastic information of traffic and energy (i.e., user density and energy arrival rate). The optimization is conducted for each period independently [13], and thus we can focus on the optimization for one period.

Two time scales are considered for the problem analysis. In the large time scale, we divide the time into T periods (e.g., $T = 24$ and the length of each time period is 1 h), and assume the average energy harvesting amount and user density remain static in each time period, but may change over different periods. During period t , the arrival of renewable energy packets is modeled as Poisson process with rate $\lambda_{E,n}(t)$ for SBSn, and the distribution of user in small cell n follows PPP with density $\rho_n(t)$.

Discrete energy model is adopted to describe the process of energy harvesting, and a unit of energy is denoted by E [14]. Denote by $\lambda_{E,n}(t)$ the arrival rate of per unit energy at SBSn and time t . The harvested energy is saved in its battery for future use. The battery is considered to have sufficient capacity for realistic operation conditions, and thus we assume no battery overflow happens. For RSBSs without grid power input, they have to be shut down when the battery runs out. Consequently, the corresponding users will be served by the upper-tier MBS for QoS guarantee. Note that handover procedure is conducted when the RSBS is shut down or reactivated, causing additional power consumption. For HSBSs, they can use the on-grid power when there is no green energy, until renewable energy arrives.

The energy supply and consumption process of each SBS can be modeled by a queue, where the queue length denotes the battery amount [15]. Based on the power consumption model of BSs (Eq. (8)), the equivalent service rate of per unit energy for SBSn is given by

$$U_{E,n}(t) = \frac{1}{E}(P_{Cs,n} + \frac{w_{ss,n}(t)}{W_s}\beta_{s,n}P_{Ts,n}) \tag{9}$$

where $P_{Ts,n}$, $P_{Cs,n}$ and $\beta_{s,n}$ are the transmit power, constant power and power amplifier coefficient of SBSn, respectively. U_E is called energy consumption rate in the rest of this paper for simplicity.

For a SBS with EH, the variation of battery can be modeled as a M/D/1 queue with arrival rate λ_E and service rate U_E given by Eq. (9). In what follows, we analyze the stable status of the energy queue. For the M/D/1 queue, the embedded Markov chain method is usually applied to analyze the stable status [16]. When $\lambda_E/U_E \geq 1$, the queue is not stable and the queue length goes to infinity, which means that the harvested energy is always sufficient. When $\lambda_E/U_E < 1$, the stationary probability distribution of L^+ can be derived by Pollaczek-Khinchin formula,

$$q_0 = 1 - \frac{\lambda_E}{U_E} \tag{10}$$

$$q_1 = (1 - \frac{\lambda_E}{U_E})(e^{\frac{\lambda_E}{U_E}} - 1) \tag{11}$$

$$q_{L^+} = (1 - \frac{\lambda_E}{U_E})\{e^{\frac{\lambda E}{U_E}} + \sum_{k=1}^{L^+-1} e^{\frac{\lambda E}{U_E}}(-1)^k \frac{\lambda_E}{U_E} \frac{\lambda_E}{U_E^{-k}} [\frac{(k \frac{\lambda_E}{U_E})^{L^+-k}}{(L^+-k)!} + \frac{(k \frac{\lambda_E}{U_E})^{b-L^+-1}}{(b-L^+-1)!}]\} \quad (L^+ > 2) \tag{12}$$

Thus, the stationary probability distribution of the energy queue length (i.e., the amount of available green energy) is derived.

3.3 Outage Probability Analysis

Service outage happens when the user’s achievable data rate is less than the requirement R_Q , we are interested in analyzing the outage probability constraint for SSUs, MMUs MSUs, and WWUs respectively, based on which the power demand can be obtained.

Service outage constraint of SSUs can be written as

$$w_{ss,nu} \tau_{ss,nu} \geq R_Q \tag{13}$$

where $w_{ss,nu}$ is the bandwidth of SSU, $\tau_{ss,nu}$ denotes the spectrum efficiency of cell edge users given by [13]:

$$\tau_{ss,nu} = \log_2(1 + \frac{P_{Ts,n}}{(\theta_s + 1)} \frac{\alpha_s + 2}{2\sigma^2 W_s} \frac{\eta}{D_n^{\alpha_s}}) \tag{14}$$

the physical meaning of Eq. (13) is that the average data rate of the non-cell-edge users (with spectrum efficiency above $\tau_{ss,nu}$) should be no smaller than R_Q .

Then

$$w_{mm,u} \tau_{mm,u} \geq R_Q \quad (15)$$

$$\tau_{mm,u} = \log_2 \left(1 + \frac{P_{Tm}}{(\theta_m + 1)} \frac{\alpha_m + 2}{2\sigma^2 W_m} \frac{\eta}{D_m^{\alpha_m}} \right) \quad (16)$$

where $w_{mm,u}$ is the bandwidth of MMU, the SBSs are considered to be uniformly distributed in the macro cell.

In addition, the area served by MBS except SBSn is

$$\pi D_{m'}^2 = \pi D_m^2 - \sum_{s \in B} \pi D_s^2 \quad (17)$$

Next, we consider an MSU. The outage probability constraint of the MSUs can be written as

$$w_{ms,u} \tau_{ms,u} \geq R_Q \quad (18)$$

where

$$\tau_{ms,u} = \log_2 \left(1 + \frac{P_{Tm}}{(\theta_m + 1)} \frac{\alpha_m + 2}{2\sigma^2 W_m} \frac{\eta}{D_{ms,u}^{\alpha_m}} \right) \quad (19)$$

$w_{ms,u}$ is the bandwidth of MSU, and $D_{ms,u}$ denotes the distance between the MBS and SBSn.

The outage probability constraint of the WWUs is

$$w_{w,u} \tau_{w,u} \geq R_Q \quad (20)$$

where

$$\tau_{w,u} = \log_2 \left(1 + \frac{P_w}{(\theta_w + 1)} \frac{\alpha_w + 2}{2\sigma^2 W_w} \frac{\eta}{D_w^{\alpha_w}} \right) \quad (21)$$

4 Energy Efficiency Maximization for Single-SBS Case

In this section, we optimize the traffic offloading for the single small cell case, where the HSBS and RSBS are analyzed respectively.

4.1 Outage Probability Analysis

For the single-HSBS case, the network energy efficiency is

$$EE = \frac{TH}{P_{sum}} \quad (22)$$

TH is the network throughput [17], the network throughput is defined as the total amount of data that is successfully received by the users per unit time and area, and is measured in bits/sec/m², P_{sum} is the total on-grid power consumption.

$$TH = I_H \left(\frac{r_{mm}}{\pi D_{m'}^2} + \frac{r_{ss,n}}{\pi D_{s,n}^2} + \frac{r_{ms,n}^a}{\pi D_{ms,n}^2} + \frac{r_{w,n}^a}{\pi D_{w,n}^2} \right) + (1 - I_H) \left(\frac{r_{mm}}{\pi D_{m'}^2} + \frac{r_{ms,n}^o}{\pi D_{ms,n}^2} + \frac{r_{w,n}^o}{\pi D_{w,n}^2} \right) \quad (23)$$

$$r_{mm} = \rho_m \pi D_{m'}^2 r_{mm,u} \quad (24)$$

$$r_{ss} = \psi_1 \rho_s \pi D_s^2 r_{ss,u} \quad (25)$$

$$r_{ms} = \psi_2 \rho_s \pi D_s^2 r_{ms,u} \quad (26)$$

$$r_w = (1 - \psi_1 - \psi_2) \rho_s \pi D_s^2 r_{ms,u} \quad (27)$$

where I_H is a 0–1 indicator denoting whether SBSn is active or not, r_{mm} is the total data rate of MMUs, r_{ss} is the total data rate of SSUs, r_{ms}^a is the total data rate of MSUs when the SBS is active, r_{ms}^o is the total data rate of MSUs when the SBS is not active. $r_{w,n}^a$ is the total data rate of WWUs when the SBS is active, $r_{w,n}^o$ is the total data rate of MMUs when the SBS is not active. ψ_1 is the traffic offloading ratio of the SBS. ψ_2 is the traffic offloading ratio of the MBS.

$$P_{sum} = P_{MBS} + P_{HSBS} + P_{wifi} \quad (28)$$

where P_{MBS} , P_{HSBS} and P_{wifi} denote the on-grid power consumptions of MBS, HSBS and wifi access points respectively. P_{MBS} , P_{HSBS} and P_{wifi} can be derived based on Eq. (8). While w_{mm} is constrained by Eq. (12), w_{ms}^a and w_{ms}^o are the corresponding bandwidth needed by the MSUs. Then we have

$$P_{MBS} = P_{Cm} + \frac{\beta_m P_{Tm}}{W_m} (w_{mm} + I_H w_{ms}^a + (1 - I_H) w_{ms}^o) \quad (29)$$

In addition, as the HSBS consumes on-grid power only when the battery is empty, we have

$$P_{HSBS} = \begin{cases} I_H q_0 (P_{Cs} + \frac{\beta_s P_{Ts}}{W_s} w_{ss}) & , \lambda_E < U_E \\ 0 & , \lambda_E \geq U_E \end{cases} \quad (30)$$

where q_0 is the probability of empty energy queue, obtained from Eq. (10).

Then

$$P_{wifi} = \frac{\beta_w P_{Tw}}{W_w} W_{ww} \tag{31}$$

Then, the network energy efficiency maximization problem of the single-HSBS case can be formulated as follows:

P1:

$$\max_{I_H, U_E} EE \tag{32}$$

s.t.

$$r_{mn,u} \geq R_Q, r_{ss,u} \geq R_Q, r_{ms,u} \geq R_Q, r_{w,u} \geq R_Q \tag{33}$$

$$0 \leq w_{mm} + I_H w_{ms}^a + (1 - I_H) w_{ms}^o \leq W_m \tag{34}$$

$$0 \leq w_{ss} \leq W_s \tag{35}$$

$$0 \leq w_{ww} \leq W_w \tag{36}$$

where Eq. (33) guarantees the QoS, Eqs. (34), (35) and (36) are due to the bandwidth limitations of MBS, HSBS, and wifi access points, respectively. U_E can be derived based on the power consumption model of HSBS Eq. (9).

In practice, the HSBS usually provides higher energy efficiency compared with the MBS, due to shorter transmission distance and lower path loss. As a result, more subcarriers should be utilized to offload more users if the HSBS is active. Besides, $w_{mm} + w_{ms}^o > W_m$ happens when the MBS is overloaded, in which case the HSBS should be activated to relieve the burden of the MBS. But the SBS can only service the amount while $w_{ss} < W_s$.

4.2 Single-RSBS Case

Unlike HSBS, RSBS do not consume on-grid power. Whereas, the SSUs have to be served by the MBS when the battery is empty, which causes handover and on-grid power consumption. The average power consumption is given by

$$P_{sum} = P_{MBS} + P_{HO} + P_{wifi} \tag{37}$$

where P_{MBS} is the power consumption of the MBS, and P_{HO} reflects the additional power consumed by SSU handover.

Denote by $I_R \in \{0, 1\}$ the ON-OFF state of the RSBS. If RSBSn is active, handover happens in the following cases: (1) RSBSn is shut down when the battery runs out; (2) RSBSn is reactivated when new energy arrives. According to the energy queueing model, the first case corresponds to the event when L^+ transits from 1 to 0, with frequency of

$q_1 A_{21} U_E$ after the energy queue becomes stable. Due to the duality between the two cases, the additional handover power consumption is given by

$$P_{HO} = I_R \cdot 2q_1 A_{21} U_E C_{HO} = \begin{cases} 2I_R(1 - \frac{\lambda_E}{U_E})(1 - e^{-\frac{\lambda_E}{U_E}})U_E C_{HO} & , \lambda_E < U_E \\ 0 & , \lambda_E \geq U_E \end{cases} \quad (38)$$

Note that SBSn may be shut down due to energy shortage even when its state is set as on, in which the MBS has to utilize more bandwidth to serve SSUn with additional bandwidth. Based on Eq. (8), the average on-grid power consumption of the MBS is given as follows:

$$P_{MBS} = P_{Cm} + \frac{\beta_m P_{Tm}}{W_m}(w_{mm} + I_R((1 - q_0)w_{ms}^a + q_0 w_{ms}^o) + (1 - I_R)w_{ms}^o) \quad (39)$$

where w_{mm} is constrained by Eq. (15), w_{ms}^a and w_{ms}^o denote the bandwidth needed by the MBS to serve MSUs when the RSBS is active and shut down, respectively.

The average on-grid power consumption of the wifi access point is given as follows:

$$P_{wifi} = \frac{\beta_w P_{Tw}}{W_w} w_{ww} \quad (40)$$

Thus, the energy efficiency maximization problem can be formulated as follows.
P2:

$$\max_{I_H, U_E} EE \quad (41)$$

s.t.

$$r_{mm,u} \geq R_Q, r_{ss,u} \geq R_Q, r_{ms,u} \geq R_Q, r_{w,u} \geq R_Q \quad (42)$$

$$0 \leq w_{mm} + w_{ms}^o \leq W_m \quad (43)$$

$$0 \leq w_{ss} \leq W_s \quad (44)$$

$$0 \leq w_{ww} \leq W_w \quad (45)$$

where the objective function is the network energy efficiency, Eq. (42) guarantees the QoS, Eqs. (43), (44) and (45) account for the bandwidth limitation of MBS, RSBS and wifi access points, respectively.

5 Energy Efficiency Maximization for Single-SBS Case

In this section, we evaluate the energy efficiency of the optimal solution for the single-SBS case. The SBSs are micro BSs, and the main simulation parameters can be found in Tables 1 and 2. Solar power harvesting devices are equipped at RSBS and HSBS.

Table 1. Power model parameters

	Transmit power $P_T(w)$	Constant power $P_C(w)$	Coefficient β
Macro	20	130	4.4
Micro	2	56	2.6
Wifi	0.025	0	1

Table 2. Simulation parameters

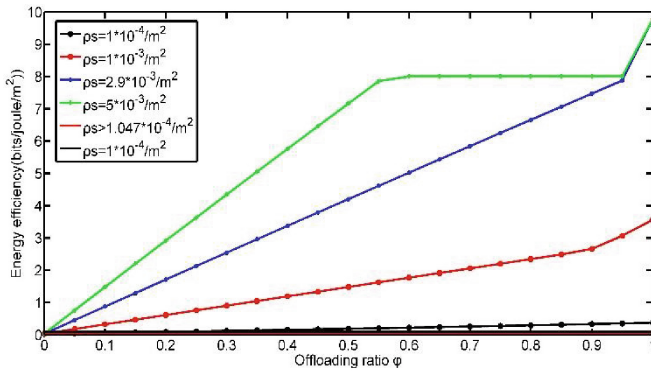
Parameter	Value	Parameter	Value
D_m	1000 m	D_s	100 m
D_{ms}	900 m	D_w	10
α_m	3.5	α_s	4
α_w	5	R_Q	300 kbps
σ^2	-104 dBm/MHZ	η	0.05
θ_s	500	θ_m	1000
θ_w	300	W_m	20 MHz
W_s	5 MHz	W_w	1 MHz

5.1 Network Energy Efficiency of Single-SBS with Different User Density

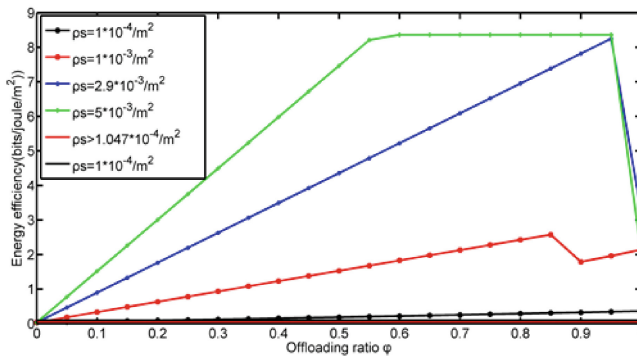
Figure 2 shows the network energy efficiency of no offloading and offloading different users with different user density under given system parameters.

Simulation shows with the amount of offloading traffic to wifi access points increasing, the energy efficiency is decreasing, regardless of the energy arrival amount. Because SBSs are powered by conventional energy and green energy, wifi access points are powered only by conventional energy and the ratio of output and power consumption decreases quickly. So the following contents are not including wifi case.

The red line and black line with no point show the no offloading case. It can be seen that energy efficiency generally increases with the increase of offloading ratio and with the increase of users, and offloading's is larger than no offloading. Besides, in the actual situation, $w_{ss} > W_s$ happens when more users are offloaded to the SBS, in which case not all users can be offloaded to the SBS for satisfying the QoS of every user, so we can choose some users whose energy efficiency is maximized to offload to the SBS. For RSBS, because of difference of user density, the energy efficiency's variation trend is different. Figure 2(b) shows when the user density is large enough, energy efficiency is maximized with the offloading ratio is not until 1.



(a)HSBS

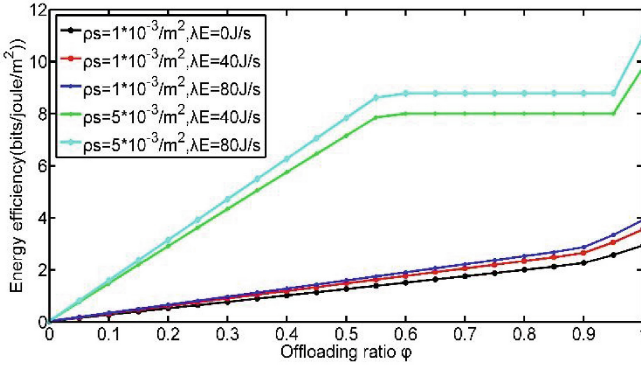


(b)RSBS

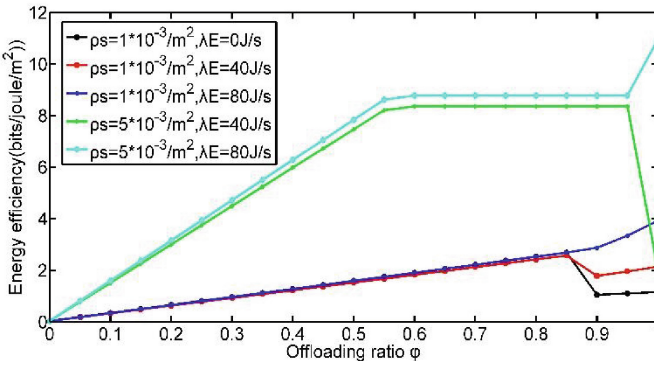
Fig. 2. The energy efficiency with different offloading ratio and different user density of single SBS. (Color figure online)

5.2 Network Energy Efficiency of Single-SBS with Different Energy Arrival Rate

Figure 3 shows the network energy efficiency of no offloading and offloading different users with different user density and different energy arrival rate under the same system parameters. Figure 3(a) shows the energy efficiency for the HSBS, which increases with the increase of energy arrival rate in the small cell and with the increase of user density. Figure 3(b) shows the energy efficiency for the RSBS. It can be seen the energy efficiency's variation trend is different with the increase of energy arrival rate, when energy arrival rate is small enough, the energy efficiency is maximized with the offloading ratio not until 1.



(a)HSBS



(b)RSBS

Fig. 3. The energy efficiency with different offloading ratio and different energy arrival rate of single SBS.

6 Conclusions and Future Work

In this paper, we have investigated the network energy efficiency through offloading traffic for green heterogeneous networks. The analytical results reflect maximized energy efficiency with different user density through traffic offloading, we also analyze offloading case of different energy arrival rate, so we can choose how much traffic should be offloaded to the SBS and wifi access points with different energy arrival rate. But we do not consider the case that all SBSs coexist, which SBS should be activated and how much traffic should be loaded, next we will achieve this with new limits.

Acknowledgment. This work was supported by the National Natural Science Foundation of China. (No. 61372117), and the State Major Science and Technology Special Projects of China under Grant 2016ZX03001017-004.

References

1. Hasan, Z., Boostanimehr, H., Bhargava, V.K.: Green cellular networks: a survey, some research issues and challenges. *IEEE Commun. Surv. Tutor.* **13**(4), 524–540 (2011)
2. Correia, L.M., Zeller, D., Blume, O., et al.: Challenges and enabling technologies for energy aware mobile radio networks. *IEEE Commun. Mag.* **48**(11), 66–72 (2010)
3. Damnjanovic, A., Montojo, J., Wei, Y., et al.: A survey on 3GPP heterogeneous networks. *IEEE Wirel. Commun.* **18**(3), 10–21 (2011)
4. Zhang, N., Cheng, N., Gamage, A., Zhang, K., Mark, J.W., Shen, X.: Cloud assisted HetNets toward 5G wireless networks. *IEEE Commun. Mag.* **53**(6), 59–65 (2015)
5. Ismail, M., Zhuang, W., Serpedin, E., Qaraqe, K.: A survey on green mobile networking: From the perspectives of network operators and mobile users. *IEEE Commun. Surv. Tutor.* **17**(3), 1535–1556 (2014)
6. Andrews, J., et al.: What will 5G be? *IEEE J. Sel. Areas Commun.* **32**(6), 1065–1082 (2013)
7. Zhuo, X., Gao, W., Cao, G., et al.: Win-Coupon: an incentive framework for 3G traffic offloading. In: *IEEE International Conference on Network Protocols*, pp. 206–215. IEEE Computer Society (2011)
8. Zhuo, X., Gao, W., Cao, G., et al.: An incentive framework for cellular traffic offloading. *IEEE Trans. Mob. Comput.* **13**(3), 541–555 (2014)
9. Usman, M., Vastberg, A., Edler, T.: Energy efficient high capacity HETNET by offloading high QoS users through femto. In: *IEEE International Conference on Networks*, pp. 19–24. IEEE Computer Society (2011)
10. Arshad, M.W., Vastberg, A., Edler, T.: Energy efficiency gains through traffic offloading and traffic expansion in joint macro pico deployment. In: *2012 IEEE Communications and Networking Conference (WCNC)*, pp. 2203–2208. IEEE (2012)
11. Dhillon, H., Li, Y., Nuggehalli, P., Pi, Z., Andrews, J.: Fundamentals of heterogeneous cellular networks with energy harvesting. *IEEE Trans. Wirel. Commun.* **13**(5), 2782–2797 (2014)
12. Zhang, S., Zhang, N., Zhou, S., et al.: Energy-aware traffic offloading for green heterogeneous networks. *IEEE J. Sel. Areas Commun.* **34**(5), 1116–1129 (2016)
13. Zhang, X., Zheng, Z., Shen, Q., Liu, J., Shen, X., Xie, L.: Optimizing network sustainability and efficiency in green cellular networks. *IEEE Trans. Wirel. Commun.* **13**(2), 1129–1139 (2014)
14. Yang, J., Ulukus, S.: Optimal packet scheduling in an energy harvesting communication systems. *IEEE Trans. Wirel. Commun.* **60**(1), 220–230 (2012)
15. Nakagawa, K.: On the series expansion for the stationary probabilities of an M/D/1 queue. *J. Oper. Res. Soc. Jpn* **48**(2), 111–122 (2005)
16. Yu, P.S., Lee, J., Quek, T.Q.S., et al.: Traffic offloading in heterogeneous networks with energy harvesting personal cells - network throughput and energy efficiency. *IEEE Trans. Wirel. Commun.* **15**(2), 1146–1161 (2016)
17. Wei, Y., Ren, C., Song, M., Yu, R.: The offloading model for green base stations in hybrid energy networks with multiple objectives. *Int. J. Commun. Syst* **29**(11), 1805–1816 (2016)

A Game-Theoretic Approach for Joint Optimization of Sensing and Access in Cognitive Cellular Heterogeneous Networks

Changqing Pan¹, Ya'nian Xiao², Yinglei Teng^{2(✉)}, Weiqi Sun²,
and Xiaoqi Qin²

¹ China Railway Test and Certification Center (CRCC),
No.2 Daliushu Road, Xizhimen-wai, Beijing 100081, China

² Beijing University of Posts and Telecommunications,
No.10 Xitucheng Road, Haidian District, Beijing 100876, China
lilytengt@gmail.com

Abstract. Cellular heterogeneous networks comprising small-cells coexisting with macro-cells have emerged as a promising solution to improve in-building coverage and capacity of wireless networks. By assuming the scenario of cognitive radio enabled cellular heterogeneous network (CCHN), where the small base stations (SBSs) carry out spectrum sensing, severe cross-tier interference are portable, however, the joint design of spectrum sensing and access poses new technology challenges. Furthermore, the joint optimization encompasses affluent heterogeneous nodes and connections, which renders the centralized paradigm messy for enormous signaling and great computation. In this paper, we propose a decentralized approach by formulating the non-cooperative power allocation game (NPAG) wherein each SBS competes for the maximization his own opportunistic throughput by joint choice of the sensing factors and the resource allocation strategy, involving interference and energy constraints. Further, the iterative water-filling (IWF) algorithm is utilized to deal with the non-convexity of the game. Simulation results show that the proposed game theoretical formulations yield a considerable performance improvement for the joint optimization problem.

Keywords: CCHN · Cognitive radio · Joint optimization · Game theory

1 Introduction

Due to the ability to bring about massive spatial reuse of frequency, the low-power, short-range mini-base stations (BSs), referred to small-cells (femto-cell, pico-cell) are increasingly important for improving network capacity. These small-cells coexist with conventional macro-cell networks, giving rise to cellular heterogeneous networks (CHNs). The structure of CHN causes interference problem to each layer. The inter-tier (inner-tier) interference (ITI) from the Macro BSs (small-cell BSs) to the small-cell users can be critical challenge to the CHN. Severely, the lower spectral efficiency (SE) and higher interference often results in great loss in the capacity and coverage. Thereby, it is necessary to improve SE and reduce interference.

Apparently, small-cells provide the flexibility of network topology while cognitive radio (CR) enables the agile usage of spectrum resource and helps small-cells avoid major interference sources. The CHN will be favored if we combine small-cell and cognitive radio technologies, which is the CR enabled Cellular Heterogeneous Networks (CCHNs). However, challenges arise for how to implement CR in CCHNs. (1) The duration of the spectrum-sensing in one slot becomes the tough dilemma. The longer sensing time helps higher sensing accuracy (SA), however, it also causes less time for the data-transmission period. (2) The sensing threshold affects SA and SE inversely, i.e., the higher sensing threshold means more accurate sensing results, but lower spectral efficiency, since access opportunities are likely to be missed. Hence, the design of the sensing factors should consider the tradeoff between SA and SE, so that the access availability should be optimized. Resource allocation strategy for reducing interference is another important issue that must be addressed to increase SE. Summarily, the mutual suppression and influence between sensing and access have motivated us to investigate the joint optimization of spectrum-sensing configuration and resource allocation in CCHNs.

The idea of considering sensing and resource allocation jointly has been investigated in conventional cognitive radio network (CRN). Several previous works [1, 2] have already considered the tradeoff between sensing capabilities and throughput of secondary users. Some researches solve the joint optimization problem using the convex optimization theory, such like [1–3], and some formulate the joint problem using the game theory, such like [4, 5]. There are still some other papers adopting smart algorithm, to name some, greedy algorithm [6], evolution algorithm [7] to solve this kind of problem.

Also, there are plenty of literatures put insights on the design of spectrum sensing method or access strategies in CCHNs. The authors of [8] present one cycle stationary-based spectrum sensing method, the design of which is based on the study of detection probability (DP), ignoring the jointing research of resource allocation. In [9], the authors provide spectrum sharing algorithm according to existing sensing results, basing on the model of ALOHA, DSMA. However, the issue of joining optimization in CCHNs has barely been addressed due to affluent heterogeneous nodes and connections, the messy interference environment, etc.

Based on the aforementioned related work, in this paper, we propose a decentralized approach by formulating the non-cooperative power allocation game (NPAG) wherein each SBS competes against the others by choosing jointly the sensing factors and the resource allocation strategy. Then, a pricing mechanism with constraints of sensing accuracy and power consumption is introduced to reduce the interference caused by the sensing errors. To deal with the non-convex issue, we compute the optimal allocation strategy under given sensing time using iterative water-filling (IWF) algorithm, then, select the optimal solution from multi groups of sensing factors. Finally, the performance of our proposed algorithm is analyzed by making comparison with average power allocation (APA) algorithm in system level simulation.

2 System Model

2.1 Network Scenario

We consider a CCHN consisting one MBS and multiple cognitive FBSs, where femto-cells coexist with macro-cell in overlay approach. Each FBS operates in the closed access mode where only authorized UEs are allowed to access to it. The sets of FBSs and MUEs are denoted by $\mathcal{S}^F = \{i, i = 1, 2, \dots, N_F\}$ and $\mathcal{S}^M = \{j, j = 1, 2, \dots, N_M\}$. The femto-cells share same spectrum while they adopt the OFDMA as the spectrum allocation strategy in each cell. Specifically, the total spectrum band is divided into N_C orthogonal sub-channels, marked as $\mathcal{S}^C = \{n, n = 1, 2, \dots, N_C\}$. We focus on block transmissions over channels which are assumed to be perfectly synchronized. With a fixed length T , the transmission frame of FBS i is divided in two slots: sensing slot τ_i and data slot as shown in Fig. 1. During sensing interval, FBSs sense the environment, looking for the spectrum holes, whereas during the data slot they possibly transmit over the licensed spectrum detected as available. The sensing and transmission phases are described in 2.1 and 2.2 respectively.

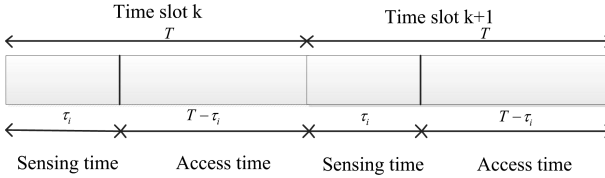


Fig. 1. Frame structure of the cognitive FBSs

The channel model follows Rayleigh fading and the large-scale path loss. The additive complex white Gaussian noise is also assumed (with mean being zero and variance being σ^2). The channel fading between FBS i and its authorized UEs on the n^{th} subcarrier is normally indicated as $|g_{i,n}|^2$. Meanwhile, $|g_{M,j,n}|^2$ represents the channel fading between MBS and MUE j on the n^{th} subcarrier, and $|g_{i,j,n}|^2$ stands for that between the FBS i and the MUE j . Besides, the channel gain between MBS and the UEs in FBS i is denoted as $|g_{M,i,n}|^2$. In CCHNs, the interference brought by the mistaken sensing between the BSs in the different tier is not considered when restricting sensing accuracy. Therefore, we just analyze the inner-tier which is depicted in Fig. 2.

The Spectrum Sensing Problem

Assume FBSs sense the licensed channels using energy detection in non-cooperative way. In sensing phase, we define the event of MBS’s occupation as follows:

H_1 : The MBS takes use of the channel.

H_0 : The MBS is idle on the channel.

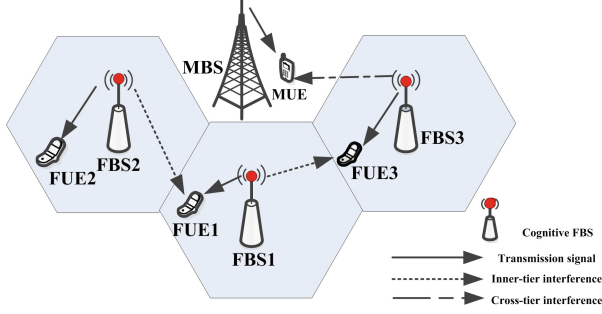


Fig. 2. The CCHN with inner-tier/cross-tier interference

The performance of the energy detector scheme is measured in terms of the DP $P_{i,n}^d(\tau_i, \varepsilon_{i,n})$ and false-alarming probability (FP) $P_{i,n}^f(\tau_i, \varepsilon_{i,n})$. DP and FP are the probabilities detecting that the channel is busy under the case H_1 and H_0 . Here, employing the results of [1], we write $P_{i,n}^d(\tau_i, \varepsilon_{i,n})$ and $P_{i,n}^f(\tau_i, \varepsilon_{i,n})$ as in (1)-(2) respectively, where τ_i denotes the sensing time of FBS i , and $\varepsilon_{i,n}$ is the decision threshold of FBS i on sub-channel n , and μ is the sampling rate. Besides, $G_n = (|g_{1,n}|^2, |g_{2,n}|^2, \dots, |g_{N_F,n}|^2)^T$ (superscript T means transpose operation). I means an identity matrix, and $Diag(G_n)$ is a diagonal matrix formed by elements in G_n . $Q(\cdot)$ is the Q-function and $\|\cdot\|_1$ of a matrix denotes its entry wise 1-norm, which is the summation of absolute values of all the elements.

$$P_{i,n}^d(\tau_i, \varepsilon_{i,n}) = Q\left(\frac{(\varepsilon_{i,n} - (\sigma^2 N_F + \|G_n\|_1))\sqrt{\mu\tau_i}}{\sigma\sqrt{2}\|\sigma^2 I + 2Diag(G_n)\|_1 N_C}\right) \tag{1}$$

$$P_{i,n}^f(\tau_i, \varepsilon_{i,n}) = Q\left(\frac{(\varepsilon_{i,n} - \sigma^2 N_F)\sqrt{\mu\tau_i}}{\sigma^2\sqrt{2}N_F N_C}\right) \tag{2}$$

Deriving from (1), $P_{i,n}^f(\tau_i, \varepsilon_{i,n})$ can be further expressed with respect to $P_{i,n}^d(\tau_i, \varepsilon_{i,n})$ as (3), where $\Sigma_n = \sigma^2 I + 2Diag(G_n)$.

$$P_{i,n}^f(\tau_i, P_{i,n}^d) = Q\left(\frac{Q^{-1}\left(P_{i,n}^d(\tau_i, \varepsilon_{i,n})\right)\sigma\sqrt{2}\|\Sigma_n\|_1 N_C + \|G_n\|_1\sqrt{\mu\tau_i}}{\sigma^2\sqrt{2}N_F N_C}\right) \tag{3}$$

In order to secure the performance of MUEs, it is rational to set system thresholds of the minimal DP and maximal FP. Note that if and only if the received power from MBS on this channel is less than the spectrum sensing threshold $\varepsilon_{i,n}$, can the FBS use the channel n . Thereby, $\varepsilon_{i,n}$ should be carefully gauged to improve the access opportunity to make sure that the MUEs do not get severe interference.

$$P_{i,n}^d(\tau_i, \varepsilon_{i,n}) \geq P_{th}^d, n \in \mathcal{S}^C, i \in \mathcal{S}^F \quad (4)$$

$$P_{i,n}^f(\tau_i, \varepsilon_{i,n}) \leq P_{th}^f, n \in \mathcal{S}^C, i \in \mathcal{S}^F \quad (5)$$

The Transmission Phase

Cognitive FBSs coexist in the network operating in a non-cooperative manner, and no centralized authority is assumed to handle the network access for the FBSs. The transmission strategy of each FBS i is then the power allocation vector $\mathbf{p}_i = \{p_{i,n}\}_{n=1}^{N_C}$ and the channel allocation vector $\boldsymbol{\beta}_i = \{\beta_{i,n}\}_{n=1}^{N_C}$ over the N_C subcarriers ($p_{i,n}$ is the power allocated over channel n , $\beta_{i,n}$ is the sub-channel allocation indicator that it equals 1 when the FBS i is allocated with sub-channel n , and zero not).

Successful detection: The goal of each FBS is to optimize its opportunistic spectral utilization of the licensed spectrum. According to this paradigm, each sub-channel n is available for the transmission of FBS i if no MBS's signal is detected over that frequency band, which happens with probability $1 - P_{i,n}^f(\tau_i, \varepsilon_{i,n})$. This motivates the use of the aggregate opportunistic throughput as a measure of the spectrum efficiency of each FBS i . Given the power allocation profile $\mathbf{p} \triangleq (\mathbf{p}_i)_{i=1}^{N_F}$ of the FBSs, the detection thresholds $\boldsymbol{\varepsilon}_i \triangleq (\varepsilon_{i,n})_{n=1}^{N_C}$, and sensing time τ_i , the aggregate opportunistic throughput of FBS i is defined as

$$R_i(\tau_i, \boldsymbol{\varepsilon}_i, \mathbf{p}_i, \boldsymbol{\beta}_i) = (1 - \frac{\tau_i}{T}) \sum_{n=1}^{N_C} \Pr(H_n^0) \left(1 - P_{i,n}^f(\tau_i, \varepsilon_{i,n})\right) r_{i,n}(p_{i,n}, \beta_{i,n}) \quad (6)$$

where $1 - \tau_i/T$ ($\tau_i < T$) is the portion of the frame duration available for opportunistic transmissions, $P_{i,n}^f(\tau_i, \varepsilon_{i,n})$ is the FP defined in (2), and $r_{i,n}(p_{i,n}, \beta_{i,n})$ is the maximum rate achievable of FBS i over channel n when no MBS's signal is detected and the power allocation of the FBSs is given. The maximum achievable rate $r_{i,n}(p_{i,n}, \beta_{i,n})$ is expressed as

$$r_{i,n}(p_{i,n}, \beta_{i,n}) = \beta_{i,n} \log\left(1 + \frac{p_{i,n} |g_{i,n}|^2}{\sigma^2 + \sum_{j \neq i} p_{j,n} |g_{j,i,n}|^2}\right) \quad (7)$$

where σ^2 is the variance of the background noise over channel n at the receiver UE associated to FBS i (assumed to be Gaussian zero-mean distributed).

As mentioned above, $P_{i,n}^f$ can be written as (3). According to [1], when $P_{i,n}^d(\tau_i, \varepsilon_{i,n}) = P_{th}^d$, (6) can achieve maximal value. Thereby, (7) can be rewritten as the following one:

$$R_i(\tau_i, \mathbf{p}_i, \mathbf{B}_i) = \left(1 - \frac{\tau_i}{T}\right) \sum_{n=1}^{N_C} \Pr(H_n^0) \left(1 - P_{i,n}^f(\tau_i)\right) r_{i,n} \quad (8)$$

Here,

$$P_{i,n}^f(\tau_i) = Q\left(\frac{Q^{-1}(P_{th}^d) \sigma \sqrt{2\|\Sigma_n\|_1 N_C} + \|G_n\|_1 \sqrt{\mu \tau_i}}{\sigma^2 \sqrt{2N_F N_C}}\right) \quad (9)$$

Energy constraints: To control the total power cost by FBSs, we propose to impose individual energy constraints. Individual constraints are provided at the level of each FBS i to limit the energy constraint. Individual energy constraints:

$$\tau_i \sum_{n=1}^{N_C} P_{i,n}^s + (T - \tau_i) \sum_{n=1}^{N_C} P_{i,n} \leq E_i^{\max} \quad (10)$$

where $P_{i,n}^s$ is the sensing power of FBS i on channel n , and E_i^{\max} is the maximum energy limitation allowed to be generated by FBS i .

Interference constraints: To control the interference radiated by the FBSs, we propose to impose interference constraints in the form of individual constraints, which is imposed at the level of each FBS i to limit the average interference generated at the MBS. Individual interference constraints:

$$\sum_{n=1}^{N_C} P_{i,n}^{\text{miss}} |g_{M,i,n}|^2 P_{i,n} \leq I_i^{\max} \quad (11)$$

where I_i^{\max} is the maximum average interference allowed to be generated by the FBS i , and $P_{i,n}^{\text{miss}} = 1 - P_{i,n}^d$ represents the probability of FBS i failing to detect the presence of the MBS on the sub-channel n and thus generating interference against the MBS.

3 Joint Spectrum Sensing and Access Optimization Strategy via Game Theory

In Sect. 2, we have defined the opportunistic throughput R_i and the individual constraints (10)-(11). In the process, we assume that FBSs aim to maximize their own throughput non-cooperatively, with the constraints holding. Therefore, a non-cooperative game theory can be introduced to build an optimization model if we regard each FBS as a game player and R_i as the player's utility. Hence, in this section, we focus on the formulation of the jointing optimization of the spectrum sensing and resource allocation of the FBSs within the framework of game theory. We propose next

equilibrium problem: games with individual constraints, and then provide a unified analysis of the game.

As mentioned above, each FBS is modeled as a game player who aims to maximize its own opportunistic throughput $R_i(\tau_i, \mathbf{p}_i, \boldsymbol{\beta}_i)$ by choosing jointly a proper power allocation strategy $\mathbf{p}_i = \{p_{i,n}\}_{n=1}^{N_c}$, carrier allocation strategy $\boldsymbol{\beta}_i = \{\beta_{i,n}\}_{n=1}^{N_c}$, and sensing time τ_i , subject to individual constraints (10).

In order to enforce the constraints (10)-(11) while keeping the optimization as decentralized as possible, we propose the use of a pricing mechanism through a penalty in the utility function of each player. To be simple, we set the price of the i^{th} player is denoted by γ_i . Assume price γ_i in (12) is given. Therefore, we have the formulation (12).

Player i 's optimization problem is to determine, for the given γ , a tuple $(\tau_i, \mathbf{p}_i, \boldsymbol{\beta}_i)$,

$$\underset{\tau_i, \mathbf{p}_i, \boldsymbol{\beta}_i}{\text{maximize}} \quad U_i(\tau_i, \mathbf{p}_i, \boldsymbol{\beta}_i) = R_i(\tau_i, \mathbf{p}_i, \boldsymbol{\beta}_i) - \gamma_i \cdot \left(\sum_{n=1}^{N_c} (\tau_i p_{i,n}^s + (T - \tau_i) p_{i,n}) \right) \quad (12)$$

s.t.

$$\tau_i \sum_{n=1}^{N_c} p_{i,n}^s + (T - \tau_i) \sum_{n=1}^{N_c} p_{i,n} \leq E_i^{\max} \quad (13)$$

$$\tau_{\min} \leq \tau_i \leq T, \quad \forall n \in \mathcal{S}^C \quad (14)$$

$$\sum_{n=1}^{N_c} P_{i,n}^{\text{miss}} |g_{M,i,n}|^2 p_{i,n} \leq I_i^{\max} \quad (15)$$

Here, (14) is derived from (2), (3), (5). $\tau_{\min} = \max(\tau_{\min}^1, \tau_{\min}^2, \dots, \tau_{\min}^{N_c})$, $\tau_{\min}^n = \frac{(Q^{-1}(P_{th}^f) \sigma^2 \sqrt{2N_f N_c} - Q^{-1}(P_{th}^d) \sigma \sqrt{2\|\Sigma_n\|_1 N_c})^2}{\mu \|G_n\|_1^2}$.

For notational simplicity, we will use $\boldsymbol{\phi}_i \triangleq (\tau_i, \mathbf{p}_i, \boldsymbol{\beta}_i)$ to denote the strategy tuple of player i .

4 Solution Analysis

This section is devoted to the solution analysis of the game (12). We start our analysis by introducing the definition of non-cooperative power allocation game (NPAG).

According to (12), we can determine the optimal sub-channel matrix $\boldsymbol{\beta}$ once the network vector \mathbf{p} is determined. In addition, to simplify the jointing problem, we compute the optimal power allocation vector with different sensing time, and then choose the optimal tuple $(\tau_i, \mathbf{p}_i, \boldsymbol{\beta}_i)$ as the optimal solution. Therefore, the jointing problem of sensing time and resource allocation turns into a power allocation problem, and the game becomes a NPAG. $\mathcal{G} = \{\mathcal{S}^F, \{\mathbf{p}_i\}_{i \in \mathcal{S}^F}, \{U_i\}_{i \in \mathcal{S}^F}\}$ as follows:

$$\text{NPAG : } \max_{\mathbf{p}_i} U_i(\tau_i, \mathbf{p}, \boldsymbol{\beta}_i) = \max \left(R_i(\tau_i, \mathbf{p}, \boldsymbol{\beta}_i) - \gamma_i \left(\sum_{n=1}^{N_c} (\tau_i p_{i,n}^s + (T - \tau_i) p_{i,n}) \right) \right) \quad (16)$$

st.

$$\mathbf{p}_i \in \mathbb{P}_i \quad (17)$$

Here,

$$\mathbb{P}_i = \left\{ \mathbf{p}_i \mid \tau_i \sum_{n=1}^{N_c} p_{i,n}^s + (T - \tau_i) \sum_{n=1}^{N_c} p_{i,n} \leq E_i^{\max}, \sum_{n=1}^{N_c} p_{i,n}^{\text{miss}} |g_{M,i,n}|^2 p_{i,n} \leq I_i^{\max} \right\} \quad (18)$$

We call a network power vector \mathbf{p} a Nash equilibrium if for every $i \in \mathcal{S}^F$, $U_i(\tau_i, \mathbf{p}_i, \mathbf{p}_{-i}, \boldsymbol{\beta}_i) \geq U_i(\tau_i, \mathbf{q}_i, \mathbf{p}_{-i}, \boldsymbol{\beta}_i)$ for all $\mathbf{p}_i \in \mathbb{P}_i$. In other words, at a Nash equilibrium, given the transmission power vectors of other FBSs, no FBS can improve its utility level by changing its own transmission power vector unilaterally.

For the given sensing time τ_i , the utility $U_i(\tau_i, \mathbf{p}, \boldsymbol{\beta}_i)$ is a convex function of \mathbf{p}_i and hence the problem is a convex problem. Therefore we can apply the Karush - Kuhn-Tucker (KKT) condition to get the solution.

The Lagrangian function of FBS i is given as follows:

$$L_i(\mathbf{p}) = \lambda_i \left(E_i^{\max} - \left(\tau_i \sum_{n=1}^{N_c} p_{i,n}^s + (T - \tau_i) \sum_{n=1}^{N_c} p_{i,n} \right) \right) + U_i(\mathbf{p}) + \mu_i \left(I_i^{\max} - \sum_{n=1}^{N_c} p_{i,n}^{\text{miss}} |g_{M,i,n}|^2 p_{i,n} \right) \quad (19)$$

Then, in the NPAG, the best response of FBS i is given by

$$p_{i,n} = \left[\frac{(1 - \frac{\tau_i}{T}) \Pr(H_n^0) (1 - P_{i,n}^f(\tau_i)) \beta_{i,n}}{\left(\gamma_i \cdot (T - \tau_i) - \lambda_i (T - \tau_i) - \mu_i p_{i,n}^{\text{miss}} |g_{M,i,n}|^2 \right) \ln 2} - \frac{\sigma^2 + \sum_{j \neq i} p_{j,n} |g_{j,i,n}|^2}{|g_{i,n}|^2} \right]^+ \quad (20)$$

$$\lambda_i \left(E_i^{\max} - \left(\tau_i \sum_{n=1}^{N_c} p_{i,n}^s + (T - \tau_i) \sum_{n=1}^{N_c} p_{i,n} \right) \right) = 0, \lambda_i \geq 0,$$

$$\mu_i \left(I_i^{\max} - \sum_{n=1}^{N_c} p_{i,n}^{\text{miss}} |g_{M,i,n}|^2 p_{i,n} \right) = 0, \mu_i \geq 0.$$

where λ_i and μ_i are the Lagrangian multipliers for the maximum energy constraint (10) and interference constraint (11). $[x]^+ = x$ if $x \geq 0$ and 0 otherwise.

Unfortunately, it is hard to find the max Lagrangian multiplier to solve the $p_{i,n}$ due to two multipliers. To get around the difficulty, we consider an iterative water-filling algorithm (IWF) mentioned in [10]. The optimal response of game can be found by computing the multipliers iteratively until they reach a certain degree of accuracy.

The details of IWF algorithm is listed in **Algorithm 1**.

Algorithm 1 IWF Algorithm For Power Allocation

1 Initialize the initial value of power, number of user-channels in power convergence state, iteration number of FBS i on channel n , the flag bit of convergence and accuracy requirement by $p_{i,n} = I_i^{\max} / N_C$, $count = 0$, $k_{i,n} = 0$, $flag_{i,n} = 0$, $\delta = 10^{-7}$ separately.

2 If $count \neq N_C N_F$

3 For $n = 1 : N_C$ **do**

4 For $i = 1 : N_F$ **do**

5 If $flag_{i,n} = 1$, $count ++$; **continue**;

6 Else

7 $\mathbf{p}_i = (p_{i,1}, \dots, p_{i,n}, \dots, p_{i,N_C})$

8 $k_{i,n} ++$; $step_ \lambda = \frac{\partial L}{\partial \lambda_i}(\mathbf{p}_i)$; $step_ \mu = \frac{\partial L}{\partial \mu_i}(\mathbf{p}_i)$;

9 $\lambda_i = \lambda_i + step \times step_ \lambda$; $\mu_i = \mu_i + step \times step_ \mu$; $p_{i,n}^* = p_{i,n}$;

10

$$p_{i,n} = \left[\frac{(1 - \frac{\tau_i}{T}) \Pr(H_n^0) (1 - P_{i,n}^f(\tau_i))}{\left(\gamma_i [(T - \tau_i) - \lambda_i (T - \tau_i) - \mu_i p_{i,n}^{miss} |g_{M,i,n}|^2] \ln 2 \right)} - \frac{\sigma^2 + \sum_{j \neq i} p_{j,n} |g_{j,i,n}|^2}{|g_{i,n}|^2} \right]^+$$

11 End If

12 If $((p_{i,n}^* \neq 0) \&\& abs(p_{i,n}^* - p_{i,n}) / p_{i,n} \leq \epsilon) \parallel k_{i,n} \geq k_{\max}$

13 $flag_{i,n} = 1$;

14 Else continue

15 End If

16 End For

17 End For

18 End If

The sub-channel allocation strategy $\beta_{i,n}$ can be achieved by the corresponding values of $p_{i,n}$. $\beta_{i,n} = 1$ when $p_{i,n} > 0$, vice versa. Furthermore, optimal solution ϕ_i can be achieved by making comparison between multiple sets of $(\mathbf{p}, \boldsymbol{\beta})$ with the given τ_i .

5 Simulation Results and Analysis

In this section, simulation results are demonstrated to illustrate theoretical findings. After testing the convergence of the proposed power allocation algorithm, performance results with respect to throughput, EE and utility function are present, with the average power allocation (APA) algorithm as comparison. The system is set up according to the following simulation parameters (Table 1):

Table1. Simulation parameters

Parameter	Value
Number of MBS N_M	1
Number of FBS N_F	3
Number of Channel N_C	5
Interference Threshold I_i^{\max}	0.1 w
Maximal Iteration Number k_{\max}	60
Accuracy Requirement δ	10^{-9}
Sampling Rate μ	8 MHz
Frame Length T	20 ms
DP Threshold P_{th}^d	0.9
FP Threshold P_{th}^f	0.2
Energy Threshold E_i^{\max}	2 mj
Sensing Power $P_{i,n}^s$	1 mw

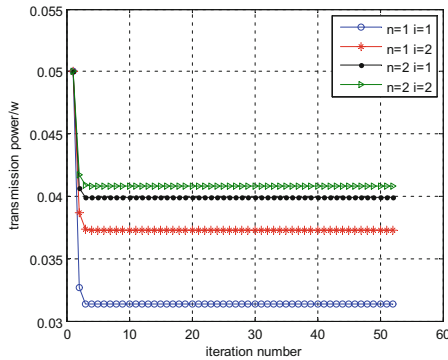


Fig. 3. Convergence of the proposed power allocation algorithm

Figure 3 presents the convergence of the proposed power allocation, where n and i denote the index of channel and FBS. It can be seen that the power of FBS on each channel declines gradually, and then keeps smooth. Meanwhile, the system gains the stable performance. In the proposed algorithm, the power converges within 10 times to achieve δ accuracy.

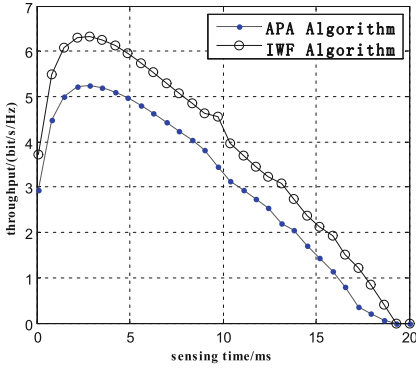


Fig. 4. The comparison of throughput versus sensing time

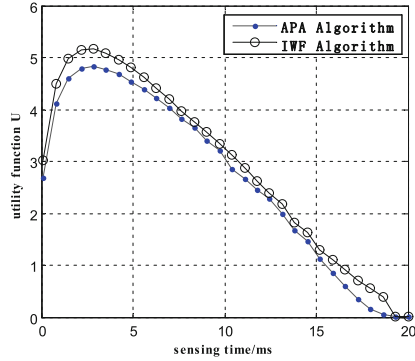


Fig. 5. The comparison of utility function versus sensing time

From Figs. 4, 5 and 6, we provide the comparison of two schemes to show the effect of sensing time on femto-cells’ throughput, utility function and the energy efficiency (EE). As depicted in Fig. 4, the throughput firstly increases with the growth of τ_i , and then decreases to the zero for the proposed IWF algorithm. That is because the higher τ_i which means the lower FP, improves the availability of spectrum resource and gains more throughput by making more FBSs access into the idle channels. However, when the sensing time reaches to some threshold, it makes little effect on FP and throughput. Contrarily, the shorter of transmission time reduces the transmission efficiency and degrade the system performance. The same trend can be found in utility function as illustrated in Fig. 5. It is not difficult to notice that the price factor λ_i will execute self-regulation according to the total power, aiming to limit the power of each FBS. In contrary to throughput, the utility function achieves a lower value due to price mechanism.

In Fig. 6, curve of EE keeps the same trend as in Fig. 5. Furthermore, IWF algorithm is better than APA algorithm. That is because, in context of guaranteeing throughput, IWF algorithm strongly reduces the total value of power allocation.

Figure 7 shows the increasing trend of throughput with the growth of inner SNR. Since the higher SNR brings higher power allocation, which improves throughput of femto-cells. While, with the increasing SNR, the inner-tier interference also become larger, which limits the improvement of throughput. Thereby, the throughput is no longer varied by the inner SNR.

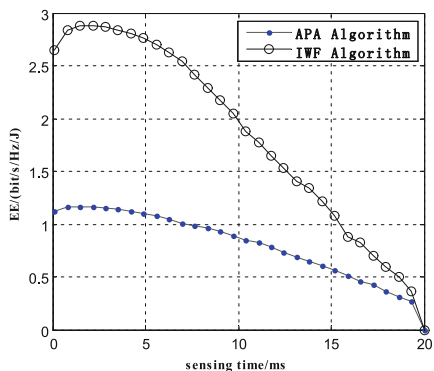


Fig. 6. The comparison of EE versus sensing time

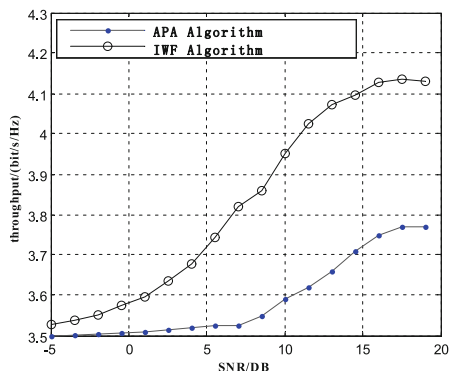


Fig. 7. The comparison of throughput versus inner SNR

6 Conclusion

In this paper, the problem of optimal multichannel sensing (with respect to sensing time and threshold) and resource allocation (with respect to channel and power) in CCHN is explored by formulating a game and the FBSs act as the players to maximize his own opportunistic throughput by choosing jointly the sensing and access configurations. A pricing mechanism that penalizes the FBSs in violating the power constraints is also provided. Finally, we deal with the non-convexity of the game by utilizing the iterative water-filling (IWF) algorithm. Simulation results show the proposed IWF algorithm gains better performance in both femto-cell throughput and EE than traditional APA algorithm.

Acknowledgement. This work was supported in part by the National Natural Science Foundation of China under Grant No. 61372117, 61302081, 61421061, and the 863 project under Grant NO.2014AA01A701.

References

1. Fan, R., Jiang, H., Guo, Q., Zhang, Z.: Joint optimal cooperative sensing and resource allocation in multichannel cognitive radio networks. *IEEE Trans. Veh. Technol.* **60**(2), 722–729 (2011)
2. Janatian, N., Sun, S., Modarres-Hashemi, M.: Joint optimal spectrum sensing and power allocation in CDMA-based cognitive radio networks. *IEEE Trans. Veh. Technol.* **64**(9), 3990–3998 (2015)
3. Zhang, N., Liang, H., Cheng, N., Tang, Y., Mark, J.W., Shen, X.S.: Dynamic spectrum access in multi-channel cognitive radio networks. *IEEE J. Sel. Areas Commun.* **32**(11), 2053–2064 (2014)
4. Wang, F., Wang, J., Li, W.W.: Game-theoretic analysis of opportunistic spectrum sharing with imperfect sensing. *EURASIP J. Wirel. Commun. Netw.* (2016)

5. Dai, Z., Wang, Z., Wong, V.W.S.: An overlapping coalitional game for cooperative spectrum sensing and access in cognitive radio networks. *IEEE Trans. Veh. Technol.* **65**(10), 8400–8413 (2016)
6. Zhang, S., Wang, H., Zhang, X., Cao, Z.: Optimal spectrum access algorithm based on POMDP in cognitive networks. *AEU Int. J. Electron. Commun.* **69**(6), 943–949 (2015)
7. Jiang, C., Chen, Y., Gao, Y., Liu, K.J.R.: Joint spectrum sensing and access evolutionary game in cognitive radio networks. *IEEE Trans. Wirel. Commun.* **12**(5), 2470–2483 (2013)
8. Bose, S., Natarajan, B.: Reliable spectrum sensing for resource allocation of cognitive radio based WiMAX femtocells. In: *The 9th Annual IEEE Consumer Communications and Networking Conference-Wireless Consumer Communication and Networking*, pp. 889–893, 14–17 January 2012
9. Cheng, S.-M., Ao, W.C., Tseng, F.-M., Chen, K.-C.: Design and analysis of downlink spectrum sharing in two-tier cognitive femto networks. *IEEE Trans. Veh. Technol.* **61**(5), 2194–2207 (2012)
10. Yu, W., Ginis, G., Cioffi, J.M.: Distributed multiuser power control for digital subscriber lines. *IEEE J. Sel. Areas Commun.* **20**, 1105–1115 (2002)

Energy Harvesting Relay Node Deployment for Network Capacity Expansion

Zhiqiang Zhang¹(✉), Yifei Wei¹(✉), Bo Gu¹, Xiaojun Wang², and Mei Song¹

¹ School of Electronic Engineering, Beijing University of Posts and Telecommunications, Beijing 100876, People's Republic of China

{zhangzhiqiang, weiyifei, gubo, songm}@bupt.edu.cn

² Dublin City University, Dublin, Ireland

xiaojun.wang@dcu.ie

Abstract. The increasing traffic demands in the past few years require further expansion of cellular network capacity. Densely deployed base stations may cause a large amount of energy consumption and lots of environmental problems. Relaying is considered as a promising cost-efficient solution for capacity expansion and energy saving due to the physical characteristics and low power requirements of the relay nodes. In this paper, we study the energy harvesting relay node deployment problem in a cellular network where the user distribution may change with time. We propose a greedy relay nodes deployment algorithm to satisfy the network capacity requirements in different time and put forward an operation optimization algorithm to make full use of renewable energy. Simulation results show that the network capacity can be increased significantly and the energy consumption can be reduced dramatically by the proposed algorithms.

Keywords: Heterogeneous cellular network · Capacity expansion
Energy harvesting · Relay node deployment

1 Introduction

In the recent years, the rapid rise in the popularity of smart devices requires a fast and ubiquitous wireless network, which makes it necessary to expand the original network capacity. However, increasing the number of macro base stations (BSs) in the cellular network significantly reduces the gain because of the elevated interference. Heterogeneous networks (HetNets) provide services across both macro and small cells to optimize the mix of capabilities and have attracted much attention in the recent years [1, 2]. Relay networks, as one kind of HetNets, is a promising solution of performance enhancement and energy saving. Relay is one of the proposed technologies in LTE-Advanced networks for coverage expansion and capacity enhancement [3]. Relay Nodes (RNs) are connected to the core network with wireless backhaul through an evolved Node B (eNB) and they usually have much smaller energy consumption than BSs.

Over the years, cellular networks have become an important source of energy consumption, reducing the network energy consumption has benefits in both economic and environmental aspects, which encourages people to look forward alternative power

supply. The usage of renewable energy sources such as wind power and photo-voltaic energy can significantly reduce traditional energy consumption. Many kinds of renewable energy sources have been studied for green networks as introduced in [4].

The improvements of network performance have been widely studied. In the paper [5], micro base stations are deployed to increase the area spectral efficiency (ASE) value. The results show that the ASE can be improved significantly when the micro base stations located at the edges of macro cells where the received signal is worst. The energy efficiency problem of cellular networks is studied in [6], excessively increasing the number of micro base stations may reduce the energy efficiency, and there exists an optimum number of deployed BSs. The capital expenditure and the total operational expenditure are considered as the base station costs in [7]. A hierarchical power management architecture is introduced in [8], the authors focus on effectively exploit the green capabilities of networks. A green base station offloading model is proposed in [9], by predicting the value of green energy collected and updating the residual energy of each BS, the maximum number of users that each BS can offload can be calculated to achieve different network performance. The article [10] mainly focuses on the energy supply aspects in the network and investigates how to optimize the using of on-grid energy to reduce the carbon emission rate. A green base station optimization algorithm is proposed in [11] to reduce the traditional power consumption, the transmission power of BSs can be adjusted to improve network performance. The deployment of RNs has been used to improve network performances in the recent years such as connectivity by [12] and lifetime maximization by [13]. The article [14] considered finite-state Markov channels in the relay-selection problem to increase spectral efficiency, mitigate error propagation, and maximize the network lifetime. These studies usually focus on the user distribution in peak periods to ensure the network performance in the worst case while ignoring the differences of traffic demands in different positions and time periods, which may cause much resource waste in the low-load state of the network.

In this paper, a more practical condition is considered. We deploy RNs to improve the network capacity where one BS has already been deployed and the changes of user distributions among different time is full considered. In addition, The RNs are equipped with energy harvesting devices so that they can harvest ambient energy. RNs still need to be connected to the on-grid power network in case that the renewable energy sources are inadequate.

The remainder of the article is organized as follows. In Sect. 2, the system model is introduced. In Sect. 3, the problem, constraints and objective function are defined. Section 4 describes the proposed algorithms for these problems. Section 5 gives the simulation parameters and results. Section 6 concludes the paper.

2 System Model

Consider a wireless network in which all users are served by one BS b . The capacity of this network needs to be expanded to satisfy the growing traffic demand by deploying RNs. The deployed RN set is denoted by R . The users, denoted by U , always connect

to the BS b or a RN r which can provide the highest signal strength to them. The signal-to-interference-plus-noise ratio (SINR) of user u can be written as

$$\Gamma_u(b) = \frac{P_{tx}(b)g_{u,b}}{\sum_{r \in R} P_{tx}(r)g_{u,r} + \sigma^2} \quad (1)$$

$$\Gamma_u(r) = \frac{P_{tx}(r)g_{u,r}}{P_{tx}(b)g_{u,b} + \sum_{r' \in R, r' \neq r} P_{tx}(r')g_{u,r'} + \sigma^2} \quad (2)$$

$\Gamma_u(b)$ and $\Gamma_u(r)$ denote the SINR of users connected to the BS b and the RN r , respectively. $P_{tx}(b)$ and $P_{tx}(r)$ denote the transmission power of BS b and RN r , respectively. $g_{u,b}$ is the channel gain from BS b to user u and $g_{u,r}$ is the channel gain from RN r to user u . Thermal noise is denoted by σ^2 . For simplicity, the shadow fading and small size decline are ignored, only the path loss is considered. Then the network capacity of user u can be calculated from SINR as

$$C_u = B_u \log_2(1 + \Gamma_u) \quad (3)$$

B_u is the bandwidth assigned to user u in equal bandwidth scheduling. This scheduling allows BSs to share the resources equally among users [15].

The power consumption of a BS consists of two parts. The first part is the static power consumed with no transmission, and the other part depends on the transmission power [16]. It can be given by

$$P(b) = P_c(b) + \alpha_b P_{tx}(b) \quad (4)$$

$P_c(b)$ is the static power of each BS and α_b scales the transmission power depending on the load.

The power consumption model of each RN is similar, however, unlike previous studies, we consider their energy harvesting abilities. With the help of energy harvesting devices, the RNs can produce energy from renewable sources such as sunlight or wind. However, renewable energy sources may be limited and the generated energy may not be enough to totally power the RNs [17]. So we define $\beta = \frac{P_{hv}}{P(r)_{\max}}$ as the energy harvesting rate, where P_{hv} and $P(r)_{\max}$ denote the average harvesting power and the maximum consumption power of each RN, respectively. The RNs can consume less on-grid power as long as $\beta > 0$ and can work for a whole day without consuming any on-grid power when $\beta \geq 1$. Thus the consumption power of each RN can be written as

$$P(r) = \begin{cases} 0 & \beta \geq 1 \\ P_c(r) + \alpha_r P_{tx}(r) - P_{hv} & 0 \leq \beta < 1 \end{cases} \quad (5)$$

$P_c(r)$ is the static power of each RN and α_r scales the transmission power depending on the load, the average harvesting power is denoted by P_{hv} .

It's assumed that users connected to the network always have data to transmit with full buffer, in addition, no power control algorithm is used. Therefore, BSs and RNs are fully utilized, α_b and α_r are constant for all BSs and RNs.

3 Problem Definition

Deploying RNs can improve the network capacity to a higher level, but it also brings extra energy consumption. By efficiently deploy RNs, we can minimize the extra energy consumption while meeting the requirement of capacity. The problem can be formulated as

$$\begin{aligned} \min \quad & \sum_{r \in R} P(r) \\ \text{s.t.} \quad & \sum_{u \in U} C_u(B \cup R) \geq \lambda \cdot C_o \end{aligned} \quad (6)$$

$C_u(B \cup R)$ denotes the capacity of user u when both BSs and RNs are deployed. C_o is the original network capacity without deploying any RNs and the multiplier $\lambda \geq 1$ is the desired increasing times over C_o after deploying RNs.

4 Solutions

Affected by user living and working conditions, the user distribution may always change with time in a day [18]. The deployment of BSs generally aims at satisfying the capacity demand in peak hours, while ignoring the resource wastes in the other hours. It has been reasonable in the past few years for the expensive costs and deployment inconvenience of traditional BSs. With the deployment of RNs, these problems matter less for low costs and high flexibilities of RNs. A whole day can be divided into several parts, each of them corresponding to a unique user distribution. Then the RNs can be deployed in each time slice to meet the capacity requirements.

There can be lots of candidate locations for RN deploying in this area and we need to select some of them. Furthermore, with the rising number of deployed RNs, the network performance may not always increase due to the interference effect, especially when the RNs are located close. The strong interference between each other even decreases the network capacity. On the other hand, influenced by the user distribution, capacity contributions from differently located RNs may vary dramatically. Therefore, the RN deployment problem is actually a combinatorial problem and it quickly becomes unsolvable when the number of candidate locations becomes large.

Thus, a greedy algorithm is proposed to select the relatively better locations of RNs. In this algorithm, a RN will be deployed at the location which can provide the most increase of network capacity. The RNs will be added iteratively until the capacity requirement is satisfied.

Algorithm 1. Greedy RN Deployment Algorithm

Initialize $R = \emptyset$
while $\sum_{u \in U} C_u(B \cup R) < \lambda \cdot C_o$ **do**
 for all $r \in R_{CAND}$ **do**
 $r_{chosen} = \arg \max_{r \in R_{CAND}} \sum_{u \in U} C_u(B \cup R \cup r) - \sum_{u \in U} C_u(B \cup R)$
 $R = R \cup r_{chosen}$
 $R_{CAND} = R_{CAND} - r_{chosen}$
 end for
end while

In Algorithm 1, the deployed RN set is denoted by R and the candidate RN set is denoted by R_{CAND} . The algorithm should be executed for every time slice. Then we can get a RN deployment schedule which consists of N sets of RNs, N is the number of time slices. One set of the RNs will work only during the corresponding time slice and will be turned off during the other time slices. All the RNs can continuously harvest energy, even in turn-off time.

Then we focus on the energy consumption problem. Long turn-off time may cause energy waste due to the limited battery capacity. One set of RNs which supposed to work only in time slice t_i actually can also work in t_j as long as they have harvested enough energy. However, the user distribution of t_j may be different and there is already one set of RNs deployed in t_j . Two sets of RNs working together may decrease the network capacity due to the interference. So we propose an optimization algorithm to merge the two sets of RNs together while satisfying the capacity requirements of both time slices. In this algorithm, the RNs deployed in two time slices are simply merged together firstly, then the nearest two RNs are replaced by a new RS which located at the middle position of them, which can effectively avoid redundant deployment and reduce the interference.

Algorithm 2. Deployment Optimization Algorithm

```

Initialize  $R_{i,tj} = R_{ti} \cup R_{tj}$ 

while  $\sum_{u \in U} C_u(B \cup R_{i,tj}) < \lambda \cdot C_{o_{ti}} \parallel \sum_{u \in U} C_u(B \cup R_{i,tj}) < \lambda \cdot C_{o_{tj}}$  do
   $minDist = \infty$ 
   $minDistRNs = \emptyset$ 
  for all  $r_x \in R_{i,tj}$  do
    for all  $r_y \in R_{i,tj}, r_y \neq r_x$  do
      if  $dist(r_x, r_y) < minDist$  then
         $minDist = dist(r_x, r_y)$ 
         $minDistRNs = r_x \cup r_y$ 
         $r_{mid} = getMidRN(r_x, r_y)$ 
      end if
    end for
  end for
   $R_{i,tj} = R_{i,tj} - minDistRNs$ 
   $R_{i,tj} = R_{i,tj} \cup r_{mid}$ 
end while

```

$R_{i,tj}$ denotes the merged RN set and will work in both time slices t_i and t_j . $dist(r_x, r_y)$ gives the distance between r_x and r_y , $getMidRN(r_x, r_y)$ gives a new RN that located at the middle position of r_x and r_y .

5 Simulation Results

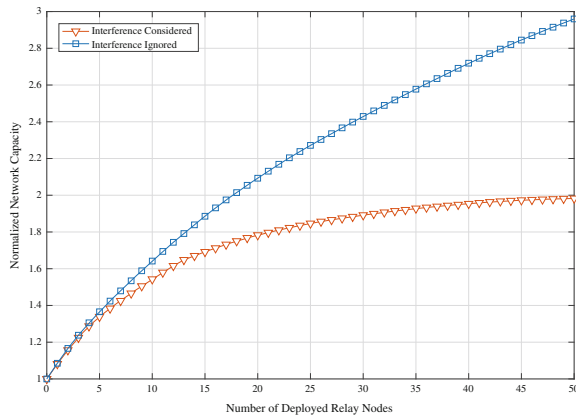
The deployment area size is 3 km \times 3 km and served by one BS. RNs need to be deployed in this area to improve the capacity. More candidate locations can get more accurate results but also brings extra calculation complexity. The number of candidate locations is set to 1600 after a set of experiments. The other parameters used in simulations are given in Table 1.

Table 1. Simulation parameters

Parameters	Values
Target capacity multiple	1.5
Number of time slices	12
Bandwidth	2 GHz
Static power of BS	168 W
Transmission power of BS	39.8 W
Static power of RN	20 W
Transmission power of RN	1 W
BS to user path loss	$128.1 + 37.6 * \log_{10}(d(\text{km}))$
RN to user path loss	$37 + 30 * \log_{10}(d(\text{m}))$
Thermal noise	-174 dBm/Hz

Firstly, we investigate the impact of RN deployment on network capacity. As is shown in Fig. 1, with the continuously deploying of RNs, the network capacity increases significantly at first, then it slows down and eventually decreases due to the gradually increasing interference. The network capacity can be influenced by interference among RNs significantly. The maximum capacity that can be reached by deploying RNs is limited. Expanding capacity to the maximum needs a large number of RNs, which may be inefficient.

The deployed positions of RNs are as shown in Fig. 2. Most of them located far from the BS due to the lower SINR there. In addition, their locations are obviously affected by the user distribution. When user distribution changes in different time, the optimum deployed positions of RNs will change accordingly.

**Fig. 1.** Increased capacity by relay nodes

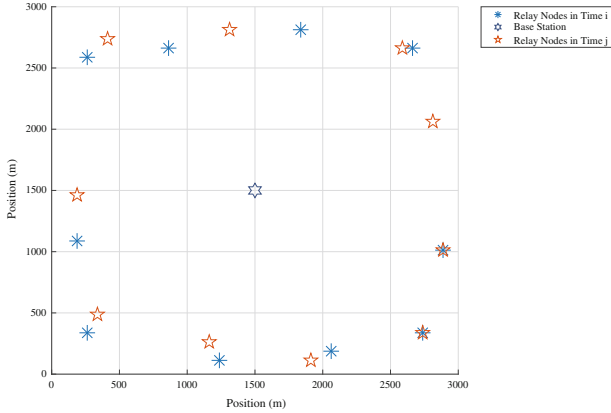


Fig. 2. Positions of deployed relay nodes

In the following experiments, we focus on the energy consumption problem. If a RN only works in non-adjacent time slices, it can make full use of its renewable energy. So we divide the time slices into many groups and each group consists of several non-adjacent time slices. The time slices in the same group has same RN deployment. If the number of time slice groups is m , then m sets of RNs will be deployed. When the energy harvesting rate is above $1/m$, our split combination solution will reach zero on-grid energy. With a certain energy harvesting rate, more groups of time slices can reduce the on-grid energy significantly. Deployment in 4 groups of time slices can save about 74.5% on-grid energy over only one group of time slices (Fig. 3).

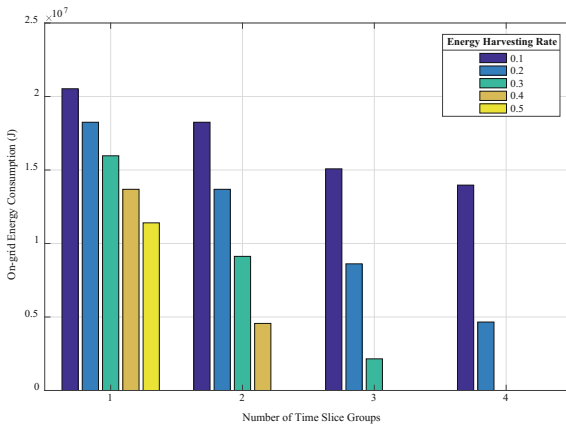


Fig. 3. On-grid energy consumption of deployed relay nodes

6 Conclusions

In this paper, we propose a greedy RN deployment algorithm and an optimization algorithm to improve the network capacity efficiently. The energy harvesting ability of RNs and user distribution changes are considered in the process of deployment. Imprudently increasing the number of RNs may decrease the network capacity due to the interference. The proposed deployment algorithm greedily selects relatively better positions from candidate locations to deploy RNs until the required capacity is satisfied. Due to the heuristic nature of the algorithm, the complexity of deployment problem is significantly reduced. Then the optimization algorithm merges different sets of RNs according to the energy harvesting ability to make full use of renewable energy. Zero on-grid energy consumption can be achieved by this algorithm. The simulation results show that the capacity demand can be satisfied efficiently and the on-grid energy consumption can be significantly reduced by the proposed algorithms.

Acknowledgments. This work was supported by the National Natural Science Foundation of China (No. 61571059).

References

1. Damjanovic, A., Montojo, J., Wei, Y., et al.: A survey on 3GPP heterogeneous networks. *IEEE Wirel. Commun.* **18**(3), 10–21 (2011)
2. Ghosh, A., Ratasuk, R.: *Essentials of LTE and LTE-A*. Cambridge University Press (2011)
3. Saleh, A.B., Redana, S., Hämäläinen, J., Raaf, B.: Comparison of relay and pico eNB deployments in LTE-Advanced. In: *IEEE 70th Vehicular Technology Conference (VTC 2009-Fall)*, USA, September 2009
4. Schmitt, G.: The green base station. In: *International Conference on Telecommunication - Energy Special Conference, VDE*, pp. 1–6 (2009)
5. Richter, F., Fehske, A.J., Fettweis, G.P.: Energy efficiency aspects of base station deployment strategies for cellular networks. In: *Vehicular Technology Conference Fall*, pp. 1–5. *IEEE Xplore* (2009)
6. Coskun, C.C., Ayanoglu, E.: A greedy algorithm for energy-efficient base station deployment in heterogeneous networks. In: *IEEE International Conference on Communications*, pp. 7–12. *IEEE* (2015)
7. Chen, Y., Zhang, S., Xu, S.: Characterizing energy efficiency and deployment efficiency relations for green architecture design. In: *IEEE International Conference on Communications Workshops*, pp. 1–5. *IEEE* (2010)
8. Wei, Y., Wang, X., Fialho, L., Bruschi, R., Ormond, O., Collier, M.: Hierarchical power management architecture and optimum local control policy for energy efficient networks. *J. Commun. Netw.* **18**(4), 540–550 (2016)
9. Wei, Y., Ren, C., Song, M., Yu, R.: The offloading model for green base stations in hybrid energy networks with multiple objectives. *Int. J. Commun. Syst.* **29**(11), 1805–1816 (2016)
10. Han, T., Ansari, N.: Optimizing cell size for energy saving in cellular networks with hybrid energy supplies. In: *Global Communications Conference*, pp. 5189–5193. *IEEE* (2012)
11. Pamuklu, T., Ersoy, C.: Optimization of renewable green base station deployment. In: *Green Computing and Communications*, pp. 59–63. *IEEE* (2013)

12. Cheng, X., Du, D.Z., Wang, L., et al.: Relay sensor placement in wireless sensor networks. *Wirel. Netw.* **14**(3), 347–355 (2008)
13. Hou, Y.T., Shi, Y., Sherali, H.D., et al.: Prolonging sensor network lifetime with energy provisioning and relay node placement. In: 2005 Second IEEE Communications Society Conference on Sensor and Ad Hoc Communications and Networks, IEEE SECON 2005, pp. 295–304. IEEE Xplore (2005)
14. Wei, Y., Richard Yu, F., Song, M.: Distributed optimal relay selection in wireless cooperative networks with finite state Markov channels. *IEEE Trans. Veh. Technol.* **59**(5), 2149–2158 (2010)
15. GPP, TR 36.814: Further advancements for E-UTRA physical layer aspects (Release 9). Technical report, March 2010
16. Richter, F., Fehske, A.J., Fettweis, G.P.: Energy efficiency aspects of base station deployment strategies for cellular networks. In: Vehicular Technology Conference Fall, pp. 1–5. IEEE Xplore (2009)
17. Han, T., Ansari, N.: ICE: intelligent cell brEathing to optimize the utilization of green energy. *IEEE Commun. Lett.* **16**(12), 866–869 (2012)
18. Nousiainen, S., Kordybach, K.: User distribution and mobility model framework for cellular network simulations. In: VTT Information Technology, pp. 518–522 (2002)

Parameters Optimization for KFKM Clustering Algorithm Based on WiFi Indoor Positioning

Zhengying Hu^{1(✉)}, Lujuan Ma², Baoling Liu¹, and Zhi Zhang¹

¹ State Key Laboratory of Networking and Switching Technology, Beijing University of Posts and Telecommunications, Beijing 100876, People's Republic of China
Zhengying_hu@163.com

² Hisense Co., Ltd, Qingdao 266061, People's Republic of China

Abstract. Kernel fuzzy K-means (KFKM) clustering algorithm is widely used to manage the fingerprint database for WiFi indoor positioning system to reduce the computational complexity of the position matching process. In this paper, we propose a novel WiFi positioning scheme based on KFKM algorithm, which can achieve a better precision by further optimizing the parameters employed in KFKM. Our proposed scheme consists of three steps. First, we choose an interval of reference points (RP) to build the fingerprint database. Then we decide an appropriate number of clusters based on the structure characteristics of fingerprint database using sample density method. During the process of clustering, we optimize the kernel parameter by approximating actual kernel matrix to a hypothetical ideal kernel matrix to improve the positioning precision. Through simulation results, we show that compared with the existing KFKM algorithm, our proposed scheme achieves 23.48% improvement in terms of positioning accuracy.

Keywords: WIFI positioning · KFKM · Parameters optimization
Fingerprint database · Clustering

1 Introduction

The basic idea of the location fingerprinting method for WiFi positioning consists of two steps. The first step is to build a database that stores pre-recorded received signal strength (RSS), or “fingerprint”, from different WiFi access points (AP) at different reference points (RP). Then, the second step is to estimate the target's location by matching real-time RSS with the offline-constructed database (Fig. 1).

The main limitation of the matching process is the high implementation cost when the database is too large to traverse. Hence, some improved clustering methods were proposed to manage the database such as K-means and fuzzy K-means (FKM) algorithms. However, non-linear data is beyond K-means method's processing power since the objective function is non-differentiable. Motivated by this, in [1], the authors came up with fuzzy K-means (FKM) method, which aim to solve the non-differentiability of the objective function; recently in [2], Saadi et al. used an un-supervised machine learning K-means clustering based on two LEDs and achieved great accuracy. In this paper, we propose a new scheme to strengthen the performance of the WiFi positioning. We first amend the data acquisition process of the database; second, we use sample

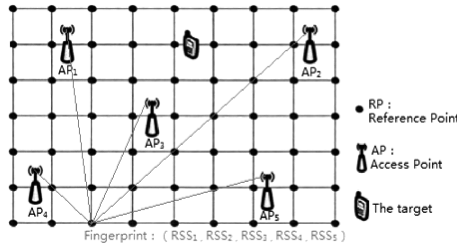


Fig. 1. The schematic diagram of database

density method to modify cluster amount to match with the characteristic of database; last, we propose an ideal kernel matrix to determine the kernel parameter σ .

2 WiFi Indoor Positioning System Based on KFKM

WQNN is an effective matching algorithm in WIFI positioning [3]. Suppose a WIFI wireless network with L access points, denoted by $\{AP_1, AP_2, \dots, AP_L\}$. There are n RP in total, denoted by $\{f_{i1}, f_{i2}, \dots, f_{in}\}^T, i = 1, 2, \dots, L$. At on-line stage, the RSSI of the target, denoted by $s = (s_1, s_2, \dots, s_L)$, will match with the fingerprint database by evaluating the Euclidean distance between s and all fingerprints. Choose Q ($Q > 2$) smallest distance and average the Q corresponding positions, the coordinate (\hat{x}, \hat{y}) is the estimated location of the target's positions, i.e.

$$(\hat{x}, \hat{y}) = \sum_{i=1}^Q \frac{\frac{1}{D_i + \varepsilon}}{\sum_{i=1}^Q \frac{1}{D_i + \varepsilon}} \times (x_i, y_i) \tag{1}$$

Where (x_i, y_i) is the coordinate of the i^{th} RP, set ε to 0.003 to prevent the “zero divisor” condition. In order to evaluate the precision of positioning test, the root-mean-square-error (RMSE) between the estimated position and the real position is proposed to measure errors. What’s more, a *RMSE* drawn from one positioning test doesn’t represent the performance of an algorithm. Hence, we collect *RMSE* from times of experiments to evaluate the algorithm comprehensively. In general, cumulative probability curve of *RMSE* is an intuitive representation for evaluation.

The Chemistry building in BNU was set to verify the optimizations of database structure would improve localization accuracy. Considering storage capacity and calculation complexity, set RP interval = 2 m and collecte RSS from 5 AP at all RP(black points) in Fig. 2, we have the database of the on-site test.

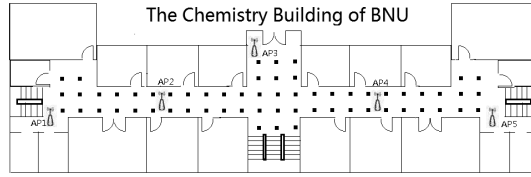


Fig. 2. Ichnography of on-site positioning test

3 Parameters Optimizations for Positioning System

In this section, we propose a series of parameter optimizations to the WiFi positioning system, including the modification of clusters amount k and kernel parameter σ of kernel function, denoted by POKFKM algorithm.

Function_1: set the cluster amount k according to the structure of RP.

The amount of clusters k plays an essential role in the performance of KFKM clustering algorithm. The main idea of sample density method [4] is to analyze all RP in the database to find out the amount of density peaks that extrude among neighbors and far from other peaks. ρ_i is the density of the i^{th} RP, δ_i is the smallest distance between the i^{th} RP and another RP with higher density, indicated as follows:

$$\rho_i = \sum_j \chi(d_{ij} - d_c), i \neq j, \delta_i = \min_{j: \rho_j > \rho_i} (d_{ij}), i \neq j \quad (2)$$

Figure 3 shows the δ - ρ situation of the on-site test database. There are 7 peaks in the upper right corner of the figure. Thus, $k = 7$ is the optimal cluster amount.

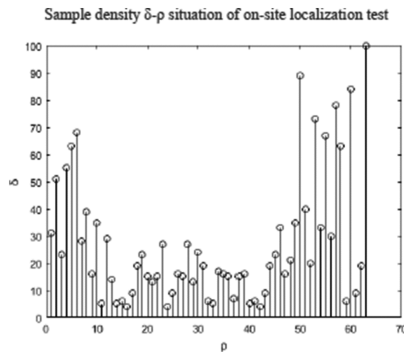


Fig. 3. Finding of density peaks to determine k value

Function_2: set the optimal kernel parameter σ to get better clustering result. Gaussian kernel function is:

$$k(x, y) = \exp\left(-\frac{\|x - y\|^2}{2\sigma^2}\right) \quad (3)$$

 Algorithm: WiFi positioning assisted by POKFKM clustering

Function Wifi_positioning(s)

while off-line stage() do

set AP amount and RP interval for fingerprints collection;

while RP ++

 collect fingerprints $x_i = [x_{i1}, x_{i2} \dots x_{iL}]$ into database $F = [x_1, x_2, \dots x_n]^T$;

end while; end while

function_1: get the cluster amount k according to the structure of RPfunction_2: set the optimal kernel parameter σ to get better clustering result

function_3: KFKM clustering

do $J(U, \theta) = \sum_{i=1}^n \sum_{j=1}^k (u_{ij})^m d(\varphi(x_i), \varphi(\theta_j))$

$$u_{ij} = \frac{\{1 / [\kappa(x_i, x_i) - 2\kappa(x_i, \theta_j) + \kappa(\theta_j, \theta_j)]\}^{1/(m-1)}}{\sum_{j=1}^k \{1 / [\kappa(x_i, x_i) - 2\kappa(x_i, \theta_j) + \kappa(\theta_j, \theta_j)]\}^{1/(m-1)}}, \theta_j = \frac{\sum_{i=1}^n u_{ij}^q \varphi(x_i)}{\sum_{i=1}^n u_{ij}^q}, i = 1, 2, \dots, n; j = 1, 2, \dots, k$$

until $|J(U, \theta)^t - J(U, \theta)^{t-1}| < \varepsilon$

end function_3

while new_arrival(s)

WQNN(s); //traverse the clusters and match with RP

end function.

While $\|\cdot\|$ means the Euclidean distance of vectors. The experiential value of σ is given by the reciprocal of sample hypersphere radius [5] or enumeration, none is optimal. Therefore, the optimal σ is supposed to approximate the actual kernel matrix to the ideal matrix [6]. K-means algorithm firstly divides the database into k clusters and gets a row vector L with n dimensions. The element $L_i = k', 1 \leq k' \leq k, i = 1, 2, \dots, n$ means the affiliation of corresponding sample.

With the purpose of making the samples within the same cluster as similar as possible and samples from different clusters as unlike as possible, the ideal kernel matrix should meet the following condition:

$$k'_{ij} = \begin{cases} 1, & L_i = L_j \\ 0, & L_i \neq L_j \end{cases} \quad (4)$$

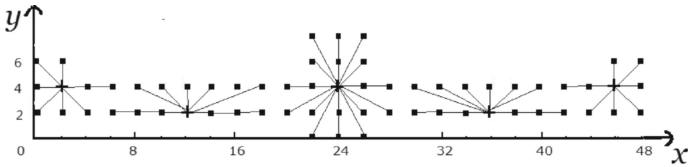
The kernel parameter that approximate the kernel matrix to the ideal one is optimal. The similarity can be quantified by the difference between k_{ij} and k'_{ij} :

$$E(k, k') = \sum_{i=1}^n \sum_{j=1}^n (k_{ij} - k'_{ij})^2 \quad (5)$$

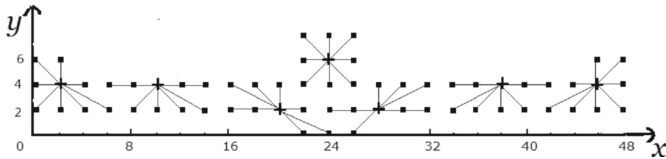
The solution to $\frac{dE(k, k')}{d\sigma} = 0$ (noted as σ_0) minimizes $E(k, k')$.

4 On-site Indoor Experiment

In order to verify the performance of POKFKM algorithm, we conduct contrast tests between (1). KFKM clustering; (2). POKFKM clustering. The Clustering result is shown in Fig. 4. Cluster centers are denoted by crosses.



1) KFKM Clustering circumstance



2) POKFKM Clustering circumstance

Fig. 4. Clustering result of original and optimized Clustering methods

After clustering, instead of matching all reference points in the database, it is capable to complete matching process by comparing real-time RSS with 7 cluster centers and 9

RP (at most) in the nearest cluster for 16 times in total after POKFKM clustering. Therefore, the computational load reduces by 74.6%.

After initialization, first position the test position RSS to the nearest cluster center, then traverse other RP within the cluster using WKNN, estimated position is the result of these two steps. We also use cumulative probability curves of RMSE of 70 times of on-site tests to illustrate the positioning accuracy of the three different clustering results above. The simulation result is illustrated in Fig. 5.

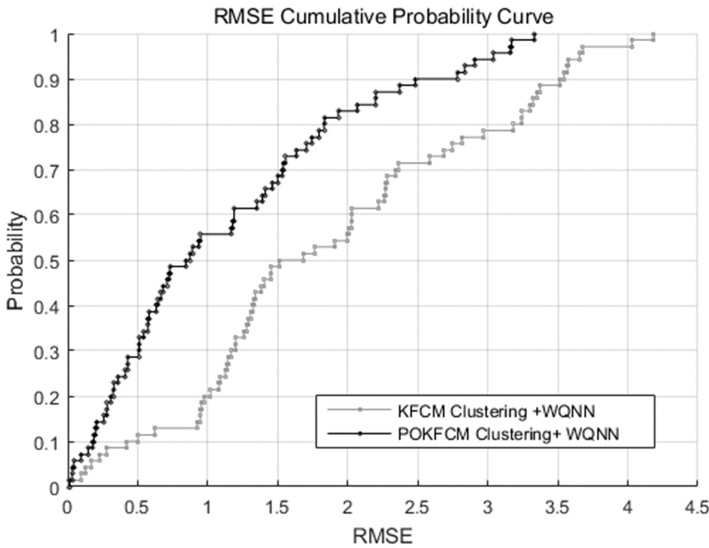


Fig. 5. KFKM, POKFKM algorithms' positioning errors

It's shown that POKFKM have better performance than KFKM clustering. The average RMSE of POKFKM is -23.48% narrowed than KFKM, which proves that POKFKM method has superior positioning precision than the KFKM algorithm. Meanwhile, POKFKM has less standard deviation of RMSE, which stands for higher robustness. KFKM Clustering method has 56.9% probability to derive expected error, while POKFCN method is more reliable with the probability of 83.3%. Hence, POKFKM clustering method largely increased the precision and the reliability of WiFi positioning system.

5 Conclusion

In this paper, three optimizations for WiFi indoor positioning system were proposed to enhance WiFi positioning. Simulation result has shown that the optimization of kernel function and cluster amount performed better than original KFKM algorithm. During on-site positioning experiments in the chemistry building in BNU, reasonable deployment of RP and AP made the database both compendious and integrate. POKFKM

algorithm was proved to be more reliable and robust and substantially increased the efficiency of WIFI indoor positioning.

Acknowledgement. This work was supported by the National Natural Science foundation of China (61421062) and Hisense Co., Ltd.

References

1. Suroso, D.J., Cherntanomwong, P., Sooraksa, P., et al.: Location fingerprint technique using fuzzy C-means clustering algorithm for indoor localization. In: TENCON 2011 IEEE Region 10th Conference, pp. 88–92. IEEE, Bali (2011)
2. Saadi, M., Ahmad, T., Zhao, Y., et al.: An LED based indoor localization system using k-means clustering. In: 2016 15th IEEE International Conference on Machine Learning and Applications (ICMLA), pp. 246–252. IEEE (2016)
3. Sadeghi, H., et al.: A weighted KNN epipolar geometry-based approach for vision-based indoor localization using smartphone cameras. In: Sensor Array and Multichannel Signal Processing Workshop (2014)
4. Rodriguez, A., Laio, A.: Clustering by fast search and find of density peaks. *Science* **344**(6191), 1492–1496 (2014)
5. Li, Z., Weida, Z.: Kernel clustering algorithm. *Chin. J. Comput.* **25**(6), 587–590 (2002)
6. Yang, H.L., Huang, Z.G., Liu, J.W., et al.: WIFI fingerprint localization based on Kernel Fuzzy C-means clustering. *J. Zhejiang Univ.* **50**, 1126–1133 (2016)

Energy Harvesting Time Coefficient Analyze for Cognitive Radio Sensor Network Using Game Theory

Mengyu Zhao^(✉), Yifei Wei, Qiao Li, Mei Song, and Ningning Liu

School of Electronic Engineering, Beijing University of Posts
and Telecommunications, Beijing 100876, People's Republic of China
{mengyuzhao, weiyifei, liqiao1989, songm,
liunn}@bupt.edu.cn

Abstract. In this paper, the cognitive radio sensor node can harvest energy from the radio frequency signal which is transmitted by the primary user. A time switching protocol was used to divide cognitive users' time into three phases: spectrum sensing mode, energy harvesting mode and data transmission mode. Therefore, the optimal energy harvesting mode time selection is a question to be solved. We consider a non-cooperative game model in which cognitive users are regarded as selfish players aiming to maximize their own energy efficiency. Then we prove the existence and uniqueness of Nash Equilibrium. A distributed best response algorithm is used to obtain the Nash Equilibrium. The simulation results prove that this algorithm can converge to the same equilibrium from different initial values. At last, we analysis the influence of various system parameters on the results of Nash Equilibrium and energy efficiency.

Keywords: Energy harvesting · Energy efficiency
Cognitive radio sensor network · Non-cooperative game
Best response algorithm

1 Introduction

In recent years, with the increase of network energy consumption and the development of green communication, energy harvesting has drawn more and more attention. Energy harvesting is a technology to keep self-sustaining and prolong network lifetime by harvesting the ambient energy (such as wind energy, solar energy, heat, etc.). Moreover, the sensor network with the capacity of harvesting energy from the ambient radio-frequency (RF) signals has received extensive research. Energy harvesting wireless sensor network (EHWSN) can greatly prolong the lifetime of the sensor nodes, which lays foundation for the development of emerging technologies such as big data and Internet of Things (IoTs) [1]. But it is worth to note that the sensor node can only work on the unlicensed spectrum band. And the unlicensed spectrum band are being more and more crowded, which limit the development of the sensor network.

Meanwhile, the survey shows the spectrum efficiency of licensed spectrum is relatively low. So energy harvesting cognitive radio sensor network (EHCRSN) has been put forward. In EHCRSN, the second user is the sensor node equipped with the ability

of spectrum sensing, which can also harvest the RF energy. But energy harvesting and data transmission of the sensor user can't be implemented at the same time. Therefore, two practical receiver methods have been proposed in [2], namely the time switching protocol (TS) and power splitting protocol (PS). In the former, the receiver harvest energy in the first period and then transmit the information in the remainder time. In PS protocol, the receiver split the received signal power into two streams: energy harvesting and information transmission.

There have been several papers in the literature that focus on the TS and PS protocol in the past years. In [3], the author research a decode-and-forward energy harvesting relay cognitive network using TS protocol. However the scenario is too specialized. [4] research the relay selection question using TS and PS protocol in cooperative cognitive radio network. [5] investigates a distributed power splitting architecture with the purpose of achieving the optimal sum-rate through selecting the power splitting ratios. RF energy harvesting in DF relay network is studied in [6]. In this paper, TS protocol, PS protocol and a hybrid TS-PS protocol are applied to compare and analyze outage probabilities and throughput.

In the aspect of cognitive radio sensor network, the author study the power allocation in cognitive sensor networks in [7]. However, no energy harvesting and TS protocol are considered in it. [8] develop a framework and propose a low-complexity algorithm in EHCRSN. [9] research the optimal mode selection question to maximize the throughput of the sensor node in EHCRSN. But to the best of our knowledge, there is seldom investigation of applying TS protocol in EHCRSN and using the best response algorithm to solve it. The main contributions of this paper are summarized as follows:

1. We propose a new cognitive radio sensor network architecture which discuss the question of how to select the energy harvesting time to balance the energy consumption and energy replenishment in EHCRSN.
2. We reply the time switching relaying (TSR) protocol into the cognitive users, which divides the time T into three parts: spectrum sensing phase, energy harvesting phase and data transmission phase. And we analysis the energy efficient maximization question through selecting the optimal energy harvesting coefficient.
3. We formulate this problem as a non-cooperative game. Then we use the best response algorithm to reach Nash Equilibrium and prove the good performance of our algorithm. At last, we get the result that different parameters variations have the different influence on the energy harvesting time and system utility.

The remainder of the paper is structured as follows. Section 2 describes the system model of primary user and cognitive user. In Sect. 3 we formulate the maximization question as a non-cooperative game and prove the existence and uniqueness of Nash Equilibrium. Then best response algorithm is introduced in Sect. 4. Finally Sect. 5 presents the numerical results and Sect. 6 concludes this paper.

2 System Model

We consider a cognitive radio sensor network with one primary user (PU) and N cognitive users (CUs) as illustrated in Fig. 1. The cognitive users, also called secondary users (SUs), are sensor node equipped with the ability of spectrum sensing. Assume that each cognitive radio sensor user can harvest energy and is equipped with the energy storage device. Denote $N = \{1, 2, \dots, N\}$ the set of CUs.

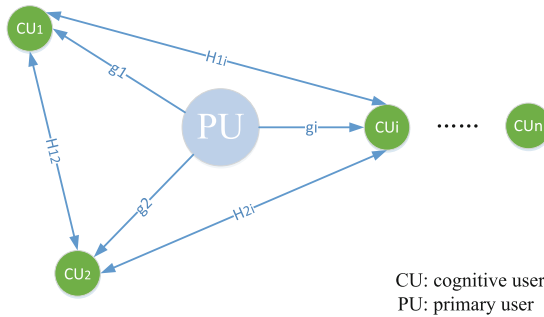


Fig. 1. The system model of the primary user and cognitive users

A. Primary user model

The primary user is work in the licensed band and shared it with cognitive users. The PU has two modes: data transmission mode and idle mode, as shown in Fig. 2(a). Because the PU’s state will always switch from transmission to idle, we consider the sum of a transmission state duration and it’s adjacent idle state duration as an analytical interval T . Assume that PU won’t always keep one state for a long time, which is the same as actual situation.

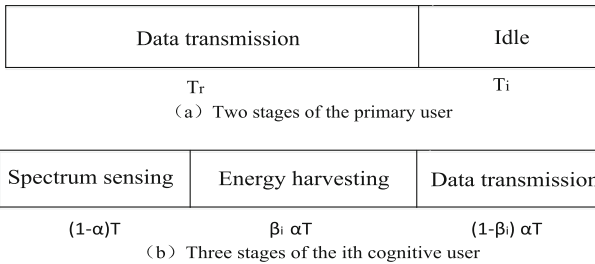


Fig. 2. The stages of primary user and cognitive users in time T

PU is regarded as a RF energy provider when it is in the data transmission. And the CUs can harvest the RF energy from the PU in this phase.

B. Cognitive user model

In Fig. 2(b), cognitive user has three states during the time T : spectrum sensing phase, energy harvesting phase, data transmission phase. Among them, α is the coefficient of spectrum sensing time and divided T into sensing phase and non-sensing phase. β is the fraction of energy harvesting time coefficient. In the first duration $(1 - \alpha)T$, CU senses the PU's state and gather the sensing result together cooperatively. In this paper, we assume the coefficient α is fixed and power consumption P_α is a constant value.

In the first duration $(1 - \alpha)T$, CU senses the PU spectrum usage information and gather the sensing result together cooperatively. In this paper, we assume the coefficient α is fixed and power consumption P_α is a constant value.

Then CU can harvest energy from the PU when the PU is in the transmission model. We consider that the CU doesn't have its own power supply and totally depends on the RF energy harvesting. And all of the CUs work in half-duplex mode, thus they can't transmit data and harvest energy at the same time. In this duration $\alpha\beta T$, the signal CUi received can be expressed as

$$y_{cui} = \sqrt{P_s} g_i x_1 + n_i^\alpha \quad (1)$$

Where g_i is the channel gain from PU to the CUi. P_s and x_1 are the fixed transmit power and the transmission information of the PU. n_i^α is the additive Gaussian noise with zero mean and $\sigma_{i,\alpha}^2$ variance. For simplicity, we ignore the influence of the Gaussian noise. The energy CUi harvested during the duration $\alpha\beta T$ can be expressed as

$$Q_i = \eta \cdot \alpha\beta_i T \cdot P_s \cdot |g_i|^2 \quad (2)$$

where η is the energy harvesting efficiency. Assume the energy Q_i will be used all to the next data transmission and spectrum sensing. The transmission power of CUi is assumed to be so small that the harvested energy is enough to use.

In the rest time $(1 - \beta_i)\alpha T$, CUi will transmit data using the harvested energy to the other CUs or the PU. Since we know the energy consumption during the sensing period is $P_\alpha(1 - \alpha)T$. We can calculate the transmission power of CUi as:

$$\begin{aligned} P_i &= \frac{Q_i - P_{\text{ses}}(1 - \alpha)T}{\alpha(1 - \beta)T} \\ &= \frac{1}{1 - \beta_i} (\eta \cdot \beta_i \cdot P_s \cdot |g_i|^2 - \frac{1 - \alpha}{\alpha} P_{\text{ses}}) \end{aligned} \quad (3)$$

C. Maximization of energy efficiency

We assumed that the cognitive users are deployed in the around of the PU. and the interference produced by other cognitive users is far greater than that from the PU. Thus the SINR of one particular cognitive user is determined by the influence of transmission power of other CUs [10]. We can write the signal-to-interference-plus-noise ratio (SINR) of the i th CU as

$$SINR_i = \frac{h_{ii} \times p_i}{\sum_{j=1, j \neq i}^n h_{ij} \times p_j + \alpha_c^2} \tag{4}$$

Where h_{ij} denote the channel gain between the CU_i and CU_j , α_c^2 is the Gaussian noise introduced by the environment. We know the $SINR_i$ is in relation to the energy harvesting coefficient vector $\beta_i = [\beta_1, \beta_2, \dots, \beta_N]$ from the Eqs. (3) and (4).

To insure the data transmission of the PU would not be affected, the interference power from CUs to PU must be limited in a tolerable range. Assume that the largest transmission power of CUs is P_{max} . Conversely, if the CUs wants to transmit information normally, its transmission power must be larger than a fixed value P_{min} . Therefore, we get the range of CU_i 's transmission power is

$$P_{min} \leq P_i \leq P_{max} \tag{5}$$

Where P_i is defined in Eq. (3), and we can get the inverse solution of β_i .

$$\frac{\alpha P_{min} + P_{ses}(1 - \alpha)}{\alpha(P_{min} + \eta P_s |g_i|^2)} \leq \beta_i \leq \frac{\alpha P_{max} + P_{ses}(1 - \alpha)}{\alpha(P_{max} + \eta P_s |g_i|^2)} \tag{6}$$

In order to simplify the description, we define the minimum and maximum value of β as β_{min} and β_{max} respectively.

On the basis of Shannon formula, we know the achievable transmission rate of CU_i is determined by the $SINR_i$ given by Eq. (4). Therefore the rate of CU_i can be obtained by

$$r_i = B \log(1 + SINR_i) \tag{7}$$

Where B is the transmission spectrum bandwidth shared by PU and CU_i . We define energy efficiency as the achievable data rate per unit power consumption [11], which can be formulated as

$$u_i(\beta) = \frac{r_i}{P_{total}} = \frac{B \log(1 + SINR_i)}{P_{ses} + P_i} \tag{8}$$

In this paper, we express the time selection problem with the goal to maximize the energy efficiency, which is a globally optimal network-wide performance problem. In actuality, this is a tradeoff of time selection between energy harvesting mode and data transmission mode. We need to solve the following network utility maximization problem

$$\begin{aligned} & \max_{\beta} \sum_{i=1}^N u_i(\beta) \\ s.t. & \frac{\alpha P_{min} + P_{ses}(1 - \alpha)}{\alpha(P_{min} + \eta P_s |g_i|^2)} \leq \beta_i \leq \frac{\alpha P_{max} + P_{ses}(1 - \alpha)}{\alpha(P_{max} + \eta P_s |g_i|^2)} \\ & 0 \leq \beta_i \leq 1 \end{aligned} \tag{9}$$

3 Non Cooperative Game and Nash Equilibrium

D. Non Cooperative Game

Game theory is a complex activity where players are contend with each other observing a series of rules [12]. In this paper, due to the interference is related to all the CUs' power, the maximization problem of each cognitive user is linking together. Make a assumption that all the CUs are selfish and rational, which means they are only interested in maximizing their own energy efficiency and have the common knowledge. Thus, question (9) can be converted as follows:

$$\begin{aligned} \max_{\beta_i} u_i(\beta_i, \boldsymbol{\beta}_{-i}) \\ \text{s.t. } \beta_i \in \mathcal{S}_i \end{aligned} \quad (10)$$

Where $\boldsymbol{\beta}_{-i} = [\beta_1, \dots, \beta_{i-1}, \beta_{i+1}, \dots, \beta_N]^T$ stands for the energy harvesting coefficients of all CUs, except the i th one. What's more, \mathcal{S}_i is the feasible set of the i th link's power splitting ratio. Next, we can model it as a non-cooperative game with N players, which can be expressed as follows:

$$g = \langle N, \{\mathcal{S}_i\}_{i \in N}, \{u_i(\rho_i, \boldsymbol{\rho}_{-i})\}_{i \in N} \rangle \quad (11)$$

- Player set $N = \{1, 2, \dots, i, \dots, N\}$: the set of N cognitive radio sensor users.
- actions $\{\mathcal{S}_i\}$: Each player i selects its energy harvesting coefficient $\beta_i \in \mathcal{S}_i$ to maximize its energy efficient. $S = \prod_{i=1}^N \mathcal{S}_i$ refer to the strategy space of N players and strategy vector $s = \{s_1, s_2, \dots, s_N\}$ is a subset of S .
- Utility function $\{u_i(\rho_i, \boldsymbol{\rho}_{-i})\}$: the utility of player i .

E. Existence of the Nash Equilibrium

Definition 1. A Nash Equilibrium (NE) exists in a non-cooperative game if and only if an strategy vectors* satisfy

$$u_i(s_i^*, s_{-i}^*) \geq u_i(s_i, s_{-i}^*) \quad \forall i \in N, \forall s_i \in \mathcal{S}_i$$

That is to say, a NE is a strategy vector with the property that any player won't have better utility by chancing its strategy. The following theorem tells us how to distinguish whether a NE exists or not for a particular game.

Theorem 1. In the game $g = \langle N, \{\mathcal{S}_i\}, \{u_i(\rho_i, \boldsymbol{\rho}_{-i})\} \rangle$, a NE exists if it have the limited players and the strategy sets \mathcal{S}_i are convex set, closed and bounded. Last the utility functions $u_i(\rho_i, \boldsymbol{\rho}_{-i})$ is continuous and quasi-concave for $\forall i \in N$.

Proposition 1. The formulated energy harvesting time selection game g exists at least one NE.

Proof. Firstly, we have mentioned that there are N players in the game totally, which meets the first condition in Theorem 1. Secondly, because the strategy sets of CUi are segments in two dimensions. It is straightforward to know that S_i is convex, closed and bounded. Besides, the utility function $u_i(\beta)$ is continuous in β . Thus, we only need to focus on the quasi concavity of $u_i(\beta)$.

If $f(x)$ is quasi-convex, $-f(x)$ is quasi-concave. So as long as we proved $-u_i(\beta)$ is quasi-convex, we can get the result that this game possesses at least one NE.

Theorem 2. A continuous function $f: \mathbb{R} \rightarrow \mathbb{R}$ is quasiconvex if and only if at least one of the following conditions is satisfied.

- f is nondecreasing.
- f is nonincreasing.
- there exists a point $c \in \text{dom } f$ which satisfy for $t \leq c$ (and $t \in \text{dom } f$), f is nonincreasing, and for $t \geq c$ (and $t \in \text{dom } f$), f is nondecreasing.

Now we perform the first-order derivative of the negative utility function,

$$f_i(\beta) = -u_i(\beta) = -\frac{B \log(1 + SINR_i)}{P_{ses} + P_i} \quad (12)$$

Through algebraic simplification, the derivative function can be expressed as

$$\begin{aligned} \frac{\partial f_i(\beta)}{\partial \beta_i} &= -\frac{\partial u_i(\beta)}{\partial \beta_i} = -\frac{\partial p_i}{\partial \beta_i} \cdot \frac{\partial u_i}{\partial p_i} = \\ &= -\frac{1}{(1 - \beta_i)^2} (\eta P_s |g_i|^2 - \frac{\alpha}{1 - \alpha} P_{ses}) \cdot B \cdot \log(e) \cdot \\ &= \frac{\frac{h_{ii} \times (p_i + P_{ses})}{\alpha_c^2 + \sum_{j=1}^n h_{ij} \times p_j} - \ln(1 + \frac{h_{ii} \times p_i}{\alpha_c^2 + \sum_{j=1, j \neq i}^n h_{ij} \times p_j})}{(p_i + P_{ses})^2} \end{aligned} \quad (13)$$

In reality, we know the primary user's transmission power is far bigger than the sensing power of CUi. So the first half of Eq. (13) $\eta P_s |g_i|^2 - \frac{\alpha}{1 - \alpha} P_{ses} > 0$ is always established and the derivative $\frac{\partial p_i}{\partial \beta_i} > 0$ is true forever. The transmission power is increasing with the increase of β_i . When the value of β_i is $\beta_a = \frac{1 - \alpha}{\alpha} \cdot \frac{P_{ses}}{\eta P_s |g_i|^2}$, we have $p_i(\beta_a) = 0$ and $\frac{\partial f_i(\beta)}{\partial \beta_i} \Big|_{\beta = \beta_a} < 0$. After analysis, we know there is only one constant β_c which satisfy $\frac{\partial f_i(\beta)}{\partial \beta_i} \Big|_{\beta = \beta_c} = 0$. And $f_i(\beta)$ is firstly decreasing and then increasing with the increasing of β_i . Therefore, we can conclude that $u_i(\beta)$ is quasi-concave and there exist at least one NE in the game.

F. Uniqueness for the NE

Definition 2. A game g is said to be supermodular if the following condition is satisfied

$$\frac{\partial^2 u_i}{\partial s_i \partial s_j} \geq 0, \forall i \neq j \in N \quad (14)$$

We have the conclusion that a NE is unique if the game is a super-modular game. Therefore, if we only need to analyze the non-negativity of differential function of the utility function. The twice differential function can be expressed as

$$\begin{aligned} \frac{\partial^2 u_i(\beta)}{\partial \beta_i \partial \beta_j} = & B \log(e) \times \frac{1}{(1 - \beta_i)^2 (1 - \beta_j)^2} (\eta P_s |g_i|^2 - \frac{\alpha}{1 - \alpha} P_{ses})^2 \\ & \times \frac{h_{ii} h_{ij} \left[p_i^2 \times h_{ii} - p_{ses} (\alpha_c^2 + \sum_{j=1, j \neq i}^n h_{ij} \times p_j) \right]}{(p_i + p_{ses})^2 (\alpha_c^2 + \sum_{j=1, j \neq i}^n h_{ij} \times p_j) (\alpha_c^2 + \sum_{j=1}^n h_{ij} \times p_j)} \end{aligned} \quad (15)$$

According to the analysis, it is concluded that whether the game is supermodular is depended on the part of $p_i^2 \times h_{ii} - p_{ses} (\alpha_c^2 + \sum_{j=1, j \neq i}^n h_{ij} \times p_j)$. After simplification, we get the necessary and sufficient condition when the above part is greater than 0.

$$SINR_i \geq \frac{p_{ses}}{p_i} \quad (16)$$

Because the sensing power is far smaller than the transmission power of cognitive users. As a result, the ratio of sensing power to the transmission power is a pretty small value and the above inequality is reasonable naturally. Finally, we can conclude that this game is a super-modular game and only exist one NE.

4 Best Response Algorithm

In this section, we will introduce a distributed best response algorithm which can achieve the unique NE from any initial state. The aim of this algorithm is to maximize the energy utility through all the users changing their energy harvesting coefficient β_i one by one until a suitable termination condition is satisfied.

First, when $t = 0$, set each player an initial value $\beta_i(0)$ from its domain and compute their utility value $u_i(0)$. Then, each player will update its energy harvesting time coefficient $\beta_i(t)$ according to Eq. (17) in a fixed sequence while other players $\beta_{-i}(t)$ remain unchanged.

$$\beta_i^* = \arg \max_{\beta_i \in S_i} u_i(\beta_i, \beta_{-i}) \quad (17)$$

Finally, the iterative process will stop until the following termination condition is satisfied.

$$\sum_{i=1}^N [\beta_i(t+1) - \beta_i(t)]^2 \leq \eta \quad (18)$$

Where η is a extremely small constant. The algorithm can be programmed as follows.

Algorithm1. Best Response Algorithm

Initialization: $t=0$, total-error=100000, $\beta_i(0) \in S_i$, $i = 1, 2, \dots, N$

while $total-error > \eta$ **do**

for $i=1:N$

find the optimal $\beta_i^*(t)$, $\beta_i(t+1) = \beta_i^*(t)$

end for

$total-error = \sum_{i=1}^N [\beta_i(t+1) - \beta_i(t)]^2$

$t \leftarrow t + 1$

end while

5 Numerical Results

In this section, we will present the numerical results to illustrate and demonstrate the superiority of the algorithm. We select eight cognitive users to analyze and the channel gain from PU to the CUs are from interval $[0.3, 0.6]$. The channel gain h_{ii} and h_{ij} between CUs vary from interval $[0.8, 1.2]$ and $[0.05, 1.15]$ independently. The recent research shows that the achieved power of RF harvester can achieve 5 mW under 1000 MHz. And we set the shared spectrum is 1000 MHz. The minimum and maximum transmission power of CU i are $P_{\min} = 0.1$ mW and $P_{\max} = 5$ mW. For the following examples if not mentioned otherwise, we set $P_s = 20$ mW, $P_{ses} = 0.2$ μ W, $\alpha = 0.2$, $\eta = 0.5$ and $\alpha_c^2 = 1$ mW.

Figures 3 and 4 show that the best response algorithm can converge to a unique NE since the initial value of CU1 choose different values. It is observed that the convergence process of CU1' energy harvesting coefficient β_1 and the utility when the initial condition is set in different values. It can be seen from Fig. 4 that the utility of CU1 is rising constantly until reaching the NE.

Figure 5 depicts the utility comparison between the initial condition and the final condition achieving the NE. It shows the result that each player's final utility is much larger than its corresponding utility in initial condition, which illustrates the superiority of our algorithm. Next, we will analysis the impacts of one parameter (e.g.: η , P_{ses} and N) change on the solution of NE and the utility value.

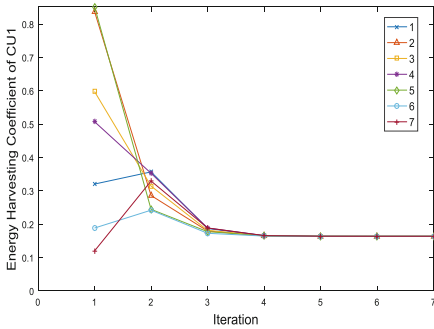


Fig. 3. Convergence process of β_1

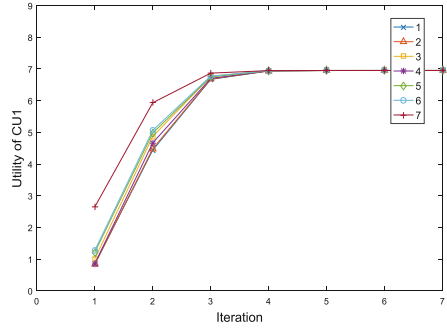


Fig. 4. Convergence process of u_1

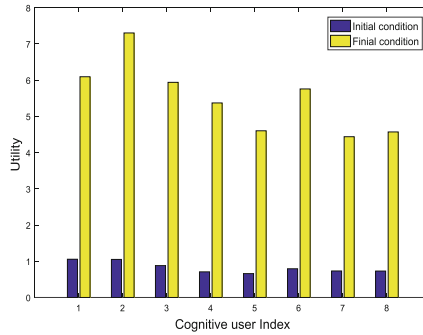


Fig. 5. Utility comparison between the initial condition and the final condition

Figure 6 show the final energy harvesting time coefficient β_i and energy efficiency u_i versus the energy harvesting efficiency η . It can be observed from Fig. 6(a) that β_i decreases as η increases, because a larger η means less harvesting time to achieve the

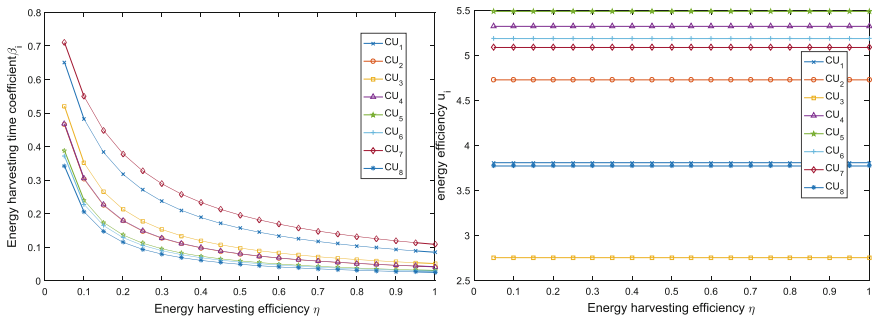


Fig. 6. The impact of energy harvesting efficiency on (a) energy harvesting time coefficient and (b) energy efficiency with $N = 8$, $P_{ses} = 0.2 \mu W$ and $\alpha = 0.2$

needed transmission power. And we can see from Fig. 6(b) that η has no effect on the final energy efficiency.

Figure 7 show the influence of CUi’s sensing power on energy harvesting time coefficient and energy efficiency. We can see that the energy harvesting time coefficient β_i keep unchanged first and then increasing with the growth of CUi’s sensing power. Meanwhile, the energy efficiency keep unchanged first and then decreasing. This is because when the sensing power is less than a certain threshold, the change of sensing power is so small in relation to the transmission power that has no effect on the NE. But with the growing of sensing power and when it is bigger enough, the CUi need more harvesting energy to support it and the energy efficiency decrease based on the Eq. (8).

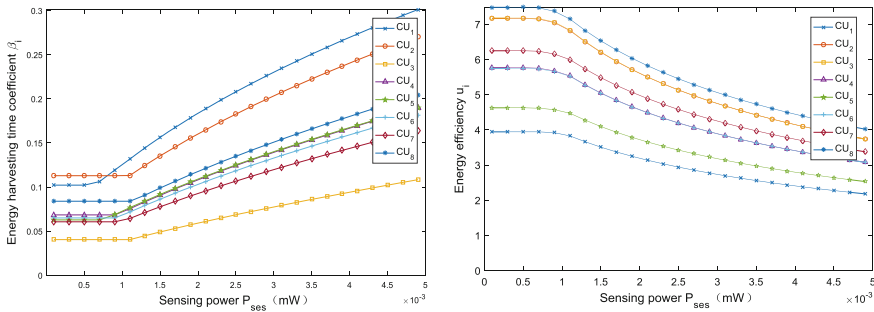


Fig. 7. The impact of CUi’s sensing power on (a) energy harvesting time coefficient and (b) energy efficiency with $N = 8$, $\eta = 0.5$ and $\alpha = 0.2$

At last, we will analysis to the final total energy efficiency $u_{all} = \sum_{i=1}^N u_i$ versus the number of cognitive users N . Figure 8 replies that the total energy efficiency of the two curve is almost the same when there are two players and then have opposite tendency. And we can see from the blue curve that with the increasing of N , the total utility after game increases first and then decreases. Because when the user number is lower than a certain value, the interference from other users is relatively small and the total utility increase with increasing the number. However, with a further increase of N , the interference become stronger, which causes the direct decreasing of the total utility.

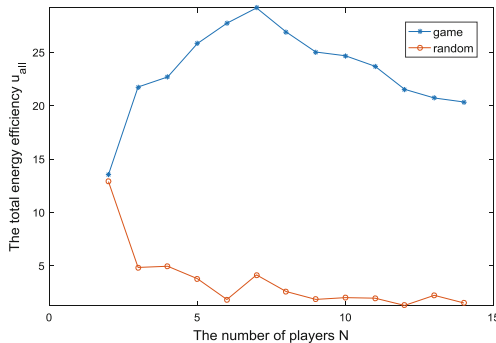


Fig. 8. The total energy efficiency versus different number of players with $P_{ses} = 0.2 \mu W$ and $\eta = 0.5$ (Color figure online)

6 Conclusion

In this paper, we have researched how to select the optimal energy harvesting time to achieve the maximize energy efficiency using non-cooperative game. First of all we proved the existence and uniqueness of Nash equilibrium, and then we got the converging process to achieve the NE with the best response algorithm. The results demonstrate that the best response algorithm can converge to the same equilibrium from different initial values. Besides, non-cooperative game yields a good utility performance to address this energy harvesting time coefficient selection question. At last we studied the effect of various system parameters on the results of Nash equilibrium.

Acknowledgment. This work was supported by the National Natural Science Foundation of China (No. 61571059), and the State Major Science and Technology Special Projects of China under Grant 2016ZX03001017-004.

References

1. Ku, M.L., Li, W., Chen, Y., et al.: Advances in energy harvesting communications: past, present, and future challenges. *IEEE Commun. Surv. Tutorials* **18**(2), 1384–1412 (2016)
2. Nasir, A.A., Zhou, X., Durrani, S., et al.: Relaying protocols for wireless energy harvesting and information processing. *IEEE Trans. Wirel. Commun.* **12**(7), 3622–3636 (2012)
3. Mousavifar, S.A., Liu, Y., Leung, C., et al.: Wireless Energy Harvesting and Spectrum Sharing in Cognitive Radio, pp. 1–5 (2014)
4. He, J., Guo, S., Wang, F., et al.: Relay selection and outage analysis in cooperative cognitive radio networks with energy harvesting. In: *ICC 2016 IEEE International Conference on Communications*, pp. 1–6. IEEE (2016)
5. Chen, H., Li, Y., Jiang, Y., et al.: Distributed power splitting for SWIPT in relay interference channels using game theory. *IEEE Trans. Wirel. Commun.* **14**(1), 410–420 (2015)
6. Elmorshedy, L., Leung, C., Mousavifar, S.A.: RF energy harvesting in DF relay networks in the presence of an interfering signal. In: *ICC 2016 IEEE International Conference on Communications*, pp. 1–6. IEEE (2016)
7. Chai, B., Deng, R., Cheng, P., et al.: Energy-efficient power allocation in cognitive sensor networks: a game theoretic approach. In: *Global Communications Conference*, pp. 416–421. IEEE (2012)
8. Zhang, D., Chen, Z., Awad, M.K., et al.: Utility-optimal resource management and allocation algorithm for energy harvesting cognitive radio sensor networks. *IEEE J. Sel. Areas Commun.* **34**(12), 3552–3565 (2016)
9. Park, S., Heo, J., Kim, B., et al.: Optimal mode selection for cognitive radio sensor networks with RF energy harvesting. In: *IEEE, International Symposium on Personal Indoor and Mobile Radio Communications*, pp. 2155–2159. IEEE (2012)
10. Wei, Y., Ren, C., Song, M., Yu, R.: The offloading model for green base stations in hybrid energy networks with multiple objectives. *Int. J. Commun. Syst.* **29**(11), 1805–1816 (2016)
11. Wei, Y., Wang, X., Fialho, L., Bruschi, R., Ormond, O., Collier, M.: Hierarchical power management architecture and optimal local control policy for energy efficient networks. *J. Commun. Netw.* **18**(4), 540–550 (2016)
12. Lasaulce, S., Debbah, M., Altman, E.: Methodologies for analyzing equilibria in wireless games. *Signal Proc. Mag. IEEE* **26**(5), 41–52 (2009)

Traffic Paralysis Alarm System Based on Strong Associated Subnet

Chen Yu^{1(✉)}, Shaohui Zhu¹, Hanhua Chen¹, Ruiguo Zhang²,
Jiehan Zhou³, and Hai Jin¹

¹ Cluster and Grid Computing Lab, Big Data Technology and System Lab,
Services Computing Technology and System Lab, School of Computer Science and Technology,
Huazhong University of Science and Technology, Wuhan 430074, China
{yuchen, hjin}@hust.edu.cn

² Siemens Ltd., Beijing, China
ruiguo.zhang@siemens.com

³ University of Oulu, Oulu, Finland
jiehan.zhou@oulu.fi

Abstract. Urban traffic congestion is a major problem for urban transportation management all over the world. However, traditional research focuses only on detection and description of urban traffic situations, which are not enough for improving urban traffic conditions. In this paper, we distinguish two types of traffic congestion: traffic paralysis and traffic jams. The former is the state that traffic is almost stagnant in a large area and on many roads, and it will take a long time before recovering the normal traffic flow. In comparison, a traffic jam has less negative effect on traffic flow and recovers easily. According to this, we propose a traffic paralysis alarm system based on strong associated subnet to alert traffic paralysis incidents. The system orients to city road network, mines association rules between road segments, constructs the strong associated subnets and detects traffic anomalies with floating car GPS data. We analyze two parameters of our proposed system with a true dataset generated by over 2000 taxicabs in Zhuhai and explain our system with a simulation experiment on VISSIM.

Keywords: Traffic paralysis · Association rule · Strong associated subnet
Alarm

1 Introduction

With the rapid development of urbanization and the remarkable improvement of living quality in China, both the population and the number of private cars has increased significantly in cities. It is reported that by the end of 2013 the urban population of China accounted for 53.73% of the total population, and urbanization is expected to reach more than 60% by 2020. In addition, the number of private cars rose from 18.48 million in 2005 to 123.39 million in 2014, according to the data from the National Bureau of Statistics of China.

Urbanization means the movement of a large part of the rural population to cities. Urbanization improves the living standards of many people, promotes economic

development, and is more conducive to improved development of industry, education, science and technology, culture, etc. But urbanization also brings with it huge challenges, such as air pollution, public health, and traffic congestion. Because of its impact on pollution and public health, traffic congestion is a key point in successful urbanization.

With the development of the *Intelligent Transportation System (ITS)*, there has been a lot of research on traffic congestion [1–3], but most of these studies are just to discriminate or describe the traffic situations. These studies are based on a two value state: traffic is either free or congested. But there is a big difference between a traffic jam and traffic paralysis. We should consider them as two different states when we analyze traffic situations in the real world.

Figure 1 is our developed traffic state transition diagram. Area A shows the traditional traffic state transition when a traffic anomaly occurs, such as a car rear-end collision, it will cause a traffic jam. Each traffic anomaly itself is random, which is why the current research on urban traffic congestion issues remains at the level of identification and description of traffic situations, and makes it difficult to carry out further research. Therefore, we re-analyze the traffic state, add a paralysis state, and then get the new traffic state transition diagram shown in Fig. 1. In the new traffic state transition diagram, a transformation from a traffic jam to a traffic paralysis does not always occur, it depends on the following three factors:

- *Spatial-temporal Location*: the time point and the location of the traffic jam occurred.
- *Road Network Topology*: the road network topology of the jammed road segment and its surrounding road segments.
- *Traffic Flow*: the size of traffic flow on the jammed road segment.

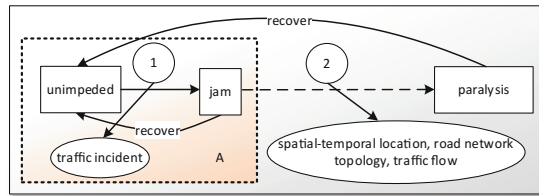


Fig. 1. Traffic state transition diagram

These three factors determine whether a traffic jam can escalate to traffic paralysis, and they provide the possibility for us to predict traffic paralysis.

We propose a traffic paralysis alarm system based on a strong associated subnet which consists of three modules, namely, data preprocessing, strong associated subnet mining, and traffic anomaly detection. The proposed system mainly depends on the strong association between the road segments in a strongly associated subnet.

2 Related Work

The proposed system is mainly related to three issues: map-matching, association rule mining, and traffic anomaly detection.

2.1 Map-Matching Problem

Irregularities in GPS positioning systems prevent the direct use of GPS data. Map-matching algorithms correct the deviation of GPS data and matches GPS data to road segments by which to render the actual trajectories of vehicles.

Typical geometric algorithms include point-point, point-line, and line-line algorithms. A point-point algorithm matches GPS data to the nearest point on surrounding road segments. The accuracy of such algorithms is unpredictable.

In [4, 5], topological algorithms consider the connectivity of the road, adjacency relationships, and other attributes (such as one-way roads) to match. Paper [5] gives a C-measure based algorithm, which uses distance, angle, and connectivity to calculate match reliability.

Advanced algorithms [6–9] generally use more complex computational models, have greater accuracy, and can meet some special needs. The ST-Matching algorithm proposed for GPS trajectories with a low-sampling-rate (e.g., one point every 2–5 min) [6], takes into account the geometric and topological structures of road networks and the temporal/speed constraints of the trajectories. Paper [7] proposes a Hidden Markov Model-based algorithm which accounts for measurement noise and the structure of the road network. In our paper, we use the algorithm proposed in [7] to correct GPS data.

2.2 Association Rule Mining

Association rule is one of the most active and widely used knowledge types in the field of data mining. Now there are many association rule mining algorithms.

Apriority is the first typical rule mining algorithm, and many other algorithms based on the idea of apriority after that. Paper [10] points out that the early iterations of Apriority-based algorithms is the dominating factor for the overall mining performance, and proposes an effective hash-based algorithm that can generate smaller candidates. FP-Growth in [11] does not generate candidates and only requires two scans of transaction database. It compresses the transaction information to the FP-tree in which the support degree of item-sets is in descending order.

There are many algorithms for different scenarios on association rule mining in the years of research and applications. For example, paper [12] presents an algorithm to mine rules in databases which are partitioned among many computers that are distributed over a wide area. Paper [13] summarizes the existing algorithms that address the issue of mining association rules from data streams.

2.3 Traffic Anomaly Detection

A traffic anomaly is anything blocking the normal traffic flow, such as broke-down vehicle, rear end collision, or other accident. There is research on detecting traffic anomalies [1, 3]. A traffic-flow-pattern based algorithm which focuses on traffic volume and velocity on roads is proposed [1]. An anomaly detected by the algorithm is represented by a subgraph of a road network where drivers' routing behaviors significantly differ from their typical patterns. An *improved nonparametric regression algorithm* (INPRA) is presented [3]. Standard Deviation Algorithm is used to calculate and check the standard deviation between prediction traffic data generated by INPRA and current traffic data: if the standard deviation is larger than a predefined threshold, the algorithm will send out a signal for a possible incident.

3 Architecture and Design

3.1 System Overview

In this section, we will present the architecture and design of the proposed system. The proposed system consists of three modules shown in Fig. 2: A. pre-processing module; B. strong associated subnet mining module; C. traffic anomaly detection module.

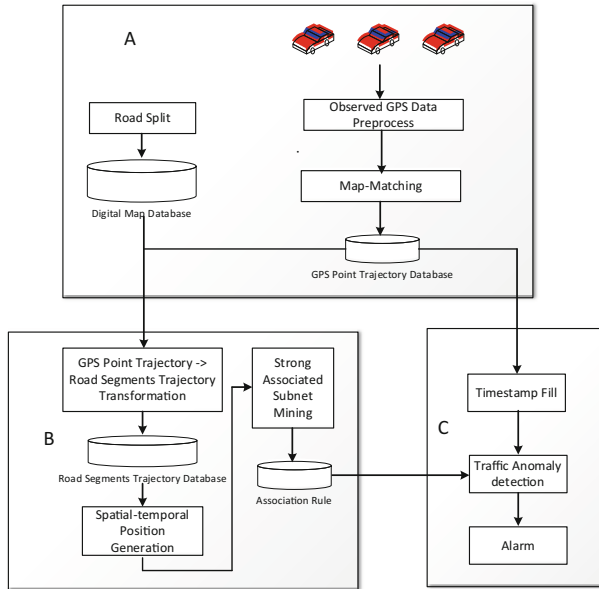


Fig. 2. Architecture of traffic paralysis alarm system

The module A mainly pre-processes digital map data, large text, and GPS data. First, a digital map database is constructed by importing digital map data into a spatial database and splitting each road into road segments. Second, the collected data must be

preprocessed because every text file of stored one-day taxi GPS data of Zhuhai city is bigger than 11 GB, and they are unordered and redundant. Therefore, we need to remove redundancy and sort by taxi ID and timestamp. Finally, deploying the map-matching server and importing GPS point data and corrected GPS point data into spatial database as GPS point trajectory database.

The main purpose of module B is to mine strong associated subnet. First, road segment trajectory database is constructed by the ways of transferring GPS point trajectories as $\{p_1, p_2, \dots, p_n\}$ to road segments trajectories as $\{r_1, r_2, \dots, r_m\}$, p_i represents a GPS point and r_i represents a road segments. Then, the most frequent passed is selected as seeds through top- k road segments and these seeds are expanded into strong associated subnets.

Module C is responsible for detecting traffic anomalies occurred at strong associated subnets. The travel speed of road segments in strong associated subnets is monitored and checked: if there occurs an extended low-speed situation, the proposed system will regard this phenomenon as a traffic anomaly and send out a signal.

3.2 Pre-processing Module

This module includes two parts: constructing a digital map database and map-matching for setting up a GPS point trajectory database.

The process of constructing a digital map database can be summarized as the following steps:

- Step 1: Install PostGIS plug-in for the PostgreSQL object-relational database.
- Step 2: Download digital map data from OpenStreetMap using QGIS tools.
- Step 3: Import digital map data into spatial database using ogr2gor tools.
- Step 4: Install PgRouting plug-in for the PostgreSQL and split road into road segments with it.

There are three steps in setting up GPS point trajectory database module:

- Step 1: Remove redundancy and sort by taxi ID and timestamp for these large text files.
- Step 2: Modify source code of *Open Source Routing Machine* (OSRM) map-matching server, then compile and deploy it.
- Step 3: Map-matching for every taxi GPS point, then import observed and corrected GPS data together into spatial database.

3.3 Strong Associated Subnet Mining Module

This module, combined with digital map database, expands the most frequent top- k road segments into strong associated subnets. As summarized by the following steps.

- Step 1: Load a corrected GPS point trajectory as $point_{Tr} = \{p_1, p_2, \dots, p_n\}$, for every point p_i of this trajectory, determine the road segment r_i that point p_i located at, then we can gain the corresponding road segments trajectory of $point_{Tr}$ as $roadseg_{Tr} = \{r_1, r_2, \dots, r_m\}$. At the same time, update the number of trajectory of r_i .

- Step 2: Save road segment trajectories to road segments trajectory database.
- Step 3: According to the number of trajectories of every road segment, select the most frequent top- k road segments as seeds.
- Step 4: Expand seeds into strong associated subnets. Finally, these strong associated subnets are used as association rules to guide the alarm system.

3.4 Traffic Anomaly Detection Module

We monitor only these road segments that strong associated subnets contain, and regard these road segments as interesting road segments. It can be summarized as three steps.

- Step 1: Select these corrected GPS point trajectories which pass through interesting road segments from GPS point trajectory database.
- Step 2: Fill timestamp of every point of the selected trajectory according to the corresponding observed GPS point trajectory.
- Step 3: For every interesting road segment, we have the trajectories passed through it. This tells us how long every taxicab passes through it and the travel distance of every taxicab. With this knowledge, we can calculate and monitor travel speed of every interesting road segment, and check the successive low speed situation.

4 Strong Associated Subnet Mining and Traffic Anomaly Detection

In this section, we will introduce two key algorithms of traffic paralysis alarm system based on strong associated subnet: strong associated subnet mining algorithm and traffic anomaly detection algorithm.

4.1 Strong Associated Subnet Mining Algorithm

We firstly define six operators used by strong associated subnet mining algorithm.

Preliminaries

Definition 1 (*cntRoadseg*): $cntRoadseg(r_x)$ is the number of the road segment trajectories that contain road segment r_x .

Definition 2 (*cntShared*): $cntShared(r_x, r_y)$ represents the number of road segment trajectories that contain both road segment r_x and r_y . It is the quantized form of the association between road segment r_x and r_y . Under the same conditions, the bigger the score of this operator, the stronger the association between road segment r_x and r_y .

Definition 3 (*cntU*): $cntU(r_x, r_y)$ represents the sum of these road segment trajectories that contain any one of road segment r_x and r_y .

Definition 4 (*support*): this operator is defined as the following:

$$support(r_x, r_y) = cntShared(r_x, r_y) / cntU(r_x, r_y) \quad (1)$$

In the process of mining strong associated subnet, we check the possibility of road segment r_y which is not in a strong associated subnet becoming a part of strong associated subnet. If road segment r_x is adjacent to r_y and is a part of strong associated subnet, $support(r_x, r_y)$ is the first we check, it must satisfy the following:

$$support(r_x, r_y) \geq \lambda \quad (2)$$

where λ is a predefined threshold and it will be analyzed in Sect. 5.1.

Definition 5 (correlation): $correlation(r_x, r_y)$ represents the correlation between road segment r_x and r_y . This operator is defined as the following:

$$correlation(r_x, r_y) = cntShared(r_x, r_y) / 2 \times (1/cntRoadseg(r_x) + 1/cntRoadseg(r_y)) \quad (3)$$

Definition 6 (cluster): The cluster degree of subnet V is the average of the correlation among these adjacent road segments in subnet V . This operator is defined as the following:

Algorithm 1: $cluster(r, V)$

Output: the cluster degree of subnet V after r added into

```

1:  $clus = 0.0$ ;
2: for  $r_x$  in  $V$  loop
3:    $listRx = loadAdjacent(r_x, V)$ ;
4:   for  $r_y$  in  $listRx$  loop
5:      $clus += correlation(r_x, r_y)$ ;
6:   end loop;
7: end loop;
8:  $clus /= 2$ ;
9:  $listR = loadAdjacent(r, V)$ ;
10: for  $r_e$  in  $listR$  loop
11:    $clus += correlation(r, r_e)$ ;
12: end loop;
13: return  $clus / (V.size + 1)$ ;

```

In Algorithm 1, $loadAdjacent(r, V)$ is used to load the adjacent road segments of r in subnet V . $cluster(r, V)$ is cluster degree of the assumed subnet which is made up of subnet V and road segment r . The second thing we check in the process of mining strong associated subnet is ensuring that cluster degree of strong associated subnet satisfies the following:

$$cluster(r, V) \geq \mu \quad (4)$$

where μ is the predefined threshold and it will be analyzed in Sect. 5.1.

Details of Algorithm

Strong associated subnet mining algorithm mainly consists of two steps. First, selecting the most frequent top-k road segments as strong associated subnet seeds. Second, checking if there exists a road segment in strong associated subnets that adjacent to one or more road segments which are not in strong associated subnets and meet the thresholds for expansion: if there exists one, we call this one as scalable road segment, and add those meeting thresholds into strong associated subnets. This process is iterative until there does not exist one meeting the requirements. More precisely, the algorithm process is the following:

Algorithm 2: SASM(minSup, minCls, maxNetsize)

```

1: generate seeds and insert them into table Subnets
2: do
3:    $r, netid = \text{loadScalable}()$ ;
4:   do
5:      $r_i = \text{loadAdjacent}(r, netid)$ ;
6:     if the size of  $netid \geq \text{maxNetsize}$  then
7:       break;
8:     end if;
9:     if  $r_i$  is already in  $netid$  then
10:      continue;
11:    end then;
12:    if  $\text{support}(r, r_i) < \text{minSup}$  then
13:      continue;
14:    end then;
15:    if  $\text{cluster}(r_i, netid) < \text{minCls}$  then
16:      continue;
17:    end then;
18:    insert  $r_i$  into Subnets;
19:     $i++$ ;
20:    while ( $i < \text{number of adjacent road segments of } r$ )
21:  while(there is still a scalable road segment )

```

4.2 Traffic Anomaly Detection Algorithm

In this section, we use the flow chart to present our successive low-speed based traffic anomaly detection algorithm. The proposed algorithm takes 30 s as a calculation cycle and computes average travel speed for every road segment in strong associated subnets in every cycle. This algorithm runs forever once started. It iteratively computes travel time and checks if there occurs a traffic anomaly.

5 Experiment and Analysis

In this section, we first analyze two parameters, λ and μ , of strong associated subnet mining algorithm. Then, a simulation experiment based on VISSIM is carried out for explaining the theory of traffic paralysis alarm system based on strong associated subnet (Fig. 3).

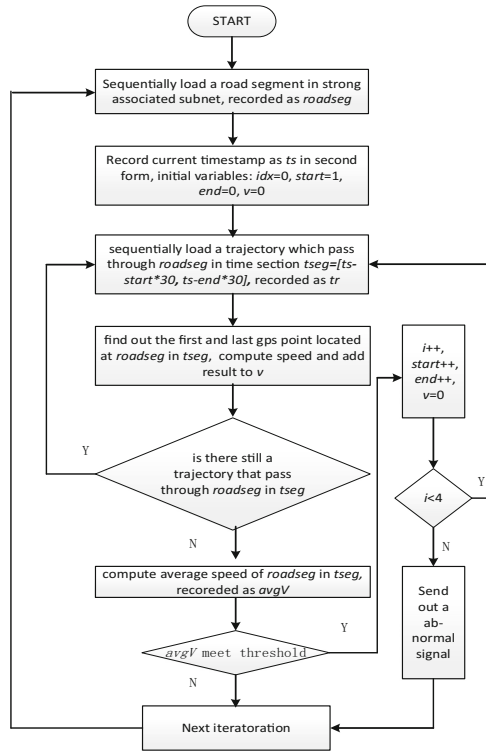


Fig. 3. A successive low-speed based traffic anomaly detection algorithm

5.1 Strong Associated Subnet Mining Algorithm Parameter Analysis

In the system testing process, we find that the scores of these operators, support and correlation, are low in most of the time, and the low score of operator correlation directly causes the score of operator cluster to be also low. Therefore, we perform an analysis based on the GPS data of Zhuhai, and get the conclusion that the smaller the sampling rate is, the smaller these operators' scores are.

The original GPS data of Zhuhai is sampled every 10 s. We manually dilute the original data and get another three datasets with sampling intervals of 20 s, 40 s, and 80 s. For each of the most frequent top-200 road segments, calculating separately average score of the operator support based on four datasets. The statistical distribution of the

average score of operator support is shown in Fig. 4. Similarly, the statistical distribution of the average score of operator correlation is shown in Fig. 5.

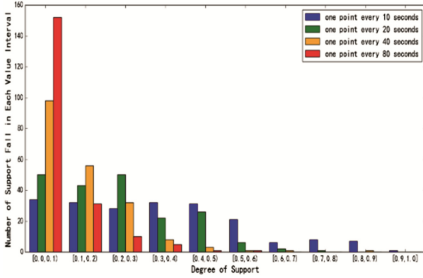


Fig. 4. Distribution of score of operator support

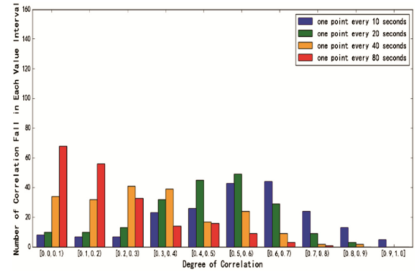


Fig. 5. Distribution of score of operator correlation

It is easy to observe from the above two figures that the sampling rate is higher, the distribution peaks are at further to the right positions.

5.2 Simulation Experiment Analysis

The idea of our proposed system is that when a traffic anomaly is detected on a strong associated subnet, alarming immediately for this subnet to reduce the traffic entering this subnet, to avoid the transformation from traffic jam to traffic paralysis. We want to discover whether reducing the traffic entering this subnet helps avoid the transformation. We perform an experiment with VISSIM and the result can be concluded as: when a traffic anomaly occurs on a strong associated subnet, reducing the traffic entering this subnet can decrease the influence of the traffic anomaly.

We simulate a traffic incident occurring at the 300th s and resolved at the 1500th s and collected a delay time dataset and a queue length dataset under different traffic volumes shown in Figs. 6 and 7.

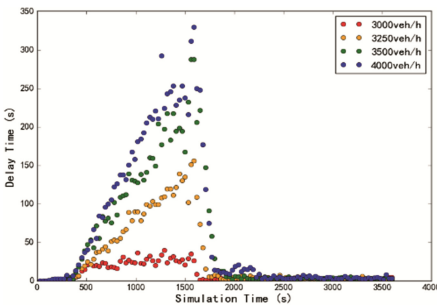


Fig. 6. Delay time under different traffic volume

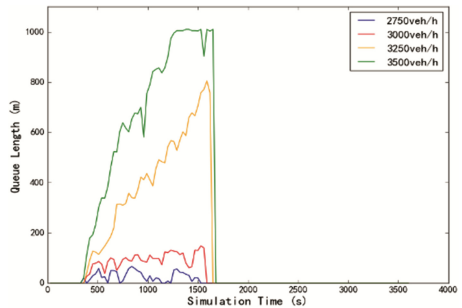


Fig. 7. Queue length under different traffic volume

It is obvious that the delay time and queue length increase remarkably as the traffic volume rises. The delay time and queue length clearly show the traffic anomaly's influence. Therefore, we can get the conclusion declared above: reducing the traffic entering this subnet can decrease the influence of the traffic anomaly.

6 Conclusion and Future Work

In this paper, we propose a traffic paralysis alarm system based on strong associated subnet. The system mainly designs and implements strong associated subnet mining algorithm and traffic anomaly detection algorithm based on the taxicabs GPS data of Zhuhai. The former is used to mining strong associated subnets with trajectories on road network, and the latter calculates travel speed of interesting road segments periodically and checks if there exists a successive low speed situation on interesting road segments: if there exists one, the algorithm sends out a signal.

Two experiments are carried out in this paper. One examines the case of low score of operators and concludes that the smaller the sampling rate is, the smaller these operators' scores are. The second experiment uses VISSIM to simulate traffic situations when a traffic incident occurred. Under different traffic volume, we analyze delay time and queue length, concluding that reducing the traffic entering this subnet can decrease the influence of the traffic anomaly.

In future work, the proposed system should be improved to solve real-time GPS data stream, how we store, pre-process, and analyze the data stream may need further research.

Acknowledgements. The work is partly supported by NSFC (No. 61472149), the Fundamental Research Funds for the Central Universities (2015QN67) and the Wuhan Youth Science and Technology Plan (2016070204010132).

References

1. Pan, B., Zheng, Y., Wilkie, D., Shahabi, C.: Crowd sensing of traffic anomalies based on human mobility and social media. In: Proceedings of the 21st ACM International Conference on Advances in Geographic Information Systems, pp. 334–343 (2013)
2. Chen, S., Wang, W., Zuylen, H.V.: Construct support vector machine ensemble to detect traffic incident. *Expert Syst. Appl.* **36**(8), 10976–10986 (2009)
3. Tang, S., Gao, H.: Traffic-incident detection-algorithm based on nonparametric regression. *IEEE Trans. Intell. Transp. Syst.* **6**(1), 38–42 (2005)
4. Velaga, N.R., Quddus, M.A., Bristow, A.L.: Developing an enhanced weight-based topological map-matching algorithm for intelligent transport systems. *Transp. Res. Part C Emerg. Technol.* **17**(6), 672–683 (2009)
5. Xu, Y., Wang, Z.: Improvement and implement of map matching algorithm based on C-measure. In: Proceedings of the 2010 2nd IEEE International Conference on Information Management and Engineering, pp. 284–287 (2010)

6. Lou, Y., Zhang, C., Zheng, Y., Xie, X., Wang, W.: Map-matching for low-sampling-rate GPS trajectories. In: Proceedings of the 17th ACM International Symposium on Advances in Geographic Information Systems, pp. 352–361 (2009)
7. Newson, P., Krumm, J.: Hidden Markov map matching through noise and sparseness. In: Proceedings of the 17th ACM International Symposium on Advances in Geographic Information Systems, pp. 336–343 (2009)
8. Yuan, J., Zheng, Y., Zhang, C., Xie, X., Sun, G.Z.: An interactive-voting based map matching algorithm. In: Proceedings of the Eleventh International Conference on Mobile Data Management, pp. 43–52 (2010)
9. Li, Y., Huang, Q., Kerber, M., Zhang, L., Guibas, L.: Large-scale joint map matching of GPS traces. In: Proceedings of the 21st ACM International Conference on Advances in Geographic Information Systems, pp. 214–223 (2013)
10. Park, J.S., Chen, M.S., Yu, P.S.: An effective hash-based algorithm for mining association rules. In: Proceedings of the 1995 ACM International Conference on Management of Data, pp. 175–186 (1995)
11. Han, J., Fu, Y.: Discovery of multiple-level association rules from large databases. In: Proceedings of the 21th International Conference on Very Large Data Bases, pp. 420–431 (1995)
12. Wolff, R., Schuster, A.: Association rule mining in peer-to-peer systems. In: Proceedings of the 3rd IEEE International Conference on Data Mining, pp. 363–370 (2003)
13. Nan, J., Le, G.: Research issues in data stream association rule mining. *ACM SIGMOD Record* **35**(1), 14–19 (2006)

Fault Recovery Algorithm Based on SDN Network

Yi Zhang^{1,2(✉)}, Yifei Wei¹, Ruqin Huang², Bo Gu¹, Yue Ma¹, and Mei Song¹

¹ School of Electronic Engineering, Beijing University of Posts and Telecommunications, Beijing 100876, People's Republic of China

{zzyy, weiyifei, gubo, mayue, songm}@bupt.edu.cn

² Institute for Network Sciences and Cyberspace, Tsinghua University, Beijing, China
15652964297@163.com

Abstract. Nowadays, diversified demand of different users is becoming a focus for improving network performance. Traditional network can't meet the demand, so we turn to Software-Defined Network architecture, which realizes virtualization and abstraction of underlying hardware resource via separation of control and data planes. First, we propose a virtual network mapping algorithm to allocate link resources, using Ant Colony algorithm to find the optimal solution. Then we develop a virtual network fault recovery mechanism to satisfy the need of end users with different fault tolerance. The mechanism is achieved by the failure recovery algorithm named NumMap Algorithm, which provide varied network reliability levels for users of varied priority. By the end of paper, we conduct simulation experiments to evaluate the algorithms with performance metrics such as failure repairing ratio, success running ratio, and working link resource utilization. The results demonstrate the superiority of the proposed algorithm compared with ResRemap and ResBackup algorithms.

Keywords: Virtual network · Software-Defined Network · Mapping algorithm

1 Introduction

Network virtualization is a new technology which can solve the problem of the internet and support the development of new technology. Important advantages of this technique is different network can share the underlying physical infrastructure. The virtual network is above the physical layer. Virtual nodes and virtual links constitute a virtual network. Network topology, the use of technology, the provision of services for different virtual networks are different.

The purpose of network virtualization is to facilitate the configuration and management and to facilitate the construction of new network technology. Resource management has become the key to achieve the advantages of the network virtualization technology. The resource management in the network virtualized environment should rationally design the management structure and the resource scheduling algorithm to realize the efficient sharing of the underlying physical network resources. In ensuring the virtual network user resource request conditions, greatly improve the network resource utilization.

The traditional network of network construction cannot meet the diverse needs of different business. Then SDN network is proposed, control and forwarding separation, to achieve the underlying hardware abstraction. SDN is a new network architecture proposed by Stanford University and is the main application architecture of this paper. With network virtualization technology, each experimental user can customize a virtual network and construct a different topology for each virtual network. The underlying physical network forms a network resource pool through node virtualization and link virtualization and allocates resources for the virtual network to improve network resource utilization.

Based on the exchange equipment, through the definition of a common standard interface to achieve data plane and control plane separation, to facilitate the researchers in the real network environment for technical research. The SDN forwarding plane is separated from the control plane. The experimenter can access the underlying physical device with a defined common protocol and programmatically control the forwarding path of the data in the network. Network virtualization technology can divide the physical network into multiple virtual networks. Each virtual network can run different routing protocols and provide different services.

The actual situation of the physical network often causes the failure due to natural causes or malicious attacks and other non-natural, affecting the normal operation of the user's business. And the previous algorithm is to enhance the physical network resource utilization, there is no study of network failure. Aiming at the reliability problem of virtual network, there is a remapping mechanism of virtual node and virtual link, which not only can improve the receiving rate of virtual network but also benefit the load balance of network. Migrating a failed virtual link to a backup path by pre-building the backup path is one of the methods. Another way, building a unified backup resource pool which can dynamically allocate backup resources for virtual links, and improve the utilization of physical resources. These algorithms use different mechanisms to improve the reliability of virtual networks. The cost of reserving backup resources in advance is too high in the first method. In the second method, a new path is found when the fault occurs, resulting in a low failure rate. In this paper, we propose a fault recovery algorithm based on the number of users for the virtual network mapping, and compare the network performance with the link remapping algorithm and the backup path construction algorithm.

2 Mapping Model Base on SDN

2.1 Network Description

Virtual network requests are mapped to the underlying physical network that is made up of different devices. The management creates a virtual network mapping request based on the needs of the user and sends the request to the physical layer. Finally, the virtual network provider can provide the customized virtual network service to the user (Table 1).

Table 1. Parameters of the mapping models

N_s	Node set
E_s	Link set
N_v	Virtual node set
E_v	Virtual link set
$N^{fwd}(n_s)$	Physical node forwarding sources $n_s \in N_s$
$N^{fwd}(n_v)$	Virtual node forwarding sources $n_v \in N_v$
$N^{ctrl}(g)$	Controller resources $n_s \in g$
$N^{ctrl}(n_v)$	The required control resources
$B(l_s)$	Bandwidth resources for each physical link $l_s \in E_s$
$B(l_v)$	The required bandwidth resources for each virtual link $l_v \in E_v$

2.2 Mapping Description

Node mapping

In the SDN network, not only the physical node can meet the forwarding resource requirements of the virtual node, but also the domain of the physical node must meet the control resource requirements of the virtual node. In addition, the most classic mapping is used. Virtual nodes and physical nodes are one-to-one mapping. The remaining resources of the physical node should more than the required forwarding resources, and the remaining control resources in the area should more than the required control resources.

$$N_r^{fwd}(n_s^j) \geq R^{fwd}(n_v^i) o_{ij} = 1 \tag{1a}$$

$$N_r^{ctrl}(g_k) \geq R^{ctrl}(n_v^i) o_{ij} = 1, n_s^j \in g_k \tag{1b}$$

$$\sum_{n_s^j \in N_s'} o_{ij} = 1 \quad \forall n_v^i \in N_v \tag{1c}$$

$$\sum_{n_s^j \in N_v} o_{ij} \leq 1 \quad \forall n_s^j \in N_s' \tag{1d}$$

Link mapping

Find all nodes that meet the requirements, select one from the node that satisfies the requirement as an endpoint. Use the Dijkstra algorithm to find the shortest path to meet the bandwidth. Finally, link mapping is implemented.

$$B_r(l_s^m) \geq R(l_v^i), \forall l_s^m \in Ph_{s,D} Ph_{s,D} = M(l_v^i) \tag{2a}$$

$$B_r(l_s^m) = B(l_s^m) - \sum_{l_s^m \in M(l_v^i)} R(l_v^i) \tag{2b}$$

2.3 Objective Function

In order to improve the efficiency of the use of physical network resources, that is, using as little physical resources as possible to carry as many virtual networks. This paper takes $S(G_s)$ as the objective function that is the residual resource value of underlying network resources.

$$S(G_s) = \alpha \left[\sum_{n_s^j \in n_s} N_r^{fwd}(n_s^j) + \sum_{g_k \subseteq G} N_r^{ctrl}(g_k) \right] + \beta \sum B_r(l_s^m) \quad (3)$$

$N_r^{fwd}(n_s^j)$ represent the remaining forwarding resources of the node, $N_r^{ctrl}(g_k)$ is the remaining control resource for the area, $B_r(l_s^m)$ A represents the remaining bandwidth resources of the link, α, β is resource conversion weight between node CPU resource and the link bandwidth. $S(G_s)$ denote the physical resources available, which is in direct proportion to the number of virtual networks supported. Therefore, set the optimization target to $\max\{S(G_s)\}$.

3 Virtual Network Algorithm

In this paper, the ant colony algorithm is used to solve the virtual network mapping problem in the software defined network model.

The Algorithm of Virtual Network

1. Initialization();
 2. VN_Creation();
 3. For i=1 to N;
 4. { Update_probability();
 5. For ant=1 to M
 6. { Node_Map();
 7. Link_Map();
 8. if(S(local_solution)>S(global_solution))
 9. global_solution=local_solution;
 10. }
 11. Update_info();
 12. }
-

According to the above algorithm, in each iteration process, select the network resource surplus value of the largest feasible solution as the current cycle optimal solution according to $S(G_s)$. Then update the pheromone of the virtual node to the physical node according to the optimal solution. After N iterations, the M feasible solutions generated by the initialization can eventually converge to the approximate global optimal solution.

The pheromone update to the physical node n_s^i is as follows:

$$\tau_{ij}(t) = \rho\tau_{ij}(t-1) + \Delta \quad (4)$$

ρ is the persistence of pheromone, Δ is the increment of pheromone.

$$\Delta = \frac{1}{S(p^{best})} \sigma \quad (5)$$

p^{best} is the optimal solution of this cycle, $S(p^{best})$ is the objective function value of the optimal solution, σ is the influence factor of the optimal solution on pheromone.

4 Fault Recovery Mechanism

4.1 Fault Recovery Algorithm Based on User Number(NumMap)

This paper presents a new fault recovery mechanism based on the previous network mapping model. The number of users is different during different period. So we can implement the strategy according to the number of users. When the number of users is low, there are more free link resources. We use the backup path construction algorithm for most users to ensure the reliability of the network as far as possible. The remaining users take the faulty link remapping algorithm when a failure occurs. When the number of users is large, the free link resources are less. So leave backup path for a small number of users. Most failed users are remapped. Most failed users should take the faulty link remapping algorithm. For each time slice, we will update the strategy based on the number of users. Change the proportion of pre-backup users to normal users. In this paper, we believe that the failure process is subject to uniform distribution.

The free link resources vary with the number of users. A fault recovery algorithm based on the number of users is proposed, that is, the traffic of the pre-backup users affected by the fault is migrated to the backup path. And the common user's faulty link is remapped. The algorithm can improve the fault repair rate and network resource utilization rate.

Mapping rules

Node mapping

$$N_r^{fwd}(n_s^i) \geq R^{fwd}(n_v^i) o_{ij} = 1 \quad (6a)$$

$$N_r^{ctrl}(g_k) \geq R^{ctrl}(n_v^i) o_{ij} = 1, n_s^j \in g_k \quad (6b)$$

$$\sum_{n'_s \in N'_s} o_{ij} = 1 \quad \forall n'_v \in N'_v \quad (6c)$$

$$\sum_{n'_v \in N'_v} o_{ij} \leq 1 \quad \forall n'_s \in N'_s \quad (6d)$$

Link mapping

For low level users, just meet

$$B_r(I_s^m) \geq R(I_v^i), \forall I_s^m \in Ph_{S,D}, Ph_{S,D} = M(I_v^i) \quad (7a)$$

$$B_r(I_s^m) = B(I_s^m) - \sum_{I_v^i \in M(I_v^i)} R(I_v^i) \quad (7b)$$

For pre-backup users, link mapping is not only required to meet bandwidth requirements, but also to ensure that there is no overlap with the backup link.

$$B_r(I_s^m) \geq R(I_v^i), \forall I_s^m \in Ph'_{SD} \quad (8a)$$

$$Ph'_{SD} \cap Ph_{SD} = \text{NULL} \quad (8b)$$

Input: $l_{SD}, W_b(l_{SD})$

Output: P_{SD}

- (1) Determine the level of the virtual network carried on the faulty link;
- (2) If it is a high level user, judge the availability of the backup path P_{SD} ;
If it is a low level user, skip to (4);
- (3) Determine if the backup path is available. If it is not available, set P_{SD} to NULL.
Skip to 7);
- (4) Remove the faulty link l_{SD} ;
- (5) Using the shortest path algorithm to find an alternative path P_{SD} . Alternative path and fault path have the same endpoint. If it is not found, set P_{SD} to NULL and skip to 7);
- (6) $B_r(I_s^m) = B_r(I_s^m) - W_b(l_{SD})$, Update the remaining bandwidth resources of the link;
- (7) If P_{SD} is NULL, the virtual network recovery failed. Otherwise, return the recovery path;

The algorithm is run one by one for all virtual networks which affected by the failure, and then the repair is complete.

4.2 ResBackup Algorithm

The res-backup algorithm is to find all the backup paths in advance and enable the backup path when the network fails. If the backup path is available, the backup path is returned. If the backup path is not available, the virtual network recovery fails. This algorithm has a high recovery rate, but the backup path takes up too much resource, resulting in reduced network utilization and degraded network performance.

S and D represent the two endpoints of the link; $W_b(l_{SD})$ indicates the bandwidth occupied by the backup resource on the link; G_l is represented as a collection of backup links. The algorithm is described as follows:

Input: $l_{SD}, W_b(l_{SD}), G_l$

Output: P_{SD}

- (1) Remove the faulty link in G_s ;
- (2) Determine if the backup path is available. If it is not available, set P_{SD} to NULL and skip to 4);
- (3) $B_r(l_s^m) = B_r(l_s^m) - W_b(l_{SD})$, Update the remaining bandwidth resources of the link;
- (4) If P_{SD} is NULL, the virtual network recovery failed. Otherwise, return the recovery path;

4.3 ResRemap Algorithm

The ResRemap algorithm is a timely repair when the link fails. When the network fails, first remove the fault link from the set, calculate whether to find the link which has the same endpoint with the faulty link. If it can be found, update the resource, restore the path, and if it was not found, the virtual network recovery fails.

Input: $l_{SD}, W_b(l_{SD}), G_l$

Output: P_{SD}

- (1) Remove the faulty link in G_s ;
- (2) Using the shortest path algorithm to find an alternative path P_{SD} . Alternative path and fault path have the same endpoint. If it is not found, set P_{SD} to NULL and skip to 4);
- (3) $B_r(l_s^m) = B_r(l_s^m) - W_b(l_{SD})$, Update the remaining bandwidth resources of the link;
- (4) If P_{SD} is NULL, the virtual network recovery failed. Otherwise, return the recovery path;

5 Simulation Parameters

5.1 Simulation Parameters

In this paper, we use MATLAB to generate the underlying physical network and virtual network request topology. 25 nodes are generated in the space of $200 * 200$, and some nodes are generated according to the random function, which are connected to each other by 0.5 probability (Table 2).

Table 2. Parameters configuration of models

Parameter	Configuration
Node control resources	a uniform distribution of [50–100]
Link bandwidth resources	a uniform distribution of [50–100]
Virtual network request	The time unit is a time window, and the intensity of the Poisson process is 4
Virtual network survival time	The mean is the exponential distribution of 10 time windows
Number of virtual network nodes	a uniform distribution of [2–10]
Required control resources	Each request is subject to uniform distribution [0–20]
Required bandwidth resources	Each request is subject to uniform distribution [0–20]
Link failure	Each request is subject to uniform distribution [0–50]
Node resource weight	Set to 1
link resource weight	Set to 1
Number of ants	70
Number of iterations	70
The persistence of pheromones (ρ)	0.7
The initial value of pheromone (τ)	5

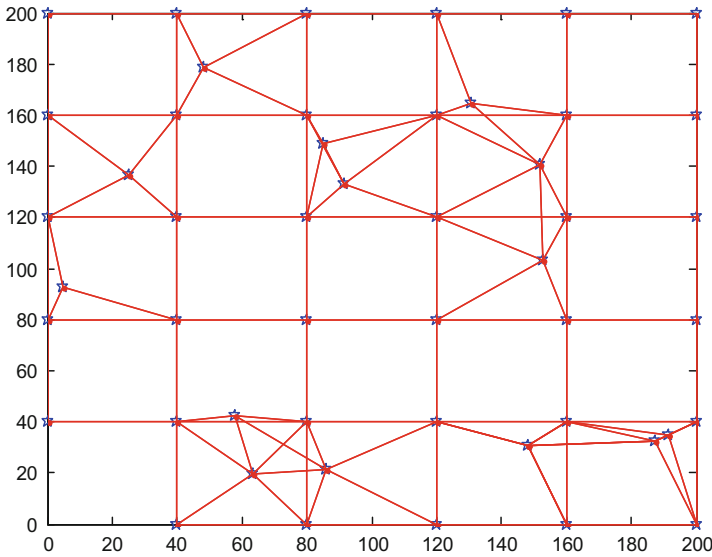


Fig. 1. Virtual network topology

5.2 Evaluation Standard

In order to evaluate the efficiency and performance of the virtual network more conveniently, we define a series of parameters as the standard to evaluate the advantages and disadvantages of the virtual network mapping algorithm (Fig. 1).

(1) Acceptance ratio

Acceptance ratio refers to how many requests are successfully mapped. It is an important criterion for evaluating the performance of the algorithm. N_{acreq} is the number of accepted requests. N_{alreq} is the number of all requests. R_{ac} is the acceptance ratio.

$$R_{ac} = \frac{N_{acreq}}{N_{alreq}} \quad (9)$$

(2) Fault recovery rate

N_{sf} is the number of failures that were successfully repaired. N_{alf} is the number of all failure. R_{fr} is the fault recovery rate

$$R_{fr} = \frac{N_{sf}}{N_{alf}} \quad (10)$$

(3) Link resource utilization

η_{lr} represent the link resource utilization. N_{norm} is the normal link resources. N_{total} indicates the total resources of links.

$$\eta_{lr} = \frac{N_{norm}}{N_{total}} \quad (11)$$

6 Simulation Results

6.1 Acceptance Ratio

When $\gamma = 0.1$ ($\gamma = \frac{\lambda_f}{\lambda}$), the request strength is not high, because the faulty link remapping algorithm does not have a backup link, so there are more free network resources, the virtual network has the highest success rate. The backup link of the ResBackup algorithm takes up many link resources, so the network running the lowest success rate. The NumMap algorithm backs up some users' links and takes up part of the additional link resources, so the R_{ac} is between the two algorithms.

The user's requests get more when $\gamma = 0.5$. The success rate of ResRemap algorithm is still the highest. But the R_{ac} decreased from 67% to 55%. And The ResBackup algorithm back up link in advance, taking up a lot of link resources, so the the change of running success rate is not obvious for virtual network. The R_{ac} of the virtual network operation of the fault recovery algorithm is slightly lower, but still between the two algorithms (Fig. 2).

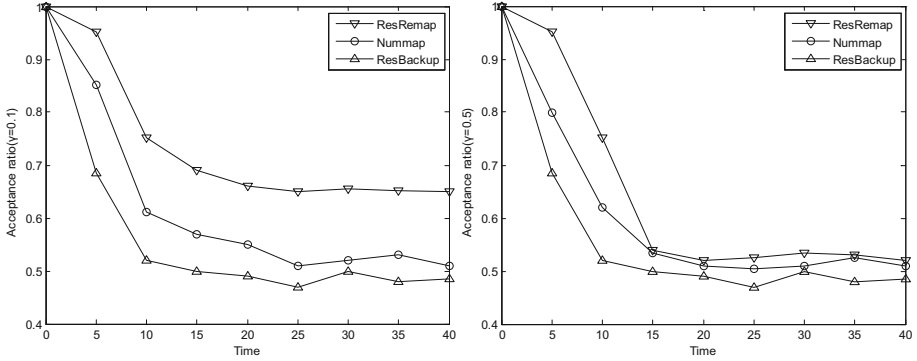


Fig. 2. Acceptance rate for three algorithms

6.2 Fault Recovery Rate

When $\gamma = 0.1$, the high-level user virtual network failure repair rate close to 100%. Low-level user fault repair rate is basically stable at 77%. The Resbackup algorithm has the highest repair rate, close to 100%. The fault repair rate of ResRemap algorithm is basically stable at 76%. When $\gamma = 0.5$, the number of users increased significantly, but the fault repair rate of the the high-level users is still about 95%, the fault repair rate of low-level users stabilized at 60% or more. The fault repair rate of ResBackup algorithm is higher. Because the backup path algorithm has set up a backup path for a virtual network that is successfully mapped before a link failure occurs (Fig. 3).

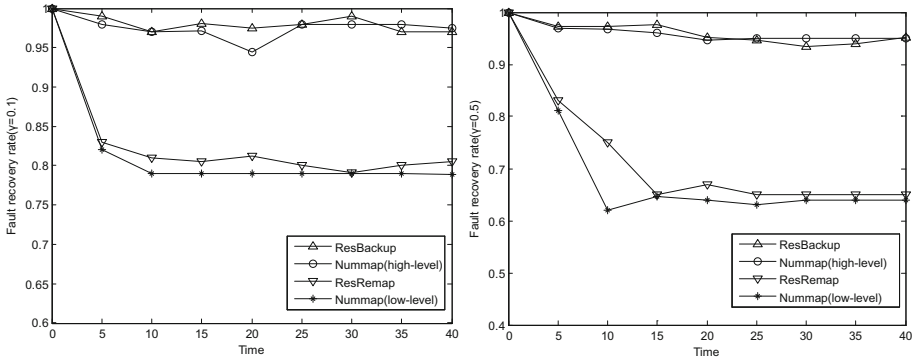


Fig. 3. Fault recovery rate for three algorithms

6.3 Link Resource Utilization

The number of users is large when $\gamma = 0.1$. Because it was when the link malfunctioned that ResRemap started to repair, there is no backup link to seize resources, so η_{lr} is the highest, reaching 50%. ResBackup takes up a lot of link resources, which backup link,

so η_r is the lowest. Fault recovery algorithm reached 45%, based on user number, backed up part of the user's link according to the number of users, which link resource rate is between the two algorithms above. In the case of $\gamma = 0.1$, link resource utilization declined (Fig. 4).

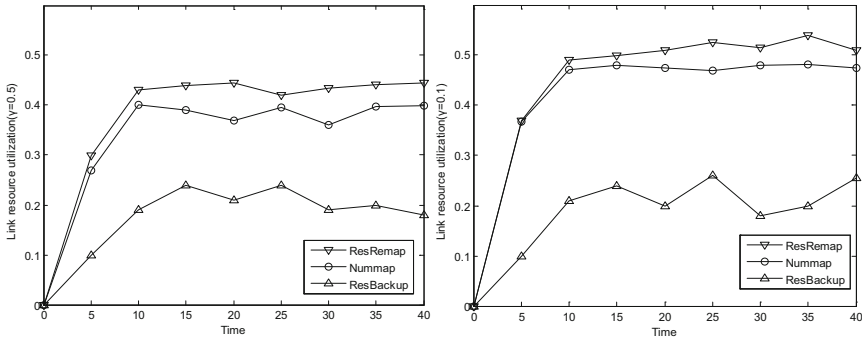


Fig. 4. Link resource utilization for three algorithms

7 Conclusion

The virtualized network represented by SDN network can meet the diversified business needs of different users, support multiple routing protocols, protect the security of user information, and promote the evolution of traditional Internet architecture to the next generation architecture. In this research, based on the premise of single link failure, which is the most prone to network in the network, based on Network reliability requirements diversity from users, we designed a fault recovery algorithm based on number. Finally, we proved the superiority of the algorithm from the aspects of virtual network fault repair rate, successful operation rate of virtual network and utilization of work link resource.

Acknowledgements. The authors would like to thank the reviewers for their detailed reviews and constructive comments, which have helped improve the quality of this paper. This work is supported by the National Natural Science Foundation of China under (Grant No. 61471055).

References

1. Karakus, M., Durrezi, A.: A survey: control plane scalability issues and approaches in Software-Defined Networking (SDN). *Comput. Netw.* **112**, 279–293 (2017)
2. Bardgett, J.A., Miguez, M.A., Wierzbowski, P.: Network management system generating virtual network map and related methods. US2015043378, 12 February 2015
3. Tootoonchian, A., Ganjali, Y.: HyperFlow: a distributed control plane for OpenFlow. In: *Proceedings of the USENIX INM Workshop on WREN* (2010)
4. Luo, Y., Chen, X., Wang, J.: A virtual network embedding algorithm for providing stronger connectivity in the residual networks. *J. Netw.* **8**(4), 779–786 (2013)

5. Yeganeh, S.H., Ganjali, Y.: Kandoo: a framework for efficient and scalable offloading of control applications. In: Proceedings of the ACM SIGCOMM Workshop on HotSDN, pp. 19–24 (2012)
6. Chai, R., Dong, X.Y., Ma, J., et al.: An optimal IASA load balancing scheme in heterogeneous wireless networks. In: 6th International ICST Conference on Communications and Networking in China, pp. 714–719 (2011)
7. Huang, T., Liu, J., Chen, J., Liu, Y.: A topology-cognitive algorithm framework for virtual network embedding problem. *China Commun.* **4**, 73–84 (2014)
8. Mijumbi, R., Serrat, J., Rubio-Loyola, J., et al.: Dynamic resource management in SDN-based virtualized networks. In: 10th International Conference on Network and Service Management (CNSM), 17–21 November 2014, Rio de Janeiro, Brazil, 1st International Workshop on Management of SDN and NFV Systems (ManSDN/NFV), 21 November 2014, Rio de Janeiro, Brazil, pp. 412–417 (2014)
9. Bays, L.R., Oliveira, R.R., Buriol, L.S., Barcellos, M., Gaspary, L.P.: A toolset for efficient privacy-oriented virtual network embedding and its instantiation on SDN/OpenFlow-based substrates. *Comput. Commun.* **82**, 13–27 (2016)
10. Khan, A., An, X., Iwashina, S.: Virtual network embedding for telco-grade network protection and service availability. *Comput. Commun.* **84**, 25–38 (2016)
11. Li, Y., Zhao, Y., Zhang, J., Yu, X., Chen, H., Zhu, R., Zhou, Q., Yu, C., Cui, R.: First field trial of Virtual Network Operator oriented network on demand (NoD) service provisioning over software defined multi-vendor OTN networks. *Optical Fiber Technol.* **33**, 22–29 (2017)
12. Xing, C., Lan, J., Hu, Y.: Virtual network with security guarantee embedding algorithms. *J. Comput.* **8**(11), 2782–2788 (2013)
13. Arakawa, S.I., Minami, Y., Koizumi, Y., Miyamura, T., Shiimoto, K., Murata, M.: A managed self-organization of virtual network topology controls in WDM-based optical networks. *J. Optical Commun.* **32**(4), 233–242 (2011)
14. Sun, G., Yu, H., Li, L., Anand, V., Di, H.: The framework and algorithms for the survivable mapping of virtual network onto a substrate network. *IETE Tech. Rev.* **28**(5), 381–391 (2011)
15. Heisswolf, J., Zaib, A., Weichslgartner, A., König, R., Wild, T., Teich, J., Herkersdorf, A., Becker, J.: Virtual networks – distributed communication resource management. *ACM Trans. Reconfigurable Technol. Syst. (TRETS)* **6**(2), 8 (2013)

Sensor Location Verification Scheme Based on Range-Free Localizations in WSNs

Chunyu Miao^{1(✉)}, Lina Chen¹, and Qingzhang Chen²

¹ College of Xingzhi, Zhejiang Normal University, Jinhua, China
netmcy@zjnu.cn

² College of Computer, Zhejiang University of Technology, Hangzhou, China

Abstract. Localization is a pivotal technology in wireless sensor networks and location information of sensor nodes is essential to location-based applications. In the beacon-based localization, the reliability of beacons' location information is critical to the quality of network service. In this paper, we study the influences of drifting beacons the network localization. So according to this scenario mentioned above, we propose a distributed and lightweight beacons locations verification algorithm based on neighborhood-similarity (BLVNS), which utilizes similarity of the beacons' neighborhood in different time slot to recognize drifting beacons. The whole algorithms can be applied to the static and dynamic WSNs to improve the accuracy of range-free localization. Experiment results show that our algorithms can recognize unreliable beacons with detection rate higher than 90%.

Keywords: WSNs · Reliable localization · Drifting beacons
Range-free localization

1 Introduction

Wireless sensor networks (WSNs), which consist of a large number of sensor nodes, have been widely used in military and human daily life, e.g. surveillance, environmental monitoring system and medical health [1]. Localization is one of the most essential research issues in WSNs because the sensed information without location is insignificant, in some scenarios such as environment monitoring, target tracking, and geographical routing [2]. To acquire the locations of sensor nodes, we can either mount nodes with GPS receiver or predefine nodes' positions manually in deployment. Because of relatively high price and energy-extensive consumption, GPS receivers may not be available for power-limited and low-price WSN, and the second method is not available for large scale WSN. As a result, we always predefine a small part of nodes' locations manually in deployment, which are called beacon nodes. And other nodes are called unknown nodes. Take the location of beacons as reference, the normal sensor nodes can estimate their locations using some certain localization algorithms. These localization algorithms can be divided into Range-Based localization algorithms and Range-Free localization algorithms [3]. The former assumes the distances between sensors and beacons can be estimated by using different measurements, such as TDoA, ToA, AoA

and RSSI [4–7]. These algorithms can usually provide higher positioning accuracy with higher hardware cost. While the latter estimates location of normal nodes based on the features of networks, such as hop counts [8], topology of network [9], etc.

In the study of localization of static WSN, we usually assume that beacons' locations are reliable. Nevertheless, for many WSN systems deployed in unstable environments, all nodes may be moved unexpectedly and Beacons have hardware failures or be captured to provide false locations. The drifting beacons are called unreliable beacons. The locations of drifting normal nodes can be re-localized by re-invoking localization algorithms. But when unreliable beacons' locations are used in re-localize process, it will seriously degrade the accuracy of re-localization and affect the quality of network service. So, recognizing and filtering out these unreliable beacons becomes one of the most important research issues in node localization of WSNs.

To solve these problems mentioned above, we proposed a distributed and lightweight beacons locations verification algorithm based on neighborhood-similarity, which use the similarity of the beacons' neighborhood in different time slot to verify which beacons are drifting.

2 Related Works

At present, the existing study of reliable localization in WSNs is divided into robust localization algorithms [10] and unreliable beacons filter algorithms [11]. The former is applicable in some scenes, where there exist the interference of ranging information or small movement of beacons. The main idea of these algorithms is reducing the environment interference of localization. The latter algorithms verify beacons locations to recognize and filter out the unreliable beacons. As a result, unreliable beacons filter algorithms are more universal and can be used in localization algorithms to ensure localization accuracy.

In [12], it proposed a point to point location verification algorithm, which can be applied to range-based algorithm. But the nodes are equipped with GPS receiver. DJ. He et al. proposed a location verification algorithm based on TOA to eliminate abnormal range value, which can be applied to Range-Based localization algorithms [13]. Kuo et al. proposed beacon movement detection (BMD) algorithm to detect the unexpected movements of beacons [14]. The basic idea of BMD algorithm is to let the beacons record the variances of RSSI measurement results between each other and report to a calculation center to determine the moved beacons. Like all other centralized algorithms, BMD algorithms will bring a heavy communication burden and need a sink node or a computer with a strong ability to calculate, which is not fit for WSN. There are also some related works, which use the location of the hidden checked nodes to verify the locations of beacons, which are also a centralized algorithm and needs involvement of additional nodes [15]. In [16], by using rigid theory to exclude the abnormal location of beacons, it can provide reliable localization results. However, the rigid theory relies on high accuracy of range and the algorithm's computation is too heavy. Ravi Garg et al. eliminated the beacons, which provide a larger descent gradient during the localization, to improve the credibility of localization. The algorithm did not consider the reference

of the Locations of normal nodes so that it can use in beacon-sparse networks [17]. Yawen Wei et al. presented a location verification probabilistic model based on the mutual observation between neighbor nodes, which achieved a better result [18]. In [19], it developed a distributed neighbor nodes score mechanism based on variation of RSSI to identify the moved beacons. However, all of above methods can't be suitable for Range-Free algorithms and solve single problem.

3 Problem Statement

3.1 System Model and Assumptions

We assume that there are two types of nodes deployed in the network: beacons and sensors. The beacons know their locations in advance. The sensors do not know their locations, which are also called unknown nodes. But they can estimate locations by using localization algorithms with beacons' locations. All nodes are mounted with RSSI transceiver. All nodes can be moved unexpectedly. Since drifting unknown nodes are always existed, we need to re-localized the network.

Besides, we assume all nodes' communication ranges have the same radius. Notice that environmental interruptions and permutations exist, so that neighborhood observation is not always symmetric. Our algorithm also can solve such asymmetry problem. In the initialized localization, we assume that beacons are reliable. And each node can participate in the algorithm calculation. During the calculation, nodes are static. In the most cases, the drifting nodes are 10%–20% of the total nodes. Unreliable beacons' percentage is not over that 50% of beacons [20]. For conveniently introducing algorithm, our notations are introduced in Table 1.

Table 1. Notations

S_i	Node i
B_i	Beacon i
$ID(i)_t$	At t time, the set of node i 's neighbors
$Nei(i, j)_t$	At t time, the common set of node i 's and node j 's neighbors
$DisRank(i, j)_t$	At t time, the actual distance coefficient between node i and node j
$EstDisRank(i, j)_t$	At t time, the estimated distance coefficient between node i and node j
$EstDis(i, j)_t$	At t time, the estimated distance between node i and node j
$IDSame(i)_{(t, t+1)}$	In the $(t, t + 1)$, the change of $ID(i)_t$ and $ID(i)_{t+1}$
$neiv(i)_t$	At t time, a vector to store $DisRank(i, j)_t, j \in ID(i)_t$
$Relation(i, j)_t$	At t time, the relationship of between node i and node j

3.2 Unreliable Beacons Models

At first, in this paper two kinds of unreliable beacons are defined as follows:

Drifting Beacons: In some application scenarios, after deployment of network and completion of localization, all nodes may be moved unexpectedly. Among these drifting

nodes, beacons are called drifting beacons. As an example, Fig. 1 shows a scenario where beacon B2 is moved, whose broadcast location doesn't match its actual location. So during re-localization, if re-invoking localization algorithms utilize B2's location, it can degrade the accuracy of re-localization.

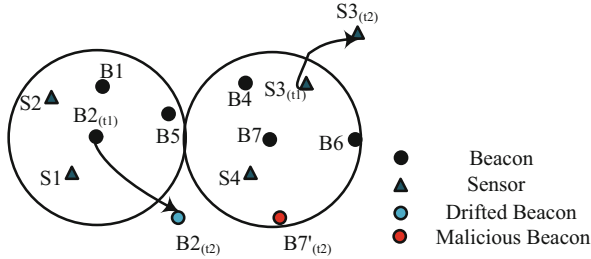


Fig. 1. Unreliable beacons models

3.3 Problem Model

Drifting beacons lead to degrade accuracy of re-localization. Before re-localizing the network, we should recognize and filter out the unreliable beacons. We assume that only a small part of beacons are unreliable beacons, the number of which is defined as h . The set of unreliable beacons is $A_d = \{a_k : k = 1 \dots h, h \ll m\}$. The set of beacons is A_d and the number of beacons is m . A'_d is denoted as the set of unreliable beacons verified by proposed verification algorithm $g(\bullet)$, so $g(A_d) = A'_d$. In this paper, we design a location verification algorithm $g(\bullet)$ to make A'_d close to A_d , i.e.:

$$\text{Min} |A_d - A'_d|$$

4 DV-Hop Localization Algorithm and Hop Count Correction

In this section, we describe the DV-Hop localization algorithm and how to correct hop count by using RSSI technology.

4.1 DV-Hop Localization Algorithm

Niculescu et al. [21] proposed the DV-Hop localization algorithm by utilizing distance vector routing mechanism. It has three phases [22]:

In the first phase, the network employ a typical distance vector routing mechanism. Beacons flood their locations throughout the network with the initial hop-count of 0. Each node that relays the message increase the hop-count by one. After the flooding procedure, every node can obtain the minimum hop-count to each other.

In the second phase, after obtaining the locations and hop-count information to all other beacons, each beacon estimates the average distance per hop. B_i calculates the

average distance per hop, called H_i , using the formula (1). Where (x_i, y_i) is the coordinate of B_i , h_{ij} is the hop-count from B_i to B_j . Then, H_i will also be flooded to sensors near to B_i .

$$H_i = \frac{\sum_{i \neq j} \sqrt{(x_i - x_j)^2 + (y_i - y_j)^2}}{\sum_{i \neq j} h_{ij}} \quad (1)$$

In the last phase, before conducting the self-localization, each sensor estimates the distance to each beacon based on its hop-count and the H to this beacon. After obtaining all the distance information, each sensor conducts the triangulation or maximum likelihood estimation to estimate its own location.

4.2 Hop Count Correction

In this section, we utilize the RSSI technology to correct the hop count between nodes, which reflects the distance proximity between nodes. In the recent study of DV-Hop localization algorithm, many papers utilize the RSSI technology to correct the hop count between nodes [22, 23]. In this paper, we use this idea to correct the hop count to help nodes get the distance proximity with their neighbors.

The coverage area of WSNs is large and the environments of different regions are different, but in some scenarios, the environment is relatively stable, such as the range of node and its neighbors. Based on this assumption, we can utilize the RSSI technology to correct the hop count.

At first, each node transmits the information of RSSI to its neighbors. So each node gets the RSSI values of its neighbors. Secondly, each node normalize the RSSI values, using the formula (2). $Rssi(i, j)_t$ represents the RSSI value between S_i and S_j , and $\min(Rssi(i, m)_t)$, $m \in ID(i)_t$, is the minimum of these RSSI values. For RSSI value is form -95 dbm to -55 dbm, the $rssi$ is a constant and set as -50 dbm. It is convenient for the proposed algorithms to calculate similarity. At last, each node gets the distance coefficients with its neighbors. Besides, if S_i can't communicate with S_j , $DisRank(i, j)_t = 0$.

$$DisRank(i, j)_t = \frac{Rssi(i, j)_t - rssi}{\min(Rssi(i, m)_t) - rssi}, m \in ID(i)_t \quad (2)$$

5 BLVNS Algorithm

In this section, we describe beacons locations verification algorithm based on neighborhood-similarity. The BLVNS uses similarity of the beacons' neighborhood in the different time slot to recognize drifting beacons. The neighborhood reflects in two aspects: the set of neighbors and the distances between the node and its neighbors. Besides, BLVNS can effectively minimize the influences of drifting neighbors.

5.1 Neighborhood Relationship

(1) *Set of neighbors*

All nodes may be moved unexpectedly. When one node is moved, its neighbors are changed. As an example, Fig. 2 shows a scenario where B_2 is moved in the (t_0, t_1) . At time t_0 , its neighbors are S_5, S_4 and S_6 . But at time t_1 , its neighbor is only S_5 . Its neighbors are changed obviously. We denote sensor S_i 's change of neighbors by $IDSame(i)_{(t,t+1)}$ in the $(t, t + 1)$, using the formula (3).

$$IDSame(i)_{(t,t+1)} = \frac{|ID(i)_t \cap ID(j)_t|}{|ID(i)_t \cup ID(j)_t|} \tag{3}$$

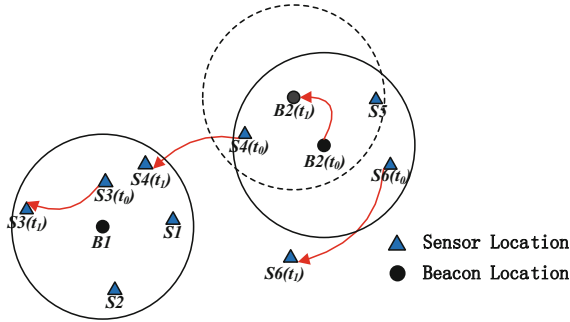


Fig. 2. The process of drifting nodes

(2) *Distances between neighbors*

If a node is moved in small distance, its neighbors are not changed completely. But the distances between node and these neighbors are likely changed. As Fig. 2 shows that after B_2 is moved, S_5 is still its neighbor. However, the distance between them is changed. Nodes hardly get the distances with their neighbors based on Range-Free localization algorithms. So In the Sect. 4.1, we calculate $DisRank(i, j)_t$ to reflect distance proximity between neighbors.

5.2 Similarity of Neighborhood Relationship

In the $(t, t + 1)$, At time t , S_i gets $ID(i)_t$ and $DisRank(i, j)_t, j \in ID(i)_t$. At time $t + 1$, S_i gets $ID(i)_{t+1}$ and $DisRank(i, j)_{t+1}, j \in ID(i)_{t+1}$. $IDSame(i)_{(t,t+1)}$ is computed by the formula (3). Neighborhood relationship of S_i and S_j 's at time t is defined as $Relation(i, j)_t$. $Relation(i, j)_t$ and $Relation(i, j)_{t+1}$ are computed by

$$Relation(i, j)_t = \begin{cases} DisRank(i, j)_t \cdot IDSame(j)_{(t,t+1)} & j \in (ID(i)_t \cap ID(i)_{t+1}) \\ DisRank(i, j)_t \cdot (1 - IDSame(i)_{(t,t+1)}) & j \in (ID(i)_t / ID(i)_{t+1}) \\ 0 & j \in (ID(i)_{t+1} / ID(i)_t) \end{cases} \tag{4}$$

$$Relation(i, j)_{t+1} = \begin{cases} DisRank(i, j)_t \cdot IDSame(j)_{(t,t+1)} & j \in ID(i)_{t+1} \\ 0 & j \in (ID(i)_t / ID(i)_{t+1}) \end{cases} \quad (5)$$

In the formula (4) and (5), to minimize the influences of drifting neighbors, $DisRank(i, j)_t$ is multiplied by $IDSame(j)_{(t,t+1)}$. When S_i is static but S_j is moved, the change of $DisRank(i, j)_t$ and $DisRank(i, j)_{t+1}$ is caused by S_j . Because of S_j 's movement, $IDSame(j)_{(t,t+1)}$ is closed to 0, which makes $Relation(i, j)_t$ and $Relation(i, j)_t$ close to 0. Besides, for $j \in (ID(i)_t / ID(i)_{t+1})$, at time $t + 1$, S_j is not S_i 's neighbor, so S_i can't get S_j 's $IDSame(j)_{(t,t+1)}$. $IDSame(j)_{(t,t+1)}$ is replaced by $1 - IDSame(i)_{(t,t+1)}$. If S_i is moved, $1 - IDSame(i)_{(t,t+1)}$ is closed to 1. If not, $1 - IDSame(i)_{(t,t+1)}$ is closed to 0. These operations can minimize the influences of drifting neighbors.

After S_i calculates $Relation(i, j)_t$ and $Relation(i, j)_{t+1}$ of each neighbor, We define vectors $RelationV(i)_t$ and $RelationV(i)_{t+1}$ to store these data. Finally, we use cosine law to calculate the similarity of $RelationV(i)_t$ and $RelationV(i)_{t+1}$ by

$$NeiSim(i) = \frac{RelationV(i)_t \cdot RelationV(i)_{t+1}}{\|RelationV(i)_t\| \cdot \|RelationV(i)_{t+1}\|} \quad (6)$$

6 Experiment and Analysis

In this section, firstly, the simulation results are presented to validate the performance and robustness of our proposed algorithms. Then, the algorithms are applied in the dynamic WSN to improve the accuracy of re-localization.

BLVNS is based on neighborhood mutual observation, so the average connectivity degree of network is more than 15. The network configuration of our simulation is set as follows: 150 nodes, including 15 beacons and 135 sensors, are deployed randomly in a 150 m \times 150 m region. The transmission range of each nodes equals to 30 m. We use the signal attenuation model to simulate the RSSI value between nodes, by using the formula (7). Where p_{kl} is the path dissipation function mattered with nodes' distance. d_{kl} is the distance between sender S_k and receiver S_l . d_0 is a reference distance and equals to 1 m. n_p is an exponent of path loss. ε is an error coefficient.

$$p_{kl} = \left(p_0 - 10n_p \lg \left(\frac{d_{kl}}{d_0} \right) \right) \cdot (1 - \varepsilon) \quad (7)$$

We use success detection rate R_s and error rate R_e to evaluate the detection performance. The calculation of R_s and R_e is given in (8) and (9), in which B_u is the set of unreliable beacons, B_{du} is the set of unreliable beacons detected by algorithms.

$$R_s = \frac{Num(B_u \cap B_{du})}{Num(B_u)} \quad (8)$$

$$R_e = \frac{Num((B - B_u) \cap B_{du})}{Num(B_u)} \tag{9}$$

The goal to this experiment is to study how the number of drifting nodes impact the performance and analyze the environmental adaptability of the verification algorithms.

At first, the measurement of RSSI does not exist any error, $\epsilon = 0$. And the thresholds of BLANS and BLATM are 0.6 and 0.45 respectively. Figure 3 shows the performance of the verification algorithms with the drifting beacons. For example, when exponent of path loss is 1.5, 2, and 2.5, respectively, R_s of two algorithms is maintained at about 95% and R_e is under the 20% with the drifting nodes increasing. So the influences of drifting sensors are small. When the measurements of RSSI exist errors, we set $\epsilon = 0$, $\epsilon \in (-0.05, 0.05)$ and $\epsilon \in (-0.1, 0.1)$ respectively. Figure 4 shows the performances of the verification algorithms with measuring errors. Compare Fig. 4 with Fig. 3, we can find their performances are similar so that the influences of RSSI measuring errors are small. The experiment shows that BLVNS is robust.

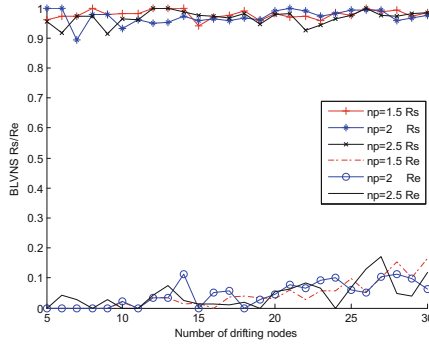


Fig. 3. Performance of BLVNS with different drifting nodes and environments

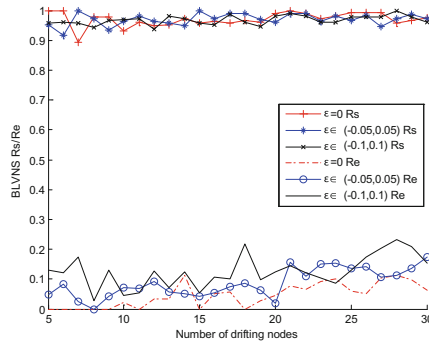


Fig. 4. Performance of BLVNS with different drifting nodes and measuring errors

7 Conclusion

In this paper, we analyze the severe impacts of the unreliable beacons on Range-Free localization algorithms, which reflects the importance of beacon location verification. To eliminate the influences of localization arise from these unreliable beacons, we propose the algorithms BLVNS which can efficiently recognize and filter out the drifting beacons. BLVNS can minimize the re-localization error and have strong anti-jamming capacity in different environments and networks. Future study will extend the location verification model to real-world experiments.

Acknowledgment. This work is supported by the National Natural Science Foundation of China under Grant (No: 61502413; 61379023), and Supported by Zhejiang provincial Top Discipline of Cyber Security at Zhejiang Normal University.

References

1. Akyildiz, F., Su, W., Sankarasubramaniam, Y., Cayirci, E.: Wireless sensor Networks: a survey. *Comput. Netw.* **38**(4), 393–422 (2002)
2. Jang, W.S., Lee, D.E., Choi, J.H.: Ad-hoc performance of wireless sensor network for large scale civil and construction engineering applications. *Autom. Constr.* **26**(10), 32–45 (2012)
3. Safa, H.: A novel localization algorithm for large scale wireless sensor networks. *Comput. Commun.* **45**, 32–46 (2014)
4. Gezici, S., Tian, Z., Giannakis, G.B., et al.: Localization via ultra-wideband radios: a look at positioning aspects of future sensor networks. *IEEE Sign. Process. Mag.* **22**(4), 70–84 (2005)
5. Patwari, N., Ash, J.N., Kyperountas, S., et al.: Locating the nodes: cooperative localization in wireless sensor networks. *IEEE Sign. Process. Mag.* **22**(4), 54–69 (2005)
6. Vempaty, A., Ozdemir, O., Agrawal, K., et al.: Localization in wireless sensor networks: Byzantines and Mitigation techniques. *IEEE Trans. Sign. Process.* **61**(6), 1495–1508 (2013)
7. Shao, H.J., Zhang, X.P., Wang, Z.: Efficient closed-form algorithms for AOA based self-localization of sensor nodes using auxiliary variables. *IEEE Trans. Sign. Process.* **62**(10), 2580–2594 (2014)
8. Wang, Y., Wang, X., Wang, D., et al.: Range-free localization using expected hop progress in wireless sensor networks. *IEEE Trans. Parallel Distrib. Syst.* **20**(10), 1540–1552 (2009)
9. Zhou, Y., Xia, S., Ding, S., et al.: An improved APIT node self-localization algorithm in WSN based on triangle-center scan. *J. Comput. Res. Dev.* **46**(4), 566–574 (2009)
10. Zhong, S., Jadliwala, M., Upadhyaya, S., et al.: Towards a theory of robust localization against malicious beacon nodes. In: *INFOCOM*, pp. 2065–2073 (2008)
11. Hwang, J., He, T., Kim, Y.: Detecting phantom nodes in wireless sensor networks. In: *INFOCOM*, pp. 2391–2395 (2007)
12. Liu, D., Lee, M.C., Wu, D.: A node-to-node location verification method. *IEEE Trans. Ind. Electron.* **57**(5), 1526–1537 (2010)
13. He, D., Cui, L., Huang, H., et al.: Design and verification of enhanced secure localization scheme in wireless sensor networks. *IEEE Trans. Parallel Distrib. Syst.* **20**(7), 1050–1058 (2009)
14. Kuo, S.P., Kuo, H.J., Tseng, Y.C.: The beacon movement detection problem in wireless sensor networks for localization applications. *IEEE Trans. Mob. Comput.* **8**(10), 1326–1338 (2009)

15. Yang, Z., Jian, L., Wu, C., et al.: Beyond triangle inequality: sifting noisy and outlier distance measurements for localization. *ACM Trans. Sens. Netw. (TOSN)* **9**(2), 26 (2013)
16. Yang, Z., Wu, C., Chen, T., et al.: Detecting outlier measurements based on graph rigidity for wireless sensor network localization. *IEEE Trans. Veh. Technol.* **62**(1), 374–383 (2013)
17. Garg, R., Varna, A.L., Wu, M.: An efficient gradient descent approach to secure localization in resource constrained wireless sensor networks. *IEEE Trans. Inf. Forensics Secur.* **7**(2), 717–730 (2012)
18. Wei, Y., Guan, Y.: Lightweight location verification algorithms for wireless sensor networks. *IEEE Trans. Parallel Distrib. Syst.* **24**(5), 938–950 (2013)
19. Xia, M., Sun, P., Wang, X., et al.: Distributed beacon drifting detection for localization in unstable environments. *Math. Prob. Eng.* (2013)
20. Alfaro, J.G., Barbeau, M., Kranakis, E.: Secure localization of nodes in wireless sensor networks with limited number of truth tellers. In: 2009 Seventh Annual Communication Networks and Services Research Conference, CNSR 2009, pp. 86–93. IEEE (2009)
21. Niculescu, D., Nath, B.: DV based positioning in Ad Hoc networks. *Netw. IEEE* **22**(1–4), 267–280 (2003)
22. Wu, J., Chen, H., Lou, W., et al.: Label-based DV-Hop localization against wormhole attacks in wireless sensor networks. *Pervasive Mob. Comput.* **16**, 22–35 (2014)
23. Guo, Z., Min, L., Li, H., Wu, W.: Improved DV-hop localization algorithm based on RSSI value and hop correction. In: Wang, R., Xiao, F. (eds.) *CWSN 2012. CCIS*, vol. 334, pp. 97–102. Springer, Heidelberg (2013). https://doi.org/10.1007/978-3-642-36252-1_10

Design and Development of Parametric System for Planetary Reducer

Yangpeng Chen, Menglun Tao, Dingfang Chen ^(✉), Bo Li, Yanfang Yang, and Boting Chen

Institute of Intelligent Manufacturing and Control, Wuhan University of Technology, Heping Road No. 1040, Wuchang District, Wuhan 430063, Hubei, China
453194287@qq.com, taomenglun@whut.edu.cn, cadcs@126.com

Abstract. For planetary reducers, most components have certain characteristics and structure. In order to obtain the 3-D models and engineering drawings of similar components which have the same characteristics and structure only different in size, a digital design system of planetary reducer is developed by parametric design method. The system is planned according to the 3-D parametric design and structural analysis of planetary reducers and the parametric operation module is also designed. In parametric operation module, 3-D models of main components of the planetary reducer are taken as templates; the parameters of template are selected and modified by using VB platform to recall controls of SolidWorks. The 3-D models and engineering drawings of similar components are output rapidly. The efficiency and correctness of planetary reducers are improved by this system, which is also provided as a reference for designers and enterprises to produce other serial products.

Keywords: Planetary reducer · Parametric design · VB · SolidWorks

1 Introduction

Most components of the mechanical product have certain characteristics and structure. Applying the parametric design method, it is helpful to improve the design efficiency and simplify the design work by using the established 3-D model library, and generate 3-D models of these components with same characteristics and structure only different in size [1].

SolidWorks is a kind of powerful 3-D modeling software [2]. And it is able to meet the specific needs of enterprises in the integration of the secondary development and the parametric design. Variables are used to replace fixed parameters of components through the parametric design in the physical modeling. The parametric design of similar components is completed through the modification of variables.

Enterprises and designers always pay attention to design, development and manufacture of planetary reducers. Especially for the aspects of standardization, serialization and generalization of planetary reducer components, it has become a general trend to achieve parametric design of reducer components [3]. The rapid development of the computer technology and CAD technology provides software with realizable conditions

for parametric design [4]. To design the planetary reducers, the mathematical model and product structure are kept the same while the parameters in size should be modified [5]. Therefore, the use of digital technology to achieve parametric design of planetary reducers helps to improve efficiency and correctness of the serial design.

2 Realization of Digital Design System

2.1 Secondary Development Based on ActiveX Automation in SolidWorks

The service program (Server) based on ActiveX Automation technology is able to be controlled and accessed by the client program (Client). In the study of secondary development of SolidWorks with Visual Basic 6.0, the service program is SolidWorks and the client program is VB [6]. The language of program is used by the client program (VB) to communicate directly with the service program (SolidWorks) and manipulate functionality of the software.

In the development of the planetary reducer system, the relationship between the service and client programs is shown in Fig. 1.

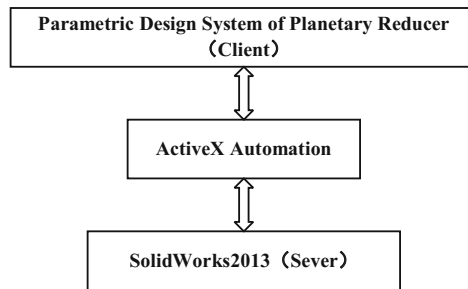


Fig. 1. The relationship between the service and client programs

2.2 Planning and Realization Process of Digital Design System

The parametric design of main components of planetary reducers is completed in the digital system planned in this paper, including overall design, 3-D modeling of main components, automatic output of engineering drawings, automatic assembly and finite element analysis of the reducer [7]. For design goals above, the digital design system is planned as shown in Fig. 2.

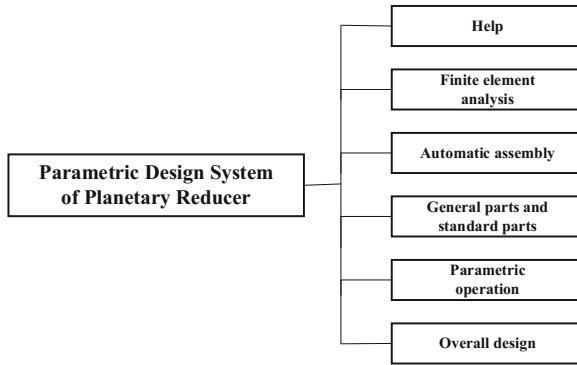


Fig. 2. Design of digital design system

In Fig. 2, the parametric operations (3-D modeling and engineering drawing), automatic assembly, and finite element analysis in the component parametric design are key modules of the digital design system.

The block diagram of the planetary reducer system is shown in Fig. 3.

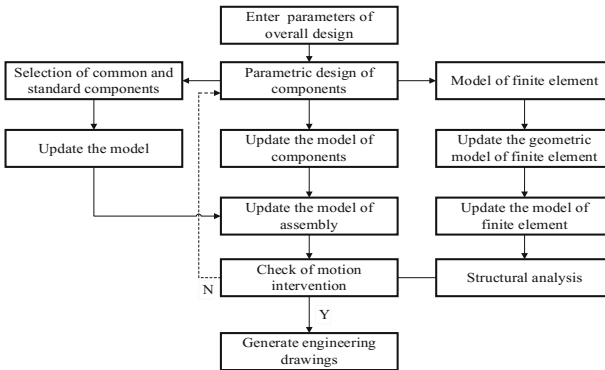


Fig. 3. Flow chart of planetary reducer digital design system

2.3 Design of Digital System

The process of secondary development for SolidWorks combined with VB is completed in this paper [8]. The parametric design of the two-stage NGW planetary reducer is taken as an example to complete the design of the digital design system.

The two parts completed are introduced as follows: main interface of the design system and parametric operation.

Figure 4 is main interface of the design system. Figures 5 and 6 are parametric operation module. The parametric operation module is one of core modules in the design system, including parametric 3-D modeling of main reducer components and automatic output of engineering drawings [9].

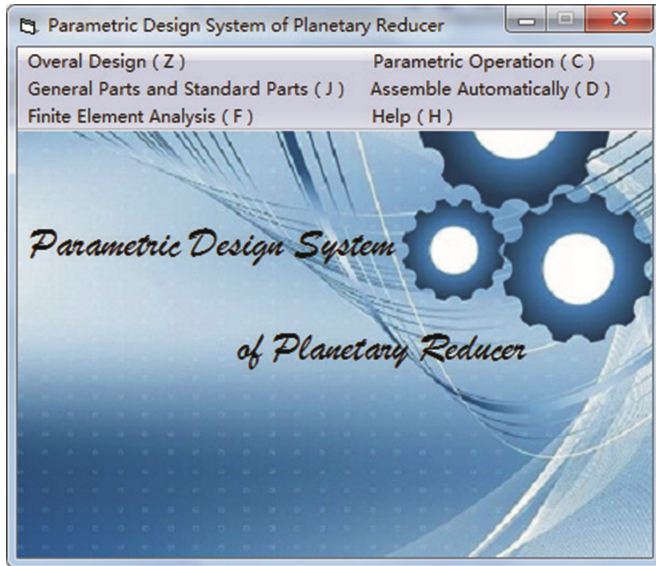


Fig. 4. Main interface of the design system

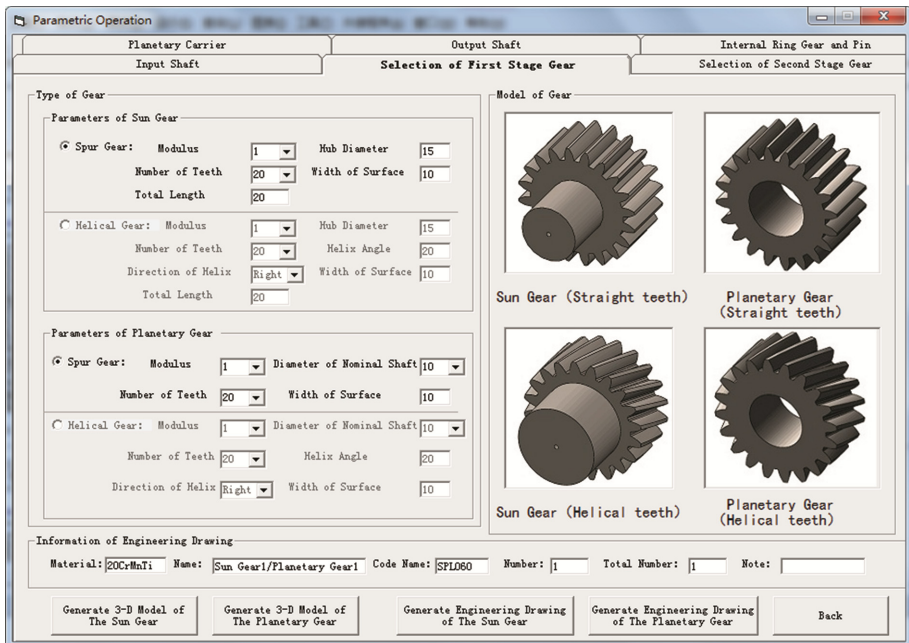


Fig. 5. Parametric design of the first stage gear

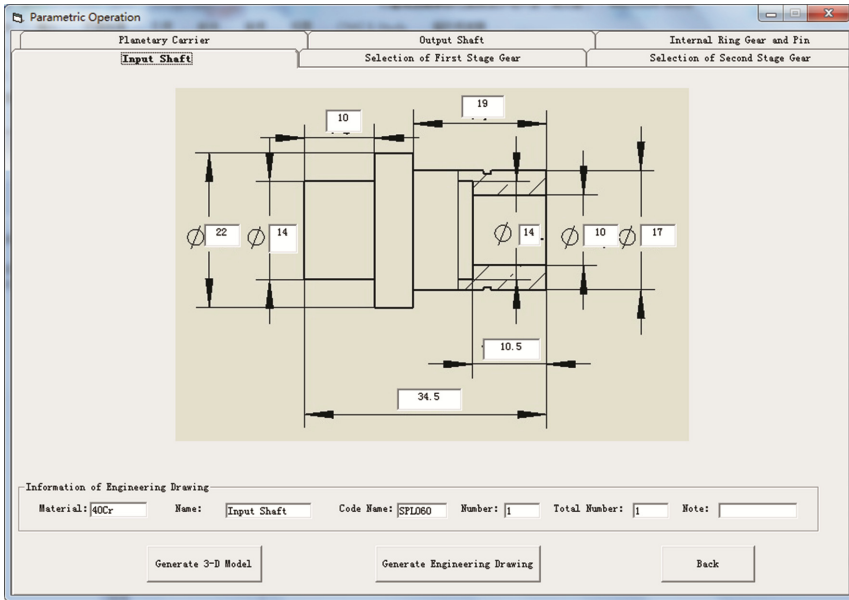


Fig. 6. Parametric design of the input shaft

Users are able to select first and second transmission system through modifying parameters of the gear to generate 3-D models and engineering drawings of new gears, and the parametric design of components is achieved as shown in Fig. 5.

After completing the selection of the gear type, the remaining components are able to be designed accordingly as shown in Fig. 6.

After modifying parameters, the new 3-D model and corresponding engineering drawing will be automatically saved to a new folder, so that the product will be viewed again and corresponding changes can be made by the user.

3 Parametric 3-D Modeling of Main Components

3.1 Parametric Modeling Method

At present, the following two methods are commonly used in parametric design [10]:

- (1) The modeling of parameter modification method: The corresponding parameters in the 3-D model template are modified through invoking program to obtain new 3-D models.
- (2) The modeling of program method: The 3-D model is built by the program fully.

The parameter modification method is used by this paper. Figure 7 is the flow chart of the parameter modification method.

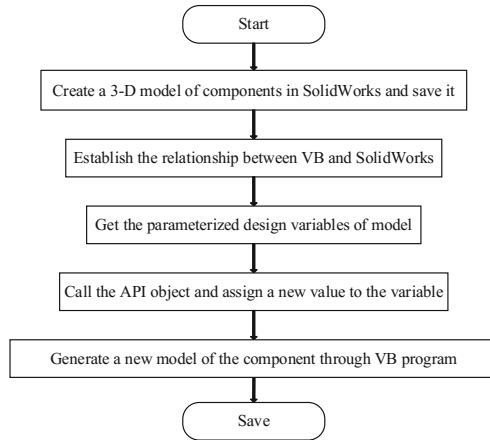


Fig. 7. Flow chart of the parameter modification method

3.2 Realization of Parametric Modeling Process Based on Characteristics

The feature-based components with same characteristics are able to be generated by using the same “template model”. These components need not to be re-modeled when the feature size changes, which is the meaning of the parametric modeling [11]. When the model with a different size is required, the “template model” is able to be used for generating the 3-D model quickly as shown in Fig. 8.

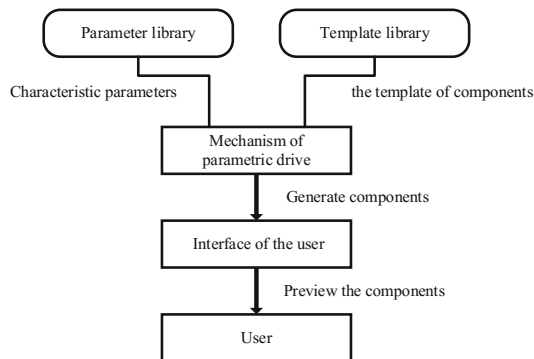


Fig. 8. Parametric method of “template model and parameter driven”

Following the mechanism of the parametric feature-based “template model and parameter driven”, users are allowed to modify size parameters of the component template and obtain components that meet requirements of the design rapidly [12]. At the same time, it can meet the needs of users for the personalized customization of components and the establishment of non-standard components.

In general, the common steps for the parametric establishment of a 3-D model are shown in Fig. 9.

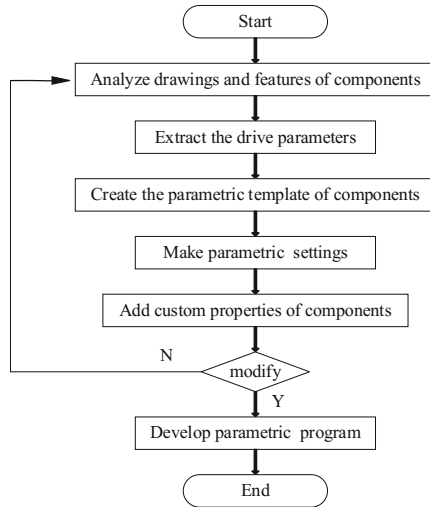


Fig. 9. Parametric modeling process based on template model

3.3 Example of Parametric Modeling

In this paper, 3-D models of main components of the two-stage NGW planetary reducer – including input shaft, sun gear, planetary gear, ring gear, planetary carrier, pin and output shaft are modeled.

Taking the output shaft of the reducer as an example, parametric modeling is performed according to Fig. 9.

The 3-D model template of the output shaft is shown in Fig. 10.

The parametric model interface of the output shaft is set up with VB to develop SolidWorks API function as shown in Fig. 11.

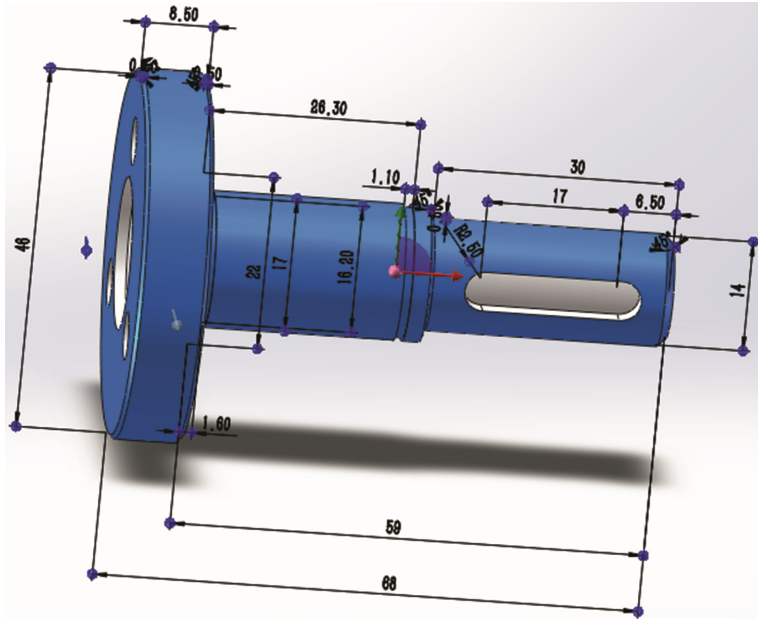


Fig. 10. 3-D model template of the output shaft

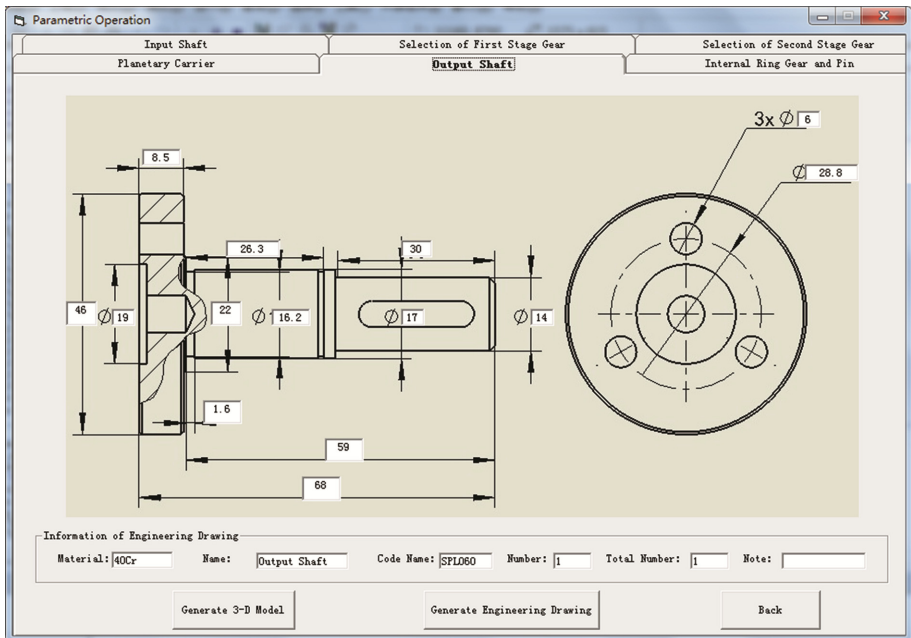


Fig. 11. Parametric modeling of output shaft

After modifying the parameters of the output shaft, according to the modification process, new parameters are transferred to corresponding parameter names of the output shaft. Then corresponding parameters in the template of the output shaft are modified and the modification of size parameters and custom properties is completed. Finally, a new 3-D model and corresponding engineering drawing of the output shaft can be generated, and the parametric operation of components is achieved [13].

4 Automatic Output of Engineering Drawing

4.1 Overall Framework of Automatic Adjustment System

After building a 3-D model, it is convenient to generate 2-D engineering drawings. But the parametric ratio of the pattern, position of view, size and notes are not processed automatically. These problems will result in defects of chaotic layouts and uncoordinated proportions, so it is not suitable for guiding the production directly [14]. Therefore, it is necessary to carry out automatic adjustments for engineering drawings from Solid-Works, so that output engineering drawings can meet the requirements of enterprise standards and facilitate rapid productions.

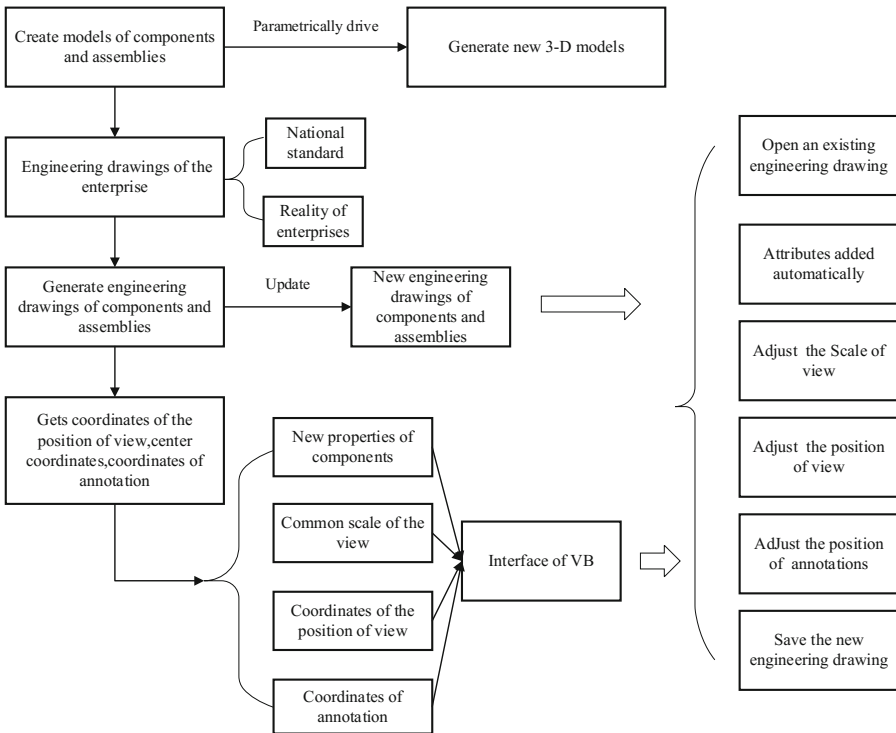


Fig. 12. The process for the automatic adjustment of engineering drawings

When the new 3-D model is generated, the functions of the adjustment of engineering drawings are able to be achieved with VB [14]. The process for automatic adjustments of engineering drawings is shown in Fig. 12.

4.2 Example for Automatical Output of Engineering Drawing

The steps for the automatical output of engineering drawings are following: (1) Establish a template for the drawing view; (2) Establish a template of engineering drawings; (3) Set custom properties for the template of engineering drawings; (4) Adjust the view for the template of engineering drawings; (5) Save and manage the template of engineering drawings.

According to the steps above, the planetary carrier of the reducer is taken as an example to complete the automatical output of the engineering drawing. Figure 13 shows the custom properties of the planetary carrier [15].

Fig. 13. The custom properties of the planetary carrier

Figure 14 is the dialog box of custom properties in SolidWorks after the custom properties of the planetary carrier is assigned.

	Property Name	Type	Value / Text Expression	Evaluated Value
1	Description	Text		
2	Material	Text	40Cr	40Cr
3	Name	Text	Planetary Carrier	Planetary Carrier
4	Code Name	Text	SPL060	SPL060
5	Number	Text	1	1
6	Total Number	Text	1	1
7	Note	Text		
8	<Type a new property>			

Fig. 14. The dialog box of the custom properties

Figure 15 is the result of the planetary carrier generated automatically.

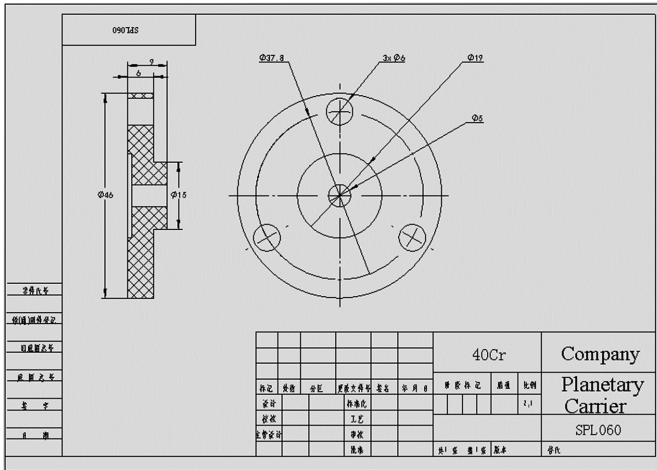


Fig. 15. The result of the engineering drawing automatically generated

5 Conclusions

Based on the understanding of the structure and design steps of the planetary reducer, the general framework of the digital design system for the planetary reducer is planned by the parametric design method. The development of the parametric operation module in the system is completed by using SolidWorks as the development platform and Visual Basic as the development tool, and the automatic output of 3-D models and engineering drawings of the same planetary reducer is realized. The system is designed to provide enterprises and designers with a way to get serial products rapidly in order to improve the efficiency and quality of design and make the product more standardized and versatile.

References

1. Hua, Z., Dingfang, C.: Application and secondary development of SolidWorks based on Visual Basic. *J. Hubei Univ. Technol.* **4**, 36–38 (2010)
2. Xiuzi, Y., Chaoxiang, C.: *SolidWorks Advanced Course. Secondary Development and API*. Mechanical Industry Press, Beijing (2007)
3. Xinhua, Z.: *Modularization and Serialization of Planetary Gear Reducer*. Dalian University of Technology (2014)
4. Fengqin, Z., Chun, Z.: Parametric programming of NGW planetary gear reducer. *Mech. Transm.* **05**, 36–38, 88 (2005)
5. Yanli, C.: *Research on Parametric Design of CAD System for NGW-S Planetary Gear Reducer*. Liaoning Technical University (2005)
6. Weiliang, L., Yixiang, W.: Parameterized design of hydraulic cylinder based on secondary development of SolidWorks. *Mach. Manufact. Autom.* **01**, 74–77 (2017)

7. Yi, W.: Parametric Design and Application of Wind Power Converter. Dalian University of Technology (2014)
8. Zhaobin, H., Lin, X., Peng, H.: Parameterization design of hydraulic cylinder based on VB and Solidworks. *Coal Mine Mach.* **12**, 254–256 (2014)
9. Junliang, Z.: Study on Three-Dimensional Optimization Design of Planetary Gear Reducer of Shearer Cutting Part. Harbin University of Science and Technology (2007)
10. Zhigeng, L.: Study on Key Technology of Parametric Design of Bridge Crane Bridge. North University of China (2007)
11. Bo, P., Yue, Y., Chunzhu, S.: Parameterization modeling of centrifugal impeller using SolidWorks API. *J. Eng. Graph.* **05**, 1–7 (2009)
12. Ke, W., Zongyan, W., Chunyue, L., Bing, Z., Zhenyu, C.: Template-based parametric design system of reducer. *Mech. Transm.* **05**, 50–52 (2014)
13. Chao, S., Yuxiang, L.: Secondary development of SolidWorks for parametric design based on VB language. *Manufact. Autom.* **15**, 137–140 (2013)
14. Yuhua, P., Zongyan, W.: Study on key technology of automatic adjustment of parametric design drawings. *Hoisting Transp. Mach.* **06**, 58–61 (2012)
15. Yuhua, P., Zhigeng, L., Zhili, H., Jingang, Y., Zongyan, W.: Three-dimensional parametric design system of main girder of bridge crane. *Mech. Eng. Autom.* **06**, 45–47 (2006)

A Dynamic Double Threshold Based Cooperative Spectrum Sensing Strategy in Heterogeneous Cognitive Radio Networks

Chongxiao Peng^{1(✉)}, Yifei Wei^{1(✉)}, Bo Gu¹, Ligang Ren², and Mei Song¹

¹ School of Electronic Engineering, Beijing University of Posts and Telecommunications, Beijing 100876, People's Republic of China

{pengchongxiao, weiyifei, gubo, songm}@bupt.edu.cn

² China Unicom System Integration Limited Corporation Beijing Branch, Beijing, China
15611030998@wo.com.cn

Abstract. Cooperative Spectrum Sensing (CSS) is the critical component of the cognitive radio technology, which could relieve the shortage of spectrum resources. The double threshold based CSS scheme was adopted to deal with the unreliability when the original energy value locates around the traditional single threshold. We utilize the dynamic double threshold based energy detection scheme, in which it can adjust the double threshold properly to respond the transformation of channel condition. This proposed dynamic double threshold based scheme could be verified by analyzing the formula and simulation, and it achieves the better performance compared with classical double threshold based CSS scheme.

Keywords: Cooperative spectrum sensing · Dynamic double threshold Energy detection · Cognitive radio

1 Introduction

The cognitive radio technologies adopt strategy which shares the frequency spectrum among the users, and the secondary user (SU) opportunistically occupy the spectrum only if spectrum hole has been detected, which means the primary user (PU) doesn't occupy the spectrum band at a certain period of time [1]. Before using shared spectrum among users, spectrum sensing is necessary to determine if there is a PU currently occupying the licensed spectrum band [2].

In this paper, we adopt dynamic double threshold method which is set dynamically according to the instantaneous SNR, so that further improve the performance of double threshold energy detection based CSS scheme.

The rest of the paper is organized as following: Sect. 2 describes the proposed system model. Section 3 demonstrates the single threshold energy detection based CSS scheme. Section 4 proposes a dynamic double threshold energy detection based CSS scheme. The simulation results and analysis are presented in Sect. 5 and the conclusion from the paper is drawn in Sect. 6.

2 System Model

There are three phases in the sensing system: sensing, reporting and broadcast. The SUs receive the signal transmitted from PU and transfer the signal into the form of energy value [3], then make the local decision or remain the original energy value. The local sensing results would be reported to the fusion center at reporting phase. This process would require some bits of data as communication overhead [4]. The finally global decision would be made in the fusion center, then all the SUs would get the final results whether PU is occupying the licensed spectrum band.

3 Single Threshold Based Cooperative Spectrum Sensing

3.1 Probability of Detection and False Alarm

We choose P_d and P_f to express the probability of detection and probability of false alarm respectively. We only consider the channel with Additive White Gaussian Noise in this article, so we can get the probability of detection and false alarm as following [5],

$$P_{di} = P\{E_i > \lambda | H_1\} = Q_M(\sqrt{2\gamma_i}, \sqrt{\lambda}) \tag{1}$$

$$P_{fi} = P\{E_i > \lambda | H_0\} = \frac{\Gamma(M, \lambda/2)}{\Gamma(M)} \tag{2}$$

where $Q_M(\dots)$ is the generalized Marcum Q function [6] and $\Gamma(\dots)$ is upper incomplete gamma function. H_0 denotes that the PU is absent of licensed spectrum band, while H_1 denotes that the PU is present of licensed spectrum band.

3.2 Fusion Decision

K out of N rule is belong to the hard fusion decision scheme, which can also be called voting rule or majority rule [7]. The fusion center deal with the local sensing results reported by each SU. Assuming that the number of SU processing spectrum sensing is N. The fusion center makes the final decision that PU is present of the licensed spectrum band only if there are at least K SU indicating the licensed spectrum band being occupied by PU. The finally global probability of detection and false alarm can be formulated as following,

$$P_{dKoutN} = \sum_{k=K}^N \binom{N}{k} \prod_{i=1}^k P_{di} \prod_{j=k+1}^N (1 - P_{dj}) \tag{3}$$

$$P_{fKoutN} = \sum_{k=K}^N \binom{N}{k} \prod_{i=1}^k P_{fi} \prod_{j=k+1}^N (1 - P_{fj}) \tag{4}$$

The Maximal Ratio Combining (MRC) [8] method adopts strategy that getting the weighted summation, in which the normalized weight factor is set according to instantaneous SNR. The method can be formulated as following,

$$P_{dMRC} = P\{E_{MRC} > \lambda_{MRC} | H_1\} = Q_M\left(\sqrt{2\gamma_{MRC}}, \sqrt{\lambda_{MRC}}\right) \tag{5}$$

$$P_{fMRC} = P\{E_{MRC} > \lambda_{MRC} | H_0\} = \frac{\Gamma(M, \lambda_{MRC}/2)}{\Gamma(M)} \tag{6}$$

where $\gamma_{MRC} = \sum_{i=1}^N \gamma_i$, $E_{MRC} = \sum_{i=1}^N w_i E_i$, $w_i = \frac{\gamma_i}{\sum_{i=1}^N \gamma_i} = \frac{\gamma_i}{\gamma_{MRC}}$.

4 Dynamic Double Threshold Based Cooperative Spectrum Sensing

For a given threshold λ , the dynamic threshold is formulated as following.

$$\lambda_{0i} = w_i \times \lambda \tag{7}$$

$$\lambda_{1i} = (2 - w_i) \times \lambda \tag{8}$$

$$w_i = \frac{\gamma_i}{\max(\gamma_1, \gamma_2, \dots, \gamma_N)} \tag{9}$$

The fusion center makes the global decision GD1 based on the local binary decision, and makes the global decision GD2 based on the original energy value. Finally, we can get the final decision which is expressed as following.

$$FD = \begin{cases} 0, & GD_1 + GD_2 < 1 \\ 1, & otherwise \end{cases} \tag{10}$$

$$GD_1 = \begin{cases} 0, & L_1 < K \\ 1, & otherwise \end{cases} \tag{11}$$

$$GD_2 = \begin{cases} 0, & E_{MRC} = \sum_{j=1}^G w_j E_j \leq \lambda_{MRC} \\ 1, & otherwise \end{cases} \tag{12}$$

where L_1 is the number of reporting binary decision which indicating the present state of the PU.

The final decision is made in the fusion center. We could compute the final probability of detection and false alarm which is formulated as following.

$$P_d = 1 - (1 - P_{dB}) \left(1 - P_{dMRC} \times \prod_{i=1}^G P_{1i} \right) \tag{13}$$

$$P_f = 1 - (1 - P_{fB}) \left(1 - P_{fMRC} \times \prod_{i=1}^G P_{0i} \right) \tag{14}$$

where P_{dB} and P_{fB} is computed by using K out of N rule, P_{dMRC} and P_{fMRC} is computed by using MRC, G is the number of original energy value reported from SU, the probability of energy located between double thresholds must be taken account, which is expressed as following.

$$P_{0i} = \frac{\Gamma(M, \lambda_{0i}/2)}{\Gamma(M)} - \frac{\Gamma(M, \lambda_{1i}/2)}{\Gamma(M)} \tag{15}$$

$$P_{1i} = Q_M(\sqrt{2\gamma_i}, \sqrt{\lambda_{0i}}) - Q_M(\sqrt{2\gamma_i}, \sqrt{\lambda_{1i}}) \tag{16}$$

5 Simulation Results and Analysis

The simulation is carried out in the assumption that channel is along with AWGN. The time bandwidth product $M = 5$. We would compare the dynamic double threshold based

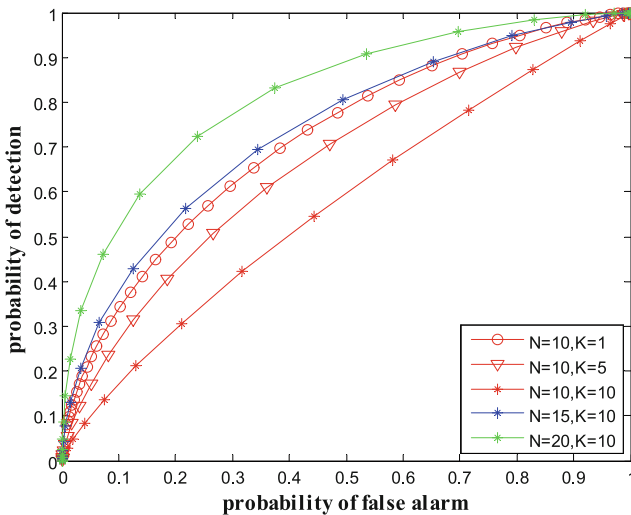


Fig. 1. Detection probability curve for single threshold based CSS using K out of N

CSS scheme with the fixed double threshold scheme in which it is set as $\lambda_0 = 0.8\lambda$, $\lambda_1 = 1.2\lambda$.

Figure 1 shows the relationship curve of probability of detection and false alarm using single threshold based CSS scheme, in which the final probability is computed by using the K out of N rule. Where the SNR is randomly generated between (-15 ~ 10) dB. We can find that the more SUs sensing spectrum is, the higher the probability is. Meanwhile the smaller the K is, the higher the probability is as expected. Figure 2 shows the changing tendency of detection probability along with false alarm probability which

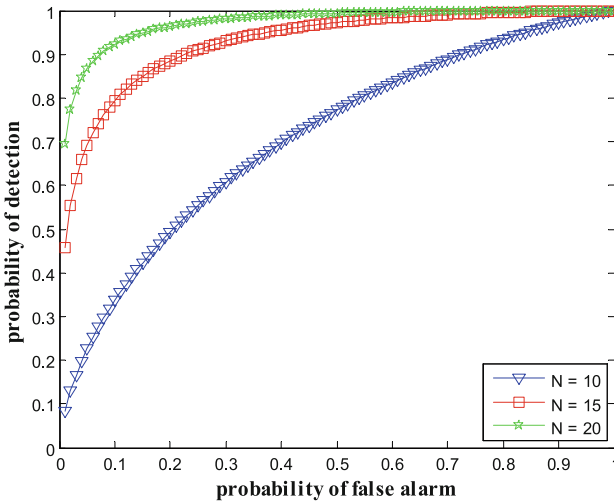


Fig. 2. Detection probability curve for single threshold based CSS using MRC

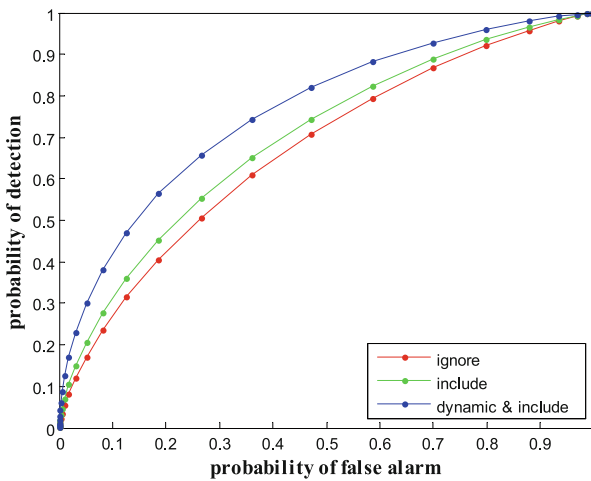


Fig. 3. Detection probability curve for dynamic double threshold based CSS

utilizes the MRC method to complete the final decision. Apparently to achieve higher detection probability it requires the number of original energy value as many as possible.

Figure 3 shows the proposed dynamic double threshold based CSS scheme under the condition ($N = 10, K = 10$), meanwhile compares with the scheme which ignores the energy value between the double thresholds and the scheme which deals with the original energy reported from the SUs further. The proposed scheme presents a better performance due to computing with the energy value between the double thresholds and adjusting the threshold according to the instantaneous SNR appropriately.

6 Conclusion

The proposed dynamic double threshold based CSS scheme could realize better performance by using MRC to deal with the original energy value between the double thresholds and utilizing K out of N rule to deal with the local binary decision, the critical factor is dynamic threshold adjusted according to instantaneous SNR.

Acknowledgement. This work was supported by the National Natural Science Foundation of China (No. 61571059).

References

1. Ghasemi, A., Sousa, E.S.: Opportunistic spectrum access in fading channels through collaborative sensing. *J. Commun.* **2**(2), 71–82 (2007)
2. Yifei, W., Yinglei, T., Li, W., Mei, S., Xiaojun, W.: QoS provisioning energy saving dynamic access policy for overlay cognitive radio networks with hidden markov channels. *China commun.* **10**(12), 92–101 (2013)
3. Urkowitz, H.: Energy detection of unknown deterministic signals. *Proc. IEEE* **55**(4), 523–531 (2005)
4. Vien, Q.T., et al.: A hybrid double-threshold based cooperative spectrum sensing over fading channels. *IEEE Trans. Wirel. Commun.* **15**(3), 1821–1834 (2015)
5. Digham, F.F., Alouini, M.S., Simon, M.K.: On the energy detection of unknown signals over fading channels. *IEEE Trans. Commun.* **55**(1), 21–24 (2007)
6. Nuttall, A.H.: Some integrals involving the Q-function. *IEEE Trans. Inf. Theor.* **21**(1), 95–96 (1972)
7. Mustapha, I., et al.: A weighted hard combination scheme for cooperative spectrum sensing in cognitive radio sensor networks. In: *IEEE Malaysia International Conference on Communications*, pp. 12–17. IEEE (2015)
8. Teguig, D., Scheers, B., Nir, V.L.: Data fusion schemes for cooperative spectrum sensing in cognitive radio networks. In: *Communications and Information Systems Conference IEEE*, pp. 1–7 (2012)

A Distributed Self-adaption Cube Building Model Based on Query Log

Meina Song^(✉), Mingkun Li^(✉), Zhuohuan Li^(✉), and Haihong E.^(✉)

Beijing University of Posts and Telecommunications, Beijing, China
{mnsong, dangshazi, lizhuohuan, ehaihong}@bupt.edu.cn

Abstract. Among the diverse distributed query and analysis engine, Kylin have gained wide adoption since its various strengths. By using Kylin, users can interact with Hadoop data at sub-second latency. However, it still has some disadvantages. One representative disadvantage is the exponential growth of cuboids along with the growth of dimensions. In this paper, we optimize the cuboid materialization strategy of Kylin by reducing the number of cuboids based on the traditional OLAP optimization method. We optimize the strategy mainly from two aspects. Firstly, we propose Lazy-Building strategy to delay the construction of nonessential cuboid and shorten the time of cuboid initialization. Secondly, we adopt Materialized View Self-adjusting Algorithm to eliminate the cuboids which are not in use for a long period. Experimental results demonstrate the efficacy of the proposed Distributed Self-Adaption Cube Building Model. Specifically, by using our model, cube initialization speed has increased by 28.5% points and 65.8% points space are saved, comparing with the cube building model of Kylin.

Keywords: Distributed OLAP · Distributed query processing system · Kylin
Query log · Materialization strategy

1 Introduction

In the era of big data, many modern companies produce huge amounts of data in their service lines. These data are used to conduct report analysis based on OLAP analysis. In order to conduct report analysis, companies need a system which can response to the query of thousands of data analysts at the same time. That requires high scalability, stability, accuracy and speed of the system. In fact, there doesn't exist a widely-accepted method in distributed OLAP field. Many query engines can also conduct report analysis, such as Presto [4], Impala [2], Spark SQL [14] or Elasticsearch [10], but they are more emphasis on data query and analysis. As a matter of fact, Kylin [7] is the specialized tool in Distributed OLAP field which is used often.

Kylin is originally developed by eBay, and is now a project of the Apache Software Foundation. It is designed to accelerate analysis on Hadoop and allow the use of SQL-compatible tools. It also provides a SQL interface and supports multidimensional analysis on Hadoop for extremely large datasets. Kylin can reach the scale of one million or

even millisecond OLAP analysis. So it is very frequently-used in the domestic IT industry.

The idea of Kylin is not original. Many technologies in Kylin have been used to accelerate analysis over the past 30 years. These technologies involve storing pre-calculated results, generating each level's cuboids with all possible combinations of dimensions, and calculating all metrics at different levels. Essentially, Kylin extends the methods of traditional OLAP field to the distributed field, generating Cube on Hadoop ecology.

When data becomes bigger, the pre-calculation processing becomes impossible even with powerful hardware. However, with the benefit of Hadoop's distributed computing power, calculation jobs can leverage hundreds of thousands of nodes [9]. This allows Kylin to perform these calculations in parallel and merge the final result, thereby significantly reducing the processing time.

Data cube [5] construction is the core of Kylin, it has two characteristics: one is the exponential growth of cuboids [5] along with the growth of dimensions; the other is the large amount of IO due to increased number of cuboids. The cube is usually very sparse, the increase of sparse data will waste a lot of computing time and memory space.

A full n -dimensional data cube could contains 2^n cuboids [5]. However, most of cuboids are not used, because most of query requested by data analyst follow the normal distribution. That's a waste of IO and memory.

In this paper, we propose a self-adaption cube building model which adopts a method called lazy-building cuboids and abandons useless cuboids based on query log. It can reduce the cube construction time and cube size a lot to save IO and memory. The paper is structured as follows. In Sect. 2, we present the background. In Sect. 3, we introduce the design and implementation details of the self-adaption cube building model. In Sect. 4, we focus on experimental evaluation. Finally, in Sect. 5, we discuss the Self-Adaption Cube Building Model and give a summary of the paper.

2 Background

2.1 Cube Calculation Algorithm

There are several strategies of data cube materialization [11] to reduce the cost of aggregation calculation and increase the query processing efficiency including iceberg cube calculation Algorithm [3], condensed cube calculation Algorithm [15], shell fragment cube calculation Algorithm [13], approximate cube calculation Algorithm [17], and time-series data stream cube calculation Algorithm [6]. They are all based on Partial Materialization [16], which means that a data sub-cube is selected and pre-calculated according to specific methods. Partial Materialization is a compromise between storage space, cost of maintenance and query processing efficiency.

In the process of iceberg cube calculation, sub-cubes which are higher than the minimum threshold are aggregated and materialized. Beyer proposed BUC algorithm [12] for iceberg cube calculation, which is widely-accepted.

According to the order of cuboid calculation, the methodologies of aggregation calculation can be divided into two categories: top-down and bottom-up.

1. Top-Down: Firstly, calculate the metric of the whole data cube, and then the recursive search is performed along each dimension. Secondly, check the conditions of the iceberg, prune branches that do not meet the condition. The most typical algorithm is BUC algorithm, it perform best on sparse data cube.
2. Bottom-Up: Starting from the base cuboids, compute high level cuboid from the low level cuboid in the search grid according the parents-children relationship. Typical algorithms are Pipesort algorithm, pipehash algorithm, overlap algorithm and Multiway aggregation algorithm [18].

However, Kylin doesn't follow the principle of partial materialization. In order to reduce unnecessary redundant calculation and shorten the cube construction time, Kylin adopts a Method called By Layer Cubing, which is a distributed version of the Pipesort algorithm, a kind of bottom-up algorithm [1].

2.2 By Layer Cubing

As its name indicates, a full cube is calculated by layer: N dimension, N-1 dimension, N-2 dimension, until 0 dimension; Each layer's calculation is based on it's parent layer (except the first, which base on source data); So this algorithm need N rounds of MapReduce running in sequence [8]; In the MapReduces, the key is the composite of the dimensions, the value is the composite of the measures; When the mapper reads a key-value pair, it calculates its possible child cuboids; For each child cuboid, remove 1 dimension from the key, and then output the new key and value to the reducer; The reducer gets the values grouped by key; It aggregates the measures, and then output to HDFS; One layer's MR is finished; When all layers are finished, the cube is calculated. The following Fig. 1 describes the workflow:

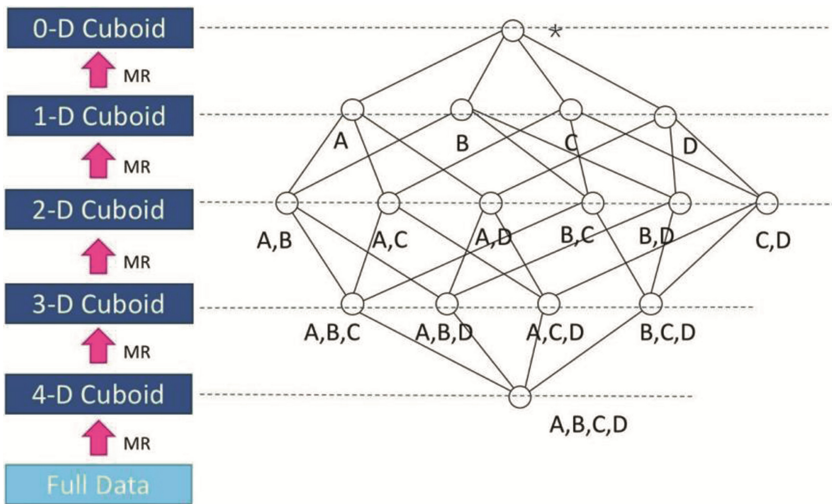


Fig. 1. By layer cubing. Each level of computation is a MapReduce task, and serial execution. A N dimensional Cube needs N times MapReduce Job at least.

It has some disadvantage:

1. This algorithm causes too much shuffling to Hadoop; The mapper doesn't do aggregation, all the records that having same dimension values in next layer will be omitted to Hadoop, and then aggregated by combiner and reducer;
2. Many reads/writes on HDFS: each layer's cubing need write its output to HDFS for next layer MR to consume; In the end, Kylin need another round MR to convert these output files to HBase HFile for bulk load; These jobs generates many intermediate files in HDFS;

All in all: the performance is not good, especially when the cube has many dimensions.

2.3 By Segment Cubing

In order to solve these shortcomings above, Kylin develops a new cube building algorithm called by segment cubing. The core idea is, each mapper calculates the feed data block into a small cube segment (with all cuboids), and then output all key/values to reducer; the reducer aggregates them into one big cube segment, finishing the cubing; Fig. 2 illustrates the flow;

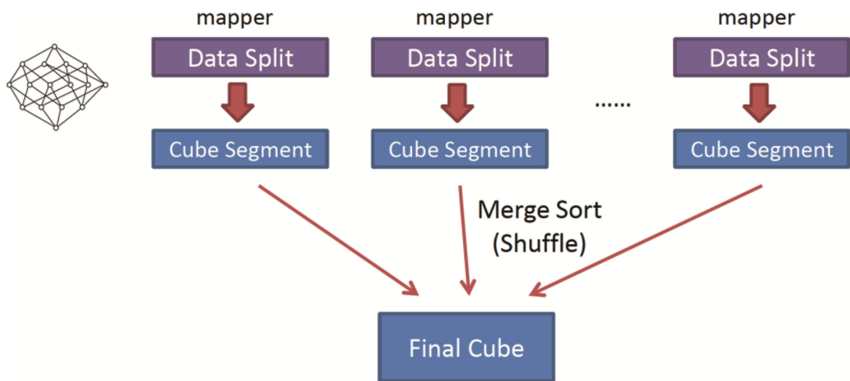


Fig. 2. By segment cubing.

Compared with By Layer Cubing, the By Segment Cubing has two main differences:

1. The mapper will do pre-aggregation, this will reduce the number of records that the mapper output to Hadoop, and also reduce the number that reducer need to aggregate;
2. One round MR can calculate all cuboids;

Based on the work mentioned above, we take advantage of both two Algorithm, and optimize cuboid materialization strategy.

3 Design and Implementation

In this section, we first introduce the architecture of Self-adaption Cube Building Model (SCBM) and the overall workflow. Then we explain cuboids Lazy-Building and the cuboid spanning tree. Finally, we describe the implementation details of the Materialized View Self-Adjusting Algorithm.

3.1 Architecture of Self-adaption Cube Building Model

The overall architecture of self-adaption cube building model is illustrated in following Fig. 3.

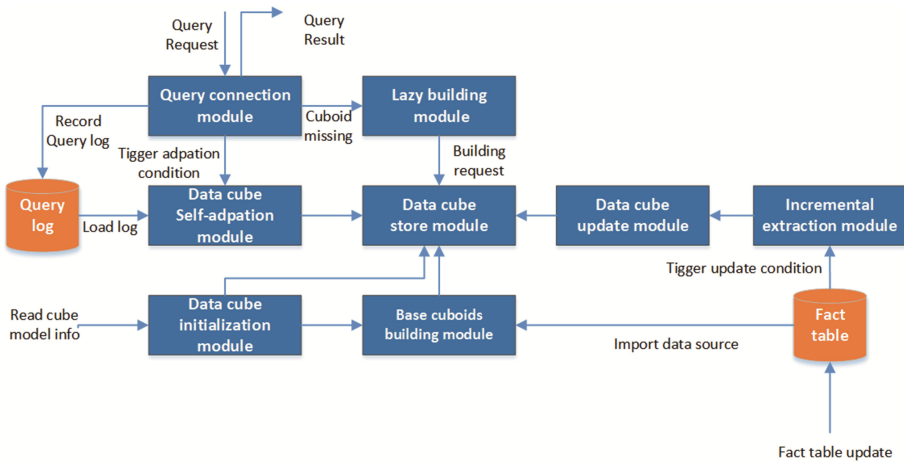


Fig. 3. Architecture of self-adaption cube building model.

Self-adaption cube building model takes fact table [5] as input of the overall system, usually the fact table is managed by distributed Data Warehouse Hive. We first set the parameters of the cube model, such as the filed for analysis, the base cuboid level and so on, then we build base cuboids in a mapper-reduce. After the construction of the base cuboids, the system can support query request, Query execution engine [7] resolves the query to find the required cuboids. If the cuboid has been generated, the query will be executed; if the cuboid is missing, the Lazy building module will be triggered to build the cuboid using the method in Sect. 3.2. When the query result returns, the system records the query log and waits for the adjustment of cube launched by Self-Adaption module according to the Materialized View Self-Adjusting Algorithm explained in Sect. 3.3. At the same time, the system maintains a dynamic cube spanning tree to store the metadata of cuboids.

3.2 Cuboid Spanning Tree and Lazy-Buliding

Cuboid Spanning Tree. In original By Layer Cubing, Kylin calculates the cuboids with Broad First Search (BFS) order, which causes a waste of memory. On the contrary, Cuboid Spanning Tree generates cuboid with Depth First Search (DFS) order to reduce the cuboids that need be cached in memory. This avoids unnecessary disk and network I/O, and the resource Kylin occupied is highly reduced;

With the DFS order, the output of a mapper is fully sorted (except some special cases), as the row key of cuboid is composed of cuboid ID and dimension values like [Cuboid ID + dimension values], and inside a cuboid the rows are already sorted. Since the outputs of mapper are already sorted, Shuffles sort would be more efficient.

In addition, DFS order is vary suitable for cuboid’s lazy building. Cuboid spanning tree also record the metadata of cuboids in every node in the tree, it provides the basis for the selection of ancestor cuboids.

Lazy-Building. Lazy-Building is a basic concept of the model. In order to reduce the number of cuboids, we adopt the strategy of generating on demand. At the same time, we persist all cuboids on the low layer in the By-Layer cubing algorithm for higher speed and lower computational complexity of Lazy-Buliding. For example: a cube has 4 dimensions: A, B, C, D; Each mapper has 1 million source records to process; The column cardinality in the mapper is Card(A), Card(B), Card(C) and Card(D). The Lazy-Buliding is demonstrated in Fig. 4.

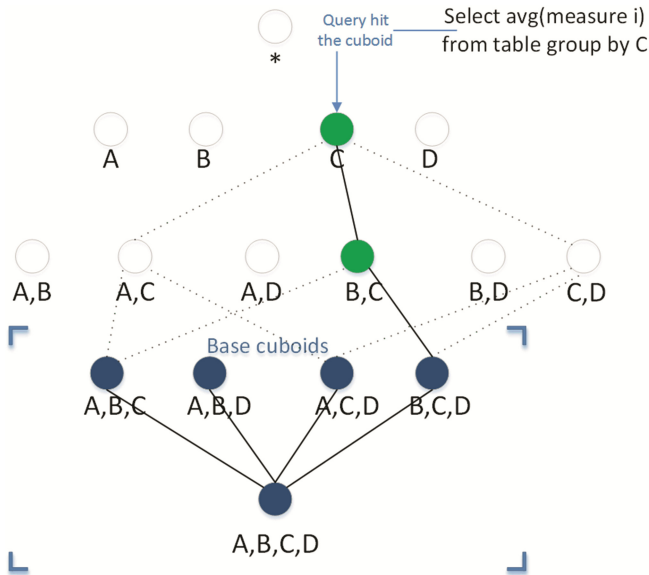


Fig. 4. Lazy-building and ancestor cuboids selection.

1. User set a base-layer parameter in cube model info to control the scale of base cuboids layer. If this parameter is not set, it will use default value $\log(\text{dimensions}) + 1$
2. Base cuboids building module import data from fact table and build the base cuboids by Cube Build Engine in Kylin.
3. Update the Cuboid Spanning Tree and save the metadata.
4. Client launch a query select avg (measure i) from table group by C which hit the missing cuboid [C]. Then, lazy building module receive request to build cuboid [C].
5. Lazy building module find a cuboid generation path according to Ancestor Cuboids Selection and build the missing cuboid to response the query as soon as possible.
6. Record the path and determine whether to build all the cuboid on the path at low load according to Materialized View Self-Adjustment Algorithm.

Ancestor Cuboids Selection. When the needed cuboids is missing, we should select an ancestor cuboid and a cuboid generation path. The basic principle is to choose the ancestor cuboid whose measures are the least to aggregate, which means we can get the minimum amount of computation and time to generate the missing cuboid. After that, we need to find a path P from ancestor cuboid to the missing cuboid in compliance with the Minimum cardinality principle.

For example, in the Fig. 4. In order to generate the missing cuboid [C], we firstly find all the candidate cuboids [A B C] [A C D] [B C D]. Then, we compare the size of the three candidate cuboids. Assuming [B C D] is selected, we generate [C] by aggregate [B C D] on dimension B, D. The cube is enough to response the query. However, for the sake of maintenance of cube according to By Layer Cubing, we need to find a path from [B C D] to [C].

When aggregating from parent to a child cuboid, assuming that from base cuboid [B C D] to 1-dimension cuboid [C], There are two paths: [B C D] [B C] [C] and [B C D] [C D] [C]. We assume $\text{Card}(D) > \text{Card}(B)$ and the dimension A is independent with other dimensions, after aggregation, the cuboid [BCD]'s size will be about $1/\text{Card}(D)$ or $1/\text{Card}(B)$ of the size of base cuboid; So the output will be reduced to $1/\text{Card}(D)$ or $1/\text{Card}(B)$ of the original one in this step. So we choose the first path, the records that written from mapper to reducer can be reduced to $1/\text{Card}(D)$ of original size; The less output to Hadoop, which means less I/O and computing and the model can attain better performance.

3.3 Materialized View Self-Adjustment Algorithm

Self-adaption module adjusts the cube according to the Materialized View Self-Adjusting Algorithm. This chapter proposes a query statistics method which takes fixed times of queries as a statistical period, and this method updates the corresponding query statistics. This method adjusts materialized views set according to the threshold of elimination and generation, stabilizes the query efficiency, and minimizes the shake of materialized view.

Query Statistics Method. A kind of Statistics Method for query.

Definition 1: Materialized view adjustment cycle T_n .

The materialized view adjustment cycle can be customized to a fixed number of queries, for example, every 100 queries for a materialized view adjustment cycle.

Definition 2: Average query statistics $E(T_n(q_i))$.

Since the actual query may change over time, the query set should also be adjusted accordingly. For example, a query that has not been executed in a couple of cycles should be removed from the query collection and the corresponding materialized view is deleted.

After many queries, the query log will accumulate a certain amount of query records, this paper presents a query statistical method based on the query log which described in the following. If there is a query set $Q = \{q_1, q_2, \dots, q_n\}$, and the query log set L , scan forward the log file from the ending of the log file and determine whether there is a query q_i in the T_n cycle, and update $E(T_n(q_i))$ according to Eq. 1:

$$E(T_n(q_i)) = \begin{cases} \alpha + (1 - \alpha)E(T_{(n-1)}(q_i)) & q_i \in L(T_n) \\ (1 - \alpha)E(T_{(n-1)}(q_i)) & q_i \notin L(T_n) \end{cases} \quad (1)$$

In the formula, α is a weighted coefficient, a constant; $L(T_n)$ is the query set in the T_n cycle. By this method, we can monitor the change of the query set Q , which can greatly reduce the shake of materialized view.

Materialized View Self-Adjustment Algorithm. The main steps of the materialized view set adjustment with the query changes are listed as follows:

1. Prior to the adjustment, initialize materialized view set $M = \{base\ cuboids\}$, the corresponding query task set to Q .
2. During the query, the query is written into the query log L , and the query counter is accumulated
3. Set the threshold of elimination T and the threshold of generation S , update the Average query statistics each life cycle T_n , and determine whether eliminate or materialize corresponding views.

The pseudo code of Materialized View Self-Adjustment Algorithm is showed in Algorithm 1.

Input: Query Log L , Materialized View M , Query Task set Q , Materialized view adjustment cycle T_n , Threshold Of Elimination T , Threshold of generation S , Path set from ancestor cuboid to the missing cuboid P

Output: Materialized View after Adjustment M

```

1 Gets the current query count value count;
2 if count %  $T_n$  then
3   for  $j = 1; j \leq T_n; j++$  do
4     scan forward the log file from the ending of the
log file  $L(T_n)$ ;
5     update query task set  $Q$  according to  $L(T_n)$  and  $P(T_n)$ ;
6   end-
7 end
8 update  $E(T_n(q_i))$  according to formula 2;
9 for each  $q_i$  in  $Q$ -do
10  if  $E(T_n(q_i)) \geq S$  then
11    materialize views  $m$  corresponding to  $q_i$ ;
12     $M.add(m)$ ;
13  end
14  else-if  $E(T_n(q_i)) \leq T$  then
15    eliminate views  $m$  corresponding to  $q_i$ ;
16     $M.delete(m)$ ;
17  end
18 end
19 Return  $M$ ;
```

Algorithm 1. Materialized View Self-Adjustment Algorithm

In the above algorithm, from line 1 to line 8, it scans the query log in a statistical period T_n , and update the query task set Q during the scanning. From line 9 to line 17, it iterate around query in Q , and determine whether eliminate or materialize corresponding views according to the comparison of threshold and the $E(T_n(q_i))$ calculated by formula 2. Suppose query task set Q contains k different query, then the time complexity of the algorithm is $O(T_n + k)$.

4 Experimental Evaluation

4.1 Dataset

To test performance, we use the standard weather dataset from the China Meteorological Data network. The dataset contains 4726499 weather records from China's 2170 distinct counties started from January 1, 2011 to January 1, 2017. The original dataset is too complicated. In order to better conduct the experiment, we select eight dimensions: Province, city, county, date, weather, wind direction, wind speed, air quality level and two measures: Maximum temperature, Minimum temperature.

4.2 Evaluation Metrics

We use cube first construction time, average query time and cube size as the evaluation metrics of our proposed method.

Cube First Construction Time refers to the base cuboids building time for self-adaption cube building model.

Average Query Time is defined as the average query time during materialized view adjustment cycle T_1-T_n . The detailed calculation is listed in Eq. 2.

$$Average\ Query\ Time = \frac{1}{NUM(Q)} \sum_{i=1}^n \sum_{j=1}^{m_{T_i}} response\ time(q_i) \tag{2}$$

Cube Size refers to the disk allocation that the whole cube takes up.

4.3 Experimental Results

We first compare the metric of cube first construction time. Because the parameter of base-layer has a great impact on this metric, in order to reflect the average condition, we use the default value $log(dimensions) + 1$. We test the model 5 times and the results were aggregated to calculate averages which can avoid the impact of MapReduce failure. Results can be seen from Table 1, the time consumption of the new model is reduced by 28.5% (Fig. 5).

Table 1. Cube first construction time

Test result	Test 1	Test 2	Test 3	Test 4	Test 5	Average
Origin Kylin cube building model	92 min	83 min	86 min	104 min	91 min	91.2 min
Self-adaption cube building model	64 min	61 min	83 min	57 min	61 min	65.2 min

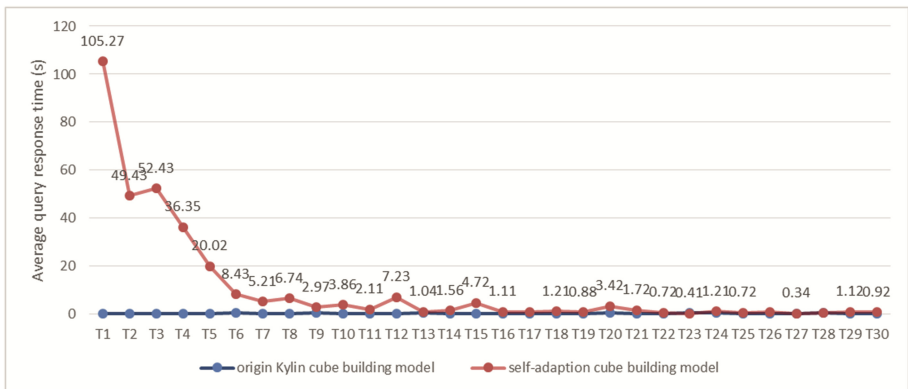


Fig. 5. Average query time trends in T_1-T_{30} .

In query time, we set Materialized view adjustment cycle T_n 50 and test 30 cycles $T_1 - T_{30}$. We can observe that Cuboid hit rate and query response time significantly increased and improved along with the increase of query requests. Finally, the query efficiency of the two models are almost on a par.

In cube size, we see that the curve that represents this metric tends to be stable after vibration in prophase from Fig. 6. Finally, the spaces consumption of the proposed model was reduced by 65.83%.

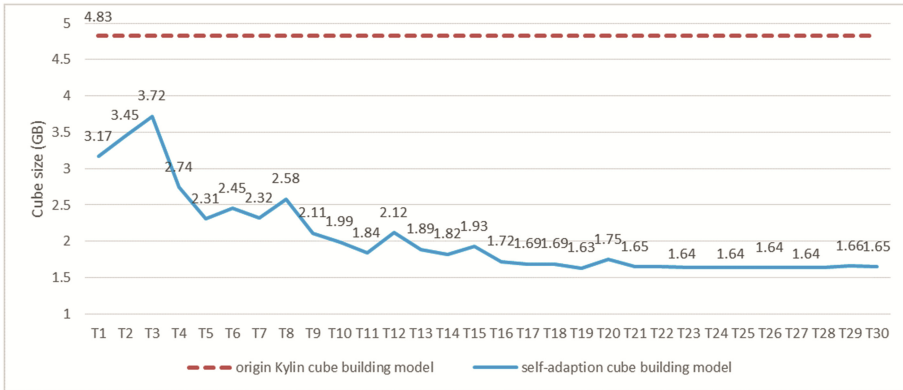


Fig. 6. Average cube size trends in $T_1 - T_{30}$.

5 Conclusion

We have presented a Distributed Self-Adaption Cube Construction Model Based on Query Log and applied it to a weather dataset to test its performance. Our model adopts a special partial materialization strategy and it can automatically adjust the cuboid set which is used in query request according to query log. Based on experimental results, the proposed model can reduce the cube construction time and cube size to a great extent at the expense of tiny query efficiency reduction. However, this model has good performance only when the query distribution is relatively concentrated. So users can choose either of the two models according to their practical business query scenario. Overall, the proposed model is of great practical significance in the application of BI tools. In the next stage, we will optimize the base cuboids generation strategy to reduce the query latency in prophase.

Acknowledgement. This work is supported by the National Key project of Scientific and Technical Supporting Programs of China (Grant No. 2015BAH07F01); Engineering Research Center of Information Networks, Ministry of Education.

References

1. Chen, Y., Dehne, F., Eavis, T., Rau-Chaplin, A.: Parallel ROLAP data cube construction on shared-nothing multiprocessors. *Distribut. Parallel Databases* **15**(3), 219–236 (2004)
2. Impala (2017). <http://impala.apache.org/>. Accessed 13 Apr 2017
3. Deshpande, P.M., Gupta, R., Gupta, A.: Distributed iceberg cubing over ordered dimensions, March 2015. US Patent App. 14/658,542
4. Presto (2017). <https://prestodb.io/>. Accessed 13 Apr 2017
5. Gray, J., Chaudhuri, S., Bosworth, A., Layman, A., Reichart, D., Venkatrao, M., Pellow, F., Pirahesh, H.: Data cube: a relational aggregation operator generalizing group-by, cross-tab, and sub-totals. *Data Mining Knowl. Disc.* **1**(1), 29–53 (1997)
6. Kalisch, M., Michalak, M., Przystalka, P., Sikora, M., Wróbel, Ł.: Outlier detection and elimination in stream data – an experimental approach. In: Flores, V., et al. (eds.) *IJCRS 2016*. LNCS (LNAD), vol. 9920, pp. 416–426. Springer, Cham (2016). https://doi.org/10.1007/978-3-319-47160-0_38
7. Kylin (2017). <http://kylin.apache.org/>. Accessed 13 Apr 2017
8. Lee, S., Kim, J., Moon, Y.-S., Lee, W.: Efficient distributed parallel top-down computation of ROLAP data cube using MapReduce. In: Cuzzocrea, A., Dayal, U. (eds.) *DaWaK 2012*. LNCS, vol. 7448, pp. 168–179. Springer, Heidelberg (2012). https://doi.org/10.1007/978-3-642-32584-7_14
9. Li, F., Ozsu, M.T., Chen, G., Ooi, B.C.: R-store: a scalable distributed system for supporting real-time analytics. In: 2014 IEEE 30th International Conference on Data Engineering (ICDE), pp. 40–51. IEEE (2014)
10. Elasticsearch (2017). <https://www.elastic.co/products/elasticsearch>. Accessed 13 Apr 2017
11. Nandi, A., Yu, C., Bohannon, P., Ramakrishnan, R.: Distributed cube materialization on holistic measures. In: 2011 IEEE 27th International Conference on Data Engineering (ICDE), pp. 183–194. IEEE (2011)
12. Shi, Y., Zhou, Y.: An improved apriori algorithm. In: *Granular Computing (GrC)*, pp. 759–762. IEEE (2010)
13. Silva, R.R., Hirata, C.M., de Castro Lima, J.: Computing big data cubes with hybrid memory. *J. Convergence Inf. Technol.* **11**(1), 13 (2016)
14. Spark SQL (2017). <http://spark.apache.org/sql/>. Accessed 13 Apr 2017
15. Wang, W., Feng, J., Lu, H., Yu, J.X.: Condensed cube: an effective approach to reducing data cube size. In: 18th International Conference on Data Engineering, Proceedings, pp. 155–165. IEEE (2002)
16. Xia, Y., Luo, T.T., Zhang, X., Bae, H.Y.: A parallel adaptive partial materialization method of data cube based on genetic algorithm (2016)
17. Yin, D., Gao, H., Zou, Z., Li, J., Cai, Z.: Approximate iceberg cube on heterogeneous dimensions. In: Navathe, S.B., Wu, W., Shekhar, S., Du, X., Wang, X.S., Xiong, H. (eds.) *DASFAA 2016*. LNCS, vol. 9643, pp. 82–97. Springer, Cham (2016). https://doi.org/10.1007/978-3-319-32049-6_6
18. Zhao, Y., Deshpande, P.M., Naughton, J.F.: An array-based algorithm for simultaneous multidimensional aggregates. *ACM SIGMOD Rec.* **26**, 159–170 (1997)

Property-Based Network Discovery of IoT Nodes Using Bloom Filters

Rustem Dautov^{1(✉)}, Salvatore Distefano^{1,2}, Oleg Senko³, and Oleg Surnin³

¹ Higher Institute of Information Technology and Information Systems (ITIS),
Kazan Federal University (KFU), Kazan, Russia

{rdautov,s_distefano}@it.kfu.ru

² University of Messina, Messina, Italy

sdistefano@unime.it

³ Kazan, Russia

Abstract. As the number of IoT devices is exponentially growing, and IoT networks are expanding in their size and complexity, timely device discovery is becoming a pressing concern. The extreme (and constantly growing) number of network nodes, dynamically connecting to and disconnecting from a network, renders existing routing techniques, such as multicasting and broadcasting, unscalable, especially when using the IPv6 128-bit addresses. To address this limitation, this paper discusses the potential of implementing the IoT device discovery, based on device properties, such as type, functionality, location, etc., and presents an approach to enable property-based access to IoT nodes using Bloom filters. The proposed approach demonstrates space- and network-efficient characteristics, as well as provides an opportunity to perform device discovery at various granularity levels.

Keywords: Bloom filter · Internet of things · Edge computing
Device discovery

1 Introduction

In the IoT context, a user (or an application) using hundreds or thousands of devices has to deal with considerably long addresses to uniquely identify and refer to network devices. This exponential growth is expected to introduce new challenges to traditional computer network protocols, such as, for example, *(i)* efficient access to a huge number of devices; *(ii)* security and privacy; *(iii)* interoperability and standardisation; *(iv)* efficient energy consumption. Moreover, given the extreme amounts of heterogeneous devices constituting the IoT ecosystem, timely and accurate device discovery based on some specific parameters such as device type, sensing/actuating capabilities, status, powering options is also seen as a pressing and challenging issue. In this light, a potential way to enable device discovery in the IoT, taking into account the size and complexity of underlying networks, could be to include additional parameters in the

routing procedure with a goal to limit the search space. More specifically, a potential solution would be able address IoT network devices not only through their IP addresses, but also through a combination of device properties, such as their type, location, sensing/actuating capabilities, available resources and so on. From this perspective, an envisaged solution could implement some kind of selective routing algorithm, which would facilitate time- and network-efficient device discovery in the IoT context. For instance, this will allow collecting information from specific sensing devices (e.g. within a single building) and apply actuation commands (e.g. turn on heating in rooms with low temperature) in a selective manner. Similarly, remote device management and maintenance would also become feasible, as users would be able to diagnose errors and patch required devices with corresponding software updates (e.g. keeping a surveillance system up to date with most recent system security updates).

Taking into considerations these desired features of a possible solution, this paper presents an approach to facilitate property-based device search and discovery in complex IoT networks using counting Bloom filters. As it will be explained below, the proposed approach benefits from the space-efficient way of storing information about devices and their properties, as well as fast calculation times when deciding whether a matching device is present in the network. Moreover, with property-based search using Bloom filters, it becomes possible to perform device discovery at various granularity levels.

2 Background: Bloom Filters

A Bloom filter, originally defined by Bloom in 1970 [1], is a space-efficient probabilistic data structure, representing a set S of m elements using an array of n bits $\mathbf{B} = (B[1], \dots, B[n])$ initialised to 0. The filter uses a set of k independent hash functions $\mathcal{H} = \{h_1, \dots, h_k\}$ with a range $\{1, \dots, n\}$ uniformly mapping each element of S to a random position over the \mathbf{B} array. More specifically, for each element $s \in S$, the bits $B[h_i(s)]$ are set to 1 $\forall i \mid 1 \leq i \leq k$. A bit can be set to 1 multiple times either through different hash functions for the same element s or different elements of S . As a result, an answer to the query ‘Is $b \in S$?’ is true, if all $h_i(b)$ are set to 1, otherwise (i.e. if at least one bit is 0), b is not in S . While the Bloom filter has many advantages, such as fast access time and a relatively small size (a few bytes per element at most), it may suffer from a possibility of false positive results on membership checks. A false positive occurs when the hashes from an element not in the Bloom filter overlap with a combination of hashes from elements that are in the Bloom Filter.

Deleting elements from a Bloom filter cannot be done simply by changing ones back to zeros, as a single bit may correspond to multiple elements. To enable deletion of elements, the so-called counting Bloom filter uses an array of n counters instead of bits. These counters are able to ‘track’ the number of elements currently hashed to that location [3]. Deletions can be safely done by decrementing the relevant counters. A standard Bloom filter can be derived from a counting Bloom filter by setting all non-zero counters to 1.

Bloom filters were originally introduced to improve data management performance, and quickly became popular in a variety of databases and storage systems [1]. Then, they have been widely used in distributed systems [6] across a wide range of application domains. In the recent years, Bloom filters experienced an increased interest by the networking and security domains [2]. More specifically, they are also widely applied in intrusion detection, virus and spam detection, access control [4], and IP traceback [5].

3 Proposed Approach

The proposed approach is based on a two-step procedure. First, all the intermediate nodes in the network hierarchy are populated with information about edge nodes. Second, once the network is populated, an IoT device can be discovered using a corresponding query.

3.1 Populating the Network

An IoT device in a network hierarchy can be represented as a tuple $D = (ID, Prop)$, where ID is a unique identifier of this device, and $Prop$ is a set of properties of this device, such as, for example, *type* (e.g. CCTV camera, environmental sensor, smartphone, etc.), *sensing capabilities* (e.g. temperature, pressure, noise, acceleration, etc.), *power supply* (e.g. solar panel, battery, power cord, etc.), *manufacturer*, *model*, *production date*, and so on. Using suitable hash functions, each set of device properties $Prop$ is converted into a corresponding Bloom filter array. Next, the network hierarchy is ‘populated’ by these newly-created Bloom filters in a bottom-up manner – i.e. edge devices provide its immediate subnet gateway with their Bloom filter representations, which are summed up in a single Bloom filter by doing the bitwise OR operation. This process is then iteratively repeated up until the very top of an IoT network hierarchy. As a result, the top-level server’s Bloom filter eventually contains Bloom filters of all individual edge nodes in its network.

3.2 Device Discovery

At the device discovery step, Bloom filters are used to represent corresponding discovery queries. More specifically, each query is represented by a tuple $Q = (ID, Prop)$, where ID is a unique identifier of this query, and $Prop$ is a set of device properties, which are expected to be discovered within the given network. These properties can be seen as search parameters, as typically used in traditional searching. Each query is then represented by a corresponding Bloom filter, using the same hash functions. Device discovery can be seen as a reverse process of populating the network hierarchy, executed in a top-down manner starting from the very top of the network topology. By performing the bitwise AND operation, the top-level server first checks with its own Bloom filter whether

there is a device, matching query parameters, in its managed network. Accordingly, if the evaluation is true, the query is sent down to lower-level network gateways, which similarly check whether a suitable device is present in their subnet. This process iterates in each subnet either (i) until reaching the very bottom level and a suitable device is discovered, or (ii) until one of the intermediate network nodes replies that no matching device is present in its subnet.

3.3 Sample Scenario

The simplified use case scenario assumes each device (and its properties) is represented by a 6-bit Bloom filter. From left to right, these bits indicate whether a device is: a camera (1), an environmental sensor (2), a smartphone (3), battery-powered (4), powered by a solar panel (5), or powered by a cord (6). It is also assumed that there are three subnets in the network, each containing three devices (Fig. 1). The three network gateways contain combined Bloom filters of their respective subnets, and the server contains the overall Bloom filter representation of the network. The goal of this scenario is to discover a camera, powered by a cord. Accordingly, the query is represented by the following Bloom filter $BF = (1, 0, 0, 0, 0, 1)$.

At the first step, the server evaluates the query against its own Bloom filter, and decides that there is indeed a matching device present somewhere down the network. Next, the query is propagated down to three subnets. The respective gateways start evaluating the query against their own Bloom filters. As it is seen from the diagram, Subnet A contains only smartphones, and Subnet B contains only environmental sensors. The query evaluation returns false, and, as a result, the network call is not propagated down the first two subnets. Gateway C, by evaluating the query, understands that there is a matching device in its subnet and sends the query to all three nodes. Two of these nodes are cameras, but only one of them – Device C3 – is actually powered by a cord. By evaluating

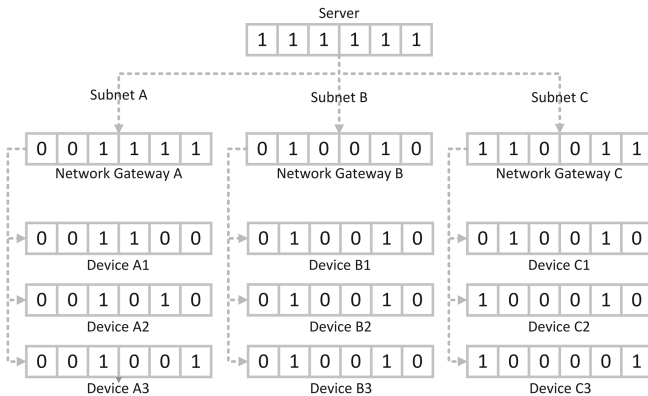


Fig. 1. Property-based network device discovery using Bloom filters.

the incoming query, it realises that it matches query parameters, and replies back with its ID and network location. The reply is then sent back to the server through intermediate hops.

The presented property-based search for IoT devices enables flexible, fine-grained discovery of IoT nodes. The more properties are specified in the query, the more precise the search is and less matching devices are discovered. On contrary, for a single specified property, the search space is expected to be wider, since more devices might satisfy the search query parameter. For example, in the simplified scenario above, searching for a solar panel-powered device will yield 6 results.

4 Discussing the Benefits

This paper presented an approach for property-based network discovery of IoT nodes using Bloom filters. Potential benefits of the proposed solution can be summarised as follows:

Flexible device discovery at different levels of granularity: as opposed to the traditional access to edge nodes in IoT environments, where IP addresses need to be known in advance, the proposed approach enables searching for devices based on their properties, such as type, sensing capabilities, powering options, etc. This kind of property-based device discovery can be performed at various levels of granularity – i.e. coarse-grained (e.g. discover any kind of camera within a network) or fine-grained (e.g. discover an outdoors CCTV camera with high resolution, powered by a solar panel). This flexibility has the potential to contribute to creation of a wide range of IoT systems, where the network topology is not static, but rather devices are constantly joining and leaving the network. Moreover, the property-based search paves the way for *interchangeable* IoT architectures, in which individual elements are described in terms of their features and functionalities. This way, one element can be substituted by a similar one based on their shared properties, in a seamless, transparent manner.

Network efficiency: a Bloom filter (as suggested by its name itself) serves to filter incoming search queries to avoid redundant broadcast calls through the whole network. If an intermediate node understands that there is no matching device within its subnet, it does not allow the query to go down that specific subnet, thus (i) decreasing the amount of time needed to discover a device, and (ii) minimising the amount of redundant network traffic and improving network latency. Moreover, the query evaluation procedure – i.e. performing the bitwise AND operation on two bit arrays – is a time-efficient operation with minimum impact on the overall device discovery process. In the presence of hundreds and thousands of edge devices and intermediate network nodes, both network- and time-efficiency is seen as considerable benefits when discovering devices (even taking into consideration the false positive rate).

Space efficiency: Bloom filters are space-efficient data structures, requiring minimum amount of memory. Even when using counting Bloom filters, resulting

arrays typically do not exceed 4 MB of storage space – a highly-relevant feature in the context of IoT environments, where individual nodes are not necessarily equipped with mass storage facilities.

High accuracy: despite potential false positive results, which may occur during the device discovery process at intermediate network nodes, the overall accuracy is not affected, since a final decision whether a matching device is present in the network or not is taken by edge devices themselves. Only if an edge device's Bloom filter matches an incoming query, a corresponding acknowledgement is sent back to the server. Otherwise, it is assumed that no matching devices were identified.

Scalability and extensibility: thanks to the ability to store large amounts of hashed values and high calculation speed, a Bloom filter can be updated with new elements with a minimum effect on the overall performance. This is especially important in the context of IoT networks, which are already constituted by millions of devices, and keep on growing in their size and complexity.

5 Conclusions

The presented solution enables flexible property-based device discovery in the context of complex IoT networks using Bloom filters. As opposed to the IPv6 routing, which requires 128 bits to encode an address, the proposed approach benefits from the space-efficient way of representing and storing data using a Bloom filter. This also contributes to decreased traffic and network latency, as the device discovery duration depends on how narrow-focused a search query is (i.e. the less devices matching the query, the less network traffic is generated). The Bloom filter decides whether a device belongs to a subnet branch or not, and can 'cut off' the entire branch before actually checking it. As a result, this considerably reduces the amount of network traffic, especially when compared to broadcast and multicast routing techniques.

References

1. Bloom, B.H.: Space/time trade-offs in hash coding with allowable errors. *Commun. ACM* **13**(7), 422–426 (1970)
2. Broder, A., Mitzenmacher, M.: Network applications of Bloom filters: a survey. *Int. Math.* **1**(4), 485–509 (2004)
3. Fan, L., Cao, P., Almeida, J., Broder, A.Z.: Summary cache: a scalable wide-area web cache sharing protocol. *IEEE/ACM Trans. Netw. (TON)* **8**(3), 281–293 (2000)
4. Foley, S.N., Navarro-Arribas, G.: A Bloom filter based model for decentralized authorization. *Int. J. Intell. Syst.* **28**(6), 565–582 (2013)
5. Snoeren, A.C., Partridge, C., Sanchez, L.A., Jones, C.E., Tchakountio, F., Kent, S.T., Strayer, W.T.: Hash-based IP traceback. In: *ACM SIGCOMM Computer Communication Review*, vol. 31, pp. 3–14. ACM (2001)
6. Tarkoma, S., Rothenberg, C.E., Lagerspetz, E., et al.: Theory and practice of Bloom filters for distributed systems. *IEEE Commun. Surv. Tutorials* **14**(1), 131–155 (2012)

The Personality Analysis of Characters in Vernacular Novels by SC-LIWC

Yahui Yuan¹, Baobin Li^{1(✉)}, Dongdong Jiao², and Tingshao Zhu²

¹ School of Computer and Control, University of Chinese Academy of Sciences, Beijing 100190, China
libb@ucas.ac.cn

² Institute of Psychology Chinese Academy of Sciences, Beijing 100101, China
tszhu@psych.ac.cn

Abstract. There are many researches on psychological text analysis, and it has been proved that the words people use can reflect their emotional states. In this paper, we introduce how to analyze the psychology of the characters in vernacular novels automatically. First, we process the dialogs with word segmentation, and analyze the segmented text with SC-LIWC. Then, a vector reflecting the psychology of the character is obtained and we map it to the big five. Finally, taking the dialogs of *the Journey to the West* as corpus, We have got the personalities of four main characters which are verified to be same as some famous comments of *the Journey to the West*, which shows that our work is effective.

Keywords: LIWC · Vernacular · The Journey to the West · The big five
Text analysis

1 Introduction

The use of words in the text can reflect the individual's psychological state and personality [1]. Linguistic Inquiry and Word Count is a tool which we can use to analyze text. The way that the Linguistic Inquiry and Word Count (LIWC) program works is fairly simple. Basically, it reads a given text and counts the percentage of words that reflect different emotions, thinking styles, social concerns, and even parts of speech.

To date, LIWC has been applied to many psychology research. It is often used to examine suicide writings in order to characterize the quantitative linguistic features of suicidal texts, in [2], the authors analyze texts compiled in Marilyn Monroe's Fragments using LIWC, in order to explore the contact between the use of different linguistic categories over the years and her suicide. The result is coincide with different theories of suicide. López-López et al. [3] analyzed the StackOverflow's answers and questions to explore the users' personality traits. They found that the top reputed authors are more extroverted than general users. Moreover, authors who got more votes express significantly less negative emotions than those who got less votes. Markovikj et al. [4] explored

the modeling feasibility of user personality based on the features extracted from Facebook. In [5], they collected a sample of 363 participants, including their written self-introductions and final course performance, the result shows that course performance could indeed be predicted by the word usage of linguistic categories.

LIWC for Traditional Chinese, TC-LIWC, is published with the authorization of Pennebaker by Huang et al. (2012). After that, SC-LIWC for Simplified Chinese [6, 7] is published on the basis of TC-LIWC, which lays the foundation for the following research [10, 12].

Recently, some researchers are concerned about automatic personalistic prediction using liwc. Personality is stable in a period of time, so a collected corpus from several months is suitable for this research. Gao [12] selects 1766 participants, first make them fill in a big five inventory for comparison, and then collect their weibo through the API of Sina. 90% of the samples are trained using liwc and the rest act as test set. In the training stage, they compute the Pearson's coefficient between the inventory and the training results, then choose features which behave well in the training. At last, the features are composed to predict personality of test set. They compute the Pearson's coefficient as before, and the results are between 0.3~0.4. While the coefficient between self-rating and rating by observers is about 0.5, hence the method has prediction ability to some extent.

We will seek method to predict the personality of characters in novels written in vernacular. Vernacular is a written language with some artistic processing. It is easy to read, but still have some features of ancient Chinese. Vernacular is generally used for literacy, especially in the novels. Vernacular novels are very popular from the beginning of Ming Dynasty. Three of the four famous Chinese novels were accomplished in Ming Dynasty. After that, vernacular novels were more and more popular. There are many excellent ancient books in China, which created numerous virtual characters, a book named *A Dream of Red Mansions* only, contains hundreds of characters. We will pay a lot of time to read books, look up in the library, to understand these figures and step into the author's inner world. If we can analyze the characters of the books automatically, it will save us much time and help us follow the books.

In this study, we use LIWC to analyze the personality of the characters in vernacular novels. The process of personality analysis of the characters in the vernacular novels is shown in Fig. 1. The rest of this paper is organized as follows. Section 2 will discuss the preprocessing work for the novel. And then in Sect. 3, we will split the dialogs obtained from Sect. 2, which will be used to analysis the personality of the characters and get the big five of characters in Sect. 4. Finally, we also present the personality change of Sun Wukong before and after the three strikes of White Bone Demon.

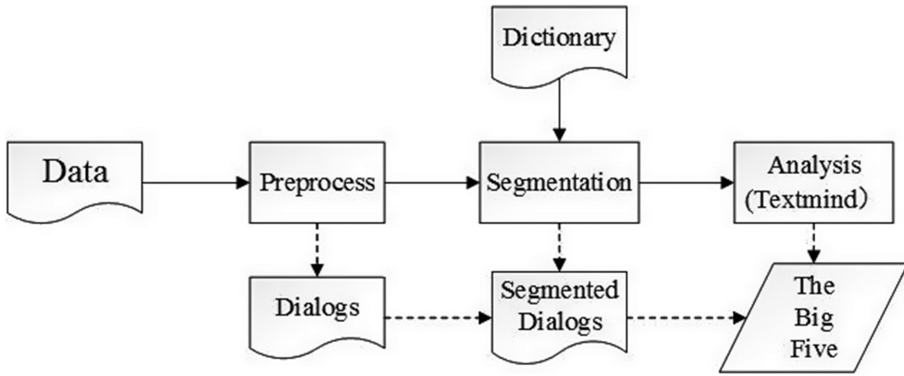


Fig. 1. The flow chart of automatic personality analysis of vernacular novels.

2 Data and Data Preprocessing

The Journey to the West is the first ancient Chinese romantic novel. The book deeply depicts the social reality of the time, mainly describes the origin of Tang priest, Sun Wukong, Zhu Bajie, Sha monk, and together with the story of pilgrimage to the west. After the spread of centuries, *the Journey to the West* has been translated into many languages, and a number of relevant research monographs have been published, which made a high evaluation of the novel. *The Journey to the West* is known as one of the four famous Chinese classics. There are four main characters in *the Journey to the West*. They are Sun Wukong, Sha monk, Zhu Bajie and their master, Tang priest.

James W. Pennebaker proved that words used in their daily lives could contains important information of psychological information [8]. Especially, he proved that not only nouns and verbs serve as markers of emotional state, social identity, and cognitive styles, particles, serve as the glue that holds nouns and regular verbs together, can also do the same things. That means we can study the particles instead of more complex methods. On the basis of his work, we decide to use the dialogs of the characters to study their personality. We select the dialogues and their inner monologues for each character respectively, and put them into 5 different files. There are a lot of descriptive verses in the text, we should delete them because they would interface the process of participation, and these verses are often said by other people, not the roles themselves, so we believe that the descriptive verse have little influence on the personality. Notice that it shouldn't include quotes on the end of the sentence. But other interval will be retained for the next step. At last we get four files.

3 Segmentation

In order to get the particles for analysis, we should first do the text segmentation. As we know, the current methods of Chinese word segmentation can be divided into three kinds: the method based on lexicons, the method based on statistics and one based on

semantics. Also there are methods mixing two or three of them in order to improve the accurate. There have been many kinds of word segmentation systems for modern Chinese. For example, LTP-CLOUD, NLPIR, jieba, and so on. These systems all have good results in Chinese word segmentation. Among these tools, LTP and NLPIR are systematic tools, while jieba only contains segmentation function. Moreover, LTP and jieba are open source tools, but NLPIR is not.

Few studies are involved in ancient Chinese segmentation. First, there is little corpus for ancient Chinese. As we all know, segmentation need a lot of corpus which has been marked manual to improve the accurate, but no one have done the work for ancient Chinese. Second, it seems that we cannot obtain any economic benefits from it. However, Hou, et al. have studied ancient Chinese segmentation [9], but the corpus is still very small, which couldn't be generalized easily.

Vernacular has the features of both ancient Chinese and modern Chinese. Therefore, we can refer to the methods for modern Chinese segmentation.

The punctuation and function words are not changed much over the years. They are also used in ancient Chinese. Besides, there are a lot of words that still exist in ancient Chinese. In addition, the Chinese word segmentation methods are able to identify new words according to statistical methods.

In order to simplify the segmentation procession, we make a simple test on the segmentation of vernacular and find, most words are segmented correctly by applying the LTP directly. But there are still many mistakes; notional words are not distinguished from others, idioms are segmented wrong, and there are other mistakes generated in the algorithm. That is mainly because of the difference between vernacular and modern Chinese. There are many words which are not used now, especially those appear only several times in the text.

A simpler and more efficient method we used to solve above questions is add a manual dictionary to the LTP. The dictionary includes notional words and some idioms. Notional words include place name, monster name, Tang priest and his three apprentices' name and nickname, gods' name and their nickname, the particular items and some words about the emperor and the dynasty.

- Place name. There are a lot of places made up by the author, such as the monster's cave, the god's mountain, the monkey's birthplace, and so on. Take these words into dictionary will make sure they are segmented correctly.
- Monster's name. Tang priest and his four apprentices meet many big monsters on *the Journey to the West*, and each of them get a nickname, even some of small monster under them get one, too. To split them correctly, we had better put them into the dictionary.
- Four characters' name and their nickname. Though only four people, each of them have many nickname. Only Tang priest has more than 5 nicknames, for example, priest, Tang priest, Xuanzang, elder, Tang elder, master, and so on. Especially they often emerge in the dialogs. Therefore, split them from other words are important.
- Gods' name and their nickname. When walking through the long way, the four meet a lot of gods. Each of them have several nickname, especially Guanyin, his nicknames even catch up with Tang priest.

- The particular items. There are many particular things in *the Journey to the West*, such as kinds of weapons, treasures, and so on. Much of them are not usually used in modesty Chinese.
- Some idioms. Idioms are fixed phrases in the ancient Chinese.
- Some words about the emperor and the dynasty.

We select 1000 characters randomly from the segmentation results for each of the four, five of our workmates check it respectively. When finished all, they vote on the contradicted ones. Table 1 shows that the error rate is about 2%~3%, in other words, the accurate rate is about 97%~98%. Though the punctuation is count into the words, the error rate will not exceed 1.2 times of the existing data. As we can see, this method is quite effective.

Table 1. The error rate of word segmentation.

	Total	Wrong	Error Rate
Tang priest	850	27	0.0318
Sun Wukong	766	21	0.0274
Zhu Bajie	1048	25	0.0239
Sha monk	753	30	0.0398

In [12], five of six feature classes are properties of Weibo, so in our work, we choose only the features of liwc. Due to the differences between ancient Chinese and modern Chinese, liwc dictionary will have corresponding change, so will the features selected based on liwc. To solve it, we get rid of the features which are not consistent with ancient Chinese. The rest features will serve as input of the model which have been trained in [12]. In order to inspect the personality more intuitive, we adopt a commonly used quantitative method in psychology—the big five personality traits [11]. In the big five traits model, the user's personality is abstracted into five dimensions, which are shown in Tables 2 and 3. The big five score of Tang priest and his apprentice is shown in Table 4.

Table 2. The big five 1. Each of them has 6 facets.

Agreeableness	Conscientiousness	Extraversion
Trust	Competence	Warmth
Straightforwardness	Order	Gregariousness
Altruism	Dutifulness	Assertiveness
Compliance	Achivement striving	Activity
Modesty	Self-discipline	Excitement seeking
Tender mindedness	Deliberation	Positive emotion

Table 3. The big five 2.

Openness to experience	Neuroticism
Fantasy	Anxiety
Aesthetics	Hostility
Feelings	Depression
Actions	Self-consciousness
Ideas	Impulsiveness
Values	Vulnerability to stress

Table 4. The big five of Tang priest and his three apprentice.

	Agree.	Cons.	Extra.	Open.	Neur.
Tang priest	13.06	11.26	7.94	3.50	25.42
Sun Wukong	9.63	4.97	1.34	0.92	1.93
Zhu Bajie	9.25	5.02	18.54	15.08	18.27
Sha monk	15.24	6.54	14.15	1.10	26.31

4 Personality Analysis of Characters

4.1 Agreeableness

As an eminent monk from Tang dynasty, Tang priest is very kind and compassionate [13]. On the Journey to the West, he tries to help others, though when he is in danger. He is modest and subject to authority, such as emperor of Tang Dynasty, and all the gods they meet on the Journey to the West. But sometimes he is egoistic, and often shifts responsibility. His agreeableness is relatively high.

Sha monk is very careful and slavish since he was surrendered by Sun Wukong. He has never been egoistic, doing his best to serve the master and help his brothers [14]. Tang priest and Sun Wukong all have deep trust on him. The agreeableness of him is highest.

Sun Wukong is capable, but his master does not trust him. He has helped many people, but that does not mean he is willing to sacrifice. If someone harms his interests, he will not hesitate to teach him a lesson. Sun Wukong is also an arrogance role, never understanding what modesty is. He is not gentle too. In conclude, his agreeableness is lowest.

4.2 Conscientiousness

Tang priest has no ability to protect himself, and has no experience to deal with monsters. He strictly abides by the doctrine, trying his best to protect it. And he has a strong will, which makes him go to the west firmly to obtain Mahayana Buddhism [13]. All in all, his conscientiousness is relatively high.

Though exiled from heaven just because knocked over a glass made of colored glaze, Sha monk not only gets no angry, but also accepts the destiny to atone for his sin. In this point, he is something like Tang priest [14]. Compared with his brothers, he seems plain, but he is better than his brothers in human nature. So his conscientiousness is relatively higher.

Sun Wukong is strongest among his brothers. He pursues the idea that the stronger should hold the power, never yielding to authority [15]. Therefore, many gods serve him as a servant. He tries his best to protect the master, not for any benefits, but for returning Tang priest's salvation. He could not restrain his aggressive instincts, and that makes Tang priest most unhappy. It is not strange that his conscientiousness is lower than his brothers.

Zhu Bajie is similar with Sun Wukong in agreeableness and conscientiousness. There is also difference: Zhu Bajie gets more score in tender mindedness, while Sun Wukong gets more in altruism [16, 17]. Zhu Bajie obeys the laws. Sun Wukong is a king of monkey before he follows Tang priest, so he has no knowledge of it. Thus in order, Zhu Bajie gets more score. But he always declares to go back to Gao Village when he encounters danger. Sun Wukong loves battle while Zhu Bajie loves women. In total, they go head in head with each other in agreeableness and conscientiousness.

4.3 Extraversion

In the point of extraversion, Zhu Bajie gets first without question. He is very lustful, showing great enthusiasm for women. He loves to eat, too [18]. Each time when they arrive to a new town, he is happiest because he can eat a lot. Zhu Bajie is outgoing compared with other people.

Sha monk is upright and honest [19]. He talks little, but what he said is very useful. When there is contradiction among the group, Sha monk is the one who tries to solve it.

Tang priest is kind and friendly when dealing with people, but not enthusiastic. He prefers quiet than noisy. So his extraversion is low.

In Table 4, Sun Wukong is lowest in extraversion. Though his warmth is not as good as his brothers, but the rest features should be better than others. The possible reason may be the dictionary we use may not be so fit with his dialogs.

4.4 Openness

Openness is an indicator of the level of intelligence. From Table 4 we can observe that Zhu Bajie gets the highest score. Zhu Bajie is always being called "fool", but that is not the case [18]. He is fond of eating and sleeping, and good at flattering in front of master, so Tang priest trusts him very much. In general, he always makes the best decision for himself.

As a leader of the group, Tang priest is well learned and behaved. But he is often cheated by monsters and confused by Zhu Bajie, and getting rid of Sun Wukong several times, who tries to protect him.

Sha monk actually is a servant of Tang priest. He is responsible for all trifles, but never complaining about it [20].

Sun Wukong is powerful and good at dealing with enemies, however, he is often fooled by Zhu Bajie. So in fact, Zhu Bajie is the most intelligent person among the group.

4.5 Neuroticism

In the term of neuroticism, Tang priest and Sha monk are similar to each other. When facing the danger, Tang priest is anxious and scared, and often bursts into tears [13]. Sha monk is puzzled, and ‘What should we do?’ is his pet phrase. Zhu Bajie helps Sun Wukong a lot in fighting, but once failed the first thing he thinks of is escaping. Sun Wukong never gives up, even if he was alone, he will fight until success.

5 The Personality Change of Sun Wukong

We also did a research on the personality change of Sun Wukong before and after the three strikes of White Bone Demon with this model. The results are shown in Table 5.

Table 5. The big five of Sun Wukong before and after his beating the White Bone Demon for three times.

	Agree.	Cons.	Extra.	Open.	Neur.
Before	6.28	3.63	2.83	19.27	6.62
After	10.56	4.99	0.39	1.03	1.19

Beating the White Bone Demon for three times was a turning point of Sun Wukong. The author explained the mind change of Sun Wukong by the words of Zhu Bajie.

Before that, Sun Wukong was very irritable, but under the constraint of Tang priest, he changed gradually. He became no more impulsive at all. It is corresponding to the decrease of neuroticism.

In the early stage, Sun Wukong despised the authority, refused to obey the discipline, and showed a clear sense of rebellion. While later he was influenced by Tang priest, no longer having a strong sense of resistance. As we can see in Table 5, his openness is greatly changed before and after the three beats of White Bone Demon.

The agreeableness is higher after the three strikes. In the respect of getting along with people, Sun Wukong changed obviously, especially to Bodhisattva, Buddha, and some others who is venerable. He was more and more courteous and no longer as arrogant as before.

In the early stage, the responsibility of Sun Wukong is not clear, he even tried killing Tang priest and attacked the Bodhisattva at first. However, he accepted his duty in the late, becoming a qualified defender.

6 Conclusion

In this paper, we make a automatic personality analysis of characters *in the Journey to the West* using LIWC, and map the feature vector into the big five to make it easy to

observe. We compare the results with many famous reviews, and compare the results between characters, and compare the results back and forward. These comparisons all show that automatic personality analysis of characters with LIWC is feasible.

References

1. Tausczik, Y.R., Pennebaker, J.W.: The psychological meaning of words: LIWC and computerized text analysis methods. *J. Lang. Soc. Psychol.* **29**, 24–54 (2010)
2. Fernándezcabana, M., Garcíacaballero, A., Alvespérez, M.T., Garcíagarcía, M.J., Mateos, R.: Suicidal traits in Marilyn Monroe's fragments: an LIWC analysis. *Crisis* **34**, 124–130 (2013)
3. López-López, E., del Pilar Salas-Zárate, M., Almela, Á., Rodríguez-García, M.Á., Valencia-García, R., Alor-Hernández, G.: LIWC-based sentiment analysis in Spanish product reviews. In: Omatu, S., Bersini, H., Corchado, J.M., Rodríguez, S., Pawlewski, P., Bucciarelli, E. (eds.) *Distributed Computing and Artificial Intelligence*, 11th International Conference. AISC, vol. 290, pp. 379–386. Springer, Cham (2014). https://doi.org/10.1007/978-3-319-07593-8_44
4. Markovikj, D., Gievska, S., Kosinski, M., Stillwell, D.J.: Mining Facebook data for predictive personality modeling. In: *AAAI International Conference on Weblogs and Social Media* (2013)
5. Robinson, R.L., Navea, R., Ickes, W.: Predicting final course performance from students' written self-introductions: a LIWC analysis. *J. Lang. Soc. Psychol.* **32**, 469–479 (2013)
6. Gao, R., Hao, B., Li, H., Gao, Y., Zhu, T.: Developing simplified Chinese psychological linguistic analysis dictionary for microblog. In: Imamura, K., Usui, S., Shirao, T., Kasamatsu, T., Schwabe, L., Zhong, N. (eds.) *BHI 2013. LNCS (LNAI)*, vol. 8211, pp. 359–368. Springer, Cham (2013). https://doi.org/10.1007/978-3-319-02753-1_36
7. Zhao, N., Jiao, D.D., Bai, S.T., Zhu, T.S.: Evaluating the Validity of Simplified Chinese Version of LIWC in Detecting Psychological Expressions in Short Texts on Social Network Services, vol. 11, p. e0157947 (2016)
8. Pennebaker, J.W., Mehl, M.R., Niederhoffer, K.G.: Psychological aspects of natural language use: our words, our selves. *Annu. Rev. Psychol.* **54**, 547–577 (2003)
9. Zeng, Y., Hou, H.: Research on the extraction of ancient texts. *J. China Soc. Sci. Tech. Inf.* **30**, 132–135 (2008)
10. Gao, R., Hao, B.B., Li, L., Bai, S., Zhu, T.S.: The establishment of the software system of Chinese language psychological analysis. In: *Psychology and the Promotion of Innovation Ability: the Sixteenth National Conference on Psychology*, p. 3 (2013)
11. de Raad, B.: *The Big Five Personality Factors: The psycholexical Approach to Personality*, pp. 309–311. Hogrefe & Huber Publishers, Ashland (2000)
12. Gao, R.: *The Research and Application of the Psychological Analysis Technology of Weibo Content*, University of the Chinese Academy of Sciences, vol. Master. University of the Chinese Academy of Sciences (2014)
13. Cao, B.J.: The reflection and critique of pure confucianism personality: a new comment of Tang priest. *Acad. J. Zhongzhou* **4**, 110–112 (1999)
14. Jiang, K., Huang, L.J.: Compromise and secularization: an image evolution of Sha monk. *J. Zibo Normal Coll.* **4**, 58–62 (2007)
15. Zhou, X.S.: The time spirit and cultural connotation of Sun Wukong. *J. Southeast Univ.* **8**, 63–73 (2006). (Philosophy and Social Science)
16. Cao, B.: Secularized Comic Image and Civil Personae 1: A New Reading of Ba Jie in A Journey to the West. *J. Huaihai Inst. Technol.* **5**, 23–27 (2007). (Social Science Edition)

17. Cao, B.: Secularized Comic Image and Civil Personae 2: A New Reading of Ba Jie in A Journey to the West. *J. Huaihai Inst. Technol.* **5**, 27–30 (2007). (Social Science Edition)
18. Liu, W.L., Qiu, H.C.: The Empiricism of Zhu Bajie. *J. Keshan Teachers Coll.* **2**, 42–46 (2002)
19. Cai, S.: Discussion on Sha monk in “Journey to the West”. *J. Educ. Inst. Jilin Province* **30**, 114–115 (2014)
20. Lu, L.: Industrious, duty, firm and persistent: a comment of Sha monk. *South J.* **11**, 98–99, 110 (2014)

Digging Deep Inside: An Extended Analysis of SCHOLAT E-Learning Data

Aftab Akram^{1,2}, Chengzhou Fu^{1(✉)}, Yong Tang¹, Yuncheng Jiang¹, and Kun Guo^{3,4}

¹ School of Computer Science, South China Normal University, Guangzhou 510631, Guangdong Province, China
aftabit39@gmail.com, fucz@m.scnu.edu.cn,
{ytang, ycjiang}@scnu.edu.cn

² University of Education, Lahore 54000, Pakistan

³ College of Mathematics and Computer Sciences, Fuzhou University, Fuzhou 350116, Fujian Province, China
gukn@fzu.edu.cn

⁴ Fujian Provincial Key Laboratory of Network Computing and Intelligent Information Processing, Fuzhou University, Fuzhou 350116, Fujian Province, China

Abstract. More and more higher education institutions are adopting computer based learning management system to boost learning of the students. Networking and collaboration through social media platforms are vital realities. Learning is not merely limited to class rooms, which is now independent of location and time. Understanding how students learn in this realm is a mighty challenge for teaching professionals. Fortunately, data is abundantly available through learning management systems and social media platforms. Analyzing this vast data could give an insight into how learning is happening in these days. Data mining techniques are vastly being used for this purpose. In this paper, we present a statistical analysis of e-learning data obtained from SCHOLAT, a scholar oriented social networking system. The analysis aims at getting data oriented perspectives of learning, e.g., which factor to what extent impacts learning. The analysis revealed factors which positively or negatively affect learning achievement of the students, i.e., course final scores.

Keywords: Data mining · Academic social network
Learning management system · Statistical analysis

1 Introduction

Self-motivated, self-directed, self-paced and collaborative knowledge construction, this is how learning can be described now and in coming future. Learning is not limited to class rooms and to individuals. In fact, apart from a fraction, most of learning takes place outside of class room settings and through collaboration [1]. Realizing this need, the modern e-learning systems are built around ‘knowledge construction by collaboration’ principle. These e-learning systems include features like wikis, forums, discussion boards, podcasts, etc., to facilitate collaborative and interactive ‘free’ learning.

Students learn more by exchanging knowledge with each other, participating in meaningful interactions and learning discourses [2]. Those who are engaged in collaborative and interactive learning activities, are more productive in terms of learning achievements [3]. Engaging students in meaningful and productive social interactions is a major concern of modern day course instructors, and the vertical social networking platforms emerged to respond. These kinds of social networking systems are built to meet demand of social interactions for a specific group of users with similar needs, for example learners and scholars. Together with the appropriate e-learning technology, this system can fulfill the demand of future learning.

The students who involve in on-line discussions and interactions can easily be distracted [4]. This is not what the course instructor has desired, nor may the learners themselves have known this. The course instructor should decide which dimension of learning process is most appropriate to be supported by social interactions [5]. This is not likely to happen until instructors analyze the course very closely. For a course supplemented by collaborative activities, the breach between instructor's intentions and students' response should be well known. By making this sure, is what guarantees a sound learning process.

The e-learning and social networking systems gather vast data as a result of users' interactions with the system, [6] termed it as gold mine of educational data. The data mining techniques can be applied to this data to get an insight into the learning process. Unlike, traditional face to face learning settings, where data is scarce and available only at the end of session, the data gathered through e-learning and social networking systems is abundant and is available beforehand. Therefore, course instructor can get useful knowledge about the current learning process. The emergence of educational data mining and learning analytics fields is response to the growing demand of analyzing the vast data produced in e-learning and social networking systems.

SCHOLAT is a vertical social networking platform built specifically for learners and scholars. SCHOLAT through its course module also facilitates building blended learning environment to promote 'beyond classroom interactions' between learners and course instructors. In this paper, we present an analysis of data retrieved from SCHOLAT-course module. We analyze this data to get an insight of the learning process and to know how the students behave. The analysis will help us understand the various dynamics of learning process and in future, will lay foundation for building more sophisticated algorithms to understand learning in a 'blended social collaborative' learning environment.

The paper is organized in the following way: Sect. 2 describes a brief review of related work, Sect. 3 provides an introduction of SCHOLAT, Sect. 4 presents data and methods used in this analysis, results of analysis are presented in Sect. 4, the results are discussed in Sect. 5 and finally Sects. 6 and 7 present future work and conclusion respectively.

2 Literature Review

Numerous studies have been conducted to demonstrate the effectiveness of collaborative and interactive learning. In essence, these studies emphasized the very fact that future learning is only by cooperative and collaborative means. The presence of modern age social media networks and their popularity highly signifies this fact. Although, researchers have recognized it quite a while ago, but now it is indispensable. In this brief review, we present some of the important studies.

Social constructivist is a learning paradigm advocating social and collaborative learning. This learning paradigm emphasizes on learner-to-learner interactions, knowledge co-construction and sharing of contents [7, 8]. According to this theory, learning process resides in social interactions. And foremost learning activities are group work and collaboration.

The collaborative activities, in fact, are supplement face to face teaching [9]. The computer based tools help to vanish spatial and temporal limitations, therefore expanding the scope of cooperation beyond classrooms to make anywhere and anytime learning possible [10]. Yu *et al.* asserted that collaborative learning helps in achieving desirable learning outcomes [11]. Another study maintained that more collaborative students achieve more in terms of their learning outcomes [12].

It is the instructor who decides the scope and limits of social interactions and collaboration. The learners are facilitated by engaging beyond classroom activities and availability of course related material outside classrooms [13]. A careful design and conduct of learning activities ensure a sound learning process. The instructor can analyze vast data generated by students' use of computer based learning system to have a close look at the learning process.

Data mining or knowledge discovery in databases (KDD) is set of techniques applied to extract implicit and interesting pattern from large collection of data [14]. Most observed data mining method are statistics, visualization, clustering, classification, association rule mining, sequential pattern mining, etc. [15]. Whereas, educational data mining (EDM) is the application of data mining techniques to a specific dataset coming from education environment to address important educational questions [21].

Data mining techniques have been used to improve e-learning process [16]. There are various uses of data mining of educational data, for example, to explore, analyze and visualize data, to find out useful patterns, to discover how students learn, etc. [17–19]. Other studies indicate some more uses of data mining, for example, recommending activities for students, getting feedback about learning process, evaluating course structure, classifying learners according to their learning needs, discovering regular and irregular patterns, adoption of computer based learning systems to user need, etc. [15].

In a previous study [20], a descriptive statistical and correlation analysis of SCHOLAT e-learning data was presented. The analysis disclosed many interesting facts about students' behavior in online learning management system. The analysis revealed higher descriptive statistics values of variables representing activities expecting to contribute towards final scores and moderate weak correlation between them. Lower descriptive statistical value and weak correlation with final scores was observed in case

of other variables. The distributional shape were skewed and outliers were present in the data.

However, previous analysis was carried out on a single class and only four variables were used (3 independent and 1 dependent). In this paper, we present an extended and diverse analysis of SCHOLAT e-learning data. We include four class in this analysis to study behavior across different students’ cohorts. Further, we use 11 variable (10 independent and 1 depended). These variables represent administrative and collaborative use of learning management system. By use of statistical and correlation analysis techniques, the analysis reveals common trends of system usage among different groups of students. We use course final scores as criteria of successful learning. We plan to use this analysis as base work for developing machine learning models representing students’ learning in blended social learning environment.

3 SCHOLAT-Past and Future

SCHOLAT is an emerging vertical social networking system designed and built specifically for scholars, learners and course instructors. It uses un-directed graphs to represent social network structure. It is bi-lingual, i.e., supports English and Chinese. The main goal of SCHOLAT is to enhance collaboration and social interactions focused around scholarly and learning discourses among community of scholars. In addition to social networking capabilities, SCHOLAT incorporates various modules to encourage collaborative and interactive discussions, for example, chat, email, events, news post, etc. Table 1 shows a comparison of SCHOLAT with other similar social networking system. SCHOLAT definitely has an advantage over them.

Table 1. Comparison of SCHOLAT and other scholar networking systems

Function	SCHOLAT	ResearchGate	SocialScholar	eScience	Scholarmate
Data space	Yes	Yes	Yes	Yes	Yes
Academic search	Yes	Yes	Yes	Yes	Yes
Team	Yes	Yes	Yes	Yes	Yes
Course	Yes	No	No	No	No
Email	Yes	No	No	No	No
Chat	Yes	No	No	No	No

Course module is a distinctive feature in SCHOLAT. The course module is built around blended social learning concept which provides its users, e.g., instructors and students, an opportunity to indulge in collaborative and interactive activities beyond class room settings. It mainly supports administrative and collaborative activities. For example, instructors can create online courses and classes, present course introduction and teaching plans on course website, make announcements, assign tasks to students like homework, upload course help materials, interact with students via online question answer, etc. The students can get up to date information about course in progress, download course help materials, submit homework, ask questions online, etc. At the time this

study is being conducted, 32758 students have been enrolled in 1785 classes of 760 courses.

SCHOLAT-course is still developing. Being a part of SCHOLAT scholar social networking system opens vast horizons for its future development. We plan to work in dimensions of social collaborative learning. We plan to study the factors affecting the learning in collaborative social learning environment. This study is start of a journey towards this destination.

In this study, we explore the statistically supported answers of four research questions: (1) what is the general pattern of system usage among four classes, (2) course administration and collaboration, what type of course support is mostly used by students, (3) is the data is normally distributed or not?, (4) which variable(s) is (are) most correlated with the course final scores.

Table 2. Variables in previous and current studies

Variables	Description
<i>Student level data independent variables</i>	
Number of logins ^{a,b}	The number of times a student has logged into the system
Number of online questions asked ^{a,c}	The number of questions asked by a student on-line
Number of on-line reply ^c	The number of replies to all questions posted by a student
Number of homework submitted on time ^{a,d}	The number of homeworks submitted within deadline
Number of homework submitted late ^d	The number of homeworks submitted after deadline
Number of homework not hand in ^d	The number of due homeworks not submitted by a student
<i>Course level data independent variables</i>	
Total number of homework ^d	The number of homework assigned by instructor
Number of hits course notice ^d	The number of times course notices were opened
Number of downloads course resources ^d	The number of times course materials were downloaded by students
Number of comments ^c	The number of comments posted. The comments can be posted by students or other users
<i>Dependent variable</i>	
Course final score ^a	The score obtained by student in a formative assesment written test

^aVariables included in previous study [20].

^bVariable for system Use.

^cVariable for collaboration.

^dVariable for course administration.

4 Data and Method

In previous study [20], the analysis was performed on one class. In present study, we include four classes. We also increase number of variables from four to eleven. These four classes were selected from three different courses, course ID165 (C Language Programming) class ID279 taught in autumn 2014, course ID520 (Introduction to Learning Sciences) class ID1149 taught in autumn 2015, and course ID206 (Software Requirement) classes ID1563 and ID1729 taught in spring 2016. The number of students enrolled in four classes was 216 out of which 188 students passed the course or took the final exam.

Table 2 shows the variable included in previous and current studies. All of these variables are quantitative values. The variables are categorized in to two types: student level data for which observations for each student was available, and course level data for which observations was only available at course level. Ten out of eleven variables are independent variable, one variable (course final score) is dependent variables. These variables were extracted from course records stored in SCHOLAT database. The course final scores were not present in the database, so the relevant course instructor was asked to provide. The main cause of selection of these four classes was availability of course final scores.

Earlier, we used two types of descriptive statistical techniques: univariate and bivariate [20]. The univariate technique was used to uncover the properties of individual variables, whereas bivariate analysis was used to discover relationship between independent and dependent variables. We intend to use same statistical techniques in this study. This study has an added advantage that results will be compared among four different classes.

The results of the analysis are presented in following three subsections.

4.1 Univariate Analysis

We perform univariate analysis on student level variables and dependent variable (course final score) as discussed in previous section. Therefore, total seven variables are included in this episode of analysis. The results of analysis are shown in Table 3. Five descriptive statistics measures have been calculated for each variable in each class. These measures include average or mean, mode, median, standard deviation and skewness. Table 3 is divided into five compartments, where each compartment presenting results for one type of descriptive statistical measure. The top row indicates the variables included in the analysis. The left most column specifies the class to which the variable corresponds to. The top row is not repeated, however, left most column is repeated in each sub section of the table. Each column (next to left most column) in the table corresponds to results of one variable, for example, column under number of logins presents results of analysis for this variable only. So if reader wants to know what is mode of number of homework submitted on time for class ID279, choose column first for this variable and then go to corresponding sub section showing mode of each variable. In this sub section, choose the row indicating the desired class, the intersection of that column and this row the required answer, i.e., 105.

Table 3. Descriptive statistics univariate mode

	No. of logins	No. of question	No. of reply	No. of homework on time	No. of homework late	No. of homework not hand-in	Final score
<i>Mean</i>							
ID279	213.34	7.94	6.38	89.65	0.03	2.96	86.94
ID1149	22.32	0.45	0.45	2.29	1.84	0.26	73.77
ID1563	664.53	0	0	5.32	3.32	1.17	82.20
ID1729	68.43	0	0	6.86	2.43	1.08	84.27
<i>Mode</i>							
ID279	0	0	0	105	0	0	90
ID1149	16	0	0	2	1	0	73
ID1563	3	0	0	4	0	0	90
ID1729	39	0	0	9	1	0	90
<i>Median</i>							
ID279	0	2	2	100	0	2	90
ID1149	19	0	0	2	2	0	73
ID1563	47	0	0	4	3	0	86
ID1729	41	0	0	8	1	0	86
<i>Standard Deviation</i>							
ID279	1667.57	13.50	21.56	28.93	0.16	2.98	11.57
ID1149	10.59	1.41	1.34	1.13	1.21	0.44	6.50
ID1563	2695.07	0.00	0.00	3.78	3.13	3.15	10.29
ID1729	168.10	0.00	0.00	3.83	2.69	2.85	8.90
<i>Skewness</i>							
ID279	8.88	3.15	7.66	-2.68	6.16	0.74	-5.60
ID1149	0.58	3.38	3.01	1.45	1.64	1.16	-0.91
ID1563	5.92	0	0	0.18	0.97	3.12	-0.76
ID1729	6.00	0	0	-0.21	1.14	3.13	-0.95

4.2 Bivariate Analysis

Table 4 shows the results of bivariate analysis performed on each of aforementioned variables. We calculated correlation co-efficient for each pair of one of the six independent student level variables and dependent variable. The structure of Table 4 is similar to Table 3 described in previous subsection with top row describing the variables and left most columns the relevant class. The right most columns under final score contain all ones since it indicates self-correlation.

Table 4. Descriptive statistics bivariate mode

	No. of logins	No. of question	No. of reply	No. of homework on time	No. of homework late	No. of homework not hand-in	Final score
<i>Correlation Co-efficient (r)</i>							
ID279	0.12	0.16	0.16	-0.12	-0.06	-0.35 ^a	1.00
ID1149	0.44 ^a	0.10	0.22	0.03	-0.39 ^a	-0.08	1.00
ID1563	-0.25	0	0	0.41 ^a	-0.06	-0.50 ^a	1.00
ID1729	0.16	0	0	0.42 ^a	-0.50 ^a	-0.19	1.00

^aSignificant at p-value < 0.05, 95% confidence interval.

4.3 Course Level Variables

Table 5 shows the obtained figures for course level variables. We did not perform any calculations on these variables like we did on student level variables, since these figures are available only at course level. However, we present a discussion on its implications in next section. The class ID1563 and ID1729 belong to same course, so in Table 5 the figures for these two classes are presented jointly.

Table 5. Course level variables

	ID279	ID1149	ID1563/ID1729
Total number of homework	105	8	13
Number of hits course notice	6041	553	54
Number of download course resources	5969	9375	2176
Number of comments	30	3	0

5 Discussion

In this section, we present discussion on results presented in previous section. The discussion is focused on finding the data supported answers of research questions presented in Sect. 3.

Table 3 presents the results of univariate analysis. Five types of statistical measures have been presented. We discuss each of them in following text.

The number of logins shows the extent of system use by the students. The mean, mode and median values given in Table 3 show different usage behavior shown by four classes. The classes ID279 and ID1563 have high average values, i.e., 213.34 and 664.53, whereas classes ID1149 and ID1729 show low usage average, i.e., 22.32 and 68.43. Mode is value mostly appearing in data [22], the classes ID1149 and ID1729 have mode values, i.e., 16 and 39, the class ID1563 has mode 3 and class ID279 has mode 0. Median is the value appearing in the center of score continuum. If the distribution is not normal, median gives a decent idea where is the center of data. The median of class ID279 is 0 (range: 0–14841) indicates highly unbalanced use of system, i.e., some

students using system not at all while some other students usage is very high. A similar trend is observed in class ID1563, i.e., median 47 (range: 0–17053). Earlier high average values for these two classes were observed. The other two classes show relatively balanced usage, i.e., median is 19 (range: 5–46) for class ID1149 and median is 41 (range: 11–1059) for class ID1729. From above discussion it can be concluded that classes ID279 and ID1563 show high and unbalanced usage while classes ID1149 and ID1729 show low but balanced usage. We also note presence of outliers in classes ID279 and ID1563. The high values of standard deviation also signify presence of varied usage behavior. The classes ID279, ID1563 and ID1729 show high variability in system usage, i.e., 1667.57, 2695.07 and 168.10. The class ID1149 has relatively consistent usage pattern and low value for standard deviation, i.e., 10.59.

The variables number of question and number of reply are indication of level of collaboration, since asking questions and getting replies promotes collaboration and interaction among students. The descriptive statistics shown in Table 3 indicate that these activities are highly overlooked by students. The mean, mode, median and standard deviation values for these two variables for classes ID1563 and ID1729 are zero. For other two classes these values are very low. The data indicates very low collaboration among the students.

The SCHOLAT course module has comprehensive facility for instructors to upload homework and for students to submit homework. Submitting homework on time is indication of good behavior whereas late submission or not submitting at all indicates procrastinating behavior which is alarming for students' learning. The three variables number of homework on-time, number of homework late and number of homework not hand-in are related to this key aspect of course administration. The statistics provided in Table 3 rather provide a satisfactory view, as mean, mode and median values for all classes indicate a healthy trend of submitting assignments on-time and to avoid procrastination. For class ID279 the mean value is 85.4% of maximum values of 105. Whereas for other classes ID1149, ID1563 and ID1729 the mean values are 28.6%, 41% and 52.3%, although lower than class ID279 but still satisfactory. The standard deviation values for all four classes are not high indicating consistent behavior of submitting homework timely. The mean, mode and median values for variables number of homework late and number of homework not hand-in indicate that the students tend not to procrastinate because it can lower their final scores. In Table 3, mostly zero and low values for mean, mode and median are observed for these variables. Further, low standard deviation values indicate that avoiding procrastination is a universal trend among all four classes.

The final score variable is indication of successful learning. The scores have a maximum value of 100. The mean, mode and median values in Table 3 indicate that despite all odds students manage to get good scores. The low standard deviation speaks of a healthy trend of getting good scores after all among all classes.

However, the distribution of data is not normal and we mostly see skewed distributions. The skewness is a measure of how much a frequency distribution is asymmetric [23]. A normal distribution has skewness values to zero, whereas positive or negative non-zero values indicate a positively or negatively skewed distribution. Table 3 indicates that most distributions are positively or negatively skewed. There are also outliers

present in data which make distribution further skewed. The skewed distribution speaks of extreme behavior by students, i.e., against a normal distribution in which an average behavior is mostly seen.

Table 4 shows the results of bivariate correlation coefficient analysis. The analysis was done to find out the strength of relation between each of independent variables in each course and the final scores. The values of correlation coefficient r illustrates the strength of positive or negative relationship, with two extreme values $+1$ or -1 (strong positive or negative relation) and value of 0 for no relation at all [24]. The variables have weak to moderate relationships. But very few significant correlations (p -value < 0.05) are observed. The course ID279 has only one significant correlation, i.e., number of homework not hand is negatively correlated with final scores ($r = -0.35$). In course ID1149, the number of logins has positive significant correlation with final scores ($r = 0.44$) and number of homework late has negative significant correlation ($r = -0.39$). In courses ID1563, the number of homework on time has positive moderate significant correlation with final scores ($r = 0.41$) and number of homework not hand-in has negative moderate significant correlation ($r = -0.50$). Finally, in course ID1729 the number of homework on-time has positive moderate significant correlation with final scores ($r = 0.42$) and number of homework late has negative moderate significant correlation ($r = -0.50$).

Next we examine the course level data. This is data either same for entire group or figures were not available for individual students. For example, total number of homework is same for all students, i.e., 105, 8 and 13 for classes ID279, ID1149 and ID1563/ID1729 respectively. For other three variables, number of hits course notice, number of downloads course resources and number of comments, the figures were not available for individual students. However, these figures are helpful to find out the extent of use of beyond class room on-line services. Since, the figures are not available for each student, we cannot use them to correlate to student's achievement.

First, we look at variable number of hits course notice. The figures of this variable for classes under study, i.e., ID279, ID1149 and ID1563/ID1729 are 6041, 553 and 54, where number of notices issued by course instructors were 30, 18 and 1 respectively. As such, we see more activity in class ID279 reading and staying in touch with course instructor. Similarly, we can view number of downloads of course resources as another indicator of on-line interactive activities. Table 5 indicates that in class ID279 students downloaded course resources 5969 times, in ID1149 9375 times, and in ID1563/ID1729 2176 times, whereas 61 resources were uploaded in ID279, 63 in ID1149 and only 18 resources were uploaded in classes ID1563/ID1729. We see rather healthy trend that the students are benefited from this facility effectively, which is indicative by the number of downloads in each class.

We observe a disappointing activity in terms of comments posted by students. For our classes, there are only 30 comments for ID279, 3 comments for ID1149 and no comment for other two classes combine. These comments can be useful for course instructors and other students willing to join the course.

6 Conclusion

The important findings of the above analysis can be summarized as follows:

- There is varied trend of system usage, i.e., in some classes students use system more and in some do not.
- Students do not take much interest in on-line collaboration activities.
- Students try their best to submit their homework and avoid procrastination.
- In each class there are different factors which are significantly related to students' learning success (course final scores). We see both positive and negative correlations.
- The distributions are skewed, which shows above or below normal behavior.

7 Future Work

In future, we intend to extend this work for building machine learning algorithm to predict students' current learning and future achievement. This would enable course instructors to take timely actions to avoid students' failures. We also intend to increase data collection ability of the system.

Acknowledgment. This work is supported by the National Nature Science Foundation of China (Grant Nos. 61272066, 61272067, 61300104), the Applied Technology Research and Development Foundation of Guangdong Province (2016B010124008), the Technology Innovation Platform Project of Fujian Province (Grant Nos. 2009J1007, 2014H2005), the Fujian Collaborative Innovation Center for Big Data Applications in Governments.

References

1. Chen, B., Breyer, T.: Investigating instructional strategies for using social media in formal and informal learning. *Int. Rev. Res. Open Distance Learn.* **13**(1), 87–104 (2012)
2. Hrastinski, S.: A theory of on-line learning as on-line participation. *Comput. Educ.* **52**, 78–82 (2009)
3. Junco, R., Helbergert, G., Loken, E.: The effect of Twitter on college student engagement and grades. *J. Comput. Assist. Learn.* **27**, 119–132 (2011)
4. Hurt, N.E., Moss, G.S., Bradley, C.L., Larson, L.R., Lovelace, M.D., Prevost, L.B., et al.: The 'Facebook' effect: college students' perceptions of online discussions in the age of social networking. *Int. J. Sch. Teach. Learn.* **6**(2), 2–14 (2012)
5. Fewkes, M., McCabe, M.: Facebook: learning tool or distraction? *J. Digital Learn. Teacher Educ.* **28**(3), 92–98 (2012)
6. Mostow, J., Beck, J., Cen, H., Cuneo, A., Gouvea, E., Heiner, C.: An educational data mining tool to browse tutor-student interactions: Time will tell!. In: *Proceedings of the Workshop on Educational Data Mining*, pp. 15–22, Pittsburgh, USA (2005)
7. Dewey, J.: *Experience and education*, New York: Collier, 1938/1963
8. Vygotsky, L.S.: *Mind in society: the development of higher psychological processes*. Harvard University Press, Cambridge Mass (1978)
9. Cole, J.: *Using Moodle*. O'Reilly, Sebastopol (2005)

10. Dawson, S.: A study of the relationship between student social networks and sense of community. *Educ. Technol. Soc.* **11**(3), 224–238 (2008)
11. Yu, A.Y., Tian, S.W., Vogel, D., Kwok, R.C.: Can learning be virtually boosted? an investigation of on-line social networking impacts. *Comput. Educ.* **55**, 1494–1503 (2010)
12. Junco, R.: Too much face and not enough book: the relationship between multiple indices of Facebook use and academic performance. *Comput. Hum. Behav.* **28**, 187–198 (2012)
13. Lamb, L., Johnson, L.: Bring back the joy: creative teaching, learning, and librarian-ship. *Teach. Librarian* **38**(2), 61–66 (2010)
14. Klossgen, W., Zytrow, J.: *Handbook of Data Mining And Knowledge Discovery*. Oxford University Press, New York (2002)
15. Romero, C., Ventura, S., Garcia, E.: Data mining in course management systems: moodle case study and tutorial. *Comput. Educ.* **51**(1), 368–384 (2008)
16. Romero, C., Ventura, S.: *Data Mining in E-Learning*. Southampton. Wit Press, UK (2006)
17. Mazza, R., Milani, C.: Exploring usage analysis in learning systems: gaining insights from visualization. In: *Workshop on Usage Analysis in Learning Systems at 12th International Conference on Artificial Intelligence in Education*, pp. 1–6, New York, USA (2005)
18. Mor, E., Minguillon, J.: E-learning personalization based on itineraries and long term navigational behavior. In: *Proceedings of the 13th International World Wide Web Conference*, pp. 264–265 (2004)
19. Talavera, L., Gaudioso, E.: Mining students data to characterize similar behavior groups in unstructured collaboration spaces. In: *Workshop on Artificial Intelligence in CSCL*, pp. 17–23, Valencia, Spain (2004)
20. Akram, A., Chengzhou, F., Yong, T., Yuncheng, J., Xueqin, L.: Exposing the hidden to the eyes: analysis of SCHOLAT E-learning data. In: *Proceedings of the 2016 IEEE 20th International Conference on Computer Supported Cooperative Work in Design*, pp. 693–698 (2016)
21. Romero, C., Ventura, S.: Data mining in education. *WIREs Data Min. Knowl. Disc.* **3**, 12–27 (2013). <https://doi.org/10.1002/widm.1075>
22. Huck, S.W.: *Reading Statistics and Research*, vol. 2(28). Pearson Education, Boston (2012)
23. Huck, S.W.: *Reading Statistics and Research*, vol. 2(24). Pearson Education, Boston (2012)
24. Huck, S.W.: *Reading Statistics and Research*, vol. 3(49). Pearson Education, Boston (2012)

Social Network Analysis of China Computer Federation Co-author Network

Chengzhou Fu¹, Weiquan Zeng^{1,2}, Rui Ding¹, Chengjie Mao¹(✉),
Chaobo He³, and Guohua Chen¹

¹ Computer Science, South China Normal University, Guangzhou, China
{fucz, zengwq, ding, chengh}@m.scnu.edu.cn, maochj@qq.com

² Computer Science, Clemson University, Clemson, USA

³ School of Information Science and Technology,
Zhongkai University of Agriculture and Engineering, Guangzhou, China
hechaobo@foxmail.com

Abstract. We extract the data set from 2010 to 2014 of the China Computer Federation (CCF (<http://www.ccf.org.cn>)) by the distributed web crawler system and build the co-author network with R language. In this co-author network, authors represent nodes and a pair of authors is connected by an edge if they have co-authored at least one paper over the entire duration. We analyze this network with social-centric and ego-centric methods to study the situation of co-author network of CCF and visualize the analysis results. Social-centric measure reveals that the co-author network density, the usage of key words, the average number of authors per article, and confirms that most authors in computer science field publish a very small number of papers but have higher collaborators than those of other fields. Ego-centric analysis discovers betweenness centrality, closeness centrality, and degree centrality, indicates that only a small percentage of the authors locate in the center of the coauthor network. Finally, we pick out eight key persons and point out the group teams where the key persons are respectively. Based on these findings, we suggest that computer science field should promote wider collaboration, encourage more authors to publish their papers.

Keywords: Co-author network · Social-centric · Ego-centric · Centrality
Key person · Visualize

1 Introduction and Motivation

CCF aims at bringing scholars together in computer research. CCF was founded in 1962, member of China Association of Science and Technology. It contains 13 kinds of journals, namely Chinese Journal of Computers, Journal of Computer-Aided Design & Computer Graphics, Journal of Computer Science & Technology, Journal of Computer Research and Development, Journal of Software, Journal of Computer Applications, Computer Engineering and Applications, Computer Technology and Development, Computer Science, Journal of Chinese Computer Systems, Journal of Frontiers of Computer Science and Technology, Computer Engineering and Science, and Computer Engineering and Design.

Social network analysis (SNA) methods have been used to study co-author network in various fields including physics, library and information service (LIS), biology, and computer science. Scholars in LIS field need strengthen communication with each other after studying the co-author network of LIS with betweenness centrality, degree centrality, and average degree features [1]. Zhu et al. [2] discovered the present situation and pattern of Chinese-foreign cooperation, simultaneously offered suggestions to the international collaboration through studying the co-author network of information system field. Sun et al. [3] figured out the most influential author and paper in the co-author network with network density, betweenness centrality methods. Shen et al. [4] applied the vector space model into the identification of scientific research teams within the co-author network, and revealed the scientific research co-author relationship by degree of similarity between author vectors. Du [5] extracted the co-author network over the past 26 years of USIT (User Interface Software and Technology), which is generally recognized as the top conferences in the Human-Computer Interaction field, and analyzed the co-author network with SNA methods. El Kharboutly and Gokhale [6] revealed the collaborative pattern of co-author from the co-author network that extracted over the entire history of the SEKE conference.

After retrieving and reading paper about social network analysis, we can deeply understand the collaboration, communication among authors. Thus, we can offer suggestions on how to improve and strengthen the collaboration and communication among authors, but no one has investigated into CCF co-author network before. Therefore, it is necessary for us to study the CCF co-author network. In this paper, the main of contribution of our work is summarized as follows:

1. Design and implement the distributed crawler system; collect the data set from CCF through the distributed crawler system; build the co-author network of CCF.
2. Discover the co-author network with social-centric and ego-centric. Social-centric analyzes the major metrics of the data set and compares the metrics with other field. Ego-centric reveals the betweenness centrality, closeness centrality, degree centrality of the co-author network.
3. According to the analysis of key words, we point out the research hotspots and research trendy, find out the key persons with the higher degree centrality, and gain the group teams where the key persons are from the co-author network.

The rest of paper is organized as follows: Sect. 2 describes data collection and pre-processing. Sections 3 and 4 discuss socio-centric and ego-centric analysis respectively. Section 5 points out key person and the group team. Section 6 concludes the paper and offers directions for future work.

2 Data Collection and Pre-processing

We extract the data set from the last recent 5 years of CCF by the distributed crawler system. Table 1 shows the major metrics of CCF co-author network. The distributed crawler system consists of a master node and several slave nodes. Master node is the core of the crawler system, and it is responsible for scheduling task, managing process

and crawling log, while every slave node is a performer of the task. Furthermore, slave node is a plug-in base on the Google browser Chrome, thus it can run on any computer that has chrome and run independently with other programs [7]. Architecture of the distributed crawler system is presented in the Fig. 1.

Table 1. Major metrics of CCF co-author network

Metric	Value	Metric	Value
Total number of authors	49453	Total number of key words	70631
Average papers per author	1.35	Average authors per papers	4.38
Average collaborators per author	4.88	Average number of key words per author	9.09
Average clustering coefficient	0.30	Density	0.0037

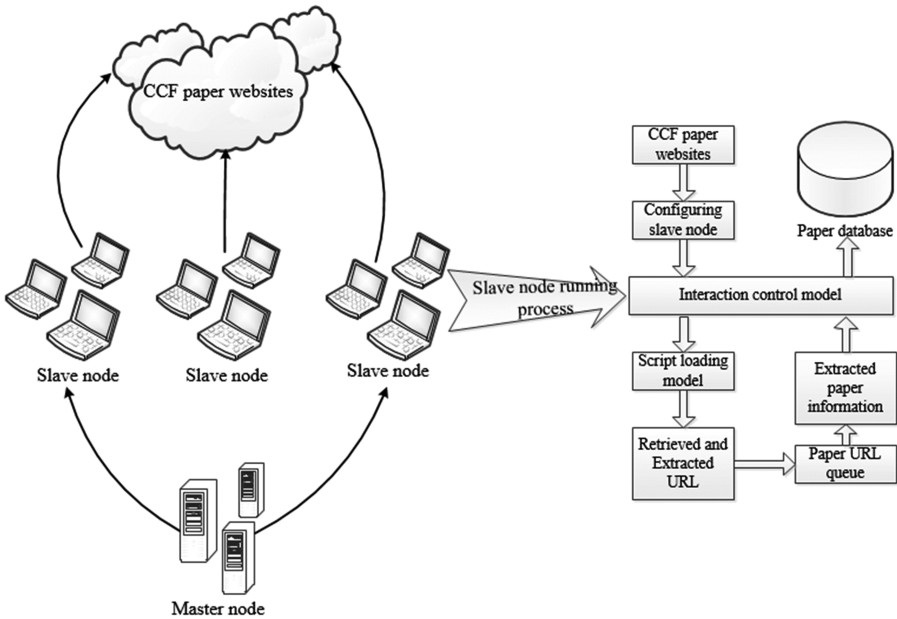


Fig. 1. Architecture of the distributed crawler system.

Since data obtained from the web by the crawler system are JSON (JavaScript Object Notation) format, we parsed and formatted data into XML format by program. Furthermore, in pre-processing we found that some (only 10–20 instances) authors share their first name and last name. We disambiguated between such authors by their emails, assuming that authors who share a name but not email represent different individuals.

After pre-processing, we build the CCF co-author network, which authors represent nodes, the pairwise of authors is connected by an edge if they have co-author at least

one paper. In addition, this analysis of CCF co-author network is an unweighted graph. That is, although authors A and B have multiple co-authored relationship, there is only one edge connect author A with author B. Figure 2 shows the overview of the co-author network graph in CCF.

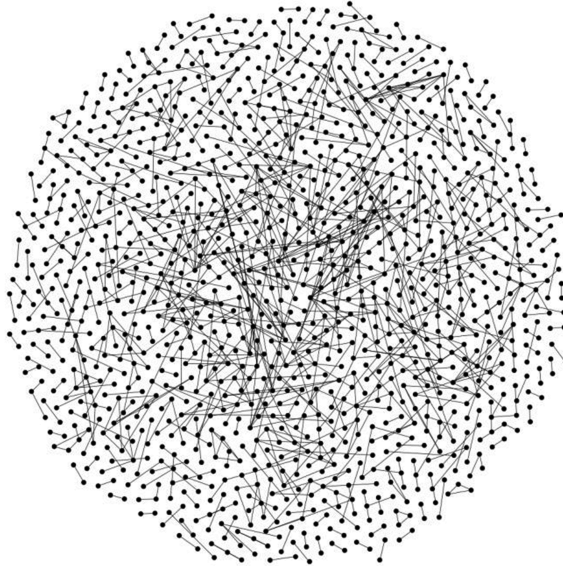


Fig. 2. The overview of the co-author network graph in CCF

3 Social-Centric Analysis

In this section, we discuss social-centric metrics that we computed overall nodes in the CCF co-author network. We compare these metrics, shown in the Table 1, with those of other fields.

3.1 Major Metrics of CCF Co-author Network

From Table 1, we know that total number of authors is 49453, and total number of key words is 70631. Furthermore we figure out that on an average a CCF author writes 1.35 articles, collaborates with 4.88 authors. Comparing with other communities within and beyond computer science, on an average a CCF author writes 1.35 articles is lower than one in LIS (2.71), biology (6.4) and physics (5.1), otherwise, on an average a CCF author collaborates with 4.88 authors is higher than one in LIS (1.57), biology (3.75) and physics (2.53) [2, 8, 9]. These differences may arise due of the nature of LIS, biology and physics. Additionally, on an average a CCF article has 4.38 authors, and on an average a CCF author has 9.09 key words.

Figure 3, which shows the distribution of number of articles per author with less than 10 articles, reveals that a very large of percentage of CCF authors have less than 3

articles. Authors with 40 or more articles are very rare, with 87 being the maximum. In order to analyze the distribution of articles per author, we extract the authors data over the entire data set where per author has 10 or more articles. Figure 4, which shows the distribution of number articles per author who has 10 or more articles further confirms that author with 40 or more articles are rare.

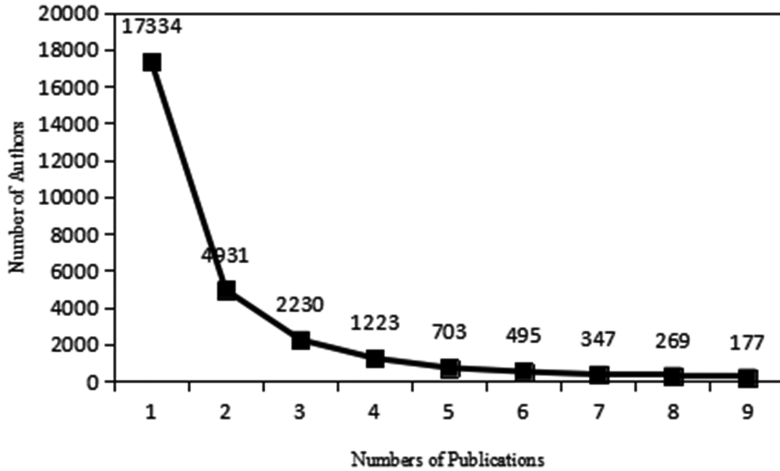


Fig. 3. Distribution of number of articles per author with less than 10 articles.

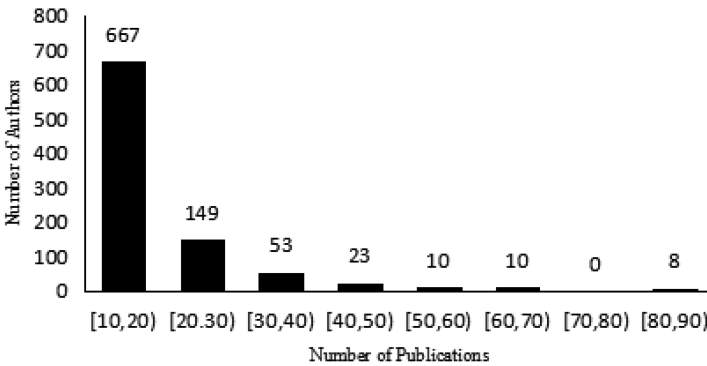


Fig. 4. Distribution of number of articles per author with 10 or more articles.

3.2 Research Major Trend

Research hotspot is the trend in special field. In CCF co-author data set, there are 70631 key words. In order to point out the research trend of computer science, all those key words, that have been use more than 1000, are referred to as Main Key Words (MKWs). Figure 5, which shows MKWs of CCF co-author, indicates that seven MKWs occupy 31.02%, which is a larger proportion than any other key words. Seven MKWs are data

mining, support vector machine (SVM), clustering, wireless sensor network, genetic algorithm (GA), segmentation, and cloud computing. Apparently, they are consistent with big data, Internet of Things (IoT), image processing, community discovery and cloud computing research major trend.

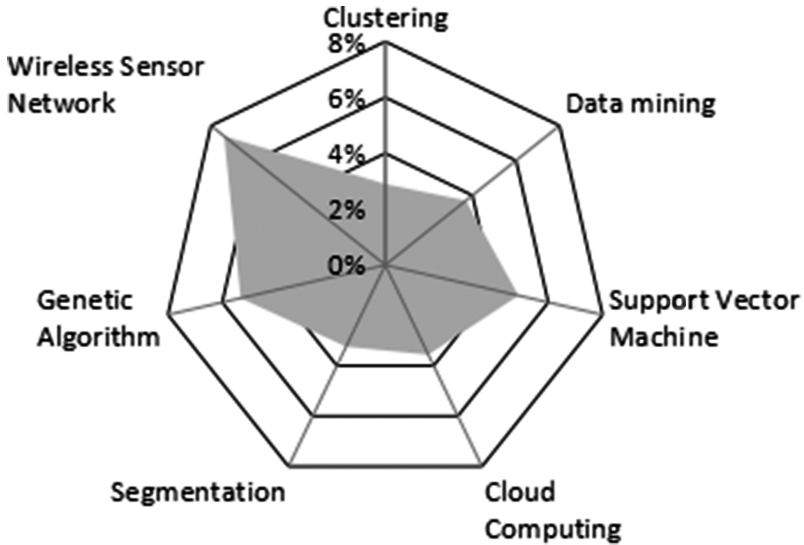


Fig. 5. Proportion of MKWs in CCF data set

3.3 Co-author Network Density

The network density (D) is defined as the number of edges E to the number of possible edges and is given by Eq. (1) [10]. The density of the CCF co-author network is 0.0037, indicating an overall very sparsely connected network.

$$D = \frac{2 * E}{N(N - 1)} \tag{1}$$

4 Ego-Centric Analysis

In this section, we discuss ego-centric metrics of centrality which is a tool to understand structure, function, and composition of the co-author network tie around the individual.

4.1 Betweenness Centrality

Betweenness centrality is used to answer the question of who controls knowledge flows. Betweenness centrality is defined as the number of the shortest paths from all authors that pass through the given author [11]. It is an indicator of an author’s centrality in a

network or an author’s ability to control the knowledge flows, resources and information [12]. Betweenness centrality of author v is given by Eq. (2), where P_{ij} is the total number of geodesic linking author i and author j , and $P_{ij}(v)$ is all the geodesics linking author i and author j which pass through author v . Authors with high betweenness centrality can play a role of “bridge” or “middleman” in the co-author network, also the author with high betweenness centrality can obtain resources, information and knowledge efficiently from other authors in the co-author network [13]. Table 2 shows the top 10 authors with betweenness centrality in CCF co-author network.

$$C_b(v) = \sum_{i,j \neq v} \frac{P_{ij}(v)}{P_{ij}} \tag{2}$$

Table 2. Top 10 authors with betweenness centrality in CCF co-author network.

Author alias	Betweenness centrality	Author alias	Betweenness centrality
28452	21029.19	25214	13763.72
9161	11182.73	4921	14594.92
6151	12469.83	20252	22731.28
5066	12623.50	30312	13731.08
28719	16091.17	851	13689.25

4.2 Closeness Centrality

Closeness centrality is used to answer the question of who has the shortest distance to other authors. Closeness Centrality is defined as the mean length of all shortest paths from a node to other nodes in the network [14]. It is measured as the average of the reciprocal distance of an author from others. Closeness centrality of an author v is given by Eq. (3), where $d(v,j)$ is the distance between authors v and j , while N is the total number of authors where author v can reach in the co-author network. Closeness centrality judges how important an author is. As we know, the higher closeness centrality is, the more important the author is. Moreover, an author with higher closeness centrality could access or obtain resources in the co-author network more efficiently than others with lower closeness centrality [15]. Additionally, an author with higher closeness centrality also indicates that an author can communicate efficiently than those with lower closeness centrality [12]. Table 3 shows the top 10 authors with closeness centrality in CCF co-author network.

$$C_c(v) = \sum_{n=1}^N \frac{1}{d(v,j)} \tag{3}$$

Table 3. Top 10 authors with closeness centrality in CCF co-author network.

Author alias	Closeness centrality	Author alias	Closeness centrality
44551	4.887e-10	43639	4.769e-10
45050	4.768e-10	36614	4.761e-10
31895	4.753e-10	45238	4.752e-10
36626	4.740e-10	18639	4.740e-10
31865	4.728e-10	18951	4.722e-10

4.3 Degree Centrality

Degree centrality is used to answer the question of who knows the most authors. It is measured as the tie of author with others. Degree centrality is defined as the number of links incident upon a node [16]. Degree centrality of author v is given by Eq. (4). Authors with higher degree centrality represent they are more central to the co-author network. Table 4 shows the top 10 authors with ten degree centrality in CCF co-author network.

$$D_d(v) = deg(v) \quad (4)$$

Table 4. Top 10 authors with degree centrality in CCF co-author network.

Author alias	Degree centrality	Author alias	Degree centrality
28452	73	13772	85
20252	71	851	58
14929	55	30312	52
28719	59	15748	53
20222	49	18169	47

5 Identifying Key Person and Group Team

Above the discussion, we try to discover key persons and group teams. According to the value of centrality, we regard the author as a key person who is in the central position of CCF co-author network. Moreover, we point out group team members who have a certain count of collaboration with the key person.

5.1 Identifying Key Person

Actually, key person indicates that he or she has high quantity and quality of their research work in coordination with other scholars and may be at the top fields currently. Above the discussion, we know that an author with higher degree centrality is more central in the co-author network and the author accesses or obtains resources and information more efficiently than other authors with lower degree centrality. Therefore, we define an author as a key person that degree centrality is higher than 50 in the CCF co-author network. Table 5, which shows the key persons with degree centrality and number

of publishes in the CCF co-author network confirms that key persons not only have higher degree centrality, but also have higher number of publications.

Table 5. Key persons with degree centrality and number of publications in CCF co-author network.

Author alias	Degree centrality	Number of publish
28452	73	85
13772	85	87
20252	71	51
851	58	47
14929	55	57
30312	52	42
28719	59	42
15748	53	56

5.2 Group Team Discovery

As usual, key person has a group team or laboratory as a support, furthermore, key person is also the soul in the group team. Therefore, we point out group teams through collaboration with key person. Firstly, group team appears as a cluster in the co-author network, that is, a key person has much collaboration with others in the group team and key person is in the center of group team co-author network. Secondly, those authors who have less than 3 co-authored relationships with key person may represent collaborations across institutions but not the member in the group team where key person is. Therefore, while selecting the group team members, we filter those who have less than 3 co-authored with the corresponding key person. Figure 6 shows eight key persons and their group team clusters in the co-author network. The bigger sizes nodes stand for the key persons, other



Fig. 6. The overview of the co-author network in group teams

sizes nodes represent other authors that have collaboration with key persons. From Fig. 6, apparently, a large proportion of collaboration exists in the group team, but there is rare collaboration across group teams. Base on the above finding, there will be fruitful produce if authors collaborate frequently with others across group teams.

6 Conclusions and Future Work

In this paper, we describe the process of extracting the data set from last resent 5 years CCF paper websites and building the co-author network of CCF. We analyze CCF co-author network using social-centric and ego-centric social network analysis methods to understand the pattern of author collaboration and communication. Otherwise, we analyze the MKWs to confirm the research trend in computer science field. Moreover, we identify the key person in the CCF co-author network through the authors' degree centrality. Finally, according to the collaboration with key person, we point out eight group teams where eight key persons are respectively.

Our future research involves co-authorship order to understand how the pattern of collaboration has been influenced. Moreover, we will deeply study group team research interest by analyzing the key words of group team members.

Acknowledgement. This work is supported by the National Nature Science Foundation of China (Grant No. 61272067), the Applied Technology Research and Development Foundation of Guangdong Province (2016B010124008).

References

1. Rong, X., Tao, Q.: Social network analysis in LIS field co-relation of empirical research. *Libr. World* **01** (2010)
2. Zhu, Q., Fan, Z., Shi, W.: Information systems and foreign co-authored research network. *Inf. Stud. Theory Appl.* **11** (2011)
3. Sun, N., Zhu, J., Cheng, H., Wu, Y.: Study co-author relationship based on social network analysis papers. *J. Suzhou Univ.* **29**(09) (2014)
4. Shen, G., Huang, S., Wang, D.: On the scientific research teams identification method taking co-authorship of collaboration as the source data. *New Technol. Libr. Inf. Serv.* **1**, 57–62 (2013)
5. Du, R.: UistViz: 26 Years of UIST Coauthor Network Visualization. *CMSC 734* (2013)
6. El Kharboutly, R., Gokhale, S.S.: Social analysis of the SEKE co-author network. *SEKE 2015-092* (2015)
7. Yang, Z., Cai, Z., Chen, G., Tang, Y., Zhang, L.: Design and implementation of distributed web crawler for open access journal. *J. Front. Comput. Sci. Technol.* **10** (2014)
8. Sarigol, E., Pfitzner, R., Scholtes, I., Garas, A., Schweitzer, F.: Predicting scientific success based on coauthorship networks. [arXiv:1402.7268](https://arxiv.org/abs/1402.7268) (2014)
9. Newman, M.E.J.: Coauthorship network and patterns of scientific collaboration. *Proc. Natl. Acad. Sci. U.S.A.* **101**(1), 5200–5205 (2001)
10. Abbasi, A., Cheung, K.S.K., Hossain, L.: Egocentric analysis of co-authorship network structure, position and performance. *Inf. Process. Manag.* **45**, 671–679 (2012)
11. Borgatti, S.P.: Centrality and network flow. *Soc. Netw.* **27**(1), 55–71 (2015)

12. Freeman, L.C.: Centrality in social networks: conceptual clarifications. *Soc. Netw.* **1**(3), 215–239 (1979)
13. Jamali, M., Abolhassani, H.: Different aspects of social network analysis. In: IEEE/WIC/ACM International Conference on Web Intelligence (2006)
14. Lu, H., Feng, Y.: A measure of authors' centrality in co-authorship networks based on the distribution of collaborative relationships. *Scientometrics* **81**(2), 499–511 (2009)
15. Borgatti, S.P.: Centrality and network flow. *Soc. Netw.* **27**(1), 55071 (2005)
16. Wasseman, S., Faust, K.: *Social Network Analysis: Methods and Applications*, vol. 8. Cambridge University Press, Cambridge (1994)

Detecting Postpartum Depression in Depressed People by Speech Features

Jingying Wang^{1,2}, Xiaoyun Sui¹, Bin Hu³, Jonathan Flint⁴(✉),
Shuotian Bai⁵, Yuanbo Gao², Yang Zhou^{1,2}, and Tingshao Zhu¹(✉)

¹ Institute of Psychology, Chinese Academy of Sciences, Beijing 100101, China
{wangjingying, tszhu}@psych.ac.cn, oswicer@163.com

² University of Chinese Academy of Sciences, Beijing 100049, China

³ School of Information Science and Engineering,
Lanzhou University, Gansu 730000, China
bh@lzu.edu.cn

⁴ Department of Psychiatry and Biobehavioral Sciences,
UCLA David Geffen School of Medicine, Los Angeles, CA 90095, USA
jf@well.ox.ac.uk

⁵ School of Information Engineering,
Hubei University of Economics, Wuhan 430205, China

Abstract. Postpartum depression (PPD) is a depressive disorder with peripartum onset, which brings heavy burden to individuals and their families. In this paper, we propose to detect PPD in depressed people via voices. We used openSMILE for feature extraction, selected Sequential Floating Forward Selection (SFFS) algorithm for feature selection, tried different settings of features, set 5-fold cross validation and applied Support Vector Machine (SVM) on Weka for training and testing different models. The best predictive performance among our models is 69%, which suggests that the speech features could be used as a potential behavioral indicator for identifying PPD in depression. We also found that a combined impact of features and content of questions contribute to the prediction. After dimension reduction, the average value of F-measure was increased 5.2%, and the precision of PPD was rose to 75%. Comparing with demographic questions, the features of emotional induction questions have better predictive effects.

Keywords: Postpartum depression · Depression · Speech features
Detecting · Classification

1 Introduction

Postpartum depression (PPD) is a kind of depressive disorder with peripartum onset, which can affect both genders after childbirth, and females usually suffer worse than males [1]. It is a heavy burden to not only patients themselves, but also their spouses, children and whole families [2]. The concept “PPD” was proposed by Pitt. B in 1968 [1], but there is still no agreement on its diagnostic criteria until now. PPD is one subtype of depressive disorder. It is liable to cause misdiagnosis between PPD and other subtypes of depressive disorder [3]. Accurate diagnosis is the critical for effective

intervention. In the case of inconsistent diagnosis, it is necessary to develop new methods to aid PPD diagnosis.

Depressive disorder has a visible influence on patients' emotions [4]. The influence of emotion on people could reflect in their voices [5]. The study of Cannizzaro [6] shown that depressed people had less verbal production and variations comparing with healthy people. Sobin and Sackeim [7] summarized some specific speech features in depression, including slow speech speed, increased pause duration, and so on. As a subtype of depressive disorder, the influence of PPD on patients should reflect on their voices as well.

The diagnosis of PPD by using voice is feasible. First of all, speech-based diagnosis did not disturb patients too much. The procedure can be set during interviewing. Patients need not finish any complex or time-consuming tasks. Secondly, the check method is easier to hide. Behavioral features are easy to become untrue, because people are able to control their behaviors [7]. The method of speech check can avoid to directly contact with patients, which is benefit for data' ecological validity.

We proposed to detect PPD from depressed patients by using speech features. The purpose of this study is to investigate the effect of detecting PPD within depression via speech features under the state of natural experiment. The voices we used were originated from the conversation between patients and doctors recorded during interviewing. Patients' voices were separated from these recordings, and divided into two group: PPD and non-PPD. Speech features extracted by OpenSMILE, and 988 features were extracted in all. We used all speech features and features after dimension reduction to predict PPD, respectively. The predictive effects of speech features were evaluated in the light of three indexes: precision, recall and F-measure.

2 Related Work

Voice is one way of emotional expression. Speech features have been found to be able to identify different emotions. Nwe et al. [8] reported that classifying voice as different emotions based on HMM (hidden markov model) had a higher accuracy rate (average 7.7%) than artificial judging, the average rate was up to 78%. Wu et al. [9] used prosodic and spectral features to identify seven emotions, with the best precision as 91.6%. From the above studies, we know emotional can be predicted based on speech features. It motivates us to identify mental illness like PPD using speech features. There have been few studies about PPD patients' voices. We think those studies about phonetic changes of depression probably can be generalized to PPD.

The sounds of depressed patients have significant changes because of their illness [6]. The diagnostic speech features of depression in DSM-5 are described as slow, volume sank, variation of tone lessen, pause duration increase [4] (P163). Experiments revealed some specific vocal indicators in depression, such as speech speed slow down [10], increased pause duration and times [10, 11], shortened duration of utterance [12], longer initiative time latency [13]. Speech features in depression express with changes of F0 such as the decreasing of bandwidth, amplitude, energy [10, 14], shrunken F0 range ($\Delta F0$) [14], weakened intensity [15], variation of frequency spectrum like shrunken second formant transition [12] and shrunken spectral energy distribution [16], and so on.

Reviewing recent findings, Cohen and Elvevåg [17] believed that computer-based assessments of natural language has the potential for measuring speech disturbances in people with severe mental illnesses. Some researchers attempted to predict depression via patients' speech. Mundt et al. [11] stated that the regression model consisted of F0, pause duration, speech speed, speech duration, etc. could predict depression, and the explanatory power of model to depression reaching 79.2%. Emerging evidence suggested that speech features have a strong performance in predicting depression, which obtained a RMSE of 10.17 well below the baseline of 14.12 [18]. The study of Cohn et al. shown that the accuracy in detecting depression was 79% for vocal prosody [19].

In our study, we choose the depressed voices collected from natural circumstance to improve ecological validity, differing from the controlled experimental environments in the previous studies. In clinical diagnosis, it is more crucial and harder to make a distinction between different mental illnesses than distinguish healthy people from psychiatric patients. To improve the differential diagnosis among depressive spectrum disorders, our detective aim is detecting PPD within depression.

3 Methods

3.1 Participants

In this study, patients' voices were secondary data which acquired from CONVERGE (China, Oxford and VCU Experimental Research on Genetic Epidemiology) project of MDD which recorded during interviewing. Our analyses were based on a total of 740 depressed patients recruited from 58 provincial mental health centers and psychiatric departments of general medical hospitals in 45 cities of 23 China provinces. All patients were female. They were excluded if they had bipolar disorder, intelligence deficiency or any type of psychosis. Patients were aged from 30 to 60, the mean age (standard deviation) of them was 44.4 (8.9). More details of this research include diagnosis and measures were described in [20].

3.2 Data Acquisition

Voices have been collected by recording pens during computer-based interviewing. All interviewers were professional medical staffs, and trained on how to carry out the interview by CONVERGE team for at least a week. The Interview (equal to the content of recordings) includes assessment of demographic, family history, life events, psychopathology (e.g. depression, anxiety, mania, psychosis, PPD) and psychosocial functioning. The interview lasted on average two hours. The answers of patients in interviews are the data what we want.

3.3 Data Preprocessing

The audios were recorded for auditing by trained editors who provided feedback on the quality of the interviews at the beginning, thus noise control had not been planned ahead. Since we only analyze the voices of patients', data preprocess is required before usage. There are three steps of data preprocessing before speech features extraction (see Fig. 1).

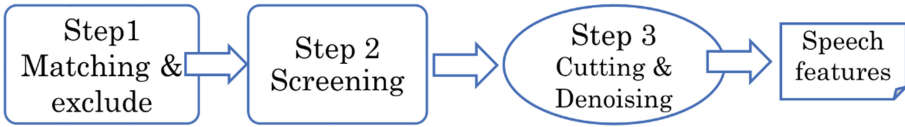


Fig. 1. The procedure of data preprocessing

The first step was matching and exclusion. First of all, we exported 11875 MP3 files from CONVERGE database. We need to match recordings with the results of psychological scales. We only left those patients who have both voice recording and questionnaire results. After matching, a total of 4243 patients were remained. The next step is exclusion. To make sure that enough recordings with enough length were used in the following steps, the short recordings should be excluded. On the basis of our experiences, we excluded those recordings which less than half an hour. Finally, a total of 3964 patients remained in this step.

The second step was screening. There were all kinds of noises in these recordings. We selected high-quality recordings to avoid the impact of noises on the predictive results. We divided all recordings into different levels according to the certain evaluation criteria (see Table 1). Finally, 774 recordings of level A were labelled, which were used for the further process.

Table 1. Evaluation criteria of voices in different levels

Level	Evaluation criteria
A	Background is quiet
B	Background has light noises
C	Noisy, hard to be cut
D	The voice of patient is not clear ^a

^aClear, means the voices are distinguishable, the content could be easily understood via hearing

In the last and most important step, our mission was cutting and denoising. We needed to separate the voices of patients from interviewers, and wiped out other noises. We recruited a few workers to engage in this part of work. The requirements of this work including: (1) the voice clips should be longer than 5 s; (2) the noises need to be cut include but not limited to ring, telephone ring, click, voices of other people, and so on. There were 740 patients remained after denoised, including 21459 voice clips. Each voice clip is equal to one answer of one patient.

3.4 Feature Extraction, Selection and Data Analysis

Open SMILE [21] was used to extract speech features. A total of 988 speech features were extracted. The procedure of feature extraction was as follows: firstly, in view of the above related work, 26 basic speech features were extracted from recordings,

including intensity, loudness, zero cross rate, voicing probability, F0, F0 envelope, eight linear spectral pair frequencies (LSP) and twelve Mel-frequency cepstral coefficients (MFCC). Secondly, to investigate the variability of voices, 26 features were turned into their first-order derivatives. Thirdly, we calculated 19 statistics of those features mentioned above, such as mean, standard deviation, range, etc. At last, we acquired 988 ($= (26 + 26) \times 19$) speech features.

It is expected that there are some irrelevant and redundant data will weaken the prediction performance. Therefore, it is not a good idea to input all speech features for prediction. Speech features should be selected before prediction. For choosing relevant features and achieving dimension reduction of speech features, we used the Sequential Floating Forward Selection (SFFS) algorithm.

Data analyses mainly includes classification and correlation analysis. Patients were divided into two groups in the light of whether they have been diagnosed as PPD or not. The group labels were considered as golden standard in classification: patients with PPD were labeled 1, without PPD were labeled 0. As classification, we implemented SVM and 5-fold cross validation for training and testing different models. To figure out whether there are salient relationships between the independent variables “number of features” and “sample size” and the predictive effects, we used partial correlation analyses to test them. In addition, paired-sample t-test was used in trying out the impacts of dimension reduction and the content of question on the predictive effects.

4 Results

4.1 Prediction

The rate of PPD group and non-PPD group was kept 1:1 to ensure that sample size has no obvious impact on predictive results. In order to directly observe the effect of dimension reduction, we used all speech features and features after dimension reduction to predict PPD, respectively. The results are respectively shown in Tables 2 and 3. We list the results of top ten best-performing questions, and order by the sample size from small to large.

In Table 2, the classification was based on 988 speech features. The best predictive result of F-measure is 65%, which is the reply to one question of depression scale. Observation of row 4–9, we found that different questions with same sample size had different predictive powers, considering the speech features used in these ten questions were the same. In addition, the predictive effects of demographic answers were common lower than the other questions.

In Table 3, the number of features were dramatically reduced after dimension reduction. The best predictive result 69% of the selected features is *PSY.3*, which is the reply to one question of psychosis scale. The average value of F-measure was increased 5.2%. By looking into row 4–9, we found that the differences of predictive effects of different questions with same sample size decreased.

Table 2. Results of classification using 988 features

Sample size	Question	Precision	Recall	F-measure
80	DEP.E24.F	0.65	0.65	0.65
90	PSY.4	0.57	0.57	0.57
120	PSY.3	0.62	0.62	0.61
120	DEP.E29	0.58	0.57	0.57
130	GAD.D64.D	0.61	0.61	0.61
130	DEP.E26	0.53	0.53	0.53
170	D2.B	0.46	0.46	0.46
170	D4.A	0.49	0.49	0.49
190	D6.A	0.55	0.55	0.55
220	D6	0.53	0.53	0.53
Average		0.559	0.558	0.557

In the second column, these abbreviations before the first point represent the corresponding questionnaire, the content after the first point represents the corresponding item (means question) number in questionnaire (except scale demographics, the content after letter “D” is the item number). DEP, depression scale; PSY, psychosis scale; GAS, scale of general anxiety disorder; D, demographics.

Table 3. Results of classification after dimension reduction

Sample size	Number of features	Question	Precision	Recall	F-measure
80	12	DEP.E24.F	0.63	0.62	0.62
90	35	PSY.4	0.61	0.60	0.59
120	15	PSY.3	0.69	0.69	0.69
120	18	DEP.E29	0.65	0.64	0.64
130	28	GAD.D64.D	0.62	0.62	0.62
130	12	DEP.E26	0.62	0.62	0.62
170	13	D2.B	0.53	0.53	0.53
170	30	D4.A	0.54	0.54	0.53
190	9	D6.A	0.63	0.63	0.63
220	12	D6	0.63	0.62	0.62
Average			0.615	0.611	0.609

In the second column, these abbreviations before the first point represent the corresponding questionnaire, the content after the first point represents the corresponding item (means question) number in questionnaire (except scale demographics, the content after letter “D” is the item number). DEP, depression scale; PSY, psychosis scale; GAS, scale of general anxiety disorder; D, demographics.

PPD and non-PPD Confusion matrixes were shown in Table 4. The precision of PPD was markedly improved after dimension reduction, reaching 75%. In contrast, the precision of non-PPD had slightly decreased after dimension reduction.

Table 4. Confusion matrixes of the most effective questions

DEP.E24.F	0	1	Precision
0	27	13	67.5%
1	15	25	62.5%

a) 988 features (0, non-PPD; 1, PPD)

PSY.3	0	1	Precision
0	38	22	63.3%
1	15	45	75%

b) 15 features (0, non-PPD; 1, PPD)

4.2 Correlation Analysis and Significance Test

Do independent variables sample size and the number of features have significant relationships with predictive effects? To figure out it, partial correlation analyses were applied in consideration of the impact of the other factor. The analyzed result between the number of features and predictive indexes exhibited that there is no salient correlation between them, after controlling the sample size (precision: $r = -0.461, p > .1$; recall: $r = -0.422, p > .1$; F-measure: $r = -0.473, p > .1$). The correlation analysis between sample size and predictive indexes (see Fig. 2) shown that sample size had a significant negative correlation with three indexes which predicted by 988 features after controlling the impact of the number of features (precision: $r = -0.697, p < .05$; recall: $r = -0.691, p < .05$; F-measure: $r = -0.691, p < .05$). However, there is no significant correlation between sample size and three indexes which calculated via reduced features.

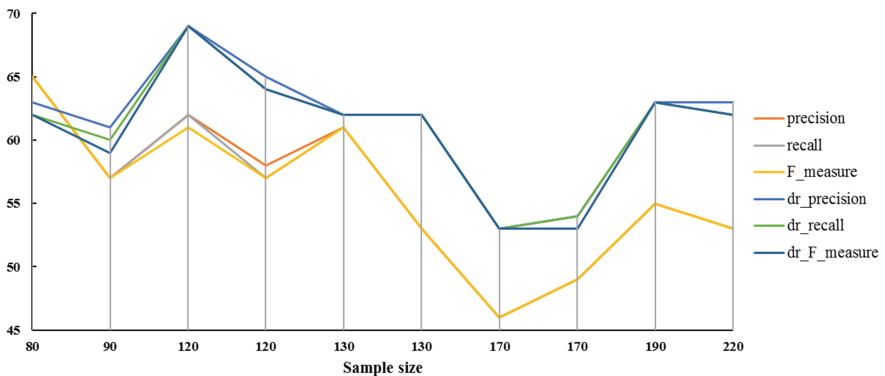


Fig. 2. The impact of sample size on predictive indexes (dr, dimension reduction)

To make it clear that if dimension reduction can evidently improve the predictive effect or not, we compared the predictive results of total features with reduced features by using paired-sample t test (Table 5 lists the means and standard deviations of

predictive indexes). The results indicated that the predictive results improved significantly after dimension reduction (precision: $t = -4.763$, $p < .01$; recall: $t = -4.31$, $p < .01$; F-measure: $t = -4.061$, $p < .01$). Further analysis, considering the impact of question, the contrast of three pairs questions with same sample size was ran by paired-sample t test. The results shown that the differences between different questions with same sample size had saliently shrank after dimension reduction (120 sample size: $t = -1$, $p = .42$; 170 sample size: $t = 7$, $p < .05$). The results of the sample size of 130 cannot test t value because their SD is zero. But their difference value's change is the largest after dimension reduction.

Table 5. The means and standard deviations of predictive indexes

	988 features			Reduced features		
	Precision	Recall	F-measure	Precision	Recall	F-measure
Mean	55.90	55.89	55.79	61.50	61.10	60.90
SD	5.92	5.88	5.77	4.77	4.64	4.86

SD, standard deviation

5 Discussion

The purpose of this study is to detect PPD in depressed patients via speech features. We used openSMILE for feature extraction, selected SFFS for feature selection, tried different numbers of features, set 5-fold cross validation for strengthening generalizability of model and applied SVM in Weka for training and testing different models. The best performance of F-measure reaching 69%, comparing with the random predictive effect 50%, which suggests that voice could be used as a potential behavioral indicator to identify depression disorder' subtypes.

We speculate there may be important influences of *the number of features*, *sample size* and *the content of question* on the predictive effect. Our results indicated that the number of features has no significant relationship with the prediction, but the predictive effect is dramatically improved after dimension reduction. The number of features among different questions are different after dimension reduction, so we think the positive impact of dimension reduction on predictive results is a combined result of number of features and content of question. It is unexpected that there is a negative correlation between sample size and predictive effect. The probable cause is demographic questions lack of the ability of emotional induction, which results in the undistinguishable neutral emotion in all patients' voices. Just as it is shown in Fig. 2, questions D2.B and D4.A make significant contributions to obvious dents of curves.

Different question has different predictive effect. We can find some clues by the most effective questions in Tables 2 and 3. The most effective question is DEP.E24.F before dimension reduction. This question asked patients to recall the state in their severest depressive episode. The most effective question is PSY.3 after dimension reduction. This question asks, "*have you ever taken medicine for your nerves or the way you were feeling or acting?*". All patients are recurrent depressive sufferers, they

must have experiences on taking anti-depressants. Thus, it is a good question to induce emotion, because the experiences about psychotropic medicine probably were negative due to medicines' side effects. In summary, the effect of emotional induction of questions has an important influence on the predictive effect.

6 Conclusion

In this study, the best predictive performance of our speech-based models is F-measure 69%, which suggests that the speech features could be used as a potential behavioral indicator to identify PPD in depressed patients. A combined impact of features and question contribute to the improvement of predictive effect. After dimension reduction, the average value of F-measure was increased 5.2%, and the precision of PPD was rose to 75%. Compared with neutral demographic questions, the features of emotional induced questions have better predictive effects.

Acknowledgments. This work was supported by the National Basic Research Program of China (973 Program) (No. 2014CB744603), and Natural Science Foundation of Hubei Province (2016CFB208).

References

1. Pitt, B.: 'Atypical' depression following childbirth. *Br. J. Psychiatry* **114**(516), 1325–1335 (1968)
2. Burke, L.: The impact of maternal depression on familial relationships. *Int. Rev. Psychiatry* **15**(3), 243–255 (2003)
3. American College of Obstetricians and Gynecologists. Committee on Obstetric Practice, Committee opinion no. 453: Screening for depression during and after pregnancy. *Obstet. Gynecol.* **115**(2 Pt 1), 394–395 (2010)
4. Accounts Payable Association: Diagnostic and Statistical Manual of Mental Disorders (DSM-5®). American Psychiatric Publishing (2013)
5. Kramer, E.: Elimination of verbal cues in judgments of emotion from voice. *J. Abnorm. Soc. Psychol.* **68**(4), 390–396 (1964)
6. Cannizzaro, M., Harel, B., Reilly, N., Chappell, P., Snyder, P.J.: Voice acoustical measurement of the severity of major depression. *Brain Cognit.* **56**(1), 30–35 (2004)
7. Sobin, C., Sackeim, H.A.: Psychomotor symptoms of depression. *Am. J. Psychiatry* **154**(1), 4–17 (1997)
8. Nwe, T.L., Foo, S.W., De Silva, L.C.: Speech emotion recognition using hidden Markov models. *Speech Commun.* **41**(4), 603–623 (2003)
9. Wu, S., Falk, T.H., Chan, W.-Y.: Automatic speech emotion recognition using modulation spectral features. *Speech Commun.* **53**(5), 768–785 (2011)
10. Ellgring, H., Scherer, P.K.R.: Vocal indicators of mood change in depression. *J. Nonverbal Behav.* **20**(2), 83–110 (1996)
11. Mundt, J.C., Vogel, A.P., Feltner, D.E., Lenderking, W.R.: Vocal acoustic biomarkers of depression severity and treatment response. *Biol. Psychiatry* **72**(7), 580–587 (2012)

12. Flint, A.J., Black, S.E., Campbell-Taylor, I., Gailey, G.F., Levinton, C.: Abnormal speech articulation, psychomotor retardation, and subcortical dysfunction in major depression. *J. Psychiatr. Res.* **27**(3), 309–319 (1993)
13. Mandal, M.K., Srivastava, P., Singh, S.K.: Paralinguistic characteristics of speech in schizophrenics and depressives. *J. Psychiatr. Res.* **24**(2), 191–196 (1990)
14. Porritt, L.L., Zinser, M.C., Bachorowski, J.-A., Kaplan, P.S.: Depression diagnoses and fundamental frequency-based acoustic cues in maternal infant-directed speech. *Lang. Learn. Dev.* **10**(1), 51–67 (2014)
15. Cohen, A.S., Kim, Y., Najolia, G.M.: Psychiatric symptom versus neurocognitive correlates of diminished expressivity in schizophrenia and mood disorders. *Schizophr. Res.* **146**(1–3), 249–253 (2013)
16. Tolkmitt, F., Helfrich, H., Standke, R., Scherer, K.R.: Vocal indicators of psychiatric treatment effects in depressives and schizophrenics. *J. Commun. Disord.* **15**(3), 209–222 (1982)
17. Cohen, A.S., Elvevåg, B.: Automated computerized analysis of speech in psychiatric disorders. *Curr. Opin. Psychiatry* **27**(3), 203–209 (2014)
18. Cummins, N., Joshi, J., Dhall, A., Sethu, V., Goecke, R., Epps, J.: Diagnosis of depression by behavioural signals: a multimodal approach. In: *Proceedings of the 3rd ACM International Workshop on Audio/Visual Emotion Challenge*, New York, NY, USA, pp. 11–20 (2013)
19. Cohn, J.F., et al.: Detecting depression from facial actions and vocal prosody. In: *2009 3rd International Conference on Affective Computing and Intelligent Interaction and Workshops*, pp. 1–7 (2009)
20. Yang, F., et al.: Clinical features of and risk factors for major depression with history of postpartum episodes in Han Chinese women: a retrospective study. *J. Affect. Disord.* **183**, 339–346 (2015)
21. Eyben, F., Wenginger, F., Gross, F., Schuller, B.: Recent developments in openSMILE, the Munich open-source multimedia feature extractor. In: *Proceedings of the 21st ACM International Conference on Multimedia*, New York, NY, USA, pp. 835–838 (2013)

Research on Network Public Opinion Propagation Mechanism Based on Sina Micro-blog

Weidong Huang^(✉), Qian Wang, and Yixuan Wang

School of Management, Nanjing University of Posts and Telecommunications,
Nanjing, Jiangsu, China
huangwd@njupt.edu.cn

Abstract. In the era of micro-blog, network public opinion has become the main expression of public opinion. Network public opinion can quickly form a network of public opinion, and promote the dissemination of information fission, with a strong interaction and effectiveness. In the case of “A girl suffered attacks in a Yitel”, we construct network propagation diagram by ucinet software and research the structural characteristics of the network public opinion propagation network based on Sina micro-blog, and the whole structure of the propagation network and the key nodes are measured. The results show that the key nodes in public opinion network propagation has a high ability to spread, so we can control the velocity of micro-blog public opinion through affecting these key nodes.

Keywords: Micro-blog · Social network analysis · Key nodes
Network structure

1 Introduction

Because of the clustering characteristics of network aggregation, the propagation of network public opinion is often sudden and explosive. With the rise of social networks, social media has become a great impetus to the formation of public opinion. By the end of 2015, the active users of Sina micro-blog have reached 236 million monthly, an increase of 34%. As one of the most rapid development of new media in recent years, Sina micro-blog becomes the main carrier of aggregation and outbreak of network public opinion due to its dual attributes of social and media.

As a medium of propagation, each user of micro-blog is the publisher and communicator of information. After the netizens release information, this information only needs to be forwarded through their huge fans group, and then, secondary forwarding again by the fans group and it will form the immeasurable reading quantity and influence. Micro-blog’s concern is based on similar preferences and habits, which makes the propagation of micro-blog’s superposition and resonance effect significant. And based on the event of public opinion in micro-blog, it is of great practical significance for the new media to study the propagation mechanism of the network public

opinion in micro-blog, and it has very important reference significance to the monitor and guide of network public opinion.

2 Research and Design of the Propagation Mechanism of Network Public Opinion Based on Sina Micro-blog

The information of Sina micro-blog spread mainly in the following ways: the release function, @ function, forwarding function and comment function [1]. These four ways can quickly and effectively release information, so that this information can spread in the Sina micro-blog and can be concerned by more users. The propagation of micro-blog's network public opinion is a very complex process, and it is not a single, linear propagation mode. However, based on the sub-public communication formed by the users' concern function, it develops into mass communication by the first level information receiver who forward information through forwarding function for the secondary spread, and then, it turns into a multi-level propagation mode with the traditional mass media platform. In this paper, we selected "A girl suffered attacks in a Yitel" as a case, and we collected data and tried to build the propagation analysis framework of micro-blog public opinion events to study the evolutionary mechanism of network public opinion.

2.1 Event Description of "A Girl Suffered Attacks in a Yitel"

April 5, 2016, the victim whose account name on micro-blog is Wanwan in her Sina micro-blog released a video of the attack in the hotel. Her unnerving story soon triggered a nationwide rage online. Through micro-blog's comment function, some users hope that the party can release the details of the development process, some users asked if the hotel would give a statement and how to deal with it after calling the police, and there are users who want more people to see this vicious incident through forwarding it to give a warning to the female friends. Due to the spread of fast and large scale, the topic of #A girl suffered attacks in a Yitel# is quickly on the hot topic list of Sina micro-blog. During this period, @Reporter_hong-tao Xue has been forwarded Wanwan's micro-blog to conduct a consultation on this issue and popularize relevant legal knowledge. @Yiteland @Homeinns Co., Lt issued a statement through micro-blog, and it said that they would investigate this vicious incident and give an account of the party and the public. @Safety Beijing, as official micro-blog of the Beijing Municipal Public Security Bureau, has been tracking this matter.

2.2 Data Collection and Processing

Set the time segment of collection and retrieval from April 5 to April 6, 2016 through the acquisition of Sina micro-blog source data. We collected Sina micro-blogs and its forwarding data by the searching method of hot topic, a total of 1900 micro-blogs. We teased out the micro-blog's forwarding relationship through Sina micro-blog's forwarding rules and identified the Sina micro-blog theme users more than 500 people of "A girl suffered attacks in a Yitel". We processed and calculated raw data and

propagation relationship between each node, and constructed the propagation network matrix of micro-blog public opinion of this event, this network matrix was anon-symmetric matrix of 502*502, and the data indicated the nodes' frequency of emergence in the sample data. Based on the matrix, using UCINET software for visualization processing of the propagation network for this event (Fig. 1).

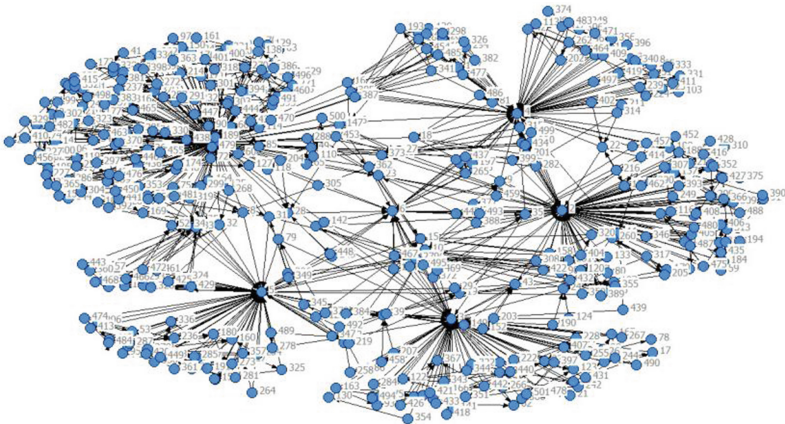


Fig. 1. Network propagation diagram of “A girl suffered attacks in a Yitel” (Numbered Edition)

2.3 The Design of Analytic Framework

To analyze the relationship of propagation node of micro-blog public opinion, we need to measure the structure of the propagation network that is composed by nodes. Social network analysis can not only measure the relationship between nodes and other nodes, but also make the researchers more intuitively grasp the behavior of nodes by visualizing the interaction between nodes.

For the micro-blog public opinion events, “A girl suffered attacks in a Yitel”, we designed the analytic framework, and it mainly included the overall network structure measurement and key nodes measurement. In the parameters that measure the overall network structure, the network density measures the compactness of network nodes through calculating the total distribution of each line and the difference between it and the complete graph; Clustering coefficients are used to reflect the structure of propagation network and the degree of aggregation between nodes.

And in measuring the key parameters of the key nodes, the structure hole index gives us the ability of nodes to control the information received by other nodes through calculating the effective size, global constraints and grades; Intermediate centrality refers to frequency, and the frequency means that shortest path of other nodes are by the way of this node, and it shows the ability of a node to act as a medium; Intermediate centrality reflects the dependence of nodes on information flow, whereas closeness centrality is a measure of the point in a graph that is not subject to other controls (Fig. 2).

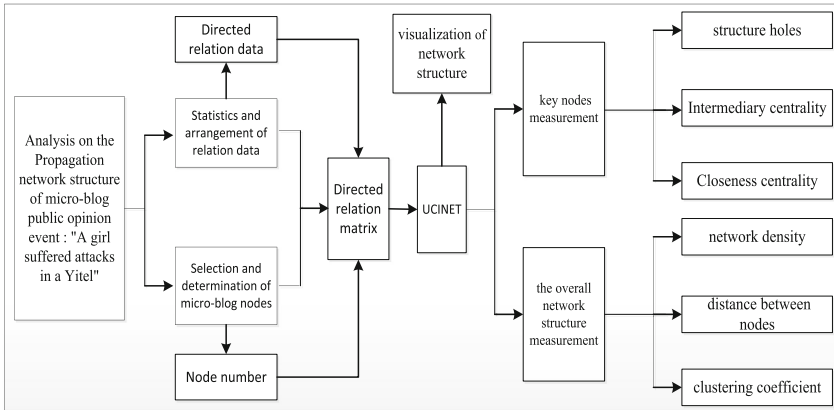


Fig. 2. Analytic framework of propagation network structure

3 Experimental Measurement and Analysis

3.1 Analysis of Key Nodes

In the propagation of micro-blog public opinion of this event, @Wanwan_2016, as a party, released the first micro-blog about encountering attack in Yitel and it soon swept across this social media platform. The official micro-blog of Yitel released a statement on it. At the same time, @Safety Beijing also reported on this incident, and it was the first government micro-blog to report the incident. In addition, @Reporter_hong-tao Xue also played a more important role in the propagation and diffusion of micro-blog public opinion. Using the key nodes analysis algorithm to form a visual description, as shown in Fig. 3, the nodes in the Figure are significantly expressed.

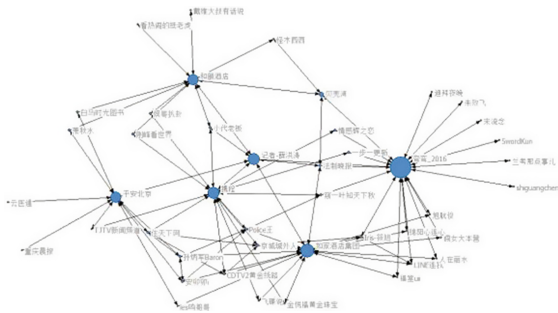


Fig. 3. Key nodes diagram of “A girl suffered attacks in a Yitel”

3.1.1 Analysis of Structural Holes

The value of the contribution to the network of the two related people who exist structural holes between nodes can be accumulated. By measurement; the degree of

structural holes in the propagation network can be analyzed [2]. By using UCINET software, we analyzed part nodes of structural holes in micro-blog public opinion propagation network of “A girl suffered attacks in a Yitel”, and we sort out the effective scale to get the Table 1. We funded that No. 1 “Wanwan_2016”, No. 2, “Ctrip”, No. 3 “Safety Beijing”, No. 5, “Homeinns Co., Ltd” and No. 4 “and “Yitel” ranked the top five. The value of effective scale reflects the position of nodes in the propagation network, and the bigger the value is, the more core the position becomes [2]. In addition to the effective scale, the limiting degree of these five nodes are relatively small, they are less than 0.2, and it also reflects that the five nodes are not easy to be controlled by other nodes and easier to access and spread public opinion.

Table 1. Analysis of propagation network structural holes of “A girl suffered attacks in a Yitel” (part)

	Nodes	Degree	Effective scale	Efficiency	Limiting degree	Grade degree
1	Wanwan_2016	199	152.078	0.764	0.176	0.904
2	Ctrip	100	76.185	0.762	0.166	0.795
3	Safety Beijing	87	64.389	0.740	0.196	0.810
5	Homeinns Co., Ltd	82	60.809	0.742	0.190	0.795
4	Yitel	77	56.717	0.737	0.198	0.787
6	Reporter hong-taoXue	28	19.286	0.689	0.223	0.451
10	Police Wang	15	9.090	0.606	0.281	0.195
7	People outside the city	15	8.825	0.588	0.306	0.273
27	Update step by step	11	5.583	0.508	0.327	0.065

3.1.2 Intermediary Centrality

Intermediate centrality is used to measure the ability of a node as a medium of propagation, that is, it measures the ability of the node as a “bridge” in the process of information propagation [3]. When a node appears on the shortest path between two nodes, the more the nodes appears, the higher the intermediate centrality of the node is, and this shows that more and more nodes have to spread information through it, and the node is also known as the “bridge node”. l_{jk} is the shortest path number from node j to node k , $l_{jk}(x_i)$ is the shortest path number that contains the node i on the shortest path from node j to node k , N is the number of all nodes in a network. In a directed network, the formula for calculating the intermediary centrality is shown in Eq. (1). The results of intermediary centrality measurements of the propagation network are shown in Table 2.

$$C_B(x_i) = \frac{\sum_{j < k} l_{jk}(x_i) / l_{jk}}{(n - 1)(n - 2)} \tag{1}$$

We can find that, “Wanwan_2016”, “Ctrip”, “Safety Beijing”, “Homeinns Co., Ltd”, “Yitel” and “Reporter_ hong-tao Xue”, the value of intermediate centrality of the six nodes is located in the top six of the data sample, it means that the six nodes play the important roles in the propagation process of micro-blog’s public opinion and take on the more important roles of the medium. They not only have a greater share of public opinion information, but also a greater degree of impact on other nodes. It can be seen from the measurement results of intermediate centrality, the party discloses the vicious incident and triggers a large number of micro-blog users to forward the information, and it leads to the information propagation. In addition, the government micro-blog, the official micro-blog of media and other celebrities have a high intermediary, while the intermediary centrality of the other nodes is generally low, which also shows that the different types of nodes have different effects on the propagation of public opinion information.

Table 2. Analysis of intermediary centrality of propagation network of “A girl suffered attacks in a Yitel” (part)

	User type	Node	Absolute intermediary centrality	Relative intermediary centrality
1	Party	Wanwan_2016	143458.422	57.498
2	Companies involved	Ctrip	67290.070	26.970
3	Government micro-blog	Safety Beijing	64621.414	25.900
5	Companies involved	Homeinns Co., Ltd	51395.484	20.599
4	Companies involved	Yitel	50695.699	20.319
6	Other celebrities	Reporter_ hong-taoXue	47793.961	19.156
27	Domestic consumer	Update step by step	7226.098	2.896
23	Domestic consumer	A glimpse of autumn	7142.234	2.863

3.1.3 Closeness Centrality

In the information propagation process of Sina micro-blog, a user may contact with many people in the network directly or indirectly. In this case, the user has a relatively high closeness centrality, that is, the user can close to a large number of other users in the network. It can be seen from the Table 3, the closeness centrality of Reporter_ hong-taoXue is highest in the propagation network of the micro-blog public opinion, and it means that this node contact with many people in the network, and it also can be found from the attributes of the node, the influence of the opinion leaders is more strong in the development of public opinion events.

From the point of view of structural holes, intermediary centrality and closeness centrality, we analyze the key nodes of the propagation network of micro-blog public opinion event of “A girl suffered attacks in a Yitel”. From the view of calculated data, “Wanwan_2016”, as the party node, Homeinns Co., Ltd and Yitel, as the involved companies nodes, their effective scale are 152.078, 60.89 and 56.717, and their limiting degree are less than 0.2. And the three nodes are the starting nodes of microblog information in “A girl suffered attacks in a Yitel”, so external nodes do not affect them.

Table 3. Analysis of closeness centrality of propagation network of “A girl suffered attacks in a Yitel” (part)

	Node	In farness	Out farness	In closeness	Out closeness
6	Reporter_ hong-taoXue	973.000	974.000	51.387	51.335
1	Wanwan_2016	1027.000	991.000	48.685	50.454
3	Safety Beijing	1105.000	1297.000	46.249	38.551
28	Legal Evening News	1203.000	1210.000	41.563	41.322
2	Ctrip	1250.000	1250.000	40.000	40.000
5	Homeinns Co., Ltd	1268.000	1269.000	39.432	39.401
305	Happy xiaoliumang	1279.000	1288.000	39.093	38.820
23	A glimpse of autumn	1290.000	1258.000	38.760	39.746

What’s more, the intermediary center degrees of “Safety Beijing”, “Reporter_ hong-taoXue” are 25.900 and 19.156 respectively, and they have relatively high closeness centrality, so it can be concluded that the two nodes are “bridge” nodes in network propagation of this micro-blog public opinion event, and they play the roles of “opinion leaders”, and they play leading roles in the propagation of public opinion information in this event and promote the transfer of public opinion information through their own influence.

3.2 Overall Network Structure Measurement

3.2.1 Network Density and Distance Between Nodes

There is a direct correlation between the network density and the strength of the relationship between nodes, and the value of the network density will decrease with the increase of the number of nodes [4, 5]. The distance between nodes in the propagation network is mainly used to measure the network structure characteristics, and the shorter the distance between nodes in the propagation network is, it means that the connection can be established between the nodes through a shorter path, and the relationship between the nodes is close, and the propagation network has a strong cohesion and the information in the network can spread rapidly.

Table 4. Measurement results of network density and distance between nodes of “A girl suffered attacks in a Yitel”

Density	Standard deviation	Average distance	Distance-based cohesion	Distance-weighted fragmentation
0.0102	0.1018	3.193	0.344	0.656

According to the statistical results in Table 4, the network density of this public opinion event is only 0.0102, the result shows that the network density is very small in the propagation process of the public opinion events, the links between nodes are more dispersed, and the exchange of information is not frequent. The distance between nodes of the propagation network is 3.193, cohesion distance-based is 0.344, and fragmentation distance-weighted is 0.656. This result shows that the propagation ability of the

public opinion information in data samples is general and cohesion is not strong. The propagation probabilities of distance from 1 to 4 are 1%, 26.1%, 25.4% and 47.4%, so, the propagation ability of sub-public propagation is general, however, the relationship links whose distance is 4 are nearly half, and it also shows that the mass communication has a huge effect in this event.

3.2.2 Clustering Coefficient

The clustering coefficient is mainly used to reflect the characteristics of the topology structure of the propagation network and the aggregation degree of the relationships among the nodes [6]. If a node j in the network has n_j neighbor nodes, then there may be a maximum of $n_j(n_j - 1)/2$ edges between the n_j nodes. We define the ratio of actual number of edges $E(j)$ between nodes n_j and the possible number of edges $n_j(n_j - 1)/2$ as the clustering coefficient of nodes $CC(j)$, that is:

$$CC(j) = 2E(j)/[n_j(n_j - 1)] \tag{2}$$

The clustering coefficient CC of the whole network is the average of the clustering coefficients of all nodes j :

$$CC = \frac{\sum_{j=1}^N CC(j)}{N} \tag{3}$$

The value of clustering coefficient ranged from 0 to 1, the greater the number of clusters is, the stronger the cohesive force of the whole propagation network is, and the links between nodes are more closely. The measure results in Table 5 show that efficient clustering coefficient is 0.1, in propagation network in the public opinion event of “A girl suffered attacks in a Yitel”. The clustering coefficient is too small, and it means that there is a relatively low level of information communication between nodes. At the same time, the network structure is relatively loose, the community structure and the state of the internal substructure are not obvious, and the connection between the nodes is relatively weak.

Table 5. Analysis of clustering coefficient of propagation network of “A girl suffered attacks in a Yitel” (part)

	Node	Clustering coefficient	Node logarithm
1	Wanwan_2016	0.014	19503
2	Ctrip	0.031	4851
3	Safety Beijing	0.031	3655
4	Yitel	0.036	2850
5	Homeinns Co., Ltd	0.034	3240
6	Reporter_hong-taoXue	0.138	351
7	People outside the city	0.275	91

Weighted Overall graph clustering coefficient: 0.100.

In this paper, we use three indexes, the network density, the distance between nodes and the clustering coefficient [7–9], in order to analyze the overall network structure of the micro-blog public opinion of “A girl suffered attacks in a Yitel”. According to measure results, the network density is very small in the propagation network of the public opinion events, it is only 0.0102, the links between nodes are more dispersed, and the exchange of information is not frequent. The propagation ability of sub-public communication is general; however, the relationship links whose distance is 4 are nearly half, so it also shows that the mass communication has a huge effect in this event. In spite of this, the cohesive force of propagation network is weak and lack of communication between nodes and nodes, and the forwarding relationship does exist, but it did not communicate with other nodes for effective communication after the forwarding, making public opinion propagation effect cease to advance. For this micro-blog public opinion event, information is more concentrated on the party and the company involved, “Wanwan_2016” and “Yitel”, and they are the key communicators of this event. For “Safety Beijing”, “Reporter_hongtaoXue” and other key nodes, etc., they only have single forward relationship rather than mutual forwarding relationship, and the connectivity between nodes is poor, so it is difficult to form a small group.

4 Conclusion

In this paper, we measured the overall network structure that are composed of nodes and the key nodes of the propagation network through statistics and arrangement on the relationship of micro-blog public opinion propagation node. Through the analysis of the measurement results, it is found that it is difficult to form a small group because of the lack of cohesion between the nodes of this event. Investigating its deep reason, the event of “A girl suffered attacks in a Yitel” is a vicious incident caused by the individual party, and in the information propagation of micro-blog public opinion, it is focused on the hotel’s indifference to violence that complained by the party, companies involved also issued a statement and it said they would investigate it to the end, in order to give the party and the public an account. Although the forwarding quantity in the short term of this incident is very high, and it also appeared the “bridge” node as the “opinion leader”, and there is a lack of cohesion between the nodes of the propagation network, and there is no small group, and the communication between the nodes is weak.

Therefore, the parties of public opinion events should actively enhance communication with other users, and it needs more media, celebrities and government micro-blog to pay attention to public opinion events so as to promote the transfer of public opinion information through their own influence. On the one hand, the parties should strengthen the communication with other users and select the representative users to forward their questions for each other after forwarding their own micro-blog. It will not only form a small group based on forwarding, but also can enhance the cohesion between the user nodes, so that public opinion information can spread rapidly. On the other hand, we can develop opinion leaders to achieve the effect of guiding public opinion. The “opinion leader” in Sina micro-blog refers to a kind of communicator that has appeal and influence in the propagation process of network public opinion. This speech of information communicator is very easy to cause the recognition

of other users, and the users use comment and forwarding function to make it spread in the micro-blog, resulting in a greater impact on public opinion, which has a greater impact on public opinion. Therefore, we need to have the opinion leaders to exert their influence and spread positive energy, in order to achieve the purpose of infects and affects other user groups.

Acknowledgment. Work described in this paper was funded by the National Natural Science Foundation of China under Grant No. 71671093. The authors would like to thank other researchers at the Nanjing University of Posts and Telecommunications.

References

1. Russo, T.C., Koesten, J.: Prestige centrality and learning: a social network analysis of an online class. *Commun. Educ.* **54**(3), 254–261 (2005)
2. Jinlou, Z., Junhui, C.: Analysis of micro-blog public opinion diffusion based on SNA: an empirical study on April 20 Ya'an Earthquake in Sichuan. *Manag. Rev.* **01**, 148–157 (2015)
3. Wei, K.: Analysis of the key nodes in public opinion spread during emergencies based on social network theory—a case study of the 7·23 Wenzhou high-speed train collision. *J. Public Manag.* **03**, 101–111, 127–128 (2012)
4. Xiaojuan, H., Nan, J., Jinjin, X.: Study on micro-blog rumor based on social network analysis—a case study on the micro-blog about food security. *Intell. J.* **08**, 161–167 (2014)
5. Wei, J.C., Bu, B., Liang, L.: Estimating the diffusion models of crisis information in micro-blog. *J. Inform.* **6**(4), 600–610 (2012)
6. Lee, C.H.: Mining spatio-temporal information on microblogging streams using a density-based online clustering method. *Expert Syst. Appl.* **39**(10), 9623–9641 (2012)
7. Nair, H.S., Manchanda, P., Bhatia, T.: Asymmetric social interactions in physician prescription behavior: the role of opinion leaders. *J. Mark. Res.* **47**(5), 883–895 (2010)
8. Xin, M.J., Wu, H.X., Niu, Z.H.: A quick emergency response model for micro-blog public opinion crisis based on text sentiment intensity. *J. Softw.* **7**(6), 1413–1420 (2012)
9. Xia, Z.Y., Yu, Q., Wang, L.: The public crisis management in micro-blogging environment: take the case of dealing with governmental affairs via micro-blogs in China. *Adv. Intell. Soft Comput.* **141**, 627–633 (2012)

Scholar Recommendation Model in Large Scale Academic Social Networking Platform

Ming Chen¹, Chunying Li², Jiwei Liu¹, Dejie Meng¹, and Yong Tang¹

¹ School of Computer Science, South China Normal University, Guangzhou, China
mchencf@163.com, {cocoliu, 2016022321, ytang}@m.scnu.edu.cn

² School of Computer Science, Guangdong Polytechnic Normal University, Guangzhou, China
zqxylcy@163.com

Abstract. A scholar-recommended model based on community division is established due to the characteristics of social intercourse of academic social network. The model was developed by GraphChi, the single version of large-scale graphic computing system which was launched by GraphLab, to find the core network in parallel on network topology map. In the established network, using self-adaptive label transmission to create labels and then according to the number of labels on the nodes to get final results of community division. Calculation is done within the community for expert recommendation services. The experiment of data-set on academic social networking platform, SCHOLAT, suggests, models not only can create community quickly, but also can gain good recommendation results by all the three personalized methods, i.e. Community Weight Recommended (CWR), Community Random Recommended (CRR) and Acquaintance Community Recommended (ACR).

Keywords: GraphChi · Community detection · Kernel sub-network
Label propagation · Scholars recommendation

1 Introduction

In recent years, with the advent of WeChat, micro-Bo, Facebook and other social networking platform, large-scale social networks have developed rapidly. The greatest charm of a social network is Social, and each social networking platform creates many explicit or hidden circle of friends [1]. With the rapid development of intelligent terminals, a rapid growth of network data has been seen in social networking platform, so people often encounter the problem of information overload when they find interested friends. Therefore, the provision of friends recommended in social networking platform can help users more quickly and more accurately find their potential friends. As a kind of social platform, academic social networking platform also need a scholars recommend system to help users brush selected interested scholars.

At present, the domestic and foreign scholars have proposed many friend recommendation algorithm to solve the mentioned above problems, which can be divided into two categories. One is the friend recommendation algorithm based on the user's existing information. In the literature [2], a friend recommendation model is established by

obtaining user's preferences and information that already exists on the social network platform, and the model explores and recommends friends who may have intersects with the user on the view of user's existing information. The algorithm in [3] analyzes the microblog content published by the user to discover the interest of the user, and then according to the user's interest to recommend it may be interested friends. The paper [4] aimed at some friends recommend algorithms, but ignored the relationship between individuals and timing factors, this paper proposed a method to model the temporal behavior among users based on the extraction of the user's existing information, so they could found the neighbour collection that have the greatest influence on the current user, and then merged the collection in-to a coordinated Itering recommendation algorithm which based on probability matrix decomposition. In the literature [5], the non-topology information were used to calculate the similarity among users, and then recommended the potential friends who were similar to the target user according to the similarity between users. Another friends recommendation algorithm was based on social network topology modeling. In the literature [6], the separation degree of each node was calculated by dividing the topological graph of the buddy relationship in the social network. Based on the degree of separation, the algorithm divided the nodes with the same degree of dissimilarity into the same community group, and then recommended nodes within the same group reciprocally.

Considering the unique social nature of academic social networks [7–9], we propose a scholars recommendation algorithm based on label community discovery, which is a friend recommendation algorithm based on social network topology modeling. The Label Propagation Algorithm (LPA) [10] proposed by Raghavan et al. in 2007 firstly, which is a community discovery algorithm based on label propagation. LPA is relatively simple. The algorithm first assigns a unique label to all the nodes, and then flushes the labels of all the nodes until the convergence requirements are reached, and finally get the non-overlapping community. In recent years, many scholars [11–13] have improved the LPA algorithm from different angles in view of its simple and high efficiency. For the LPA can only be applied to the discovery of non-overlapping community problems, Gregory proposed the Community Overlap Propagation Algorithm (COPRA) [14] algorithm in 2009, which was applicable to overlapping communities. Concerning the problem that community detection algorithm based on label propagation in complex networks has a pre-parameter limit in the real network and redundant labels, LI Chunyin proposed the Adaptive Label Propagation Algorithm (ALPA) [15]. The algorithm used the adaptive threshold to eliminate the unreasonable label in the iterative process, and finally classified the node with the same label into a community. ALPA algorithm has achieved good results, especially in the academic social network. But it is not ideal when dealing with social networks with large user population and complex user relationships, because the time complexity of the algorithm is relatively high in this case. To solve this problem, this paper proposes Community Detection Based on GraphChi (CDBG) algorithm which is a community discovery scholars recommendation algorithm based on GraphChi system. CDBG uses the characteristics of GraphChi system to achieve ALPA algorithm in parallel, and then uses the community clustering results to achieve friend recommendations. This algorithm improves the response speed of friends recommendation.

2 Recommended Approach

The main idea of the model is to explore the community according to the topology diagram of the user relationship in the social network, and then recommend a friend in the community. Finding out core networks and then building the community by tag propagation is a better-performing and easy-to-implement approach. However, it is very time-consuming to find the core network in the massive graph data, which makes the recommendation system unable to meet the user's psychological response time. Therefore, it is very important to improve the search strategy of the core network. The strategy of this paper that to use the concurrent mechanism of Graphchi system to split the topography of the buddy relationship, and then find out the core network from each part. Each local topology to find out the core network. As the number of local nodes is much smaller than the whole, it improves the speed of finding the core network, thus improving the response time of the whole recommendation system.

2.1 GraphChi

The Graphchi system is a stand-alone version of the large-scale graphing system introduced by GraphLab Labs. Although it is not based on the popular distributed architecture, the efficiency of this system is very high, and it is not inferior to the distributed computing system [16] in dealing with large-scale data. The ingenious design allows Graphchi to efficiently process large-scale map data. In order to speed up the efficiency of the system, Graphchi load the data into memory. This approach is similar to other large scale computing systems. Since the memory is very limited in stand-alone environment, it is impossible to load all the data into memory when it encounters large graph data. So Graphchi first cut into a number of small map, and then load the sub-graph data into the memory for each calculation. Loading each subgraph one after the other can complete an iteration. After several rounds of iterations, you can complete the task of graph calculation. The above process is the main idea of Parallel Sliding Windows (PSW).

The running process of PSW has completed the update of the sub graph data. Each round diagram update process includes three main steps: the loading of sub-graph data, the concurrent implementation of node update function, write back the updated sub-map data. When Graphchi completes the three sequential steps mentioned above, it completes the update of a subgraph. When all the P intervals are updated, a round of iteration of the entire graph is completed.

As can be seen from the above algorithmic flow, the key of Graphchi to handle massive amounts of data in a single-machine environment is the data is sliced and then stored in memory. Because only need to read a piece of information at a time, so long as the external memory space is large enough to be able to adjust the value of P to make the memory to meet the computing requirements. Graphchi uses a vertex-centric programming model in which adjacent vertices pass messages between edges. Developers only need to consider a single vertex update function, and Graphchi framework to solve specific details such as vertex-parallel.

2.2 Community Detection Based on GraphChi (CDBG)

2.2.1 Establish Core Network

Definition 1: Complete graph. The topological graph of social network user relations is represented by graph $G = \{V, E\}$, where V represents the set of user nodes in the topology graph. E is the edge set of the topology graph, which represents a collection of friend relationships among users. If graph G_s is a subset of graph G and any pair of different vertices in G_s have exactly edges connected, then G_s is called a complete graph.

Definition 2: Core network. In graph $G = \{V, E\}$, assume that A and B are any two nodes in V that are not tagged. If A and B are the maximum degree and unmarked nodes of each other, then the edges A to B are used to find the complete graph for the initial edge. If $G_s \in G$ and there is no any complete graph $G_t \in G$ making $G_s \in G_t$, then G_s is a core network of graph G .

Definition 3: Community consolidation. There are two sets of G_i and G_j representing two different communities. G_i is a subset of G_j that represents the community G_j contains the community G_i . The behavior of deleting the community G_i is referred to as merge communities G_j and G_i .

The core network is the core unit of the community, and the nodes in the same core network must be in the same community. Because this algorithm is based on the core network of relationships to build the community, so the algorithm must first look for the core network. This is the initialization phase of the algorithm. Specific steps are as follows.

1. Assign 0 to all nodes in V ;
2. Select a node U_i with value of 0 in the data fragment, then find the node U_j with the largest degree and value of 0 in the adjacent node of the node U_i ;
3. If the value of node U_i is 0 and U_i is the adjacency node with the largest degree of U_j , then choose $e(U_i, U_j)$ as the initial edge to find the core network according to Definition 2;
4. If the condition of step 3 is satisfied, then the node number with larger degree in U_i and U_j is regarded as the core network number and assigned to all the nodes in the core network found in step 3;
5. If the condition in Step 3 is not true, go back to Step 2 and select another node.
6. Repeat steps 2–5 until there is no change in the core network, and the process of finding the core network is stopped.

According to the above-mentioned rules, the network topology diagram shown in Fig. 1 is taken as an example to illustrate the process of establishing the core network. According to the above process, a total of 2 core networks are found in the topology map, which are the core networks of 4 and 7: $M_4 = (3, 4, 2, 5)$, $M_7 = (6, 7, 8)$. Finally, the core network assigned to all the nodes, that is, 4 is assigned to the node 3, 4, 2, 5, and the 7 is assigned to the node 6, 7, 8. In this algorithm, the node's value is the label of the node. Figure 1 shows the topology which has established the core network.

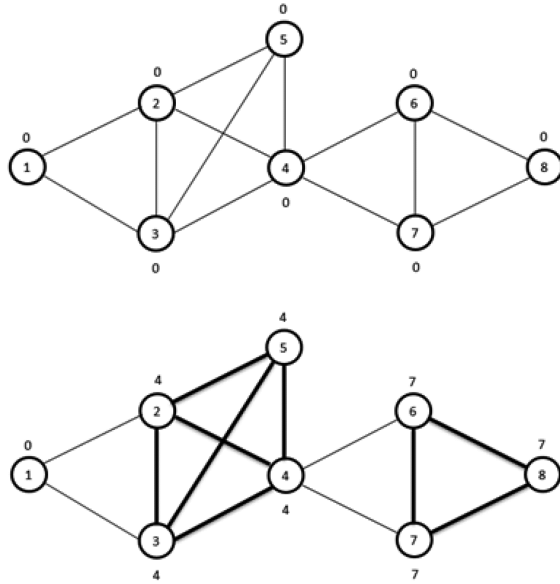


Fig. 1. After the establishment of the core network

2.2.2 Label Update

When the core network is established, each node in the network is assigned a unique value. The value on the node is the label of the node, which is the original label. The value is also the number of the core network to which it belongs. The core network is the influential circle of friends in the community, and the core of the topological relationship of the community is the core network. Therefore, the algorithm spreads the label with the core network as the center. In order to reduce the redundant tags and avoid the excessive spread of tags and improve the stability of the algorithm, the algorithm automatically removes some labels with less weight in the process of label propagation, so as to self-adaptively propagate the notes. Specific rules are as follows.

1. The weight of each node in the core network is set to 1, which corresponds to the original label of the node;
2. In each iteration, the label of any node v in V is updated with the following rules:
 - (a) The nodes v check the labels of its neighbors one by one. If v node and its adjacent node v_a have the same label L_1 , update the label in v : $L_1 = W_v + (W_1/d)$. Where W_v is the weight of the label L_1 in v , W_1 is the weight of the label L_1 in the adjacent node, and d is the degree of v . If the adjacent node v_a has the label L_2 but the node v does not have the label, then label v as $L_2 = W_2/d$. Where W_2 is the weight of label L_2 in v_a ;
 - (b) Assume that the number of labels is C . If C is greater than 1, the label with weight less than $1/C$ is deleted. If all the label values satisfy the condition, the label with the largest weight is retained and the remaining labels are deleted. If the weight of the largest have more than one label, you can keep a random;

- (c) Normalize the labels in node v , and finally make the sum of the weights in each node equals to 1.
- 3. Repeat steps 2–4 until all nodes have at least one label;
- 4. Traverse all nodes and classify nodes with the same label as the same community. If a node has more than one label, it is categorized into multiple communities;
- 5. Community consolidation based on Definition 3.

According to the above rules, now take the Fig. 1 as an example to update the label. Eventually generated two communities, namely $C_1 = \{1, 2, 3, 4, 5\}$, $C_2 = \{6, 7, 8\}$. The results of community detection are shown in Fig. 2.

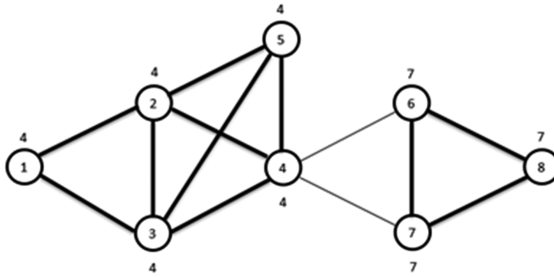


Fig. 2. Results of community detection

2.3 Scholars Recommend

In a social network, users in the same community tend to have similar interests or areas of work, and users in the same community are more likely to accept it. Therefore, the recommendations in this paper are carried out in the divided communities. The CDBG algorithm is used here to classify communities. After the community division, this model uses three methods to make personalized recommendation, namely: Community Weight Recommendation (CWR), Acquaintance Community Recommendation (ACR) and Community Random Recommendation (CRR).

After the establishment of the scholar community using the CDBG algorithm, each scholar may belong to several different communities. In the CWR recommendation mode, all the scholars who are in the same community as the target scholar A and not the friends of A are sorted by weight from high to low. Then the former N highest weight scholars recommended to the scholar A , which is a CWR recommendation. This recommendation is suitable for recommending scholars to Ph.D. and professors because we assume that highly educated user groups are more likely to accept influential scholars in the same community. The ACR recommended method selects the community with the least number of nodes among the communities to which the target scholar A belongs, and ranks the users of the community in descending order of weight, and then recommends the first N highest weight scholars to the scholar A . This recommendation is recommended for scholarships for Masters and below, as these users have limited communication and academic skills and are more willing to accept scholars in acquaintance communities. For example, a college counselor is more willing to accept the college

clerk and other college counselors in her acquaintance community than a well-known scholar in a field. CRR recommended method is the most simple. The CRR randomly recommends nodes that are in the same community as Target A and whose weights are higher than the specified value. This approach is suitable for those who have just joined the academic social networking platform and friends and team information is scarce. It is a cold start recommended way. Take the CWR method as an example, the process of Scholar Recommendation is illustrated below:

1. Input

$G = \{V, E\}$: G represent the initial community topology,

A: A represent the ID of the target scholar,

N: N represent the number of recommended scholars,

2. Recommended procedure

(1) Community Detection (CDBG)

```

foreach iteration do
  shards[] ← InitializeShards(P)
  for interval ← 1 to P do
    subgraph ← LoadSubgraph(interval)
    parallel foreach vertex in subgraph:vertex do
      CDBG_updateVertex (vertex)
    end
    shards[interval].UpdateFully()
    for s in 1, ..., P, s ≠ interval do
      shards[s].UpdateLastWindowToDisk()
    end
  end
end

```

(2) Scholars Recommend

```

foreach iteration do
  shards[] ← InitializeShards(P)
  for interval ← 1 to P do
    max_n (vertex. edges)
  end
end

```

3. Output

1, 2, 3, ..., N, The top n users with the highest

3 Experimental Results

In this part, we first introduce the data set used in the experiment, and then explain the evaluation method of the experiment. Finally, we give the experimental results of CWR, CRR and ACR, and analyze the experimental results.

3.1 Description of Dataset

The data set used in the experiment is the friend relationship data set of the academic social network platform (SCHOLAT) on October 12, 2016. The data set records the relationship between scholars and friends on the social network platform. After denoising the data set, there are 5168 users whose information is disclosed and 22284 user relations.

3.2 Evaluation Method

In the experiment, we used four general indicators [17] to evaluate the recommended results, namely: Precision, Recall, F-measure and MAP. These four methods are the standard to measure the accuracy of the recommendation system, and reflect the accuracy of the recommendation system to the specified users, where Precision is the accuracy of the recommended system recommendations, and it can be defined as follows:

$$P = \frac{1}{T} \sum_u \frac{N_t}{L} \quad (1)$$

Where T is the number of experimental test samples, and N_t is the number of recommended objects the user likes in each recommendation, and L is the recommended list length in a recommendation.

Recall expresses the possibility that the user's favorite object is recommended by the recommended system, and it can be defined as follows:

$$R = \frac{1}{T} \sum_u \frac{N_t}{A_u} \quad (2)$$

Where A_u represents the total number of objects in the test set that are accepted by the recommended user.

F-measure is the weighted harmonic average of Precision and Recall, and when the value is high, the test result is more effective. It can be defined as:

$$F_1 = \frac{(a^2 + 1)P * R}{a^2(P + R)} \quad (3)$$

When $a = 1$, the formula is the most common F_1 -measure, and it defined as:

$$F_1 = \frac{2 * P * R}{P + R} \quad (4)$$

The final evaluation criterion is MAP, which reflects the average accuracy of the recommended system and is the probability of recommending an object to be accepted. it can be defined as:

$$MAP = \frac{1}{T} \sum_{j=1}^T \left(\sum_{k=1}^L \frac{p(L_{jk})}{m_j} \right) \quad (5)$$

Where $p(L_{jk})$ represents the ratio of the number of users preferred in the first K recommended objects in the j th recommendation to k . j represents the number of objects that the user likes in the j th recommendation. L represents the length of the recommended list, and we get $L = 10$ and $L = 5$.

3.3 Result Analysis

In the data set described above, we use the community recommendation model proposed in this paper to generate a total of 442 communities, with the largest community having 1986 user nodes and the smallest community having 3 nodes. The total time it takes to generate the community is 1.508 s. In order to verify the validity of this model and compare the advantages and disadvantages of CWR, CRR and ACR recommendations, we calculate the Precision, Recall, F-measure and MAP by questionnaire survey. These questionnaires are divided into two categories, one with a recommended length of 10 and another of 5; Table 1 gives the experimental results for $L = 10$ and $L = 5$. From Table 1, we can see that no matter which kind of recommendation method, the recommended accuracy rate is above 55%, and the average accuracy MAP can be maintained above 55%. Additionally, when the ACR recommended method is adopted, the accuracy can reach 77.68% and the MAP can reach 81.63% under the recommended length $L = 10$. In this way, when the recommended length $L = 5$, the accuracy is 84%, MAP is 85.84%. This is a very good result, and at the same time, it proves the effectiveness of the proposed model in this paper.

Table 1. Comparison of experimental results.

Description	L = 10			
	Precision	Recall	F1-measure	MAP
CWR	0.5503	0.4825	0.5141	0.5634
CRR	0.6335	0.4994	0.5585	0.6228
ACR	0.7768	0.5007	0.6089	0.8163
Description	L = 5			
	Precision	Recall	F1-measure	MAP
CWR	0.5234	0.4670	0.4935	0.5709
CRR	0.6021	0.4969	0.5445	0.6359
ACR	0.8467	0.5093	0.6360	0.8584

By comparing the results in Table 1, it can be seen that the CWR recommendation method has the worst performance among the three methods. There are two reasons for this situation. First of all, in the scholar network social network platform, the weight of a scholar is not exactly the same as the scholar has great influence, because some scholars often use the scholar network platform for teaching, thus accumulating a large number of students friends to increase their weight, but this weight does not affect the choice of other people; In addition, a highly qualified scholar does not guarantee that he is well known by other scholars, nor can he guarantee that the direction of his research is to accept the recommendation of users interested in. And the majority of users of social networking platform is a master’s degree, so the user’s academic social and research areas are relatively limited. So the CWR method is more suitable to recommend scholars to doctoral and professors and other highly educated users. As can be clearly seen in Table 1, the ACR method is most effective. The reason for this result is that there is a high possibility that users have a connection in acquaintance communities, so the user is more inclined to accept a scholar in the community. In addition, by comparing the two results of $L = 10$ and $L = 5$, it can be seen that there is no significant difference in the effect of CRR between the two lengths. However, CWR perform better at $L = 5$, but ACR at $L = 10$ gives better results. This just verifies the above analysis.

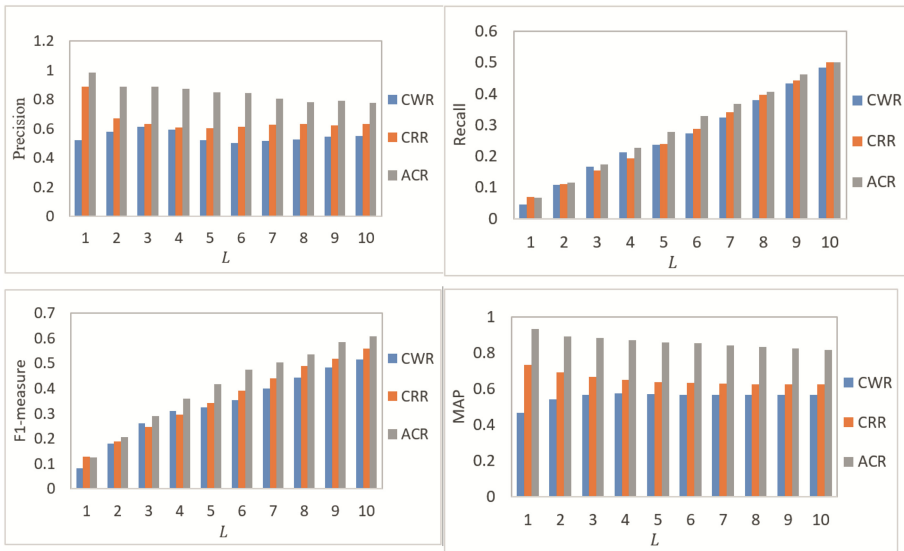


Fig. 3. Results of community detection

Figure 3 shows the change in the recommended results with the length of the recommended list. As can be seen from the figure, Recall and F_1 -measure are more sensitive to the recommended list length, while Precision and MAP are less affected by the recommended length. In addition, it can be seen from the diagram that the ACR method can achieve better results under different recommended lengths. It can be seen that the use of ACR recommended in many cases can get the best results. But the ACR method

obviously has his shortcomings. The acquaintance community recommendation can improve the acceptance of the recommendation object by the user, but such recommendation lacks novelty and unexpectedness, and the coverage rate is low, so that the user's satisfaction can not be guaranteed. WRR also has these deficiencies. CRR is not the best, but its randomness is high, and can provide enough freshness and accident, and have a higher coverage rate. In summary, if the user is a doctor or professor, you can choose CRR and CWR mode. If you want to recommend scholars to the MS and the following user groups, the best choice is ACR.

4 Conclusion and Discussion

In this paper, we propose a community-based recommendation model for large-scale social networks. The model firstly uses the graphchi framework to divide the community and obtains the core network of the network structure. Then, the core network is used as the core to transmit the tags. The nodes are updated by using the synchronous adaptive label propagation mode. Eventually forming multiple communities and recommending scholars in these communities. In the stage of recommending buddies, this paper provides three methods, which are community weight recommended (CWR), community random recommended (CRR) and acquaintance community recommended (ACR). Through the analysis of the experiment, we can see that the overall effect of CRR is the best, and the effect of ACR is the second.

The lack of the CRR approach in the recommended scholarly stage is precisely the advantage of the ACR. In the next work, we intend to study how to combine the two recommended ways to further improve the effectiveness of recommendations.

Acknowledgment. This work is supported by the Applied Technology Research and Development Foundation of Guangdong Province (No. 2016B010124008), the Science and Technology Planning Project of Guangdong Province (Nos. 2016A030303058, 2015B010109003).

References

1. Zhang, Z., Li, Q.: Questionholc: hot topic discovery and trend analysis in community question answering systems. *Expert Syst. Appl.* **38**, 6848–6855 (2011)
2. Colace, F., Santo, M.D., Greco, L., Moscato, V., Picariello, A.: A collaborative user-centered framework for recommending items in online social networks. *Comput. Hum. Behav.* **51**, 694–704 (2015)
3. Armentano, M.G., Godoy, D., Amandi, A.A.: Followee recommendation based on text analysis of micro-blogging activity. *Inf. Syst.* **38**, 1116–1127 (2013)
4. Sun, G.F., Wu, L., Liu, Q., Zhu, C., Chen, E.H.: Recommendations based on collaborative filtering by exploiting sequential behaviors. *J. Softw.* **24**, 2721–2733 (2013)
5. Debnath, S., Ganguly, N., Mitra, P.: Feature weighting in content based recommendation system using social network analysis. In: *International World Wide Web Conference*, pp. 1041–1042 (2008)

6. Silva, N.B., Tsang, I.R., Cavalcanti, G.D.C., Tsang, I.J.: A graph-based friend recommendation system using genetic algorithm. In: *Evolutionary Computation*, pp. 1–7 (2010)
7. Gruzdz, A., Staves, K., Wilk, A.: Connected scholars: examining the role of social media in research practices of faculty using the UTAUT model. *Comput. Hum. Behav.* **28**, 2340–2350 (2012)
8. Nández, G., Borrego, Á.: Use of social networks for academic purposes: a case study. *Electron. Libr.* **31**, 781–791 (2013)
9. Gu, F., Widén-Wulff, G.: Scholarly communication and possible changes in the context of social media: a finnish case study. *Electron. Libr.* **29**, 762–776 (2011)
10. Raghavan, U.N., Albert, R., Kumara, S.: Near linear time algorithm to detect community structures in large-scale networks. *Phys. Rev. E Stat. Nonlinear Soft Matter Phys.* **76**(3 Pt 2), 036106 (2007)
11. Liu, X., Murata, T.: Advanced modularity-specialized label propagation algorithm for detecting communities in networks. *Physica A Stat. Mech. Appl.* **389**, 1493–1500 (2010)
12. Cordasco, G., Gargano, L.: Community detection via semi-synchronous label propagation algorithms, pp. 1–8 (2011)
13. Xie, J., Szymanski, B.K.: Community detection using a neighborhood strength driven label propagation algorithm. In: *IEEE NSW*, pp. 188–195 (2011)
14. Gregory, S.: Finding overlapping communities in networks by label propagation. *New J. Phys.* **12**, 2011–2024 (2009)
15. Li, C., Huang, Y., Tang, Z., Tang, Y., Zhao, J.: Adaptive label propagation algorithm to detect overlapping community in complex networks. *Int. J. Future Gener. Commun. Netw.* **9**, 317–326 (2016)
16. Kyrola, A., Blelloch, G., Guestrin, C.: GraphChi: large-scale graph computation on just a PC. In: *Usenix Conference on Operating Systems Design and Implementation*, pp. 31–46 (2012)
17. Lichtenwalter, R.N., Lussier, J.T., Chawla, N.V.: New perspectives and methods in link prediction. In: *ACM SIGKDD International Conference on Knowledge Discovery and Data Mining*, Washington, DC, USA, July, pp. 243–252 (2010)

Research on Simulation for Fuel Consumption of UAV

Zongpu Jia¹, Yonghui Shi², Songyuan Gu^{3(✉)}, and Shufen Liu³

¹ College of Computer Science and Technology, Henan Polytechnic University, Jiaozuo, China
jiazongpu@126.com

² China Shipbuilding Information Technology Co., Ltd., Beijing, China
shiyh@csit.net.cn

³ College of Computer Science and Technology, Jilin University, Changchun, China
gusongyuan614@163.com, liusf@mail.jlu.edu.cn

Abstract. To enhance the sense of reality of Unmanned Aerial Vehicle (UAV) simulation, factors influencing fuel consumption of UAV are analyzed in this paper in detail. On the basis of these factors, a fuel consumption model of UAV is presented, and finally fuel consumption simulation in UAV simulation control system could be implemented employing the presented model.

Keywords: Unmanned Aerial Vehicle · Fuel consumption · Simulation model
Energy balance

1 Introduction

Technologies concerning Unmanned Aerial Vehicle (UAV) areas developed significantly in recent years, and UAV simulation appears great theoretical and applied importance [1]. The instrument monitoring areas display the flight status of UAV during missions in real-time, the areas contain a series of data, e.g. fuel consumption, propeller speed, propeller temperature, link state, etc. The series of data is of great references to estimate whether the UAV is in normal flight state. As important one of instrument monitoring areas, fuel gauge displays the fuel consumption level of UAV in real time, which is extremely valuable for flight status monitoring and flight mission planning [2]. A fuel consumption model of UAV on the basis of detailed analyzed influencing factors in Sect. 2 is presented in Sect. 3. Fuel consumption simulation of instrument monitoring areas in UAV simulation control system could be implemented employing the presented model.

2 Influencing Factors Analysis of Fuel Consumption of UAV

2.1 Fundamental Aerodynamic Parameters

Aerodynamic parameters contain lift coefficient, drag coefficient, lift-drag ratio, etc. Fundamental aerodynamic parameters of UAVs with different types or different performance would vary as temperatures and speeds differ. However, the correlations among those fundamental aerodynamic parameters are complex and could hardly be

described in functions, and thus are measured by wind tunnel test or test flight, which are shown in Figs. 1 and 2.

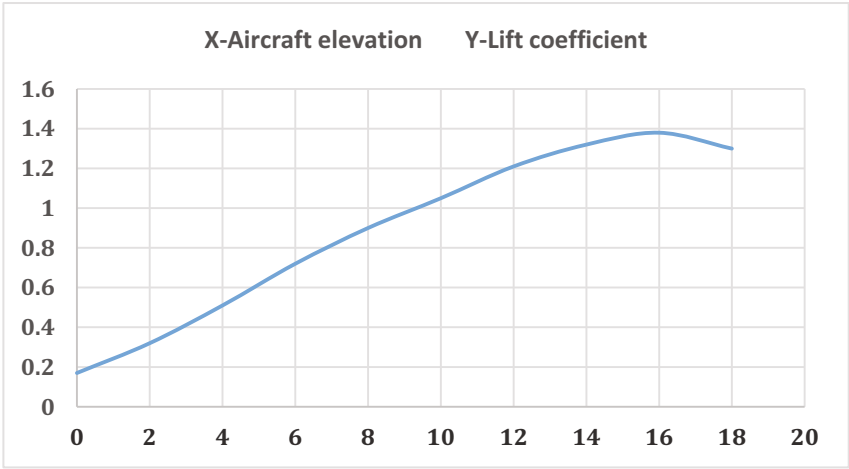


Fig. 1. Relation curve of aircraft elevation and lift coefficient

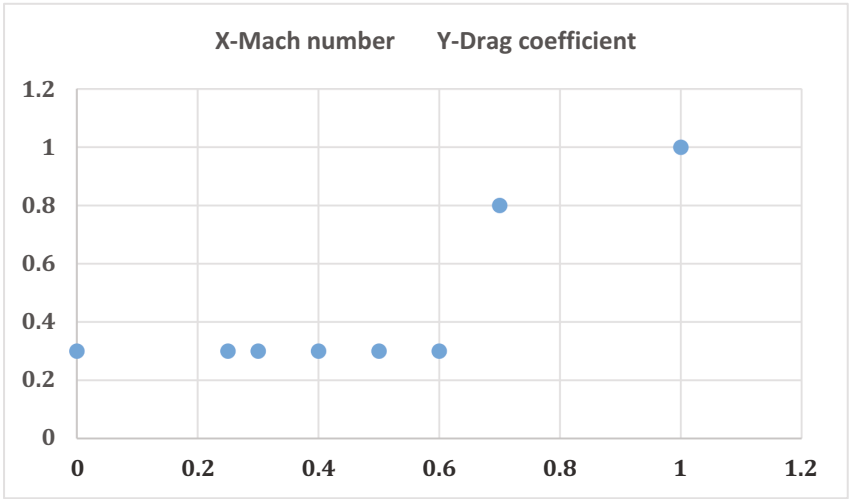


Fig. 2. Scatter plot of Mach number and drag coefficient

2.2 Engine Performance Parameters

The performance of engine is linear with respect to the fuel consumption; the fuel consumption of engine is determined by UAV type, speed and altitude. One of the most important indexes is the Thrust specific fuel consumption (TSFC) [3]. The TSFC of

engine, which is different from fundamental aerodynamic parameters, is a function of speed, altitude and thrust.

2.3 Flight Trajectory

The flight trajectory of UAV is shown on Head up display (HUD) [4], which includes speed, altitude, pitch angle, roll angle, deflection angle, acceleration, course, etc. These indexes are all factors influencing fuel consumption.

2.3.1 Speed

The speed to be considered here is the level flight speed of UAV. There are two speed units in aviation field: the commonly used km/h, and the Mach number. Speed relates directly to fuel consumption of UAV.

2.3.2 Pitch Angle

The fuselage of a UAV would be at a certain angle to horizontal while the UAV is ascending or is descending. The UAV is nosing up during ascent, and the angle which is designated positive is defined as elevation angle; on the contrary, the UAV is nosing down during descent, and the angle which is designated negative is defined as depression angle. When ascending, greater thrust is required to overcome the gravity and to generate upward acceleration, as a consequence, the fuel consumption would increase; when descending, the thrust reduces, the fuel consumption decreases accordingly [5, 6].

2.3.3 Roll Angle and Deflection Angle

The UAV would subject to centrifugal force, gravity and drag, and would tilt at an angle when it makes a turn. The tilt angle is defined as roll angle. Turning radius and turning rate of an aircraft are determined by the roll angle. The deflection angle is the course change caused by the nose of a UAV when turning. More thrust is needed to maintain

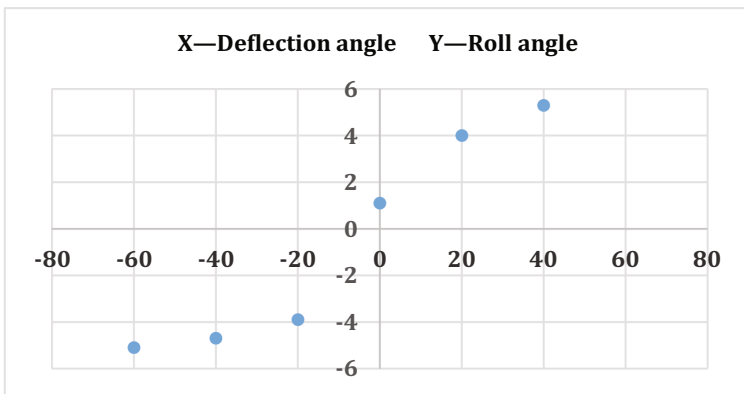


Fig. 3. Scatter plot of roll angle and deflection angle

circling when the UAV makes a turn. Figure 3 shows a series of roll angles and deflection angles sampled in a turning process.

2.3.4 Acceleration

The acceleration of an aircraft consists of horizontal acceleration and vertical acceleration. Figure 4 shows scatters of vertical acceleration and fuel consumption sampled during UAV missions.

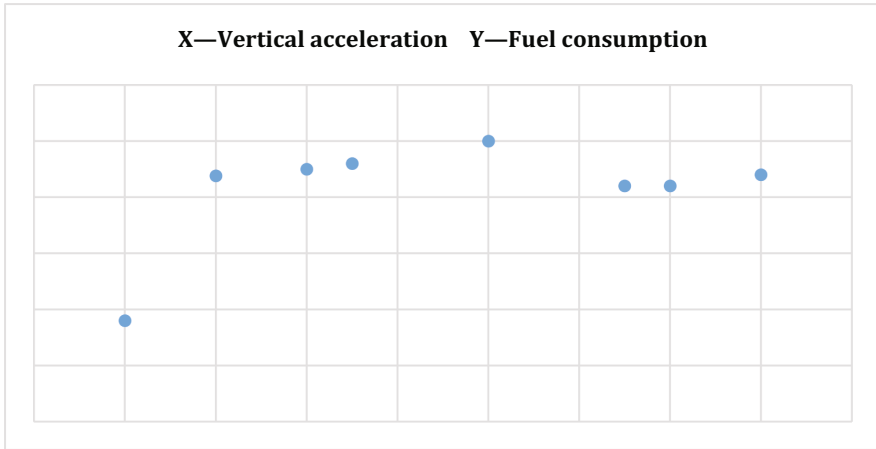


Fig. 4. Scatter plot of vertical acceleration and fuel consumption

2.4 Weight

The weight of a UAV is the sum of fuselage weight and load weight. The heavier the UAV weighs, the greater thrust is needed, accordingly the fuel consumption increases. When in a UAV mission, the UAV weight would reduce as the fuel consumption increases. In fuel consumption calculation, therefore, the flight process should be divided into several stages, weight deduction in each stage is neglected, and thus simplified calculation is proceeded minimizing calculation error in accordance with aforementioned assumption.

2.5 Atmospheric Parameters

Atmospheric parameters mainly include temperature, density, pressure, etc. These parameters are evenly distributed on horizontal surface, but are with considerable variation on vertical surface. Temperature and pressure are main factors influencing fuel consumption; standard atmosphere would be utilized to execute simulation in aviation field.

3 Computational Model for Fuel Consumption

Fundamental aerodynamic parameters are complex variables in factors influencing fuel consumption discussed in Sect. 2: firstly, aerodynamic parameters differ as UAV types are different; secondly, the correlations between different aerodynamic parameters could hardly be described in functions. Hence, aerodynamic parameters won't be considered in fuel consumption modeling in this paper.

Because of the linear relationships between engine performance parameters and TSFC (relative with speed v , altitude h and thrust F), engine performance parameters could be used to model fuel consumption.

Flight trajectory parameters relate most directly to the fuel consumption, speed, altitude, pitch angle, roll angle, etc. could be all used to model fuel consumption, and therefore we further involve these parameters into the fuel consumption modeling.

Since the accurate acquisition and uncomplicated calculation of the fuselage weight and the load weight of a UAV, we also involve the total weight of a UAV as one of parameters into fuel consumption modeling.

Normally, atmospheric parameters have certain influence on fuel consumption. However, due to the little critical difference of the altitude in level flight, atmospheric parameters have little relationship to fuel consumption modeling; hence atmospheric factor won't be considered in fuel consumption model establishment.

The following assumptions are presented based on principle of energy balance before fuel consumption modeling:

1. The weight change caused by fuel reduction in UAV mission doesn't affect the fuel consumption calculation;
2. The accelerated motion of UAV is deemed as uniformly accelerated motion, i.e. the variations of speed and altitude are linear;
3. Energy generated from fuel consumption is all for UAV motion, ignoring energy supply for other components at the same time. In fact, energy for other components is provided by battery in UAV;
4. A complete UAV mission includes 5 stages, i.e. taxiing, climbing, cruising, landing and taxiing. Though the fuel consumption in each stage is different, since taxiing, climbing and landing make up small proportions of time throughout the mission, only fuel consumption in cruising would be taken into account when modeling.

Model description of fuel consumption of UAV on vertical surface employing the principle of energy balance is shown in Fig. 5.

Let altitude be h , speed be v , acceleration of gravity be g , the UAV mass be m_1 , the load mass be m_2 , thrust generated from engine be T , aerodynamic drag be f , lift be L , pitch be α , roll angle be γ , and abscissa and ordinate of the UAV be x and y . Then the following equation set could be set up

$$m \times \frac{dv}{dt} = T \times \cos \alpha - f - (m_1 + m_2)g \times \sin \gamma \tag{1}$$

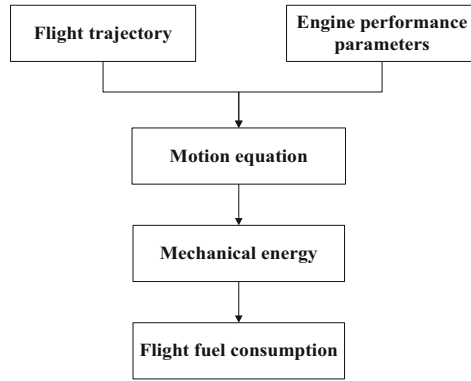


Fig. 5. UAV fuel consumption model on vertical surface

$$m \times v \times \frac{d\gamma}{dt} = T \times \sin \alpha + L - (m_1 + m_2)g \times \cos \gamma \tag{2}$$

$$\frac{dy}{dt} = v \times \sin \gamma \tag{3}$$

$$\frac{dx}{dt} = v \times \cos \gamma \tag{4}$$

The energy height of the UAV is following

$$E = h + \frac{1}{2g} \times v^2 \tag{5}$$

The total energy equals to the product of the energy height and the UAV mass, thus the state model based on principle of energy balance could be obtained as follows

$$\begin{cases} E = h + \frac{1}{2g}v^2 \\ E = \frac{v \times (T \times \cos \alpha - f)}{mg} \\ x = v \times \cos \gamma \end{cases} \tag{6}$$

The formula of fuel consumption Mf is as follows

$$dMf = C_e P dt \tag{7}$$

where C_e is the TSFC of UAV; P is the rated thrust of engine.

Therefore, the formula of fuel consumption and energy height is as follows

$$\frac{dE}{dMf} = \frac{dE/dt}{dMf/dt} = \frac{dE/dt}{C_e P} \tag{8}$$

where the TSFC of engines varies according to aircraft types: the TSFC of an airliner is generally 0.1–0.5; the TSFC of a fighter is generally 0.7–1.5; and the TSFC of the UAV in this paper is about 0.1. Fuel consumption of a UAV in cruising stage could be derived from formula 3.6 and formula 3.8.

4 Conclusion

Factors influencing fuel consumption of UAV are analyzed in detail above all in this paper, and then on the basis of these factors, a fuel consumption model of UAV is presented. Employing the presented model, fuel consumption simulation in UAV simulation control system could be implemented.

References

1. Huang, K.M., Zhang, M.Y., Wang, T.: The design of UAV simulation model system based on component modeling technology. *Ship Electron. Eng.* **12**, 86–89 (2015)
2. He, Y.C., Liu, K., Shen, X.Y., et al.: Simulation study of aircraft fuel consumption estimates model. *Comput. Simul.* **32**(5), 33–36 (2015)
3. Shirley, C.M., Schetz, J.A., Kapania, R.K., et al.: Tradeoffs of wing weight and lift/drag in design of medium-range transport aircraft. *J. Aircraft* **51**(3), 904–912 (2014)
4. Perez-Rodriguez, D., Maza, I., Caballero, F., et al.: A ground control station for a multi-UAV surveillance system: design and validation in field experiments. *J. Intell. Robot. Syst.* **69**(1–4), 119–130 (2013)
5. Zhang, Y.X.: *Research on Mission Flight Path Planning and Optimization Method for Fixed-wing UAV*. Zhejiang University (2016)
6. Xu, M.X., Zhu, X.P., Zhou, Z., et al.: Exploring an effective method of thrust allocation for solar-powered UAV with multiple propellers. *J. Northwest. Polytechnical Univ.* **4**, 505–510 (2013)

Research on Meteorological Data Simulation

Zhenglun Wu, Shufen Liu, and Tie Bao^(✉)

Jilin University, Changchun, China

497564655@qq.com

Abstract. This paper proceeded with simulating the meteorological data. Based on the meteorological data that has been collected, this paper puts forward the simulation method where the meteorological data can be classified into discrete data and continuous data which can be simulated respectively. By establishing the mathematical model of meteorological variables and the employment of the relevant knowledge, the simulation of meteorological data can be achieved. The simulated relationship among meteorological data accord with the relationship among the real data. In other words, the simulated result approach the real meteorological data to a certain extent. Moreover, this result guarantees the application of the unmanned aerial vehicle in logistics, disaster relief, medical care etc.

Keywords: Meteorological data · Simulation · Mathematical model
Discrete

In UAV simulation training, the weather is a very important factor, Changes in weather will greatly affect the operation and flight of UAV in simulation environment. In order to improve simulation level of the simulation training system, the simulation of meteorological data needs to be studied. The objective of Ref. [1] was to develop and validate a simulation model of the evaporation rate of a Class A evaporimeter pan. Daily weather data and three climatic variables for four cities in China were gathered, investigated and analyzed, and the sensitivity of climatic variables on building energy consumption was discussed [2]. An experimental embankment was constructed, and the first objective is to investigate the influence of climatic changes on the soil response such as changes in water content and temperature [3]. The main contribution of Ref. [4] is an analysis of requirements for a wind power infeed model used in a power system simulator from a meteorological viewpoint. The WARMF model was applied to the Catawba River watershed of North and South Carolina to simulate flow and water quality in rivers and a series of 11 reservoirs [5]. The data generated in Ref. [6], can be directly applied to the EIA prediction model and serve for EIA. Edgar et al. [7] analyze the performance of the physically based snow model SNOWPACK to calculate the snow cover evolution with input data commonly available from automatic weather stations. A system for observing meteorological data based on a wireless sensor network is designed to fulfill the business requirements for meteorological data observation in unattended areas [8]. This paper puts forward the simulation method where the meteorological data can be classified into discrete data and continuous data which can be simulated respectively. This paper proceeded with simulating the meteorological data. Based on the meteorological data that has been collected. Task deducing and simulated training are conducted by coordinating with the comprehensive task control system and the result is satisfactory.

1 Meteorological Data Collection and Sorting

Under the condition that the way of establishing statistic model has been determined, appropriate meteorological data can be collected according to the types of meteorological data which is required to simulate. Table 1 shows the daily meteorological data of one of the districts in Changchun.

Table 1. The daily meteorological data of one of the districts in Changchun

Time	Weather condition	Temperature (°C)	Relative humidity	Air pressure (hpa)	Wind force	Wind direction
8 am	Fine	21	56	991	2	South
9 am	Fine	23	47	991	1	South
10 am	Fine	25	41	991	2	Southwest
11 am	Fine	25	41	991	2	West
12 am	Fine	27	39	990	0	North
13 pm	Fine	27	37	990	2	Northwest
14 pm	Fine	28	35	989	1	West
15 pm	cloudy	27	38	989	1	Northwest
16 pm	cloudy	28	39	989	0	North
17 pm	Fine	25	45	989	0	North
18 pm	Fine	21	50	989	0	North
19 pm	Fine	19	64	989	0	North
20 pm	Fine	18	73	989	0	North
21 pm	Fine	17	76	989	0	North
22 pm	Fine	16	79	990	0	North
2 pm	Fine	15	83	990	0	North
24 pm	Fine	15	86	990	0	North
1 am	Fine	14	88	990	0	North
2 am	Fine	14	88	990	0	North
3 am	Fine	14	87	990	2	West
4 am	Fine	14	88	991	1	South
5 am	Fine	13	87	991	1	East
6 am	Fine	13	91	991	0	North
7 am	Fine	16	69	991	1	South

2 Initial Meteorological Data Analysis

Meteorological data variable mainly consists of six types which are meteorology, temperature, relative humidity, air pressure, wind power, wind direction. According to the meteorological knowledge, initial analysis will be conducted on the types of variable as well as the value range. Atmospheric phenomenon generally includes the sky condition, rainfall, snowfall which are usually described as fine, rain, fog, snow. Meteorology names physical quantity that measures the degree of the hot and cold as

air temperature, international standard temperature unit of measurement is Celsius. Relative humidity is the specific value of absolute humidity and saturated absolute humidity under the same air temperature, it is also a percentage. Air pressure is the hydrostatic pressure on a specific point which is generated by air. The resource of the air pressure is gravity of the atmosphere, known as atmospheric pressure on unit square. The measurement unit is hpa. Meteorology defines the direction that the wind blows from as wind direction which normally falls in to sixteen directions. Wind speed is usually represented as the level of wind. Wind level is determined by the degree of effect that the wind generates on the ground objects. In meteorology, wind power can be classified in to thirteen levels. Two kinds of variables can be concluded based on the initial analysis of these variables. The first type of variable includes weather condition, wind power and wind direction, their value ranges belong to set value which are defined as discrete variables. The second type of variable includes temperature, relative humidity and air pressure. They are numeric variables which are defined as continuous variables.

3 Simulation of the Discrete Data

Markov process is such a kind of process: In the process of $x(t)$, every transfer of the state is related to the state of the previous moment but not the past state. In other words, there is no after effect during the state transfer process, hence, such a state transfer process is called Markov process. Markov chain is a discrete Markov process in the time discretization state.

Markov chain is a sequence of random variables like X_1, X_2, X_3, X_4 . The range of these variables called state space is the set of all their possible values and the value of X_n represents the state in time n . If X_{n+1} is a function of X_n with respect to the conditional probability distribution of the past state, then

$$P(X_{n+1} = x | X_0, X_1, X_2, \dots, X_n) = P(X_{n+1} = x | X_n)$$

This identical equation represents the characteristic of the Markov chain. In the Markov chain, n -step transition probability has the following characteristic:

$$P_{ij}^{(n)} = \sum_{k \in I} P_{ik}^{(l)} P_{kj}^{(n-l)}$$

This equation is called Norman-Kolmogorov Equation which solves the relationship between n -step transition probability and one-step transition probability and its matrix format is: $\mathbf{P}^{(k+m)}(n) = \mathbf{P}^{(k)}(n) \mathbf{P}^{(m)}(n+k)$.

Then we take an example of the weather condition to illustrate the process of the data generation. Firstly, we assume that weather condition at time $a + 1$ is only correlated to the weather condition at time a but has nothing to do with the previous weather condition. This process is consistent with Markov process, then Markov Chain can be used to calculate probability transition.

3.1 Generate Initial Value

Statistics of the Meteorological data can help figure out the frequency of each kind of weather condition and calculate the probability of each kind of weather condition, the results are shown in Table 2.

Table 2. The frequency and probability of each kind of weather condition table

Weather condition	Fine	Partly cloudy	Cloudy	Overcast	Rainy
Frequency	83	20	7	5	3
Probability	69.1%	16.6%	5.8%	4.1%	2.7%

Divide the value range of the random number into corresponding interval according to the probability and then stochastic number p is generated. Then, the interval of the stochastic number p can be estimated while the initial value of the meteorology can also be determined. For example, stochastic number range [1–100] can be divided into fine [1,69], partly cloudy [70,86], cloudy [87,93], overcast [93,97], rainy [98,100]. The generated stochastic number 19 suggests that the initial value of the weather condition is fine.

3.2 Calculate Probability Transition Matrix

Then statistics of the meteorology data also contributes to obtaining the transition frequency and the matrix F .

$$F \begin{bmatrix} f_{clear\ to\ clear} & f_{clear\ to\ partly} & f_{clear\ to\ cloudy} & f_{clear\ to\ overcast} & f_{clear\ to\ rainy} \\ f_{partly\ to\ clear} & f_{partly\ to\ partly} & f_{partly\ to\ cloudy} & f_{partly\ to\ overcast} & f_{partly\ to\ rainy} \\ f_{cloudy\ to\ clear} & f_{cloudy\ to\ partly} & f_{cloudy\ to\ cloudy} & f_{cloudy\ to\ overcast} & f_{cloudy\ to\ rainy} \\ f_{overcast\ to\ clear} & f_{overcast\ to\ partly} & f_{overcast\ to\ cloudy} & f_{overcast\ to\ overcast} & f_{overcast\ to\ rainy} \\ f_{rainy\ to\ clear} & f_{rainy\ to\ partly} & f_{rainy\ to\ cloudy} & f_{rainy\ to\ overcast} & f_{rainy\ to\ rainy} \end{bmatrix} = \begin{bmatrix} 74 & 6 & 3 & 0 & 0 \\ 3 & 14 & 1 & 1 & 1 \\ 0 & 4 & 3 & 0 & 1 \\ 0 & 0 & 2 & 3 & 0 \\ 0 & 0 & 2 & 0 & 1 \end{bmatrix}$$

Then, transition probability matrix p can be generated according to the matrix F .

$$P = \begin{bmatrix} 0.89 & 0.07 & 0.04 & 0 & 0 \\ 0.15 & 0.7 & 0.05 & 0.05 & 0.05 \\ 0 & 0.5 & 0.375 & 0 & 0.125 \\ 0 & 0 & 0.4 & 0.6 & 0 \\ 0 & 0 & 0.66 & 0 & 0.34 \end{bmatrix}$$

By employing Norman-Kolmogorov Equation, we can calculate n-step transition probability matrix $P^{(1)}, P^{(2)}, \dots, P^{(23)}$.

3.3 Generate Data from Transition Probability

The way of generating the weather condition at time n is similar to the way of generating the initial value of the weather condition. Divide the value range of the stochastic number into corresponding intervals according to the transition probability of the initial value in matrix $P^{(n)}$, and then stochastic number p and its interval can be obtained. Hence, the value can be determined.

4 Continuous Data Simulation

Linear regression analysis is the common method of establishing meteorology application model. The relationship exists among many of the meteorology variables through relevant meteorology knowledge. Moreover, linear regression analysis is thoroughly complete from model establishment to authentication method theory. Meteorological data can be forecast and analyzed by employing this model.

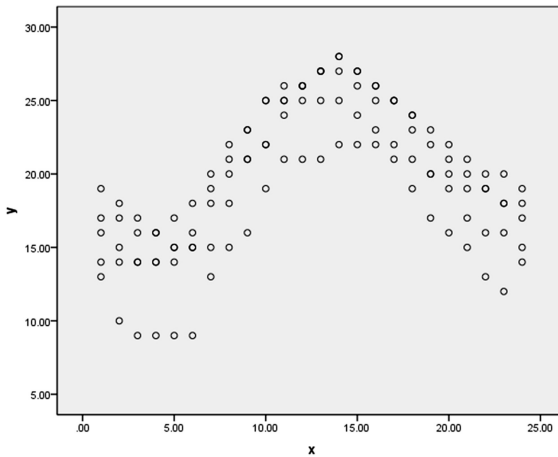


Fig. 1. Temperature and time scatter figure

For continuous variables, existing meteorological data can be used to conduct multiple linear regression analysis and establish the mathematical relationship among meteorological data. Substitute the generated variables into the equation in order to generate continuous variables. The following temperature example is to introduce the process of generating continuous variables by employing the multiple linear regression analysis. By screening out the factors, choose time and weather condition as the dependent variables in the regression analysis of temperature, the scatter diagram of time and temperature is shown as Fig. 1.

From the above Fig. 1, temperature is in a steadily increasing trend from 2 pm to 2 am; However, temperature is decreasing from 3 am to 1 pm. Thus, it is necessary to conduct multiple linear regression analysis on these two time periods.

We need to endow meteorological value with numerical meanings in order to quantify the factors, the result is shown as Table 3.

Table 3. Meteorological quantify table

Weather condition	Fine	Partly cloudy	Cloudy	Overcast	Rainy
Value	1	2	3	4	5

The following explanation is the process of establishing regression model of temperature from 2 pm to 2 am:

$$y = \beta_0 + \beta_1 x_{1i} + \beta_2 x_{2i} + \varepsilon_i, \quad i = 1, 2, 3 \dots n \quad (n \text{ is the number of value})$$

where ε_i is mutually independent and follow normal distribution $N(0, \sigma^2)$.

The 65 times records can be written as:

$$\begin{cases} y_1 = \beta_0 + \beta_1 x_{11} + \beta_2 x_{12} + \varepsilon_1 \\ y_2 = \beta_0 + \beta_1 x_{21} + \beta_2 x_{22} + \varepsilon_2 \\ \dots \dots \\ y_n = \beta_0 + \beta_1 x_{n1} + \beta_2 x_{n2} + \varepsilon_n \end{cases}$$

If transfer this equation set into matrix, then: $Y = XB + \varepsilon$

Where matrix:

$$Y = \begin{pmatrix} y_1 \\ y_2 \\ \cdot \\ \cdot \\ \cdot \\ y_{65} \end{pmatrix} = \begin{pmatrix} 28 \\ 28 \\ \cdot \\ \cdot \\ \cdot \\ 15 \end{pmatrix} X = \begin{pmatrix} 1 & x_{11} & x_{12} \\ 1 & x_{21} & x_{22} \\ \cdot & \cdot & \cdot \\ \cdot & \cdot & \cdot \\ \cdot & \cdot & \cdot \\ 1 & x_{65} & x_{65} \end{pmatrix} = \begin{pmatrix} 1 & 14 & 1 \\ 1 & 15 & 1 \\ \cdot & \cdot & \cdot \\ \cdot & \cdot & \cdot \\ \cdot & \cdot & \cdot \\ 1 & 26 & 1 \end{pmatrix} B = \begin{pmatrix} \beta_0 \\ \beta_1 \\ \beta_2 \end{pmatrix} \varepsilon = \begin{pmatrix} \varepsilon_0 \\ \varepsilon_1 \\ \cdot \\ \cdot \\ \cdot \\ \varepsilon_{65} \end{pmatrix}$$

For the equations above, we can use the least square method to find the solutions. The fundamental principle of the least square method is to find $b_0, b_1, \dots b_n$ which can minimize the residual sum of square between observation and regression value. It is equivalent to find the solutions of the equations:

$$\begin{aligned} \frac{\partial}{\partial \beta} (Y - X\hat{\beta})'(Y - X\hat{\beta}) = 0 & \quad \frac{\partial}{\partial \beta} (Y'Y - \hat{\beta}'X'Y - Y'X\hat{\beta} + \hat{\beta}'X'X\hat{\beta}) = 0 & \quad \frac{\partial}{\partial \beta} (Y'Y - 2Y'X\hat{\beta} + \hat{\beta}'X'X\hat{\beta}) = 0 \\ -X'Y + X'X\hat{\beta} = 0 & \quad X'Y = X'X\hat{\beta} & \quad \hat{\beta} = (X'X)^{-1}X'Y \end{aligned}$$

We can obtain the estimations b_0, b_1, b_2 of $\beta_0, \beta_1, \beta_2$ which are 42.9, -1.08, -0.85. Therefore, the regression equation of temperature is: $y = 42.9 - 1.08x_1 - 0.85x_2$. Then, it is required to proceed with the test of significance of the regression equation.

4.1 Certainty Coefficient of the Equation

The certainty coefficient of the equation represents the explanation degree of independent variables against dependent variables, the certainty coefficients of the regression equation are shown as Table 4:

Table 4. The deterministic coefficient of the regression equation table

Item	R	R ²	Adjusted R ²
Value	0.905	0.819	0.813

From the diagram, it can be known that the coefficient of R is 0.905, the coefficient of R² is 0.819, the coefficient of adjusted R² is 0.813, we have to preferentially consider adjusting the coefficient of R². Since 0.813 is bigger than 0.05 and approaches 1, the explanation degree of the independent variables against dependent variables is high.

4.2 Significance Test of the Linear Relationship of the Regression Equation

Variance analysis is a way of decomposing the sum of squares of deviations and its degree of freedom and examining the linear relationship between independent and dependent variables by employing statistical magnitude F. The variance analysis is shown as Table 5:

Table 5. The variance analysis table

Source of variance	Sum of square	Degree of freedom	F value
Regression	1037.914	2	140.536
Residual value	228.947	62	
Total	1266.862	64	

$$\text{Assume: } \left\{ \begin{array}{l} H_0 : \beta_1 = \beta_2 = 0 \\ H_1 : \beta_1, \beta_2 \text{ at least one nonzero} \end{array} \right\}$$

We can identify significance level $\alpha = 0.05$ and find the rejection region. We find $F_{0.05}(2, 60) = 3.15$ by referring to the table,

$$F = 150.536 > F_{0.05}(2, 60) > F_{0.05}(2, 62)$$

By rejecting H_0 and assuming to accept H_1 , we can believe that the linear relationship between independent variables and dependent variables is significant.

4.3 Significance Test of the Regression Coefficient of the Regression Equations

The purpose of significance test is to identify the significant linear relationship between independent variable and dependent variable by testing the significant difference between regression coefficient and 0.

t-test on regression coefficient:

Given level of significance $\alpha = 0.05$, calculate the value of the test statistic t:

$$t = \frac{\text{Estimation of regression coefficients}}{\text{The standard deviation of the regression coefficients}}$$

$$t_1 = -16.698, t_2 = -3.477.$$

$t_{\alpha/2}(n-m-1) = t_{\alpha/2}(62) = 1.999$, $|t_1| > t_{\alpha/2}(62)$, $|t_2| > t_{\alpha/2}(62)$. Reject null hypothesis, then linear relationship between independent variable and explained variable is significant which should be in the equation.

4.4 Introduce Normal Distribution Error

The result generated from the formula is obviously the ideal value. Meteorological data has only several sets of values since fixed independent value will also contribute to fixed dependent variable. In order to make the data more closed to the real value, random error of normal distribution would be introduced once the value of variable has been generated. Box-Muller is a widely used calculation method which is normally distributed. It is efficient and simple in calculating. In Box-Muller method, two evenly distributed random numbers n_1, n_2 whose value range is $(0,1)$ are required:

$$N = \sqrt{-2 \ln(n_1)} \cos(2\pi n_2).$$

Generate a normally distributed random number $N(0,1)$. A normally distributed random number whose mean value is a and standard error is sd can be obtained by doing the following transformation: $X = a + (N * sd)$.

5 Conclusion

This paper mainly focuses on the simulation method of the meteorological data. These meteorological data can be classified into discrete variable and continuous variable according to their own characteristics and respectively simulated. This paper begins by collecting and analyzing the data. Then, Markov model is introduced to generate discrete data. Finally, multiple regression model is required to analyze both generated variables and processing continuous variables. This paper provides a reliable data simulation method for the application of UAV in logistics, disaster relief, medical care.

References

1. Molina Martínez, J.M., Martínez, A.V., González-Real, M.M., Baille, A.: A simulation model for predicting hourly pan evaporation from meteorological data. *J. Hydrol.* **318**(1), 250–261 (2006)
2. Gao, Q., Liu, J., Yang, L.: Sensitivity studies on elements of meteorological data for building energy simulation in China. In: International Building Performance Simulation Association, pp. 217–222 (2007)
3. Cui, Y.J., Gao, Y.B., Ferber, V.: Simulating the water content and temperature changes in an experimental embankment using meteorological data. *Eng. Geol.* **114**(3), 456–471 (2010)
4. Brose, N.: Specification of meteorological data requirements for a wind power infeed model used in power system simulator. In: 12th International Conference on Environment and Electrical Engineering, pp. 140–144 (2013)
5. Herr, J.W., Vijayaraghavan, K., Knipping, E.: Comparison of measured and MM5 modeled meteorology data for simulating flow in a mountain watershed. *J. Am. Water Resour. Assoc.* **46**(6), 1255–1263 (2010)
6. Wang, Q., Li, S., Ding, F., Zhao, X.: Simulation of high-altitude meteorological data used to environment impact assessment by MM5 model. *Procedia Environ. Sci.* **2**, 1713–1716 (2010)
7. Edgar, S., Christoph, M., Charles, F., Michael, L.: Evaluation of modelled snow depth and snow water equivalent at three contrasting sites in Switzerland using SNOWPACK simulations driven by different meteorological data input. *Cold Reg. Sci. Technol.* **99**, 27–37 (2014)
8. Reza, A., Zhiliang, Z., Shuang, Z.: Design and simulation of a meteorological data monitoring system based on a wireless sensor. *Int. J. Online Eng.* **12**(5), 27–32 (2016)

Anti-data Mining on Group Privacy Information

Fan Yang¹, Tian Tian¹, Hong Yao¹, Xiuyu Zhao^{1(✉)},
Tinggang Zheng¹, and Min Ning²

¹ Computer School, China University of Geosciences, Wuhan 430074, China
planesail@163.com, {tiantian,yaohong}@cug.edu.cn,
2829936010@qq.com, 2289067224@qq.com

² Founder International Software (Beijing) Co., Ltd., Beijing 100080, China
ningmin@founder.com

Abstract. In the big data era, privacy preserving is a vital security challenge for data mining. Common object of privacy preserving is personal privacy, which should be kept unrevealed while data mining on group information. However, for a few sensitive groups, such as suffering from some particular disease, engaging in some special occupation or having some peculiar hobby, even if every personal data is processed for privacy preserving, group specificity can be still exposed. Therefore, we propose the concept and method of anti-data mining on group privacy information. By adding, swapping data according to our rules, the minable characteristic and group specificity of original data is destroyed and eliminated to prevent group privacy from data mining.

Keywords: Anti-data mining · Group privacy information
Privacy preserving · Group specificity

1 Introduction

The concept of “big data” has appeared in the field of physics, biology, environment ecology, finance and communication for several years. In 2011, the well-known consulting company Mckinsey predicted that “the era of big data” was coming for the first time [1]. Big data is a term for data sets that are so large or complex that traditional data processing application software is inadequate to deal with them [2]. The lifecycle of big data includes data extraction and integration, data analysis and interpretation, among which data analysis is the core [3]. Different from conventional data, big data possesses the features of “4V”, which are Volume, Velocity, Variety and Value [4]. Consequently, the common ways of data analysis aren’t suitable for big data anymore.

Data mining is defined as the procedure of extracting or excavating useful knowledge from vast data stored in database [5]. Pattern and feature contained in big data is so valuable that almost all industries, such as enterprises, telecom operators and governments, are engaged in data mining. Sometimes, science and technology is a double-edged sword. Data mining on big data brings forth both mass valuable information and huge privacy leakage risk. The data mining algorithms are bound to collect abundant users’ data for a long term to conclude the behavioral habits behind [6].

The concept of privacy preserving data mining (for short, PPDM) was firstly presented in [7] to resolve the conflict between the precise excavation of knowledge rule and the privacy protection of original information. Lindell indicated the need to protect data privacy while ensuring data accuracy [8]. Evfimeievski used randomization to establish an accurate data mining model for aggregated data [9]. In 2004, Vaidya introduced how data mining should be changed to accommodate the attacks of privacy advocates [10]. To solve the problem of constructing aggregated data without accurate data, Zhang Nan describes the related technologies such as reconstruction [11]. By 2005, Vaidya has proposed a relatively systematic idea and solution in [12], including a variety of corresponding models. Lindell focused on the decision tree algorithm, especially the ID3 algorithm [13]. Most recently, Saranya conducted extensive surveys of different PPDM algorithms and analyzed the representative technologies [14]. In addition, since PPDM is a highly integrated cross-cutting topic, there have been significant progress for PPDM in statistics, machine learning, etc. [15–17]

Common object of PPDM is personal privacy, which should be kept unrevealed while data mining on group information. But for a few sensitive groups, such as suffering from some particular disease, engaging in some special occupation or having some peculiar hobby, even if every personal data is processed for privacy preserving, group specificity can be still exposed. Group privacy refers to the private information shared inside the group, but unwilling to reveal to ones outside the group. Anti-data mining indicates destroying the minable specialty of raw data and invalidating data mining to protect the covert information contained in big data.

The rest of this paper is formed as following. Section 2 lists the technological classification of PPDM, compares existing corporate privacy and anti-data mining to ours. Section 3 explains our concrete algorithms. Section 4 conducts a series of experiments to state the validity of above algorithms. Section 5 draws a conclusion.

2 Background and Related Work

2.1 Classification of PPDM

According to the mainstream technologies of the raw data transformation, PPDM can be classified into five dimensions [18]:

- (i) Data distribution
- (ii) Data modification
- (iii) Data mining algorithms
- (iv) Data or rule hiding
- (v) Privacy preservation

The first dimension of data distribution can be classified as centralized data and distributed data scenarios [19]. Distributed data scenarios can also be divided into horizontal data distribution [20–22] and vertical data distribution [23–25]. Generally, the raw data needs to be modified before releasing to the public for privacy. The data modification of second dimension is divided into perturbation [26, 27], blocking [28], aggregation/merging, swapping [29] and sampling [30]. The third dimension refers to

the data mining algorithms, among which relatively important ones are decision tree inducers [31], association rule mining [32, 33], clustering algorithms [34], rough sets [35] and Bayesian networks [36]. The fourth dimension refers to whether raw data or aggregated data should be hidden. To achieve higher utility and protect privacy, selective modification is essential. The last dimension of privacy preservation to modify data includes heuristic-based techniques [37], cryptography-based technique [38], reconstruction-based techniques [39] and so on.

2.2 Group Privacy and Anti-data Mining

In China, a piece of news raised wide concern that 275 HIV-infected patients from 30 provinces declared the reception of fraud calls for the leak of authoritative AIDS database in July 2016 [40]. For this special group, any sensitive item revealed from the database may label members as HIV or AIDS, probably resulting in discrimination, losing job, even suicide. Even individual data is processed for privacy preservation, message from group members still carries the group specificity. Once the mass fragments are excavated and pieced together as integrated information, the group privacy will be exposed in the end. Consequently, protecting the individual privacy of group is far from enough. For this reason, we propose the protection on group privacy information.

The traditional PPDM means learning the group pattern and assuring the individual privacy secret by limited data mining [41], while our anti-data mining prevents the group specificity from data mining to protect group privacy. “Corporate privacy” mentioned in [42] protects data from distributed sources by secure multiparty computation instead of the trusted third party, while we centrally pre-process the raw data to hold back data mining on group privacy. Different from the anti-data mining in [43, 44], where noise data is added to personal information, our method is applied to group attributes.

3 Anti-data Mining on Group Privacy

3.1 Scenario Description

We present anti-data mining on group privacy to solve the dilemma from the following scenario. There are many active social networks based on common hobby, belief or anything else. For example, there exists a network community among which are all AIDS patients, meeting the social need for this special group. But this community is quite vigilant against outside for the real world still discriminates them. Existing data mining tools may collect the google searching records to find out the keyword (AIDS) of this community. Here comes the requirement that protects the common feature of this group. Our work pre-processes the searching records so that both the needs of acquiring information and protecting group privacy are met.

3.2 Method Feasibility

Group specificity distinguishes group members from other random members, implying the existing of a special group and the common privacy. Once we lessen or eliminate the specificity, the group privacy can be protected. On the premise of not obstructing the regular communication with outside, we pre-process the data issued by group memberships. The material methods are adding and swapping according to some rules so that it can't be clustered as before. At last, the transformational searching records lose their original group specificity completely. The more approximate are the results to searching records of random user, the greater effect does we get.

Our model is the agency of searching engine between group and outside Internet, preprocessing the searching requests from group individuals and returning the results back by converse progress. The preprocessing aims to convert the searching records with obvious group specificity into so random ones that data mining on such records can't get the group characteristics about AIDS. Meanwhile, the effect of information retrieval remains insusceptible, i.e., the converse process can filter the rough searching results into the interested information about AIDS for group individuals from seemingly random result pool.

3.3 Relevant Definition

Clustering is a division of data into groups of similar objects. Each group, called cluster, consists of objects that are similar between themselves and dissimilar to objects of other groups [45]. The similarity is measured by the distances between the described objects. As searching record is the main study object of our thesis, complex text clustering need calculation of nonmetric similarity function. So, we introduce Jaccard index. Given two sets, A and B, the Jaccard index is defined as the ratio of intersection and union about A and B.

Definition 1. Point of Searching Record. Point of searching record refers to the set of searching keywords that the individual of special group submits in Internet, denoted as PSR as below. There are n searching records in PSR, denoted as r_i .

$$PSR = \{r_1, r_2, \dots, r_n\} \quad (1)$$

Definition 2. Point Similarity. Point similarity of two PSRs are defined as the Jaccard index of two sets. For set A and B,

$$PS(A, B) = \frac{|A \cap B|}{|A \cup B|} = \frac{|A \cap B|}{|A| + |B| - |A \cap B|} \quad (2)$$

Definition 3. Clustering Score. Clustering score indicates the proportion of special individuals in clustering result vs the random distribution. Suppose that n is the number of target records in cluster after clustering, s is the size of result cluster, r_a is the ratio of total target record in total searching records. We use the following equation to normalize the clustering score into the interval of $[-1, 1]$.

$$CS = \begin{cases} \frac{\frac{n}{s} - r_a}{s} & \text{when } \frac{n}{s} < r_a \\ \frac{r_a}{s} & \\ \frac{\frac{n}{s} - r_a}{s} & \text{when } \frac{n}{s} \geq r_a \\ 1 - r_a & \end{cases} \quad (3)$$

Definition 4. Average Clustering Score. Average clustering score indicates the average of absolute value sum about all result clusters. Assume that there are m final clusters, then ACS is defined as below.

$$ACS = \frac{|CS_1| + |CS_2| + \dots + |CS_m|}{m} \quad (4)$$

3.4 Algorithm Description

Different to the common data mining, anti-data mining makes the result of clustering unapparent by variation process. Our method follows the general approach of data mining except the process of variation, indicating the core of group privacy preservation. By different clustering algorithms, patients of same kind tend to gather together into one or a few clusters unequally. We grade the clustering result, rank and vary it, after which it's graded again to judge whether the mixing is uniform. If not, we loop to vary and cluster again, or else output the result. In ideal condition, the target patients spread evenly in all result clusters, indicating the data mining on group privacy is invalid.

3.4.1 Clustering

We use clustering algorithm to testify the effect of anti-data mining. The distance calculation of two points is the proportion of common entries to total entries in the clustering procedure as the Jaccard index in Eq. (2). The central point is a virtual and auxiliary one containing the most frequently used entries, whose length is the average of all points inside a cluster. This parameter is used frequently in the following steps.

3.4.2 Grading

Grading refers to the hidden extent of target expressed by the uniformity degree distributed in every cluster. Based on the expectation distribution of targets in the cluster, calculate the deviation coefficient to the expectation. The calculation follows Eq. (3), where the result CS falls into the interval of $[-1,1]$. The value is closer to 1, the better the clustering effect is. The result of 1 means all records in the cluster are target. The value is closer to -1 , the worse the clustering effect is. The result of -1 means no records in the cluster are target. But for anti-data mining, the perfect result is 0, meaning final target after clustering approximates to the random distribution.

3.4.3 Variation

Before variation, rank the clusters in descending order according to the above grades. The variation consists of two situations: adding and swapping. In the former adding, match a pair clusters of the correspondent high and low grades every time. Then, randomly select a keyword of central point from the other to add into one of its own real records. If the keyword number of the added record is more than the maximum allowable value, then replace the newly added one. By adding uncorrelated noise to change the clustering characteristics of original records, the records belonging to one or a few clusters intensively can be randomly scattered into clusters as many as possible. In the latter swapping, exchange a keyword pair from two neighboring clusters every time, where the two keywords both come from the central point sets of each cluster. By reducing the occurrence of high-frequency words, the clustering results can be altered.

4 Experiments

4.1 Construction of Experimental Data

At the beginning, two dictionaries are built artificially. One includes 100 entries about AIDS keywords, such as HIV, homosexuality, incubation period, sex and so on, named as target dictionary. The other includes 400 entries selected from everyday vocabulary randomly, named as common dictionary. Next, we should construct ten original clusters, where the first cluster is all about AIDS and the other nine are non-AIDS. The AIDS cluster contains 1000 records, where each record consists of one to twenty entries picked from the target dictionary. Other nine original clusters are built as above from the common dictionary.

4.2 Disposal of Anti Data Mining

Using k-means algorithm on 10000 records from above ten original clusters, in which k ($k = 5$) indicates the number of result clusters.

Table 1. Clustering condition before variation (adding only).

Generation	Cluster 1	Cluster 2	Cluster 3	Cluster 4	Cluster 5	ACS
0	4806/308	693/0	2612/0	1197/0	692/692	0.871827
0	5396/332	2915/0	680/0	341/0	668/668	0.8769458
0	4707/310	2615/0	306/0	1682/0	690/690	0.8682812
0	5033/1000	1043/0	1978/0	623/0	1323/0	0.8219308
0	4795/326	2043/0	1519/0	969/0	674/674	0.864025
0	4867/1000	2777/0	387/0	682/0	1287/0	0.8234368
0	5850/1000	509/0	327/0	2228/0	1086/0	0.8157644
0	5120/1000	2328/0	1582/0	301/0	669/0	0.8211806

In Experiment 1, we gather statistics of running generation, target distribution in 5 result clusters and Average Clustering Score on eight independent tests, given the ending

condition of $ACS \leq 0.1$. In this experiment, we test our method on two variation ways: adding only vs both adding and swapping. Tables 1 and 2 list the clustering conditions before and after variation (adding only). Figures 1 and 2 illustrate the target distributions in clusters before and after variation (adding only).

Table 2. Clustering condition after variation (adding only).

Generation	Cluster 1	Cluster 2	Cluster 3	Cluster 4	Cluster 5	ACS
7	2517/265	1749/175	2771/315	1401/105	1562/140	0.075076
3	2986/318	1297/100	2770/287	1569/143	1378/152	0.0680522
5	4252/446	1256/118	2479/269	1489/113	524/54	0.0639792
5	3069/334	3038/320	1918/173	1088/101	887/72	0.0747442
5	3414/378	2009/209	1387/142	405/26	2785/245	0.0994694
6	2833/287	2239/105	1277/112	1163/93	2488/303	0.0866714
5	4045/459	2507/243	821/68	1848/157	779/73	0.086152
6	4027/347	2825/274	1592/184	780/101	776/94	0.0483918

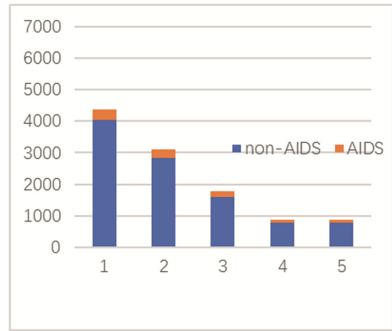
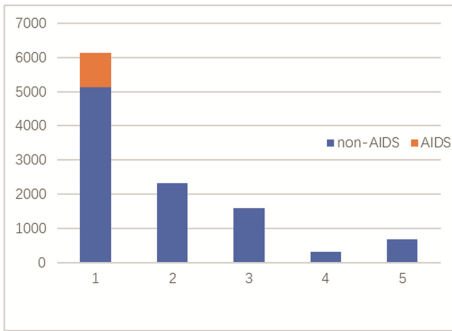


Fig. 1. Distribution of target before variation **Fig. 2.** Distribution of target after variation

Comparing Tables 1 and 2, before variation, the clustering gathers the target records into one or two clusters intensively and the ACS approximates 0.9 indicating the distribution is uneven. After variation, every cluster has target records and the ACS approximates 0.1. As our experimental data includes 1000 target records and 9000 normal records, 0.1 implies so random distribution that data mining is without effect on group privacy. We choose the data of last line in Tables 1 and 2, showing the distributions in histograms of Figs. 1 and 2. From these two figures, we find before variation, the sizes between clusters are quite different. While after variation, every cluster is more similar in scale than before and the target records have uniform distributions.

Table 3 lists the clustering condition after variation (both adding and swapping). For this variation includes adding and swapping, the effect is more obvious than Table 2 in that the ACS and running generations are less. In particular, adding only is suitable for the relative centralization of target data in early variation, while adding and swapping is appropriate for the relative uniformity of target data in late variation.

Table 3. Clustering conditions after variation (Adding and Swapping).

Generation	Cluster 1	Cluster 2	Cluster 3	Cluster 4	Cluster 5	ACS
3	3548/365	567/48	3270/346	1019/94	1596/147	0.0639128
5	2764/251	2239/207	3458/382	1003/118	536/42	0.0830066
6	4099/392	826/95	2046/206	1531/192	1498/115	0.0643302
5	2053/195	2436/241	3241/379	1178/99	1092/86	0.0903424
6	2402/238	2268/232	2507/286	1927/167	896/77	0.060269
3	2684/307	2355/261	1618/130	2290/206	1053/96	0.082661
4	2773/289	2129/187	2370/212	1608/190	1120/122	0.0523848
5	3432/391	2837/294	1499/153	1341/73	891/89	0.095712

In Experiment 2, we gather statistics of running generation, target distribution in 5 result clusters and Average Clustering Score on eight independent tests, given the ending condition of running generation = 10. In this experiment, we test our method on two variation ways: adding only vs both adding and swapping. Table 4 lists the ACS of adding only vs adding and swapping. Comparing the two columns, we can find adding and swapping is better than adding only for ACS is much less in average.

Table 4. ACS of adding only vs adding and swapping (generation = 10).

ACS (adding only)	ACS (adding and swapping)
0.118620	0.071738
0.176082	0.058726
0.062426	0.084542
0.115515	0.028413
0.070112	0.102586
0.057862	0.052701
0.628860	0.107852
0.132182	0.055899

Figure 3 illustrates the two scatter diagrams of Experiment 1 and 2. According to the two variables: running generation (x-axis) and ACS (y-axis), we get two curves of linear regression. In common, two experiments fit a power function with a negative exponent. In early variation, y decreases rapidly with the increase of x and the rate of decrease slows down continually later. In comparison, the tendency of decline tends to be gentle when generation >=5 for adding only, while the generation threshold is 4 for adding and swapping. Given the same running generation, adding and swapping gains smaller ACS. The derivative is larger than adding only proving the blue curve decline to nearly horizontal more quickly than the red one. In conclusion, adding and swapping is better than adding only in variation effect.

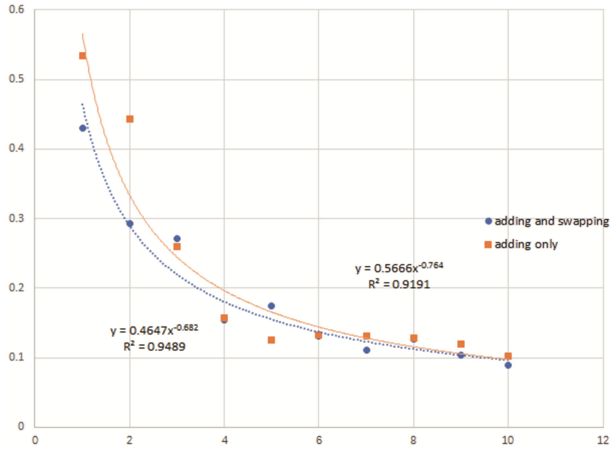


Fig. 3. Scatter diagrams of Experiment 1 and 2

5 Conclusion

This paper puts forward the concept and realization of anti-data mining on group privacy information. Transforming the clustering process by adding and swapping, the group specificity is altered and the data mining becomes ineffective. The validity of our idea is testified by a series of experiments.

In the era of big data, anti-data mining is of practical significance for privacy preserving and data security. We will research further on this theme in the near future.

Acknowledgement. The project was supported by the National Natural Science Foundation of China under Grant 61502440 and the Open Research Project of The Hubei Key Laboratory of Intelligent Geo-Information Processing under Grant KLIIGIP1610.

References

1. Brown, B., Chui, M., Manyika, J.: Are you ready for the era of “big data”? <http://www.mckinsey.com/business-functions/strategy-and-corporate-finance/our-insights/are-you-ready-for-the-era-of-big-data>
2. https://en.wikipedia.org/wiki/Big_data
3. Meng, X., Ci, X.: Big data management: concepts, techniques and challenges. *J. Comput. Res. Dev.* **50**(1), 146–169 (2013)
4. Mauro, A.D., Greco, M., Grimaldi, M.: A formal definition of big data based on its essential features. *Libr. Rev.* **65**(3), 122–135 (2016)
5. Han, J., Kamber, M.: *Data Mining: Concepts and Techniques*, 2nd edn. Morgan Kaufmann Publishers, San Francisco (2006)
6. Zetlin, M.: *The Latest Privacy Invasion: Retailer Tracking* (2012)
7. Agrawal, R., Srikant, R.: Privacy preserving data mining. In: *Proceedings of SIGMOD 2000*, New York, pp. 439–450. ACM (2000)

8. Lindell, P.: Privacy preserving data mining. *J. Cryptol.* **15**(3), 177–206 (2002)
9. Evfimievski, A., Gehrke, J., Srikant, R.: Limiting privacy breaches in privacy preserving data mining. In: PODS, pp. 211–222 (2004)
10. Vaidya, J., Clifton, C.: Privacy-preserving data mining: why, how, and when. *IEEE Secur. Priv. Mag.* **2**(6), 19–27 (2004)
11. Zhang, N.: Privacy-preserving data mining. Texas A&M University, pp. 439–450 (2006)
12. Vaidya, J., Zhu, Y.M., Clifton, C.W.: *Privacy Preserving Data Mining. Advances in Information Security.* Springer, New York (2005)
13. Lindell, P.: *Privacy Preserving Data Mining.* Springer, New York (2006)
14. Saranya, K., Premalatha, K., Rajasekar, S.S.: A survey on privacy preserving data mining. In: *International Conference on Electronics and Communication Systems*, pp. 1740–1744. IEEE (2015)
15. Aggarwal, C.C., Yu, P.S.: A general survey of privacy-preserving data mining models and algorithms. In: Aggarwal, C.C., Yu, P.S. (eds.) *Privacy-Preserving Data Mining. ADBS*, vol. 34, pp. 11–52. Springer, Boston (2008). https://doi.org/10.1007/978-0-387-70992-5_2
16. Matwin, S.: Privacy-preserving data mining techniques: survey and challenges. In: Custers, B., Calders, T., Schermer, B., Zarsky, T. (eds.) *Discrimination and Privacy in the Information Society. SAPERE*, vol. 3, pp. 209–221. Springer, Heidelberg (2013). https://doi.org/10.1007/978-3-642-30487-3_11
17. Xu, L., Jiang, C., Wang, J., et al.: Information security in big data: privacy and data mining. *Access IEEE* **2**, 1149–1176 (2014)
18. Verykios, V.S., Bertino, E., Fovino, I.N., et al.: State-of-the-art in privacy preserving data mining. *ACM Sigmod Rec.* **33**(1), 50–57 (2004)
19. Li, F., Ma, J., Li, J.H.: Distributed anonymous data perturbation method for privacy-preserving data mining. *J. Zhejiang Univ. Sci. A* **10**(7), 952–963 (2009)
20. Kantarcioglu, M., Clifton, C.: Privacy-preserving distributed mining of association rules on horizontally partitioned data. *IEEE Trans. Knowl. Data Eng.* **16**(9), 1026–1037 (2004)
21. Inan, A., Sayg, Y., Savas, E., et al.: Privacy preserving clustering on horizontally partitioned data. *Data Knowl. Eng.* **63**(3), 646–666 (2007)
22. Ouda, M.A., Salem, S.A., Ali, I.A., et al.: Privacy-preserving data mining (PPDM) method for horizontally partitioned data. *Int. J. Comput. Sci.* **9**(5) (2012)
23. Dwork, C., Nissim, K.: Privacy-preserving datamining on vertically partitioned databases. In: Franklin, M. (ed.) *CRYPTO 2004. LNCS*, vol. 3152, pp. 528–544. Springer, Heidelberg (2004). https://doi.org/10.1007/978-3-540-28628-8_32
24. Muthulakshmi, N.V., Sandhya Rani, K.: Privacy preserving association rule mining in vertically partitioned databases. *Int. J. Comput. Appl.* **39**(13), 29–35 (2012)
25. Malik, M.B., Ghazi, M.A., Ali, R.: Privacy preserving data mining techniques: current scenario and future prospects. In: *Third International Conference on Computer and Communication Technology*, pp. 26–32. IEEE Computer Society (2012)
26. Liu, K., Kargupta, H., Ryan, J.: Random projection-based multiplicative data perturbation for privacy preserving distributed data mining. *IEEE Trans. Knowl. Data Eng.* **18**(1), 92–106 (2006)
27. Kargupta, H., Datta, S., Wang, Q., et al.: On the privacy preserving properties of random data perturbation techniques. In: *IEEE International Conference on Data Mining*, p. 99. IEEE Computer Society (2003)
28. Sugumar, R., Jayakumar, C., Rengarajan, A.: An efficient blocking algorithm for privacy preserving data mining. *J. Comput.* (2011)

29. Fienberg, S.E., McIntyre, J.: Data swapping: variations on a theme by Dalenius and Reiss. In: Domingo-Ferrer, J., Torra, V. (eds.) PSD 2004. LNCS, vol. 3050, pp. 14–29. Springer, Heidelberg (2004). https://doi.org/10.1007/978-3-540-25955-8_2
30. Li, G., Wang, Y.: Privacy-preserving data mining based on sample selection and singular value decomposition. In: International Conference on Internet Computing & Information Services, pp. 298–301. IEEE (2011)
31. Fang, W.W., Yang, B.R., Yang, J., et al.: Decision-tree model research based on privacy-preserving. *Pattern Recogn. Artif. Intell.* **23**(6), 776–780 (2010)
32. Oliveira, S.R.M., Zaiane, O.R., Saygin, Y.: Secure association rule sharing. In: Dai, H., Srikant, R., Zhang, C. (eds.) PAKDD 2004. LNCS (LNAI), vol. 3056, pp. 74–85. Springer, Heidelberg (2004). https://doi.org/10.1007/978-3-540-24775-3_10
33. Agrawal, R., Srikant, R.: Fast algorithms for mining association rules in large databases. In: International Conference on Very Large Data Bases, pp. 487–499. Morgan Kaufmann Publishers Inc. (2000)
34. Kumar, P., Varma, K.I., Sureka, A.: Fuzzy based clustering algorithm for privacy preserving data mining. *Int. J. Bus. Inf. Syst.* **7**(1), 27–40 (2011)
35. Pawlak, Z.: *Rough Sets: Theoretical Aspects of Reasoning about Data*. Kluwer Academic Publishers, Dordrecht (1991). <https://doi.org/10.1007/978-94-011-3534-4>
36. Iqbal, K., Asghar, S., Fong, S.: A PPDM model using Bayesian Network for hiding sensitive XML Association Rules. In: IEEE International Conference on Digital Information Management, ICDIM 2011, Melbourne, Australia, September, pp. 30–35. DBLP (2011)
37. Ferguson, D., Likhachev, M., Stentz, A.: A guide to heuristic-based path planning. *Comput. Knowl. Technol.* (2005)
38. Pinkas, B.: Cryptographic techniques for privacy-preserving data mining. *ACM Sigkdd Explor. Newsl.* **4**(2), 12–19 (2002)
39. Agrawal, R., Srikant, R.: *Privacy-Preserving Data Mining. Foundations and Advances in Data Mining*, pp. 36–54. Springer, Berlin Heidelberg (2005)
40. <http://news.china.com/domestic/945/20160718/23079010.html>. [DB/OL]
41. Fang, B., Jia, Y., Aiping, L.I., et al.: Privacy preservation in big data: a survey. *Big Data Res.* (2016)
42. Brugger, S.T., Kelley, M., Sumikawa, K., et al.: Defining privacy for data mining. In: National Science Foundation Workshop on Next Generation Data Mining, pp. 126–133 (2002)
43. Chen, T.S., Chen, J., Kao, Y.H., et al.: A novel anti-data mining technique based on hierarchical anti-clustering (HAC). In: Eighth International Conference on Intelligent Systems Design and Applications, pp. 426–430. IEEE Computer Society (2008)
44. Chen, T.S., Chen, J., Kao, Y.H.: A novel hybrid protection technique of privacy-preserving data mining and anti-data mining. *Inf. Technol. J.* **9**(3), 500–505 (2010)
45. Berkhin, P.: A survey of clustering data mining techniques. *Grouping Multidimension. Data* **43**(1), 25–71 (2006)

Big Data Analysis of Reviews on E-commerce Based on Hadoop

Qiaohong Zu^(✉) and Jiangming Wu^(✉)

School of Logistics Engineering, Wuhan University of Technology,
Wuhan 430063, People's Republic of China
zuqiaohong@foxmail.com, 1752398990@qq.com

Abstract. With the increasing popularity of online shopping, it has brought with its massive online consumers and the growth of merchandise information data. In order to deal with the demand for big data processing, building an analysis system of e-commerce reviews base on Hadoop software framework. The reviews of Internet commodity are chosen to be the samples of study. Choosing Navie Bayesian classification to analyze the attributed values are discrete. The classification algorithms in accordance with MapReduce parallel computing theory designed and run on Hadoop platform. Constructing the Naive Bayesian sentiment classifier, and make the classifiers on the Hadoop platform to achieve commodity reviews mining job. Result shows that it can improve the efficiency of the commodity reviews analysis by using the Hadoop distributed platform.

Keywords: Hadoop · MapReduce · Big data · Emotion tendency

1 Introduction

According to *Chinese Online Shopping Market Research Report in 2015* [1], which CNNIC published in 2016, China's online sales continue to maintain the high growth rate. With online shopping becoming more and more popular, it has also brought the explosion of commodity review texts, produced huge amounts of data information, so the demand for the analysis of the Internet commodity reviews is higher efficiency. For automatic text sentiment analysis, traditional single machine has some limitations. This project takes advantages of the MapReduce programming model of distributed computing, based on Hadoop, compared with single machine, it has more CPU kernel number and bigger RAMs. Under the lots of data reviews text information, with Hadoop distributed computing framework in the review of text information has important significance.

2 Analysis of Review Texts and the Research of Hadoop

2.1 Analysis of Review Texts

The text emotion analysis is also called opinion mining, it refers to the machine learning, statistics, natural language processing and other techniques to automatically extract,

define or describe a content containing emotional information, achieves to make classification judgments of the emotional tendencies of overall text or of some subjective [2, 3]. In order to judge the emotional tendencies of the reviews. Naive Bayesian is chosen to be classification method. Naive Bayesian classification model has the following advantages: (1) algorithm theory is simple, high accuracy; (2) classification time is shorter; (3) support for different kinds of data types, the algorithm is more stable.

Bayesian theorem is actually applied as follows, suppose a purchase experiment E , X is a description of N attributes value of a customer, such as age, gender, annual income and other statistical values, H represents the purchase hypothesis, $H = 0$ means the purchase, $H = 1$ means no purchase. Which $P(H | X)$ represents the probability that H occurs when condition X is known, and $P(H | X)$ is the posterior probability. $P(H)$ is the probability of occurrence of event and $P(X)$ is the probability of occurrence of event X , they are called the prior probability (unconditional probability) and $P(X | H)$. The three probability values can be obtained from the historical data, the probability of user purchasing a product need to be predicted, i.e. the probability of event $P(H | X)$. According to the Bayesian theorem, the equation is available.

$$P(H | X) = \frac{P(X | H)P(H)}{P(X)} \quad (1)$$

The above pilot knowledge can be used to illustrate a simple Bayesian classification problem. Here is a training set of samples D , where each row of data represents a training tuple and the tuple class attribute value label, each tuple with an n -dimensional attribute vector represents $X = \{a_1, a_2, \dots, a_{n-1}, a_n\}$, $\{a_1, a_2, \dots, a_{n-1}, a_n\}$ represents the measured value of $A_1, A_2, \dots, A_{n-1}, A_n$ corresponding to the n characteristic attributes. Also assume there are m class variables $C_1, C_2, \dots, C_{m-1}, C_m$.

Assuming tuple vector X is known, classifier needs to predict class C_i of X belongs to, in fact, obtain the maximum posteriori probability of $P(C_i | X)$ and classification prediction result for test set X can be obtained from Eq. (2). It is the value of C_i when $P(C_i | X)P(C_i)$ get the maximum value

$$class(X) = \arg \max \{P(X | C_i)P(C_i)\} = \arg \max \left\{ P(C_i) \prod_{k=1}^n P(x_k | C_i) \right\} \quad (2)$$

2.2 Research of Hadoop

Hadoop distributed software framework is designed to solve the problem of large data computing, through distributed data storage and distributed computing. Therefore, Hadoop's basic platform is the core structure of HDFS distributed storage system and the distributed data processing model and execution environment of MapReduce [4].

HDFS can automatically divide large files into many parts, and then upload these parts to the computer node of the same Hadoop cluster. Users only need to log in to the HDFS root directory to view all the shared files in the system, rather than knowing which

computer is the part of the file belong to. At the same time large-scale file block storage is the base of achieve mass data parallel computing. HDFS distributed file system has the advantages of detecting data node failure, setting file copy, high availability and low operating costs and so on. MapReduce parallel computing model needs to implement Map and Reduce two functions, with the way of “divide and rule” to achieve the idea of distributed parallel computing [5]. Map function part of the MapReduce calculation program is mapped to the part of the data stored on the machine to calculate the Reduce function phase based on the actual data situation. Reduce function phase based on the actual data situation, generate a number of Reduce tasks on the Map phase of the data protocol, processing.

3 Design and Development of Review Texts Analysis System

3.1 Architecture Design of Review Texts Analysis System

In this study, a analysis system of e-commerce review texts is designed, under distributed storage of Hadoop platform and framework of parallel computing, which is based on the needs of businessmen’s automatic acquisition of product reviews, secure storage and emotional analysis. Based on the B/S architecture WEB management system, the system is divided into Hadoop distributed cluster product review data analysis module, data storage module and data display module.

Data analysis module is the core module of the whole system. Its main job is divided into three parts: first part is preprocessing and distributed storage the date of the product sales and review. Second part is the implementation of Mapreduce parallel computing framework analysis mining commodity review data information, the processed data transferred to the database server. Third part is the data migration work. Soop is chosen to be the cross-platform data migration tool, it is good at dealing with transporting the data of HDFS distributed storage system to the database server.

3.2 Design of Review Texts Analysis

According to the design requirements of analysis system of e-commerce reviews, emotional tendency classifier based on Naive Bayesian classification algorithm is realized under Hadoop platform. The system architecture of the naive Bayesian affective classifier is shown in Fig. 1, which includes classifier a learning stage and a classification stage.

According to different kinds of products, reviews of the commodity may show a big difference. Therefore, combining the corpus to build the product ontology library for the corresponding product.

3.2.1 Construction of Review Texts’ Lexicon

Major brands of chocolate is selected as the object of research, chocolate brands contains Dove, Ferrero and so on. The corresponding product page of the product reviews are randomly selected to analyze, based on frequency of the word frequency statistics,

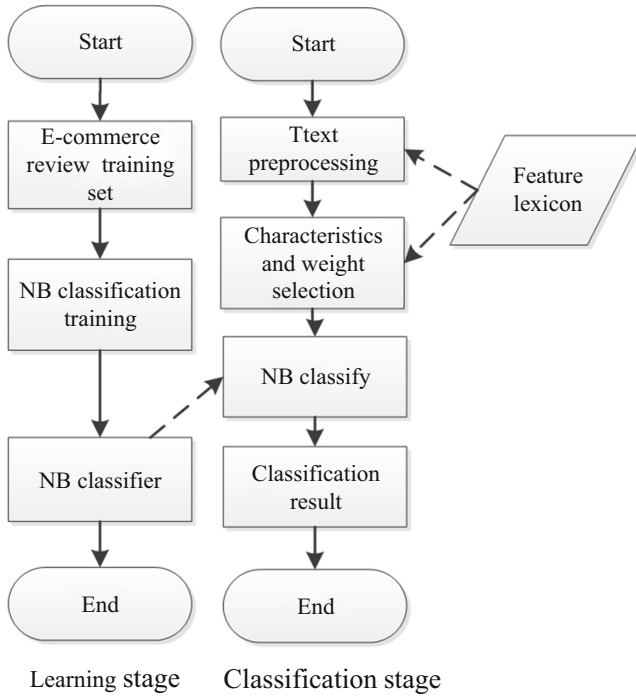


Fig. 1. System architecture of the naive Bayesian affective classifier

according to analytic hierarchy process to determine the weight of the Review elements, constructing review elements and weight table, the results are shown in Table 1.

Table 1. Review elements and weight table

Review elements	Weighted value (N)
Product	9
Price	8
Logistics	7
Public praise	6
Pack	5
Promotion	4
Other	3

At the same time, it has been observed that there are many elements of reviews are not directly described, but are described by other words, taking into account the lack of elements. Therefore, it is necessary to establish a classification table for the review elements, which can be classified into the corresponding review elements when matching the words of the classification table. Table 2 shows the review elements.

Table 2. Review element classification table

Review elements	Related words
Product	Product, taste, taste, delicious, Ø
Price	Cheap, affordable, cost-effective, expensive
Logistics	Speed, express
Public praise	Genuine, fake, come again, just so so
Pack	Packaging, grade, exquisite
Promotion	Promotions, discount
Other	Attitude, service, reply

According to the review element words contained in each review text, the weights of the review elements are calculated according to the weight table of the review factor words. The calculation is shown in Eq. 3:

$$P_i = \frac{N_i}{\sum_{i=1}^n N_i} \tag{3}$$

In Eq. 3, N_i represents the weight setting of the i -th review element in the review, $\sum_{i=1}^n N_i$ represents the sum of the weight values of all the review elements analyzed in the review, and P_i is the weight proportion that represents the i -th review element in the review of this process.

The effective factors in the review mainly include emotional words, negative words and turning words. Combined with *Chinese Emotional Vocabulary Ontology Library* [6], according to the review to improve the emotional word annotation, it is shown in Table 3.

Table 3. Emotional poles vocabulary table

Emotion tendency	Words	Marking
Neutral	In general, okay, gray	0
Commendatory	Good, like, authentic, beautiful	1
Derogatory	Garbage, silent, bad, poor	2

In judging the emotional tendencies of the review document, it is often determined not only by the emotional polarity category of the emotional vocabulary in the text, but rather by the common use of the words used in the emotional vocabulary [7, 8]. So negative vocabulary is shown in Table 4. Turning vocabulary marked as Table 5.

Table 4. Negative vocabulary table

Whether it contain negative words?	Vocabulary	Marking
Yes	No, not, inferior to, incompatible, will not	1
No	∅	0

Table 5. Turning vocabulary table

Whether it contains a turning words?	Vocabulary	Marking
Yes	But, well, however, but, yet, still, just	1
No	∅	0

In a commodity review sentence, although all the review elements are not evaluated, there are often include two or more concerns, positive or negative. If all for the same emotional tendencies, the emotional polarity of the sentence is easy to judge. But if there are two kinds of emotional tendencies, the general approach is to take a simple weighting approach to evaluate the weight of the elements, but this approach tends to have an erroneous effect on the results [9]. Therefore, during the emotional analysis of weighted calculation, a turning word before the review element, the weight of the previous clause can be weaken or strengthen the weight of themselves. When there are three or more review elements, the weakening of the previous term will increase the number of calculations, combined with Table 1 to evaluate the elements of the word and the weight table, using Eq. 4 to calculate the influence of the turning point on the weighting elements of the review element.

$$\left\{ \begin{array}{l} P_i = \frac{N_i}{\sum_{i=1}^n N_i} (1 + \theta) \\ \theta = 1 - \frac{N_i}{\sum_{i=1}^n N_i} \end{array} \right. \quad \theta \in (0, 1) \quad (4)$$

3.2.2 Naive Bayesian Classification

It can be known that the Naive Bayesian classification algorithm only needs to calculate the maximum value of $P(X | C_i)P(C_i)$ for the text emotion classification, from the Eq. 2, and can predict the emotional tendency of the data to be classified. The classified tuples data is called X and the attribute value of X is obtained by text preprocessing, feature and weight selection, $P(C_i)$ is called the prior probability of class C_i , and $P(X | C_i)$ is called the probability of vector X under class C_i . The probability values of $P(C_i)$ and

$P(X | C_i)$ are unknown, the prior probabilities of class C_i , which can be obtained from training set data, Naive Bayesian algorithm is to calculate the prior probability and conditional probability value, Fig. 2 shows the algorithm flow.

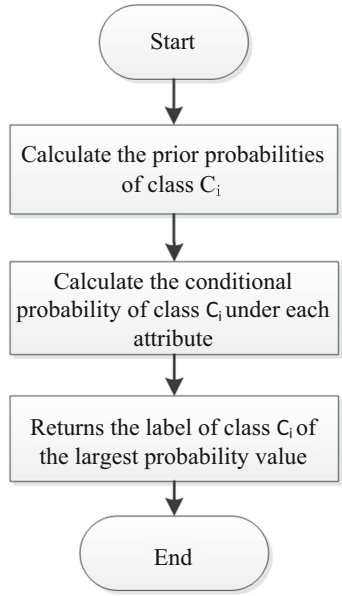


Fig. 2. Bayesian classification algorithm flow

After calculating the priori probability, calculating probability $P(X | C_i)$ of the tuple data X in class C_i . It can be known that the attributes of X are independent of each other, from the Naive Bayesian assumption, and $P(X | C_i)$ is obtained by multiplying the conditional probability of each attribute value under class C_i .

According to different types of reviews, using the algorithm to deal with, various categories of $P(X | C_i)$ probability value can be obtained. By comparing the size of $P(X | C_i)P(C_i)$, it can predicted the label of current data tuple X class. When a review text has multiple review elements, the emotional tendency of whole sentence can be determined by comparing $P(X | C_i)P(C_i) * w_i$ (w_i represents the weight value) with the weighted value.

3.3 MapReduce Parallel Computing Module

MapReduce parallel computing module is that the calculation of the classification stage is integrated into the Hadoop platform, to achieve the emotional classification of parallel processing. In general among the Hadoop clusters in MapReduce parallel computing, Map phase is responsible for the main data processing work, Reduce phase is primarily responsible for data protocol operations, such as statistical operations, maximum fetched

operation. And training set of naive Bayesian emotional classifier construction stage is artificially annotated, and the amount of data is not large. The massive training set of data may also cause over-fitting problems. So the structure of classifier and classification stage are processed in the Map phase, classified statistic results is processed by the Reduce phase. The MapReduce parallel computing flow is shown in Fig. 3.

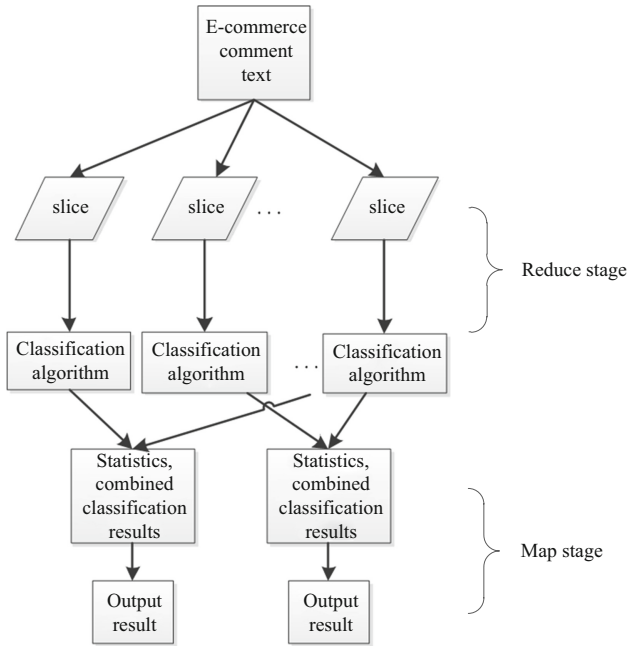


Fig. 3. MapReduce parallel computing flow

4 Achievement of Review Texts Analysis System Based on Hadoop

4.1 Achievement and Test of Review Texts Analysis System

4.1.1 Data Selection and Evaluation Standard of Experiment

Hadoop distributed cluster has a total of six servers, and these six servers to run as virtual machines build on the two desktop computers through VMware software.

The experimental data set is a commodity review text of the chocolate brands that is collected on different platforms. Training set and test set are constructed by artificial annotation method. Before the data is marked out, the effective data is selected, and the data set is marked according to the lexical ontology database which has been constructed. Finally, Constructed one hundred compliment comments, fifty derogatory comments, thirty neutral comment data sets, according to 1:1 ratio of ninety assigned to the training set and test set.

In the review of the effectiveness of the classification of commodity reviews, the following review indicators are often used: the precision is recorded as P ; the recall rate is denoted by R ; the calculation of the next two indicators is described below (Table 6).

Table 6. Product review test set classification example table

Category	The number of reviews of “good reviews”	The number of reviews of “bad reviews”
The number of reviews judged to be “good reviews”	a	b
The number of reviews judged to be “bad reviews”	c	d

The precision ratio P is the proportion of the correct value of the classification a in the classification result a and b . Then the precision P calculation equation as shown in Eq. 5:

$$P = \frac{a}{a + b} \tag{5}$$

The recall rate R is the correct value of the classification a in the test set attributable to “praise” the proportion of a and c . The recall rate R is calculated as shown in Eq. 6:

$$R = \frac{a}{a + c} \tag{6}$$

4.1.2 Design and Result Analysis of Experiment

In order to verify the classification accuracy of the emotion classifier and the classification efficiency under the Hadoop platform, following experiment was designed: ninety test data was chosen to be the study object, the emotion classification of ninety test set data was analyzed, verify the accuracy of classification analysis. The experiment runs the program on the Hadoop platform to classify the review texts test set data. The result of experimental classification result is shown in Fig. 4.

0006	e0003	2015-06-08	00005	t0001	6	0	0
0006	e0003	2015-06-08	00006	t0001	18	0	0
0006	e0003	2015-06-08	00007	t0001	12	0	0
0006	e0003	2015-06-08	00010	t0001	36	0	0

Fig. 4. Result of experimental emotional classification results

Figure 4, from left to right are the product brand code, electricity business platform coding, date, review category code, commodity category code, and the statistics of commodity, medium and bad reviews. The recall rate P of the experiment is zero point eight six two and the recall rate R is zero point eight eight. The experimental results

show that the accuracy rate of the classifier is more than eighty-five percent, which means the system is good at predicting the emotional tendency of the review texts.

After analyzing the output result, it is found that the classification result is more accurate when the review text has only one review factor or only include emotional word. When the review text has multiple review factors, the classification result is prone to appear classification error, which leads to the decrease of classification accuracy.

5 Conclusion

Under the background of online shopping normalization and big data age, the e-commerce reviews are chosen to be the object of study, to analyze the review texts features, and designs the system of information retrieval based on Hadoop data processing technology. Extraction, analysis of additional business information from a large number of unstructured reviews text data, providing the important reference basis for merchants to adjust production and sales strategy. Although the work of the corresponding research is completed, getting a better analysis of the results, but there are some deficiencies, following aspects need to be improved:

- (1) Only the naive Bayesian classification algorithm is adopted. Although it is better to classify the commodity in the text, it can not get all the attribute characteristics of the text when it is large.
- (2) Hadoop platform is good at dealing with massive data, due to limited hardware, only in the virtual machine to achieve a real cluster structures, its efficiency in large-scale data can not be effectively tested.

Acknowledgment. This paper was supported by the project in the Hubei Science and Technology Pillar Program (No. 2015BKA222).

References

1. CNNIC. Chinese Online Shopping Market Research Report of 2015 [EB/OL] (2016). http://www.cnnic.net.cn/hlwfzyj/hlwzxbg/dzswbg/201606/t20160622_54248.htm
2. Liu, B.: Sentiment Analysis and Opinion Mining. Synthesis Lectures on Human Language Technologies, vol. 5, no. 1, pp. 1–167 (2012)
3. Mao, C., Hu, B., Wang, M., Moore, P.: Learning from neighborhood for classification with local distribution characteristics. In: 2015 International Joint Conference on Neural Networks (IJCNN), pp. 1–8. IEEE, July 2015
4. Welcome to Apache Hadoop! [EB/OL] (2015). www.hadoop.apache.org
5. Dittrich, J., Quiané-Ruiz, J.A.: Efficient big data processing in Hadoop MapReduce. Proc. VLDB Endowment **5**(12), 2014–2015 (2012)
6. Xu, L., Lin, F., Yu, P., et al.: The structure of emotional vocabulary ontology. J. Intell. **27**(2), 180–185 (2008)
7. Zhao, P., Zhao, H., Tao, X., et al.: Based on the semantic model of TriPos Chinese subjective and objective analysis method. Res. Comput. Appl. **29**(9), 3285–3288 (2012)

8. Chen, J., Hu, B., Moore, P., Zhang, X., Ma, X.: Electroencephalogram-based emotion assessment system using ontology and data mining techniques. *Appl. Soft Comput.* **30**, 663–674 (2015)
9. Xie, S., Liu, B., Wang, T.: Apply the semantic relation to construct the emotional dictionary automatically. *J. Natl. Univ. Defense Technol.* **36**(3), 111–115 (2014)

Analysis on Structural Vulnerability Under the Asymmetric Information

Mingshu He^{1,2(✉)}, Xiaojuan Wang^{1,2}, Jingwen You^{1,2}, and Zhen Wang^{1,2}

¹ Electronic Engineering Institute, Beijing University of Posts and Telecommunications,
Beijing 100876, China
hms_bupt@163.com

² Electronic Engineering Institute of PLA, Heifei 230000, China

Abstract. Network attack can invalidate the connectivity of the resource network topology composed of routers, switches and other resources. This type of structural vulnerability which is caused by increasing scale of nodes in the network is a hotspot of current researches. In order to integrate the random attack and the targeted attack, we proposed an asymmetric information attack model which is closer to reality. In this attack model, we use the attack range and the node detection degree to adjust the attack mode and these two parameters extend the attack mode more than the random attack and the targeted attack. In this paper, we apply our attack model to attack BA network, ER network and Router network under different parameters. Then we find the random attack is better than other attack modes with nonzero node detection degree in ER network. And BA network is fragile to nonzero node detection degree attack mode. In addition, we also notice that although the distribution of Router network and BA network both satisfy the power law distribution, they show different structural vulnerability. The random attack has a better effect than the asymmetric information attack with nonzero node detection degree and attack range. Router network has the same structural vulnerability with ER network, which means Router network also has randomness.

Keywords: Structural vulnerability · Asymmetric information
Random attack · Targeted attacks

1 Introduction

With the rapid development of the information society, some information systems such as the distributed network equipment, computers, databases and the application software has attracted particular interests, they have higher resources sharing speed and stronger coordinated ability but meanwhile the structure may be complex. To analyze the influence of resources topology to communication, we need to detect the basic network topology. We are capable of sending data packets to any place through a computer terminal. By changing the survival time of the data packet we can find IP of routers. This process can be realized by the computer tool “Traceroute” [1]. Then we can use this tool to combine up a great deal of node’s routing tracking paths to detect the whole

network topology [2]. In addition, we can refer to the routing list information stored in routers to complete the whole network topology. The so-called routing list information is the connected relationship with other routing in the network. Rather than studying the routing of the network, we would like to pay more attention to the connectivity and other properties of the network. The present researches on the complex information system mostly concentrated on the connectivity of the network.

In an ideal world, network topology is connected. Meanwhile the number of network attack rises, such as Trojan, botnets, computer viruses, worms, denial of service attacks, web page tampering, domain name hijacking and so on. These can lead to nodes or links failed. Single node or link which is removed from the network can cause damage to the original connected network and result in communication failure. The robust of the network is that the network still has strong connectivity after deleting several nodes or links. On the contrary, if the network is no longer connected due to the emergence of a large number of isolated nodes, we consider the network to be vulnerable. The vulnerability caused by the change of network topology is called the structural vulnerability. Considering that the influence of the failure of nodes and links to the network is equal, in this paper, we just talk about the failure of nodes. There are two main types of existing way of attack: Random attack [3, 4] and Targeted attack [5, 6]. Random attack randomly selects the nodes in the network to attack and this attack way has strong randomness. Targeted attack is ranging the nodes in network by the nodes centrality and select the most important nodes to delete. Many researches [7–9] compared two attack methods but they did not point out the relationship between them. We think that these two attack forms can use a common attack model to combine together. How to put forward a common attack model to combine two attack methods is our research focus.

We also studied the researches about the structural vulnerability. Albert [10] found that, in the random network, when removed node number exceeds a threshold, the network will become fragmented and lose the network connectivity. And in scale-free networks when the threshold phenomenon disappears, deleted node number and largest number of nodes in the connected subgraph synchronously reduce in proportion. Li [11] proposed an attack method based on the Maximal Vertex Coverage and conducted a lot of experiment simulations to prove that different networks have different network structural vulnerability in MVC attack forms. Li [12] used Percolation Theory to analyze network reliability. The failure of network can be regarded as a percolation process. Effective nodes are corresponded to occupied nodes in percolation process and failure nodes are corresponded to blank nodes in percolation process. Through the network simulation analysis he got the lifetime of the network nodes, and when the scale of the nodes is larger, the network has a longer life. Ye [13] reconstructed the network to relatively small scale-free networks in order to increase the robustness of the network. Tanizawa [14] described random attack and targeted attack as a series of waves, so as to put forward a series of anti-destroying ability optimization schemes. But most researches focus on comparing network structural vulnerability under a specific attack mode, and assume that the network is known, ignoring the fact that the attacker may not get the whole information of the network, and the differences between the defenders and attackers. In the process of actual attack, the detected network and real network are different due to some factors such as technology and resources. This reflects the information asymmetry between the attackers and defenders.

In order to acquire a better understanding of the structural vulnerability, we need to verify the simulation results from the aspects of theory. But the study on network structural vulnerability theory has only a few number of researches. Karrer [15] completed the theoretical derivation of percolation theory in sparse network. The percolation process simulation is a process of information transmission. This provided theoretical basis for the spread of disease and network attack. Newman [16] analyzed the max connected component in random network and the result showed max connected component represent the network connection. Di [17] combined assortativity and percolation theory together, and he thought if the independence of the nodes in the network is added, the robustness of the network can effectively increase. This part of the theoretical research, however, cannot completely fit the simulation results, and sometimes it is not feasible in large-scale networks.

Accordingly, in view of the information differences between attacker and defender, we put forward an asymmetric information model in this article. Based on the model we proposed, we simulate in different networks and find that BA networks show vulnerability under the asymmetric information of nonzero degree of node detection. From simulations on the Routing network, the degree distribution of BA network and Routing network meets the power law distribution, but Routing network shows the different structural vulnerability to BA network and the same to ER network. This suggests that with the node scale of the network increasing the real network will show some randomness.

The chapters are arranged as follow. Section 2 introduces the random attack and the targeted attack, and puts forward the asymmetric information attack model, to model the network attack. Section 3 uses the proposed attack model to measure the network structural vulnerability. By attacking BA network we observe the correlation between coefficients in the model and different performances under different attack forms. After that, we verify the Routing network and BA network both meet the power law distribution and we do simulations on the Router network and compare the results between other networks. Section 4 summarizes the research achievements of this paper.

2 Attack Mode

The targets of the network attack are generally the topology of network resources such as routes and switches, which can be abstracted as the graph $G(N, E)$. Here N represents the nodes in the network while E represents the edges. Let adjacency matrix A stand for the connectivity of the network. A is an $N \times N$ matrix. If node i and node j are connected, $a_{ij} = 1$, else $a_{ij} = 0$. When the nodes are under the attack caused by system vulnerability or other reasons and fail in the topology of controlled resources, a disturbance occurs and the adjacency matrix A will change into $A_{N-k} = A - A_k$. Here, k is the proportion of removed nodes. The analysis of structural vulnerability is equivalent to analyze the connectivity difference between A and A_{N-k} . We introduce R to represent the index of evaluating the attack performance and R has many different definitions. In this paper, we choose the largest connected branch as the major measuring object and use the local redundancy of specific node as a supplement. Concrete expressions will be shown in Sect. 3.

2.1 Random Attack and Targeted Attack

In the network under a random attack, nodes are deleted and the value of R would be changed. To compare different indexes side by side, we normalize R to R^* . The boundary values of R^* can be defined as follow.

$$R^*_{\min}[k] = \{\min[R^*(\frac{1}{N})], \min[R^*(\frac{2}{N})], \dots, \min[R^*(1)]\} \tag{1}$$

$$R^*_{\max}[k] = \{\max[R^*(\frac{1}{N})], \max[R^*(\frac{2}{N})], \dots, \max[R^*(1)]\}, \tag{2}$$

where k in $R^*[k]$ represents the proportion of removed nodes. We can get mean values denoted as,

$$R^*_{avg}[k] = \{E[R^*(\frac{1}{N})], E[R^*(\frac{2}{N})], \dots, E[R^*(1)]\} \tag{3}$$

It can be confirmed that finding a node set to minimize the $R^*[k]$ is a NP hard problem [18], and the random attack fits the mean value of $R^*[k]$. In the case of a specific network topology, we can get the probability of each node being selected when the nodes attacked are randomly chosen, which can be denoted as,

$$P_N = \left\{ \frac{1}{N}, \frac{1}{N}, \frac{1}{N}, \dots, \frac{1}{N} \right\} \tag{4}$$

This kind of attack doesn't need too much algorithm complexity, and can finish the choosing process quickly. But the attack effect is not ideal in some networks, this will be reflected in the following simulations.

Targeted attack is to delete the nodes according to node centrality. That means the attacker has to detect the whole network first. This attack method has high algorithm complexity and needs to compare each node in the network. The node centrality [19, 20] includes degree centrality, closeness centrality and betweenness centrality, etc. In this paper, we apply the degree centrality. That is to say, the node with a higher degree value has a greater priority to be deleted. Targeted attack has different effects in different networks. The first step is to sort the nodes according to the degree value in the detected network.

$$\text{Centrality}\{n_1, n_2, \dots, n_N\} \quad n_1 \geq n_2 \geq \dots \geq n_N \tag{5}$$

At this time, to all nodes in the network, the probability distribution of being chosen is $P\{1,0,0,\dots,0\}$. Targeted attacks only select one node as the target at a time which ensures the accuracy of the attack. We can assume that the targeted attack fits the minimum value of R. We will do simulations and further explanations in Sect. 3.

2.2 Asymmetric Information Attack

In the process of the network attack, the attacker cannot get the entire topology information of the network. The amount of information he gets depends on his resource, technology and so on. The adjacency matrix the attacker detects A' must have a perturbation denoted as $A' = A + A\sim$. $A\sim$ is the error caused by the limitation of attacker's technology or resources. The attacker evaluates the node importance and deletes the nodes based on the information he has got. At this time the effect to the detected network will reflect on the real network. This whole process is called the asymmetric information attack. The attacker cannot get the whole information of the network and the defender cannot know the choice of the attacker or what he knows about the network. Therefore we should model this process.

To attack network $G(N, E)$ with nodes $N\{n_1, n_2, n_3 \dots n_k\}$, we should sort nodes by centrality to confirm the attack performance. In this paper, we apply the degree centrality as the importance of nodes. And we assume the attacker is a rational person and has restricted resources. That is to say, in the attack to a specific network, he cannot know the entire topology of the network and will choose a certain number of nodes to delete. Based on that, we put forward two parameters as follow.

- (1) Attack range H . First we calculate the degree of all nodes and sorting them. H represents the proportion of the detected nodes. We define $H = i/n$. And i represents the number of detected nodes, n represents the number of all nodes in the network.
- (2) Detection degree of node F . When attacking network, A and A' are different. There must be error between them. We use the percentage to represent detection degree of node F . F is the ratio of the detected network information to the whole network topology information, ranging from 0 to 1.

With restricted resource, F and H must belong to 0 to 1. It is easy to know that if we want to get higher F and H , we must spend more resource. So we define the resource cost coefficient as follow.

$$C = H \times F \quad C \in [0, 1] \tag{6}$$

It can be seen that when C is higher, the algorithm is more complex and the time cost is more. So we can know for the random attack $C = 0$ and for the targeted attack $C = 1$. Assuming that the attacker spends the same resource on each deleted nodes denoted as G . x is the number of deleted nodes. And we can get that the optimal attack plan must meet

$$P\{Max[\Delta Con]|Min[G(x - i) + R(i)]\} \tag{7}$$

where $R(i) = G'(i + C \times i)$ is the resource spent under the asymmetric information attack. ΔCon is the effect to the connectivity of the network.

2.3 Attack Model

From the definition of the asymmetric information attack, we can find that it includes both the random attack and the targeted attack. As shown in Fig. 1, light red nodes represent the undetected nodes and red nodes are the detected nodes with high degree under the certain

F. We can see that when F is not big enough, the attacker cannot find all nodes with big degree. The lack of the amount of the information attackers acquires leads to inaccurate attacks.

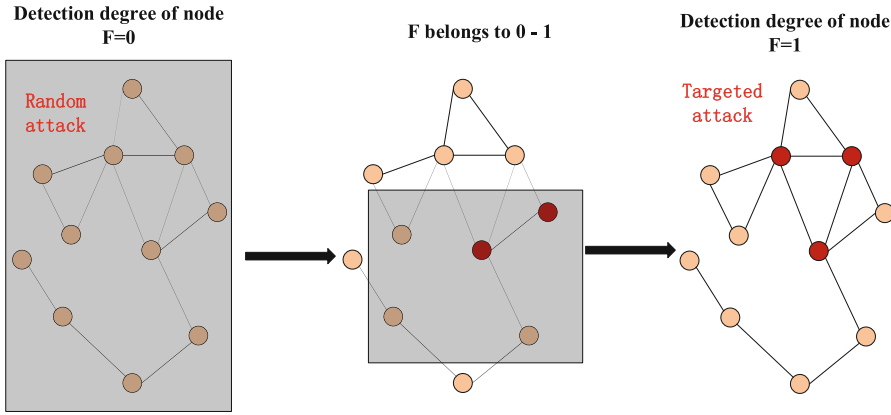


Fig. 1. Asymmetric information attack graph (Color figure online)

From Table 1, we can further understand the relationship between parameter and attack mode. When $F = 0$, the attack mode is random attack. At this time H becomes meaningless. When $F = 1$, the mode turns into the targeted attack. At this time, H is actually the number of the deleted nodes. When $F \in (0, 1)$, it is the asymmetric information attack. The probability of selecting important nodes depends on F . Attack range H corresponds to the number of selected nodes. It can be observed that bigger H can make up for F . This phenomenon will be showed and analyzed in later simulation.

Table 1. The mapping relationship between parameter and attack mode

H	F	Attack mode
0	0	Random attack
1	1	Targeted attack
(0, 1)	(0, 1)	Asymmetric information attack

According to attacker’s resource we can get H and F , and the number of deleted nodes x . To prevent nodes with big degree from repeatedly showing up in the sample, we module the whole simulation process as the non-return unequal probability sampling. The whole attack process is defined as follow:

- Step 1: Based on H , we calculate the number of sample nodes i , which meets $i = H \times N$
- Step 2: Calculate all nodes’ degree in the network and sort them.
- Step 3: Respectively give all the nodes in the network the sample rate. For the node with the biggest degree, F is the sample rate. Other nodes’ sample rates are calculated as follow,

$$N_j = (1 - F)^{j-1} F \tag{8}$$

- Step 4: Select one node according to the sample rate. Then compare the number of the sample nodes with i . If smaller, go to Step 2, else go next.
- Step 5: When $x \leq i$ just delete x nodes of the sample nodes. When $x > i$ first delete the sample nodes, then delete $x-i$ nodes randomly.

In the real world, when the attacker launches an attack against a network, the attacker cannot get the whole information of the network and the defender cannot know the choice of the attacker or what he knows about the network. Supposed that the attacker is rational and his resource is limited, his best choice is to attack the most important nodes in the network. The importance of the node depends on two aspect, the attacker’s knowledge of the network and the index of the importance. For the first aspect, we proposed two parameters, the attack arrange H and the detection degree of node F , which represents the proportion of the detected nodes and the ratio of the detected network information to the whole network topology information respectively. Or simply, H shows how many nodes have been detected and F shows, for the detected nodes, how much the attacker knows. As for the second aspect, the indicator of the importance is usually the centrality of the nodes. In this paper, we use the degree value, and it is obvious that for a single node, more degree value means it is connected to more nodes. And that means if the node is attacked, there will be a greater effect. Thus, we say the more the degree value of the node is, the more important the node is.

3 Structural Vulnerability Measurement and Impact Analysis

3.1 Attack Performance Evaluation Indicators

R measures the connectivity of the network. The common measurement of the connectivity of the network is the number of the nodes that belongs to the largest connected component. The redundancy of the network is also used to measure the network, especially the robustness of the network. R has two definitions explained as follow. R_m is the number of nodes in the largest connected branch

$$R_m = \{n_j | \text{iff} \exists n_i \in R_m \wedge e_{ij} = 1\} \tag{9}$$

The largest connected branch is the carrier of the network traffic. The number of nodes in the largest connected branch measures the connectivity of the whole network after the network is attacked, and is also an important index to judge whether the network is failed.

R_v is the local redundancy of the specific node in the network. It can show the robustness of the node against the attack. It is also a measurement of connectivity. It is defined as follow.

$$R_v = \frac{1}{|S|} \sum_{j \in V(\Gamma_v^2)} \min\{d(v), d(j)\} \tag{10}$$

Node redundancy rate refers to the ratio of the number of the paths a node goes through to arrive to its “neighbors’ neighbors” to the number of the paths in the complete graph. Γ_v represents the set of neighbor nodes. Γ_v^2 is the set of nodes’ “neighbors’ neighbors”. $|S|$ is the complete graph consisting of the nodes, Γ_v and Γ_v^2 .

3.2 Structural Vulnerability Analysis on BA Network

In order to test different performances of the network under various attack modes, we use BA network for simulations. BA network is a sparse network with 5000 nodes and 5000 edges. In simulations, we use Spyder as the simulation software and python as the simulation platform. Besides we use networkx module to call the specific function to generate BA networks. During the experiments we assume that the attacker prepares to delete 100 nodes. Then we adjust the value of H and F and observe the change of parameters in the network, and based on the simulation results we analyze the different properties of the network vulnerability under different H and F. In order to guarantee the experimental accuracy, we do each experiment for 50 times, then average them as the final results and plot curves.

Table 2. Asymmetric information attack algorithm

Input: {G,N,H,F,x}

Output: {G', $\rho(\rho_0, \rho_1, \rho_2 \dots \rho_i)$, Figure }

- 1: Input {G,N,H,F,x}
- 2: edges(l),nodes (k), linklist
- 3: calculate i
- 4: sorted degree $N_k = [n_1, n_2, n_3, \dots n_k]$
- 4: $p_k = [p_1, p_2, p_3, \dots p_k]$
- 5: use distr.rvs choose n_i refer to p_k
- 6: if $n < i$ go to 4 else go next
- 7: delete n_i in order and get ρ
- 8: Figure show
- 9: return {G', $\rho(\rho_0, \rho_1, \rho_2 \dots \rho_i)$, Figure}

Table 2 is the algorithm for using the number of the nodes belong to the largest connected component to measure the connectivity of the network after the network attacked.

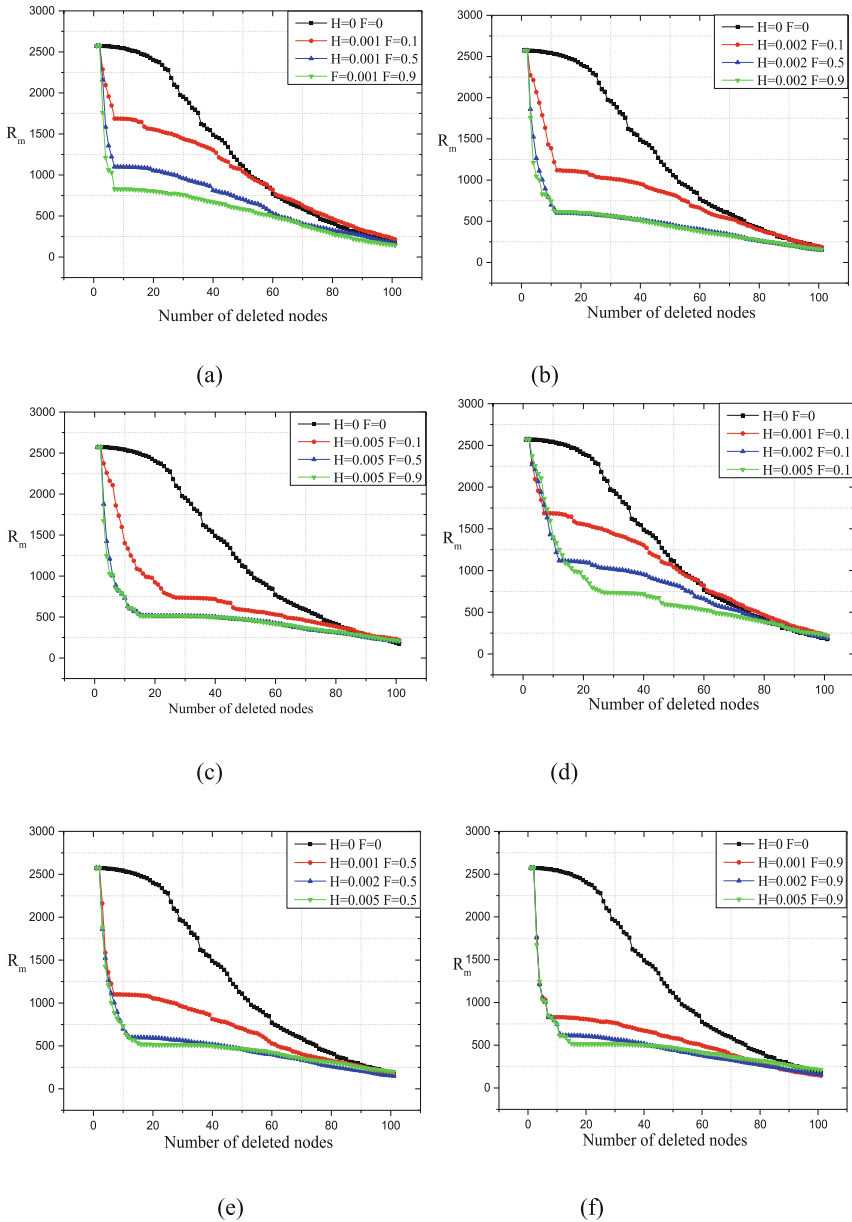


Fig. 2. The change of R_m under different H and F in BA network

First we simulate the attack on the BA network (Fig. 2). The attack range H is respectively 0.001, 0.002 and 0.005, and the detection degree of node is respectively 0.1, 0.5 and 0.9. In figures, the horizontal axis represents the number of the deleted nodes and the vertical axis is the number of nodes in the largest connected branch. Based on the simulation results it can be found that:

- (1) As a whole, no matter what strategy the attack process is based on, after deleting 100 nodes, the curve tends to be gentle and the network shows its robustness. That is to say, BA network will not be directly completely broken after deleting a certain number of nodes. However, at this time, the network may not be able to communicate. Therefore, to the attacker, it is not necessary to delete all 100 nodes to destroy the network.
- (2) Comparing 2-a, 2-b, 2-c we can find that when H and F are big enough, the curves go down rapidly, and then go to a plain. At this time the network is failed. When $H = 0.005$ $F = 0.9$, deleting 20 nodes is enough to make the network failed. It is obvious that these 20 nodes are important to the whole network connectivity. The attacker is a rational person with limited resources, as a result he will choose the most important nodes to attack.
- (3) For the supplement effect (H and F), it can be proved from the aspect of algorithm. From 2-a, 2-b, 2-c, when H is fixed, F just need to reach a certain value to make network failed quickly. As in figures, curves ($F = 0.5$ $F = 0.9$) are close to each other. From 2-d, 2-e, 2-f when F is fixed, H reaches a certain value to make curves close to each other. We use the resource cost coefficient C to evaluate the attack performance. Obviously when C is smaller, the attack cost is lower and correspondingly, the protect cost is lower. How to balance the relationship between the cost and the effect is a big issue. We can also find that the BA network is a multi-center network. After deleting several center nodes, the network tends to be broken.

3.3 Compared with Other Indicators

Figure 3 is the change of redundancy of the specific node (the node is same as 3.2). From this figure we can find that the specific node's local redundancy falls much. It indicates that the attacker deletes many neighbor nodes or 'neighbor's neighbor' nodes of the specific node. Eventually, the lines all become to flatten, which shows certain robustness.

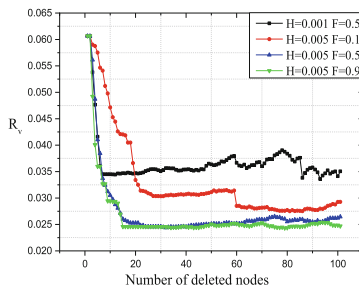


Fig. 3. The change of redundancy in BA network

Comparing R_m with R_v , we can find that the two indicators can both be used to measure the connectivity of the network, and can both reflect the robustness of the network. The difference between the two indicators is that they indicate the properties of the network from different aspects. R_v is used to analyze single node's connectivity and R_m is used to measure the whole network's connectivity. The connectivity of single node and the whole network are different but relevant. When there is a need for evaluating important nodes, we will select the R_v to be the indicator. When we need to evaluate the robustness of the network structure, we select the R_m . From the analysis of BA network, the effect of the nonrandom attack ($F > 0 H > 0$) is better than random attack ($F = 0 H = 0$). When F and H are bigger, the attack effect is more obvious. And in the beginning of the attack, the connectivity of the network reduces quickly. When the network shows robust and the curves become gentle, the effect of the random attack and the nonrandom attack ($F > 0 H > 0$) are tend to be the same.

3.4 Simulations on Router Network

From analysis of Sect. 3 we can get the structural vulnerability of BA network. We can compare real network with BA network to get more information about the structural vulnerability. Router network has 192244 nodes and 609066 edges.

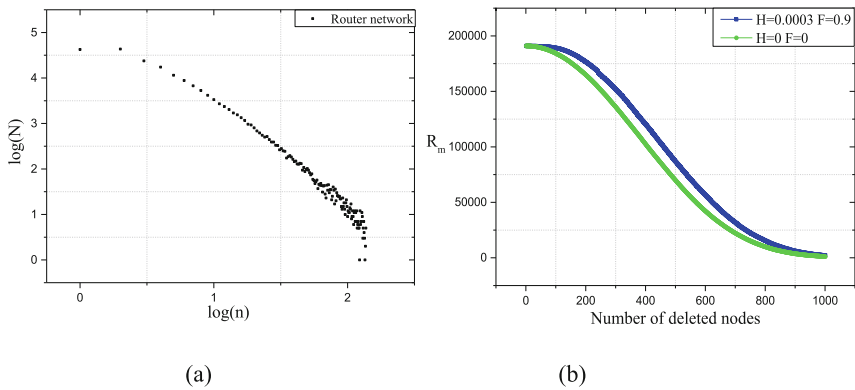


Fig. 4. Simulations on Router network. (a) the degree distribution of Router network (b) the change of R_m during the attack of Router network

Figure 4a is the degree distribution of Router network. And x axis is degree; y axis is the number of nodes. Degree and number of nodes meet linear relationship. So the degree distribution of Router network and BA network obey power law distribution. From Fig. 4b we can see after deleting 1000 nodes, the network becomes to be failed. The curve at the top is the asymmetric information attack which has $H = 0.0003$ and $F = 0.9$, and the random attack ($F = 0, H = 0$) is under the curve ($H = 0.0003, F = 0.9$). So the effect of the random attack is better than the asymmetric information attack. We can conclude that the effect of the asymmetric information attack in BA network is opposite to that in Router network. But the degree distribution of the two networks both

obey the power law distribution. So the structural vulnerability does not only depend on the degree distribution. In order to fully understand the reason of this phenomenon, we do simulations on ER network which has different structural vulnerability with BA network.

ER network has 5000 nodes and 12500 edges. Corresponding parameters m, n are 5000 and 0.0005. Here we attack ER network (Fig. 5) we can find that.

- (1) From Fig. 5a random attack ($H = 0, F = 0$) is at the bottom which states that the effect of random attack on ER network is best. And the bigger F is, the worse the effect is.
- (2) In Fig. 5b three curves almost coincide. It indicates that when the H is less than a certain value F has no influence. This is because the effect of the asymmetric information attack ($F > 0$) is tiny in ER network.

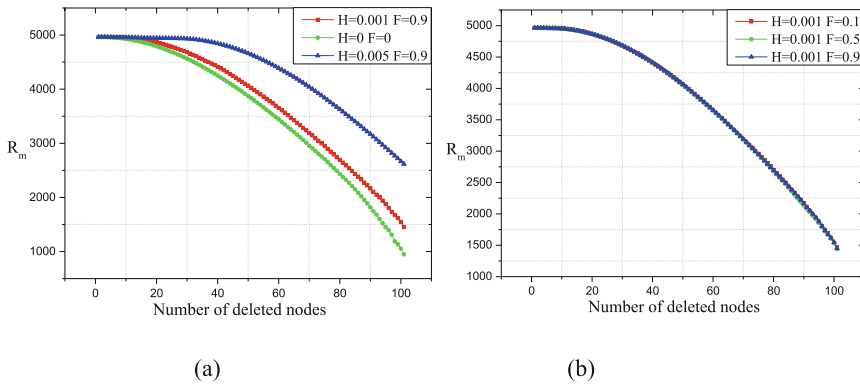


Fig. 5. The change of R_m under different H and F in ER network

The result shows that ER network is robust against the attack ($F > 0$) and the random attack has the best effect on ER network. ER network is a random network. The nodes of the network have similar degree value, and the status of each node is the same. If we use the asymmetric information attack ($F > 0$), can not improve the attack effect not only, rise instead counteractive. Compared with BA network the curves of attack ($F > 0$) are above the random attack so the targeted attack cannot fit $R_{\min}[k]$.

Thus, the effect of the asymmetric information attack on ER network is opposite to that on BA network but is same with that on Router network. Although Router network shares the same degree distribution with BA network, its structural vulnerability is more close to ER network. This shows that the real network has certain randomness.

4 Conclusion

In this article, through the analysis of the random attack and the targeted attack, we proposed an asymmetric information attack model, and the random attack and the targeted attack are special cases of the attack model. Using node degree as the indicator,

we do simulations on the ER, BA and Routing network, and analyze the contact among the random attack, the targeted attack and the asymmetric information attack. Based on the results, we reveal different structural vulnerability of different networks. Simulation shows that BA network is fragile to the asymmetric information attack ($F > 0$). And ER network shows robust to the attack ($F > 0$). Because the scale of the real network is large and the real network has randomness, it is robust to the asymmetric information attack ($F > 0$) when the attack uses degree centrality to measure nodes' importance.

References

1. Burch, H., Cheswick, B.: *Computer* **32**(4), 97 (1999)
2. Guo, R.R., Song, R.S.: *Comput. Eng. Appl.* **38**(10), 162 (2002)
3. Trajanovski, S., Martín-Hernández, J., Winterbach, W., Mieghem, P.V.: *J. Complex Netw.* **1**(1), 44–62 (2013)
4. Scellato, S., Leontiadis, I., Mascolo, C., Basu, P., Zafer, M.: *Proceedings of INFOCOM, Shanghai, China*, pp. 1–5. IEEE (2011)
5. Huang, X., Gao, J., Buldyrev, S.V., Havlin, S., Stanley, H.E.: *Phys. Rev. E* **83**, 065101 (2011)
6. Wang, J., Jiang, C., Qian, J.: *J. Netw. Comput. Appl.* **40**(7), 97 (2014)
7. Byungjoon, M., Do, Y.S., Kyu-Min, L., Goh, K.-I.: *Phys. Rev. E* **89**(4), 042811 (2014)
8. Pin-Yu, C., Shin-Ming, C.: *Phys. Rev. E* **91**(2), 19 (2015)
9. Xie, F., Cheng, S.Q., Chen, D.Q., Zhang, G.Q.: *J. Tsinghua Univ. (Sci. Technol.)* **10**, 1252 (2011)
10. Albert, R., Jeong, H., Barabási, A., Albert, R.: *Nature* **406**(6794), 378 (2000)
11. Li, R.H., Yu, J.X., Huang, X., Hong, C., Ze, C.S.: *Inf. Sci.* **278**(10), 685 (2014)
12. Li, D., Zhang, Q., Zio, E., Havlin, S., Kang, R.: *Reliab. Eng. Syst. Saf.* **142**, 556 (2015)
13. Ye, B., Jia, J.-J., Zuo, K.-W., Ma, X.P.: *Int. J. Mod. Phys. C* **26**(4), 1550040 (2015)
14. Tanizawa, T., Paul, G., Cohen, R., Havlin, S., Stanley, H.E.: *Phys. Rev. E Stat. Nonlinear Soft Matter Phys.* **71**(4), 047101 (2005)
15. Karrer, B., Newman, M.E.J., Zdeborová, L.: *Phys. Rev. Lett.* **113**(20), 208702 (2014)
16. Newman, M.E.J.: *Phys. Rev. E* **76**(4), 70 (2007)
17. Zhou, D., Stanley, H.E., D'Agostino, G., Scala, A.: *Phys. Rev. E* **86**(6), 066103 (2012)
18. Dinh, T.N., Xuan, Y., Thai, M.T., Pardalos, P.M., Znati, T.: *IEEE/ACM Trans. Networking* **20**(2), 609 (2011)
19. Ronald, S.B.: *Am. J. Sociol.* **110**(2), 349 (2004)
20. Fu, L.D.: Ph.D. dissertation (Xidian University) (2012). (in Chinese)
21. Dueñas-Osorio, L., Craig, J.I., Goodno, B.J., Bostrom, A.: *J. Infrastruct. Syst.* **13**(3), 185 (2007)

Combining Link and Content Correlation Learning for Cross-Modal Retrieval in Social Multimedia

Longtao Zhang^(✉), Fangfang Liu, and Zhimin Zeng

Beijing Laboratory of Advanced Information Networks,
Beijing University of Posts and Telecommunications, Beijing, China
{zhanglongtao, fliu, zengzm}@bupt.edu.cn

Abstract. With the rapid growth of multimedia data, cross-modal retrieval has received great attention. Generally, learning semantics correlation is the primary solution for eliminating heterogeneous gap between modalities. Existing approaches usually focus on modeling cross-modal correlation and category correlation, which can't capture semantic correlation thoroughly for social multimedia data. In fact, the diverse link information is complementary to provide rich hints for semantic correlation. In this paper, we propose a novel cross-modal correlation learning approach based on subspace learning by taking heterogeneous social link and content information into account. Both intra-modal and inter-modal correlation are simultaneously considered through explicitly modeling link information. Additionally, those correlations are incorporated into final representation, which further improve the performance of cross modal retrieval effectively. Experimental results demonstrate that the proposed approach performs better comparing with several state-of-the-art cross-modal correlation learning approaches.

Keywords: Cross-modal retrieval · Correlation learning · Social multimedia
Heterogeneous networks

1 Introduction

With the rapid development of multimedia technology, there has been a massive explosion of multimedia data on social media websites, which makes the traditional social media show the trend of multimedia [1]. In face of large amounts of complex social multimedia data, retrieving valuable information is of great significance. Consequently, cross-modal retrieval attracts considerable attention, in which users can input any modalities data at hand to query relevant information of other modalities. Different from traditional single-modal retrieval, it is more comprehensive and can meet the increasing user demands. Generally, learning semantic correlation is the main solution for eliminating heterogeneous gap between modalities for cross-modal retrieval. Nevertheless, these data do not exist in isolation in social multimedia, which makes correlation learning more challenging. On the one hand, different modalities of multimedia data are usually in coexistence. For example, in image sharing website, users usually share images accompanied by some text to illustrate. On the other hand,

these multimedia data are closely associated with the multi social factors, such as user, group and location information, which connect different social components into heterogeneous social multimedia networks.

Although, several efforts have been paid to correlation learning. Most of existing methods focus on modeling cross-modal correlation and category correlation, such as canonical correlation analysis [2], cross-modal factor analysis [3] and semantic correlation matching [4]. However, those methods fail to model the correlation thoroughly for social multimedia data. Much social correlation between two objects is not exploited adequately. For instance, image and text may be connected by the same user, which indicates they have some semantic correlation. In fact, the complex heterogeneous link structure is complementary to provide the rich hints for semantic correlation and can be exploited to bridge the heterogeneous gap to some extent. Therefore, both link and content information are should be captured to improve the retrieval performance.

In this paper, we propose a novel correlation learning approach based on subspace learning. It jointly considers both heterogeneous link and multimedia content, which is ignored by previous works. In this learning framework, firstly, multiple social links are transformed into both intra-modal and inter-modal correlation via heterogeneous networks. Then heterogeneous modalities are projected into a unified subspace according to those correlation so that the similarity between different modalities can be measured through projection matrices. The proposed approach is experimentally evaluated better than other prevailing approaches on a cross-modal dataset.

Along this line of research, there are two main contributions of proposed approach. On one hand, instead of treating each semantic link equally, we design a weight learning approach keeping link structure consistence with content information. On the other hand, we propose incorporating heterogeneous link structure and content information into the unified feature representation which are not only helpful to bridge the heterogeneous gap, but also robust to noise.

The remainder of this paper is organized as follows. The related work on correlation learning for cross-modal retrieval is reviewed in Sect. 2. Then we present the proposed combining link and content correlation learning approach in Sect. 3. In Sect. 4, experiments are shown to verify the effectiveness of proposed method. Finally, we conclude this paper in Sect. 5.

2 Related Works

It is of considerable challenge to learning semantic correlation of heterogeneous modalities. Generally speaking, existing efforts are roughly divided into two aspects: the one is mapping the different features into a unified feature space based on subspace learning so that similarity between heterogeneous modalities can be computed, and the other is modeling the probability that learns a set of shared latent topics for different modalities.

For subspace learning, there are many representative approaches like canonical correlation analysis, deep canonical correlation analysis [5], and partial least square [6]. Those methods usually maximize the correlation between two different modalities and learn the joint feature representation. While most of them do not take high-level

semantic correlation into account. To consider label information, Rasiwasia et al. propose combining subspace and semantic modeling to improve retrieval accuracy. Huang and Peng [7] present exploiting fine-grained correlation by taking entity level into account to construct high-level concepts. Moreover, further study jointly model labeled information and unlabeled information with graph regularization in a semi-supervised learning framework [8]. As for probabilistic model, Jia et al. [9] proposed a probabilistic model seen as Markov random field of topic models, which establish correlation among modalities based on their similarity. Han and Thomas [10] proposed matching images and sounds with tags which treated as shared latent variables by combining Latent Dirichlet Allocation and Correspondence Latent Dirichlet Allocation model. However, these methods often take strict assumptions that there exist the same topic proportions or pairwise topic correspondences between different modalities, which are not satisfied for social multimedia data.

Generally, there is an important principle for correlation leaning. It is the both inter-modal and intra-modal correlation that should be preserved [11]. That is, if two objects are closely related in original space, they should be closed to each other in latent subspace. The coexistence information is usually taken as intermodal correlation. The intra-modal correlation is usually provided by high-level category information. In this paper, we transform the rich link structure into the intra-modal and inter-modal correlation, which can further improve the performance of semantic correlation.

3 Combining Link and Content Correlation Learning

3.1 Overview of Proposed Framework

To begin with, the problem formulation is defined in this section. Given a set of training dataset $D = \{X, Z\}$, in which $X = \{x_1, x_2, \dots, x_n\}$ denotes images, $Z = \{z_1, z_2, \dots, z_n\}$ denotes texts. While $\mathbf{X} = \{\mathbf{x}_1, \mathbf{x}_2, \dots, \mathbf{x}_n\} \in \mathbb{R}^{d_1 \times n}$ and $\mathbf{Z} = \{\mathbf{z}_1, \mathbf{z}_2, \dots, \mathbf{z}_n\} \in \mathbb{R}^{d_2 \times n}$ represent the image and text feature matrix respectively. In this case, the number of training samples is n , and the feature dimensionalities of image and text are d_1 and d_2 respectively. The main goal of correlation learning is to learn two projection matrices $\mathbf{U} \in \mathbb{R}^{d_1 \times r}$ and $\mathbf{V} \in \mathbb{R}^{d_2 \times r}$ for image and text domain, so that the similarity between projected objects $Sim(\mathbf{U}^T \mathbf{x}_i, \mathbf{V}^T \mathbf{z}_j)$ can be computed. In other words, the semantic correlation is built among heterogeneous modalities in same dimensional subspace, so that cross-modal retrieval can be performed.

Next, an effective and concise learning framework of proposed approach is introduced briefly as illustrated in Fig. 1. This approach mainly consists of two phases. For the first step, the heterogeneous social multimedia network is treated as a kind of heterogeneous information network [12], in which the link-based similarity could be measured by meta-path. After that, heterogeneous network is transformed into multiple homogeneous networks and bipartite networks. Therefore, the link-based similarity relationship is encoded into intra-modal and intermodal correlation. For the second step, it learns projection matrices according to those correlation for each modal based on subspace learning. To state conveniently, we take two modalities for example in this

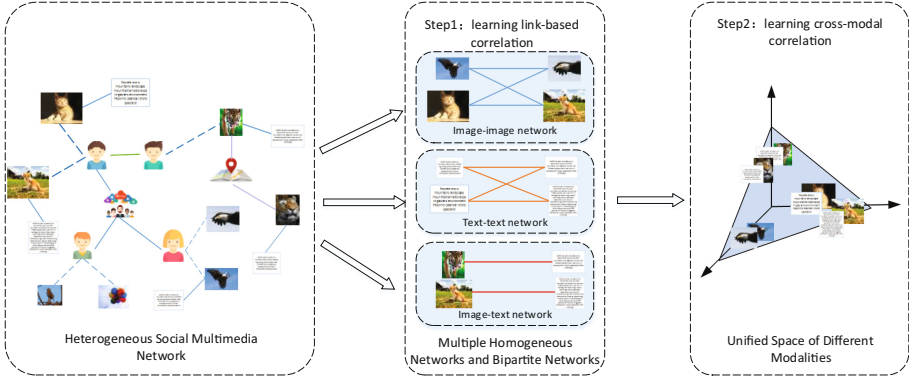


Fig. 1. The framework of the proposed method.

framework, while it can easily extend to multi-modalities case. Based on this framework, the details are depicted for each step as follows.

3.2 Learning Link-Based Correlation

As mentioned above, similarity relationship should be preserved to learning semantic correlation. Nevertheless, existing study [13] has shown that content-based similarity sometimes may not reliable to determine the similarity between two objects. Thus, only content-based correlation may lead to unsatisfying results for correlation learning. Of course, the link-based correlation is also uncertain and contingency. Intuitively, link and content are complementary to each other, so combining them will achieve more robust performance. In this paper, we embed link-based correlation into content-based correlation to obtain more effective yet efficient feature representation.

It is reasonable to assume that semantic relationship exist between two objects, if there exist link explicitly. Given a heterogeneous network, there are many semantic links to connect two objects, which are defined as meta-paths. Different meta-paths imply different semantic meanings. For example, if two images are uploaded by the same user, they are connected via “image $\xrightarrow{\text{upload}^{-1}}$ user $\xrightarrow{\text{upload}}$ image” path, thus it can be assumed that the two images are partially similar through common user. Besides, there are many other meta-paths, such as “image $\xrightarrow{\text{favor}^{-1}}$ user $\xrightarrow{\text{favor}}$ image” path, “image $\xrightarrow{\text{upload}^{-1}}$ user $\xrightarrow{\text{contact}}$ user $\xrightarrow{\text{upload}}$ image” path, “image $\xrightarrow{\text{locate}}$ location $\xrightarrow{\text{locate}^{-1}}$ image” path, and “image $\xrightarrow{\text{upload}^{-1}}$ user $\xrightarrow{\text{belong}}$ group $\xrightarrow{\text{belong}^{-1}}$ user $\xrightarrow{\text{upload}}$ image” path. The link-based similarity can be computed based on meta-path like Pathsim [14] which similarity measure formula is defined as follows,

$$s^P(x_i, x_j) = \frac{2 * |\{p_{x_i \rightarrow x_j} : p_{x_i \rightarrow x_j} \in P\}|}{|\{p_{x_i \rightarrow x_i} : p_{x_i \rightarrow x_i} \in P\}| + |\{p_{x_j \rightarrow x_j} : p_{x_j \rightarrow x_j} \in P\}|} \quad (1)$$

where x_i and x_j are the same type, P is a meta-path, $|P_{x_i \rightarrow x_j}|$ is the number of path instances between x_i and x_j , $|P_{x_i \rightarrow x_i}|$ is that between x_i and x_i , and $|P_{x_j \rightarrow x_j}|$ is that between x_j and x_j .

Different meta-paths reflect different aspects of image or text similarity. Instead of treating each meta-path equally, we design a novel algorithm to learn different weights. The latent hypothesis is the link-based similarity $s(x_i, x_j)$ is consistence with content-based similarity $c(x_i, x_j)$. The set of meta-paths are denoted as $\mathbf{p} = [p_1, p_2, \dots, p_m]$ and the weights of different meta-paths are denoted as $\mathbf{w} = [w_1, w_2, \dots, w_m]$. We minimize the following objective function to learn different weights,

$$L(\mathbf{w}) = \sum_{i=1}^n \sum_{j=1}^n \left(c(x_i, x_j) - \sum_{d=1}^m w_d s^{p_d}(x_i, x_j) \right)^2 + \alpha \|\mathbf{w}\|_2^2 \quad (2)$$

where the first component ensures that link-based similarity is consistence with content-based similarity, and the second term is L2 regulation. It is worth paying attention that these similarities are normalized in $[0, 1]$. The above objective unction can solved by many off-the-shelf methods, such as Newton method or stochastic gradient decent method.

After having all the weights for each meta-path, the link-based similarity can be computed by combining all the similarities that based on different meta-paths. Therefore, link-based correlation can be modeled by three weight matrices, of which each element w_{ij} is expressed as below,

$$w_{ij} = \begin{cases} \sum_{d=1}^m w_d s^{p_d}(i, j) & i \text{ and } j \text{ are of the same type} \\ c_{ij} & \textit{otherwise} \end{cases} \quad (3)$$

where the c_{ij} denotes whether the link exist or not. In this paper, if there exist meta-path “*image* $\xrightarrow{\textit{coexist}^{-1}}$ *text*” between i and j , we set $c_{ij} = 1$, otherwise we set $c_{ij} = 0$. Furthermore, multi-modal fusion is performed to get a common w_{ij} for image and text domain in this research.

3.3 Learning Cross-Modal Correlation

So far, we have encoded the complex link information into both inter-modal and intra-modal correlation. Our ultimate target is realizing cross-modal retrieval, so we embed link-based correlation into content-based unified representation to learn semantic correlation in the common subspace.

Essentially, similar objects should have similar feature representation. Then, the higher of the correlation between two objects, the distance between them in the joint subspace should be more close to each other. As mentioned above, to obtain better semantic correlation and more robust representation, both intra-modal and inter-modal

similarity relationship should be preserved when learning the common subspace. Hence, the loss function is formed by Frobenius norm as follows,

$$\begin{aligned} & \min_{\mathbf{U}, \mathbf{V}} \sum_{i \in X, j \in Z} w_{ij} \|\mathbf{U}^T \mathbf{x}_i - \mathbf{V}^T \mathbf{z}_j\|_F^2 \\ & + \lambda \sum_{i, j \in X \text{ or } Z} w_{ij} \left(\|\mathbf{U}^T \mathbf{x}_i - \mathbf{U}^T \mathbf{x}_j\|_F^2 + \|\mathbf{V}^T \mathbf{z}_i - \mathbf{V}^T \mathbf{z}_j\|_F^2 \right) \end{aligned} \quad (4)$$

where the first term is the distance between different modalities in the projected space and the second term is that between same modality, λ is the parameter for balancing the inter-modal and intra-modal correlation.

However, there are no obvious semantic meanings in the above projected space. In fact, the semantic label information can offer some useful guide information. Motivated by this, we also add the label consistent term into above loss function. So our ultimate objective function is defined as follows,

$$\begin{aligned} & \min_{\mathbf{U}, \mathbf{V}} \sum_{i \in X, j \in Z} w_{ij} \|\mathbf{U}^T \mathbf{x}_i - \mathbf{V}^T \mathbf{z}_j\|_F^2 \\ & + \lambda \sum_{i, j \in X \text{ or } Z} w_{ij} \left(\|\mathbf{U}^T \mathbf{x}_i - \mathbf{U}^T \mathbf{x}_j\|_F^2 + \|\mathbf{V}^T \mathbf{z}_i - \mathbf{V}^T \mathbf{z}_j\|_F^2 \right) \\ & + \beta \left(\|\mathbf{U}^T \mathbf{X} - \mathbf{Y}_X\|_F^2 + \|\mathbf{V}^T \mathbf{Z} - \mathbf{Y}_Z\|_F^2 \right) + \mu \left(\|\mathbf{U}\|_{2,1} + \|\mathbf{V}\|_{2,1} \right) \end{aligned} \quad (5)$$

here, \mathbf{Y}_X and \mathbf{Y}_Z are the initial label matrices on image and text domain respectively. $\|\cdot\|_{2,1}$ denote $l_{2,1}$ -norm, which is used to sparse feature selection on projection matrices. β and μ are the balancing parameters.

To solve the objective function in Eq. (5), we firstly simplify it. Inspired by Laplacian regularizer, we may arrive at a corresponding compact form as in Eq. (6).

$$\begin{aligned} & \min_{\mathbf{U}, \mathbf{V}} \|\mathbf{U}^T \mathbf{X} - \mathbf{V}^T \mathbf{Z}\|_F^2 + \lambda \text{tr}(\mathbf{F}(\mathbf{D} - \mathbf{W})\mathbf{F}^T) \\ & + \beta \left(\|\mathbf{U}^T \mathbf{X} - \mathbf{Y}_X\|_F^2 + \|\mathbf{V}^T \mathbf{Z} - \mathbf{Y}_Z\|_F^2 \right) + \mu \left(\|\mathbf{U}\|_{2,1} + \|\mathbf{V}\|_{2,1} \right) \end{aligned} \quad (6)$$

where $\text{tr}(\cdot)$ denote the trace of matrix, \mathbf{D} is a diagonal matrix with $d(i, i) = \sum_j w_{ij}$, and $\mathbf{F} = (\mathbf{X}^T \mathbf{U}, \mathbf{Y}^T \mathbf{V})$. Note that the parameter λ have been changed to 2λ . While it does not affect the result, so we still use λ for convenience.

The above objective function can be optimized by an iterative algorithm, which solves for one variable while keeping the others fixed. Hence, the solution of \mathbf{U} and \mathbf{V} can be expressed in each iteration by Eqs. (7) and (8),

$$\mathbf{U} = \left((1 + \beta)\mathbf{X}\mathbf{X}^T + \mu\mathbf{R}_u + \lambda\mathbf{X}(\mathbf{D} - \mathbf{W})\mathbf{X}^T \right)^{-1} (\beta\mathbf{X}\mathbf{Y}_X^T + \mathbf{X}\mathbf{Z}^T\mathbf{V}) \quad (7)$$

$$\mathbf{V} = \left((1 + \beta)\mathbf{Z}\mathbf{Z}^T + \mu\mathbf{R}_v + \lambda\mathbf{Z}(\mathbf{D} - \mathbf{W})\mathbf{Z}^T \right)^{-1} (\beta\mathbf{Z}\mathbf{Y}_Z^T + \mathbf{Z}\mathbf{X}^T\mathbf{U}) \quad (8)$$

Where \mathbf{R}_u is a diagonal matrix [15], each element is defined as in Eq. (9), \mathbf{R}_v has analogous representation with \mathbf{R}_u as in Eq. (10).

$$r_u(i, i) = \frac{1}{2\sqrt{\sum_j \|U_{ij}\|_2^2 + \varepsilon}} \quad (9)$$

$$r_v(i, i) = \frac{1}{2\sqrt{\sum_j \|V_{ij}\|_2^2 + \varepsilon}} \quad (10)$$

in which ε is a smoothing term, and we set it to be a small constant value to avoid the denominator being zero.

Once projection matrices for heterogeneous low-level features are learnt, all the data are readily projected into unified feature space. To perform cross-modal retrieval, the similarity between the query and the other modalities can be computed directly.

4 Experiments

In this section, experiments are conducted to verify effectiveness of our method and investigate the performance by comparing with several state-of-the-art methods.

4.1 Dataset

We perform the experiments for cross-modal retrieval based on the large-scale NUS-WIDE dataset [16]. Each image is associated with some tags, which can be regarded as text information. The dataset contains almost 270,000 images with 5,018 unique tags collected from Flickr website. We firstly find 10 largest classes and crawl the list of users who upload or favor a given image according to the image ID. Then, we choose the users owing more than 10 images and obtain 6487 unique users including 1418 authors and 5069 favorite users. What's more, we also crawl the groups and contacts information for each author.

In the learning link-based correlation stage, in order to catch the link-based intra-modal correlation as much as possible, we chose 5 kinds of meta-paths for images and texts as mentioned above. While, we only consider one meta-path “*image* $\xrightarrow{\text{coexist}^{-1}}$ *text*” as inter-modal correlation. As for low-level feature, we take 500-dimensional SIFT feature vectors for images and 1000-dimensional tag feature vectors for texts. Besides, we random select 80% of the image-text pairs used for training and 20% for testing to conduct experiments.

4.2 Comparison Methods and Evaluation Metrics

To verify the effectiveness, we compare our method with several state-of-the-art correlation learning methods including both unsupervised and supervised setting.

- (1) Canonical Correlation Analysis (CCA): A traditional unsupervised method maximizes the correlation in the common subspace to learn the correlation matching between two heterogeneous features. Note that there are no obvious semantic meanings in the latent subspace.
- (2) Semantic Matching (SM): This approach is a supervised methods, which learns the correlation though transform the heterogeneous feature to the common semantic subspace. Thus the similarity between two objects can be computed according to the probability belonging to the same class.
- (3) Semantic Correlation Matching (SCM): This approach is also a supervised method, which combines CCA and SM. Firstly, it learns cross-modal correlation through maximize the correlated subspaces, and then logistic regression is performed to get the probability of each object belonging to all the classes. Both correlation analysis and semantic abstract are considered in this method.

In addition, since the dataset is a multi-labeled dataset, we use mean average precision (MAP) to evaluate the retrieval performance which is a rank-based evaluation metric and widely used to multi-label classification. Moreover, precision-recall (PR) curves are also plotted to investigate the performance of different approaches.

4.3 Experimental Result

In this section, we compare the proposed combining link and content correlation (CLCC) approach with several prevailing approaches. Figure 2 shows the MAP performance of different approaches on two different cross-modal retrieval task, i.e. image to text retrieval task and text to image retrieval task. As can be seen that the method of SCM achieves better performance than CCA and SM which both consider correlation matching and semantic matching. It is also clear that our approach significantly outperforms other approaches, demonstrating the effectiveness of proposed approach. It is reasonable because we not only exploit the rich link structure to improve correlation, but also consider semantic projection in the subspace during the training stage. Note that different tasks may have different performance for an approach. While our approach obtains better performance for both retrieval tasks comparing with its several counterparts.

Additionally, further analysis of the results is presented in Fig. 3 in terms of precision-recall curves. Obviously, SCM obtains higher precision than CCA and CM at all levels of recall for text to image retrieval task and almost levels of recall for image to text retrieval task. The same insight can be acquired about the performance improvements. Comparing the PR curves of CLCC with others, we can see that the precision of our method is higher than others at all levels of recall for both forms of cross-modal retrieval.

In short, we can conclude that the semantic correlation can be exploited fully by combining link and content information for cross-modal retrieval.

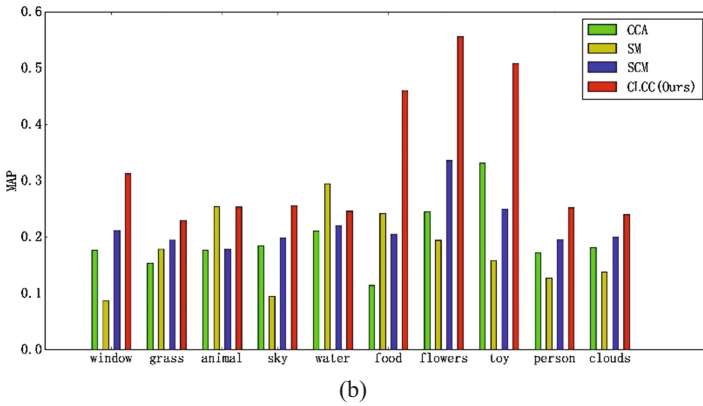
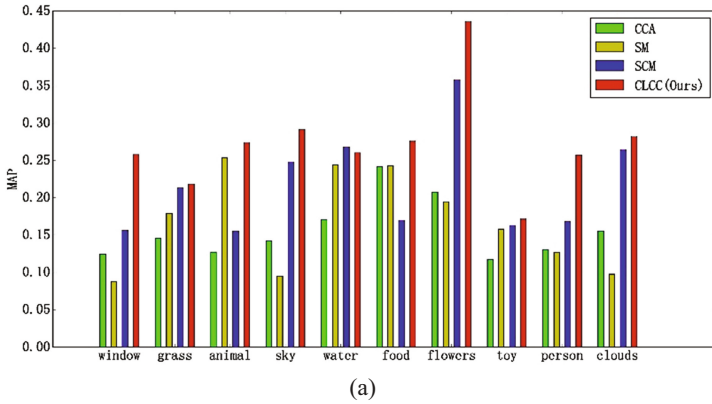


Fig. 2. MAP performance of (a) image to text and (b) text to image retrieval task for each category.

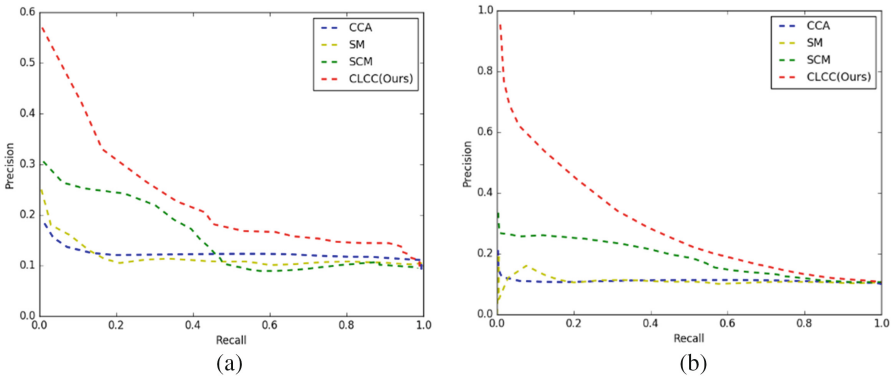


Fig. 3. Precision recall curve of (a) image to text and (b) text to image retrieval task.

5 Conclusion

In this paper, we examined the problem of correlation learning for cross-modal retrieval in heterogeneous social multimedia networks. We have proposed an effective learning approach by combining link and content information into together to improve the performance of semantic correlation in a unified projection subspace. Different from traditional approaches, we integrate rich link structure to obtain accurate and robust representation. Furthermore, there are obvious semantic meanings in the unified space through embedding semantic label information. Extensive experiments have verified the better performance of proposed approach comparing with several prevailing approaches. In the future, we intend to exploit nonlinear projection to obtain unified feature representation.

Acknowledgments. This work is supported by Chinese National Nature Science Foundations (61501050).

References

1. Sang, J., Xu, C., Jain, R.: Social multimedia mining: from special to general. In: IEEE International Symposium on Multimedia, pp. 481–485 (2016)
2. Hardoon, D.R., Szedmak, S., Shawe-Taylor, J.: Canonical correlation analysis: an overview with application to learning methods. *Neural Compute.* **16**(12), 2639–2664 (2004)
3. Li, D., Dimitrova, N., Li, M., Sethi, I.: Multimedia content processing through cross-modal association. In: Proceedings of ACM International Conference on Multimedia, pp. 604–611 (2003)
4. Rasiwasia, N., Pereira, J.C., Coviello, E., Doyle, G., Lanckriet, G., Levy, R., Vasconcelos, N.: A new approach to cross-modal multimedia retrieval. In: Proceedings of the ACM International Conference on Multimedia, pp. 251–260 (2010)
5. Andrew, G., Arora, R., Bilmes, J., Livescu, K.: Deep canonical correlation analysis. In: Proceedings of the 30th International Conference on Machine Learning, pp. 1247–1255 (2013)
6. Rosipal, R., Krämer, N.: Overview and Recent Advances in Partial Least Squares. In: Saunders, C., Grobelnik, M., Gunn, S., Shawe-Taylor, J. (eds.) SLSFS 2005. LNCS, vol. 3940, pp. 34–51. Springer, Heidelberg (2006). https://doi.org/10.1007/11752790_2
7. Huang, L., Peng, Y.: cross-media retrieval by exploiting fine-grained correlation at entity level. *Neurocomputing* **236**, 123–133 (2017)
8. Peng, Y., Zhai, X., Zhao, Y., Huang, X.: Semi-supervised cross-media feature learning with unified patch graph regularization. *IEEE Trans. Circuits Syst. Video Technol.* **26**(3), 583–596 (2016)
9. Jia, Y., Salzmann, M., Darrell, T.: Learning cross-modality similarity for multinomial data. In: Proceedings of the 11th International Conference on Computer Vision, pp. 2407–2414 (2011)
10. Han, X., Thomas, S.: Toward artificial synesthesia: linking images and sounds via words. In: NIPS Workshop on Machine Learning for Next Generation Computer Vision Challenges (2010)
11. Wang, S., Huang, Q.: Research on heterogeneous media analytics: a brief introduction. *J. Integr. Technol.* **4**(2), March 2015

12. Sun, Y., Han, J.: Mining heterogeneous information networks: a structural analysis approach. *SIGKDD Explor.* **14**(2), 20–28 (2012)
13. Jin, X., Luo, J., Yu, J., Wang, G., Joshi, D., Han, J.: Reinforced similarity integration in image-rich information networks. *IEEE Trans. Knowl. Data Eng.* **25**(2), 448–460 (2013)
14. Sun, Y., Han, J., Yan, X., Yu, P., Wu, T.: Pathsim: meta path-based top-k similarity search in heterogeneous information networks. *VLDB* **4**(11), 992–1003 (2011)
15. Wang, K., He, R., Wang, W., Wang, L., Tan, T.: Learning coupled feature spaces for cross-modal matching. In: *IEEE International Conference on Computer Vision*, pp. 2088–2095 (2013)
16. Chua, T., Tang, J., Hong, R., Li, H., Luo, Z., Zheng, Y.: NUS-WIDE: a real-world web image database from National University of Singapore. In: *Proceedings of ACM International Conference Image Video Retrieval*, pp. 1–9 (2009)

The Research on Touch Gestures Interaction Design for Personal Portable Computer

Qing Sheng^{1,2}, Ting Liu^{1,2}, Wenjun Hou^{1,2(✉)}, and Gengyi Wang^{1,2}

¹ School of Digital Media and Design Art, Beijing University of Posts and Telecommunications, Beijing, China

25389640@qq.com, hou1505@163.com

² Network System and Network Culture Key Laboratory of Beijing, Beijing, China

Abstract. This paper studies the gestures interaction of personal portable computer with user defined methods on different operating objects. According to the data analysis on experimental result, we developed a set of gestures for personal portable computer which can meet different users' needs. In accordance with touch gestures, we can divide touch gestures into three categories: basic gestures, symbol gestures and combination gestures. Based on this gestures database, developer and designer can design touch gestures interaction which match the product features quickly and in a reasonable way.

Keywords: Touch gestures · Interaction design · Personal portable computer

1 Related Researches

Touch screen technology has been applied to mobile phones for 16 years and the exploration of touch gesture interaction has always been the focus of researchers. «User-Defined Gestures for Surface Computing» [1] written by Jacob O. Wobbrock etc. defined the commonly used gestures and basic gestures of desktop large screen, deeply discussed the influence of human cognitive behavior on hand gesture interaction. Based on user defined design method in intuitive interaction domain, foreign scholars designed Interactive behaviors on touch screen mobile phone, somatosensory operation device. Besides, there are also many scholars study on the pain point of the touch screen interaction [2–4], such as “click low precision”, “fat finger” and so on. Cedric Foucault et al designed a two-handed interaction model “Spad” [5] to enhance the productivity of tablet, this interactive model adopts non master hand to activate the functional mode and use a tablet application “Spad” interactive control mode cooperate with context components in “Keynote” to complete the same task. By comparing the operations confirmed that “Spad” completes the task more efficiently without increasing the complexity. But “Spad” requires that all tasks be divided into four groups. Each of groups contains three buttons that brings functional limitations.

To draw a conclusion, researchers have proposed their own design methods and solutions to the pain points of mobile phone touch screen gesture interaction. However, there is no research on the design of large screen personal portable computer to provide a unified guidance for personal portable computer touch screen gesture interaction.

2 Experimental Study

2.1 Experimental Subject

We invited 12 college students to participate in the experiment, all of them were graduate students, among them, 5 were female, and the others are male. Their age ranged from 20–25. In the formal experiment, there were no long time intense hand movements. All of them had used touch screen equipment in the past and are familiar with the touch operation. The subjects had 3 min to know the page layout and basic operations before task.

2.2 Experimental Task

The experiment presented three kinds of common operation tasks, which were the basic operation, the shape operation and the text operation while different target tasks had different pre conditions. In order to facilitate the experiment, the extracted tasks were divided into three usage scenarios. In order to avoid the contextual effects caused by different tasks, we arranged the sequence of the task process. This also could avoid interrupting some continuous operation tasks, such as Copy and Paste task (Table 1).

2.3 Experimental Equipment

The device used in the experiment were iPad Pro (12.9 in.), the operating system platform was IOS10.0, having smart keyboard.

2.4 Experimental Process

Subjects had 3 min to get familiar with the layout of the user interface. In the formal experiment. The task interface in the scene has prompt message which didn't contain the contents of the gestures. Subjects needed to define gestures themselves to complete the corresponding task. In the experiment, sounding thinking was adopted, the subjects need to inform the main reason of some gestures. After each task, the subjects were asked to score the subjective perceptions of gestures, including the matching degree between the gestures and target task, the accessibility of operations etc.

2.5 Data Treating

564 motion data were recorded in the experiment. Based on the data, we summarized the frequency, the predictability, the consistency and the subjective evaluation of the gestures.

2.5.1 Frequency

Select the most frequent gestures as standard of experiment task and remove the gestures in poor consistency, we achieved the target collection of gesture. The corresponding gestures and their frequency are shown in below tables (Tables 2, 3 and 4).

Table 1. Experimental task operation

	Situation 1	Situation 2	Situation 3
Pre condition	None	Select single, multiple, all shapes	Select textbox
	Create Slide	Copy shape	Active edit status
Experimental task	Create slide with the same format	Paste shape to the specified location	Move cursor position
	Create new position to new slide	Shear shape	Select word
	Create a copy for the slide	Delete shape	Select phrase
	Copy slide to the specified location	Get into the state of editing	Select line text
	Move slide	Rotate shape	Choose the sentence
	Switch to browse view	Change size	Select whole segment
	Switch to normal view	Modify fill color	Copy
	Previous one	Modify border color	Paste
	Next one	Modify border's type of line	Shear
		Combination	
	Play slide in current position		Delete
	End playing slide	Cancel combination	Align (left, middle, right, both sides)
	Play slide from beginning	Revision level	Change font
	Delete slide		
	Revoke		
	Redo		
	Zoom in this slide		
	Zoom out this slide		
	Check page object hierarchy		

Table 2. Basic operation gestures



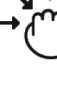





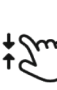










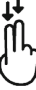


Task	Gestures	Operating mode	Frequency
Building a new default format slide		Double-click the blank area	4
Specified location building a new default format slide		Double-click the interval area	5
Move the slide		Press and hold to drag	10
Switch to the slide show view		Five fingers grasping	4
On one piece		underscore	9
The next		On the cross	9
The slide start playing from the current position		Double-click	5
Exit the slides		Double-click	5
Delete the slides		Hold and slip out of the screen	5
Back out		Counterclockwise	7
Reform		Clockwise	7
Zoom in slide on this page		Expand	11
Zoom out slides on this page		Shrink	11

Table 3. Shape operation gestures

Pre condition	Task	Gestures	Operating mode	Frequency
-	Access edit text state		Double-click	7
	Delete		Hold and slip out the screen	7
Multiple choice	Rotating		Compatible with three kinds of rotation	7
	Zoom in shape		Two fingers extended	8
	Reduce the shape		Two fingers pinched	8
-	Copy		Two fingers drag into the clipboard	-
Multiple/all	Cut		One finger into the clipboard	-
-	Paste		One finger drag the clipboard	-

Due to the current page layout will be trimmed by the more frequent task like copy, cut and paste, the page layout framework will have an impact on the process of user defined gestures, therefore, the final data of these three tasks are eliminated in the data statistics.








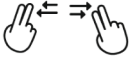



2.5.2 Predictability

Through gestures set and the frequency of each gesture, the Predictability of the gestures set can be calculated:

$$G = \frac{\sum_{s \in S} |P_s|}{|P|} \cdot 100\%$$

In the formula: G stands for Predictability, P represents the total number of actions defined by the user in task, P_s represents the number set of “S”. s is a subset of S, the predictable sequence of tasks is shown in the following figure (Fig. 1).

Table 4. Text operation gestures

Cursor calibration	Choice	Task	Gesture	Operating mode	Frequency
		delete		Hold and slip out the screen	5
		Zoom in the words		Two fingers extended	7
		Zoom out text		Two fingers pinched	7
		Alignment		Drag and drop two points to target alignment direction	5
		Copy		Two fingers drag into the clipboard	-
		Cut		One finger drag into clipboard	-
		Paste		One finger drag out of clipboard	-

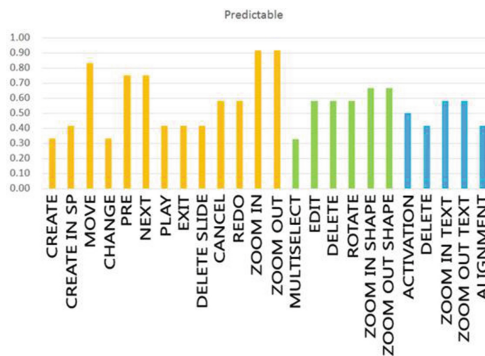


Fig. 1. Predictable sequence of gestures for each task

2.5.3 Uniformity

After calculating the predictable nature of gesture set, the consistency of gesture set can be calculated.

$$A = \frac{\sum_{r \in R} \sum_{P_i \subseteq P_r} \left(\frac{|P_i|}{|P_r|} \right)^2}{|R|} \cdot 100\%$$

In this formula: A indicates consistency score, R represents the total number of actions for the target task defined by the user, r is a character for the target mission R, P represents the total number of actions for a task R, P_i is a subset of P_r that represents the number of an actions (Fig. 2).

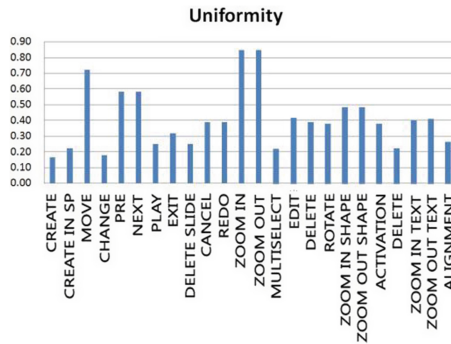


Fig. 2. Sequence of gestures for each task

2.5.4 User’s Subjective Evaluation

From the following table, we can see the matching degree and accessibility scores. Creating a new slide, moving the slide, switching the slide, deleting the slide, slide zoom, activating text edition, shape zoom got higher scores, indicating the task operations in the gesture set are easily understood and implemented by the user at the cognitive level. While switching the slide and playing the slides are easy to implement, but the matching degree is low. Through the interviews we know that this is because the subjects afraid to conflict with the operating system in the process of defining the gesture, so that the results were also affected (Fig. 3).

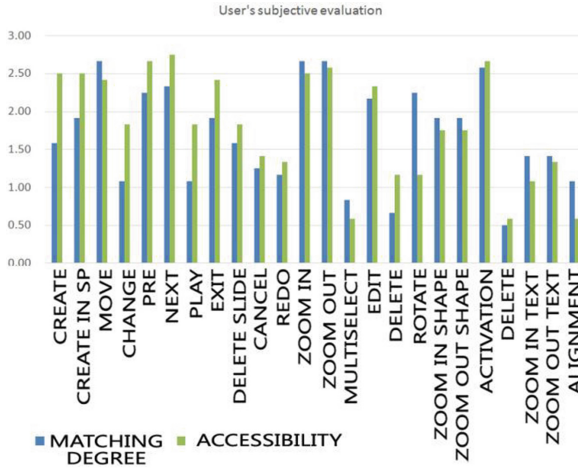


Fig. 3. User's subjective evaluation of each task

3 Personal Portable Device Resture Ttype

By summarizing the experimental data further, generally, the gestures can be used in personal portable computer are divided into: basic gestures, symbol gestures, combined gestures.

3.1 Basic Gestures

Basic gestures including: click, press, swipe, drag, zoom, rotates, complete the functional operation of common application, such gestures are versatile (Table 5).

3.2 Basic Gestures

Symbolic gestures follow the user's daily life and graphical interface experience, continue to use the book written symbols or icon that from graphical user interface to the touch screen interface. For example, most users use the counterclockwise circle shape to represent revoking, the symbol is similar to the revoke icon in the graphical interface, and counterclockwise circle also gives the user a psychological hint of time reversal. In this way, you can extend the other gesture definitions of other functions, such as text bold, tilted, underlined function can be expressed through the gesture to draw the graphics that similar to the icon, for example, using "B", "I", "U" to manipulate text attributes. Symbolic gestures rely on the user's experience in the daily life and graphical interface experience, the symbol that can be used is limited, and its scalability is relatively low (Fig. 4).

Table 5. Symbolic gestures

	Main screen	In list	Thumbnail	Detailed view	Control	Text editing	Picture editing	Shape editing	Form	
Click	Open / Adjust the corresponding item	Adjust the corresponding item / Stop the sliding item			Active control function	Move cursor position	Select			
Double click	—	—	—	Scale / Switch view	—	Intelligent phrase selection	Select	Enter input status		
Triple click	—	—	—	—	—	Select whole segment	—	—	—	
Long press	Active application editing	Corresponding items get into edit status, Activate hidden functions			—	Activate hidden functions				
Single finger drag	Mobile shortcut location	Move project location /Delete		Delete	—	Move cursor position like fisheye / Delete	Move position/Delete			
Double finger drag						copy		copy		
Horizontal sliding	Switch main screen	Transfer delete	Switch to another sibling page	Horizontal movement / Switch to another	Operation control	—	—	—	—	
Vertical slip	Open Notification bar / toolbar	Vertical moving to certain page		Vertical moving /Switch to another sibling page	Operation control	—	—	—	—	
Four finger slip	Switching application / View the background running APP									
Zoom	—	—	Return to previous level	Two finger retraction Three or four finger switch view	—	Scale			—	
Five finger zoom	Close the application back to the main screen									
Rotate	—	—	—	Rotate the picture	—	Rotate			—	

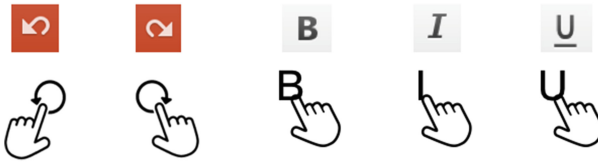


Fig. 4. Symbolic gesture manipulation

3.3 Combination Gestures

Combination gestures refer to the simultaneous completion of gestures through two hands or the completion of two different types of gestures in one hand, including three types of gestures: hands combination of homogeneous anisotropy gestures, hands combination of heterogeneous gestures, and one hand heterogeneous combination gestures.

3.3.1 Hands Combination of Homogeneous Anisotropy Gestures

Hands input requires the user to interact with hands of a high degree of coordination, coherence, avoiding the challenge of “Draw a circle with one hand, and draw a square with the other”. On the other hand, the input of both hands requires a high degree of concentration of the user, if the task is too complicated that the cognitive burden in the implementation of the task will be increased. So in most cases, the hands interactive gestures are mostly through the hands to complete the anisotropy homogeneous gesture operation, such as the “rotation” “text center alignment” “text on both sides of the alignment” etc.

3.3.2 Hands Heterogeneous Combinations

Hands heterogeneous combinations refer to the completion of static gestures by one hand, the completion of dynamic gestures by the other hand. Guiard believes that the operating mechanism of both hands is based on the co-operation and asymmetry of both hands [6]. The movement of the non-conventional hand is more granular than that of the conventional hand. Therefore, the non-conventional hand can be used to activate the operation mode of some function and the master hand can be used to operation or do some fine adjustment. In the experiment, users complete the multi-election operation through the “one finger long press, one finger click” or “one finger long press, one finger drag”, complete the “shape rotation” operation through “one finger hold the shape, one finger rotate the shape”. Such gestures increase the user’s ability to activate the gesture memory of the functional modifiers for non-master controls, but can improve the operational performance of the expert user.

3.3.3 One Hand Heterogeneous Combination

One hand heterogeneous combination refers to a group of different combinations of gestures that completed by one hand, such as the continuous touch gestures that Google created for Android device. In Google’s gestures, users are allowed to draw the letters “g” and circle the target search term continuous, or cover the target search with the combination shape of “g” and “o”, you can search for the target vocabulary quickly.

4 Conclusion

At present, as a “productivity tool”, large-screen personal portable computer has not yet formed a complete and systematic touch-screen operation model in the people’s understanding. We applied the method put forward by Wobbrock and others in the personal portable computer gestures interactive design, summarized a set of gesture set that for different operators of the personal portable computer. We also divided the personal portable computer gestures are into three categories of basic gestures, symbol gestures, and combined gestures in accordance with the gesture operation model, and summed up the specialty of three types of gestures. Based on this gesture set, it is convenient for the personal portable computer designers to build gestures that conform to the user’s mental model, and giving the user a more natural and intuitive interaction experience.

References

1. Wobbrock, O., Morris, M.R., Wilson, A.D.: User-defined gestures for surface computing. In: Proceedings of CHI, no. 9, p. 183 (2009)
2. Wobbrock, O.: Maximizing the guessability of symbolic input. In: CHI Extended Abstracts, no. 5, pp. 69–72 (2005)
3. Ruiz, J., Li, Y., Lank, E.: User-defined motion gestures for mobile interaction. In: Proceedings of the SIGCHI Conference on Human Factors in Computing Systems, Vancouver. ACM (2011)
4. Abadi, H.G.N., Peng, L.Y., Zadeh, A.M.H.: Guessability study on considering cultural values in gesture design for different user interfaces. In: International Proceedings of Economics Development & Research, no. 4, pp. 76–80 (2012)
5. Foucault, C.: Spad:a bimanual interaction technique for productivity applications on multi-touch tablets. In: CHI, no. 4, pp. 1879–1884 (2014)
6. Guiard, Y.: Asymmetric division of labor in human skilled bimanual action: The kinematic chain as a model. *J. Motor Behav.* **19**(4), 486–517 (1987)

Research on Mobile User Dynamic Trust Model Based on Mobile Agent System

Weijin Jiang^{1,2,3} and Yuhui Xu¹(✉)

¹ School of Computer and Information Engineering,
Hunan University of Commerce, Changsha 410205, China
nudtjwj@163.com, 363168449@qq.com

² Electronic Information Engineering Department, Changsha Normal University,
Changsha 410100, China

³ School of Computer Science and Technology,
Wuhan University of Technology, Wuhan, China

Abstract. For mobile Internet people's personalized service needs, how to move from the vast number of mobile information in real time, accurate access to mobile users really interested in the content. In order to obtain more accurate mobile user's preferences to meet the requirements of personalized services, this paper propose a new mobile user's preference prediction method based on trust and link prediction by analyzing the mobile user behavior. Firstly, this paper propose a method to calculate the trust of mobile users by analyzing the behavior of mobile users; Then according to the similarity of the mobile user's trust and the mobile user's score, the approximate neighbor of the mobile user is selected; we use the link prediction method to calculate the correlation between mobile users and mobile network services and determine mobile network services that needed predict; Finally, we use this method to predict the user's preference. The research shows that the prediction accuracy of this method is better than traditional method of Collaborative Filtering recommendation, which solves the sparsity problem to some extent.

Keywords: User's personality feature · Mobile agent system
Collaborative Filtering (CF) · Trustworthiness · Mobile internet

1 Introduction

Due to the rapid development of mobile communication technology and intelligent mobile devices, mobile phones have become one of the main platforms for people to obtain information. With the development of multimedia technology and mobile information loading, mobile transmission capability, mobile e-commerce and mobile Internet Service Mall is also more people to use, but the huge mobile network service information for mobile users has brought serious overload problems of mobile information. Therefore, how to get the real interest of mobile users in real-time and accuracy from mobile information has become a difficult problem to be solved in personalized mobile network service [1, 2]. Among the many methods for predicting user preferences, the collaborative filtering algorithm is the most classic and the most widely used.

However, when user preference prediction is carried out by using the traditional collaborative filtering method, the prediction accuracy of the user preference is relatively low due to the sparsity problem. At the same time, due to the limited input and output capability of mobile phones and the characteristics of mobile user's real-time access to information, mobile network users have higher demand on mobile users' forecasting accuracy [3]. Traditional user preference forecasting methods are not suitable for personalized mobile network service system.

The basic idea of collaborative filtering is to find the nearest neighbor of the target user by calculating the similarity between the users and then to predict the interest preference of the target user by the nearest interest preference of the neighbor. However, with the expansion of data size, data sparsity problems gradually appear, it leads to algorithm efficiency and accuracy reducing. Some scholars mitigate this problem by integrating trust relationships between users into traditional collaborative filtering. In literature [4], the trust relationship between mobile users is calculated by the mobile user's explicit score. However, in the mobile communication network, because the mobile phone's input and output capability is limited, the explicit evaluation information between mobile users is relatively small, Generally, we use the implicit calculation method to obtain the trust relationship among mobile users. In literature [2], for the characteristics of mobile communication networks, the trust relationship between mobile users is introduced into the traditional collaborative filtering, and the trust relationship between mobile users is analyzed by analyzing the communication behavior between mobile users and gives a linear calculation method to calculate the trust of mobile users. In literature [5], it describes an e-mail-based social network computing method, which analyzes the communication behavior between users to build a social network, and through experiments to prove that based on the logarithm function to calculate the user trust relationship is more accurate than that through the linear function [6].

In addition, some researchers solve the sparsity problem from another aspect. In literature [7], it propose a collaborative filtering improvement method based on link prediction, which builds a network model that connects users and project nodes and by analyzing the relation between the user and the project can effectively reduce the sparsity problem existing in the traditional collaborative filtering. In the traditional link prediction method, node only represents the user/project, edge only represents the relationship between the user/project, and the literature [7] improved the traditional link prediction methods, nodes in the network represent users and items, and edges represent relationships between the user and the project. Although the literature [7] reduces the sparsity problem of collaborative filtering through link prediction, it does not consider the impact of trust on mobile user preference prediction for the characteristics of mobile communication network.

In this paper, we analyze the mobile user behavior to calculate the trust degree between mobile users and select the approximate neighbor of the target user by combining with the similarity of the mobile user's preference; Then, the improved link prediction method is used to calculate the correlation information between the mobile user and the mobile network service, and the mobile network service which the target user is most likely to use is determined according to the calculated correlation; Finally,

based on the above research, a mobile user preference prediction method based on trust and link prediction is proposed.

2 Mobile User Preference Prediction Model

In order to improve the accuracy of mobile user preference forecasting, this paper introduces the trust degree between mobile users and the correlation between mobile user-mobile network services into the mobile user preference prediction model [8].

2.1 Data Model

There are a large number of user communication and interactive information in the mobile communication network, mainly including the communication records such as voice communication, short message, flying letter and some evaluation information of the mobile network service by the mobile users. In this paper, we build the data model based on these data, including four data set [8]:

- (1) Mobile user Set: $U = \{u_i | i \in [1, N]\}$, in this collection N is the number of mobile subscribers
- (2) Mobile Web Services Set [9]: $S = \{s_j | j \in [1, M]\}$, The mobile network service includes basic communication service and value-added service, such as downloading software, browsing web page, e-commerce, receiving and sending mail, customizing service. M denotes the number of mobile network services.
- (3) Mobile subscriber service network [10]: The evaluation behavior of the mobile user in the set U to the mobile network service in the set S is denoted by $G_{us} < V_{us}, E_{us} >$, V_{us} represents the set of mobile users and the set of all mobile network services that need to be processed, the edge $e < u, s > \in E_{us}$ denotes the mobile network service s used by the mobile user u . For the weights $w < u, s >$ between the edges, it is the rating of the mobile user u for the mobile network service s . The mobile users 'rating of mobile network services is extracted from the feedback, evaluation and other records of the mobile services used by the mobile users, and combined with the mobile user's usage of the related mobile services.
- (4) Mobile users trust network [11]: The trust relationship between mobile users in the set U is expressed by $G_{uu} < V_{uu}, E_{uu} >$, Which V_{uu} denotes a set of all mobile communication network users, $e < u_i, u_j > \in E_{uu}$, indicating that there is a trust relationship between the mobile users u_i and u_j . For the weight $w < u_i, u_j >$ between the edge and the edge, it represents the trust degree of the mobile user u_i to the mobile user u_j . The trust degree between the mobile users is obtained by analyzing the communication behavior among the mobile users. If there are more connections between mobile users u_i and u_j , the trust between mobile users u_i and u_j is high, and on the contrary, is relatively low.

2.2 Mobile User Trust Calculation

Combining the characteristics of mobile communication behavior and the transitivity of trust, this paper defines direct trust and indirect trust as follows:

Definition 1 (direct trust): If there is communication between mobile users, and trust is greater than the set threshold λ , then there is a direct trust relationship between mobile users.

Definition 2 (indirect trust): If there is no direct trust relationship between mobile users, but there is a common trust neighbor, then there is an indirect trust relationship between users.

The calculation procedure of trust among mobile users in mobile communication network is as follows:

- (1) Preprocessing mobile user communication behavior, deleting incomplete data and noise data;
- (2) According to the communication behavior between mobile users, the initial mobile user trust network $G_{uu1} < V, E >$ is constructed, that is, if there is a call or text message between the mobile user u_i and u_j , u_i and u_j are connected. Because the degree of trust between users is asymmetric, so $G_{uu1} < V, E >$ is a directed weighted graph [11].
- (3) Calculate the direct trust between mobile users: With the increase of the amount of traffic, the trust degree between the mobile users tends to be stable with the increase of the amount of traffic, which is consistent with the theory of marginal utility decreasing. Therefore, this paper uses logarithmic function to express the relationship between the them. For example, the mobile user u_i , in his communication record is mainly for text messages and call information statistics. First, the total number of statistical messages p and the number of messages p_{u_j} corresponding to the mobile user u_j serving as the receiving party are counted, and then the total time q of the user u_i is counted, the total number of calls r and the mobile user u_j serving as the called party and the total time q_{u_j} , the total number of calls r_{u_j} . Define $T(u_i, u_j)$ as the trust of u_i for mobile user u_j , define $T(m_{u_j}, m)$ as u_i or u_j trust in a communication behavior. In it, $m_{u_j} \in \{p_{u_j}, q_{u_j}, r_{u_j}\}$, and $m \in \{p, q, r\}$, so $T(m_{u_j}, m)$ can be expressed as

$$T(m_{u_j}, m) = \frac{2(1 - 1/\ln m_{u_j})(1 - 1/\ln(m - m_j))}{2 - 1/\ln m_{u_j} - 1/\ln(m - m_{u_j})} \tag{1}$$

- (4) The direct trust between mobile users can be expressed as

$$T(u, u_j) = \frac{T(p_{u_j}, p) + T(q_{u_j}, q) + T(r_{u_j}, r)}{3} \tag{2}$$

So, In $G_{uu1} < V, E >$, The weight between $e < u_i, u_j >$ is $T(u_i, u_j)$;

- (5) Each user node in U repeat (3) to form $G_{uu2} < V, E >$;
- (6) Calculate the indirect trust between mobile users. In the Mole Trust algorithm proposed in document [8], we introduce the attenuation factor into the trust calculation, and think that the trust degree is declining in the transmission process. According to Definition 2, when calculating the indirect trust degree, because there may be multiple co-trust neighbors between the two mobile user nodes, the indirect trust degree can be calculated by the method of trust synthesis [12]. Let the confidence factor in the transmission process is D , taking the mobile user nodes u_i and u_k as an example, if the node u_j is the common trust neighbor, the indirect trust degree of u_i through u_j and node u_k can be expressed as

$$T_j(u_i, u_k) = D \times \text{Min}(T(u_i, u_j), T(u_j, u_k)) \tag{3}$$

For each of the mobile users u_i and u_k , the trust neighbor u_j calculates $T_j(u_i, u_k)$, and finally obtains the indirect trust degree of u_i and u_k . The formula can be expressed as

$$T(u_i, u_k) = \sum_j^L T_j(u_i, u_k) / L \tag{4}$$

Where L represents the total number of mobile users u_i and u_k common trust neighbors.

- (7) For each pair of mobile user nodes satisfying Definition 2 for $G_{uu2} < V, E >$ carried out (5), forming a complete mobile user trust network $G_{uu3} < V, E >$.

2.3 User - Service Dependency Calculations Based on Link Forecasting

Traditional collaborative filtering mainly predicts user preferences by calculating the similarity between users or between projects, and less consideration of the relationship between users and projects. In document [7], the data model established by link prediction shows the relationship between the two, and the improved link prediction method is given. Jaccard's Coefficient is one of the commonly used methods in link prediction [7], but this method does not apply to the calculation of user-service relevance in link forecasting model, so this paper redefines it and gives the user-service correlation calculation formula

$$\text{corr}(u, s) = \frac{|\Gamma(u) \cap \bar{\Gamma}(s)|}{|\Gamma(u) \cup \bar{\Gamma}(s)|} \tag{5}$$

where $\Gamma(u)$ represents the set of neighbor nodes of node u , $\Gamma(s)$ represents the set of neighbor nodes of node s and $\bar{\Gamma}(s) = \bigcup_{c \in \Gamma(s)} \Gamma(c)$.

2.4 Mobile User Similarity Calculation

In this paper, the Pearson correlation coefficient is used to calculate the similarity between mobile users [13]. The formula is expressed as

$$\text{sim}(u_i, u_j) = \begin{cases} \frac{\sum_{s \in Su_i u_j} (r_{u_i, s} - \bar{r}_{u_i})(r_{u_j, s} - \bar{r}_{u_j})}{\sqrt{\sum_{s \in Su_i u_j} (r_{u_i, s} - \bar{r}_{u_i})^2 \times \sum_{s \in Su_i u_j} (r_{u_j, s} - \bar{r}_{u_j})^2}}, & |Su_i u_j| \geq t \times \min(|Su_i|, |Su_j|) \\ 0, & |Su_i u_j| < t \times \min(|Su_i|, |Su_j|) \end{cases} \quad (6)$$

Where Su_i and Su_j represent the scoring service set of mobile users u_i and u_j respectively, $Su_i u_j$ represents the service set, $r_{u_i, s}$ and $r_{u_j, s}$ of the common score of mobile user u_i and u_j , respectively represent the score of mobile user u_i and u_j to the service, \bar{r}_{u_i} represents the average score of the mobile user u_i for the rating service.

2.5 Mobile User Preference Prediction

In order to improve the prediction result of mobile user preference [8, 11], this paper improves the traditional collaborative filtering method because of the low accuracy and sparseness of traditional collaborative filtering technology. In the approximate neighbor search target user, fusion as approximate neighbor weights will move the similarity between trust and mobile user preferences between users; and then through the link prediction method to determine the mobile network services for mobile users are most likely to use; finally improved by preference prediction formula to predict the mobile user preferences. Specific methods are as follows:

(1) Determine the approximate neighbor set of the mobile user

In the process of mobile user preference prediction, this paper not only considers the impact of similarity between mobile user preferences on forecasting results, but also considers the impact of mobile users' trust on mobile user preferences and the harmonic neighbor is used to select the approximate neighbor set of the target user. Reconciliation weights are determined by the degree of similarity of scoring and the degree of trust of the user. When the trust between mobile users is relatively large (for example, mobile users u_i and mobile users u_j is a good friend), the trust of the weight value is relatively large; When the trust between mobile users is relatively small (for example, mobile users u_i and mobile users u_j is strangers), the similarity of the weight value is relatively large. So the formula for the harmonic weight is expressed as

$$W(u_i, u_j) = \begin{cases} \alpha_1 \text{sim}(u_i, u_j) + \beta_1 T(u_i, u_j), & T(u_i, u_j) \geq \lambda \\ \alpha_2 \text{sim}(u_i, u_j) + \beta_2 T(u_i, u_j), & T(u_i, u_j) < \lambda \end{cases} \quad (7)$$

Where $W(u_i, u_j)$ represents the harmonic weight of the mobile user u_i and the mobile user u_j ; $\text{sim}(u_i, u_j)$ represents the similarity degree of the mobile user u_i and the mobile user u_j ; $T(u_i, u_j)$ represents the trust of the mobile user u_i and the mobile user u_j , $\alpha_1, \alpha_2, \beta_1, \beta_2$ are the harmonic factors, and $\alpha_1 + \beta_1 = 1, \alpha_2 + \beta_2 = 1, \lambda$ is the trust threshold.

When determining the approximate neighbor set of mobile users, the approximate neighbor of $t\%$ is selected as the approximate neighbor set of the target user. When $t = 0$, the approximate neighbor set is empty set, $t = 100$, then the approximate neighbor set includes all the mobile users in the data set, so we cannot get the desired

result when the value of t is too small or too large. In this paper, according to a number of experimental results to select a reasonable value of t .

(2) Identify the target mobile network service set that needs to be predicted

According to literature [14], the higher the correlation between the mobile user and the mobile network service, the greater the possibility that the mobile user will use the corresponding mobile network service in the future. Therefore, when determining the target mobile network service set that needs to be predicted, selecting the relevance of the former $h\%$ of the mobile network services as the target user is most likely to use a collection of mobile network services.

(3) Predict mobile user preferences

Combining the harmonic weight with the traditional preference prediction formula, the weighted average forecast formula [15] is

$$r_{u_i,s} = \bar{r}_{u_i} + k \sum_{\substack{u_j \in N_{u_i} \\ s \in S_{u_i}}} (W(u_i, s, u_j) \times (r_{u_j,s} - \bar{r}_{u_j})) \quad (8)$$

Where N_{u_i} is the nearest neighbor node set for mobile user u_i , S_{u_i} is the set of mobile network services needed for mobile user u_i , k is a normalization factor $k = 1 / \sum_{\substack{u_j \in N_{u_i} \\ s \in S_{u_i}}} 6W(u_i, s, u_j)$.

3 Experiment and Analysis

3.1 Introduction to Data Sets

In order to verify the feasibility and validity of the proposed method in the mobile network service environment, the experimental data were validated by two data sets. One is the MIT data set based on mobile communication behavior provided by Massachusetts Institute of Technology (MIT); One is publicly available for movie score data sets Filmtipset. The disadvantage of the MIT dataset is that the number of mobile users is relatively small. The number of mobile network services is relatively small. Therefore, in order to further verify the validity of the method, the filmtipset dataset is used to verify. Although the Filmtipset data set is not for the mobile network to collect, but the data set contains a user score for the project as well as the user's social relationship, so you can verify the validity of the method in a certain extent

- (1) The MIT data set [16] is public data provided by the Massachusetts Institute of Technology media lab set, the data set is a collection of 94 mobile users, mobile user behavior information from September 2004 to June 2005 a total of 9 months, including mobile communication and mobile Internet services using mobile users, mobile context information related to the user's friends and relations.
- (2) Filmtipset [17] is Switzerland's largest film recommendation community, which has more than 80000 registered users and more than twenty million movie rating

data. The Filmtipset community not only provides the relevant scoring information based on user records, but also includes the social relations between users. In this paper, we randomly selected 500 of the users and these users to make the evaluation of the 1000 films for the experiment.

Since the MIT data set does not include the user’s evaluation of the mobile network service, the data set is processed as follows before the experiment: By using the behavior of the mobile service for all users in the nine months, the user’s preference for the mobile service is sorted in the order of time, and the user’s preference information is quantized in the form of scores (1 to 10).

During the experiment, the two data sets are processed in the same way, each data set is divided into five groups randomly, each group is divided into two parts, one is the training set, the other is the test set, which training set accounts for 80% of each group of data, test set accounted for 20%.

3.2 Evaluation Standard

In this paper, Mean Absolute Error (MAE) [3] and F measure [18] were used as the evaluation criteria.

The MAE measures the accuracy of the forecast by calculating the deviation between the predicted user score and the actual user score. The smaller the MAE value, the higher the accuracy of the prediction. Assume that the predicted score set is represented as $\{p_1, p_2, \dots, p_n\}$, The corresponding actual score set is expressed as $\{q_1, q_2, \dots, q_n\}$, MAE is defined as

$$MAE = \sum_{i=1}^n |p_i - q_i|/n \tag{9}$$

The F indicator is a comprehensive assessment of the accuracy and recall rate, The higher the F index is, the higher the accuracy is, In this paper, according to the experimental results evaluation criteria for the precision and recall rate is redefined as follows:

$$P(u) = (u \text{ number of trusted users})/(u \text{ the number of contacts}) \tag{10}$$

$$R(u) = (u \text{ number of trusted users})/(u \text{ the number of good friends}) \tag{11}$$

among them $u \in U$, F index:

$$F(u) = (2 \times P(u) \times R(u))/(P(u) + R(u)) \tag{12}$$

3.3 Analysis of Experimental Results

(1) Comparison of the accuracy of trust and trust threshold selection

This experiment is carried out on the MIT data set, this paper mainly compares the accuracy of the trust degree calculated by the logarithm function and the degree of trust

based on the linear function. The range of the indirect trust attenuation factor D is set to [0.5, 1.0), the step size is 0.05, according to the experimental results, the D is set to 0.55. The threshold value of the confidence threshold is set to [0.1,0.9] and the step length is 0.1. The experimental results are shown in Fig. 1. You can see from Fig. 1, based on the logarithmic function of trust calculation method is superior to linear function calculation method based on trust, this is because between user preference and traffic with diminishing marginal utility theory, the logarithmic function can better reflect the relationship between them.

You can see from Fig. 1, the F index is less than 0.6 in a general increasing trend, in the case of more than 0.6 overall decreasing trend, this is because when a value is small, too many users trust, when is large, remove too much trust users, both caused a decline in trust the degree of accuracy. The results show that when the threshold of trust is 0.6, the F index is larger. In this paper, the trust threshold is set to 0.6.

(2) Harmonic weighting parameter selection experiment

This paper makes use of genetic algorithm in Matlab (Genetic Algorithm GA) toolbox respectively on the two datasets, the parameter α_1 and β_1 and α_2 and beta β_2 tuning experiments. The fitness function of genetic algorithm is defined as follows:

$$\zeta_{MRE} = \left(\sum_{i=1}^n \frac{|p_i - q_i|}{q_i} \right) / n \tag{13}$$

In this paper, the range of the harmonic eights α_1 and α_2 in the Eq. (7) is set to $\alpha_1 \in (0,1)$ and $\alpha_2 \in (0,1)$, while $\beta_1 = 1 - \alpha_1$ and $\beta_2 = 1 - \alpha_2$. The optimal parameter values obtained by genetic algorithm optimization are shown in Table 1.

Table 1. Tuning parameter values

Parameter name	MIT data set	Filmtipset data set
α_1	0.42	0.38
β_1	0.58	0.62
α_2	0.71	0.67
β_2	0.29	0.33

From the experimental results, we can see that in determining the mobile user approximate neighbors, if the trust is greater than a given threshold, the trust plays a major role. If the degree of trust is less than a given threshold, the score similarity plays a major role. This is because people are always more trusted about the more familiar people, and their preferences are more likely to be affected by the surrounding people (such as family, friends, etc.), and for relatively unfamiliar people, their preferences are primarily influenced by user preferences that are similar to their ratings. When the trust is greater than a given threshold, mobile users are more likely to be family members, friends, etc., and trust is less than a given threshold, the mobile users are more likely to be strangers [19, 20].

(3) Preference prediction experiment based on public data set

In this study, the following 3 methods were used to predict the user's preference in the two data sets: Tradition Collaborative Filtering, TCF; Preference Prediction based on UserTrust, PPUT (i.e., only the use of (1) and (3) in Sect. 2.5, the method of using link prediction) and Preference Prediction based on User Trust and Link Prediction, PPUTLP (The method proposed in this paper). Experimental results shown in Figs. 2 and 3, according to a number of experimental results, select $t = 25$.

As can be seen from Figs. 2 and 3:

- (1) For the MIT dataset, the PPUTLP method has the highest accuracy when $t = 15$; for the Filmtipset dataset, when $t = 25$, the PPUTLP method has the highest accuracy. This is because when the value of T is too small, the user's data is deleted too much. When the value of T is too large, it contains too much noise data. In these two cases, the accuracy of prediction is reduced. In addition, for different data sets, the proportion of the approximate neighbors is not the same, we need to select the size of the approximate neighbor data set according to the specific circumstances of the experimental data set.
- (2) For the two data sets, compared with the TCF and PPUT methods, the PPUTLP method has a lower MAE value in the case of different neighbors. This is because the user's preference is not only related to the similarity of the score, but also by the surrounding people (such as family, friends, etc.), The TCF method does not consider the trust relationship between users when determining the user's approximate neighbors, but only considers the similarity of the scores. PPUT method in determining the approximate neighbor users, not only consider the similarity score effect on user preference, also consider the surrounding personnel (such as family, friends etc.) impact on user preferences, so the prediction accuracy of PPUT method is better than that of TCF method. PPUTLP method on the basis of PPUT method, first through the link prediction to select the user may use the project, to a certain extent, ease the sparsity problem, so PPUTLP method is better than the PPUT prediction method.
- (3) On the MIT dataset, the PPUTLP method has an average improvement of 8.4% on the MAE compared to the TCF method. Compared with the PPUT method, the PPUTLP method has an average improvement of 3.12% on the MAE [21]. On the Filmtipset dataset, the PPUTLP method has an average improvement of 4.03% on the MAE compared to the TCF method. Compared with the PPUT method, the PPUTLP method has an average improvement of 1.94% on the MAE. The prediction accuracy of MIT data set is generally larger than increase based on the Filmtipset data set based on this is because of the unique characteristics of mobile network, according to the communication behavior of mobile users to obtain more reliable than the Internet in social relations, so the trust relationship between users get more credible, the prediction accuracy is better user preference.

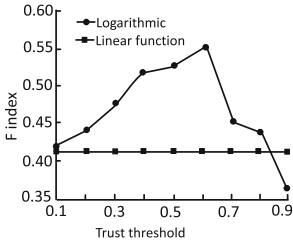


Fig. 1. Comparison of the accuracy of trust based on the MIT data set

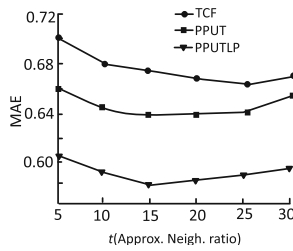


Fig. 2. Comparison results based on MIT datasets

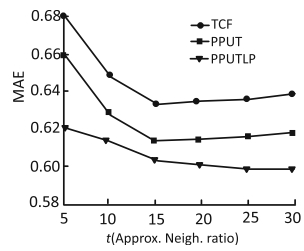


Fig. 3. Comparison results based on the Filmtipset dataset

4 Conclusion

Based on the characteristics of mobile communication network, this paper proposes a mobile user preference prediction method based on trust and link prediction. By analyzing the potential social relations in mobile communication networks, the trust between mobile users is calculated, and the relevance information between mobile users and mobile network services is explored by using link forecasting technology, finally, the mobile user preference is predicted by the mobile user rating similarity. The experimental results verify the feasibility of the proposed method in mobile user preference prediction. The method proposed in this paper can obtain more accurate mobile user preferences, so it can provide mobile users with accurate personalized mobile network services.

In the course of this study, we do not consider the privacy and security of mobile users. In the follow-up study, we will consider how to accurately predict the preference of mobile users while ensuring the privacy of users.

Acknowledgments. This work was supported by the National Natural Science Foundation of China (61472136; 61772196), the Hunan Provincial Focus Social Science Fund (2016ZBB006) and Hunan Provincial Social Science Achievement Review Committee results appraisal identification project (Xiang social assessment 2016JD05).

References

1. Ricci, F.: Mobile recommender systems. *J. Inf. Technol. Tourism* **12**(3), 205–231 (2011)
2. Wuhan, H., Xiangwu, M., Licai, W.: Collaborative filtering algorithm based on user socialization relation mining in mobile communication network. *J. Electron. Inf. Technol.* **33** (12), 3002–3007 (2011)
3. Jiang, W., Zhang, L., Wang, P.: Research on grid resource scheduling algorithm based on MAS cooperative bidding game. *Sci. China F* **52**(8), 1302–1320 (2009)
4. Wang, H.M., Yin, G., Xie, B., et al.: Research on network-based large-scale collaborative development and evolution of trustworthy software. *Sci. Sin. Inf.* **44**, 1–19 (2014)

5. Fengling, X., Xiangwu, M., Licai, W.: Collaborative filtering recommendation algorithm based on mobile user context similarity. *J. Electron. Inf. Technol.* **33**(11), 2785–2789 (2011)
6. Ding, Y., Wang, H., Shi, P., et al.: Trusted cloud service. *Chin. J. Comput.* **38**(1), 133–149 (2015)
7. Jiang, W., Yusheng, X., Guo, H., Zhang, L.: Dynamic trust calculation model and credit management mechanism of online transaction. *Sci. China F Inf. Sci.* **44**(9), 1084–1101 (2014). <https://doi.org/10.1360/N112013-00202>
8. Zhang, S.B., Xu, C.X.: Study on the trust evaluation approach based on cloud model. *Chin. J. Comput.* **36**(2), 422–431 (2013)
9. Jiang, W.J., Zhong, L., Zhang, L.M., Shi, D.J.: Dynamic cooperative multi-agent model of complex system based-on sequential action' logic. *Chin. J. Comput.* **36**(5), 115–1124 (2013)
10. Lim, S.L., Finkelstein, A.: StakeRare: using social networks and collaborative filtering for large-scale requirements elicitation. *IEEE Trans. Softw. Eng.* **38**(3), 707–735 (2012)
11. Xu, J., Si, G.N., Yang, J.F., et al.: An internetware dependable entity model and trust measurement based on evaluation. *Sci. Sin. Inform.* **43**, 108–125 (2013)
12. Yuxiang, W., Xiuquan, Q., Xiaofeng, L.: Research on the mechanism of mobile social service selection based on context. *J. Comput. Sci.* **33**(11), 2126–2135 (2010)
13. Weijin, J.: *Dynamic Modeling and Quantification Trust More Research Methods Agent*. Science Press, Beijing (2014). 6
14. Wang, J., Li, S.-J., Yang, S., Jin, H., Yu, W.: A new transfer learning model for cross-domain recommendation. *Chin. J. Comput.* **40**(33), 1–15 (2017). Online publication number
15. Zhang, W.-L., Guo, B., Shen, Y., et al.: Computation offloading on intelligent mobile terminal. *Chin. J. Comput.* **39**(5), 1021–1038 (2016)
16. Eagle, N., Pentland, A., Lazer, D.: Inferring friendship network structure by using mobile phone data. *Proc. Natl. Acad. Sci.* **106**(36), 15274–15278 (2009)
17. Fernando, D., Chavariaga, J., Pedro, G., et al.: Movie recommendations based in explicit and implicit features extracted from the Filmtipset dataset. In: *Proceedings of the Workshop on Context-Aware Movie Recommendation*, Barcelona, Spain, pp. 45–52 (2010)
18. Xiong, C.Q., Ouyang, Y., Mei, Q.: Argumentation model based on certainty-factor and algorithms of argument evaluation. *J. Softw.* **25**(6), 1225–1238 (2014)
19. Huang, D.J., Arasan, V.: On measuring email-based social network trust. In: *Proceedings of the Global Telecommunications Conference (GLOBECOM)*, Miami, FL, pp. 1–5 (2010)
20. Xiuquan, Q., Chun, Y., Xiaofeng, L.: A trustworthiness method based on user context in social network service. *J. Comput. Sci.* **34**(12), 2403–2413 (2011)
21. Benchettara, N., Kanawati, R., Rouveirol, C.: Supervised machine learning applied to link prediction in bipartite social networks. In: *International Conference on Advances in Social Networks Analysis and Mining*, Odense, pp. 326–330 (2010)

A Group Decision-Making Method Based on Evidence Theory in Uncertain Dynamic Environment

Weijin Jiang^{1,2,3(✉)} and Yuhui Xu¹

¹ School of Computer and Information Engineering,
Hunan University of Commerce, Changsha 410205, China
nudtjwj@163.com

² Electronic Information Engineering Department,
Changsha Normal University, Changsha 410100, China

³ School of Computer Science and Technology,
Wuhan University of Technology, Wuhan, China

Abstract. A debate model based on evidence theory is proposed to solve the problem of group decision-making under uncertain conditions. First, the framework of the debate system is constructed. The internal structure of the argument is composed of preconditions and conclusions. There is not only an attack and a support relationship between the arguments, but also to support or oppose such attacks and support relationships. Then we introduce the evidence theory to describe the uncertainty of the argument, apply the evidence mapping method to the uncertainty process of the debate process, and realize the numerical calculation of the reliability of the argument. Finally, a simulation example is given to demonstrate the effectiveness of the model.

Keywords: Evidence theory · Uncertainty · Argumentation model
Evidence mapping

1 Introduction

In the dynamic environment, the information obtained by the decision-making body is usually incomplete and inconsistent, so there must be conflict and disagreement among the subjects, and the debate is an effective way to resolve the conflict [1, 2] and has become the field of artificial intelligence research Hot issues. The abstract debate framework proposed by Dung [3] is a large-scale debate model, after which many scholars have extended the abstract debate framework, such as the rule-based debate framework [4], the bipolar debate framework [5], the expansion of bipolar debate Framework, etc. [6].

The above model is mainly applied to the reasoning of the debate under certainty, and the actual debate process there is uncertainty. In recent years, scholars at home and abroad have studied the debate model under uncertainty conditions, such as the preference-based debate framework proposed by Amgoud and Vesic [7], Tang et al. [8] proposed a debate based on Dempster-Shafer theory, Xiong et al. [9, 10] based on the credibility of the debate model and evidence theory based on the debate model.

The above model achieves the uncertainty description of the debate model in different ways, but it is not comprehensive enough to construct the relationship between arguments in the debate system.

This paper expands the description of the relationship between the arguments by referring to the model of the literature [11] in the description of the internal structure of the argument. There is not only a mutual attack and support relationship between the arguments, but also to support such attacks and support relationships. Against the theory of evidence is used to analyze the reasoning process of uncertainty under the condition of uncertainty, and the quantitative description of the reliability of the argument is realized.

2 Group Discussion Framework

Group discussion is carried out through dialogue among speakers, and the arguments (views) generated during the dialogue process constitute the content of the whole study. The research framework is a formal description of the research arguments, including the description of the internal structure of the argument and the interrelationship between the arguments. Based on the literature [11], this paper proposes an extended research model, which includes not only the attack and support relationship between the arguments, but also the support or opposition to such attacks and support relationships.

Definition 1. [11] The statement is a description of things, it can be objective data, subjective judgments, factual phenomena, theoretical knowledge, etc., constitute the basic constituent units of the argument, recorded as h .

Definition 2. [11] Reasoning argument is a tuple of $A_t = (H, h)$, Among them, $H = \{h_1, h_2, \dots, h_n\}$ is a statement, and satisfy: (1) H is consistent, namely $\nexists h_i, h_j \in H, h_i \equiv -h_j$; (2) Logically, H infers the h , denoted as $H \Rightarrow h$. The H is called the premise of the reasoning argument, the h is called the reasoning argument, and the set of all arguments is denoted as \mathcal{A}_t .

Definition 3. [11] The definition is provided with two theories of $A_t = (H_1, h_1)$, $B_t = (H_2, h_2)$: (1) if $\exists h \in H_2, h_1 \equiv -h$, A_t attack B_t , denoted by $A_t \rightarrow B_t$ or $(A_t, B_t)^-$; (2) if $\exists h \in H_2, h_1 \equiv h$, A_t support B_t , denoted as $A_t \rightsquigarrow B_t$ or $(A_t, B_t)^+$. The relationship between attack and support relationship referred to as an argument-the argument relation, denoted as $r_{ll} = (A_t, B_t)$, as shown in Fig. 1. All the arguments-the set of arguments are recorded as \mathcal{R}_{ll} .

Definition 4. The rule argument is a two tuple $A_g = (H, r_{ll})$, where H is a set of statements, r_{ll} is an argument-argument relationship, and satisfies: (1) H is compatible, (2) Logically H inference out of r_{ll} , denoted as $H \Rightarrow r_{ll}$. The set of all rules argument is denoted as \mathcal{A}_g .

Definition 5. A rule $C_g = (H_1, r_1)$, argument-argument relationship $r_2 = (A_t, B_t)$: (1) if $r_1 \equiv -r_2$, C_g against r_2 , denoted as $C_g \rightarrow r_2$ or $(C_g, r_2)^-$; (2) if $r_1 \equiv r_2$, C_g support r_2 , denoted as $C_g \rightsquigarrow r_2$ or $(C_g, r_2)^+$. The support and opposition of the argument to

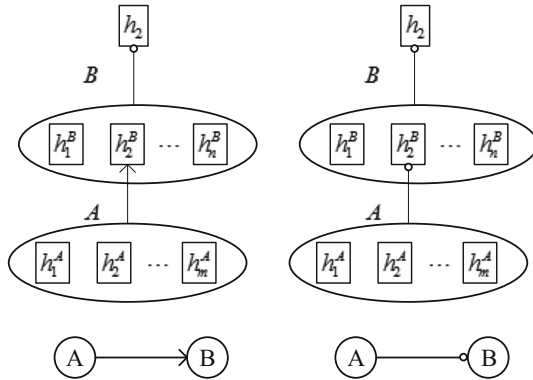


Fig. 1. Diagram of relations between reasoning arguments

argument-argument relation is called argument rule relation, denoted as $r_{lg} = (C_g, r_2)$. The set of all arguments-rule relations is denoted by \mathcal{R}_{lg} . The four types of argument-rule relations are shown in Fig. 2.

Figure 2(a) indicates that the C_g is against A_t attacks on B_i ; Fig. 2(b) indicates that the C_g supports A_t attacks on B_i ; Fig. 2(c) indicates that C_g is opposed to A_t support for B_i ; Fig. 2(d) indicates that C_g supports A_t support for B_i .

Definition 6. The debate-based research framework is a two-tuple $AG = (\mathcal{A}, \mathcal{R})$, where $\mathcal{A} = \mathcal{A}_t \cup \mathcal{A}_g$ is the argument set and $\mathcal{R} = \mathcal{R}_{ll} \cup \mathcal{R}_{lg}$ is the relation set.

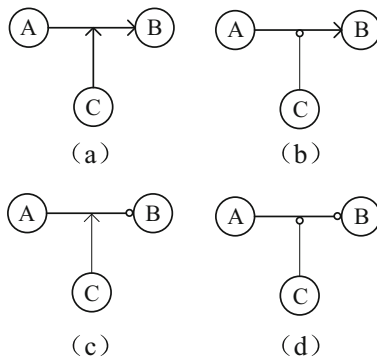


Fig. 2. Diagram of relations between arguments and rules

3 Debate Model Based on Evidence Theory

In a dynamic environment, the relationship between the argument and its arguments is uncertain. The evidence theory is an effective method to express and deal with the uncertainty reasoning. This paper analyzes the argument and the relationship of the research model based on the evidence theory.

3.1 The Uncertainty Representation of the Argument Premise

Definition 7. [12] For a verdict, the complete set of all possible answers is $\Theta = \{\theta_1, \theta_2, \dots, \theta_n\}$, and the elements in Θ are mutually exclusive, then Θ is the recognition frame. The power set of Θ is denoted by 2^Θ .

Definition 8. [13] For any proposition $A \in 2^\Theta$, the definition of mapping $m : 2^\Theta \rightarrow [0, 1]$ satisfies the following conditions:

- (1) $m(\emptyset) = 0$
- (2) $\sum_{A \subseteq \Theta} m(A) = 1$

Then we called m for Θ on the basic belief assignment (basic belief assignment, BBA).

Definition 9. [14] Assuming that the two independent evidence m_1 and m_2 under frame Θ are identified, $m = m_1 \oplus m_2$ is defined as

$$m(A) = \begin{cases} \frac{\sum_{A_i \cap B_j = A} m_1(A_i)m_2(B_j)}{1-K}, & A \neq \emptyset \\ 0, & A = \emptyset \end{cases} \tag{1}$$

according to the Dempster combination rule, where $K = \sum_{A_i \cap B_j = \emptyset} m_1(A_i)m_2(B_j)$ is the degree of conflict between the evidence m_1 and m_2 .

Definition 10. The truth of a statement h as a question to be judged, construct a statement recognition framework, recorded as $\Theta_h = \{True, False\}$, where *True* represents the statement is true, *False* on behalf of the statement is false.

Definition 11. For the statement recognition frame $\Theta_h = \{True, False\}$, the reliability assignment function $m_h : 2^{\Theta_h} \rightarrow [0, 1]$ defined on 2^{Θ_h} , where $m_h(True) = \alpha_h$ is the reliability of the statement that the statement is true according to the current situation, $m_h(False) = \beta_h$ indicates that the statement is false, $m_h(\Theta_h) = \gamma_h = 1 - \alpha - \beta$ is the confidence of the statement unknown reliability, the confidence vector of statement h is denoted as $w(h) = (\alpha_h, \beta_h, \gamma_h)$.

Definition 12. The authenticity of a certain premise $H = \{h_1, h_2, \dots, h_n\}$ as a pending decision, the premise of the framework to identify the framework, denoted as $\Theta_H = \{True, False\}$.

The reliability vector of the premise H is denoted as $w(H) = (\alpha_H, \beta_H, \gamma_H)$. When the current H is the combination of multiple statements, that is $H = h_1 \wedge \dots \wedge h_n$, then $w(H) = w(h_i)$, where i satisfies: $\alpha_{h_i} = \min_{j \in \{1, \dots, n\}} \{\alpha_{h_j}\}$, that is, the premise of the reliability of the value of the vector from the lowest credibility of the statement. When the current H is the recursion of multiple statements, that is $H = h_1 \vee \dots \vee h_n$, then $w(H) = w(h_i)$, where i satisfies: $\alpha_{h_i} = \max_{j \in \{1, \dots, n\}} \{\alpha_{h_j}\}$, that is the prerequisite reliability vector is determined by the highest degree of confidence.

3.2 The Reasoning of Uncertainty in Argument Conclusion

3.2.1 Reasoning Rule Representation Based on Evidence Mapping

Definition 13. [10, 15] Evidence mapping refers to the mapping of the prerequisite framework Θ_H to the conclusion recognition framework Θ_h , which describes the reasoning relationship between the elements in Θ_H and the elements in Θ_h . Evidence mapping from Θ_H to Θ_h is expressed as $\Gamma : \Theta_H \rightarrow 2^{2^{\Theta_h} \times [0,1]}$. The evidence mapping for each element in Θ_H is expressed as

$$\Gamma(\theta_{H_i}) = \left\{ (\theta_{h_{i1}}, f(\theta_{H_i} \rightarrow \theta_{h_{i1}})), \dots, (\theta_{h_{im}}, f(\theta_{H_i} \rightarrow \theta_{h_{im}})) \right\} \tag{2}$$

where θ_{H_i} is the prerequisite element, $\theta_{h_{ij}}$ is the element of the conclusion, and $f(\theta_{H_i} \rightarrow \theta_{h_{ij}})$ is the rule strength of θ_{H_i} supporting $\theta_{h_{ij}}$.

Make $\Theta_{H_i} = \bigcup_{j=1}^m \{\theta_{h_{ij}}\}$ a prerequisite for θ_{H_i} to infer all the conclusion of the collection.

Equation (2) satisfies the following condition:

- (1) $\theta_{h_{ij}} \neq \emptyset \quad j = 1, 2, \dots, m$
- (2) $0 < f(\theta_{H_i} \rightarrow \theta_{h_{ij}}) \leq 1$
- (3) $\sum_{j=1}^m f(\theta_{H_i} \rightarrow \theta_{h_{ij}}) = 1$

3.2.2 The Calculation of the Conclusion of Reasoning

Under the condition of uncertainty, for the reasoning argument $A_t = (H, h)$, the rule relations between the prerequisite H and the conclusion h include the following: $H \rightarrow h, H \rightarrow \neg h, \neg H \rightarrow h, \neg H \rightarrow \neg h$. The corresponding regular strength is: $Hh = f(H \rightarrow h), H\neg h = f(H \rightarrow \neg h), \neg Hh = f(\neg H \rightarrow h), \neg H\neg h = f(\neg H \rightarrow \neg h)$.

Definition 14. [10] For the reasoning $A_t = (H, h)$, we define the mapping matrix $R(A_t) = (r_{ij})_{3 \times 3}$ from the premise H to the conclusion h , and the row headings are $H, \neg H$ and the complete set Θ_H ; the column headings are $h, \neg h$ and the complete set Θ_h . The specific form of $R(A_t)$ is

$$R(A_t) = \begin{bmatrix} Hh & H\neg h & 1 - r_{11} - r_{12} \\ \neg Hh & \neg H\neg h & 1 - r_{21} - r_{22} \\ r_{31} & r_{32} & 1 - r_{31} - r_{32} \end{bmatrix}$$

among which,

$$r_{31} = \begin{cases} (r_{11} + r_{21})/2, & r_{11} \times r_{21} \neq 0 \\ 0, & r_{11} \times r_{21} = 0 \end{cases} \tag{3}$$

$$r_{32} = \begin{cases} (r_{12} + r_{22})/2, & r_{12} \times r_{22} \neq 0 \\ 0, & r_{12} \times r_{22} = 0 \end{cases} \tag{4}$$

According to the reliability value vector $w(H)$ and the mapping matrix $R(A_t)$ of the premise H , the reliability value vector

$$w(h) = w(H) \cdot R(A_t) \tag{5}$$

of the conclusion h can be obtained.

Assuming that there are multiple prerequisites pointing to the same conclusion h , we can fuse the multiple confidence values of h according to the Dempster combination rule to get $w(h) = w(h)_1 \oplus w(h)_2 \oplus \dots \oplus w(h)_k$.

3.2.3 The Calculation of the Conclusions of the Rules

For the rule argument $A_g = (H, r_{ll})$, where $r_{ll} = (A_t, B_t)$, $A_t = (H_1, h_1)$, $B_t = (H_2, h_2)$, we can see the argument-argument relation r_{ll} , whose essence corresponds to the mapping matrix $R(A_t)$ of A_t . Therefore, the relationship between the premise H and the conclusion r_{ll} is the relationship between H and $R(A_t)$, including the following: $H \rightarrow f(H_1 \rightarrow h_1)$. The corresponding regular intensity is recorded as $H(H_1h_1)$, $H(H_1\neg h_1)$, $\neg H(H_1h_1)$, $\neg H(H_1\neg h_1)$, $H(\neg H_1h_1)$, $H(\neg H_1\neg h_1)$, $\neg H(\neg H_1h_1)$, $\neg H(\neg H_1\neg h_1)$.

Because the relationship between the premise H and the conclusion r_{ll} is more complex, it is divided into two categories (the first four categories, the second category for the last four) were calculated and then synthesized.

Definition 15. For the rule argument $A_g = (H, r_{ll})$, the mapping matrix defined by the prerequisites H to $R(A_t)$, the first row $R(A_t)^{(1)}$, is $R_1 = (r_{ij})_{3 \times 3}$, and the row headings are $H, \neg H$ and the complete set Θ_H ; the column heading is the rule strength deduced by H_1 , followed by $H_1h_1, H_1\neg h_1$ and complete works Θ_{H_1} . The specific form of R_1 is

$$R_1 = \begin{bmatrix} H(H_1h_1) & H(H_1\neg h_1) & 1 - r_{11} - r_{12} \\ \neg H(H_1h_1) & \neg H(H_1\neg h_1) & 1 - r_{21} - r_{22} \\ r_{31} & r_{32} & 1 - r_{31} - r_{32} \end{bmatrix}$$

where r_{31} and r_{32} are calculated by the same formula (3) and (4).

According to the reliability value vector $w(H)$ and the mapping matrix R_1 of the premise H , the first behavior

$$R(A_t)_H^{(1)} = w(H) \cdot R_1 \tag{6}$$

of the mapping matrix $R(A_t)$ can be obtained.

Definition 16. Similarly, the mapping matrix defined by the second row $R(A_t)^{(2)}$ of the prerequisites H to $R(A_t)$ is $R_2 = (r_{ij})_{3 \times 3}$. The row headings are $H, \neg H$ and the complete set of Θ_H ; the column heading is the intensity of the rules deduced by $\neg H_1$, followed by $\neg H_1 h_1, \neg H_1 \neg h_1$ and the complete set $\Theta_{\neg H_1}$. The specific form of R_2 is

$$R_2 = \begin{bmatrix} H(\neg H_1 h_1) & H(\neg H_1 \neg h_1) & 1 - r_{11} - r_{12} \\ \neg H(\neg H_1 h_1) & \neg H(\neg H_1 \neg h_1) & 1 - r_{21} - r_{22} \\ r_{31} & r_{32} & 1 - r_{31} - r_{32} \end{bmatrix}$$

where r_{31} and r_{32} are calculated as follows (3) and (4). The second row of the mapping matrix $R(A_t)$ can be obtained

$$R(A_t)_H^{(2)} = w(H) \cdot R_2 \tag{7}$$

Thus, under the influence of H , the original mapping matrix $R(A_t)$ is updated to:

- (1) Update the first row of $R(A_t)$ according to the Dempster combination rule:
 $R(A_t)_{new}^{(1)} = R(A_t)_H^{(1)} \oplus R(A_t)^{(1)}$;
- (2) Similarly, the second line of $R(A_t)$ is updated as $R(A_t)_{new}^{(2)} = R(A_t)_H^{(2)} \oplus R(A_t)^{(2)}$;
- (3) The third line of $R(A_t)$ is calculated by the same formula (3) and (4).

3.3 Declaring the Update of the Reliability

In the course of the study, when there is a new reasoning argument A_2 , if there is an argument-argument relation (A_2, A_1) , then A_2 will change the confidence value of a statement h_{1i} in the premise H_1 of A_1 , thus changing the reliability of the conclusion h_1 of A_1 . As the study continues, the relation (A_3, A_2) is generated, then A_3 changes the confidence value of a statement h_{2j} in the premise H_2 of A_2 , thus changing the confidence value of the conclusion h_2 of A_2 (that is, h_{1i}), and the final conclusion of the reliability of A_1 change h_1 . In addition, when a new rule argument A_4 is generated, if there is an argument-rule relation $(A_4, (A_2, A_1))$, then A_4 changes the mapping matrix R_{21} of A_2 to A_1 , thus changing the confidence value of A_2 's conclusion h_2 (that is, h_{1i}), and eventually changing A_1 's conclusion h_1 's reliability value. Thus, for each new argument, the correspondence value of the corresponding statement on the entire argument chain will change.

- (1) When adding a reasoning argument, the algorithm described in the framework of the reliability update is as follows:

Step1: Generate a reasoning argument $A_t = (H_A, h_A)$, set the initial confidence value of each statement h_{Ai} in the preamble $H_A = \{h_{A1}, h_{A2}, \dots, h_{An}\}$ to $w(h_{Ai})^0 = (\alpha_{h_{Ai}}, \beta_{h_{Ai}}, \gamma_{h_{Ai}})^0$, calculate the reliability value $w(H_A)^0$ of H_A , and generate the inference rule mapping matrix R_A from H_A to h_A .

Step2: Calculate the confidence value $w(h_A) = w(H_A) \cdot R_A$ of h_A , and if h_A is the target statement for the whole debate, the stated reliability value is updated. If h_A

belongs to the premise of an argument $B_t = (H_B, h_B)$, that is $h_A = h_{Bj} \in H_B$, then h_A updates the reliability value of h_{Bj} to $w(h_{Bj})_{new} = w(h_{Bj})^0 \oplus w(h_A)$, the reliability value $w(H_B)_{new}$ of H_B is updated, and the reliability value $w(h_B) = w(H_B)_{new} \cdot R_B$ of h_B is calculated.

If h_B is still a prerequisite for an argument, follow the steps 2 above to proceed with the update until the entire statement of the debate is updated.

- (2) When adding a rule to the argument, the discussion within the framework of the reliability value update algorithm is as follows:

Step1: Produce a rule argument for $C_g = (H_C, r_C)$, where the premise is $H_C = \{h_{C1}, h_{C2}, \dots, h_{Cn}\}$, the relationship is $r_C = (A_t, B_t)$. The initial reliability value of each statement h_{Ci} is set to $w(h_{Ci})^0 = (\alpha_{h_{Ci}}, \beta_{h_{Ci}}, \gamma_{h_{Ci}})^0$, the reliability value $w(H_C)$ of H_C is calculated, the initial mapping matrix of A_t is $R(A_t)_0$, and the updated post-mapping matrix is $R(A_t)_{new}$.

Step2: Calculate the update reliability value $w(h_A)_{new} = w(H_A) \cdot R(A_t)_{new}$ of h_A , and then h_A updates the reliability value of h_{Bj} to $w(h_{Bj})_{new} = w(h_{Bj})^0 \oplus w(h_A)_{new}$, and then update the reliability value of h_B .

3.4 The Acceptability of the Statement

If the confidence vector of statement h is $w(h) = (\alpha_h, \beta_h, \gamma_h)$, it is possible to determine whether it is acceptable according to the following three rules (Table 1):

Rule1: If $\alpha_h > \alpha_0$, statement h is acceptable.

Rule2: If $\beta_h < \beta_0$, statement h is acceptable.

Table 1. Arguments of the discussion

Argument	Argument premise	Argument conclusion	Prerequisites initial reliability values	Reasoning rule strength
A_1	$h_{11} \wedge h_{12}$	h	$w(h_{11}) = (0.7, 0.2, 0.1)$ $w(h_{12}) = (0.85, 0.1, 0.05)$	$H_1 \rightarrow h(0.9)$ $\neg H_1 \rightarrow \neg h(0.8)$
A_2	$h_{21} \wedge h_{22} \wedge h_{23}$	h_{11}	$w(h_{21}) = (0.8, 0, 0.2)$ $w(h_{22}) = (0.9, 0.1, 0)$ $w(h_{23}) = (0.7, 0.1, 0.2)$	$H_2 \rightarrow h_{11}(0.9)$
A_3	$h_{31} \wedge h_{32}$	h_{23}	$w(h_{31}) = (0.8, 0.1, 0.1)$ $w(h_{32}) = (0.7, 0, 0.3)$	$H_3 \rightarrow \neg h_{23}(0.8)$
A_4	$h_{41} \wedge (h_{42} \vee h_{43})$	h_{12}	$w(h_{41}) = (0.6, 0.1, 0.3)$ $w(h_{42}) = (0.8, 0.2, 0)$ $w(h_{43}) = (0.7, 0.1, 0.2)$	$H_4 \rightarrow \neg h_{12}(0.8)$
A_5	$h_{51} \wedge h_{52}$	$r(A_4, A_1)$	$w(h_{51}) = (0.9, 0, 0.1)$ $w(h_{52}) = (0.8, 0.2, 0)$	$H_5 \rightarrow (H_4 \rightarrow h_{12})(0.5)$

Time node 1 produces argument A_1 , the reliability value $w(H_1)^1 = w(h_{11})$ of the premise H_1 , the rule mapping matrix $R_{11} = \begin{bmatrix} 0.9 & 0 & 0.1 \\ 0 & 0.8 & 0.2 \\ 0 & 0 & 1 \end{bmatrix}$, the confidence value $w(h)^1 = w(H_1)^1 \cdot R_{11} = (0.63, 0.16, 0.21)$ of the conclusion h .

Time node 2 produces argument A_2 , the reliability value of $w(H_2)^2 = w(h_{23})$ of the premise H_2 , and the confidence value $w(h_{11})^2 = w(H_2)^2 \cdot R_{21}$ of the conclusion h_{11} . The reliability value of h_{11} is updated to $w(h_{11})^2_{new} = w(h_{11})^2 \oplus w(h_{11}) = (0.8730, 0.0847, 0.0423)$. In this case, the reliability value of H_1 is $w(H_1)^2 = w(h_{12})$, the reliability value of h is updated to $w(h)^2 = w(H_1)^2 \cdot R_{11} = (0.7650, 0.0800, 0.1550)$. It can be seen that the reliability of A_1 conclusion h is improved by support of A_2 for A_1 .

Time node 3 produces argument A_3 , A_3 reduces the credibility of A_2 premise, and thus reduces the credibility of h_{11} , the final h of the reliability value is updated to $w(h)^3 = (0.7267, 0.1027, 0.1706)$.

The time node 4 produces the argument A_4 , $w(h_{12})^4_{new} = w(h_{12})^4 \oplus w(h_{12}) = (0.7466, 0.2095, 0.0439)$, the confidence degree of h_{12} , is reduced by A_4 , and the reliability value of h is updated to $w(h)^4 = (0.6720, 0.1676, 0.1605)$.

The time node 5 produces the argument A_5 , A_5 against the attack of A_4 to A_1 , and the first row of the mapping matrix R_{41} of A_4 is updated to $R_{41new}^{(1)} = R_{41H}^{(1)} \oplus R_{41}^{(1)} = (0.1176 \ 0.7059 \ 0.1765)$. Thus the reliability value of h is updated to $w(h)^5 = (0.7018, 0.1442, 0.1540)$.

Assuming that the acceptability of the statement is discriminated by rule 1, if the threshold is $\alpha_0 = 0.7$, then h is acceptable at the end of the study.

In the whole study, the update process of the presentation reliability value is shown in Table 2.

Table 2. The renewal process of the reliability values of statements

Statement	Time 1	Time 2	Time 3	Time 4	Time 5
h	(0.63,0.16, 0.21)	(0.7650,0.0800, 0.1550)	(0.7267,0.1027, 0.1706)	(0.6720,0.1676, 0.1605)	(0.7018,0.1442, 0.1540)
h_{11}	(0.70,0.20, 0.10)	(0.8730,0.0847, 0.0423)	(0.8074,0.1284, 0.0642)	(0.8074,0.1284, 0.0642)	(0.8074,0.1284, 0.0642)
h_{12}	(0.85,0.10, 0.05)	(0.85,0.10,0.05)	(0.85,0.10,0.05)	(0.7466,0.2095, 0.0439)	(0.7797,0.1803, 0.0400)
h_{21}	–	(0.80,0,0.20)	(0.80,0,0.20)	(0.80,0,0.20)	(0.80,0,0.20)
h_{22}	–	(0.90,0.10,0)	(0.90,0.10,0)	(0.90,0.10,0)	(0.90,0.10,0)
h_{23}	–	(0.7,0.1,0.2)	(0.4565,0.4130, 0.1304)	(0.4565,0.4130, 0.1304)	(0.4565,0.4130, 0.1304)
h_{31}	–	–	(0.8,0.1,0.1)	(0.8,0.1,0.1)	(0.8,0.1,0.1)
h_{32}	–	–	(0.7,0,0.3)	(0.7,0,0.3)	(0.7,0,0.3)

(continued)

Table 2. (continued)

Statement	Time 1	Time 2	Time 3	Time 4	Time 5
h_{41}	–	–	–	(0.6,0.1,0.3)	(0.6,0.1,0.3)
h_{42}	–	–	–	(0.8,0.2,0)	(0.8,0.2,0)
h_{43}	–	–	–	(0.7,0.1,0.2)	(0.7,0.1,0.2)
h_{51}	–	–	–	–	(0.9,0,0.1)
h_{52}	–	–	–	–	(0.8,0.2,0)

4 Conclusion

In this paper, the debate model based on evidence theory is constructed for the problem of group decision-making under uncertain conditions. First, a more comprehensive framework of the debate system is defined, which defines the relationship between the internal structure of the argument and the argument, which not only includes attacks and support relationships, but also allows for support or opposition to such attacks and support relationships. Then we introduce the theory of evidence to describe the uncertainty of the argument, apply the evidence mapping method to the uncertainty process of the debate process, and realize the transmission and renewal of the reliability of the argument.

Acknowledgments. This work was supported by the National Natural Science Foundation of China (61472136; 61772196), the Hunan Provincial Focus Social Science Fund (2016ZBB006) and Hunan Provincial Social Science Achievement Review Committee results appraisal identification project (Xiang social assessment 2016JD05).

References

1. Amgoud, L., Prade, H.: Using arguments for making and explaining decisions. *Artif. Intell.* **173**(3–4), 413–436 (2009)
2. Chen, Y., Xiang, D., Zhao, Y.: Argumentation-based group discussion modeling and decision approach. *Syst. Eng. Theory Pract.* **33**(7), 1633–1639 (2013)
3. Dung, P.M.: On the acceptability of arguments and its fundamental role in nonmonotonic reasoning, logic programming and n -person games. *Artif. Intell.* **77**(2), 321–357 (1995)
4. Caminada, M., Amgoud, L.: On the evaluation of argumentation formalisms. *Artif. Intell.* **171**(5–6), 286–310 (2007)
5. Cayrol, C., Lagasquie-Schiech, M.C.: Bipolarity in argumentation graphs: towards a better understanding. *Int. J. Approximate Reasoning* **54**(7), 876–899 (2013)
6. Chen, J.L., Wang, C.C., Chen, C.: Extended bipolar argumentation model. *J. Softw.* **23**(6), 1444–1457 (2012)
7. Amgoud, L., Vesic, S.: A new approach for preference-based argumentation frameworks. *Ann. Math. Artif. Intell.* **63**(2), 149–183 (2011)
8. Tang, Y., Hang, C.W., Parsons, S., et al.: Towards argumentation with symbolic Dempster-Shafer evidence. In: *Proceedings of the Computational Models of Argument (COMMA 2012)*, Vienna, Austria, pp. 462–469. IOS Press (2012)

9. Xiong, C.Q., Ouyang, Y., Mei, Q.: Argumentation model based on certainty-factor and algorithms of argument evaluation. *J. Softw.* **25**(6), 1225–1238 (2014)
10. Xiong, C.Q., Zhan, Y.F., Chen, S.B.: An argumentation model based on evidence theory. In: *The 10th International Conference on Computer Science and Education (ICCSE 2015)*, Cambridge University, UK, pp. 451–454. IEEE Press (2015)
11. Xiong, C.Q., Li, D.H.: Model of argumentation. *J. Softw.* **20**(8), 2181–2190 (2009)
12. Zhang, X., Mu, L.H.: Evidence combination rule based on local conflict elimination. *Syst. Eng. Electron.* **38**(7), 1594–1599 (2016)
13. Han, D.Q., Yang, Y., Han, C.Z.: Advances in DS evidence theory and related discussions. *Control Decis.* **29**(1), 1–11 (2014)
14. Shafer, G.: *A Mathematical Theory of Evidence*. Princeton University Press, Princeton (1976)
15. Liu, W., Hughes, J.G., McTear, M.F.: Representing heuristic knowledge in DS theory. In: *Proceedings of the Eighth International Conference on Uncertainty in Artificial Intelligence*, pp. 182–190. Morgan Kaufmann Publishers Inc. (1992)

Analysis and Estimate the Effect of Knowledge on Software Reliability Distribution

Chunhui Yang^{1,2(✉)}, Yan Gao^{2,3(✉)}, Xuedong Kong², Dingfang Chen¹,
Shengwu Xiong¹, and Jianwen Xiang¹

¹ Wuhan University of Technology, Wuhan, China
yangch@ceprei.com, cadcs@126.com, {xiongsw, jwxiang}@whut.edu.cn

² Software Center, CEPREI, Guangzhou, China
kongxd@ceprei.com

³ Key Laboratory for Performance and Reliability Testing of Foundational Software
and Hardware, MIIT, Guangzhou, China
thegoldfishwang@163.com

Abstract. Software knowledge plays an important role in software testing and software reliability model. This paper proposes that software knowledge affects the software reliability distribution significantly based on the theoretical analysis on the Weibull distribution of defect density, and proof that the software knowledge amount mainly affects from the scale parameter c of Weibull distribution, while c can be expressed as a quantitative expression of software knowledge amount. In this paper, engineering experiment is carried out to verify the proposed conclusion, which shows that more knowledge testers have, the smaller the scale factor c of Weibull distribution becomes. Furthermore, according to the degree of the software knowledge, the trend of the problems found in testing can be predicted, so as to evaluate the reliability of the software.

Keywords: Software knowledge · Software test · Reliability model
Weibull distribution

1 Introduction

Software reliability is the possibility of software runs successfully according to the design requirement under a given time interval and required environment condition [1–3]. While software product is released, the reliability and latent fault of software product can be predicted and estimated through the software reliability theory, which includes two reasons: (1) It can be used as the objective statement of product quality. (2) It can be used for the resource planning in software maintenance phase.

Software reliability model plays an important role in software reliability theory, which includes two types as static model and dynamic model. In static model [4, 5], the coefficient is estimated from previous data of software products, while relative software product can be the supplement observation for the total project. Static model did not consider the time factor, but actually is a quality model. Dynamic model [6–8] is mainly used in the software development phase and software reliability testing phase. The Rayleigh model is a typical model used in the development phase, while exponential

growth model and other reliability growth model is used in the test phase. All dynamic reliability models can be denoted as a function of time or its logic in the development phase.

Knowledge can provide guidance for software testing and many studies have been carried out. Xu [9] indicated that the cause of software errors is the errors of knowledge used and its usage in the software system, and proposed software testing method based on the knowledge by practice analysis, which can make up the inadequacy of testing method adequacy and suitability effectively. Vijaykumar [10] proposed the concept of Reference Ontology of Software Testing by identifying and reuse of the ontology in the software testing process, which can give semantics to a large number of software testing information, so as to support the knowledge management in the software testing process.

However, the research of the effect of Software knowledge on software reliability is very few. How to describe the relationship between knowledge and software reliability, so as to achieve high quality of software testing with knowledge, and improve software quality and reliability, scientific and quantitative analysis is necessary. Therefore, this paper estimates and is focus on the relationship between the software knowledge and software reliability.

The remainder of this paper is structured as follows. In Sect. 2, Weibull distribution is briefly summarized. The relationship between the software knowledge and software reliability are derived in detail, and a formalization expression of the relationship are described briefly in Sect. 3. Engineering Experiments results and analysis are reported in Sect. 4 and Sect. 5 concludes this paper.

2 Software Reliability Distribution

Weibull distribution [11, 12] is used for reliability analysis in various engineering fields for many years, which from bearing fatigue life of the deep groove ball to the tube fault and river flood. Weibull distribution is one of the three famous extreme value distributions. The significant feature of Weibull distribution is that the probability density gradually tends to zero. Figure 1 shows the Weibull probability density curves with different shape parameter m values.

The Cumulative Distribution Function(CDF) and Probability Density Function(PDF) of Weibull distribution can be formulated as:

$$\text{CDF: } F(t) = 1 - e^{-(t/c)^m} \quad (1)$$

$$\text{PDF: } f(t) = \frac{m}{t} \left(\frac{t}{c}\right)^{m-1} e^{-(t/c)^m} \quad (2)$$

where m denotes the shape parameter, c denotes scale parameter, t denotes time.

Rayleigh model is special case of the Weibull distributions which shape parameter m is equal to 2. The CDF and PDF are expressed as:

$$\text{CDF: } F(t) = 1 - e^{-(t/c)^2} \quad (3)$$

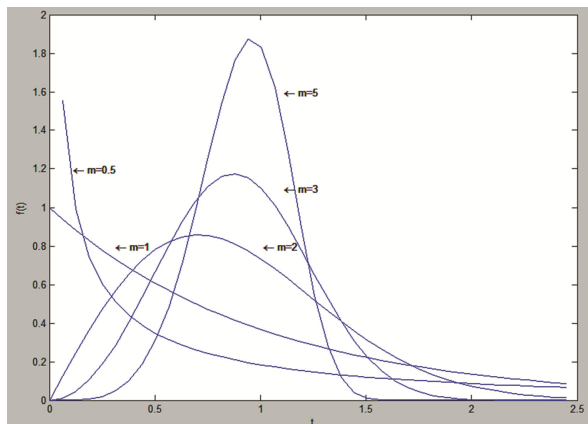


Fig. 1. Several typical curves of Weibull distribution

$$\text{PDF: } f(t) = \frac{2}{t} \left(\frac{t}{c}\right)^2 e^{-(t/c)^2} \tag{4}$$

Exponential model is another special case of the Weibull distributions which shape parameter m is equal to 1. Exponential model is suitable for statistical process that monotonous decline to progressive values. The CDF and PDF are expressed as:

$$\text{CDF: } F(t) = 1 - e^{-(t/c)} = 1 - e^{-\lambda t} \tag{5}$$

$$\text{PDF: } f(t) = \frac{1}{c} e^{-(t/c)} = \lambda e^{-\lambda t} \tag{6}$$

In engineering practice, the above formulations need to be multiplied by the total defect number or total defect cumulative probability K , where K is an estimated parameter for deriving specific model from the dataset.

3 Analysis of Knowledge and Reliability

3.1 Relationship Derivation

Observed from the engineering practice, the experience and knowledge of testing team can affect the testing efficiency and problems found. Generally, high level testing team can find problem more quickly and the problems found are subject to certain mathematical distribution.

Two Weibull functions are used in the application of software reliability usually that, Rayleigh distribution is used to describe the defect distribution in development phase, exponential distribution is used to describe the fault distribution in system test phase or after product delivery. Due to the significant correlation between the knowledge of testing team and testing efficiency from engineering practice, this paper analysis the quantitative relationship of knowledge and fault distribution by Weibull function.

This paper takes the system testing phase for example, where the shape parameter m is equal to 1. There are three hypotheses as follow.

- Hypothesis 1:** The knowledge quantity of testing team A and B are S_A and S_B correspondingly.
- Hypothesis 2:** Testing team A and B test the same software product respectively, while they can find out all defects through learning and experience accumulation.
- Hypothesis 3:** The fault distribution of software product is subject to Weibull distribution in software reliability field.

Assuming the fault set $X = \{x_1, x_2, x_3, \dots\}$ is the sum of all kind fault modes found at t moment.

$$X = K \cdot f(t) = \frac{K}{c} e^{-t/c} \tag{7}$$

where K denotes the total defect number, c denotes scale parameter.

As observed from the engineering practice, the experience and knowledge of testing team can affect the test efficiency and the found problems. Therefore, the knowledge quantity of testing team is positively related to the amount of defects can be found.

$$K = K(S) \propto S \tag{8}$$

By plugging Formula (8) to Formula (7), the following formula is obtained as:

$$X = \frac{K(S)}{c} e^{-t/c} \tag{9}$$

which means that the defect number X found at moment t is related to knowledge quantity S and scale factor c . X can be expressed by S and c as:

$$X = X(S, c, t) \tag{10}$$

Assuming the fault probability distribution of testing team A and B are $f_1(t, c_1)$ and $f_2(t, c_2)$ correspondingly:

$$X_1 = K(S_A) \cdot f_1(t) = \frac{K(S_A)}{c_1} e^{-t/c_1} \tag{11}$$

$$X_2 = K(S_B) \cdot f_2(t) = \frac{K(S_B)}{c_2} e^{-t/c_2} \tag{12}$$

Subtract Formula (11) and (12) after logarithmic, the following formula is obtained as:

$$\ln X_1 - \ln X_2 = \ln K(S_A) - \ln K(S_B) - \ln c_1 + \ln c_2 - t * \frac{c_1 - c_2}{c_1 c_2} \tag{13}$$

Formula (13) can be rewritten as:

$$\Delta \ln X = \Delta \ln K - \Delta \ln c - t * \frac{c_1 - c_2}{c_1 c_2} \tag{14}$$

High-level testing team can find problem faster and more, which means that if $S_A > S_B$, $c_1 < c_2$. For any moment t as a constant, team A finds more faults and more efficient than team B. Team A reaches the testing goal faster than team B at the end of the test timing.

Because $\Delta \ln K$ is a constant, the relationship of $\Delta \ln X$ and $|\Delta \ln c|$ can be shown in Fig. 2.

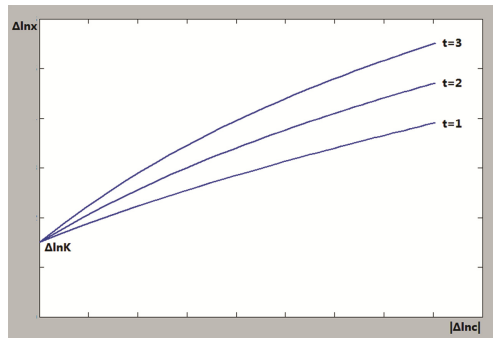


Fig. 2. Relationship between defect number X and scale parameter c

From Fig. 2, $\Delta \ln X$ is proportional to $|\Delta \ln c|$. Due to $c_1 < c_2$, so that X is inversely proportional to c . Moreover, Formula (13) indicates that X is proportional to the knowledge quantity S testing team have, therefore, the knowledge quantity S testing team have is inversely proportional to c , and the knowledge quantity S required is proportional to c .

Therefore, software knowledge mainly affects the scale parameter c in Weibull distribution. The smaller c is, the more knowledge testers have, the less knowledge they need to obtain; the larger c is, the less knowledge testers have, the more knowledge they need to obtain. c can be expressed as a quantitative expression of knowledge quantity needed.

$$c = \lambda g(D, A^D, R, A^R, H, I) \tag{15}$$

where D denotes the concept set of software knowledge, A^D denotes the attribute set of software knowledge, R denotes the relationship and rules of knowledge, A^R denotes attribute set of knowledge relationship, H denotes the level of knowledge concept, I denotes instance set, λ denotes coefficient. Function $g()$ denotes the measurement of the knowledge quantity needed in software development or testing, which is proportional to the scale parameter c .

3.2 The Effect of Knowledge Analysis

This subsection analyses the effect of knowledge on size parameter c from development phrase and testing phrase respectively.

For the software development phase, assuming that the software development and testing activities are ongoing, the effect of knowledge on the software development phase is shown in Fig. 3.

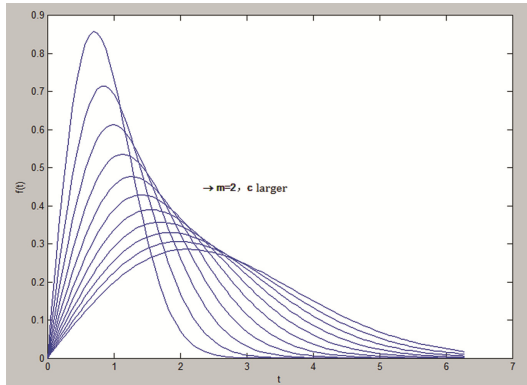


Fig. 3. The effect of knowledge on development phase

The knowledge quantity required by software testers has direct effect on the test. If the tester's understanding of the software system is more comprehensive and profound, the less knowledge quantity required, the smaller scale parameter c is, which makes software fault detection faster and software reliability can be improved effectively. On the contrary, if the knowledge and experience of tester is weak, the more knowledge quantity required and the larger c is, which makes fault detection slower.

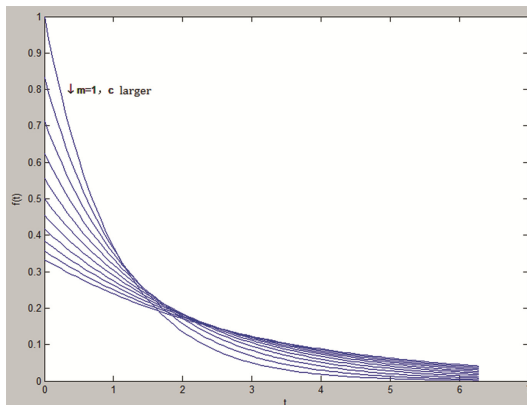


Fig. 4. The effect of knowledge on the testing phase

Similarly, the effect of knowledge on the software testing phase is shown in Fig. 4. The less of knowledge quantity tester requires, the smaller scale parameter c is, which makes software fault found timely and effectively. On the contrary, if the knowledge and experience of tester is weak, the more knowledge quantity required, the larger scale parameter c is, which makes fault detection slower.

4 Experiments

In this section, software engineering testing of a certain Linux operation system is carried out, in order to verify the proposed conclusion of the relationship between knowledge and software reliability.

There are total 10 round testing designed, the test strategies are shown as follow:

- (1) Each round is independent.
- (2) For each round, the found problems and fault modes are concluded as knowledge.
- (3) For each round, test cases are added based on the increased problems and fault modes of the previous round.
- (4) For each round, test case distribution is improved based on the fault mode distribution of all previous rounds.

The test results of 10 rounds are shown in Table 1, and the analysis is shown in Fig. 5. Firstly, tester can find more faults by learning the software product more as the testing going on. The knowledge of tester can be enriched after analyzing these defects and faults. Secondly, the number of test problems and fault modes are increased each round, while the increasing speed decreases and fault mode tends to 35 finally, which means that the knowledge of tester has been improved.

Table 1. The test results of 10 rounds

Round	Result			
	Fault mode num	Test case num	Test problem num	Fault mode added
1	20	240	92	/
2	23	328	97	3
3	26	368	108	3
4	28	392	114	2
5	29	421	123	1
6	32	450	140	3
7	34	489	145	2
8	35	520	151	1
9	35	531	156	0
10	35	543	170	0

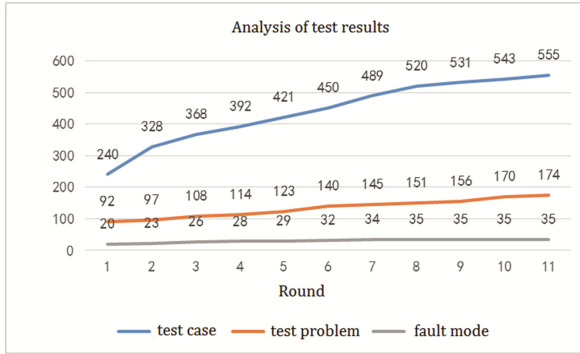


Fig. 5. Analysis of the test results

According to Formula (7), K and c of Weibull cumulative defect distribution are estimated with the fault mode number (20, 23, 26, 28, 29) of the first five test rounds.

$$X = K \cdot f(t) = \frac{K}{c} e^{-(t/c)} \tag{16}$$

The simulation result by Matlab tool is shown in Fig. 6, which $K = 27.943$, $c = 0.911$.

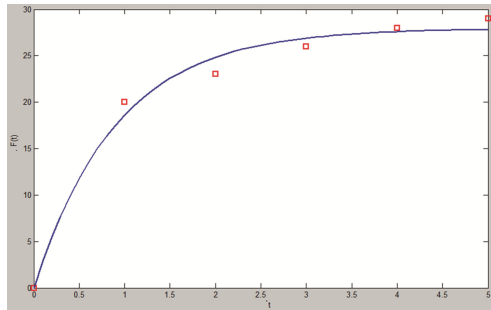


Fig. 6. The fitting distribution curve of the first 5 rounds

Similarly, according to Formula (7), K and c of Weibull cumulative defect distribution are estimated with the fault mode number (32, 34, 35, 35, 35) of the last five test rounds.

The simulation result by Matlab tool is shown in Fig. 7, which $K = 34.841$, $c = 0.404$.

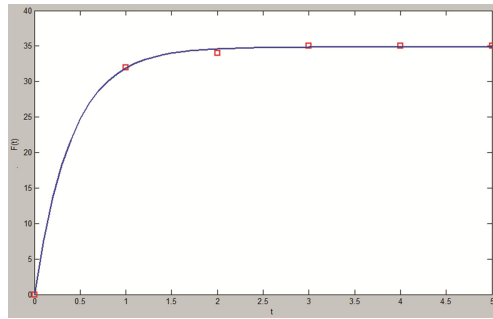


Fig. 7. The fitting distribution curve of the last 5 rounds

By plugging the above two c into the probability density function of Formula (7), two probability density curves are obtained as shown in Fig. 8.

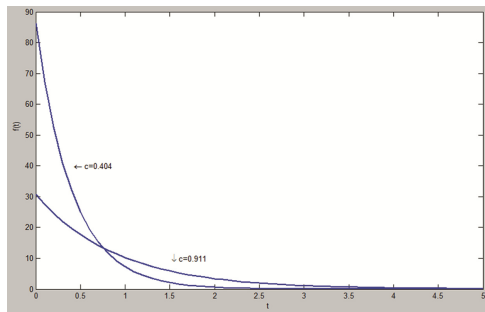


Fig. 8. The probability density curves of different c

With the knowledge increasing of tester, more defects are found, and smaller the scale parameter c is, which means that the knowledge mainly affect the scale parameter c of software reliability distribution.

5 Conclusion

On the basis of the theoretical analysis and derivation on the Weibull distribution of defect density, this paper gives the conclusion that the knowledge qualification varies inversely to scale parameter c of Weibull distribution via the analyses of the quantitative relation between the tester knowledge level and defect distribution. Accordingly, the proposed relationship can help to analysis the effect of software test team on the product reliability curve, so as to predict the trend of finding problems along with software reliability, and determine the end time of the test process.

References

1. Lyu, M.R.: Handbook of Software Reliability Engineering. McGraw Hill and IEEE Computer Society Press, New York (1996)
2. Bansal, A., Pundir, S.A.: Review on approaches and models proposed for software reliability testing. *Int. J. Comput. Commun. Technol.* **4**(2), 7–9 (2013)
3. Xavier, J., Macêdo, A., Matias, R., et al.: A survey on research in software reliability engineering in the last decade. In: Proceedings of the 29th Annual ACM Symposium on Applied Computing, pp. 1190–1191. ACM (2014)
4. Duran, J.W., Wiorowski, J.J.: Capture-recapture sampling for estimating software error content. *IEEE Trans. Softw. Eng.* **1**, 147–148 (1981)
5. Nathan, I.: A deterministic model to predict “error-free” status of complex software development. In: Workshop on Quantitative Software Models for Software Reliability, Complexity and Cost: An Assessment of the State of the Art
6. Musa, J.: Operational profiles in software-reliability engineering. *IEEE Softw.* **10**(2), 14–32 (1993)
7. Littlewood, B., Verrall, J.L.: Likelihood function of a debugging model for computer software reliability. *IEEE Trans. Reliab.* **30**(2), 145–148 (1981)
8. Goel, A.L., Okumotu, K.: Time-dependent error detection rate model for software reliability and other performance measures. *IEEE Trans. Reliab.* **28**(3), 206–211 (1979)
9. Xu, R.: The testing method based on software knowledge. *J. Wuhan Univ. (Nat. Sci. Edn.)* **46**(1), 61–62 (2000)
10. de Santiago Jr., V.A., Vijaykumar, N.L.: Generating model-based test cases from natural language requirements for space application software. *Softw. Qual. J.* **20**(1), 77–143 (2012)
11. Kan, S.H.: Metrics and models in software quality engineering (2003)
12. Covert, R.P., Philip, G.C.: An EOQ model for items with Weibull distribution deterioration. *AIIE Trans.* **5**(4), 323–326 (1973)

Development of Virtual Reality-Based Rock Climbing System

Yiming Su, Dingfang Chen^(✉), Congxing Zheng,
Sihan Wang, Liwen Chang, and Jie Mei

Institute of Intelligent Manufacturing and Control,
Wuhan University of Technology, Wuhan, China
953477859@qq.com

Abstract. In this paper, development of virtual reality-based rock climbing system is demonstrated. As virtual reality possesses immersive, synchronous and interactive characteristics, the VR technology has been widely used in many engineering areas. Through the combination of multi-path variable amplitude rock climbing machine and the virtual reality technology, the users can do the rock climbing sports in room environment with immersive experience. The virtual rock climbing scene is developed based on the Unity3D engine to achieve the interaction among the user, the rock climbing machine and the virtual reality environment. The system utilizes virtual reality technologies such as HTC Vive, Leap Motion and Unity3D game engine in an attempt to simulate an immersive rock climbing experience. The rock climbing machine is designed that capable of changing the path or amplitude automatically, which overcomes the defects of indoor climbing machine with fixed route. With the VR technology, it greatly improves the indoor climbing experience.

Keywords: Virtual reality · Unity3D · Leap Motion · Rock climbing

1 Introduction

Virtual reality (VR) typically refers to computer technologies that use VR headsets to generate the realistic images, sounds and other sensations, through which users can interact with virtual objects or stimuli that are modeled from the real world. VR environments have been used extensively in a variety of fields, such as cinema and entertainment, healthcare and clinical therapies, engineering, education and training and so on which offers users numerous advantages and benefits such as immersive, interactive and cost-efficient experiences [1]. The study of VR technology possesses an interdisciplinary characteristic. Through the advancement of interface technologies, VR will eventually become widely popular, changing our lifestyle and making our work easier [2–4].

There are many commercial indoor rock climbing machines available in the market [5–7]. The Treadwall series indoor climbing machine, released at 2012, is one of the most widely used climbing machine, which is the first generation of the track format climbing machine. However, its climbing path is single and repeated which lacks immersive sense. Currently, there are more and more research and development work

using VR techniques to construct virtual environments combined with mechatronic for different physical education applications. Widerun is the first fully interactive bike trainer specifically designed to deliver engaging fitness sessions through VR headsets and external screens, delivering a responsive, immersive, biking experience with unlimited virtual 3D worlds featuring games and bike tracks.

In this research, the VR environment was developed to connect to the rock climbing machine and provide a nearly real experience [8, 9]. HTC Vive was utilized as the VR helmet, Leap Motion was used to recognize user’s hands and Vive Tracker to track the position and orientation of the rock climbing machine. To satisfy the function of immersive rock climbing system, a suitable development engine is necessary, which should work well with HTC Vive, Leap Motion and Vive Tracker with accessory hardware devices. Unity3D engine is chosen as it can meet all above needs at the same time [10, 11]. The system combines rock climbing fitness and social networking, to provide users with immersive rock climbing experience, and give users a scientific feedback report of health.

2 Development

The developed VR system consists of following components, which include the user control interface, 3D geometric model of the entire environment and the correspondence of the virtual and real.

The overall VR system architecture is illustrated in Fig. 1. A number of software tools as well as hardware interfaces are used to develop the VR environment.

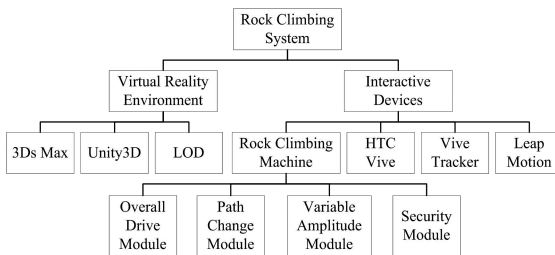


Fig. 1. Overall system architecture

2.1 The Control Interface and the Program Design

The Control Interface consists of four main interfaces, which are Log in Interface, Mode Selection Interface, Setting Interface and Mountains Selection Interface. Each main interface is built in different scene using UGUI [12] (Fig. 2).

Control interface is the windows for information exchanging between user and the system. User can interact with it according to his/her needs. Each main interface contains one or more sub-interfaces. All of them form the application interface level that implements the system function operation.



Fig. 2. Four main interfaces of the Control Interface

So as to accomplish the login function, we create a database with two sheets. They are user base information sheet: users: id, username, avatar and user authorization information sheet: user_auths: id, user_id, identity_type, identifier, credential. When the user sends the mailbox/username/phone number and password request to log in, we first determine the type then check the credential. For example, someone use username “xiaoming” to login, part of the code is shown below:

```
SELECT * FROM user_auths WHERE identity_type = 'username' and identifier='xiaoming'
```

It will return user_id when password match with credential.

When user is in the scene “SelectMount” and select a mount, the program will load the ‘LoadingScene’ at first, then start the Coroutine ‘BeginLoading’ on its Start function. Part of the code is shown below:

```
IEnumerator BeginLoading ()
{
    asyn = SceneManager.LoadSceneAsync(MountName);
    yield return asyn;
}
```

The progress of “asyn” will be shown in “LoadingScene” as shown in the Fig. 3.



Fig. 3. Loading progress of a mountain scene

The Setting Interface, which consists of video settings and audio settings, enable user to change the effect of mountain scene and the sound of system (Fig. 4).

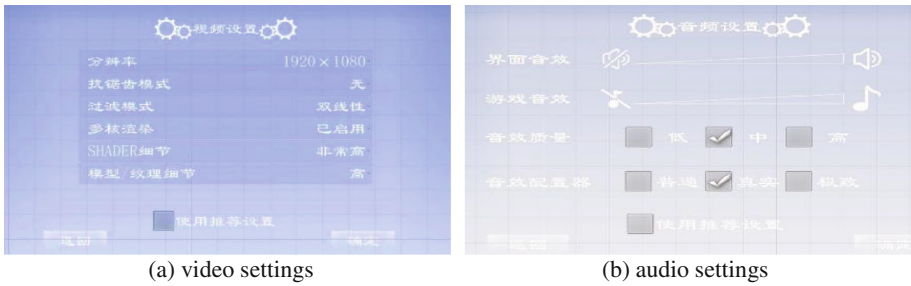


Fig. 4. Two sub-interface of the Setting Interface

The video settings allow user to set the resolution, the anti-aliasing mode, the filtering mode or shader to tell system how to render. The audio settings are for adjusting the volume and quality of all sounds in the entire climbing system, giving the user the most comfortable sound experience.

2.2 Geometric Model

2.2.1 Construction of Large-Scale Outdoor Rock Climbing Scene Modeling

The virtual scene model is the 3D data foundation of the virtual reality system [13]. The fidelity of the model and the data precision are the key factors to the successful construction of the virtual reality system. In this paper, the construction process of large-scale outdoor rock climbing scene and the key technology of large-scale virtual scene for VR application are systematically studied. Finally, the construction of large-scale immersive rock climbing scene is completed. The building process is shown in Fig. 5.

Step 1: Select the real outdoor climbing peaks for parametric analysis. Study the corresponding terrain appearance to provide data and graphics support for the establishment of virtual mountain model.

- Step 2: Using the Terrain tool in Unity3D to draw the rough model of the mountain, and then build the detailed model to shape it to be similar with the real mountain appearance.
- Step 3: Map the model and improve the mapping quality. Add the sky, sunlight, trees and other natural elements to increase the reality degree and improve the immersive experience.
- Step 4: To determine whether the virtual rock climbing scene is similar to the real peak scene. If there is a big gap, it is necessary to continue to optimize the model to develop the immersion sense. If it meets the requirements, the scene is supposed to be completed.

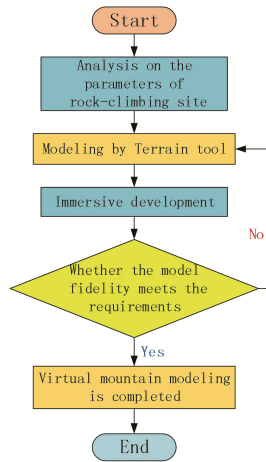


Fig. 5. Large-scale outdoor rock climbing scene modeling process

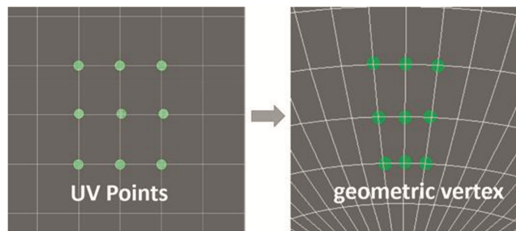


Fig. 6. UV mapping principle

2.2.2 Development of Immersive Scene

For a three-dimensional model, there are two most important coordinate systems, one of which is the position of the vertex (X, Y, Z) and the other for the UV coordinates [14]. As shown in Fig. 6, the UV texture map defines the location information in the map, which is associated with the 3D model and the location of the model surface texture. The UV texture mapping technology is different from the traditional plane projection

map. Each point of the image is accurately matched to the surface of the model object, and the gap between the two adjacent points is processed by the smooth interpolation of the image.

In the 3ds MAX 3D modeling software, polygon modeling technology is utilized to build the rock model, as shown in Fig. 7(a). The rock texture map is obtained by contrasting it to the real rock appearance. Through the UV mapping technology, the rock model map is rendered to derive the final model, which is shown as Fig. 7(b).

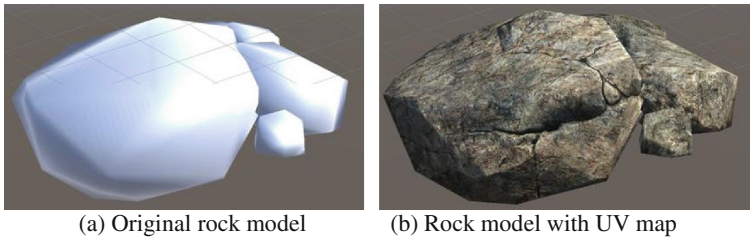


Fig. 7. Rock model built by polygon modeling technology and UV map method

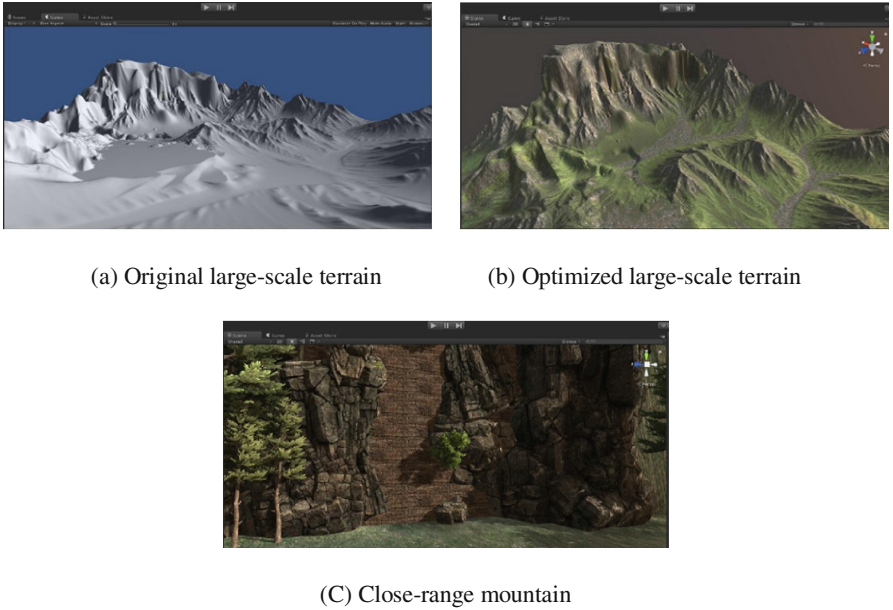


Fig. 8. Mountain modeling

The brush tool of the terrain editor is utilized to build the mountain model. By referring the model to the actual mountain surface of the Roraima, the mountains, valleys and plains in the real peaks as shown in Fig. 8(a) are carved out. By using Photoshop software to deal with the color map and the normal map of the environment, the corresponding textures are obtained. Then the terrain editor tool is adopted to select the

different materials on the terrain mapping. The model effect is shown in Fig. 8(b). The close-range mountain is shown in Fig. 8(c).

2.2.3 LOD Technology

In the process of running virtual reality system, the hardware system has to do real-time rendering, which puts forward higher requirements to complex scene optimization. LOD technology can guarantee the visual effect. With the virtual point of view and the target model object distance data changed, the system shows models of different levels. LOD follows the principle that rough model is drawing for long range and detailed one is for close range. The LOD principle is designed as shown in Fig. 9.

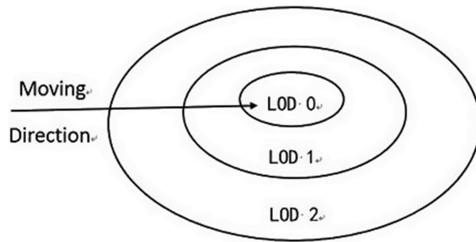


Fig. 9. LOD schematic

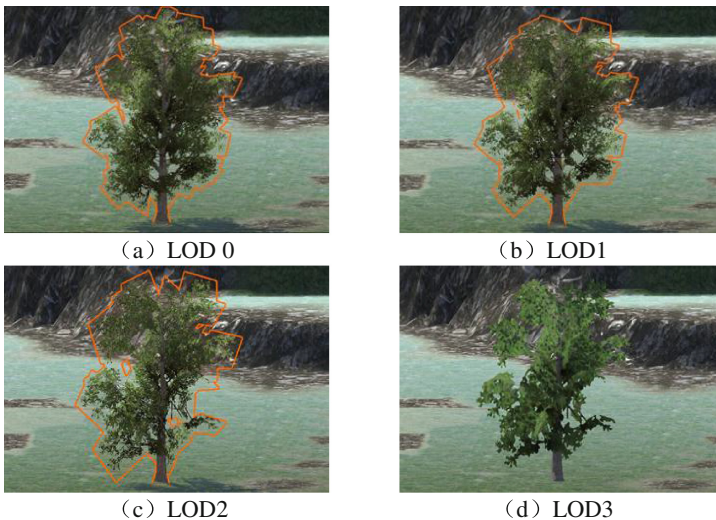


Fig. 10. LOD rendering models

Through the establishment of different level of detail complex models and drawing corresponding levels, it can realize the optimization of computing resources on the basis of ensuring visual effects. The system is based on Unity3d engine. By applying LOD Group components and add different level models, optimal resource adjustment is

achieved. Taking the tree model as an example, the LOD level detail rendering technique is designed as shown in Fig. 10.

2.3 Correspondence of the Virtual and Real

2.3.1 Correspondence of the Climbing Surface

When the machine's amplitude changes, the position and rotation of the tracker will change at the same time. Since the rotation center or axis of the virtual mountain surface or the rock climbing surface is different, it is necessary to transform the position and rotation of the tracker then set it as the virtual mountain surface's ones in order to superimpose the virtual mountain surface on the rock climbing surface after the machine's amplitude changed.

A script, named *Accessory.cs*, is attached to the virtual mountain surface in order to fix the relative position and rotation of Vive Tracker and the rock climbing machine. Part of the code is shown below [15]:

```
//Get current Tracker pose

Vector3 tracker_position =
SteamVR_Controller.Input(deviceIndex).transform.pos +
GameObject.Find("LMHeadMountedRig").transform.position;

Quaternion tracker_rotation =
SteamVR_Controller.Input(deviceIndex).transform.rot *
GameObject.Find("LMHeadMountedRig").transform.rotation;

//Transform current Tracker pose to Accessory pose

this.transform.rotation = tracker_rotation * delta_rotation;

this.transform.position = tracker_position + (tracker_rotation *
delta_rotation) * delta_displacement;
```

2.3.2 Correspondence of the Climbing Holds

In order to match the hold in the virtual system, it is necessary to convert the plane position data to the position data of the hold relative to the starting point. We firstly obtain the relative position of the tracker and the zeroth hold on the zeroth plate, and thus deduce the position where the virtual hold should be, and then use this as the starting point for the virtual holds. In the virtual scene, we create an empty *GameObject* as the plane where all holds are placed, named *HoldsGroup*. We load each hold in accordance with the distance, converted from the path file, of the hold relative to the starting point, and make it perpendicular to the *HoldsGroup* plane. Finally, we superimpose the

HoldsGroup plane on the virtual mountain surface so that the virtual hold can coincide with the real hold.

Besides, we acquire the running speed of the rock climbing machine by using encoder during the operation of it, and send it to PC via Serial Port. When the machine is running, the rock climbing surface will rotate and the real holds will continuously move down. We move up the Room in the VR environment at the speed received from machine so as to match the virtual hold with the real hold through.

3 Interactive Device

3.1 Leap Motion

Leap Motion is use as hands and fingers tracking device [16]. In order to use Leap Motion normally, we need to install Leap Motion Orion software and download and import the *UNITY CORE ASSETS* package to the Unity3D “IndoorClimbing” project. Then we drag a *LMHeadMountedRig* into the scene from the path: LeapMotion/Prefabs. The *LMHeadMountedRig* prefab uses the camera location provided by Unity to place the *LeapHandController* at the correct position in the virtual world. The coordinates in the tracking data are then transformed from Leap space to Unity space relative to the position and orientation of the *LeapHandController* game object.

We import the UI Input module as well in order to control the standard Unity UI widgets by naked hands. The primary component of the UI input module is the *LeapEventSystem* prefab. The *LeapInputModule* script component of this prefab implements a Unity Input Module that uses tracking data to allow the user to manipulate standard UI controls with their hands.

3.2 Vive Tracker

Vive Tracker have many modes to communicate with PC, the mode we used is that track moving objects using a wireless interface in VR, with the accessory (refer to the rock climbing machine) passing data to a PC via ‘FATFS-SDIO-USB’ [15]. The dongle is used to transfer tracking data from the Vive Tracker to a PC, but the accessory transfers data to/from a PC directly for a specific purpose based on our design that transfer the

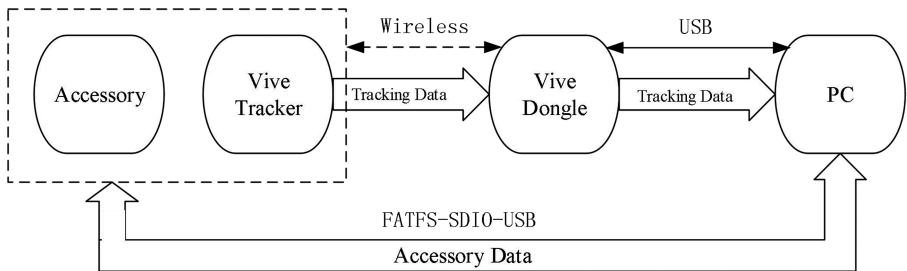


Fig. 11. The communication mode

path file to the rock climbing machine's controller. The communication mode is shown in Fig. 11.

3.3 The Rock Climbing Machine

We have designed a rock climbing machine that is compatible with the immersive rock climbing system. The developed virtual reality-based machine enables interaction with the immersive rock climbing environment. There are four functional modules that were designed to achieve the experience of the indoor climbing as similar as outdoor climbing by superimposing virtual mountain surface on the rock climbing surface (Fig. 12).

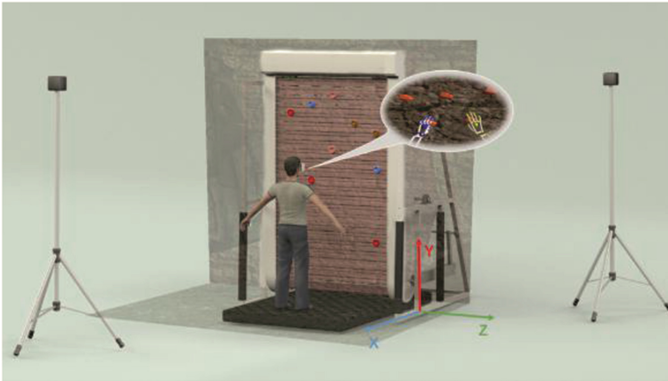


Fig. 12. The virtual mountain surface superimposed on the rock climbing surface

The overall drive module controls the rock climbing machine to work through human body weight as well as hydraulic resistance, to achieve the dynamic balance of people climbing process. The path change module is used to achieve the path change of the rock climbing process during climbing. We design the variable amplitude module to change the slope of climbing machine through the worm gear mechanism in order to simulate the different slope of the rock in the real outdoor rock climbing. The security module is used to reduce the risk of the user during the climbing process and the failure rate of the machine.

4 Conclusion

Virtual Reality Technology as Emerging Technology has a huge development prospects. Climbing movement as a new movement is also increasingly favored by the masses. The immersive rock climbing system not only effectively solves the problem of rock climbing site, but also puts forward a good solution to the problem of repeated path of indoor climbing machine and dull experience. The system combines rock climbing machine with virtual reality technology to achieve the experience of indoor rock climbing more intense, more authenticity. The system make the climbing movement, whose risk factor is large, into a safe indoor movement, and broaden the range of people who can enjoy the rock

climbing. Users can stay at home to enjoy the beauty of the world's major famous climbing mountains via this system. This project is of great significance to the development of rock climbing and the combination of virtual reality technology and sports [17].

References

1. Chen, D.: *Colorful Virtual Reality World*. China Water & Power Press, Beijing (2015)
2. Yu, X.: *Virtual Reality Technology Basic Tutorial*. Tsinghua University Press, Beijing (2015)
3. Shen, Y.: *Virtual Reality Technology*. Tsinghua University Press, Beijing (2009)
4. Wang, H.: *Virtual Reality: Leading the Future Human-Computer Interaction Revolution*. China Machine Press, Beijing (2016)
5. Magiera, A., Rocznio, R.: The climbing preferences of advanced rock climbers. *Hum. Mov.* **14**(3), 254–264 (2013)
6. Hinch, T.: “It’s a place to climb”: place meanings of indoor rock climbing facilities. *Leisure/loisir* **38**(3–4), 271–293 (2014)
7. Udrea, P.E.: *Rock climbing exercising machine*. CA, CA 2794590 A1 (2014)
8. Zulj, S., Seketa, G., Dzaja, D., Celic, L., Magjarevic, R.: Virtual reality system for assisted exercising using WBAN. In: *IFMBE Proceedings of 6th European Conference of the International Federation for Medical and Biological Engineering*, vol. 45, pp. 719–722 (2014)
9. Zhang, L., Liu, Q.: Application of simulation and virtual reality to physical education and athletic training. In: Pan, Z., Cheok, A.D., Müller, W., Chang, M., Zhang, M. (eds.) *Transactions on Edutainment VII. LNCS*, vol. 7145, pp. 24–33. Springer, Heidelberg (2012). https://doi.org/10.1007/978-3-642-29050-3_3
10. Jerald, J., Giokaris, P., Woodall, D., Hartbolt, A., Chandak, A., Kuntz, S.: Developing virtual reality applications with unity. In: *Virtual Reality*, pp. 1–3. IEEE (2014)
11. Linowes, J.: *Unity Virtual Reality Projects*. Kybernetes, vol. 29, no. 3 (2015)
12. Jackson, S.: *Unity3D UI Essentials* (2015)
13. Mooney, T.: *3ds Max Speed Modeling for Games*. Packt Publishing, Birmingham (2012)
14. Xudong, Q.: *Research on 3D Model Codec*. (Doctoral dissertation, University of Science and Technology of China)
15. HTC Corporation: *HTC Vive Tracker Developer Guideline* (2017)
16. Nandy, A.: *Leap Motion for Developers*. Apress, New York (2016)
17. Chang, L., Chen, D.: The development of immersive rock climbing system based on virtual reality technology. In: *National Conference on Intelligent Manufacturing*. Chinese Association of Artificial Intelligence (2016)

Kinematics and Simulation Analysis of a 3-DOF Mobile Handling Robot Based ADAMS and MATLAB

Jingbo Hu, Dingfang Chen^(✉), Lijie Li, Jie Mei, Qin Guo, and Huafeng Shi

School of Logistic Engineering, Wuhan University of Technology, Heping Road No.1040,
Wuchang District, Wuhan 430063, Hubei, China
cadcs@126.com

Abstract. A 3 Degree-Of-Freedom (DOF) mobile handling robot model is designed by SolidWorks package. The link coordinate system and kinematics equation is established by the D-H parameter method. The kinematics and inverse kinematics is solved and it offers theoretical foundation. And then, the kinematics simulation analysis of the robot is carried by using ADAMS–multi-body dynamic simulation software. Finally, the trajectory planning is carried out by MATLAB. It establishes the foundation for the structure design, dynamic analysis and control system of the robot.

Keywords: D-H parameter method · Handling robot · Kinematic
Adam simulation · Coordinate system

1 Introduction

The handling robot made in KUKA, ABB and so on has been used in the production process of assembly, welding, handling and etc. [1]. With the robot technology gradually becoming mature, handling robots have presented an important support in the field of industrial production [2]. In microelectronics manufacturing, welding, packaging and many other areas, handling robots have been widely used [3]. At present, the handling robot has been widely used in the national economy in all important aspects [4]. But, there are less robots which combines motion and handling. In fact, robots combining motion and handling are necessary and can play important role in many fields.

In this paper, a mobile handling robot model is established. And in the end the displacement of the joints is analyzed, which provides the basis for the debugging of handling robot, saving the on-site debugging time and protecting the handling robot in an extent [5].

2 Kinematics Models of 3-DOF Mobile Handling Robot

The robot designed in this paper is a 3 DOF mobile handling robot. Three manipulators are rotating joints and the rotation axes are parallel to each other. As shown in Fig. 1, the front mobile platform (1) is equipped with a servo for the steering of the mobile platform, and the servo implements the forward and backward commands of the

platform. The joints (7), (8), (9) are individually driven by a servo to achieve steering. All servos are controlled by the controller (3). The end part of the arm (6) can be provided with different clamping mechanisms depending on the work object. In the actual process, through the mobile platform, the object can be held and moved from the target point 1 to the target point 2.

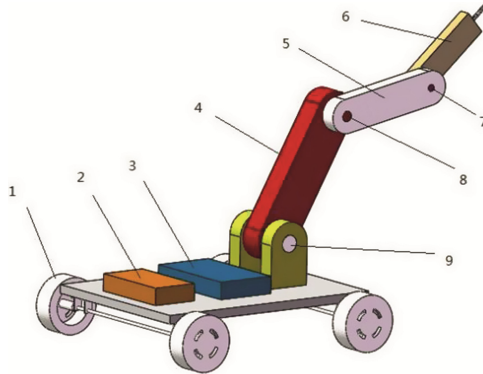


Fig. 1. Three - dimensional simplified model of mobile handling robot. 1-Mobile platform, 2-Additional weight, 3-Controller, 4-Big arm, 5-Middle arm, 6-End arm, 7-Joint 3, 8-Joint 2, 9-Joint 1

As the robot actually works, the movement and handling are not carried out at the same time. Therefore, the model can be simplified in the analysis of the robot’s handling characteristics. The mobile part of the robot can be neglected temperately, and only manipulator is analyzed. According to the D-H parameter method, the coordinate system of the links in the manipulator is built. The coordinate system of each joint is established at the end of the link. Each coordinate system draws only two axes in the Fig. 2.

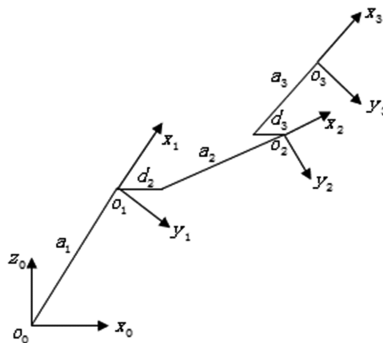


Fig. 2. Link coordinator system of the mobile handling robot

According to the link coordinate system established in Fig. 2, the corresponding D-H parameter table can be obtained, as shown in Table 1.

Table 1. D-H parameter table of the mobile handling robot

Joint (<i>i</i>)	$a_i(\text{mm})$	$\alpha_i(^{\circ})$	$d_i(\text{mm})$	$\theta_i(^{\circ})$
1		-90	0	θ_1
2	a_2	0	d_2	θ_2
3	$a_1 a_3$	0	d_3	θ_3

According to above table, the posture transformation matrix is obtained as:

$${}^0_3T = {}^0_1T {}^1_2T {}^2_3T = \begin{bmatrix} n_x & o_x & a_x & p_x \\ n_y & o_y & a_y & p_y \\ n_z & o_z & a_z & p_z \\ 0 & 0 & 0 & 1 \end{bmatrix} \tag{1}$$

In the analysis, the geometric and joint variables of links are supposed to be known, and the position and posture of the robot terminal actuator relative to the reference coordinate system can be solved [6]. The inverse kinematics means that the position and posture of the robot terminal actuator are provided to derive the joint parameters. In order to control the robot arm, the inverse kinematics solution is the basis of the robot movement [7]. It is because that in the practically work, the variables of all joints are determined according to the position of target point.

For a given position and posture, the transformation matrix of robot is deduced as formula (1), The values of the joint variable $\theta_1, \theta_2, \theta_3$ can be solved by using corresponding inverse transformation matrix multiply Eq. (1), as shown in Table 2:

Table 2. The algebraic solution of each joint

$\theta_i(^{\circ})$	The algebraic solution
θ_1	$\arctan (a_x/a_y)$
θ_2	$\arctan ((a_x c\theta_1 - a_z s\theta_1)/(a_z c\theta_1 + a_x s\theta_1))$
θ_3	$\arccos (c\theta_2(n_x c\theta_1 - n_z s\theta_1) - s\theta_2(n_z c\theta_1 + n_x s\theta_1))$

3 Kinematics Analyses

Virtual Prototyping Technology is a digital design method based on virtual prototyping, which can shorten product development cycles, improve product quality [8]. A three-dimensional simplified model of the robot is imported into an ADAMS virtual prototype for simulation [9]. Adam simulation is carried out to get the displacement curve of the marker points relative to the earth, as shown in Figs. 3, 4, 5 and 6

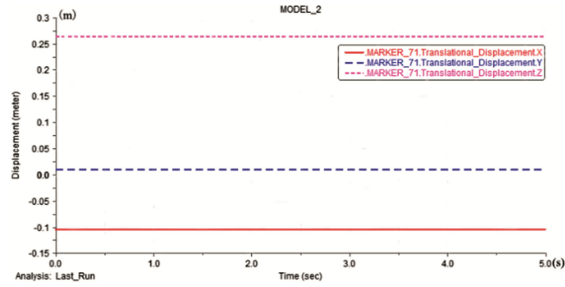


Fig. 3. The marker point displacement curve of joint 1

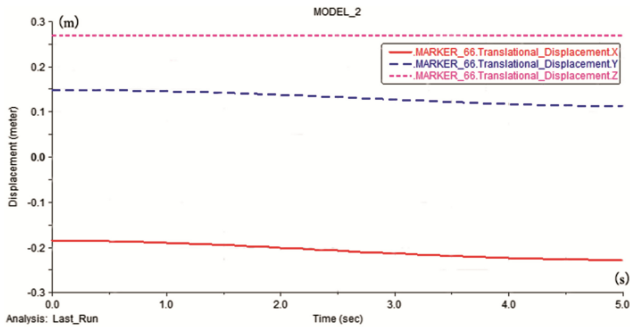


Fig. 4. The marker point displacement curve of joint 2

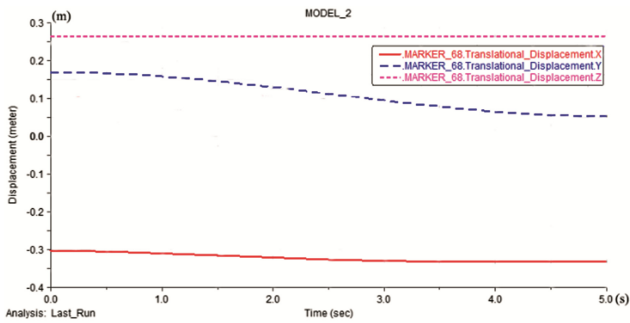


Fig. 5. The marker point displacement curve of joint 3

As it can be seen from Fig. 3, the displacement of the mark point 1 does not change because the joint shaft 1 is connected to the seat (i.e., the base), so that the displacement does not change. From Figs. 4, 5 and 6, it is found that the displacement of the marker points in the Z direction does not change and there is no movement in the Z direction. In the X, Y direction, the displacement curve approximates in the form of a sin function. The results of the above ADAMS simulation are in accordance with the actual situation, which verifies the rationality of the designed structure. The kinematics analysis and research provide the theoretical and simulation basis for the subsequent product design.

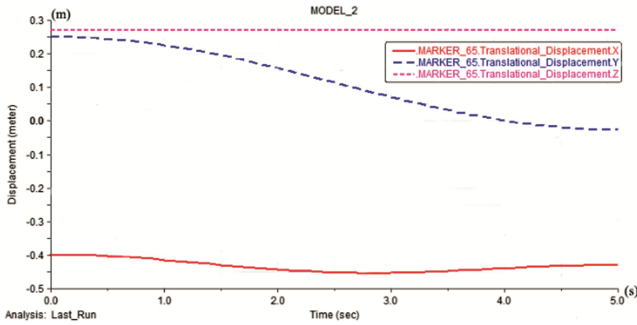


Fig. 6. The marker point displacement curve of terminal link 3

4 Trajectory Planning

The trajectory planning is to map each joint variable to a smooth time function [10], which includes Cartesian space planning and joint space planning. The Cartesian space planning is to use the Cartesian coordinate points' sequences of the end effector position to constitute a trajectory, which may reach the singularity. But the situation does not appear in the joint space planning. In this paper, the trajectory planning of robot is carried out by using the joint space planning method (Fig. 7).

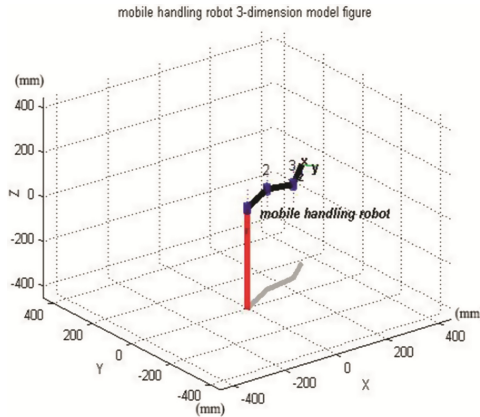
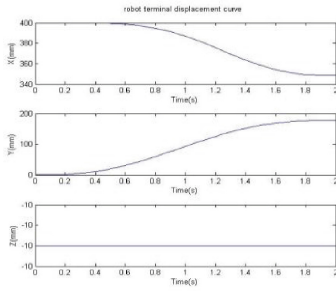
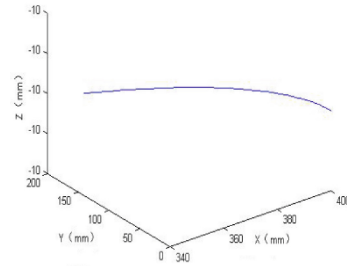


Fig. 7. Space model of robot

As can be seen from Fig. 8, the kinematic curve in the x, y direction of the terminal manipulator can be seen as a trigonometric function, and the kinematic curve in the z direction can be considered basically no change, which is the same as the previous Adam simulation results. If the image is furtherly solved, the correlation graph of velocity and acceleration can be obtained. It can be seen that the trajectory is in accordance with the operational requirements of the mobile manipulator robot, indicating that the path planning method is reasonable.



(a) Displacement curve



(b) Three-dimensional space trajectory

Fig. 8. Terminal manipulator

5 Conclusion

In this paper, the displacement curves of the three joints and the end point of the robot are obtained, and the rationality of the structural design is verified, which provides the theoretical and simulation basis for the next step of the robot design. The two-dimensional and three-dimensional displacement curves of the end of the manipulator further validate the rationality of the mechanism and the correctness of the Adams simulation. It establishes the foundation for the structure design, dynamic analysis and control system of the robot.

References

1. Miao, D.: Design and Dynamic Performance Analysis of Heavy Load Handling Robot. Hefei University of Technology (2014)
2. Li, R.: Development strategy of industrial robot industrialization in China. *Aviat. Manuf. Technol.* **9**, 32–37 (2010)
3. Li, C., Yang, Z., Cai, T.: A motion planning of moving robot based on ADAMS simulation. *Mech. Transm.* **9**, 28–31, 37 (2016)
4. Song, D.: Application of industrial robot in manufacturing industry. In: China Automotive Industry and Equipment Manufacturing Industry Development Forum (2008)
5. Han, X., Li, C., Yu, X., Zhao G.: Modeling simulation of arc welding robot based on ADAMS/view. *Weld. J.* **4**, 69–72, 116 (2013)
6. Cai, Z., Xie, B.: Robotics, 3rd edn. Tsinghua University Press, Beijing
7. Ding, L., Li, E., Tan, M., Wang, Y.: Design and kinematics analysis of five-DOF moving robot system. *J. Huazhong Univ. Sci. Technol.* **S1**, 19–22 (2015). (Natural Science Edition)
8. Chen, Z., Dong, Y.: Characteristics and Examples of MSC Adams Simulation of Multi-Body Dynamics. China Water Resources and Hydropower Press, Beijing (2012)
9. Ma, R., Hao, S., Zheng, W.: Research on joint simulation of manipulator based on MATLAB and ADAMS. *J. Mech. Des. Manuf.* **4**, 93–95 (2010)
10. Wang, Y., Yu, X., Li, N., Zhu, W.: Kinematical analysis of ROBONOVA-1 robot. *J. Xihua Univ.* **03**, 6–9, 22 (2009). (Natural Science Edition)

A New Type of 3D Printing Nozzle with PET Wire as Raw Material

Yawei Hong, Shaobo Li^(✉), Shupeí Wu, Tianhao Huang, Guang Liu, Liwen Chang, and Yang Zhang

Yujiatou Campus, Wuhan University of Technology, Wuhan, Hubei, China
1985296054@qq.com

Abstract. In this paper, the wasted PET bottles were analyzed. With the experiment analysis and the related literature, we determine the feasibility of the wasted PET plastic bottles as 3D printing materials. We design and introduced the principle of the 3D print nozzle of using the positive and negative screw to extrude material. The feasibility of the design is demonstrated by three - dimensional modeling, physical experiment analysis and ANSYS simulation analysis.

Keywords: FDM technology · PET material · Positive and negative screw
The modification of material

1 Introduction

The “No.1” plastic bottle which is made of the PET material accounts for more than half of the plastic bottle market. The output is huge, but its recovery rate is low [1]. The PET material can be used as an excellent printing supplies, because of its strong adhesion between the layers, good mobility, easy carbonation and other advantages. However, due to the crystallization rate of the PET material is slow, the PET material can't meet the requirements of 3D printing technology rapid prototyping.

In recent years, FDM technology is the most used 3D printing technology, many open source desktop 3D printers are mostly using this program [2]. FDM printing supplies are mostly ABS and PLA [3], supplies are expensive, and ABS in the printing process will release toxic gases. The use of ABS and PLA for FDM printing has some shortcomings. For example, it is easy to break the wire, poor extrusion molded product and product strength is not enough and the surface accuracy is poor. To improve the printing performance, Kannan [4] added iron powder to the ABS, the addition of surface active agent material made of iron powder or ABS composite. You Shu studied the effect of 3D printing conditions on the mechanical properties of PLA plastics [5].

In this paper, we first studied the modification of materials. We have designed a nucleating agent addition device, positive and negative threaded screw extrusion device, heating and cooling system. The feasibility of the design is demonstrated by three-dimensional modeling, physical experiment analysis and ANSYS simulation analysis.

2 The Study on Modification of Materials

The experiment two types of mainstream PET plastic bottles on the market were DSC experiments, the experimental results shown in Figs. 1 and 2. From the DSC experimental data obtained, wasted PET material T_m is 240°C – 255°C , the difference between pure PET plastic bottle is not much, and it can be used for secondary processing.

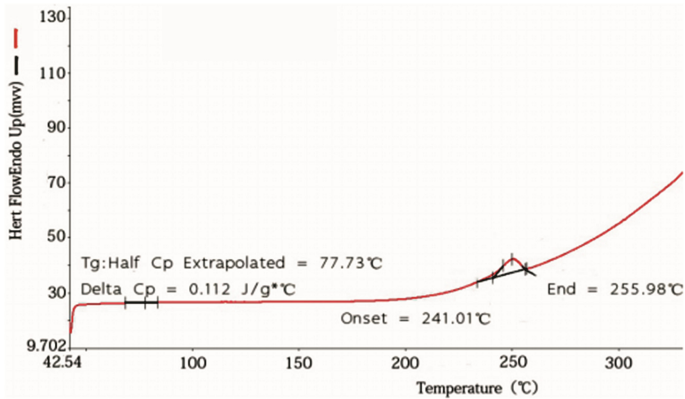


Fig. 1. Nongfushanquan

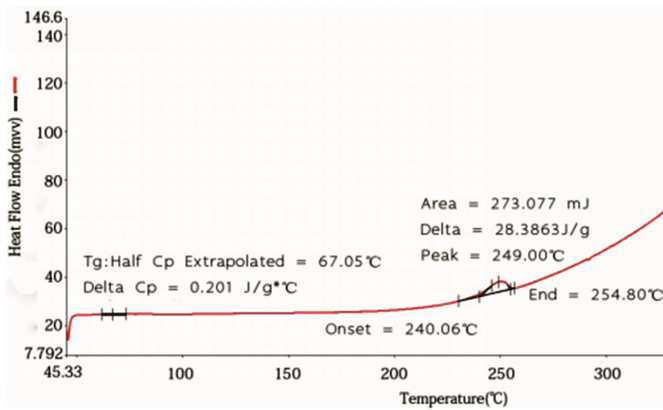


Fig. 2. Yibao

It is helpful to increase the crystallization rate and improve the mechanical properties of the finished product by adding nucleating agent to PET during the melting process [6]. The results showed that the use of inorganic nucleating agent talc powder to modify the PET material, when the nucleating agent to add the quality ratio of 5% [7], the crystallization effect is better, the printing effect is the best.

3 Nozzle Mechanical Structure

3.1 Overview of the Overall Structure

The design of new nozzle structure includes nucleating agent addition device, positive and negative threaded screw extrusion device, heating and cooling system. Figure 3 is a graph model for explosion.

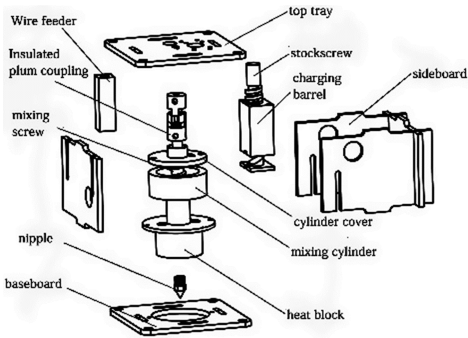


Fig. 3. Model explosion diagram

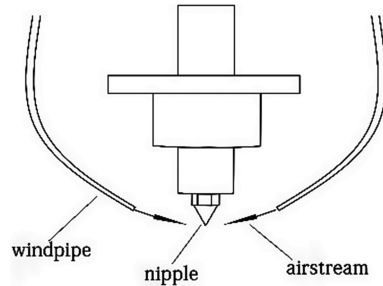


Fig. 4. Schematic diagram of heat dissipation

The nucleating agent adding device comprises a feeding screw rod and a material cylinder. It can achieve the purpose of accurately and stably adding nucleating agent. The extruding device is composed of a mixing cylinder and a positive and negative threaded screw extrusion device.

The heating device is arranged outside the mixing cylinder and is heated by a heating rod, and the temperature is accurately controlled by a temperature sensor. The heat dissipation system adopts the principle of air pump blowing. The heat dissipation effect is better, the energy consumption is lower, and the noise is smaller. A schematic diagram of the heat sink is shown in Fig. 4.

3.1.1 Nucleating Agent Adding Device

Because the amount of nucleating agent is small, and the amount of added material is larger, it needs to be accurately controlled. In this paper, the screw feeding mechanism is used for feeding, the nucleating agent is stored in the material bed and sent to the feed bed continuously through an external device to ensure that the nucleating agent can be continuously transported to the pet cylinder. The feed screw of the nucleating agent is driven by a micro reduction motor, and the rotation speed of the motor is controlled accurately through the PWM wave, so that the nucleating agent in the screw thread gap can be accurately and stably added to the print nozzle.

3.1.2 Positive and Negative Thread Extrusion Device

Device section view as shown in Fig. 6 and screw thread. Both ends of the thread is the thread, the thread and the inner wall of the sleeve is tightly attached at both ends of a

thread feeding extrusion effect. The middle part is anti thread, and the screw thread and the inner wall of the sleeve are buffered by a certain clearance between the threads and the inner wall of the sleeve. PET sheet material into the above material inlet, PET material into the molten state, it will melt the screw thread of PET material is transported downwards and the formation of certain anti back flow in the thread, and after the nucleating agent is fully mixed, melted PET material is down from the nozzle at the lower end of the screw extrusion molding.

3.1.3 Heating and Cooling System

The heating device is arranged around the nozzle and is heated by the mixing device, and the inner part is connected with a heating rod and a temperature sensor. The heating rod when heating block temperature increases when the temperature is higher than the preset temperature, the heating rod stops working. When the temperature is lower than the preset temperature, the heating rod starts working, heating block temperature rise. By this dynamic adjustment process, the internal temperature of the screw extruder is maintained at about 250 °C by controlling the extrusion of the screw.

The heat transfer is installed on the nozzle frame to dissipate heat at the nozzle, so as to ensure that the pet material can be crystallized and cooled in time when the nozzle is extruded.

3.2 Experiments and Simulation Analysis

3.2.1 Positive and Negative Screw Experiment Analysis

First of all, the simulation results show that the positive and reverse directions screw can mix up the PET material with Polymer Nucleators. The experimental process is shown in Fig. 5. The screw can squeeze the molten PET smoothly. In addition, it is verified that the anti-thread can achieve the purpose of mixing.

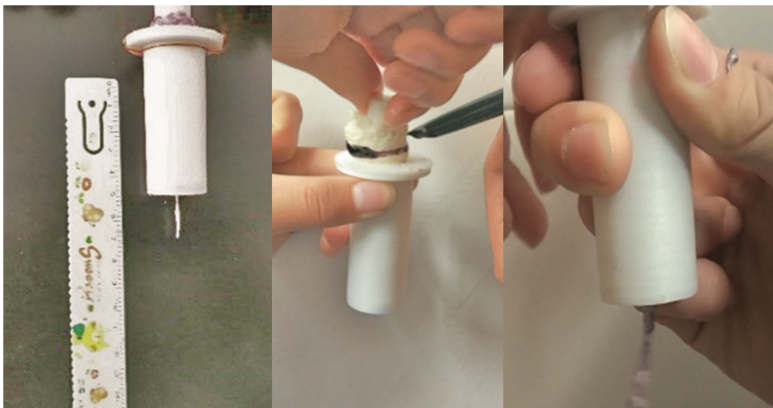


Fig. 5. Test simulation process

Figure 6 is the positive and negative screw in kind. Figure 7 shows the nozzle's working process.



Fig. 6. The positive and negative screw

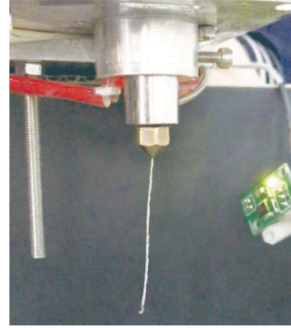


Fig. 7. The nozzle's working process

By analyzing the experiment results, We can obtain that:

- (1) The rate of discharging of the molten PET material depends on the screw's speed. The faster the screw's speed is, the faster the extrusion rate of molten PET material is.
- (2) The molten PET material flows simultaneously in the cartridge and can be well blended with the nucleating agent.
- (3) The flow velocity is relatively stable and PET can extrude smoothly at the nozzle.

3.2.2 Simulation Analysis of Heating and Cooling System

We conduct thermal analysis of the nozzle's heating and cooling modules by ANSYS Workbench [8]. Nozzle, heating block, mixing cylinder's material is brass. Their thermal conductivity is $45 \text{ W}/(\text{m}^*\text{K})$. Screw's material is stainless steel. Its thermal conductivity is $14.6 \text{ W}/(\text{m}^*\text{K})$. We know that the melting temperature of pet is between $245\text{--}255 \text{ }^\circ\text{C}$. The optimum heating temperature of heating rod is obtained by thermal analysis. Nozzle surface's convective heat transfer coefficient is set to $50 \text{ W}/(\text{m}^2*\text{K})$. The heating block is set to $35 \text{ W}/(\text{m}^2*\text{K})$. Mixing cylinder is set to $20 \text{ W}/(\text{m}^2*\text{K})$. By setting different heating temperatures for analysis. When the temperature of the heating rod is set to $270 \text{ }^\circ\text{C}$, the internal temperature of the mixing cylinder reaches $250 \text{ }^\circ\text{C}$. Through the heat pump nozzle, the temperature dropped to $230 \text{ }^\circ\text{C}$. This is consistent with the actual temperature requirement for pet melting during actual printing.

Figure 8 is the temperature distribution nephogram, Fig. 9 is the picture of pressure nephogram.

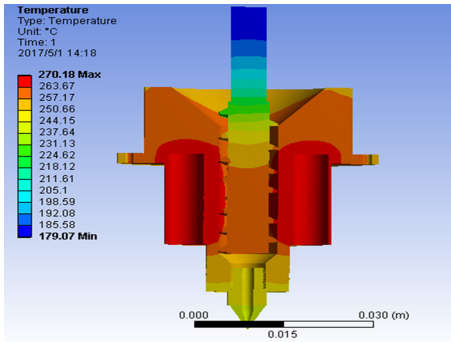


Fig. 8. Temperature distribution nephogram

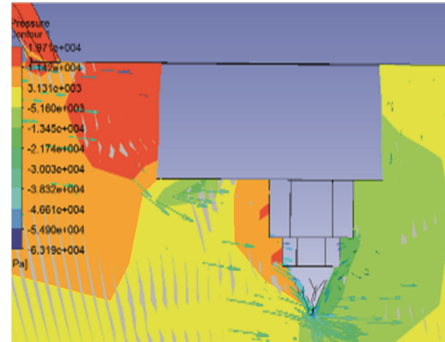


Fig. 9. Pressure nephogram

4 Conclusion

The nozzle we designed completes the modification and extrusion molding of waste PET material. The whole process from the plastic bottle to the actual model can be realized. PET material does not produce toxic substances during printing which is more environmentally friendly Compared to ABS. However the melting range is too narrow. Suitable temperature is an important indicator to measure the printing effect. How to control the printing temperature accurately is a problem we need to solve. Due to the complex internal mechanical structure of the nozzle, the vibration amplitude of the nozzle has a great influence on the model printing accuracy. It is the important direction of mechanical debugging to make the printing more smoothly. This design has solved the current printer can't use PET material as 3D printing raw materials. Waste PET material is cheap, the cost of printing is reduced by about 90% Compared to ABS and PLA materials which provides a new opportunity for the development and wide application of 3D printing technology [9].

References

1. Tang, G., Hu, B., Kang, Z.: Current situation and problems of waste plastics recycling. *Renew. Resour. Recycl. Econ.* **6**(1) (2013)
2. Guo, K.: Three-dimensional printing equipment and data processing software a number of key technology research. Huazhong University of Science and Technology (2008)
3. Melnikova, R., Ehrmann, A., Finsterbusch, K.: 3D printing of textile-based structures by Fused Deposition Modelling (FDM) with different polymer materials. *Mater. Sci. Eng.* **62**(1), 12–18 (2012)
4. Kannan, S., Senthilkumaran, D., Elangovan, K.: Development of composite materials by rapid prototyping technology using FDM method. In: *International Conference on Current Trends in Engineering and Technology*, vol. 13, pp. 281–284 (2013)
5. You, S., Hu, Y., Wei, Q.: Effects of 3D printing conditions on the mechanical properties of degradable polylactic acid. *Plastics* **29**(3), 91–94 (2015)

6. Legras, R., Dekoninck, J.M., Vanzieleghem, A., Mercier, J.P., Nield, E.: Crystallization of poly (ethylene terephthalate) induced by organic salts: model compound study of the mechanism of action of the nucleating agent. *Polymer* **27**, 109–117 (1986)
7. Ailan, Z.: Application of nucleating agents in crystallization of PET. *Polyester Ind.* **05**, 1–5 (2011)
8. Gao, J.: FDM rapid prototyping machine temperature field and stress field numerical simulation
9. Sun, J., Tong, Z., Ying, Z.: Analysis of the market development prospect and application of 3D printing technology. *Wuhan Univ. Technol.* **6**(1), 1672–3918 (2014)

When Partitioning Works and When It Doesn't: An Empirical Study on Cache Way Partitioning

Hanfeng Qin^(✉)

School of Computer Science and Technology, Huazhong University of Science and Technology,
Wuhan 430074, China
hanfengtsin@hust.edu.cn

Abstract. Virtualization and cloud computing technologies enable modern data centers to consolidate various services and applications with the prevalent multi-core processor to improve resource utilization. However, service consolidation has the risk of degraded quality-of-service (QoS) due to uncontrolled contention for the shared *last-level caches* (LLC). Cache partitioning techniques are promising to improve resource utilization as well as guarantee QoS. As the capacity of LLC in data center is ever growing and there have been some practical cache partitioning techniques implemented in production system. Although the partitioning schemes have been explored extensively, how to make effective use of partitioning is still an important problem in data center and not well understood. Given the varying cache configurations, the complex workload mixes of diverse memory characteristics, and the different overheads of partitioning algorithms, we do not always gain performance improvement with cache partitioning. In this paper, we are seeking to explore when partitioning. We investigate the impact of cache configurations, memory characteristic of program, and partitioning variation to the performance gain under partitioning. We also identify several interesting findings and implications which help us in future cache system design and optimization for cloud data centers.

Keywords: Cache partitioning · Memory architecture · Empirical study

1 Introduction

The poor resource utilization in data centers increases the *total cost of ownership* (TCO) of IT service. For example, the average utilization achieves only around 6% to 12% in Google's data center [10]. Recent efforts in virtualization and cloud computing technologies are promising to improve resource utilization by consolidating many services on the same server in data centers. However, co-locating more applications has the risk of degraded *quality-of-service* (QoS) due to uncontrolled contention for shared resources, primarily the *last-level caches* (LLC) [18, 19]. Researchers leverage cache partitioning techniques [17] to address the arbitrary access to the shared LLC. As an important performance isolation mechanism, cache partitioning has been proposed to restrict the available amount of shared cache lines that an applications can access when it co-runs with other workloads. Depending on the optimization target, generally, a cache

partitioning technique consists of a line allocation policy and a partitioning-enable mechanism, which determine the amount of lines a program receives, and enforce such allocation to be actually executed, respectively. Prior works explored many cache partitioning schemes implemented by hardware [8, 14, 15, 19], software [9, 20], or co-designed hardware and software [4, 6].

As the capacity of last-level cache (LLC) in modern x86 processors is ever growing, there have been some practical cache partitioning technologies implemented in production system and markets [4, 6]. It is important to understand how to make effective use of cache partitioning techniques in data center. Despite that cache partitioning techniques have been extensively explored, given the varying cache configurations, the complex workload mixes of diverse memory characteristics, and the different overheads of partitioning algorithms how to use cache partitioning effectively is still a problem and not well understood. We carry an experimental case study that we consolidate various quad-core workload mixes to co-run on the same multicore server that supports cache partitioning, and find that cache partitioning does not always work as an expected winner. Partitioning vanishes its expected performance gains for some workloads, even worse, results in unexpected performance degradation.

We are very interested in the unexpected behavior of cache partitioning which has not ever been studied in prior work. In this paper, we are seeking to explore when partitioning works and when it does not, and how to make effective use of it. With an empirical study on a commonly used way-partitioning technique, we perform a thorough evaluation with the SPEC CPU2006 suite. We group the total 29 programs into 11 subsets based on memory intensity analysis and way sensitive analysis, and construct 77 workloads with various memory characteristics in terms of memory access intensity and associative way sensitivity. We investigate the impact to partitioning performance of many possible factors spanning from cache configurations, memory characteristic of program, and partitioning variations to the performance gain under partitioning. We also identify several interesting findings and implications which help us in future cache system design and optimization for cloud data centers.

We highlight our key contributions here:

- We identify an important problem on how to make effective use of cache partitioning technology which has not ever been well understood by prior studies. To seek answers to this problem, we perform a detailed empirical study on a commonly used way-partitioning technology for a variety of workload mixes with different memory access intensity and associative way sensitivity, and study the impact of cache configurations, memory characteristics of program, and the partitioning variation to the performance gain under partitioning quantitatively.
- We identify several interesting findings and implications which help us in future cache system design and optimization for cloud data centers. (i) There is a close correlation between cache configurations and the performance gains from cache partitioning where cache partitioning does not work in caches of small capacity. Increasing the set number can improve the performance gains of cache partitioning. Moreover, it is not beneficial to design high-associative caches in data center because they do not make cache partitioning work better. (ii) Consolidating services in data centers should take the memory characteristics of programs into account. It degrades

performance when cache partitioning is applied to programs that have less similarity in memory access intensity of high memory intensity. Co-scheduling programs of heterogeneous cache way sensitivity can make effective use of cache partitioning. (iii) The overhead of dynamic partitioning adjustment impacts the performance gains of cache partitioning. Design a partitioning algorithm with a steady partitioning size from less frequently adjustment can improve performance.

2 Motivation

Cache partitioning is an important performance isolation mechanism in use of guaranteeing QoS. Table 1 summarizes the commonly used partitioning schemes during the past research efforts. *Hardware*-based implementations require architecture modification and are performance efficient. *Software*-based schemes are based on page coloring theory that leverage dynamic page allocation in OS to enforce pages to be scattered in contiguous caches. *Co-HW/SW*-based solutions combine the flexibility and efficiency of both software and hardware with low-level architecture extensions and a group of programming control routines.

Table 1. Cache partitioning technologies

Implementation	Partitioning schemes
Hardware	Way-partitioning [8, 14, 15, 19]
Software	Page coloring [9, 20]
Co-HW/SW	Intel CAT [6]

As the capacity of last-level cache (LLC) in modern x86 processors is ever growing. It is important to understand how to make effective use of cache partitioning techniques in data center. For example, Intel releases Xeon E7-8893 v4 processor equipped with an LLC of 60 MB, and IBM Power 8 associates a larger LLC of 96 MB. It is important to understand how to make effective use of cache partitioning techniques in data center. Although has been proposed for a decade around, way-partitioning has still been an active baseline in cache partitioning research [1, 12, 19], even in complex workload in context of cloud computing [3] and warehouse computer [7]. In practical production system and market, Intel releases a cache allocation techniques (CAT) [4, 6] in Haswell SKUs processor, which is also based on way-partitioning.

Although cache partitioning techniques have been extensively explored, how to use cache partitioning effectively is still a problem and not well understood. We carry an experiment and find that cache partitioning does not always work as an expected winner. We consolidate various quad-core workload mixes to co-run on the same multicore server that supports CAT, and measure their performance under the baseline LRU and a CAT-based partitioning policy, respectively. Figure 1 reports the results under the baseline system and CAT-based partitioning. We find that cache partitioning has diverse impact on performance for different workload mixes. For some workloads cache partitioning outperforms LRU indeed as expected. But for some workloads, the expected benefits of partitioning vanish. Even worse, it result in unexpected performance

degradation for some workloads under partitioning. We are very interested in seeking the answer to this unexpected behavior which has not ever been reported in prior work. In this paper, we are motivated to explore when partitioning works and when it does not, and how to make effective use of it.

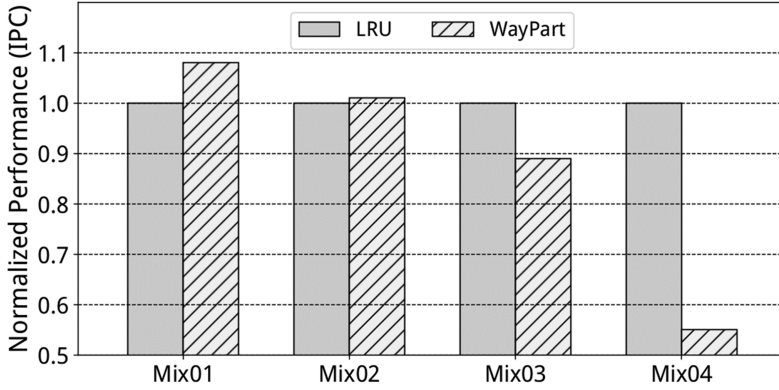


Fig. 1. Performance comparison for various workload mixes under the baseline LRU and the Intel CAT-based partitioning replacement policy

3 Experimental Methodology

3.1 Simulator

We use an event-driven ZSim [16] to model our baseline multicore system. ZSim is a fast x86 micro-architecture simulator based on Intel Pin [11]. We closely model an Intel Sandy-bridge processor, of which configuration parameters are detailed

Table 2. Simulation configurations of baseline multicore system

Components	Parameters
Processor	4-core, 2.6 GHz, Out-of-Order, 4-issue width, 168-entry ROB, 64-entry load queue, 32-entry store queue
L1 Cache	32 KB, split instruction/data cache, 4-way associative, 64-byte block size, 4-cycle latency, LRU replacement
L2 Cache	256 KB, unified cache, 8-way associative, 64-byte block size, 8-cycle latency, LRU replacement
L3 Cache	4 MB, unified cache, 16-way associative, 64-byte block size, 28-cycle latency, LRU replacement
Memory	1 channel, 8 ranks, 8 banks, 64-bit bandwidth, 1333 MHz bus frequency, 64-entry read queue, 64-entry write queue, open page management, 1 KB row buffer, $t_{RCD} = 15$ ns, $t_{CL} = 15$ ns, $t_{RP} = 15$ ns, $t_{WTR} = 7.5$ ns, $t_{WR} = 15$ ns, $BL/2 = 4$, FR-FCFS request scheduler

presented in Table 2. Each core has its private split 32 KB 4-way associative L1 instruction and data cache, and a unified 256 KB 8-way associative L2 cache. A unified 4 MB 16-way associative L3 cache (LLC) is shared by all cores. The default LLC replacement policy in our baseline system is LRU. We choose *Utility Cache Partitioning* (UCP) [14] as way-partitioning candidate, and implement an UCP-based replacement policy, labeled as *WayPart* in Sect. 4. We configure UCP with a per-core 256-line 16-way associative UMON circuits, and enforce the *Lookahead* algorithm to dynamically resize the partitions every 5000 cycles, similar as [14].

3.2 Workloads

The SPEC CPU2006 [5] suite is used to perform evaluation. We compile each program using GCC 6.2.1 with an optimization flag of `-O3`, and feed them with a single reference input. A representative slice of 500 million instructions for each program is identified with PinPoint [13]. To characterize the memory behavior, we perform both way sensitivity analysis and memory intensity analysis for the total 29 programs, respectively.

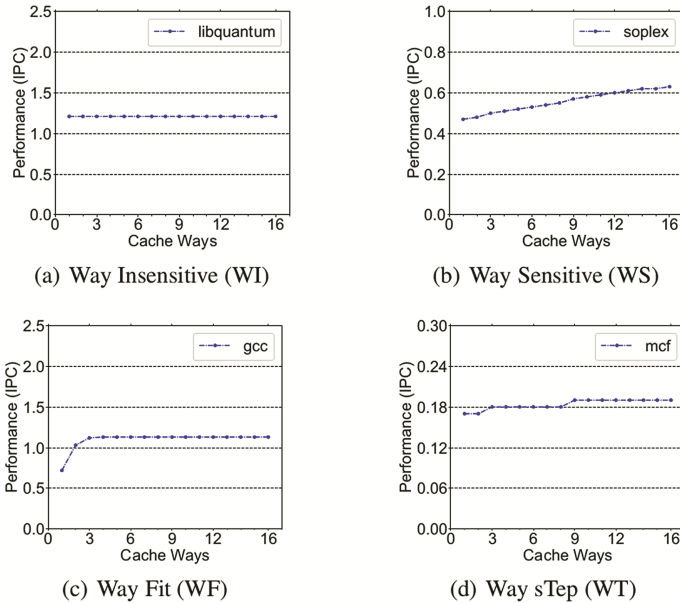


Fig. 2. Sensitivity of performance in terms of IPC to cache ways

Way Sensitivity Analysis. We observe both the varied performance in terms of instructions per cycles (IPC) as we change the available way number a program can access. We classify these programs into four categories: *Way insensitive* (WI) programs do not experience performance improvement as cache way increases. *Way sensitive* (WS) programs have a positive correlation between performance improvement and increased ways. *Way fit* (WF) programs also improve performance as cache way

increases, but would not increase any more at some point even more ways are assigned. *Way step* (WT) programs improve performance as cache way increases, and they show an increased steady phase. Figure 2 depicts the correlation curves of performance and cache ways for typical workload within these categories.

Memory Access Intensive Analysis. We also study the memory access intensity in terms of *misses per thousand instructions* (MPKI) and classify programs into four categories: *High intensive* (HI) programs have MPKI larger than 30, thus generate very high memory pressure. *Medium intensive* (MI) programs have MPKI larger than 10 but less than 30. *Low intensive* (LI) programs have MPKI larger than 1 but less than 10. *Non-intensive* (NI) programs have lower MPKI than 1 and thus they do not contend for the memory bandwidth.

Combining both memory intensity and way sensitivity, we group the total 29 programs into 11 subsets as shown in Table 3. We perform evaluation with a total of 77 quad-workloads mixed with programs from these categories by varying memory intensity and way sensitivity.

Table 3. Memory characteristics of SPEC CPU2006 in a 4 MB shared LLC

#	Memory intensity	Way sensitivity	Benchmarks
G01	HI	WT	429.mcf, 473.astar
G02	HI	WF	470.lbm
G03	MI	WT	437.leslie3d, 482.sphinx3, 459.GemsFDTD
G04	MI	WS	450.soplex, 471.omnetpp, 483.xalancbmk
G05	MI	WI	462.libquantum, 433.milc
G06	LI	WT	434.zeusmp, 445.gobmk, 436.cactusADM
G07	LI	WF	447.dealII
G08	NI	WT	400.perlbench, 435.gromacs
G09	NI	WF	458.sjeng, 403.gcc, 444.namd, 481.wrf, 465.tonto, 453.povray, 416.gamess
G10	NI	WS	401.bzip2, 456.hmmer, 464.h264ref
G11	NI	WI	410.bwaves, 454.calculix

3.3 Simulation Control

We leverage a most common simulation control mechanism used in the past researches in cache memories [8, 14, 16]. We have caches warmed up with the subsequent 1 billion instructions, and have each program detailed executed at least 500 million instruction. If some program finishes earlier, they continue to run to contend for shared cache with other co-running programs. We only report performance for the first 500 million instructions interval. Performance are measured with weighted speedup [2] calculated as

$$\text{Weighted Speedup} = \sum \frac{IPC_i^{\text{shared}}}{IPC_i^{\text{alone}}},$$

where both the IPC_i^{shared} and IPC_i^{alone} are performances of the i -th program when it co-runs with other programs, and that when it runs alone, respectively.

4 Empirical Studies

In this section, we report the results of our empirical studies. We are restricted to present the evaluation to a subset of these workloads due to page limit instead of the total 77 workload mixes, nevertheless, the results are also applied to the remaining workloads. Specially, we perform evaluations on workload mixes of medium memory intensity and varying way sensitivity as shown in Table 4 in studying the impact of cache configuration, cache way sensitivity, and partitioning variations to performance. We use workload mixes of way step sensitivity and varying memory intensity as shown in Table 5 to investigate the impact of memory intensity to performance.

Table 4. Workload mixes of medium memory intensity and varying way sensitivity

Category	Workload mixes	Category	Workload mixes
4WS	(450,471,483,471)	4WT	(437,482,459,437)
4WI	(462,433,462,433)	3WS + 1WI	(450,471,483,462)
3WS + 1WT	(450,471,483,459)	2WS + 2WI	(471,483,462,433)
2WS + 1WI + 1WT	(483,450,433,459)	2WS + 2WT	(471,483,437,482)
1WS + 1WI + 2WT	(450,462,437,482)	1WS + 3WI	(450,462,433,462)
1WS + 2WI + 1WT	(471,462,433,459)	1WS + 3WT	(471,437,482,459)

Table 5. Workload mixes of way step sensitivity and varying memory intensity

Category	Workload mixes	Category	Workload mixes
1HI + 3LI	(473,434,445,436)	1HI + 1MI + 1LI + 1NI	(473,459,436,435)
1HI + 3MI	(429,437,482,459)	1HI + 1MI + 2LI	(473,437,434,445)
2HI + 2MI	(429,473,437,482)	1HI + 1MI + 2NI	(429,482,435,400)
2HI + 2LI	(429,473,445,436)	1HI + 2MI + 1LI	(429,482,459,434)
2HI + 2NI	(429,473,435,400)	1HI + 2MI + 1NI	(473,437,482,400)
3HI + 1MI	(429,473,429,482)	2HI + 1MI + 1LI	(429,473,459,434)
3HI + 1LI	(429,473,429,436)	2HI + 1MI + 1NI	(429,473,437,435)
3HI + 1NI	(429,473,429,435)	2HI + 1LI + 1NI	(429,473,445,400)
1HI + 3NI	(429,400,435,400)		

4.1 Impact of Cache Configuration

Cache Set Number. Figure 3 reports the normalized performances across a group of cache size from 4 MB to 16 MB by increasing the number of cache sets while keeping a fixed cache way number. We can see that the set number has a direct impact of performance gains of way-partitioning. To our surprised, the baseline LRU outperforms way-partitioning for most workloads (7 out of 12) with a small cache of 4 MB. As we

increase the set number, way-partitioning improves these workloads gradually. When the cache size is increase to 16 MB, besides 2 workloads which have the similar performance under both partitioning and LRU, way-partitioning wins LRU for 10 out of the total 12 workloads, including the 7 workloads which has poor performance in small caches of 4 MB. Way-partitioning achieves a normalized performance improvement to LRU at a geometric mean of 11.5% in the large cache of 16 MB.

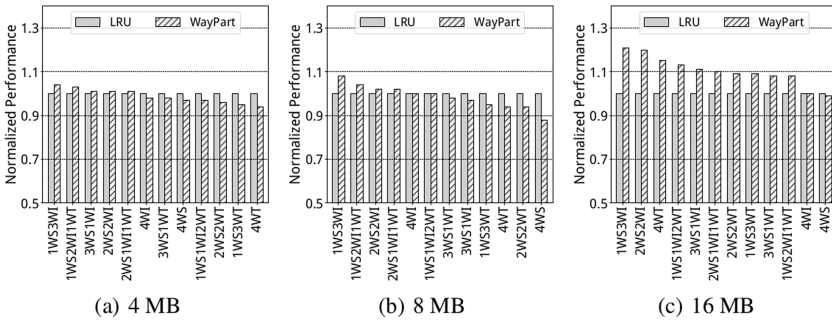


Fig. 3. Normalized performance of way-partitioning to LRU in LLC of the same way numbers but different set numbers

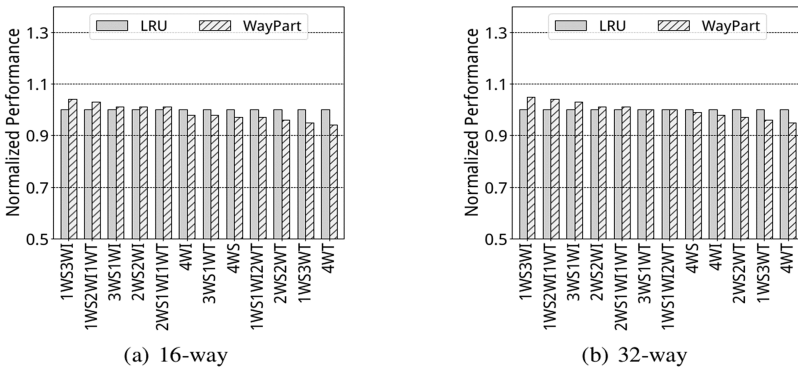


Fig. 4. Normalized performance of way-partitioning to LRU in LLC of the same set numbers but different way numbers

Cache Way Number. We set a fixed cache size of 4 MB but varying the associativity to 16-way and 32-way, respectively. Figure 4 reports the normalized performances of way-partitioning to LRU with an associativity of 16-way and 32-way. Considering that the workloads used in this evaluation are picked in terms of cache way sensitivity, we expect to see performance improvement for workload mixes containing more cache way sensitive programs under a high associative cache. However, we hardly observe any performance improvement for all workload mixes, only by a geometric mean of 1%, as we increase the cache associativity. Compared with the impact of increasing the cache

set number, the performance improvement from increasing cache way number is tiny (1% v.s. 11.5%).

The different impact of cache set number and cache way number attributes to the amount of conflict misses. As the cache set number increases, the address stream is scattered among more cache sets, consequently, decreases the conflict misses within a cache set. However, increasing the cache way number decreases capacity misses but does not prevent conflict misses. Excessive conflict misses diminish the performance gains from cache partitioning.

4.2 Impact of Memory Characteristics

Memory Access Intensity. We investigate the impact of memory access intensity with the mixed workloads of way step sensitivity and various memory intensity shown in Table 5. The normalized performance of cache partitioning to LRU are presented in Fig. 5. We observe an unexpected performance degradation for almost all of the workloads with cache partitioning. Compared with LRU, the performance loss in way-partitioning reaches by a geometric mean of 17% and at most by 38%. Obviously, for this group of workload mixes, cache partitioning does not work at all. Further, we find that there is a negative correlation of performance loss with the similarity in memory access intensity of the mixed workloads. It is highly likely to suffer performance degradation when programs that have less similarity are co-scheduled. For example, the workloads labeled as 1HI3LI and 3HI1LI both contain programs of high memory intensive and low memory intensive. The large diversity in memory access intensity, consequently, makes them suffer significant performance loss. In contrast, the performance of workloads labeled as 3HI1MI and 3MI1HI has little impact because they have smaller diversity in memory access intensity. This negative correlation can be explained with the extra misses from partitioning interference. We compare the cache misses in LRU and way-partitioning for each program in the workload mixes of 3HI1LI as shown in Table 6. We can see with partitioning, the misses in 429.mcf decreases but the misses for the remaining programs increase. The misses in 436.cactusADM increases by 20x. Due to partitioning interference, extra misses are pushed to the co-scheduled partners.

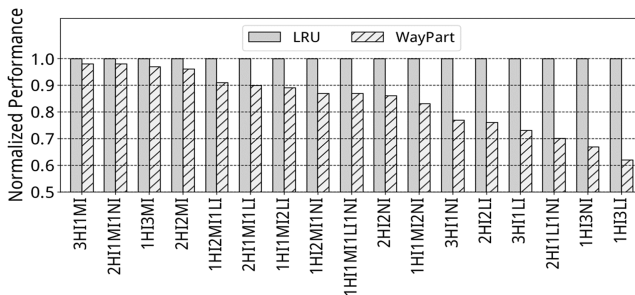


Fig. 5. Normalized performance of way-partitioning to LRU for workload mixes of cache way step sensitivity programs under different memory intensities

Table 6. Cache misses comparison of workload mixes with high diverse memory access intensity under LRU and way-partitioning

Cache misses	473.astar	429.mcf	473.astar	436.cacutsADM
LRU	45.38	68.27	45.38	5.04
WayPart	48.29	64.60	48.28	102.74

Associative Way Sensitivity. We evaluate the impact of associative way sensitivity by enforce mixed workloads of fixed medium memory intensive while varying associative way sensitivities. Figure 3(a) shows the normalized performance of way-partitioning to that of LRU. *Firstly*, we observe a similar performance in a 4 MB shared LLC on average under either LRU or way-partitioning. *Secondly*, we observe that way-partitioning outperforms LRU for some workloads as a result of effective use of the allocated ways. For example, for workload mixes labeled as 1WS3WI, an extra performance of 3% to 4% can be gained with cache partitioning. *Thirdly*, we observe that workload mixes that benefit from way-partitioning contain at least one way insensitive program, which is necessary but not sufficient. Way insensitive programs do not benefit from the extra lines received. For example, 462.libquantum accesses cache lines with a streaming pattern and does not see any performance gains on receiving more ways. Consequently, cache partitioning preserve less ways for these programs, typically only 1 way. The remaining ways can be devoted to those highly utilize caches. Thirdly, we find performance is highly dependent on co-runners when way insensitive program are scheduled with others. Workload mix labeled as 1WS1WI2WT has a performance lost due to the excessive line contention from programs of way step sensitivity.

4.3 Impact of Partitioning Variation

To correlate performance with programs that benefit from cache partitioning, we review the dynamic number of cache blocks each program receives during co-running. Figure 6 presents the number of blocks allocated by the *Lookahead* algorithm in UCP for a workload mix labeled as 1WS3WT consists of 450.soplex, 437.leslie3d, 482.sphinx3, and 459.GemsFDTD. *Firstly*, we observe a negative correlation of partitioning size variation with cache size. In a 4 MB LLC, the number of allocated blocks varies frequently, which results a frequent partitioning adjustment, consequently, the overhead of partitioning increases. With the increment of cache set to 8 MB and 16 MB, the variation comes down gradually. *Secondly*, we see that more performance improves as more steady the partition is. It implicates that frequent partition variation does not improve performance due to extra overhead of partitioning adjustment.

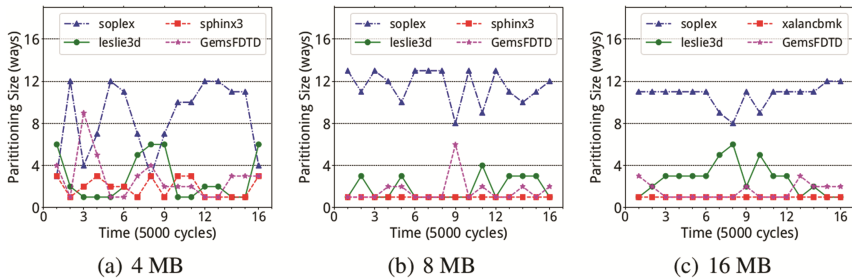


Fig. 6. Cache blocks received by each program in a medium memory intensive workload mixes consisting of one way sensitive and three way step sensitive programs under the Lookahead partitioning algorithm

4.4 Implications

We summarize our findings and their implications to future cache system design or effective cache resource exploration for cloud data centers as follows.

- Cache partitioning does not work in caches of small capacity. Increasing capacity by increasing the set number instead of the way number can improve the performance gains of cache partitioning. Considering the design complication, high overhead and energy of associative lookup, it is not beneficial to design high-associative caches in data center because they do not make cache partitioning work better.
- Consolidating services in data centers should take the memory characteristics of programs into account since they have direct impact on performance gains of cache partitioning. It degrades performance when cache partitioning is applied to programs that have less similarity in memory access intensity of high memory intensity. Co-scheduling programs of heterogeneous cache way sensitivity can make effective use of cache partitioning.
- The overhead of dynamic partitioning adjustment impacts the performance gains of cache partitioning. Design a partitioning algorithm with a steady partitioning size from less frequently adjustment can improve performance.

5 Conclusion

Service consolidation is promising to improve the poor resource utilization in cloud data centers but at a risk of suffering performance due to uncontrolled access to shared last-level cache. Although cache partitioning schemes have been exploited extensively, how to make effect use of cache partitioning is still not well understood. In this paper, we are seeking to explore when partitioning works and when it does not with an empirical study on a commonly used way-partitioning policy for a variety of workloads. We investigate the impact of cache configuration, memory characteristic of program, and partitioning variation to the performance gain under partitioning. We identify several interesting findings which help us in future cache system design and optimization for cloud data centers.

References

1. Cook, H., Moreto, M., Bird, S., Dao, K., Patterson, D.A., Asanovic, K.: A hardware evaluation of cache partitioning to improve utilization and energy-efficiency while preserving responsiveness. In: Proceedings of ISCA, pp. 308–319 (2013)
2. Eyerman, S., Eeckhout, L.: System-level performance metrics for multiprogram workloads. *IEEE Micro* **28**(3), 42–53 (2008)
3. Ferdman, M., Adileh, A., Kocberber, O., Volos, S., Alisafae, M., Jevdjic, D., Kaynak, C., Popescu, A.D., Ailamaki, A., Falsafi, B.: Clearing the clouds: a study of emerging scale-out workloads on modern hardware. In: Proceedings of ASPLOS, pp. 37–48 (2012)
4. Funaro, L., Ben-Yehuda, O.A., Schuster, A.: Ginseng: market-driven LLC allocation. In: Proceedings of ATC, pp. 295–308 (2016)
5. Henning, J.L.: SPEC CPU2006 benchmark descriptions. *ACM SIGARCH Comput. Archit. News* **34**(4), 1–17 (2006)
6. Herdrich, A., Verplanke, E., Autee, P., Illikkal, R., Gianos, C., Singhal, R., Iyer, R.: Cache QoS: from concept to reality in the Intel® Xeon® processor e5-2600 v3 product family. In: Proceedings of HPCA, pp. 657–668 (2016)
7. Kanev, S., Darago, J.P., Hazelwood, K., Ranganathan, P., Moseley, T., Wei, G.Y., Brooks, D.: Profiling a warehouse-scale computer. In: Proceedings of ISCA, pp. 158–169 (2015)
8. Kasture, H., Sanchez, D.: Ubik: efficient cache sharing with strict QoS for latency-critical workloads. In: Proceedings of ASPLOS, pp. 729–742 (2014)
9. Lin, J., Lu, Q., Ding, X., Zhang, Z., Zhang, X., Sadayappan, P.: Gaining insights into multicore cache partitioning: bridging the gap between simulation and real systems. In: Proceedings of HPCA, pp. 367–378 (2008)
10. Lo, D., Cheng, L., Govindaraju, R., Barroso, L.A., Kozyrakis, C.: Towards energy proportionality for large-scale latency-critical workloads. In: Proceedings of ISCA, pp. 301–312 (2014)
11. Luk, C., Cohn, R., Muth, R., Patil, H., Klauser, A., Lowney, G., Wallace, S., Reddi, V.J., Hazelwood, K.: Pin: building customized program analysis tools with dynamic instrumentation. In: Proceedings of PLDI, pp. 190–200 (2005)
12. Pan, A., Pai, V.S.: Imbalanced cache partitioning for balanced data-parallel programs. In: Proceedings of MICRO, pp. 297–309 (2013)
13. Patil, H., Cohn, R., Charney, M., Kapoor, R., Sun, A., Karunanidhi, A.: PinPointing representative portions of large Intel® Itanium® programs with dynamic instrumentation. In: Proceedings of MICRO, pp. 81–92 (2004)
14. Qureshi, M.K., Patt, Y.N.: Utility-based cache partitioning: a low-overhead, high performance, runtime mechanism to partition shared caches. In: Proceedings of MICRO, pp. 423–432 (2006)
15. Sanchez, D., Kozyrakis, C.: Vantage: scalable and efficient fine-grain cache partitioning. In: Proceedings of ISCA, pp. 57–68 (2011)
16. Sanchez, D., Kozyrakis, C.: ZSim: fast and accurate microarchitectural simulation of thousand-core systems. In: Proceedings of ISCA, pp. 475–486 (2013)
17. Suh, G.E., Rudolph, L., Devadas, S.: Dynamic partitioning of shared cache memory. *J. Supercomput.* **28**(1), 7–26 (2004)
18. Tang, L., Mars, J., Vachharajani, N., Hundt, R., Soffa, M.L.: The impact of memory subsystem resource sharing on datacenter applications. In: Proceedings of ISCA, pp. 283–294. *ACM* (2011)

19. Yang, H., Breslow, A., Mars, J., Tang, L.: Bubble-Flux: precise online QoS management for increased utilization in warehouse scale computers. In: Proceedings of ISCA, pp. 607–618 (2013)
20. Ye, Y., West, R., Cheng, Z., Li, Y.: COLORIS: a dynamic cache partitioning system using page coloring. In: Proceedings of PACT, pp. 381–392 (2014)

Track Maintenance Feedback Mechanism Based on Hadoop Big Data Analysis

Yong Zhu^(✉), Jiawei Fan^(✉), Guangyue Liu^(✉), Mou Wang^(✉), and Qian Wang^(✉)

Intelligent Manufacturing and Control Institute, Wuhan University of Technology, Wuhan, China
zhuyong2016@gmail.com, 1228915795@qq.com, 491534654@qq.com,
137078388@qq.com, 775316545@qq.com

Abstract. With the rapid development of economy and the people's growing material needs, increased frequency and intensity of railway transportation, the requirement of increasing the railway maintenance, security is becoming more and more attention. The current routine of daily maintenance is done mainly by manual and large rail inspection vehicles. The maintenance method is of high strength, low efficiency, high risk and low maintenance accuracy. Based on the above background, the project team has designed an efficient track inspection machine based on the collaborative working method of the mother-machine. The railway maintenance and data collection is achieved through the collaborative work of the mother-machine. In this case, the mother machine detects and collects the data, the sub-machine repairs and collects the data, the upper machine implements the coordination, the big data processing and the feedback system. Data collected by a railway big data, to take advantage of these data, the team set up big data processing system based on hadoop, adopting clustering analysis, integrated analysis and time prediction analysis method, experience about defect distribution map, so as to optimize the workings of a composite aircraft, constantly improve the maintenance system based on composite aircraft performance. The design of the project team is based on the system of the railway maintenance system, which is intelligent and timely. Can be automated and dehumanized, realize railway maintenance, and can improve the efficiency of railway maintenance system and reduce cost.

Keywords: Railway maintenance · Zipper · Big data analysis
Intelligent system · Feedback optimization

1 The Background Under the Time of Big Data

Recent years, China's railway development is rapid as China's economy continues to rise. According to the data of the Ministry of Railways Statistics Center, China's railway operating mileage of 91,000 km, while the annual passenger traffic volume up to 167609 million passengers, the total amount of 364.27 million tons of cargo sent. China's railway system is now six times a large area of acceleration transformation project, the introduction and development of high-speed railway speed of 350 km/h or more.

What's more, the safety factor of the railway is highly demanded with the continuous improvement of the railway. The daily maintenance of the track is mainly on the track

irregularity, orbital defect, bolt looseness and other issues detection and maintenance. However, because of the wide distribution of China's railway and large the number of long tracks, China's railway sector mainly rely on artificial or semi-automated machinery inspection method to detect and repair rail damage. Under this background, the project team designed an efficient rail maintenance machine which based on the coherent work mode of the parent machine. At the same time, the machine can also achieve the rail detection and maintenance of automation and intelligence. The most important is, people could establish a big data processing system on the hadoop based on the process of detection and maintenance of this machine.

Although the current equipment has data collection and data feedback, but it did not achieve real-time interaction, the two part are distributed with a certain lag. The data can not be timely fed back to the data processing system through the host computer after the collection. And the data which has been dealt by the data processing terminal could not be sent back to the work of equipment in time, so it could not met the requirement of immediate maintenance.

Through the collection of big data on the railway, the Hadoop for data processing and integration, and by the hadoop system for information feedback, the equipment could examines the defects of the relevant data more accurately according the relevant data. Besides, people could start a directional work through the integration of information and the types of defects and multiple locations. So the fixed section of the railway can be detected, and the efficiency can be improved.

2 Data Detection and Acquisition

From the background of railway's development, we can see that there are two kinds of information on the existing railway tracks. Among them, irregularity refers to the orbital geometry, size and spatial position of the deviation. In the broadest sense, the position of the center line of the linear track, the height of the track, deviates; the curve center curve deviation; curvature, high, gauge value, slope changes in the size of the deviation, collectively referred to as the track is not smooth. Track surface defects include cracks of rail surface, abrasions, blocks, and the surface appears dark or black lines and so on.

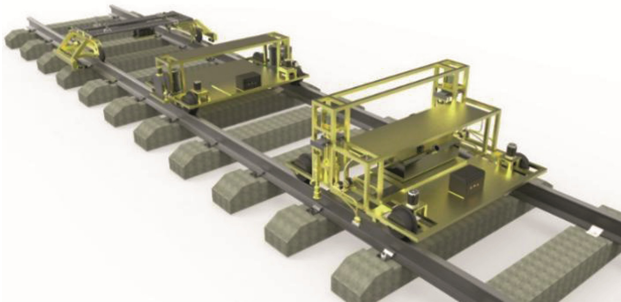


Fig. 1. Track maintenance machine

This information, needs to work through the way composite machine to work to collect. Track maintenance machine is as shown in Fig. 1 [1].

The acquisition process is divided into three parts. The first is the image, instrument and other information of data acquisition. Then these directly collected information, through the processing of data conversion, into the corresponding digital information. Finally, the data finished, and through digital-analog conversion, the digital information combined with positioning information into a digital group, and through the FPI bus-4G communication networks to the host computer. The concrete data of detection and acquisition methods are as follows:

2.1 Uneven Information Detection

In order to obtain the information of irregular, we are in accordance with the category of irregular, different types of track irregularity using different instruments for testing. Orbit irregularities can be divided into vertical orbit irregularities, transverse orbit irregularities and complex orbit irregularities (Fig. 2).

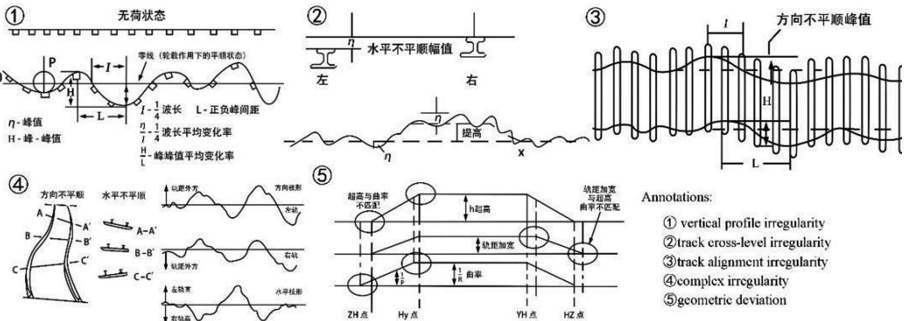


Fig. 2. All sorts of schematic schematics

In order to obtain the above non-smooth information, we use the parent machine in the detection of the parent machine for data collection. For different types of irregularities, we use different data collection. At work, each testing hardware works simultaneously. Using displacement sensors to measure displacement variables, the actual gauge values are added to the standard gauge. Using gyroscope to get the machine's side rolling Angle, the high value is calculated through trigonometric relation. The lateral acceleration of the vehicle is measured by the transverse acceleration sensor, and the integral is obtained by the horizontal displacement deviation. By using the vertical acceleration sensor, the vertical acceleration of the body is measured, and the integral obtains the vertical displacement offset, and the calculation is high and low [2].

2.2 Defect Information Detection

Track surface defects include the cracks of rail surface, abrasions, blocks, and the surface appears dark or black lines and so on. The causes of defects can be divided into two

categories: One is the limitation of the manufacturing process, the defects of the steel rail during the forging process; The other is generated by the high intensity and high density fatigue wear of the locomotive and rail.

As a result, we use machine vision technology to detect defects caused by this instability. By CCD camera track surface image acquisition in the first place, again by FPGA combined with single chip microcomputer to feature extraction, image through image processing the final defect type and location. Then, according to the image pixel information, you can coordinate the defect [3].

2.3 Location Information Detection

Location information is mainly through GPS and encoder to achieve the absolute positioning of geographic information and relative positioning. The GPS absolute positioning is mainly the approximate range of the framing machine, the detected uneven information and defect information. Coding counter relative positioning is mainly based on the initial operation of the sub-machine positioning information and rail along the direction of information to achieve the relative positioning of detection information. Finally the use both of them to achieve the location of the defect location.

After obtaining the above three kinds of information, through the FPGA to achieve the information of digital signal conversion, and through the FPI bus-4G network communications to the host computer, to achieve data collection and further processing.

3 The Detection Data Processing and Analysis

After the data collection is the corresponding data processing, in this project, the most important is the analysis of these data analysis and data feedback after this, you can simplify the construction process of maintenance machinery in the railway track, improve the efficiency of rail maintenance and management.

For the railway track data can be divided into structured data and unstructured data two categories. Unstructured data refer to the data tracked by the rail maintenance machine in this project, the most important of which is the generating data after the image processing, and the processing of this part of the data is the key to the project.

3.1 Big Data Characteristics

As we collect and maintain data on railway maintenance, we accumulate large data resources. For these big data, we need to analyze it to get the distribution of the railway service. The big data has the following characteristics:

(1) The amount of data

Rail traffic is a wide range of distribution, long distance, daily life is essential a data entity, so in order to collect data from the railway track, traditional data-processing software can't store or process such a huge amount of data, requiring large data to meet the project's requirements.

(2) Data type diversification

With the deepening of the project, the railway situation is intricate, so big data diversity the data type characteristics of the project to meet the early stage of the data processing.

(3) The rapid spread of data

In this project, it is hoped that the processing of the data on the railway situation will be sent to the staff's hand-held equipment in order to respond quickly to the abnormal state of the rail.

(4) Low the data density

Big data in the process of processing may need to deal with most of the nonsignificant data, and ultimately will reflect it contains that part of the high value of the data or results.

3.2 Big Data Processing Technology Based on Hadoop

The data of the railway track is a lot of data, so the transmission and storage of these data are key problems to be solved. In the data transmission, data compression can effectively reduce the amount of network data transmission and improve the storage efficiency. We use the fault transient process of ascension based format signal compression and reconstruction algorithm of real-time data, using linear integer transform biorthogonal wavelet filter combination Huffman encoding method of track detection of real-time data compression and decompression. Then, we need to decompress the data after the data arrived in the monitoring center, it needs appropriate computing and storage platform. In the data storage, because the orbital data on the real-time requirements are not very high, so the amount of data that can be detected can be stored using Hadoop's HDFS storage system. To meet the hadoop of the big data technology to the number of processing, we can continuously optimize the railway track detection system according to the data feedback mechanism, such as after long-term detection, we can determine the frequency of different location defects, so we can set a different detection frequency, to meet the detection and efficient management.

4 The Data Analysis and Optimization

In the sub-machine work together for some time, it will inevitably produce a large number of railway maintenance data, the analysis and optimization of the massive data have certain influence on the distribution and proportion of the work on the railway. Therefore, we are for the detection and collection of data, data processing, the analysis, to obtain big data based on the railway maintenance profile, that is, "track spectrum." Through the data analysis of the track spectrum, we find the frequency distribution rule of the daily maintenance work, so as to optimize the working scheduling of the cooperating sub-machine, realize the principle of the twenty-eight in the course of railway daily maintenance, improve the efficiency of overhaul and reduce the cost of maintenance.

Data monitoring and analysis platform as shown in Fig. 3.



Fig. 3. Monitoring platform

In order to analyse the data, we use two methods of clustering analysis and integration analysis on the basis of Hadoop, and carry out the comprehensive evaluation and analysis of the data by the two types of data and the state of track maintenance. Maintenance of the real state and its forecast analysis, and targeted adjustment of the proportional number of sub-machine maintenance and distribution of the scope of work. In the following, two analytical methods will be briefly introduced:

4.1 Clustering Analysis of Prediction Intensity

The clustering analysis is divided into two parts: the test set and the training set. The detailed analysis is as follows, Fig. 4.

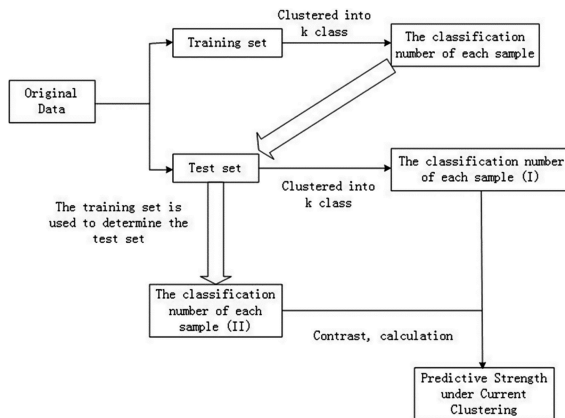


Fig. 4. Clustering analysis

Through the prediction of strength, we can get predictive state distribution of railway track defects and irregularities and bolts loosening, based on Hadoop, so as to make corresponding repair and distribution rules for the occurrence rate of defects of different frequency in different regions, and further to achieve the principle of twenty-eight, to improve the efficiency of railway railways daily maintenance, reduce the cost of railway railways daily maintenance.

4.2 Integration Analysis

Integration analysis is also an effective way to solve the problem of “big p small n”. so it is necessary to study the integration and analysis of different data sets in the era of big data [4].

Due to scattered data clustering analysis, analysis of incoherent, overall analysis is not comprehensive, we adopted the combination of integration analysis, for railway track maintenance and repair of large data analysis, realize the whole track along the integrity of big data analysis.

4.3 Comprehensive Analysis

Based on the results of the above two analyzes, we can obtain the comprehensive distribution of railway track defects, irregularities, bolts and other information, and predict the occurrence rate and time of occurrence of railway rails. For different regions, different intensity and the frequency of maintenance planning, improve the efficiency of maintenance sub-machine, reduce the corresponding cost, in order to achieve the railway track maintenance operations really “twenty-eighty principle.” Maintenance machine feedback workflow is shown as Fig. 5.

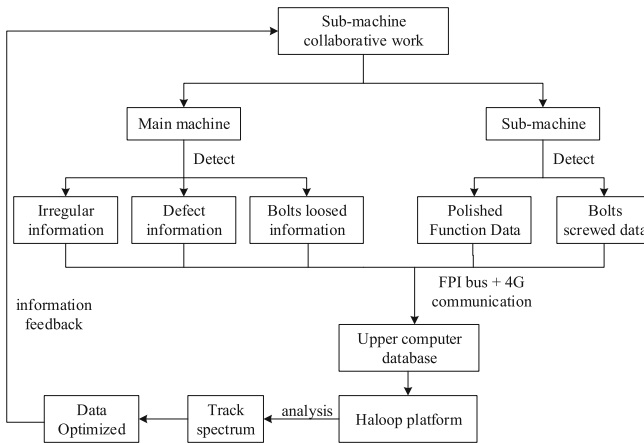


Fig. 5. Clustering analysis

5 Summary

Today, the main way of railway maintenance is still labour, it exists high duration, difficult and other defects. The current machinery can only be automated, can not be intelligent, can not meet today's needs.

This project designed a highly efficient intelligent rail maintenance machine, and based on this design based on the hadoop for big data processing system, and its collection, processing, analysis and feedback maintenance machine to detect the massive data, the project has the following innovations:

- (1) Mechanical structure design adaptive strong, can be automatically detected maintenance operations
- (2) Modular, integrated, systematic design can be adapted to a variety of complex operating requirements
- (3) Design of the data and instructions two-wire transmission function, to achieve the machine's online detection and status monitoring, and real-time access to the state of the rail changes
- (4) Designed data on-line analysis and big data processing platform to achieve the analysis of the state of the railway maintenance and sub-machine work mechanism feedback, shorten costs and improve efficiency

The project team uses cloud computing as a platform for heterogeneous and diversified data storage and analysis and the platform after the operation of the massive data based on the maintenance of state maintenance, system feedback optimization, isolated information system interoperability Support, and become a candidate after integration. This work has a low cost, good system scalability (unlimited storage capacity), high reliability, parallel analysis and so on, will become one important system of intelligent way of railway maintenance in the future.

References

1. Chen, C., Kong, J., et al.: *Modern Mechanical Designer Manual*. Mechanical Industry Press, Beijing (2014)
2. Wang, Y., Yu, Z., Bia, B., Xu, X., Zhu, L.: Study on crack identification algorithm of metro tunnel based on image processing. *J. Instrum.* **07**, 1489–1496 (2014)
3. Wang, Y.: Study on key technology of big data processing flow based on Hadoop. *Inf. Technol.* **09**, 143–146, 151 (2014)
4. Ma, S., Wang, X., Fang, K.: Integration analysis of big data. *J. Stat. Res.* **11**, 3–11 (2015)
5. Cao, Y.: *Hadoop Performance Optimization in Big Data Environment*. Dalian Maritime University (2013)
6. Tang, D.: Hadoop-based affine propagation big data clustering analysis method. *Comput. Eng. Appl.* **04**, 29–34 (2015)

Crowdsourcing and Stigmergic Approaches for (Swarm) Intelligent Transportation Systems

Salvatore Distefano^{1,2(✉)}, Giovanni Merlino¹, Antonio Puliafito¹,
Davide Cerotti³, and Rustem Dautov²

¹ Università degli Studi di Messina, Messina, Italy
{sdistefano,gmerlino,apuliafito}@unime.it

² Social and Urban Computing Group, Kazan Federal University, Kazan, Russia
{s_distefano,rdautov}@it.kfu.ru

³ Politecnico di Milano, Milano, Italy
davide.cerotti@polimi.it

Abstract. In the last decades, the impact of Information and Communication Technologies (ICT) on transportation systems radically changed them, identifying in the Intelligent Transportation Systems (ITS) a new research area. A problem often addressed in ITS is vehicle routing, for which plenty of solutions have been already defined in literature. Vehicle routing problems are usually NP hard, therefore these are mainly heuristic solutions. A requirement for them is to be deployed and run in navigation systems, ready to react to sudden changes in a (quasi) real-time way. Hence, to reduce the latency is still an open issue, not only depending on the complexity of the solution but also on other parameters, such as the traffic update latency in traffic-aware vehicle routing. A way to solve them is by exploiting distributed, collaborative approaches, establishing a proper collaboration platform and algorithms able to use it. Mobile Crowdsensing, on the one hand, and collective and swarm intelligence approaches, on the other, can fill this gap. This paper is a first attempt in this direction, aiming at defining a new class of (swarm) the Intelligent Transportation Systems (SITS), on top of a crowdsourcing-based infrastructure.

Keywords: MANETs · Mobile crowdsensing · Stigmergy
Traffic engineering · ITS

1 Introduction and Motivations

With an ever growing availability of embedded, mostly personal and mobile computing devices for everyday tasks, there is an almost limitless potential for tapping onboard resources, especially sensing-related ones, as well as corresponding compute nodes to be exploited for locally executable tasks. Mobile CrowdSensing (MCS) comprises by definition a category of applications where individuals carrying sensor-hosting embedded computers (e.g. smartphones) get collectively

engaged in information gathering and sharing efforts in order to analyze and georeference events which may be interesting for individuals and communities alike. MCS is already establishing itself as a trendy paradigm, but most efforts go into the direction of easing *participatory* (e.g. manned) patterns. Apart from privacy and security issues, where anonymization and sandboxing respectively are key countermeasures, as most engagement chances should be meant to be *opportunistic* to let MCS be truly widespread, inexpensive and wholly disruptive as a paradigm. In this context problems lie foremost in enabling unassisted deployments, as well as accommodating for peer-oriented communication and distributed self-organization, mostly due to real-world constraints, e.g. intermittently (WAN-)disconnected operation.

One of the main advantages of MCS is the possibility to conduct sample collection, data mining, etc., without accounting for the corresponding experiments in advance, just leveraging natural daily life patterns arising from human activities as they happen and leave behind breadcrumbs in form of samplings ready to be collected. Aim of this kind of enablement then is putting this power at the fingertips of developers or would-be entrepreneurs, ready to kickstart whichever effort in next to no time. In particular self-provisioning and autonomous cooperation are needed to avoid long setup times for experiments, disruptions beyond careful planning and sizing, as well as aiding coders in developing less custom logic.

Most existing typical MCS applications currently feature a common, simplified architecture, made up of two main components, one running on the embedded device in order to collect and disseminate measurements, and a second one as backend hosted on e.g. the Cloud for data mining, analytics and other business intelligence according to the requirements of the application at hand. Each application gets designed mostly from scratch with no common ground despite every implementation tackling, of necessity, overlapping challenges in scheduling, sampling, and communication duties, among others. A few drawbacks of such siloed pattern deserve to be pointed out as severe hindrances despite the promise of the underlying paradigm:

- wasted development efforts, due to mostly ground-up coding every time, including OS and platform-dependent adaptations
- unoptimized runtime, as multiple applications would execute on the same nodes without taking into account such configuration, possibly duplicating sensing or processing activities on resource-constrained devices, thus also limiting scalability of the platform
- no exploitation of proximity or density in topologies, by e.g. cooperation across nodes.

In particular this last point is crucial, as any kind of high-density scenario, especially if with real-time constraints, e.g. Intelligent Transportation Systems (ITS) as we will see in the following, needs a smart approach to proactively take advantage of proximal nodes and crowded areas instead of crumbling under the weight of such scale. Indeed, such a strategy could translate either in (self-)throttling redundant devices or even letting node aggregates preprocess data and shape

traffic accordingly by e.g. network coding strategies, otherwise leaving the back-end (and the network itself) prone to scalability issues over huge population scenarios.

Given the paradigm, i.e. MCS, and forthcoming use cases, with specific regard to ITS where mobility is really going to match crowds at scale, we conceived a design pattern. Such a scheme may lend resilience when faced with big swarms, while at the same time helping DevOps with their coding and deployment strategies. More specifically, collaborative approaches, collective and swarm intelligent ones could be good metaheuristics than can provide effective solutions to ITS problems such as vehicle routing, usually NP-hard. The collaboration of multiple agents is the best solution available in the ITS scenario to reduce latency and be effective in addressing the routing problem also when traffic conditions must be considered. This perfectly matches with crowdsourcing based paradigms as MCS, mainly aiming at supporting applications able to exploit the collective intelligence and their emerging properties in problem solving. In this paper, we propose to address the routing problem adopting a swarm intelligence approach able to take into account the road traffic conditions. It mainly consists of an ant colony optimization (ACO) algorithm implemented and deployed on mobiles constituting an MCS-contributed infrastructure, able to interact each other following an opportunistic patterns. We therefore framed our approach in the class of Swarm ITS (SITS).

In the following, we are going to first lay out an overview of ITS systems, then discussing MCS solutions for them. After that, we focus on swarm intelligence, stigmergy and ACO, coming up with SITS. This way, we define our traffic-aware vehicle routing solution based on a modified version of an ACO. This SITS solution is thus evaluated by a simulator which preliminary results are discussed. Finally some remarks and hints for future work close the paper.

2 Intelligent Transportation Systems

Intelligent transportation systems (ITS) are the coherent combination of advanced systems, and services which aim at providing as a whole innovative solutions related to typically metropolitan and regional mobility based on multiple modes of transport, by means of traffic management, as well as enabling users belonging to whichever category to be up-to-date, thoroughly informed and aware of any (transient or structural) issues, in order to make safer, more coordinated, and ‘smarter’ use of transport networks. A directive by the European Union Commission defines ITS [1] as *“systems in which information and communication technologies are applied in the field of road transport, including infrastructure, vehicles and users, and in traffic management and mobility management, as well as for interfaces with other modes of transport”*.

From the ICT perspective, we may envision ITS embracing any advanced solution for transport engineering that integrates live data and other feedback from a number of heterogeneous sources, such as parking guidance and information systems. In particular, efforts related to ITS seem naturally poised to

have as target high-population density areas considering a consistent orientation of such networks towards multimodal systems of transportation, be those either personal vehicles, shared vectors such as buses or trains.

ITS naturally spans a wide range of technologies, in particular ICT ones, starting from basic management systems such as navigation ones, possibly to be augmented in the future by systems where artificial “co-drivers” may assist humans during their duties [2]. Yet, there are many other examples of instances of subsystems prone to be enhanced through ICT, e.g., traffic signal control systems, which may leverage some kind of system-optimal routing algorithm for road networks as well, such as game-theory based ones [3]. Moreover, from a technological viewpoint, any delay in information dissemination for vehicle-to-vehicle communication networks [4], so called VANETs [5], considering a traffic-dense configuration as the relevant scenario, can be identified as one of the main challenges to be overcome for any coordination system to really work as expected. Some authors [6] have leveraged Deep Learning to predict traffic flows by dealing with Big Data sources. Such problems were also analyzed by model-based solutions: for instance in [7] a stochastic (hazard-based) model to evaluate the impact of a reliability-safety tradeoff on the travel-time is proposed.

3 A Crowdsourcing Infrastructure for ITS

Typical MCS applications mainly implement a client-server interaction pattern where a service provider offers MCS-based services to end users, leveraging contributor willingness to provide their physical (sensing) resources [8]. Data are therefore collected and processed by (backend and frontend) servers to carry out aggregate analytics and feed back relevant results to end users.

Starting from the lowest level, through heuristics and algorithm design, local analytics may provide a category of functions, among which simple ones are interpolation, extrapolation and outlier filtering, which may enhance a standard MCS application. This aspect is summarized and depicted in Fig. 1, where the main differences against the traditional MCS approach are highlighted in red. Indeed, the differentiation is related to an opportunistic, collaborative approach, where nodes may interact one another to aid local computations and perform distributed optimizations on a small/medium scale. This way, end users may leverage an MCS application, server interaction issues notwithstanding, by just exploiting cooperation among nodes.

These designs may be quite application-specific, e.g., different crowdsensing applications would coexist, each bringing independently operating local analytics, yet still possibly accessing the same readings or applying comparable inference strategies. Anyway, local analytics provide data about a relatively confined area. There are applications with a different set of requirements, where some kind of aggregate analytics is needed, to be run at the backend. The main task in this case is extracting patterns from huge sets of sensor-provided data, originating from large populations of mobile devices. Patterns may highlight features of certain physical (or social) environments of interest, also helping in building models about observed phenomena, a way to improve in forecasting.

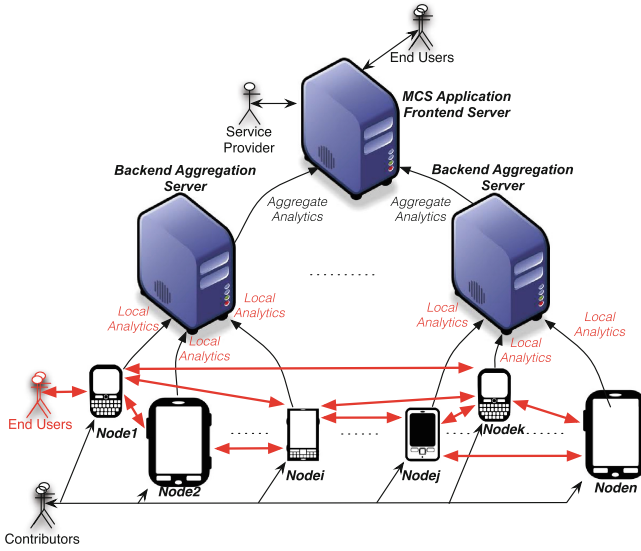


Fig. 1. The MCS reference scenario. (Color figure online)

Identifying patterns from large datasets means resorting to data mining, which calls for one of two approaches, according to either the size of incoming data or the limits imposed by applications on delays. In the first case measurements are preliminarily stored in a database, to apply mining algorithms against whole datasets and detect patterns. When the input stream is continuous and overwhelming in terms of storage, or even when applications would require fast pattern recognition techniques, “streaming” algorithms for mining may be the only viable solutions to identify patterns from streams in flight, independently from subsequent treatment such as long-term storage strategies. Data mining algorithms usually require domain-specific expertise.

4 Swarm Intelligent Transportation Systems

Over such a set of (dynamic) meshes, we propose a stigmergic approach for cooperation and optimization. Let’s first tackle swarm optimization alone.

Ant Colony Optimization. Ant colony optimization (ACO) [9] is a relatively recent metaheuristic based on the behavior of ants seeking a path between their colony and a source of food. In nature wandering ants have exhibited in this sense a provable capability to discover optimal paths. The collective intelligence of the swarm relies on ants exchanging information indirectly via the environment (the so-called *stigmergy*). While traveling to search for food, ants lay down pheromones on their way back to the nest (i.e. home colony) only when sources

of food are found. As other colony members step into pheromone trails, they tend to stick to the beaten path accordingly. Moreover, the trace gets reinforced as individuals follow the same trail, leaving pheromone of their own, in turn resulting increasingly attractive for other ants. For any complex problem which can be reduced to a search for optimal paths, ACO may work as a probabilistic solver, by emulating such naturally occurring behavior. The probability p_{ij}^k for an artificial ant k , placed in vertex i , to move toward node j is defined as follows:

$$p_{ij}^k = \frac{\tau_{ij}^\alpha \cdot \eta_{ij}^\beta}{\sum_{l \in N_i^k} (\tau_{il}^\alpha \cdot \eta_{il}^\beta)} \quad (1)$$

where τ_{ij} corresponds to the quantity of pheromones laid over arc a_{ij} , η_{ij} to a-priori attractiveness of the move, computed by some heuristic embedding the cost of choosing arc a_{ij} along the path that leads to the destination, and N_{ik} is the set of neighbours in node i for ant k , i.e., the nodes available for the ant to move in. Coefficients α and β are global parameters for the algorithm. According to typical ACO variants, ants bring food back home (i.e. nest) after being done with their movement. Denoting T_k as the tour of ant k , C_k is defined as the length of T_k , and used to specify the amount of pheromones to be placed by ant k on each arc on the trail that led to the food source:

$$\Delta\tau_{ij}^k = \begin{cases} \frac{1}{C_k} & \text{if arc } (i, j) \text{ belongs to } T^k \\ 0 & \text{otherwise} \end{cases} \quad (2)$$

$$\tau_{ij} = \tau_{ij} + \sum_{k=1}^m \Delta\tau_{ij}^k. \quad (3)$$

At the end of a round, after each ant has completed a move, the extent of pheromones laid over each arc gets reduced (e.g. evaporates), according to:

$$\tau_{ij} = (1 - \rho)\tau_{ij} \quad (4)$$

where ρ is a global parameter as well. Such simplified form of the ACO is defined an “ant system” (AS). In Fig. 2 the pseudocode for an AS of size n is listed.

ACO algorithms yield their best performance when some form of local search algorithm is employed.

Modified ACO for Traffic-Aware Route Planning. To adapt ACOs to MCS applications, we propose here a novel version of an ACO, MoCSACO, extending the algorithm of Fig. 2 into the one of Fig. 3, where an ant corresponds to a (physical) mobile device, i.e., a *real-world agent*.

We are also redefining the general objective of finding the shortest path on a (weighted) graph in terms of reusing common, state-of-the-art and readily available heuristics for path discovery. The A* search algorithm is such a solution, and leaves us free to confine stigmergy to weighting only, e.g. the admissible heuristic function in case of A*, where each arc has a cost (e.g., weight) defined

```

1: generate initial pheromone matrix  $P$  with respect to the graph topology
2:  $generation \leftarrow 0$ 
3: while termination criteria not met do
4:   place  $m$  ants randomly on graph vertices. set the amount of collected food for
   each ant to 0
5:   foreach ant do
6:     move forward in the graph. follow the probabilistic rule from eq. (1)
7:     compute the amount of collected food corresponding to ants trail
8:   end foreach
9:   find ant with largest (smallest) amount of collected food (traversed arcs). let
   the ant lay pheromones in  $P$  on his trail (back) according to eq. (3)
10:  evaporate pheromones in  $P$  according to eq. (4)
11:   $generation \leftarrow generation + 1$ 
12: end while

```

Fig. 2. The behavior of ant system in pseudocode.

```

1: place  $m$  ants randomly on graph vertices. Set the amount of collected
   food for each ant to 0
2:  $generation \leftarrow 0$ 
3: while termination criteria not met do
4:   foreach ant do
5:     ant_routing()
6:   end foreach
7:    $generation \leftarrow generation + 1$ 
8: end while
(a) MoCSACO

```

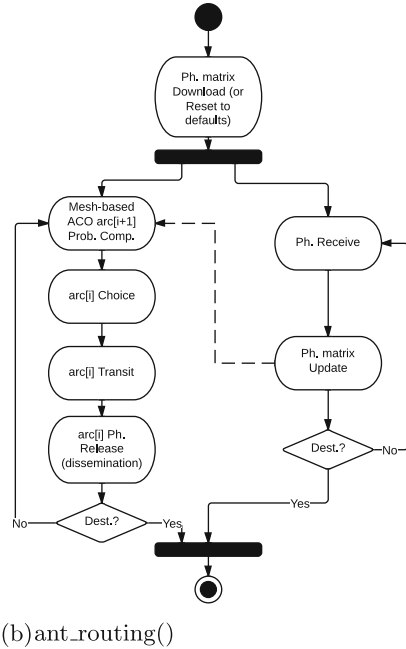


Fig. 3. The behavior of modified ant system in pseudocode.

by a certain metric. In its turn, weight directly correlates to the quantity of pheromones, as in:

$$w_{ij} = \gamma \cdot \tau_{ij} \quad (5)$$

where w_{ij} is the weight of the arc, γ is a constant of proportionality and τ_{ij} represents the amount of pheromones placed on arc a_{ij} .

In order to make the a-priori cost (i.e., of choosing an arc along the path towards destination) explicit, we first define:

$$c_{i \rightarrow d}^j = c_{ij} + c_{jd} \quad (6)$$

the distance (i.e., cost) c_{ij}^d from node i towards destination d along node j as the sum of that between i and j , c_{ij} , and that from j to destination, c_{jd} . Then we specify the cost over a certain arc a_{ij} :

$$c_{ij} = h_{ij} / w_{ij} \quad (7)$$

as the ratio between a certain property we want to use as metric, h_{ij} , and its weight, w_{ij} .

Given all the above, the value of the a-priori gain, $\eta_{i \rightarrow d}^j$, for a certain choice leading to destination d is computed according to the following formula:

$$\eta_{i \rightarrow d}^j = \delta / c_{i \rightarrow d}^j \quad (8)$$

where the relationship is inversely proportional with respect to the (weighted) distance, and δ is just a constant of proportionality.

Following this pattern, one more fix, also applicable to the standard ACO variant, would consist in relaxing the requirement that agents travel back home after finding food, in its stead by leveraging the communication bus for near-instant swarm-wide dissemination of pheromone trails.

Thus, a newly defined probability p_{ij}^d for any artificial ant, placed in vertex i , to move toward node j , according to destination d , is defined as follows:

$$p_{i \rightarrow d}^j = \frac{\tau_{ij}^\alpha \cdot \eta_{i \rightarrow d}^j^\beta}{\sum_{l \in N_i^k} (\tau_{il}^\alpha \cdot \eta_{i \rightarrow d}^l^\beta)} \quad (9)$$

where τ_{ij} corresponds to the quantity of pheromones laid over arc a_{ij} , η_{ij} to a-priori attractiveness of the choice, computed by some heuristic embedding the cost of choosing arc a_{ij} along the path that leads to the destination, and N_{ik} is the set of neighbors in node i for ant k , i.e., the admissible transitions for the ant.

The amount of pheromone to be deposited depends on a metric for posterior costs, in general with no relation to h as defined in Eq. 7. Even in this case, pheromone gets updated as defined in Eq. 3.

As choices are unpredictable and there cannot be a notion of rounds for real-world agents, pheromone laid over each arc evaporates, still according to Eq. 4, but on a time basis, by setting timers.

Even in this case, far from the solution from losing generality, on the contrary the modification expands the scope of applicability, by relaxing constraints over the scenario.

5 Preliminary Evaluation

To evaluate our proposed technique, we examined the traffic of an urban area, near down-town the city of Messina. Arcs weights represent the length l_{ij} of each road segment such that, using Eqs. 6 and 7 we can compute for each destination d the cost to take the arc (i, j) in the path towards node d without considering the road traffic. Providing these values as a metric to define the heuristic function of the A* search algorithm, we can find the shortest path length, which can be very different from the optimal path when the traffic is considered. We then implemented a simulator of the overall system. The evaluation of the model will provide a different metric to the heuristic function of the A* search algorithm that takes in account also the traffic.

In the evaluation through the simulator we considered two scenarios where either we take into account the pheromone value or not. According to Eq. 9 this can be obtained by setting either $\alpha = -1$ or $\alpha = 0$. According to the results thus obtained, in both cases the flows of traffic concentrate on the neighbors of the specific destination and are directed towards it, thus confirming that the messages go in the right directions. In the case not taking into account pheromones we can observe a strong flow from node 1 to node 3 which is justified by the presence of a source in node 1. Moreover, the preferred paths used to reach node 3 are clearly visible. However, as expected, the pheromone effect

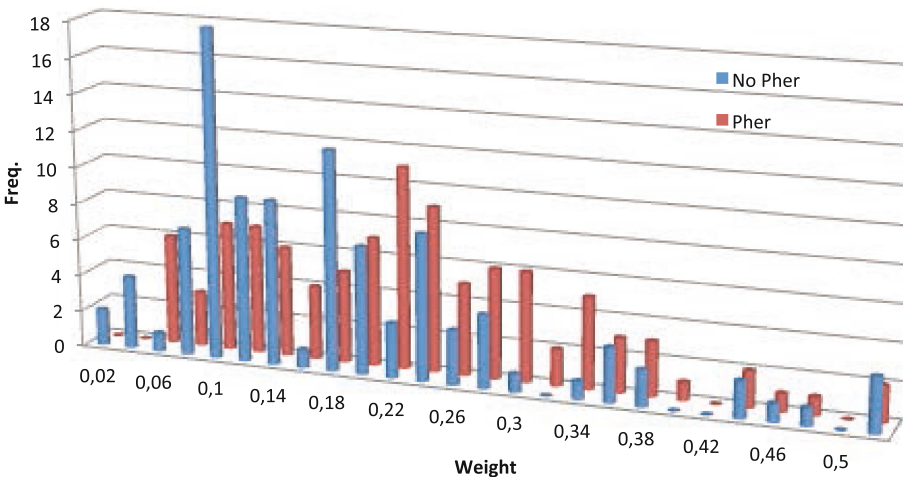


Fig. 4. Frequency distribution of the aggregated traffic obtained by simulation of the solutions with (Pher) and without pheromone (No Pher).

is to redistribute the traffic. In such case the flow on congested arcs decreases indeed, while underexploited arc one increase.

To evaluate the effectiveness of the proposed approach in distributing the overall traffic on the graph, we investigated the distribution of the aggregated traffic (i.e. related to all destinations) for all the arcs. Since the traffic is evaluated as a rate of an exponential process, we can compute the aggregated one just as the sum of the traffics of each destination.

The resulting frequency or probability mass functions of the traffic with and without pheromone are shown in Fig. 4. It can be observed that the pheromone improves the distribution of the overall traffic intensities. Indeed, without pheromone, several arcs present a high-intensity traffic, especially around the values 0.2 and 0.55. The distribution thus obtained appears to be bimodal. When the pheromone is considered, the traffic results more evenly distributed, with a peak around the value 0.6. From these values, we can argue that the pheromone allows the overall traffic to be more evenly distributed than when the pheromone is not considered.

6 Conclusions

People, crowds and critical masses are becoming more and more powerful, not only from an abstract point of view related to the opinion they express, but also in more physical terms, due to their work potential. Indeed, volunteer and crowd-based approaches are spreading like wild-fire across different disciplines and sciences. Example are crowdsourcing, crowdfunding, geocomputing and volunteer geographic information, just to name a few in different areas. A very fertile ground for new approaches and technologies is computer science and engineering, where volunteer and crowd-based ones have gained solid roots as in the cases of crowdsourcing, crowdsearching, crowdsensing. In particular, Mobile Crowdsensing is a very promising approach for involving people, citizen, crowds into sensing campaigns according to participatory and/or opportunistic schemes. Although the Mobile Crowdsensing paradigm is quickly rising interests and funds, there is still untapped potential, as well as unexplored solutions this paradigm may empower.

This paper tries to partially fill this gap by first defining a scenario and identifying some specific features for a novel opportunistic, distributed, self-organizing approach, applied to a specific class of MCS application, tackling local optimization problems, in the ITS domain. The solution proposed adapts and extends an ant colony optimization algorithm to a problem of pathfinding and graph traversal according to a given distance metric. This way a new class of intelligent transportation systems is identified: the swarm intelligent transportation systems - SITS - one.

References

1. European Parliament: Directive 2010/40/EU, Brussels (2010)
2. Da Lio, M., Biral, F., Bertolazzi, E., Galvani, M., Bosetti, P., Windridge, D., Saroldi, A., Tango, F.: Artificial co-drivers as a universal enabling technology for future intelligent vehicles and transportation systems. *IEEE Trans. Int. Transp. Syst.* **16**(1), 244–263 (2015)
3. Groot, N., De Schutter, B., Hellendoorn, H.: Toward system-optimal routing in traffic networks: a reverse stackelberg game approach. *IEEE Trans. Int. Transp. Syst.* **16**(1), 29–40 (2015)
4. Du, L., Dao, H.: Information dissemination delay in vehicle-to-vehicle communication networks in a traffic stream. *IEEE Trans. Int. Transp. Syst.* **16**(1), 66–80 (2015)
5. Lee, E., Lee, E.-K., Gerla, M., Oh, S.: Vehicular cloud networking: architecture and design principles. *IEEE Commun. Magaz.* **52**(2), 148–155 (2014)
6. Lv, Y., Duan, Y., Kang, W., Li, Z., Wang, F.-Y.: Traffic flow prediction with big data: a deep learning approach. *IEEE Trans. Int. Transp. Syst.* **16**, 1–9 (2014)
7. Hamdar, S., Talebpour, A., Dong, J.: Travel time reliability versus safety: a stochastic hazard-based modeling approach. *IEEE Trans. Int. Transp. Syst.* **16**(1), 264–273 (2015)
8. Ganti, R., Ye, F., Lei, H.: Mobile crowdsensing: current state and future challenges. *IEEE Commun. Magaz.* **49**(11), 32–39 (2011)
9. Dorigo, M., Stützle, T.: *Ant Colony Optimization*. Bradford Company, Scituate (2004)

Research on Visual Feedback Based on Natural Gesture

Wenjun Hou^{1,2}, Shupeng Zhang^{1(✉)}, and Zhiyang Jiang¹

¹ School of Digital Media and Design Art, Beijing University of Posts and Telecommunications, Beijing 100876, China

hwj1505@bupt.edu.cn, super_bupt@126.com

² Network System and Network Culture Key Laboratory of Beijing, Beijing 100876, China

Abstract. **Objective** To study some problems of visual feedback on user cognition and satisfaction in virtual and real interaction with inconsistent input and output. **Method** Based on natural gestures, experiments were designed to study user's perception of different visual feedback and satisfaction in virtual grasping, with the Ergo LAB physiological auxiliary testing equipment. **Conclusion** In the virtual and real interaction visual feedback, the feedback form of visual expression is superior to the performance of movement, and the color is the main form. The feedback form of movement performance is stronger in physiological stimulation, deformation is the most feedback way of human cognition, which can increase the sense of immersion. In the interaction involving a variety of visual feedback, it is suggested giving priority to the classification of the same form of expression.

Keywords: Virtual grasping · Virtual and real interaction · Visual feedback
Variable analysis · Physiological index

1 Introduction

Virtual and real interaction is a new and emerging form of human-computer interaction, highlighting the virtual reality and augmented reality. With the help of powerful computing and graphics capabilities of computers, it achieves more intelligent understanding of human order and enables more input modes [1].

Various input modes expand the interaction between virtual and real worlds. In the virtual and real interaction, the most reasonable and efficient interaction should be natural gestures. It allows users to abandon the external devices and interact with the virtual scene.

There are plenty forms of feedback during virtual and real interaction, such as vision, hearing, touch, space conversion etc. In virtual and real interaction, the content is mainly based on the three-dimensional scene and model objects, and the input and output of information are different.

The input of visual information accounts for more than 80% of the total intake of information, and can provide interactive feedback immediately, which has a positive

effect on reducing the user's cognitive load. Since the feedback comes from the perception of vision [2], environment and input gestures, the visual feedback plays an important role in virtual and real interaction.

2 Related Work

In view of the current research, the study of visual feedback among the virtual and real interaction was divided into the following three directions: hardware development and extensions, hardware algorithm based on recognition accuracy and natural gestures design.

Mores Prachuabrued et al. explored the visual feedback when fingers penetrating virtual objects during virtual grasping and evaluated the performance (penetration, finger release time, accuracy) of several common visual feedbacks. Results showed that recommend visual feedback is color change [3]. And another experiment showed the combination of touch and visual feedback is optimal [4].

Faieza Abdul Aziz et al. studied visual feedback mechanism, they found out that users achieved higher efficiency in finishing assigned tasks with visual feedback. In addition, the results showed that color changes are more effective than text prompts [5].

Based on previous studies, YingKai designed visual feedback for virtual hand and grasping objects. She finally concluded: 1. overall performance was better than the local performance. 2. visual change of objects was more effective than the change of virtual hand, 3. red color obtained the best feedback [6].

Zhang Wei et al. presented that static color recognition efficiency in virtual environment is far higher than in the real world, and suggested using dynamic [7] visual feedback in the virtual scene.

Previous research had laid a certain foundation for related fields, but it also exposed some shortcomings. In the virtual and real interaction visual feedback, it is not enough only to study the changes of static visual feedback, and in the course of experiment, the level of the user's operation is not accurately regulated, so it is necessary to use the auxiliary information of other channels to authenticate of conclusions under single visual feedback.

In order to improve the research content in this field, on the basis of previous research, we conducted an experimental study on natural grasping gestures in the virtual reality interaction with respect to visual feedback. This paper mainly studied the difference and validity of visual feedback form of the target object. The feedback form variables include object color, transparency, flashing, highlight, rotation, shaking, scale, and deformation. Besides, auxiliary electromyography and heart rate test were applied for evaluation. Experimental results were analyzed.

3 Experiment Design

First, we define natural gestures. Natural gestures refer to gestures that do not add any markings, do not wear any auxiliary equipment, and use bare hand to interact with

objects directly. According to Wu and his co-author [8], a gesture includes Three stages, concluding the following Fig. 1:

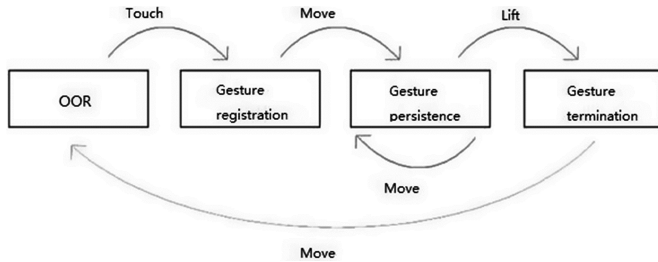


Fig. 1. Three stages of the gesture input, OOR means the device “out of range”

We defined the natural grasping gesture; sub-action can be divided into “encounter object” and “pick up the object”. We introduced the way of visual feedback.

So how do you judge the validity of different visual feedback types in virtual reality interactions? In fact, it is the in process of the grab gesture from “encounter object” to “pick up the object”. From the “encounter object”, to see the visual feedback, and then quickly “pick up the object”, the moment of seeing the visual feedback will differ because of the different kinds of visual feedback; this difference can represent the difference of feedback ways, and then we can analyze its effectiveness. On this basis, we construct the experimental platform, and do the experimental study.

3.1 Design Experiment

The experiment used Unity 5.4 as the platform, C# as the programming language, and Leap Motion camera to input the gesture coordinates and use grasping gestures to perform experimental operations and record data.

At the same time, the Ergo LAB physiological detection equipment was used to detect the EMG and heart rate in the experiment. The physiological indexes of the subjects were recorded under different visual feedback conditions (Fig. 2). The EMG detector (sEMG) electrode was pasted at the extensor carpi radialis brevis muscle of the right arm [9], which was the main muscle of the activity in the operation of the grasping gesture.



Fig. 2. Based on leap motion system and Ergo LAB, visual feedback - cognitive experiment

In this study, we use controlled-variable single factor inner-group comparison experiment and inter-group comparison experiment. Inner-group comparison experiments included the use of Leap Motion to achieve the virtual grab of the ball without feedback and in eight control variables of feedback, a total of nine groups. Inter-group comparison experiment included grabbing empty and grabbing solid table tennis, a total of two groups.

3.2 Control Arguments

Object color, transparency change - For the feedback form in this study, the independent variable of object color change was red, the self-variable of object transparency change was alpha equal to 0.4 concluding from the literature [6].

Object flashing - For the feedback form in this study, the independent variable of object blink control was the red and transparent alternation of the object in this paper [7].

Object highlighting – The paper [10] suggested that in the three-dimensional virtual scene, the use of highlighted form to interact with object was desirable. So, we designed highlighting color selection red, display on the edge of the small ball.

Rotation, shaking, and scaling of objects – The author [11] used scaling, translation and rotation operations in interactive operations of 3D models in virtual reality, so we chose these three ways in the experiment.

Object deformation - When the virtual finger is grasping, the places where fingers and small ball collide will have deformation [12], which control the deformation of the radius and the intensity in the appropriate range, in order to achieve the deformation of the feedback form. The interface was shown in Fig. 3.

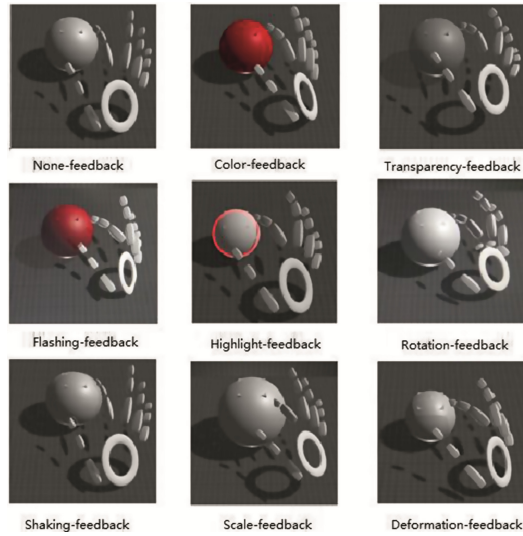


Fig. 3. Visual feedback experimental interface overall (Color figure online)

3.3 Experiment Process

After pre-tests and screening, 20 participants were selected: 10 boys and 10 girls, aged from 20 to 25 (mean age 23.4), were all right handed and familiar with computer operation. All participants were in good health and no symptoms of physical fatigue such as massive exercise before the test. All participants were willing to accept the experiment voluntarily.

Before the start of experiment, the Ergo LAB device will be fixed, and the heart index detector (HRV) was clamped on the left index finger (HRV) of the subject, wipe the right side of the arm extensor parts with alcohol and fixed the electromyography (sEMG).

The experiment will begin after the detection of heart rate and myoelectric physiological signal remaining stable. The experiment was divided into 2 groups and 11 experiments. Each process requires 3 s of rest after the participant completes each grasping, each procedure include 5 times of this process. After each procedure, let the participant take a short break while saving Ergo LAB physiological data. And so on, followed by the implementation of 11 experimental process, the data will automatically be saved in the local file. After the experiment was completed, the subjects were graded on the satisfaction of several visual feedback methods, and they were graded from -2, -1, 1, and 2 by Likert 5 scale.

3.4 Experiment Data

The experimental data included response time ΔT , satisfaction S , mean electromyography $Y_{Average}$, mean muscle contraction $Y_{Variance}$ and mean heart rate $AVHR$.

Reaction time $\Delta T = T1 - T2$, which T1 was the time when the subject encounters the ball to the release of the ball, T2 was the time when the user begin performing the grasping gesture to the release. Therefore, ΔT could be expressed as the user to see the feedback to the beginning of the implementation of the time difference, that is, the reaction time, as the form of feedback effectiveness of the important indicators. Satisfaction S was the satisfaction of the user after the completion of the experiment, the evaluation of the eight variables of the satisfaction score, respectively, -2, -1, 0, 1, 2, post-data analysis was standardized, all returned to 0 to -1 score.

The physiological signal data were sorted out in the Ergo LAB analysis software, and the fragments from the signal equalization change to the signal equalization change were selected and processed for analysis. Analysis of sEMG signal according to the literature [13] selected these three data indicators commonly used in time domain and frequency domain analysis. Of this, YAverage represented the average level of the physiological signal amplitude of the segment, YVariance represented the amplitude variance of the physiological signal of the fragment. They all obey to the zero mean Gaussian distribution, proportional to the degree of muscle contraction; AVHR represents the mean heart rate of the segment.

4 Experiment Design

4.1 Inner-Group Analysis

After 20 person-times of experiments, a large amount of statistical data was obtained. After the invalid data was eliminated, the data were consolidated and imported into the SPSS software for analysis and processing. The first test of the ΔT and S data obey normal distribution, results all meet. Descriptive statistics are then given in Table 1 below.

Table 1. Descriptive statistics of variable response time and satisfaction

	Cases	The average of ΔT	The average of S	Standard deviation
Color-feedback	20	.646497	1.30	.1102680
Transparency -feedback	20	.635995	0.250	.1800684
Flashing-feedback	20	.708847	-0.20	.1707118
Highlight-feedback	20	.615964	1.40	.1706103
Rotation-feedback	20	.763828	-0.65	.1851743
Shake-feedback	20	.756642	-0.95	.1803534
Scale-feedback	20	.775068	-0.55	.2113159
Deformation-feedback	20	.738598	0.35	.1518762
None-feedback	20	.960270		.2135176
Effective case number	20			

It can be seen from the chart that the first ΔT without feedback was much larger than that of the other eight feedback modes, indicating that the operational efficiency value in the form of visual feedback was improved and the visual feedback mode is reasonable and necessary;

The ΔT of the highlight-feedback was the smallest, and the user satisfactions were also the highest. The ΔT of these four modes of feedback such as rotation-feedback, shake-feedback, scale-feedback, and deformation-feedback were too large, and customer satisfaction were relatively low, the initial description of these the form of feedback was inappropriate.

In order to test the rationality of the ΔT and S data results, ΔT and S were tested for paired samples T, and the results showed that, in addition to the transparent and deformed feedback methods, the other six feedback patterns had a significant correlation in the relevance of the sample sig <0.05, showing a high degree of correlation, which was also consistent with the description of the statistical feedback time is small and high satisfaction Feedback time and satisfaction with low consistency.

In the process of data analysis, we found that the results of different variables showed a certain consistency, such as color, transparency, highlight the feedback method are better. And rotation, scaling, shaking, deformation of these feedback methods was relatively poor, but the results were also close to the guess may also be a certain degree of relevance. Therefore, cluster analysis was performed and the clustering results were shown in Fig. 4.

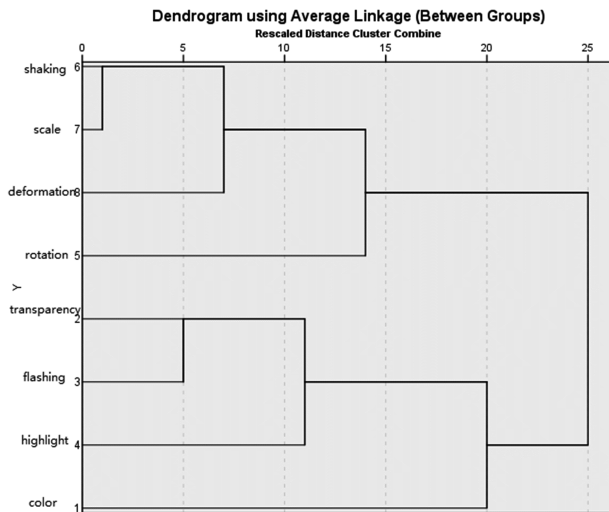


Fig. 4. Systematic clustering result pedigree

As you can see, shake-feedback, scale-feedback, deformation-feedback, and rotation-feedback are automatically clustered together, and the flashing-feedback, transparency-feedback, highlight-feedback, and color-feedback came together. The eight variables could be classified into two types, summed up the visual display and movement performance.

4.2 Inter-group Analysis

Considering that single visual input information could be deceptive, it was necessary to continue to analyze and validate from the perspective of physiological indicators, refer to Figs. 5 and 6.

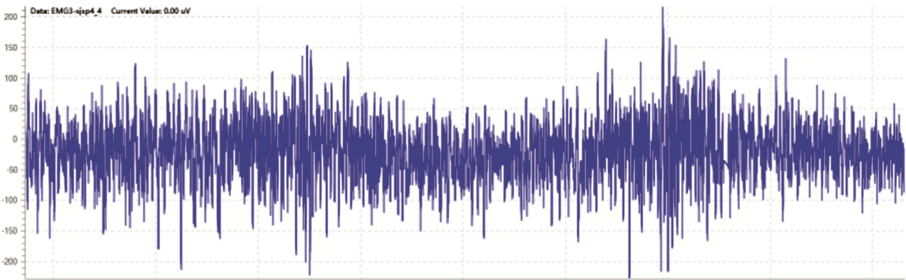


Fig. 5. Diagram of sEMG and HRV signals

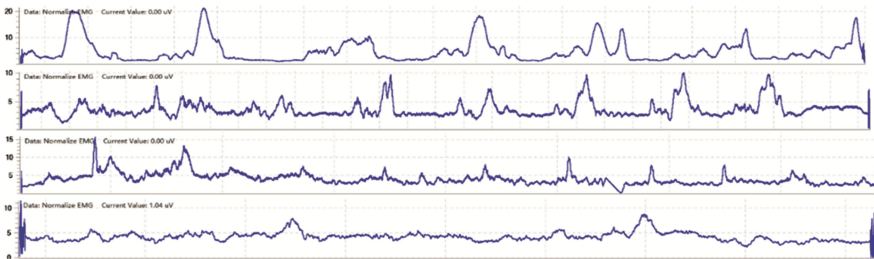


Fig. 6. sEMG in different experimental grasping processes, empty-grasping, grasping table-tennis, none-feedback and highlight-feedback

The data of the physiological indexes after the errata was sorted out, and the mean value of the case variables was output. At the same time, the satisfaction score was normalized and the overall data results were presented in Table 2.

From the overall analysis, the physiological index data of different feedback forms was different, we could guess that there existence a certain psychological model between the visual and tactile perception.

Table 2. Experimental data cross table

	ΔT	S	YAverage	YVariance	AVHR
Empty-grasping			3.7294	1.5835	71.4375
Grasping table-tennis			3.7106	1.3006	70.4
Color-feedback	0.5194	0.825	3.7456	1.6041	73.1875
transparency-feedback	0.5851	0.5625	3.8839	3.2312	75.0667
Flashing-feedback	0.6705	0.45	3.6828	2.0161	76.7143
Highlight-feedback	0.563	0.85	3.9522	1.5965	75.3571
Rotation-feedback	0.7157	0.3375	3.8833	1.995	71.1875
Shake-feedback	0.7333	0.2625	3.9244	1.4994	75.1429
Scale-feedback	0.7153	0.3625	4.0394	1.4412	71.4667
Deformation-feedback	0.7078	0.5875	4.6644	3.8787	71.7143
None-feedback	0.8869		3.665	1.8639	66.2143

The average EMG and reaction time of visual feedback was positively related to the reaction time, the greater the average EMG value is higher, but the effectiveness of the feedback form is small;

The heart rate associated with visual feedback, visual feedback was more intense, the heart rate is higher, but the effectiveness is not high, the use of context information, such as presentation, warning effect, interaction effects etc.;

The muscle fatigue and cognition, more familiar and more acceptable form of feedback of the lower degree of muscle fatigue, exercise performance was better than the intuitive, people were more likely to perceive, but the effect was not good.

5 Conclusion

Through inner-group analysis and inter-group analysis, the data were analyzed by horizontal and vertical, respectively, summarized as follows:

- (1) In general, the feedback form of visual expression was superior to the performance of movement;
- (2) The more obvious the physiological index, the strongest the stimulus. The color feedback and highlight feedback performance were the best, and also had the highest subjective satisfaction;
- (3) The flashing feedback was the most intense stimulus, but it was not applicable in interactive feedback, and subjective satisfaction was low;
- (4) The deformation feedback was the most consistent cognitive approach to grasp gestures, and was recommended in the virtual scene collision detection;
- (5) The scale feedback was not the best in cognition, but it could reduce the user's operation fatigue and reduce the user's learning process in interactive operation;

In summary, the form of visual feedback was suggested as follows:

In the virtual and real interaction, it was best to use the visual expression of visual feedback form, mainly color, local performance and overall performance should be considered;

In scene content design, the dynamic visual feedback was more easily perceived than the static;

In the multimodal input and output model, visual feedback of motor form was better and more in line with human cognition;

In the multi-channel information input and output mode, the visual feedback of motor expression form is better and more consistent with human cognition;

When there were a lot of visual feedback forms in the interaction of virtual and real interaction, priority should be given to using a consistent and consistent feedback method to select the correct form of visual expression and the performance of movement;

6 Summary and Future Work

In this paper, we studied the effects of different visual feedback forms on cognitive and user subjective satisfaction under the natural gesture. At the same time, we used physiological detection equipment to detect the physiological characteristics of the experiment process and concluded that visual feedback affects user reaction and user experience to some extent, and found that there was a relationship between physical characteristics and visual feedback.

In this paper, the study of the type of visual feedback was still at the initial stage. The variable level of scaling and deformation feedback was derived from the actual project, the selected deformation parameters needed further study. In addition, visual feedback had more dimensions and angles of variable types that need further study.

References

1. Zhao, Q.: Virtual reality review. *Sci. China Ser. F Inf. Sci.* **39**(1), 2–46 (2009)
2. Zhao, Z.: Virtual reality based on human-computer interaction. *J. Wuhan Univ. Sci. Technol.* (2007)
3. Prachyabrued, M., Borst, C.W.: Visual feedback for virtual grasping. In: *IEEE Symposium on 3D User Interfaces (3DUI)* (2014)
4. Prachyabrued, M., Borst, C.W.: Virtual grasp release method and evaluation. *Int. J. Hum Comput Stud.* **70**(11), 828–848 (2012)
5. Prachyabrued, M., Borst, C.W.: Visual interpenetration tradeoffs in whole-hand virtual grasping. In: *Proceedings of IEEE 3DUI*, pp. 39–42 (2012)
6. Ying, K.: Visual feedback for natural interaction study. *Beijing University of Posts and Telecommunications* (2016)
7. Meng, F.-X., Zhang, W.: Way-finding during a fire emergency: an experimental study in a virtual environment, vol. 57(6), June (2014). Taylor & Francis, Oxon. ISSN:0014-0139
8. Wu, M., Shen, C., Ryall, C., Balakrishnan, R.: Gesture registration, relaxation, and reuse for multipoint direct-touch surfaces. In: *Proceedings of the First IEEE International Workshop on Horizontal Interactive Human-Computer Systems (TABLETOP 06)*, pp. 183–190 (2006)
9. Lin, Y., Zhang, F.: Carpi brevis tendon twin countershaft one case. *Chin. J. Clin. Anat.* **23**(6), 582 (2005)
10. Chen, D.: Interactive real-time rendering of three-dimensional scene style of lead color. *Nanjing University* (2016)

11. Li, S.-S.: Interactive 3D model of operational studies. Dalian University of Technology (2009)
12. Hou, W., Guo, Y., Li, T.-M., et al.: Research on three - dimensional object deformation technology for natural interaction
13. Wang, J.: Research progress on signal analysis and its application of sEMG. J. Phys. Educ. **20**(4), 56–60 (2000)

Information Security Technology and Application in Logistics Traceability System of Aquatic Products Based on QR Code

Qiaohong Zu and Rui Chen^(✉)

School of Logistics Engineering, Wuhan University of Technology,
Wuhan 430063, People's Republic of China
780225537@qq.com

Abstract. In view of the security hidden danger of the business data in the logistics traceability system of aquatic product, the design of the information security strategy is carried out from the two angles, which are data collection and transmission. Firstly, the aquatic traceability code is designed. Then the data encryption algorithm is studied, and the data security transmission of information security protection system is built. In the intelligent collection of traceability data, QR Code is used to express the logistics trace data, then uses the improved data encryption algorithm to encryption storage about QR Code. In the transmission of traceability data, the HTTPS protocol is used to construct the client-server transmission encryption channel to ensure the integrity of the data. Finally those information security technologies about Logistics traceability data are used in a logistics traceability system of aquatic product, and the effectiveness of RC4-RSA hybrid encryption algorithm is verified. And the integrated applications enhance the system's information security.

Keywords: Logistics traceability system of aquatic product · Data security
Data encryption technology · RC4-RSA hybrid algorithm

1 Introduction

In the logistics system, the importance of information security is increasing gradually [1]. Those technologies of information security, two-dimensional information encryption based on random shift [2], encoding encryption key of GPS location information [3], secure data aggregation based on homomorphic encryption scheme [4], encryption the key of AES algorithm with ECC [5], sustained data protection mechanism based on virtual storage technology and others have been born on. For logistics traceability system of aquatic products, the data of aquaculture, processing, transportation and sales are stored in the bar codes in the form of encoding. With the development of network technology, the encryption algorithm must be upgraded and the data storage and backup must be strengthened, to ensure the information security during the logistics traceability process.

2 Risks Analysis on Information Security of Aquatic Logistics Traceability System

The logistics traceability system of aquatic products is a distributed processing environment which is a multi-module, multi-role, multi-service information system. With the increasing of logistics business, the security risks increase. Analyzing the hidden security about the logistics traceability system of aquatic products from four layer of the acquisition control, data, application and user, the security problems of logistics business data mainly exist in the two aspects of data acquisition and transmission.

In order to improve the data security of the aquatic products traceability system, and ensure the integrity and availability of information, the author put forward a solution from the point of technology security combining with the hidden data security in the collection and transmission process.

In the logistics traceability system of aquatic products, data collection is mainly based on bar code identification technology, wireless data transmission and wireless tag (RFID) technology [6]. Among them, the bar code technology is more widely used in logistics system than RFID technology because of its low using cost. The two-dimensional code-QR Code is widely used in the current aquatic logistics traceability system. Therefore, this paper only focuses on the encryption of QR Code as a representative research object in the data collection section. Through the encryption to QR Code, avoid the direct exposure of information carried by the two-dimensional code.

3 Research on Two-Dimensional Encoding and Encryption About Traceability Data of Aquatic Logistics

3.1 Logistics Data Collection Code Generation Encryption

3.1.1 QR Code Encoding Encryption Design

(1) QR Code encryption location selection

Through the analysis on the encoding process of the QR Code, data can be encrypted at all levels before the final information is constructed, as shown in the Fig. 1.

Analysis on different positions, encryption after the data encoding, which is related to the complex process of coding generation, cannot guarantee that the original structure is not affect by the encrypted data. The poor flexibility affect the generation of the two-dimensional code. Wrong coding function cannot be guaranteed. So, the paper takes the encryption at position 1 to prevent information from being tampered with criminals.

(2) Encryption algorithm selection

Both the security of the information and the complexity of encoding and decoding should be took into account in a QR Code encryption strategy. Table 1 compares several common cryptographic algorithms in some important reference dimensions.

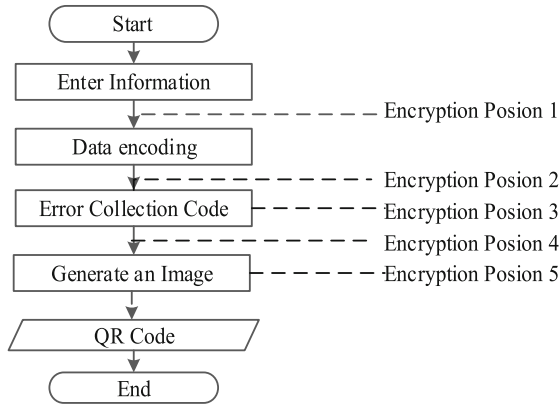


Fig. 1. QR Code multiple encryption

Table 1. Comparison of common encryption algorithms

Encryption algorithm	Category	Operation speed	Security	Resource consumption
DES	Symmetric	Faster	Low	Middle
AES	Symmetric	Fast	High	Low
RC4	Symmetric (Streaming encryption)	10 times faster than DES	High	Low
RSA	Asymmetry	Slow	High	High
DSA	Asymmetry	Slow	High	Digital signatures only

Symmetric encryption algorithms suit for a large amount of data encryption because of its low complexity of decryption and fast encryption speed, but they also have key shortcomings. Asymmetric algorithms have the feature for the high security, simple public key public key management, but relatively slow encryption speed.

QR Code using in the aquatic products logistics traceability, information read a large amount of encrypted data more, speed and security of encryption to protect data, using symmetric encryption algorithm and asymmetric encryption algorithm combination. Through the comparison of common algorithms in 3–1, this paper uses RC4 algorithm and RSA algorithm for QR Code hybrid, the original plaintext data is encrypted by RC4 algorithm, improve the speed of encryption and decryption of the RC4 algorithm, key is encrypted using the RSA algorithm, to ensure the security of the key, solve the problem of key distribution and management, further to improve the security of encryption.

(3) Encryption scheme for QR Code

Use RC4 and RSA algorithms in the encoding link of QR Code, to encrypt the data. The QR Code encryption process is shown in Fig. 2.

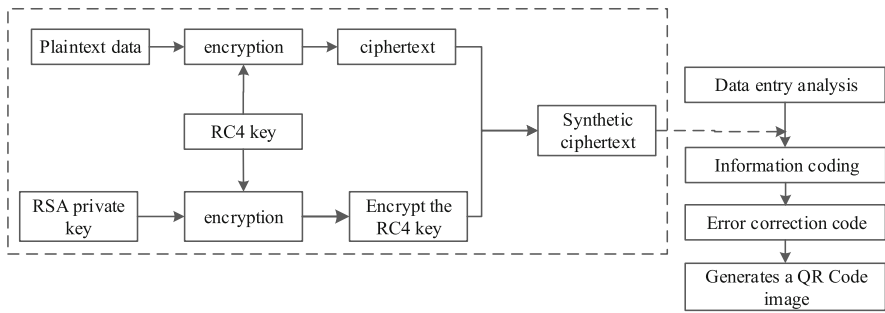


Fig. 2. QR Code encryption process

The QR Code decoding process is a reverse process of encoding, decryption process of the decryption algorithm is shown in Fig. 3.

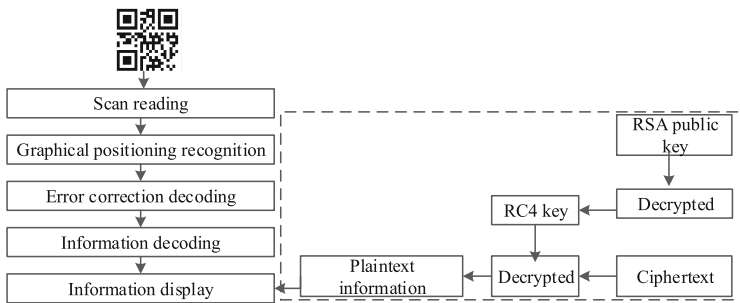


Fig. 3. QR Code decryption process

Through the mixed encryption with RC4 and RSA algorithm, the speed and security are improved while the security requirements of QR Code encryption and decryption are ensured. When QR Code is used in the aquatic traceability system, the aquatic enterprise uses the RSA algorithm to generate the public key and the private key, in which the public key can be made public, and the private key is reserved inside the enterprise for encryption. In the QR Code generating process, according to the encrypted data, enterprise distribute RC4 key or randomly generate, guarantee different QR Code using different encryption keys, dynamically generated QR Code encryption, and improve system security. The logistics staff read or write information by professional equipment with QR Code decryption algorithm, input the information to aquatic product traceability system, and data acquisition and encryption to achieve traceability to logistics supply chain, enhance the security of information.

3.1.2 Chaos Improvement of RC4 Algorithm

The QR Code encryption program for RC4 algorithm encryption is to take the XOR (exclusive OR) operation, once the sub-password is repeated, it is easy to be cracked. In addition, the randomness and ergodicity of the algorithm is not good enough, and it

is a low-diffusion state. Therefore, the RC4 algorithm has some weak keys and is vulnerable to attack.

In order to improve the security of RC4 algorithm in QR code encryption, the Logistic chaotic map is used to improve the randomness of pseudo-random sub-code generation, which make a better diffusion effect and reduce the occurrence of weak key. The so-called chaos is the disorder and random phenomenon in a deterministic system, the chaotic sequence generated by the chaotic system has unpredictability [7].

Logistic one-dimensional mapping which is widely used is a chaos mapping of mathematical form, the mathematical expression is:

$$X_{i+1} = \mu X_i(1 - X_i) \tag{2.1}$$

The ranges of values for the initialization parameter μ and X_0 are: $0 < \mu < 4, 0 < X_0 < 1$.

When $3.5 < \mu < 4$ the system is in a discrete state, that is, reaching the chaotic state. The value X_i have the characteristics of non-convergence and non-periodic, the value can traverse the whole interval of $(0, 1]$, the sequence generated outside the interval will converge to a specific value. The closer the μ is to 4, the better the proliferation.

After a large number of experiments, the parameters used in this scheme are: $X_0 = 0.8755, \mu = 3.99919$. The chaotic state reached at this time is shown in Fig. 4.

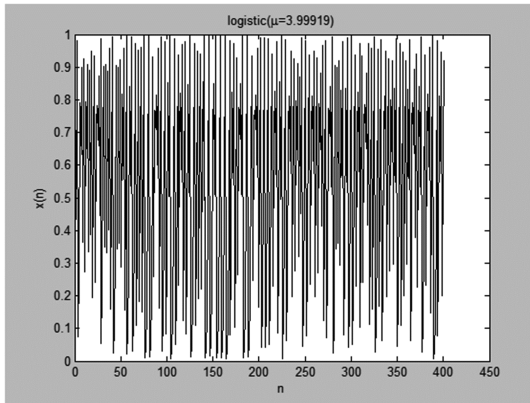


Fig. 4. The chaotic mapping when $X_0 = 0.8755, \mu = 3.99919$

After the chaotic map, the RC4 algorithm is improved as follows:

- ① Calculate the chaotic value based on the setting initial value of Logistic map.

$$y = \mu X_0(1 - X_0) \tag{2.2}$$

- ② Generate the random key sequence by substituting the chaotic value and iteration in the RC4 key scheduling algorithm.


```

y=u*x(1-x);

x=y;

j=(j+S[i]+T[i]+ y*256)mod256;

swap(s[i],s[j]);

```

- ③ Recursive execution after adding chaotic maps during the process of generation and replacement of Pseudo-random sub-code.

```

i=(i+1) mod 256;

y=u*x(1-x);

x=y;

j=(j+S[i]+y*256)mod 256;

swap(S[i],S[j]);

t=(S[i]+S[j])mod 256;

key[r]=S[t];

```

Do the XOR operation for the sequence generated by the third step with the plaintext, until the algorithm encryption step is completed. And the randomness of the random code generation is greatly improved after using the Logistic mapping.

The encryption security of QR Code information is improved by RC4 based on chaotic mapping and RSA algorithm, which are used to encrypt and decrypt the QR Code. It can effectively prevent the forgery and tampering of logistics business data and ensure the security of data in data acquisition and generation rooting.

4 Integrated Application of Aquatic Logistics Traceability Data Security Technology

In this example, the aquatic logistics traceability system is based on the background of an aquatic product processing enterprises in Hubei Province, and it is constructed according to the actual needs of the enterprises. The two-dimensional bar code is used to collect the information intelligently and realize the resource sharing of aquatic products. In the event of aquatic products quality problems, a quick inquiry to trace the relevant breeding distribution information can found where the problem is through the information contained in the two-dimensional code.

From the logistics business data security considerations, use QR Code data encryption to protect the security of data in the supply chain information transmission, and the HTTPS protocol to ensure the safety of data transmission channel.

4.1 Application of QR Code Encryption Technology in Aquatic Logistics Traceability System

4.1.1 Coding Design for QR Code in Aquatic Traceability

The core of aquatic logistics traceability is the construction of unique traceability code. Through the traceability coding rules, QR Code is used as label carrier to cover aquatic raw materials, breeding, processing and distribution process.

Combine the aquatic enterprises, product categories, production and breeding information organically to construct the only aquatic traceability code by using sub-rules. The aquaculture tracing a total of 24, is as shown in Fig. 5.

Vendor identification code	Aquatic product identification code	Unique traceability code			Check code
		Batch class number	Time	Serial number	
$N_1N_2N_3N_4$	$N_5N_6N_7N_8N_9N_{10}$	$N_{11}N_{12}N_{13}$	$N_{14}N_{15}N_{16}N_{17}N_{18}N_{19}$	$N_{20}N_{21}N_{22}N_{23}$	N_{24}

Fig. 5. Aquatic traceability code 24 bit structure

A unique identification of aquatic traceability code must be constructed, in order to truly achieve the retrospective query of aquatic logistics, processing, distribution and other information.

4.1.2 Encryption Implementation of Aquatic Traceability QR Code

QR Code stores the processing and distribution information of aquatic products. If the information is directly exposed to the two-dimensional code, it is easy to cause the information to be tampered with, so the QR Code information needs to be encrypted when printing. According to the distribution processing part of the trace code to generate encrypted QR Code.

Through the processing and distribution tracking code “123401020300216090800087”, the processing phase of the relevant information can be queried. According to the pre-assigned RC4 algorithm key “txttest” click to encrypted QR code can be generated by clicking to the pre-assigned RC4 algorithm key “txttest”. During the QR Code encryption process, the aquaculture enterprise retains the RSA unique private key for encrypting the RC4 key to make an intermediate key. The staff will posted the generated QR Code on the corresponding aquatic packaging to make user-friendly query.

When the aquatic products transported to the processing site, the staff get the aquatic product details through scanning the QR Code by the built-in decryption program PDA/mobile terminal. The built-in the RSA public key of aquatic enterprise is opening in the handheld terminal program, to convenient for staff or consumers to scan and decrypt. Using the RSA public key in the decryption program to decrypt the RC4 algorithm

intermediate key formed in the encryption process, and according to the decrypted RC4 key to obtain the original of the processing information. Using of ordinary scanning software without decryption procedures and RSA public key, can just access to a meaningless garbled.

The effect before and after the QR Code encryption is shown in Fig. 6.

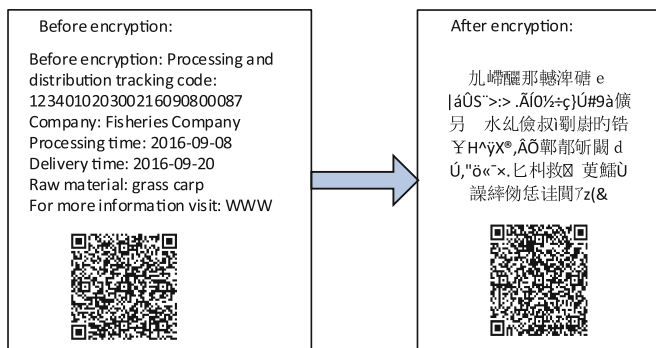


Fig. 6. QR Code encryption effect diagram

4.2 Result Analysis

4.2.1 Stochastic Analysis of the Improved RC4 Algorithm

For the improvement of RC4 algorithm in the QR Code generation encryption process, this paper adopts frequency test and run length test to verify the random performance of the improved algorithm.

The measure of randomness is P-Value, and statistic X obeyed $\chi^2(n)$ distribution, significance level $\alpha \in [0.001, 0.01]$. When $P\text{-Value} \geq \alpha$, then the sequence is random, which take $\alpha = 0.01$.

(1) Frequency Test

The frequency test is to test the proportion of 1 and 0 in the entire random sequence, and whether the two are close.

The frequency test formulas are:

$$P - \text{Value} = \text{erfc}\left(\frac{x}{\sqrt{2}}\right), x = |S_n|/\sqrt{n} \tag{3.1}$$

$$\text{erfc}(x) = \frac{2}{\sqrt{\pi}} \int_x^\infty e^{-u^2} d\mu \tag{3.2}$$

$\text{erfc}(x)$ is the complementary error function, and S_n is the result of the addition of the random sequence to -1 and 1 . By running the RC4 algorithm in MATLAB to obtain the random sequence, and then conversion and addition to get S_n , the value of S_n into

the formula, get *P* – Value, as shown in Fig. 7. It can be seen from the figure *P* – Value > 0.01, in line with the requirements of the ideal random sequence.

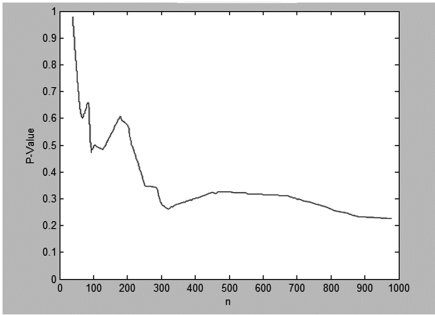


Fig. 7. Frequency test

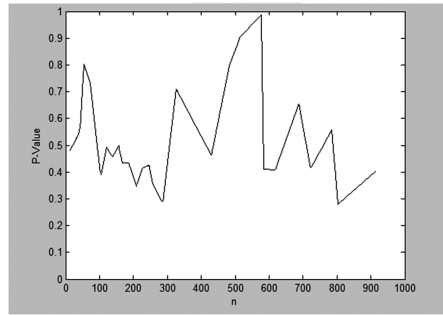


Fig. 8. Run test

(2) Run Test

Run test is a coherence test, the run is a two-part total, in the RC4 randomness test it is the uninterrupted sub-sequence constituted by the same bit sequence. The purpose of the run test is to determine whether the number of runs of 0 and 1 is consistent with the random sequence (Fig. 8).

The run test formula is:

$$P - Value = \text{erfc}(x), x = \frac{|V_n(\text{obs}) - 2n\pi(1 - \pi)|}{2\sqrt{2n\pi(1 - \pi)}} \tag{3.3}$$

$V_n(\text{obs})$ represents the sum of all 0 and 1 values in the random sequence of the RC4 algorithm, and n is its length. Replace the relevant parameters in MATLAB, to calculate *P* – Value. As can be seen from Figs. 3 and 4, *P* – Value > 0.01.

Through the frequency test and run test, the *P* – Value obtained is greater than the NIST specified 0.01, in line with the requirements of the ideal random sequence.

5 Conclusion

Under the background of supply chain logistics system, this paper analyzes the hidden dangers of aquatic logistics traceability system in business data, and constructs data acquisition and coding encryption. For the RC4 algorithm based on chaotic mapping is used in QR code encryption process, the author made the randomness test, and the test results show that the randomness is in accordance with NIST.

Through the QR Code encryption technology, using different RC4 key, the dynamic encryption of aquatic supply chain traceability can be achieved, fully guarantee the uniqueness of aquatic logistics data in the whole supply chain system, and avoid the forgery of others, improve the safety of aquatic system information from the root.

But the study only QR Code as a representative of the logistics information carrier research, Future research can also expand the data acquisition information carrier object, from the grid intrusion detection, trusted computing point of view, more adequate protection of the logistics system information security.

Acknowledgment. This paper was supported by the project in the Hubei Science and Technology Pillar Program (No. 2015BKA222).

References

1. Li, J.: The security challenge of network information reflected by “Prism” and its strategic thinking. *Inf. Theory Practice* **37**(4), 48–52 (2014)
2. Cheng, D.S., Wu, K.K., Liu, Z.Y.: Image encryption algorithm based on chaotic pseudorandom match shift. *Inf. Commun.* **8**, 7–9 (2016)
3. Prasad, R.P., Sudha, K.R., Sanyasi Naidu, P.: Information system with interlacing, key dependent permutation and rotation. *Int. J. Comput. Netw. Secur.* **2**(5), 86 (2010)
4. Soufiene, B.O., Abdullah, A.B., Abdelbasset, T.: Confidentiality and integrity for data aggregation in WSN using homomorphic encryption. *Wirel. Pers. Commun.* **80**(2), 867–889 (2015)
5. Liao, C.Z., Xu, J.W.: Research on AES and ECC mixed encryption algorithm. *Softw. Guide* **15**(11), 63–64 (2016)
6. Zhao, Q., Peng, H., Hu, B., Liu, Q., Liu, L., Qi, Y., Li, L.: Improving individual identification in security check with an EEG based biometric solution. In: Yao, Y., Sun, R., Poggio, T., Liu, J., Zhong, N., Huang, J. (eds.) *BI 2010. LNCS (LNAI)*, vol. 6334, pp. 145–155. Springer, Heidelberg (2010). https://doi.org/10.1007/978-3-642-15314-3_14
7. Niu, C., Yang, Y.J., Mao, X.Q.: Protection mechanism of continuous data based on virtual storage technology. *Comput. Eng. Des.* **34**(4), 1207–1211 (2013)

Quantified Self: Big Data Analysis Platform for Human Factor Efficacy Evaluation of Complex System

Chaoqiang Li¹, Wenjun Hou^{2,3(✉)}, Xiaoling Chen², and Hao Li²

¹ China Electronic Science Research Institute, Beijing, China

² School of Digital Media and Design Arts, Beijing University of Post and Telecommunications, Beijing 100876, China
hou.1505@163.com

³ Beijing Key Laboratory of Network and Network Culture, Beijing University of Post and Telecommunications, Beijing 100876, China

Abstract. By analyzing the factors affecting the airborne mission system, this paper applied the method of Quantified Self to the evaluation of human effectiveness in the military airborne mission system. According to the depth of interaction between people and information, we divide the information circumstance into four aspects including individual, equipment, network and environment. Then we construct a complete individual Quantified Self information interaction system by collecting physiological data, cognitive data, behavioral data and environmental data. Finally, the functional architecture and composition of the ergonomic evaluation platform are given in combination with the airborne mission system.

Keywords: Quantified Self · Complex information system · Big data

1 Introduction

With the development of information technology such as the internet of things, cloud computing, mobile Internet, “Natural Interaction” and “Intelligent Decision” have become important concepts in various information system. Developing of the information technology also lead to the explosive growth of data, which has had a profound effect and even gradually change the original knowledge production mode and cognitive framework. Big data analysis has become an integral method in many fields, and one of the big data analysis trend is Quantified Self (Fig. 1).

The airborne cabin is an important campaign environment in high-tech war. The working space of the cabin is airtight and narrow, and the operation environment is complex. Noise, vibration, electromagnetic field will affect the working condition and operation ability of operators to varying degrees, which will affect the combat effectiveness. So, the main problems we have to face are:

- (1) Large amount of data: With the development of sensors, the amount of data will become larger, the types of data will become more diverse and the update speed of data will become faster.



Fig. 1. Conception of future combat cabin

- (2) High complexity of tasks: There are many kinds of tasks, such as searching, tracking, and monitoring. The information capacity of these tasks interface is enormous, and the structural relationship of these tasks is complicated, and these tasks have the characteristic of uncertain and difficult to predict, which is easy to cause the disorder of cognitive and affect the judgement of the operator.
- (3) Change of the working mode: The working mode of the operators is mainly converted from operation to surveillance and decision making, which results in a sharp increase in imbalances between the human cognitive and the interface information encoding [2].

The information warfare requires both commanders and operators to perform tasks accurately and in real-time. It is a key link for improving the individual performance and the team decision-making ability to establish a real-time and high-precision state awareness model for combatants, which can detect the cognitive state of the commanders and soldier combatant states in real time and adjust them in a timely manner. At the same time, the information warfare also requires more dominant, autonomy and intelligent. Building a decision support system that provides operators with inferences about current and upcoming behavior and assigning tasks autonomously between operators and system.

2 Related Work

Quantifying self, as one of the big data analysis methods, can discover valuable information and implicit relationships in human-computer-environment system by analyzing various data associated with human activities, which can help to improve current states.

The emergence and development of the concept of “quantifying self” was only a few years ago and mainly in the field of health. It is used to track and record individual behaviors such as sports, sleep, diet, mood by using multiple device such as computers, portable sensors and smart phone. Then the collected data were used to discover valuable information in fitness, daily physiology and diseases treatment which can be used to improve the people’s living condition. With the development of micro sensors and

intelligent mobile technology, quantifying self will become an important method for ergonomics research, information visualization and human-computer interaction research.

At present, western countries led by the United States are in absolute leading position in the research field of complex systems. The key technology program of United States Department of Defense not only lists human-computer interaction interfaces as an important part of software technology development, but also specially adds human-computer system interface which is juxtaposed with software technology. A new project of the DARPA hopes to improve the cognitive ability by changing the information display mode, which can improve operators' efficiency, and the cognitive ability is reflected by the cognitive enhancement. The US Navy Research institute used eye tracking technology to solve problems in the ship pilot train [6]. The following work had been done:

- (1) The researchers organized a large number of experienced crew and ordinary students to simulate operations such as navigation, berthing and emergency avoidance. And the researchers collected eye movements, behavioral data and some electrophysiological data from them throughout the missions.
- (2) The researchers identified different eye movements patterns between experienced crew and ordinary students by detailed analyzing above data, and established a quantitative model of eye movements pattern.
- (3) The model is applied to training students. By monitoring the eye movement data of students, the system can automatically calculate whether the students deviate from the correct mode of operation and give timely feedback according to the model.

At present, the system has been applied to the simulation training of American Navy drivers, and has achieved good results. The study of human efficacy has entered a new stage in China, too. Quantitative research, as an important method to study human efficiency and user experience, has been carried out in many fields such as ships, tanks, aircraft driving and civil aviation control. User experience is also attached great importance in the development of civil information systems such as the Internet. A large number of quantitative research has been carried out. For example, Wen-jun Hou and Xiao-yu Gao of the Beijing University of Posts and Telecommunications studied a method based on measurement of pupil satisfaction. [4] This paper analyzed the relationship between the pupil size and the user satisfaction in usability tests. And they discovered that there is a linear significant negative correlation between the user satisfaction and user's pupil diameter standard deviation rate, and build a model to describe this relationship.

3 Classification of Quantified Self Data

According to the depth of interaction between people and information, we divide the information circumstance into four aspects including individual, equipment, network and environment [3]. Then we construct a complete individual Quantified Self

information interaction system by collecting physiological data, cognitive data, behavioral data and environmental data [3].

The physiological data include height, weight, blood oxygen, blood pressure, heart rate, etc. These data reflect the health condition of the operator. The harsh cabin work environment, limited space, noise, vibration, electromagnetic fields have a serious impact on physical and mental health of operators. The narrow space makes the operator stay in a fixed position for a long time, which will lead to blood in the legs, causing swelling, stiffness and discomfort. Operators not only have to face complex and diverse information, but also perform complex tasks, which can easily lead to fatigue. According to the corresponding physiological indexes, work intensity are reasonably arranged so as to achieve the best operation safety and performance.

The cognitive load caused by the mental energy consumption in the process of information processing has become an important indicator of the reliability evaluation of human-computer interaction system. Many researchers have realized that the cognitive load is a very serious threat for job performance and operational safety. Facing the large screen display and the global visual interface of beyond sight distance, in order to obtain the situation of the whole system, the operator must enter the interface of different functions through the interface management task to master all the information needed. When cognitive load is overloaded, the operator cannot successfully complete the task due to the insufficient supply of cognitive resources, which leads to decreased accuracy, prolonged reaction time and even accidents. However, the effective control of cognitive load does not mean to blindly reduce the cognitive load. Because when the cognitive load is too low, especially when in a monotonous boring situation, the operator is likely to become unresponsive and lead to more errors.

The environmental data, such as temperature and humidity, will have a great impact on the operators. For example, if under insufficient illumination condition, operators need repeated identification. The vision continues to decline, cause eye fatigue and even systemic fatigue. Human beings have different behavioral responses in human-computer interaction in different environments. The environment affects not only people's working ability, and also the performance and reliability of the machine. On the other hand, people and machines also affect the state of the environment. Therefore, the environmental factors are no longer excluded as a passive interference factor outside the system, but as a positive active factor into the system, and become an important part of the system research.

Behavior is the process of conscious decision making. Behavior is influenced by many factors, such as personal habits, emotions, brain state, and so on. Under long-term training, the operators' proficiency will gradually increase along with the efficiency and speed. During the process, they form individual operation habits combine with their inherent personalities. It's necessary to meet the common habits of people to improve the speed and also need to compatible with the differences of habits to reduce the difficulty of operation. At the same time, the high efficiency behavior pattern is certainly need to be promoted, and inefficient behavior patterns should be avoided by the operator.

4 The Ergonomic Evaluation Platform

We build up a scientific assessment of environmental ergonomics based on large data mining, machine learning and artificial intelligence technology to solve the problems of small data in small world. Through the ergonomic evaluation platform, we apply the methods of Quantified Self to collect operators' overall data which is based on objective data and supplemented by subjective data. Through the machine learning, a comprehensive multidimensional assessment model of the complex system is proposed with the use of continuous accumulation of data and the mediated by working load (physiological load and cognitive load) (Fig. 2).

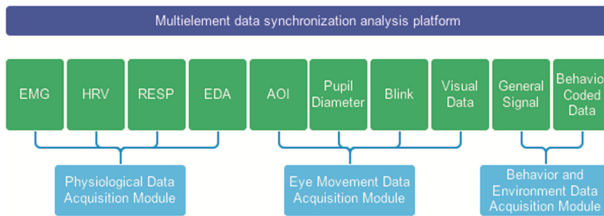


Fig. 2. Ergonomic evaluation platform

The system combines eye movement with motion capture and physiological synchronization technology. It uses wearable data acquisition technology and wireless data transmission technology to let operators can completely free from any interference when collecting data. Human-environment synchronization platform is capable of: Recording, tracking and analyzing real-time psychological and physiological changes of users, such as ECG, skin electricity and other indicators; analyzing people's attention, cognitive load, fatigue; Synchronizing real-time records involved human behaviors, equipment running information and the environmental information, such as temperature and humidity.

The system collects and analyzes the causal relationship between the changes of human-computer-environment interaction, and realizes real-time simultaneous recording and analysis of human-environment data. Therefore, it accomplishes multi-dimensional data visualization analysis. At the same time, for the effective data extraction and visualization presentation, we improve the human-computer interaction interface and system process to build an effective monitoring and evaluation methods. According to the different design for the information display interface of the aircraft system, the indicators such as the physiology and eye movement of the operator are analyzed. Meanwhile, the time, the number of occasions and the path of the operation task are explored and analyzed. We found out the good and bad of the operation interface and tried to improve the interface to become a standard of intelligent human-computer interface.

5 Conclusion

Quantified Self combining with big data technology can be applied to the evaluation of complex information system, which greatly promotes the development of China's military strategy. It not only can improve the airborne information system interface and the operation efficiency but also provides more possibilities in real-time monitoring, combat multi-distributed data acquisition and other aspects. Furthermore, sufficient and comprehensive data contribute to display interface design, flexible layout and adaptive reconfiguration. The system makes an effort on establishing a real-time and high-precision model of combat personnel state perception based on physiological data and neural calculation real-time analysis. Moreover, it increases the accuracy of automatic online analysis based on deep learning training.

References

1. What will Royal Navy warships look like in 2050? Jonathan Beale Defense correspondent, BBC News, 31 August 2015
2. Jing, L.: Encoding information of human-computer interface for equilibrium of time pressure. *J. Comput. Aided Des. Comput. Graphics* **25**(7), 1022 (2013)
3. Wang, H.: In the information age, human-computer interaction design of complex system are very important. *China Aviation News* (2016)
4. Hou, W.: Customer satisfaction evaluation model based on pupil size changes. *Space Med. Med. Eng.* **05**, 001 (2013)

Application of Speech Recognition Technology in Logistics Selection System

Tianzheng Fu^{1(✉)} and Bin Sun²

¹ Wuhan Second High School, Wuhan 400010, China
22836099@qq.com

² Zhen Kun Hang Industrial Supermarket, Shanghai 201716, China

Abstract. Speech recognition technology is designed to be used in the logistics picking system. Picking personnel start picking receive voice command from system, he feedbacks “check code” by voice, finish man-machine dialogue, choose terminal equipment to capture the “checksum” for identification. After successful verification, complete the sorting operation. When speech recognition technology is used in logistics picking system, walking time can be reduced, the work flow will simplified and the data transmission accuracy and picking efficiency will be improved, it is conducive to promote logistics service level, enhance the economic efficiency of logistics enterprises and customer satisfaction.

Keywords: Speech recognition technology · Logistics picking system
Check code · Picking efficiency

1 Introduction

Order picking based on product barcode is widely adopted in automatic logistics and warehouse management systems. However, barcode order picking presents several disadvantages when the order number increases significantly. Firstly, as the number of order increases, system capacity does not scale-up easily, leading to delay in order delivery. Secondly, currently barcode order picking systems may still rely heavily on human labors. As a result, the entire system becomes error-prone and inconsistent in system efficiency. In the present paper, we propose a voice recognition based order picking system. It is our contention that the introduction of voice recognition and voice based control system can significantly reduce the physical activity at the order picking production line. This proposed approach, therefore, is applicable in labor intensive and high throughput retail warehouse/distribution and logistics centers, in particular, those that are not equipped with automatic and semiautomatic systems.

2 Speed Recognition Technology

Automatic Speech Recognition (ASR) refers to a whole raft of technologies that aim to collect and process human speech and digitise such data into computer understandable

and actable data and/or instructions. Based on retrained models, computers should be able to performed the entire process without or with very limited human intervention.

Upon receiving human speech signal, ASR systems process the data based on features such as ambient/background signals, timbre, pitch, etc. Figure 1 depicts the key components of an ASR system. An ASR system normally consists of 5 modules, preprocessing, feature extraction, model training, model scoring and selection, and post-processing. The workflow can be largely divided into model training and model application.

- (1) Preprocessing module: Speech signal includes filtering, A/D conversion, filtering, demonising, speech enhancement, signal smoothing, end-point detection, etc.
- (2) Feature extraction: After preprocessing, speech signals are subject to time-frequency analysis, Cepstral analysis and wavelet transformation. This is to extract from the signal data such features as: timbre, language, and voice contents.
- (3) Model training: Features extracted by the previous module are then fed into training algorithms to obtain language models. Model training normally is an iterative process wherein features are evaluated, re-processed and optimised so as to construct models that can reflect all features of the input data. Trained models are stored in a model library.
- (4) Model scoring and selection: When ASR system is in application mode, features extracted from speech signal are utilised to identify and retrieve the best model from the model library. A predefined scoring scheme can guide the selection of best matching models.
- (5) Post-processing: Natural languages are ambiguous. In order to improve the system performance, it may be necessary to introduce linguistic and semantic analysis to the output of selected speech signal model.

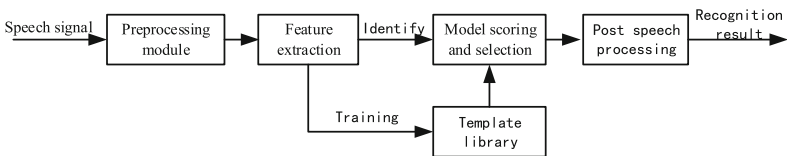


Fig. 1. Chipset for speech recognition

3 Chipset for Speech Recognition

The envisaged use case of the proposed system is that the speech recognition system should be a portable device that the order picking staff can easily carry along without hindering their normal work routines. Such a scenario derives a plethora of requirements on speech processing speed and accuracy, device portability, device energy consumption profile. In the present paper, we focused on local dialects and opt for non-specific speech recognition chip. We also tuned the model library based on the core user population, ambient and environmental noise, and typical use cases of the distribution centre where the system will be evaluated and put into production.

Currently, widely used non-specific speed recognition chips include ASR M08, LD3320 and LingYang 61A. Such chips do not require pre-recording of speech signals for initialisation and validation and are suitable for our envisaged use case [1].

LD3320 speech recognition module is a specialised processor with external circuits including AD, DA converters, microphone interface, audio output interface, and parallel and serial interface. It benefits from small physical size and low power consumption, lending itself to mobile applications. LD3320 embeds speech recognition module trained based on a large amount of speech data. It provides an off-the-shelf solution for many use cases. LD3320 provides a versatile of external control and interfaces, including dynamic editing of the recognised keywords. LD3320, therefore, facilitates further development of speech recognition functionalities and customisation against specific application context [2].

End users of the proposed speech recognition system are order picking staff in labour intensive manual warehouse/distribution centres. The speech recognition system is expected to be worn by the users while they are moving between aisles, staging areas, order picking lines and storage spaces. It, therefore, should be light weight, low energy consumption, easy to carry and highly responsive [3]. Meanwhile, as the staff turnover rate is very high in such a working environment, the speech recognition module should be non-specific [4].

LD3320 presents the following key features:

- (1) Integrated Flash and RAM. This eliminates the needs for external storage and thus reduce the complexity and cost of the system and overall energy consumption profile.
- (2) Embedded speech recognition models. The on chip models are already suitable for many generic application scenarios. It therefore presents a low learning curve for adoption.
- (3) Parameter tuning on distance and sensitivity.
- (4) No requirement on prior training and recording.
- (5) Dynamic keyword editing allows easy extension and adaption to new scenarios.
- (6) High accuracy rate (95%) against a list of as many as 50 keywords.
- (7) Integrated A/D, D/A convertors, Integrated amplifier circuit and a 550 mW speaker interface for playback; parallel and serial interface for further development.
- (8) Can easily switch between sleep and activate states to reduce energy consumption.
- (9) Working power supply of 3.3 V. LD3320 can be powered by three AA batteries to meet the power supply needs for portable systems.

LD3320 ICRout is based on keyword recognition. Figure 2 illustrates key components of LD3320.

LD3320 collects speech signal through the integrated microphone (MIC). The signal is then subject to spectrum analysis, feature extraction and feature engineering so as to be ready for keyword extraction. A trained speech recognition model will then be applied to the processed signal, outcome of which are candidate words which will be compared against a predefined list provided to the system. During the final step, the system will compute a score for each candidate keywords and output the one(s) with the highest

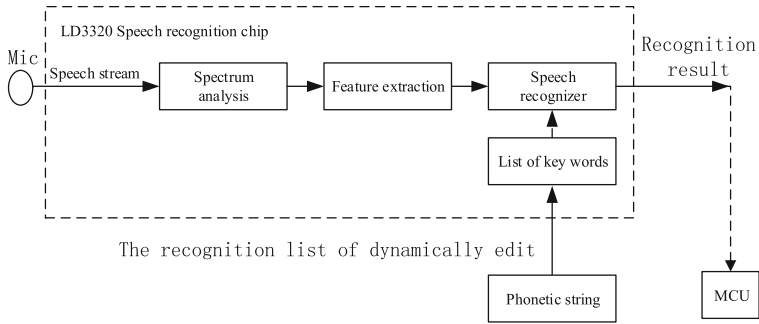


Fig. 2. The working principle of speech chip

score(s). Human intervention is possible by dynamic keyword editing through Micro Control Unit (MCU).

LD3320 is equipped with two speech signal collection and recognition modes:

- (1) Fixed Interval based: Based on a predefined interval (e.g. 3 s), LD3320 collects and records all speech signal data during the given time window. At the end of a time window, data collection is put on hold and keyword detection is only performed on signals collected within the time window.
- (2) Continuous analysis: LD3320 leverages a voice activity detection technology (VAD) to identify the beginning and end of human speech out of environmental and ambient sound. All speech signals between these two points are collected, upon which further processes are applied.

Due to the ambiguity caused by multiple matchings, when processing input speech signals, LD3320 considers any matching as interim results and does not output the identified keywords until the input speech signal stops (i.e. the end point of human speech is identified or a predefined time interval ends). When a signal ending condition is reached, LD3320 deems the input signal complete and thus the optimal keyword matching results are returned. For instance, the keyword list may contains “201” and “2017”. When processing speech signal, when “1” is detected, the best matching keyword is “201” with “2017” as a candidate with high probability. LD3320 will proceed as follows:

- (1) if input signal ends, output “201”;
- (2) if input signal continues and “7” is detected, recomputes “2017” as the best match. In the end, if not speech signal after “7”, “2017” is deemed best matching keywords and returned to end users.

4 Application of Speech Recognition in Order Picking

Speech recognition enabled order picking proceeds as follows:

- (1) order picking staff initiates the device by instructing “start operation”. Once receiving the initiation instruction, the portable device starts to “read” out the region

- number, aisle number, and shelf number of the first order. It also instruct the order picking staff to read out bar code of the picked items.
- (2) When the item is located, order picking staff reads the barcode. The portable terminal compares recognised barcode with the one in the picking order. If matches, portable terminal will pronounce quantity of item for the order; otherwise, portable terminal will read out location information again.
 - (3) When the current order is finished, order picking staff instruct the device with “task complete”. The portable device changes the status of the current order and moves to the next one in the order queue. If the order queue is empty, the portable terminal pronounces “operation complete”.

Barcode comparison in step two acts as a key checking point. This is to avoid potential cost introduced by human errors. If the barcode does not match, order picking staff will be remaindered the correct location information or provided means to manually double-check the order details.

The envisaged order picking scenario limits the keyword search space to reduce system complexity. As shown above, interactions between human order picking staff and portable terminal are restricted to the following keywords: “start operation”, “repeat”, “task complete” and digits based item barcodes. Apart from barcodes, the other instruction speech patterns can be preloaded, tuned and stored locally in the portable terminal to enable offline non-specific speech signal recognition. Terminal and server communication is only needed for handshaking, system initialisation, and downloading order details. Downlink and uplink bandwidth can be kept to minimum and thus improve system performance by reducing network latency.

5 Evaluation and Discussion

A preliminary evaluation and comparative study has been carried out. Figure 3 demonstrates the difference between conventional and speech recognition based order picking workflows.

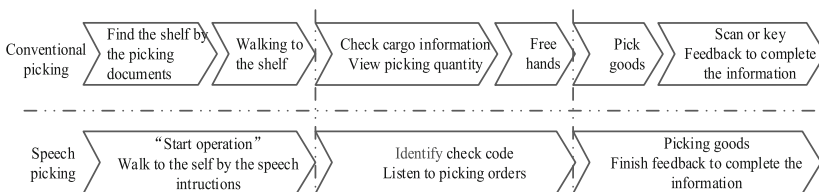


Fig. 3. The difference between conventional and speech recognition based order picking workflows

It is evident that our proposed solution can significantly reduce physical activities that are inevitable in conventional approach based on barcode or RF scanning. Reduced physical activity leads to improved work efficiency and reduced human errors due to fatigue and negligence. Speech recognition also simplified the overall workflow from

original six steps to three by integrating and removing such activities as operating scanners. The reduced steps also contributed to cost reduction through paperless work space, per order time reduction, and reduced error-rate.

The speech recognition based terminal optimises human system interface. The underlying system efficiency needs to be based on route optimisation and shelving and stock optimisation which are beyond the scope of this paper [5].

6 Conclusion

The application of speech recognition in warehouse and logistics is beneficial in the following aspects:

- (1) Significantly reduce travel distance of order picking staff
- (2) Simplify the order picking workflow
- (3) Reduce errors due to human factors
- (4) Increase efficiency of order data broadcasting

Jointly, the above lead to increased efficiency of order picking and thus reduced overall cost.

References

1. Qingxiu, M., Zhengyun, R.: Voice picking system based on indoor positioning technology of RFID. *Artif. Intell.* **18**, 50–53 (2015)
2. Qin, Y., Yong, L.V.: *Speech Signal Processing and Recognition*, pp. 7–9. National Defense Industry Press, Beijing (2015)
3. Jinping, L.: Simulation analysis of picking path and storage allocation strategy in distribution center. *Simul. Intell.* **04**, 310–315 (2015)
4. Zhao, Q., Hu, B., Shi, Y., Li, Y., Moore, P., Sun, M., Peng, H.: Automatic identification and removal of ocular artifacts in EEG—improved adaptive predictor filtering for portable applications. *IEEE Trans. Nanobiosci.* **13**(2), 109–117 (2014)
5. Qingguo, Z., Lihua, H., Rongrong, W., et al.: The application of speech picking technology in drug storage work. *Chin. Pharm.* **27**, 501–503 (2014)

Author Index

- Abramov, Vitaly 158
Akram, Aftab 410
- Bai, Shuotian 433
Bao, Tie 472
- Cai, Weiwei 108
Cerotti, Davide 616
Chang, Liwen 571, 588
Chen, Boting 364
Chen, Dingfang 364, 561, 571, 582
Chen, Guohua 422
Chen, Hanhua 330
Chen, Lina 354
Chen, Ming 453
Chen, Mo 76
Chen, Qingzhang 354
Chen, Rui 638
Chen, Xiaoling 648
Chen, Yangpeng 364
Cheng, Yuan 108
- Dautov, Rustem 183, 394, 616
Deng, Zhongliang 245
Ding, Jundong 258
Ding, Lei 189, 201
Ding, Rui 422
Distefano, Salvatore 183, 394, 616
- E., Haihong 382
- Fan, Jiachen 245
Fan, Jiawei 608
Feng, Chunyan 118
Flint, Jonathan 433
Fu, Chengzhou 410, 422
Fu, Haohui 164
Fu, Tianzheng 654
- Gafarov, Fail 158
Gao, Qian 64
Gao, Sihua 252
Gao, Yan 561
- Gao, Yuanbo 433
Gong, Ping 1
Gu, Bo 301, 342, 376
Gu, Songyuan 465
Guo, Da 274
Guo, Kun 410
Guo, Qin 582
Guo, Xing 265
- Han, Xiao 118
Han, Zhian 201
He, Chaobo 422
He, Fazhi 108
He, Mingshu 503
Hong, Yawei 588
Hou, Chunping 95
Hou, Wenjun 527, 627, 648
Hu, Bin 433
Hu, Jingbo 582
Hu, Kai 53
Hu, Neng 265
Hu, Zhengying 311
Huang, Ruqin 342
Huang, Tianhao 588
Huang, Weidong 443
- Jia, Zongpu 465
Jiang, Weijin 538, 550
Jiang, Wenchao 85
Jiang, Yuncheng 410
Jiang, Zhiyang 627
Jiao, Dongdong 400
Jiao, Jichao 245
Jin, Hai 330
- Kang, Zhongfeng 215
Kong, Xuedong 561
Kugurakova, Vlada 158
- Li, Baobin 400
Li, Bo 364
Li, Chaoqiang 648
Li, Chuanjie 85

- Li, Chunying 453
 Li, Dawei 139
 Li, Hao 150, 648
 Li, Lijie 582
 Li, Lu 76
 Li, Mingkun 382
 Li, Qiao 274, 318
 Li, Ruonan 258
 Li, Shaobo 588
 Li, Xuejing 164
 Li, Yibin 130
 Li, Zhuohuan 382
 Lian, Jian 130
 Lin, Dexi 85
 Lin, Jinjiao 130
 Lin, Sui 85
 Lin, Xiaorong 164
 Liu, Baoling 311
 Liu, Fangfang 118, 516
 Liu, Guangyue 588, 608
 Liu, Jiwei 453
 Liu, Mengmeng 34
 Liu, Ningning 23, 318
 Liu, Shufen 13, 23, 201, 252, 465, 472
 Liu, Ting 527
 Liu, Xiyu 1, 46, 102, 208
 Lu, Kaining 173
 Lv, Xiao 108
- Ma, Lujian 311
 Ma, Tongtong 95
 Ma, Yue 342
 Man, Yi 76, 232
 Mao, Chengjie 422
 Mei, Jie 571, 582
 Meng, Dejie 453
 Merlino, Giovanni 616
 Miao, Chen 13
 Miao, Chunyu 354
- Ning, Min 481
- Pan, Changqing 288
 Peng, Chongxiao 376
 Pu, Haitao 130
 Puliafito, Antonio 616
- Qi, Feng 34
 Qin, Hanfeng 595
 Qin, Xiaoqi 288
 Qin, Yajuan 164
- Ren, Ligang 232, 376
 Ren, Liyan 28
- Sabitov, Almaz 158
 Senko, Oleg 394
 Sheng, Qing 527
 Shi, Huafeng 582
 Shi, Yonghui 465
 Song, Meina 274, 301, 318, 342, 376, 382
 Su, Yiming 571
 Sui, Xiaoyun 433
 Sun, Aobing 85
 Sun, Bin 654
 Sun, Weiqi 288
 Surnin, Oleg 394
- Tan, Wen'an 53
 Tang, Anqiong 53
 Tang, Yong 410, 453
 Tao, Menglun 364
 Teng, Yinglei 288
 Tian, Tian 64, 481
- Wang, Baoliang 173
 Wang, Gengyi 527
 Wang, Jingying 433
 Wang, Mou 608
 Wang, Pan 53
 Wang, Qian 443, 608
 Wang, Qiang 139
 Wang, Sihan 571
 Wang, Xiaojuan 301, 503
 Wang, Xinyi 118
 Wang, Yanhua 46, 208
 Wang, Yixuan 443
 Wang, Zhen 503
 Wei, Yifei 274, 301, 318, 342, 376
 Wu, Jiangming 492
 Wu, Kaili 274
 Wu, Shupeii 588
 Wu, Zhenglun 472

- Xiang, Jianwen 561
Xiang, Laisheng 46, 102, 208
Xiao, Ya'nan 288
Xiong, Shengwu 561
Xiong, Yuping 252
Xu, Weifeng 150
Xu, Wenyuan 150
Xu, Yuhui 538, 550
- Yang, Bo 215
Yang, Chunhui 561
Yang, Fan 64, 481
Yang, Yanfang 364
Yang, Yang 95
Yao, Hong 64, 481
Yao, Susu 173
Yao, Zhilin 13
You, Jingwen 503
Yu, Chen 330
Yu, Meng 139
Yuan, Yahui 400
Yue, Guanghui 95
- Zang, Wenke 28
Zeng, Weiquan 422
Zeng, Zhimin 516
Zhang, Bao 102
- Zhang, Duo 232
Zhang, Longtao 516
Zhang, Ruiguo 330
Zhang, Shupeng 627
Zhang, Xingang 189
Zhang, Xinjia 23
Zhang, Yang 588
Zhang, Yi 342
Zhang, Yong 258
Zhang, Zhewei 164
Zhang, Zhiqiang 301, 311
Zhao, Huizhen 173
Zhao, Liang 258
Zhao, Mengyu 318
Zhao, Xiuyu 481
Zhao, Xuehui 189
Zheng, Congxing 571
Zheng, Kun 64
Zheng, Tinggang 481
Zheng, Wanbo 189, 201
Zhou, Jiehan 330
Zhou, Yang 433
Zhu, Shaohui 330
Zhu, Tingshao 400, 433
Zhu, Yemei 252
Zhu, Yong 608
Zu, Qiaohong 492, 638